TERN

NCRIS
National Research
Infrastructure for Australia
An Australian Government Initiative

A TERN Landscape Assessment Initiative

EFFECTIVE FIELD CALIBRATION AND VALIDATION PRACTICES

A practical handbook for calibration and validation of satellite and model-derived terrestrial environmental variables for research and management.

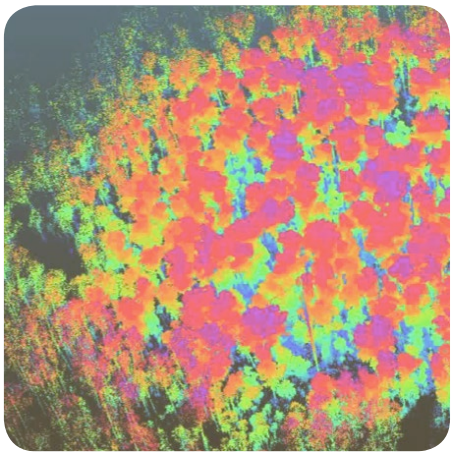

Version 1.3
August 2018

tern.org.au

Table of Contents

Acknowledgements ii

Foreword iii

Acronyms iv

Chapter 1 Introduction 1

Chapter 2 Review of validation standards of biophysical Earth Observation products 8

Chapter 3 Field data collection and management for Earth Observation image validation 29

Chapter 4 Calibration of optical satellite and airborne sensors 52

Chapter 5 Effective guidelines for calibration and validation of SAR data and derived biophysical products 69

Chapter 6 Overview of ground based techniques for estimating LAI 83

Chapter 7 Validation of Australian Fractional Cover Products from MODIS and Landsat Data 110

Chapter 8 Persistent Green Vegetation Fraction 125

Chapter 9 Satellite Phenology Validation 146

Chapter 10 Estimating foliar chemistry of individual tree crowns with imaging spectroscopy 167

Chapter 11 Tree Crown delineation 179

Chapter 12 Measurement of above ground biomass 189

Chapter 13 Vegetation spectroscopy 206

Chapter 14 The Spectroscopy Dataset Lifecycle: Effective Practices for Exchange and Dissemination 218

Chapter 15 Quality Assurance Steps for Landscape Assessment Hyper-Spectral Data 233

Chapter 16 Airborne LiDAR Acquisition and Validation 244

Chapter 17 Australian examples of field and airborne Landscape campaigns 276

Chapter 18 A calibration and validation framework to support ground cover monitoring for Australia 308

Chapter 19 Terrestrial LiDAR for measuring above-ground biomass and forest structure 321

ISBN 978-0-646-94137-0

TERN Australia
The University of Queensland
Goddard Building (Bld #8)
St Lucia QLD 4072
Australia

Tel: 61-7-3346-7021
Fax: 61-7 3365-1423
Email: tern@uq.edu.au
Web: www.tern.org.au

TERN Landscape Assessment
CSIRO Agriculture and Food
EcoSciences Precinct
41 Boggo Road
Dutton Park QLD 4102
Australia

Tel: 61-7-3833-5590
Email: info@auscover.org.au
Web: www.auscover.org.au

Front cover image credits
(Clockwise from left)

Suzanne Long
Yincai Zhou
Will Woodgate
Mark Grant
WorldView-2 Satellite Imagery
Peter Scarth

Back cover image credit
Darwin Centre for Bushfire Research

Acknowledgements

This handbook is the result of the generous contributions of multiple researchers and practitioners from various levels of government, research institutions, academia and private industry around the world. We wish to express our deep appreciation to all authors and contributors to this handbook, who shared their experience gained through years of effort in the field. The calibration and validation of environmental data products, and indeed the successful operation of any scientific facility, can only be done through collaborative work. Although too many to list, we would like to thank all of those who have been involved with the collection, processing and use of information derived from field, airborne, and satellite sensors in Australia and overseas. We also acknowledge the support of the Australian Government Department of Education and Training National Collaborative Research Infrastructure Strategy (NCRIS) for the establishment and ongoing funding of Australia's Terrestrial Ecosystem Research Network (TERN), whose goal is to provide open access for researchers to Australia's land-based ecosystem monitoring infrastructure, data and research tools and thus contribute to a broader understanding and long-term sustainable management of Australia's ecosystems.

Last but not least, we would like to thank the external reviewers for their constructive comments and suggestions.

Foreword

Earth Observation data are regarded as critical and essential information across multiple sectors in most countries around the world. However, for the EO data to be useful, to support decision making and reporting activities, the collection of image and field data sets needs to be accurate, precise and able to be reproduced following appropriate procedures.

TERN's Landscape Assessment platform (also known as TERN Landscapes) operates an open national capability that provides access to verified, science-quality dynamic soil and land surface data in which will be continuously improved with high end data analytics tools. TERN Landscape Assessment integrates TERN-wide observations to meet the needs of ecosystem researchers and support the use of factual information for policy makers and nature resource managers. Additionally, TERN Landscape Assessment will identify the need for and provide access to an appropriate suite of dynamic information infrastructure relevant to biomass, biodiversity and land use dimensions of terrestrial ecosystem research and management.

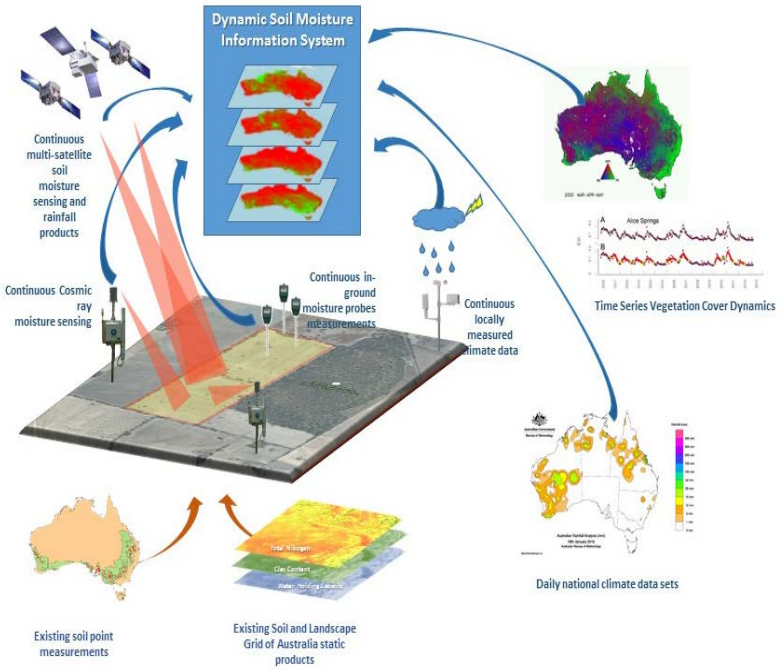

Data Model Integration Product by TERN Landscape Assessment

This handbook, structured around a unique collaboration across the remote sensing community in Australia developed by TERN (www.tern.org.au), collates information related to calibration and validation (Cal/Val) activities of remote sensing derived products that is scattered across the literature. It collates effective calibration and validation practices that link closely with internationally agreed protocols, such as those set by the Committee on Earth Observations (CEOS) – Working Group on Cal/Val. The methods outlined in this resource are based on collaborations across various levels of government, research institutions, academia and private industry entities involved with the collection, processing and use of information derived from satellite and airborne sensors. They build on protocols developed in other national environmental data facilities within TERN, where vegetation structure, composition and ground cover information is collected using systematic and clearly defined methods. It has been designed to serve as a resource for conducting environmental science, mapping and monitoring using satellite and airborne image data.

This handbook is intended to act as a starting point for information on effective Calibration/Validation practices. It is intended to present state of the art knowledge and promote discussion and criticism. To reflect the broader focus of TERN's Landscape Assessment platform, especially in soil science infrastructure, this manual will be refined and updated in 2019 with expanding chapters covering model-data assimilation, descriptors of soil water characteristics, soil moisture products and inland water, just to name a few. We commend you to read, assess, and contribute to this resource which endeavours to ensure that a sound link between ground and image data is maintained. This will allow EO data to be used for ecosystem science and management.

Acronyms

AAS/AATSE	Australian Academy of Science and the Australian Academy of Technological Sciences and Engineering
AATSR	Advanced Along Track Scanning Radiometer (ESA)
ABARES	Australian Bureau of Agricultural and Resource Economics and Sciences
AC	Atmospheric Correction
ACORN	Atmospheric CORrection Now
ADEOS-II	Advanced Earth Observing Satellite 2
AGB	Above Ground Biomass
AGL	Above Ground Level
AGOS	Australian Geophysical Observing System
AHD	Australian Height Datum
ALOS PALSAR	Advanced Land Observing Satellite Phased Array L-band
ALS	Airborne laser scanning
AMSR-E	Advanced Microwave Scanning Radiometer - Earth Observing System
ANDS	Australian National Data Service
ANZLIC	Australia New Zealand Land Information Council
AOD	Aerosol Optical Depth
ARA	Airborne Research Australia
ARI2	Anthocyanin Reflectance index
ASCWG	Australian Satellite Calibration Working Group
ASD	Analytical Spectral Devices
ASPRS	American Society for Photogrammetry and Remote Sensing
ATREM	Atmospheric REMoval program
AusCover	The remote sensing data facility of TERN
AusPlots	Plot based monitoring program of TERN
AVHRR	Advanced Very High Resolution Radiometer (NOAA)
BIL	Band Interleaved by Line
BIP	Band Interleaved by Pixel
BRDF	Bidirectional Reflectance Distribution Function
BS	Bare soil
BSQ	Band Sequential
Cal/Val	Calibration and Validation
CC	Canopy Cover
CCD	Charge-coupled Device
CEOS	Committee on Earth Observation Satellites
CEOS-WGCV	Committee on Earth Observing Satellites Working Group on Calibration and Validation
CHM	Canopy Height Model
CP	Check Point
CR	Continuum Removal
CRCSI	Cooperative Research Centre for Spatial Information
CSIRO	Commonwealth Scientific and Industrial Research Organisation
dB	Decibels
DBH	Diameter at Breast Height
DEM	Digital Elevation Model
DGPS	Differential Global Positioning System

DHF	Hierarchical Data Format
DHP	Digital Hemispherical Photography
DN	Digital Number
DOI	Digital Object Identifier
DSM	Digital Surface Model
DWEL	Dual Wavelength Echidna Lidar
EC	Eddy Covariance method for measurements of CO2, H2O and energy flux
ECV	Essential Climate Variable
EDM	Euclidian Distance Map
EGS	End of Growing Season
ENVI	Environment for Visualizing Images
EO	Earth Observation
EOS	Earth Observation Systems
ESU	Elementary Sampling Unit
ETM+	Enhanced Thematic Mapper (Landsat 7)
EVI	Enhanced Vegetation Index
ExG	Excess green – RGB camera index
fAPAR	fraction of Absorbed Photosynthetic Active Radiation
FCM	Fractional Cover Model
fCover	Fractional Cover
FLAASH	Fast Line-of-site Atmospheric Analysis of Spectral Hypercubes
FOV	Field of view
fPAR	Fraction of Photosynthetic Active Radiation (also known as fAPAR)
$fPAR_{NPV}$	fPAR from the non-green fraction of vegetation
$fPAR_{PAV}$	fPAR from the active (green) fraction of vegetation
FPC	Foliage Projective Cover
FTIR	Fourier Transform Infrared Spectoscopy
FTP	File Transfer Protocol
FVC	Fractional Vegetation Cover
Fveg	Fraction of vegetation
GCP	Ground Control Point
GDA94	Geodetic Datum of Australia 1994
GDM	Green dry matter
GEP	Gross Ecosystem Productivity
GEPsat	GEP at saturation
GIS	Geographic Information System
GLI	Global Imagery
GLT	Geographic Lookup Table
GNSS	Global Navigation Satellite System
GPS	Global Positioning System
GPS/GNSS	Global Positioning System / Global Navigation Satellite System
GRS80	Geodetic Reference System 1980
ICSM	Intergovernmental Committee for Surveying and Mapping
IDL	Interactive Data Language
IFOV	Instantaneous Field of View
IGBP	International Geosphere-Biosphere Program
IGM	Input Geometry Data

IMU	Inertial Measurement Unit
ISO	International organization for standardization
JPEG	Joint Photographic Experts Group (image format)
K	light extinction coefficient
K&C	Kyoto and Carbon
KML	Keyhole markup language
LAI	Leaf Area Index
LAI_e	Effective Leaf Area Index
Landsat ETM	Landsat Enhanced Thematic Mapper
Landsat OLI	Landsat Operational Land Imager
Landsat TM	Landsat Thematic Mapper
LAS	LASer file format
LC	Land Cover
LCI	Land Condition Index product
LDCM	Landsat Data Continuity Mission (Landsat 8, NASA)
LGS	Length of active Growth Season
LIA	Local Incidence Angle
LiDAR	Light Detection and Ranging
LPV	Land Product Validation
LTER	Long term Ecological Research sites
LUE	Ecosystem Light Use Efficiency
MAE	mean absolute error
MERIS	MEdium Resolution Imaging Spectrometer
MGA94	Map Grid of Australia 1994
MNLI	Modified non-linear vegetation index
MODIS	Moderate Resolution Imaging Spectroradiometer
MODLAND	MODIS Land Discipline Team
MODTRAN	MODerate resolution atmospheric TRANsmission (for radiative transfer through the atmosphere)
MPLS	Modified partial least squares
MSL	Mean Sea Level
MSPN	Multi-scale Plot Network
MSR	Modified Simple Ratio
NBAR	Nadir BRDF-Adjusted Reflectance
NCAS	National Carbon Accounting System
NCI	National Computing Infrastructure
NDVI	Normalized difference vegetation index
NEON	National Ecological Observatory Network
NGO	Non-governmental Organization
NIR	Near-Infrared
NIRα	albedo NIR
NIST	National Institute of Standards and Technology (USA)
NLI	Non-linear vegetation Index
NPG	Non-Photosynthetic Vegetation
NPP	Net Primary Production
NPS	Nominal Post Spacing
NPV	Non-green Fraction of Vegetation (see PAV)
NSRSN	National Scientific Reference Site Network

NT	Northern Territory
NVIS	National Vegetation Information System
ODK	Open Data Kit
OHS	Occupational Health and Safety
OLIVE	On Line Interactive Validation Exercise
PAI	Plant Area Index
PAI_e	Effective Plant Area Index
PAR	Photosynthetic active radiation
PAR_{in_cpy}	Incoming PAR measured inside the canopy
PAR_{in_soil}	PAR incident to the soil surface
PAR_{in_top}	Incoming PAR measured at the top of the canopy
PAR_{out_soil}	Soil reflected PAR
$PAR\alpha$	Albedo PAR
PAV	Active (green) fraction of vegetation (see NPV)
Pc	Photosynthetic Capacity
PGS	Peak period of Growing Season, point in time of maximum vegetation activity
PLSR	Partial least squares regression
POLDER	Polarization and Directionality of the Earth's Reflectances
PRI	Photochemical reflectance index
PV	Photosynthetic Vegetation
QA	Quality Assurance
QA^4LiDAR	Compliance and Quality Assurance Tool for Airborne LiDAR
RAW	Image format that contains minimally processed data from the image sensor (e.g. digital camera)
RCS	Radar Cross Section
RE	Regional Ecosystem
RGB	Red-Green-Blue (refers to cameras)
RINEX	Receiver Independent Exchange format
RIO	Region of Interest (refers to subsampling of an image)
RMSE	Root Mean Square Error
RSMA	Relative Spectral Mixture Analysis
SAI	Surface area Index
SAR	Synthetic Aperture Radar
SAVI	Soil Adjusted Vegetation Index
SBA	Stand Basal Area
SDSM	Solar Diffuser Stability Monitor
SeaWIFS	Sea-Viewing Wide Field-of-View Sensor
SECV	Standard error of Cross-Validation
SGS	Start of Active Growing Season
SIS	Spectral Information System
SLA	Specific Leaf Area
SLATS	State Land and Tree Survey
SLC	Scan Line Corrector
SMATS	Spectral Mixture Analysis Time Series
SNV	Standard Normal Variate
SQL	Structured Query Language
SR	Simple Ratio

SRCA	Spectroradiometric Calibration Assembly
SRTM	Shuttle Radar Topography Mission
SSU	Secondary Sampling Unit
SVC	Supervised vicarious calibration
SW_{in}	Incoming short wave radiation
SWIR	Shortwave Infrared
SZA	Solar Zenith Angle
Ta	Air temperature
TEFLON	White reference material
TERN	Terrestrial Ecosystem Research Network
THREDDS	Thematic Real-time Environmental Distributed Data Services
TIC	Terrain Illumination Correction
TIDA	Tree Identification and Delineation Algorithm
TIFF	Tagged Image File Format
TIN	Triangulated Irregular Network
TLS	Terrestrial Laser Scanning
TM	Thematic Mapper (Landsat 5)
UEP	Ultimate eroded point
USGS	United States Geological Survey
UTC	Coordinated Universal Time
UTM	Universal Transverse Mercator
VALERI	Validation of Land European Remote sensing Instruments
VI	Vegetation Index
VIS	Visible
VNIR	Visible and Near-infrared
WBI	Water Band Index
WGCV	Working Group on Calibration and Validation
WGS	World geodetic system
WGS84	World Geodetic System 1984
WRS2	Worldwide Reference System 2

Chapter 1. Introduction

A.Held[1], S.Phinn[2], M. Soto-Berelov[3,4], S. Jones[3,4]

[1] CSIRO Centre for Earth Observation, Astromony and Space Science

[2] Remote Sensing Research Centre, School of Geography, Planning and Environmental Management, The University of Queensland

[3] Remote Sensing Centre, School of Mathematical and Geospatial Sciences, RMIT University

[4] Cooperative Research Centre for Spatial Information

*Corresponding author:
Alex.Held@csiro.au

1.1 Background

Images collected from aircraft or satellites and transformed to produce maps of features of the surface of the earth are commonly referred to as Earth Observation (EO) data. They are one of the most widely used sources of information and are used globally for mapping, monitoring and modelling our environments and their changes over time (e.g., Loveland and Dwyer, 2012; Magurran et al., 2010; Mathieu and O'Neill, 2008; Purkis and Klemas, 2011; Wulder et al., 2012). However, an intrinsic component of high quality remote sensing or EO data is the explicit link between the satellite or airborne image data and corresponding sampled ground measurements used for producing mapped products (e.g. biomass, ground cover, Leaf Area Index or LAI). This involves the calibration of sensors, application of mapping algorithms, and validation of the products. In some cases, this is referred to as "ground truthing". However, it should be recognised that field measurements are still not "truth", as all data are collected using sampling approaches and their match to satellite and airborne data is often not exact.

The aim of this handbook is to present effective practice methods for the collection and use of suitable ground measurements that can be used to calibrate and validate airborne and satellite image based data and derived mapped products. To date, there has been little effort in documenting the different aspects involved in field and airborne campaigns used to calibrate and validate EO data in a single source. Although a large body of knowledge surrounding Calibration and Validation (Cal/Val) exists, it is often scattered across government reports that are highly specific to a particular project, location, and data type. There is often no explicit coverage of this topic in textbooks on remote sensing, image processing and/or ecological and bio-geophysical mapping and modelling. "Effective Field Calibration and Validation Practices: A practical handbook for calibration and validation of satellite and model-derived terrestrial environmental variables for research and management." is designed to provide practical advice on generally accepted field-based measurement standards, calibration, and validation protocols for remote sensing data and derived products.

1.2 Accurate, Precise and Repeatable Environmental Monitoring Requires Image and Field Data

Earth Observation data are regarded as critical information across multiple sectors including government (at various levels), non-governmental organisations (NGO), research institutions, and private companies. They underpin a wide a wide range of activities across these sectors in Australia and around the world (ACIL 2008). But to improve the ability to obtain accurate representations of the earth and its processes, EO data must be calibrated and validated following appropriate procedures. These have been published across scientific papers and grey literature, but have not been compiled in a format specifically designed to guide such activities so they deliver accurate, precise and repeatable environmental information. Data should be accurate in that the ground measurements match the type of variable being estimated, and the location in time and space is the same. The measurements should be precise, in that they measure the same environmental variable at the same level of detail. The measurements should also be taken using specific instruments, techniques, and analytic procedures. This handbook has been designed to serve as a resource for conducting environmental science, mapping and monitoring using satellite and airborne image data. It covers a spectrum of image and field data sets and RS data products.

1.3 Collaborative, Shared Infrastructure, Algorithms and Data

This handbook has been structured around a unique collaboration across the remote sensing community in Australia developed by Australia's Terrestrial Ecosystem Research Network (TERN, www.tern.org.au). The goal of TERN is to provide open access for researchers to Australia's land-based ecosystem monitoring infrastructure, data and research tools and thus contribute to a broader understanding and long-term sustainable management of Australia's ecosystems. A central component is an explicit link between field (Figure 1.1a) and satellite/airborne image collection (Figure 1.1b), processing, and analysis that result in the delivery of maps of environmental properties. This is done by TERN's Landscape Assessment platform, delivered primarily by the TERN facility formerly known as TERN AusCover - http://www.auscover.org.au/), following the schema shown in Figure 1.1. This approach has triggered collaboration across various levels of government, research institutions, academia and private industry entities involved with the collection, processing and use of information derived from satellite and airborne sensors.

(a)

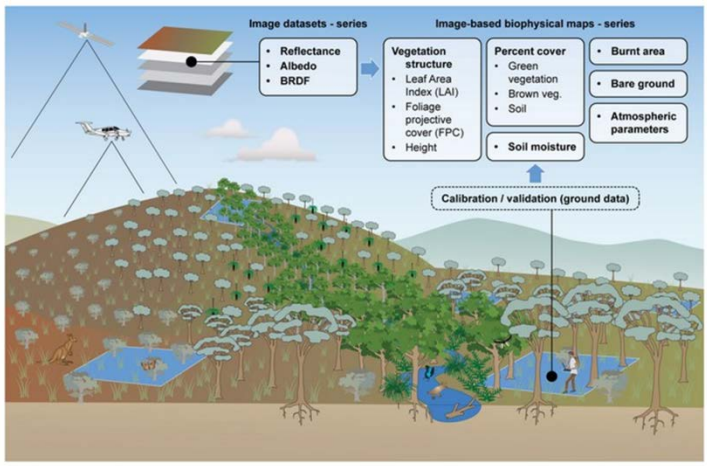

(b)

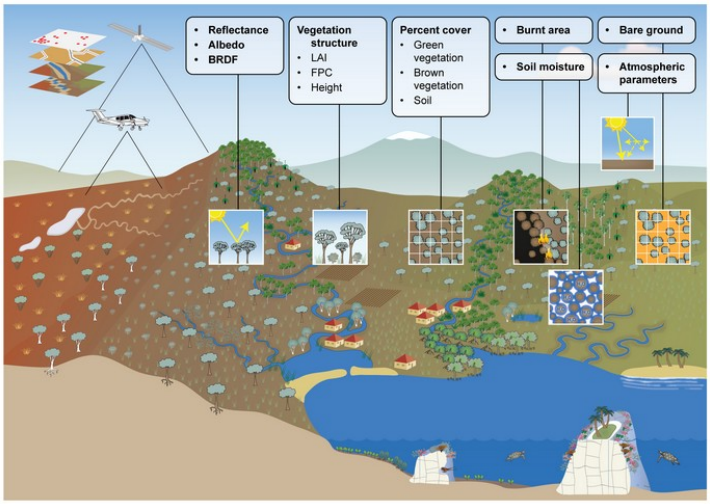

Figure 1.1

(a) Field data collection activities in TERN Landscape Assessment used to collect data for calibration and validation of satellite/airborne image maps of environmental properties.

(b) Satellite and airborne image data collection and processing activities for deriving Australian mapped products.

The methods outlined in this resource are based on such collaborations amongst the Australian remote sensing community. The handbook also makes reference to international guidelines and is built on protocols developed in other national environmental data facilities within TERN, where vegetation structure, composition and ground cover information is collected using systematic and clearly defined methods. An example is integration between TERN's two other observatory platforms TERN Ecosystem Surveillance and TERN Ecosystem Processes.

1.4 How to Engage, Use and Contribute to this Resource

This handbook provides direct guidance on how to collect field and image data sets required for producing accurate and repeatable maps of environmental properties. The protocols and approaches presented aim to link closely to internationally agreed protocols, such as those set by the Committee on Earth Observations (CEOS) – Working Group on Cal/Val (CEOS-WGCV). The intention is to present state of the art knowledge, promote discussion, and act as a starting point for collating information on Cal/Val. As such, this should not be a static resource and should be refined and updated periodically. To facilitate continual revision and addition as the field develops and as new data and methods arise, it is also presented in digital format. We commend you to read, assess, and contribute to this resource which endeavours to ensure that a sound link between ground and image data is maintained. Since we have not been able to cover all of the essential components of Cal/Val of different EO derived products, the next revision of this handbook intends to include Cal/Val activities for land cover, reflectance, burned area, and soil/geologic products. Although the handbook includes topics on Cal/Val from the general literature, examples and recommendations mainly focus on Australian ecosystems.

1.5 Outline of the Handbook

The outline of the handbook is shown in Figure 1.2. After a brief introduction, Chapter 2 summarises some of the major aspects involved when using ground-reference data to validate biophysical products derived from satellite imagery. Aspects such as site selection, site extent, and sampling design are discussed within the context of international and national validation campaigns. The authors also draw recommendations from the Committee on Earth Observing Satellites Working Group on Calibration and Validation (CEOS-WGCV).

Calibration and validation activities frequently require data to be independently collected across different scales using a range of instrumentation. For the data to be of value across the scientific community it needs to be managed appropriately. Chapter 3 summarises guidelines that promote good practice field data management and delivery. The author covers different topics associated with in-situ data collection and stresses the importance of quality assurance and data quality aspects. Data collected should be reportable to international standards and shared openly where possible.

The next two chapters focus on calibration. Key components related to the calibration of optical satellite data, including atmospheric correction, are covered in Chapter 4. The geometric and radiometric calibration of Synthetic Aperture Radar (SAR) derived biophysical products such as forest and land-cover are then presented in Chapter 5, which also includes validation aspects associated with SAR data and derived biophysical products.

The following chapters are devoted to the validation of specific EO derived products. Chapter 6 discusses the validation of Leaf area index (LAI) and Fraction of absorbed photosynthetic active radiation (f_{APAR}), closely related biophysical parameters that are often measured and validated in tandem. This chapter includes a review of some of the major global LAI and f_{APAR} product validation programs and a discussion of methods and instruments that can be used to collect measurements. It concludes by presenting a methodology designed for validating the MODIS collection 5 LAI product across Australian ecosystems.

Figure 1.2 Logical progression of image and field data collection, processing and integration as followed in this resource.

The validation of three national fractional cover products created using different sensor technologies (MODIS and Landsat) is then presented in Chapter 7. This is followed by the validation of a national Persistent green vegetation fraction product (which shows the fraction of persistent green vegetation between 2000 and 2010) using airborne LiDAR derived estimates of vertically projected cover (Chapter 8).

The next chapters focus on activities associated with validating different vegetation parameters. Chapter 9 is concerned with the validation of MODIS derived phenology metrics. These are obtained by timing and measuring the magnitude of seasonal changes in vegetation indices. Chapter 10 outlines a methodology for estimating foliar nutrients and plant secondary metabolites at an individual tree-crown level with imaging spectroscopy data. Chapter 11 reviews the most common algorithms used to delineate individual tree crowns and presents a step by step case study using image segmentation techniques. A *biomass estimation* chapter then provides a review of different validation methods that include remote sensing and *in situ* biomass measurement techniques. Chapter 13 (*Vegetation spectroscopy)* covers guidelines required for acquiring spectral measurements in the field. After presenting some basic theory surrounding the interaction of photons and vegetation, the authors warn readers about aspects that can perturb the spectral signal of vegetation. These include soil background or the viewing and illumination geometry. With this in mind, the necessary steps for obtaining field spectroscopy measurements are discussed (e.g., sampling design, data collection, associated metadata and data storage).

In today's information age, spectroscopy data management is a significant consideration for researchers and practitioners presenting challenges imposed by multi-disciplinary data producing activities. When data are created, published, exported, imported, transformed and shared by different parties and used for different

purposes, these actions form a data lifecycle. Creating a conceptualised model of this data lifecycle helps to better understand the nature of the data and the integration of previously disparate implementation efforts. Chapter 14 presents the newly enhanced AUS-SPECCHIO(V3) spectral information system within the context of a spectroscopy data lifecycle model for remote and proximal sensing activities, through a common set of lifecycle phases, features and roles established as best practice procedures.

Airborne sensors are frequently deployed for high-resolution mapping programs *per se*, but often also as part of satellite calibration programs and field campaigns. For example, high resolution hyperspectral, radar and LIDAR data can be used to upscale ground gathered observations, or to help calibrate satellite sensors passing overhead. Chapter 15 provides step by step information on how to georeference and atmospherically correct hyperspectral data. It also offers suggestions for assessing the quality of the georeferenced products; the spatial coverage of the data set; and the spectral at-surface reflectance image pixel values when compared against in-situ spectrophotometer measurements of ground calibration targets. Chapter 16 provides a brief review of LiDAR sensors; discusses the major considerations that impact a LiDAR survey (e.g., extent, vertical accuracy, point spacing, ground cover types and temporal variations); offers guidance regarding technical specifications; outlines a series of validation checks to assess the quality of LiDAR products; and presents a LiDAR Compliance and Quality Assurance Tool.

The handbook concludes by presenting a series of case studies that report on field validation campaigns that have taken place in Australia. Chapter 17 presents several TERN Landscape Assessment campaigns (formerly known as AusCover campaigns) carried out across TERN's 12 ecosystem process monitoring SuperSites, where sites that are representative of different ecosystems have been intensively characterised using data collected across multiple scales (ground based, airborne, and satellite). Chapter 18 presents a national validation campaign of ground cover conducted/collected to validate two of the Fractional Cover products presented in Chapter 7. Chapter 19 presents the uptake of terrestrial laser scanning (TLS, or terrestrial LiDAR) technology for monitoring ecosystems. This chapter describes data acquisition and analysis tools for (i) geometric modelling and (ii) gap probability monitoring.

These last three chapters cover a variety of topics associated with the collection of field data used to calibrate and validate EO data (from the planning to the implementation phase). We wish to express our deep appreciation to all authors and contributors of this handbook, who shared their experience gained through years of effort in the field. We also acknowledge the support of the Australian Government's National Collaborative Research Infrastructure Strategy (NCRIS) for the establishment and ongoing funding of TERN. The growing network of remote sensing experts and TERN will strive to keep this handbook updated and scientifically current. Lastly, we ask readers that have Cal/Val related protocols or papers to share them with us so we can include in our references in updated versions.

References

AAS & AATSE (2009a). An Australian Strategic Plan for Earth Observation from Space. Canberra.

AAS & AATSE (2009b). Decadal Plan for Australian Space Science 2009-2019. Canberra.

ACIL-Tasman (2010). Economic Value of Earth Observation from Space. Canberra.

ACIL (2008). The Value of Spatial Information: The impact of modern spatial information technologies on the Australian economy. CRC Spatial Information, ANZLIC- The Spatial Information Council. Melbourne, Australia: 171.

CSIRO (2012). Continuity of Earth Observation Data for Australia: Research and Development (2012, CEODA-R&D) G. Australia. Canberra.

Lindenmayer, D., E. Burns, N. Thurgate & Lowe, A. J. (2013). Monitoring Environmental Change. Canberra, CSIRO Publishing.

Loveland, T.R. & Dwyer, J.L. (2012). Landsat: Building a strong future. *Remote Sensing of Environment*, 122, 22-29.

Magurran, A.E., Baillie, S.R., Buckland, S.T., Dick, J.M.P., Elston, D.A., Scott, E.M., Smith, R.I. , Somerfield, P.J., & Watt, A.D. (2010). Long-term datasets in biodiversity research and monitoring: assessing change in ecological communities through time. *Trends in ecology & evolution,* 25 (10), 574-582.

Mathieu, P.P. & O'Neill, T. (2008). Data assimilation: From photon counts to Earth System forecasts. *Remote Sensing of Environment*, 112, 1258-1267.

Purkis, S., & Klemas, V. (2011). Remote Sensing and Global Environmental Change. London, Wiley-Blackwell.

Wulder, M.A., Masek, J.G., Cohen, W.B., Loveland, T.R., & Woodcock , C.E. (2012). Opening the archive: How free data has enabled the science and monitoring promise of Landsat. *Remote Sensing of Environment*, 122, 2-10.

Chapter 2. Review of validation standards of biophysical Earth Observation products

M. Soto-Berelov *[1,2], S. Jones [1, 2], E. Farmer[1], W. Woodgate[1,2]

[1] Remote Sensing Centre, School of Mathematical and Geospatial Sciences, RMIT University
[2] Cooperative Research Centre for Spatial Information

*Corresponding author:
Mariela.Soto-Berelov@rmit.edu.au

Abstract

In the context of remote sensing, validation refers to the process of assessing the uncertainty of higher level, satellite sensor derived products by analytical comparison to reference data, which is presumed to represent the true value of an attribute. Biophysical products characterise and map biotic and abiotic factors that influence the survival, development and evolution of organisms within the environment. Naturally, validation is an essential component of any earth observation program, since it enables the independent verification of the physical measurements obtained by a sensor as well as any derived products. After presenting some relevant definitions, this chapter draws on international and national validation campaigns to summarize some of the major components involved when using ground-reference data to validate biophysical products derived through Earth Observation (EO) data. These include site selection, site extent, and sampling design. Major Australian and international validation campaigns are exemplified for Leaf Area Index (LAI) and Foliage Projective Cover (FPC) vegetation products. The process of up-scaling, which enables the validation of coarse resolution products via the comparison of measurements made at various scales (i.e., ground-based, intermediate-airborne) is also reviewed. The chapter concludes with a brief section on alternative validation methods.

Key Points

- The Committee of Earth Observing Satellites (CEOS) has identified four stages of validation, each of which is progressively more comprehensive.
- Satellite derived products can be validated directly using an independent data source that is representative of the target values or indirectly through product inter-comparison and/or by collecting measurements across various scales and upscaling.
- Sites chosen for validation should meet certain criteria, including the following: be accessible to researchers; encompass existing facilities such as flux towers which collect measurements of biophysical variables over extended periods of time; have long-term commitment to scientific studies; represent significant areas of homogenous or uniformly mixed land cover.
- The site extent of a validation site must be large enough to represent the pixel size of the sensor being validated.
- The sampling design implemented for ground-based measurements is driven by two main factors: (a) the footprint of the field measurements and (b) up-scaling process used to integrate the field measurements and high resolution imagery.
- Field activities should be carried out within a week of satellite/airborne acquisition to prevent significant changes in vegetation. However, the rate at which the state of the vegetation evolves varies for different ecosystems and is also influenced by its successional stage.
- When devising a sampling design, many projects choose a sampling scheme based on elementary and secondary sampling units. Elementary sampling units (ESU) aim to capture the variability of the product being validated across the study site (this can be determined from a current land cover or floristic map, surface reflectance as characterised by recently acquired satellite imagery). Secondary sampling units (SSU) are distributed across the ESU and represent the specific locations where measurements are recorded. Different sampling designs can be implemented within SSU including fixed pattern, transect, randomised designs.
- Up-scaling is generally achieved via the integration of field measurements and a high-resolution image, which results in the production of a high resolution map of the parameter measured in the field.

2.1 Introduction

In 1984, the Committee on Earth Observing Satellites (CEOS) was established following a recommendation by the Economic Summit of Industrialized Nations Working Group on Growth, Technology, and Employment's Panel of Experts on Satellite Remote Sensing (http://www.ceos.org), to coordinate space-borne observations across the planet that help address current and critical scientific research questions. CEOS endeavors to optimise the benefits of space-borne Earth Observation (EO) by planning missions through the collaborative participation of its members, which include space agencies and both national and international EO organisations. In addition, CEOS is directly involved in planning and developing accessible and compatible data products, formats, services, applications and policies (CEOS WGCV Work Plan 2011-2016, 2014) that relate to EO data and missions.

CEOS, in consultation with end user organisations, helps specify EO product requirements. The desired product requirements are primarily driven by user needs, which include the key factors of: temporal resolution, spatial resolution, accuracy and stability. Accuracy is defined as the closeness of agreement between product values and true or reference values (GCOS, 2011). Stability is the systematic error of a product over a long period of time, typically a decade or more (GCOS, 2011). Both accuracy and stability of a product can be assessed using proficiency testing through ISO-13528, which sets out a framework for comparison of reference values with estimated or product values (e.g. Widlowski et al., 2013).

To be able to quantify data derived from EO missions and compare sensors and products and ultimately use these to tackle pressing scientific questions, CEOS established the Working Group on Calibration and Validation (WGCV) in 1984. The WGCV undertakes and promotes activities to coordinate and advance the calibration and validation of EO missions and data (Dowman 2004), so they can be of use across wide international user communities. When validating moderate resolution global products created from EO data such as MODIS, CEOS has identified four stages of validation (Table 2.1), each of which is progressively more comprehensive.

Table 2.1 CEOS Validation hierarchy (WWW2).

Stage	Description
Stage 1 Validation	Product accuracy has been estimated using a small number (typically < 30) of independent measurements obtained from selected locations and time periods and ground-truth/field program effort.
Stage 2 Validation	Product accuracy has been assessed over a widely distributed set of locations and time periods via several ground-truth and validation efforts. The spatial and temporal consistency of the product has been evaluated over globally representative locations and time periods. Results are published in peer-reviewed literature.
Stage 3 Validation	Product accuracy has been assessed over a globally distributed set of locations and time periods via several ground-truth and validation efforts. Product uncertainties have been well-established via independent measurements made in a systematic and statistically robust way that represents global conditions. Results are published in peer-reviewed literature.
Stage 4 Validation	Validation results for Stage 3 are systematically updated when new product versions are released and as the time-series expands.

The WGCV supports six subgroups. Each of these focuses on different technical areas (Table 2.2): land product validation; atmospheric composition; Synthetic Aperture Radar (SAR); microwave sensors; terrain mapping; infrared and visible optical sensors.

Table 2.2 Mission view of CEOS WGCV (CEOS WGCV five year working plan, 2012).

Subgroup	Mission
Land product validation	Foster quantitative validation of higher-level global land products derived from remote sensing data and report results so they are relevant to users.
Atmospheric composition	Ensure accurate and traceable calibration of remotely-sensed atmospheric composition radiance data and validation of higher level products, for application to atmospheric composition, land, ocean, and climate research.
Synthetic aperture radar	Foster high-quality synthetic aperture radar data from airborne and spaceborne systems through precision calibration in radiometry, phase and geometry, and validation of higher level products.
Microwave sensors	Foster high quality calibration and validation of microwave sensors for remote sensing purposes. These include both active and passive types, airborne and spaceborne sensors.
Terrain mapping	Ensure that characteristics of digital terrain models produced from Earth Observation sensors at global and regional scale are well understood and that products are validated and used for appropriate applications.
Infrared and visible optical sensors	Ensure high quality calibration and validation of infrared and visible optical data from Earth Observation satellites and validation of higher-level products.

Given this handbook recommends guidelines for the validation of terrestrial biophysical products, the Land Product Validation (LPV) subgroup is of particular relevance. The LPV is also subdivided into focus areas that represent terrestrial Essential Climate Variables[1] (ECV). The full list of ECV's that are technically and economically feasible for systematic observation comprises: Leaf Area Index (LAI)[2], Fraction Absorbed Photosynthetic Active Radiation (fAPAR)[3], river discharge, water use, groundwater, lakes, snow cover, glaciers and ice caps, ice sheets, permafrost, albedo, land cover (including vegetation type), above-ground biomass, soil carbon, fire disturbance, and soil moisture (GTOS, 2008).

This chapter focuses on the field survey techniques utilised to collect validation data and only briefly considers the up-scaling of these recorded measurements. International validation campaigns from major earth observing programs such as MODLAND (MODIS land discipline team) and ESA VALERI (Validation of Land European Remote Sensing instruments, Baret et al., 2006) are used as examples, given their focus on validating medium resolution satellite products (i.e., MODIS, MERIS) related to land cover and vegetation (e.g., LAI, Foliage Projective Cover or FPC, Fractional Vegetation Cover or FVC).

2.1.1 Validation in Australia

Earth Observation data are critically important to a number of Australian research, environmental, and government monitoring programs. The reliability and use of such data depend on the extent to which such data have been calibrated and validated. International calibration and validation (Cal/Val) programs are biased towards northern hemisphere vegetated ecosystems, leaving many of Australia's unique terrestrial ecosystems under-represented. The Australian Academy of Technological Sciences and Engineering

[1] Essential Climate Variables (ECV) can be defined as measurements of atmosphere, oceans, and land that are needed to meet the United Nations Framework Convention on Climate Change and requirements of the Intergovernmental Panel on Climate Change (Stitt et al., 2011).

[2] Leaf area index or LAI is typically defined as the total one-sided area of leaf tissues per unit of ground surface area (Watson, 1947)..

[3] fAPAR is defined as the fraction of photosynthetically active radiation (PAR) in the 400-700 nm wavelength range, that is absorbed by a canopy.

(AAS/AATSE) review of EO in Australia recognises that Cal/Val of earth observation systems (EOS) data for the Australian region is a fundamentally important scientific activity. Accordingly, there is a need for EO data to be calibrated and validated against high quality surface-based measurements across the continent following specific internationally agreed scientific criteria (AAS 2009).

Previous Australian involvement in international Cal/Val activities has allowed Australian scientists to join international EOS science teams and has provided early access to important satellite data streams. Although there are major land cover monitoring exercises such as Australia's National Carbon Accounting System (NCAS) and the Queensland government State Land and Tree Survey or SLATS (Kuhnell et al., 1998) that have dedicated validation components, the national coordination and funding of Cal/Val activities has been limited and ad hoc in the past (AAS 2009).

During recent years, Cal/Val activities in Australia have been coordinated by TERN's Landscape Assessment platform. TERN Landscape Assessment is responsible for providing a new nationally consistent approach for collecting, validating and distributing biophysical products related to land cover and land surface (Figure 2.1) derived from time-series remote sensing systems. These products can then be used to support ecosystem research and resource management within Australia.

Figure 2.1 Representation of biophysical products provided by TERN Landscape Assessment

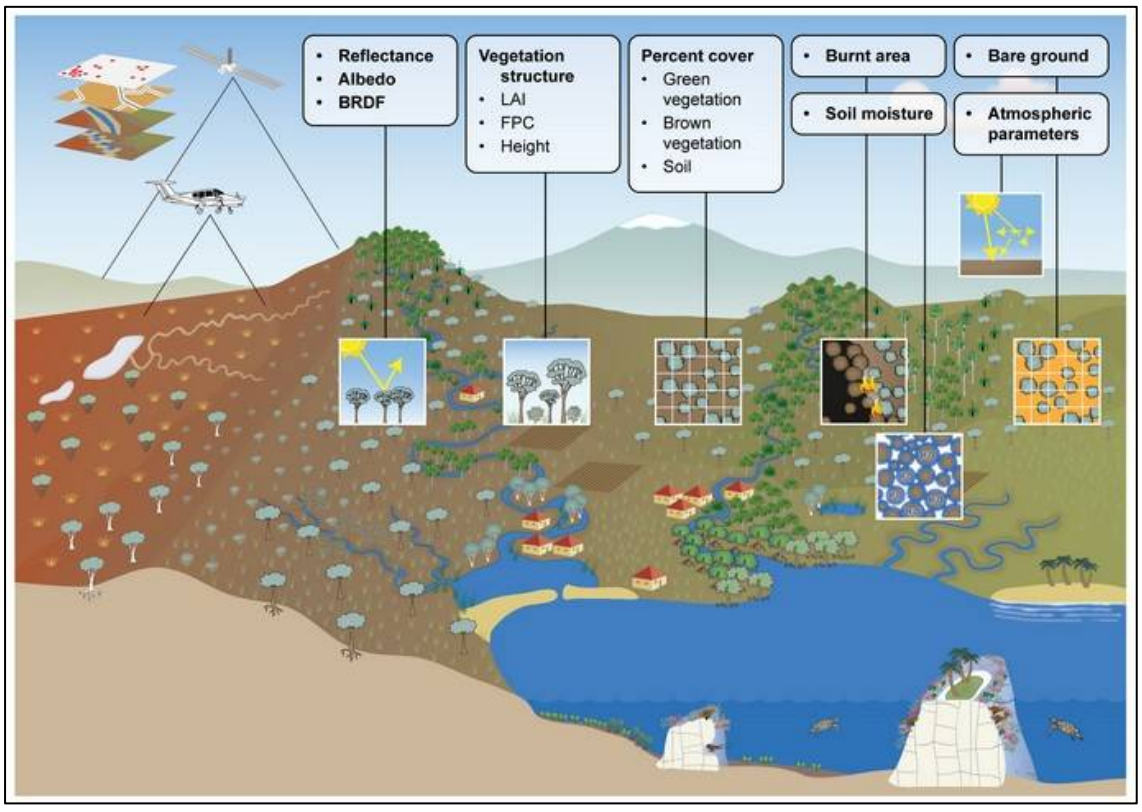

TERN's Landscape Assessment platform has set up a national calibration and validation program to provide for the Cal/Val of biophysical products. In this context, TERN's validation activities aim to utilise independent field data, aerial and satellite data to assess the quality of a range of terrestrial land surface products (Figure 2.1). This assessment will contribute to Stage 4 validation (CEOS WGCV), the highest of the CEOS defined hierarchical validation levels (Table 2.1). At this level, validation aims to comprehensively establish product uncertainties via the utilisation of independent measurements which are made in a systematic and statistically robust way and which are representative of global conditions. Chapter 17 presents several examples of TERN Landscapes validation campaigns throughout TERN's National Scientific Reference Site Network (NSRSN).

Validation activities also draw extensively on Cal/Val knowledge from international groups and campaigns (e.g., CEOS WGCV, EOS-MODIS Bigfoot CAL/VAL, ESA VALERI, National Ecological Observatory Network or NEON). In addition to the international expertise, Landscapes also incorporates local knowledge from existing projects with dedicated validation schemes (e.g., NCAS, SLATS). Some of these are discussed in this handbook. Chapter 18, for instance, presents a nationally coordinated effort for the validation of fractional cover that is led by the Australian Bureau of Agricultural and Resource Economics and Sciences or ABARES.

2.1.2 Terminology

In the context of remote sensing, validation refers to a process of assessing the uncertainty of higher level, satellite sensor derived products by analytical comparison to reference data, which is presumed to represent the target or true value of an attribute. To achieve this, conventional, ground-based observations are required using calibrated and traceable field instrumentation and associated methods. This allows for the verification and improvement of the algorithm/s used to derive the product. In a similar way, the CEOS WGCV defines validation as the process of assessing the uncertainty contained within satellite derived products via an analytical comparison to reference data (http://lpvs.gsfc.nasa.gov).

When validating a product, the accuracy or uncertainty contained within satellite derived products (e.g., land cover or LAI) can be assessed directly or indirectly. Direct validation implies using an independent data source that is representative of the target values or surface conditions (Justice et al., 2000). This allows for an 'absolute' quantification of uncertainties. Unfortunately, direct validation is often limited by the number and quality of available reference data, thus limiting the spatial coverage. To counter this, products can be inter-compared (indirect validation) to provide an indication of gross differences and possible insights into the reasons for the differences (Justice et al., 2000). Such validation procedures consider (a) the internal spatial/temporal consistency of a data product; and (b) the consistency of a given data product relative to existing data products at a comparable spatial scale (i.e. inter-comparison). Although this has the potential to provide a more extensive evaluation of consistencies/differences between products, it lacks a link to quantitative reference data (direct validation).

Products can also be validated indirectly through a two-stage process that involves the collection of measurements across various scales. At a large scale, ground observations are collected across an area that is representative of the resolution of the product that is being validated. The ground measurements can then be up-scaled to an intermediate scale using high resolution imagery (Morisette et al., 2006) and then compared to the product of interest.

2.2 Validation site requirements

The Moderate Resolution Imaging Spectroradiometer (MODIS) Land Discipline team (MODLAND), which leads validation efforts for MODIS derived biophysical products, has established a globally representative network of sites used for validation activities. In other words, sufficient sites were included to be representative of a given biome/ecosystem. Such representativeness was achieved by considering the distribution of sites both within the physical and meteorological space (Morisette *et al*., 2002). Despite a need for a globally representative framework, MODLAND recognised that given limited resources for data collection and analysis, the project should leverage on existing resources. This is achieved via the utilisation of, and partnerships with, existing (a) field programs (such as Long term Ecological Research sites or LTER); (b) science data networks (i.e., fluxnet); and (c) national and international research efforts (i.e., Morisette *et al*., 2002).

In selecting validation sites MODLAND established a series of criteria that define the optimum site location for satellite product validation (Morisette *et al.*, 2002). According to these criteria, a validation site should:

- be accessible to researchers;
- encompass existing facilities such as flux towers, which collect measurements of biophysical variables over extended periods of time;
- have a long history and long-term commitment to scientific studies;
- represent significant areas of homogenous or uniformly mixed land cover;
- be representative of extensive biomes globally;
- be complementary to existing validation sites.

To validate products derived from medium resolution satellites VALERI provides high spatial resolution maps of biophysical variables (e.g., LAI, fAPAR, fCover) that are estimated from ground measurements and high spatial resolution images like SPOT or Landsat ETM+. As part of their methodological framework, they rely on a network of sites distributed throughout the globe. These sites also need to be relatively homogenous (Baret *et al* 2006) within an area that is large enough (at least 3km x 3km) to represent the spatial resolution of the sensor. In other words, variation in the biophysical variable of interest (and associated radiometric values) should be minimal across the study area extent (as you move from one area that represents $1km^2$ to another within the 3km x x3km site). Sites should also be representative of different biomes (dependent on available local support for field activities). Ideally, sites should also have relatively small topographic variation in order to simplify the interpretation of both the ground measurements and acquired satellite imagery (Baret *et al.*, 2006).

In Australia, TERN Landscapes Cal/Val activities encompass an extensive large area validation campaign (>1000 sites) that takes advantage of sites surveyed by TERN's two other observatory platforms. An example is TERN Ecosystem Surveillance which has established a network of permanent plots across rangeland areas throughout the Australian continent (spanning across 52 bioregions, Thackway and Cresswell 1995). Fractional cover and LAI measurements (along with other metrics) are recorded in these plots using the SLATS transect sampling method (discussed below). In addition, TERN Landscapes makes use of TERN's intensively characterised national network of 12 ecosystem process monitoring SuperSites that are suitable for multi-instrumental land product validation and algorithm development. TERN Ecosystem Processes sites are also located across significant biomes within Australia and include representative areas of sclerophyll forests, savanna woodlands, grasslands and tropical forests.

Some of the key criteria that need to be met for these sites to be chosen include:

- being representative of an important land cover and Australian biome;
- being spatially homogenous over a 5km x 5km footprint area so they can be scaled-up to validate large area remotely sensed products
- being easily accessible;
- wherever possible, incorporate existing research facilities (e.g., flux towers).

2.3 Site extent

Within current validation projects the site extent, or area over which field measurements are collected, varies. Generally speaking, the extent of the site must ensure the representation of the pixel size of the sensor. The smallest possible site extent is the minimum area compatible with the spatial resolution of the sensor to be validated, typically 1km x 1km within current LAI products (Morisette et al., 2006). However, multiple authors conclude that a 1 km^2 area extent is too small given issues associated with the point spread function and geo-locational uncertainties of the sensors (Morisette et al., 2006). These issues have been minimised, in multiple studies, via the (a) positioning of sample sites within homogenous areas; and (b) definition of larger, typically 3km x 3km and 5km x 5km site extents.

When choosing the site extent, another important consideration is the available resources required for field work. Ideally, a site should be surveyed within a week of satellite/airborne image acquisition in order to prevent the significant evolution of the vegetation from the date of data capture (Baret et al., 2006) or occurrence of destructive events (e.g., fire). Nevertheless, the rate at which the state of the vegetation evolves varies for different ecosystems and is also influenced by its successional state.

In Australia, large area sites that are used for calibration and validation activities are 5km x 5km in extent (Figure 2.2). These are representative of different biomes and Australian forest ecosystems. Across these sites, airborne full waveform Light Detection and Ranging (LiDAR) and hyperspectral optical imagery are collected synchronously with ground-based data using a variety of instruments that measure biophysical products like LAI, Canopy Cover (CC), and Foliage Projective Cover (FPC) (see Chapter 17 for more information on Landscapes validation campaigns). An example schematic of a validation site and data collected during a validation campaign is shown in Figure 2.3.

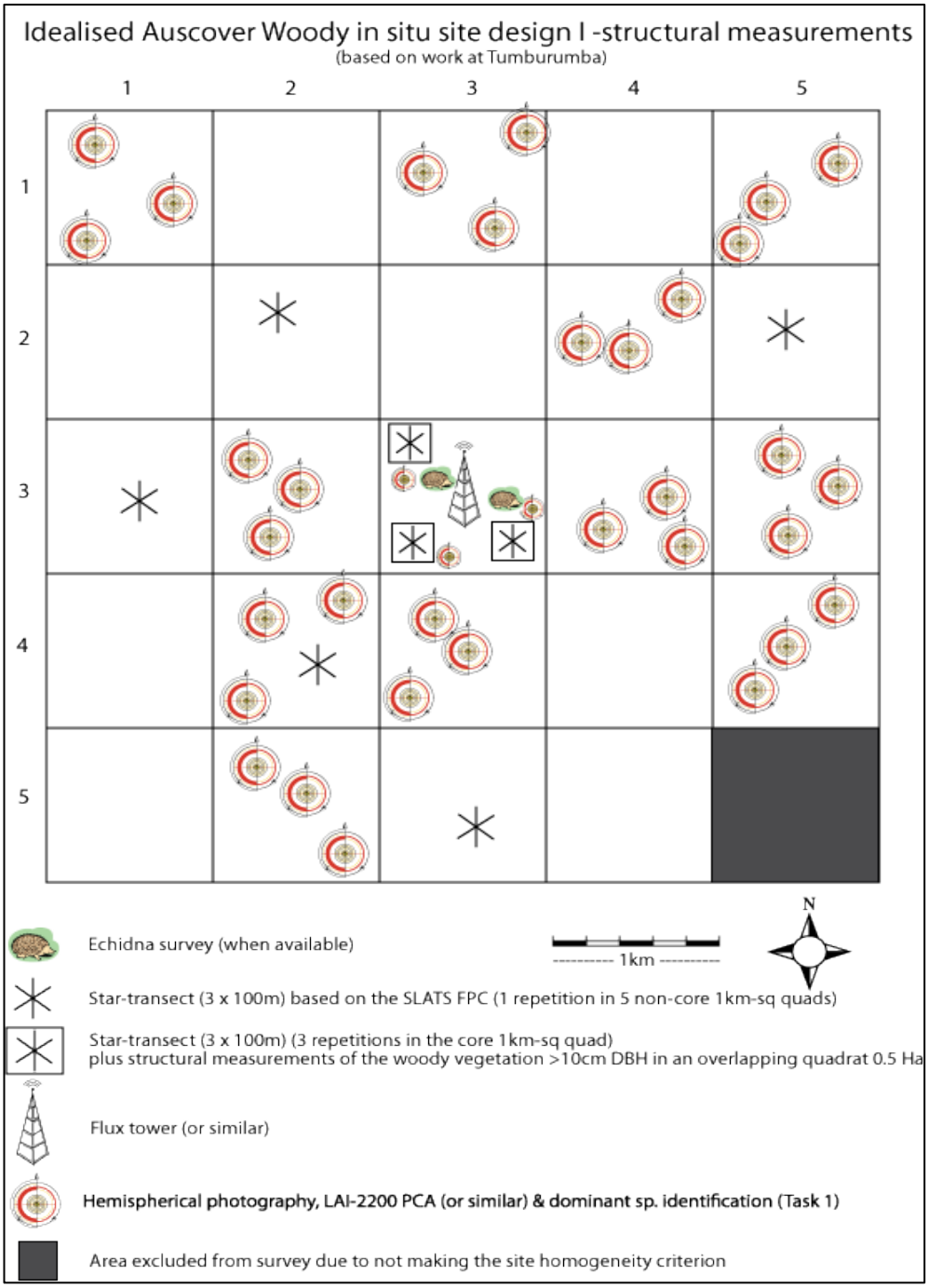

Figure 2.3 Schematic diagram of an Landscape large area (5km x 5km) validation site.

2.4 Sampling design

The sampling design implemented for ground-based measurements is driven by two main factors: (a) the footprint of the field measurements and (b) up-scaling process used to integrate the field measurements and high resolution imagery (see Table 6.3 for examples on sampling designs applied for LAI product validation). Conversely, the in-situ measurements can be compared directly to the EO product for direct Cal/Val (Cihlar *et al.*, 1997). Multiple projects choose a multi-scale, two-tier sampling scheme based on elementary and secondary sampling units (e.g., Baret *et al.*, 2006, Hufkens *et al.*, 2008).

Elementary sampling units (ESU), also defined as primary sampling units, aim to capture the variability of the product being validated across the study site. The number and distribution of ESU across the study site varies between projects as a consequence of several factors including the site area, ESU extent, and site variability (Morisette *et al.*, 2006). Site variability, within the ESU, can be defined according to a current land cover map, floristically, or using variability in the land surface reflectance as characterised by recently acquired satellite imagery.

Secondary sampling units (SSU) are distributed across the ESU and represent the specific locations where measurements are recorded. The distribution of these second-stage sampling units varies between projects and as a consequence of the (a) footprint of the product measurement device and (b) the land cover (or canopy type) being studied. Different sampling designs can be implemented within the ESU (Morisette *et al.*, 2006) such as those shown in Figure 2.4 (e.g., fixed pattern, Figure 2.4a; transect, Figure 2.4b; randomised design, Figure 2.4c).

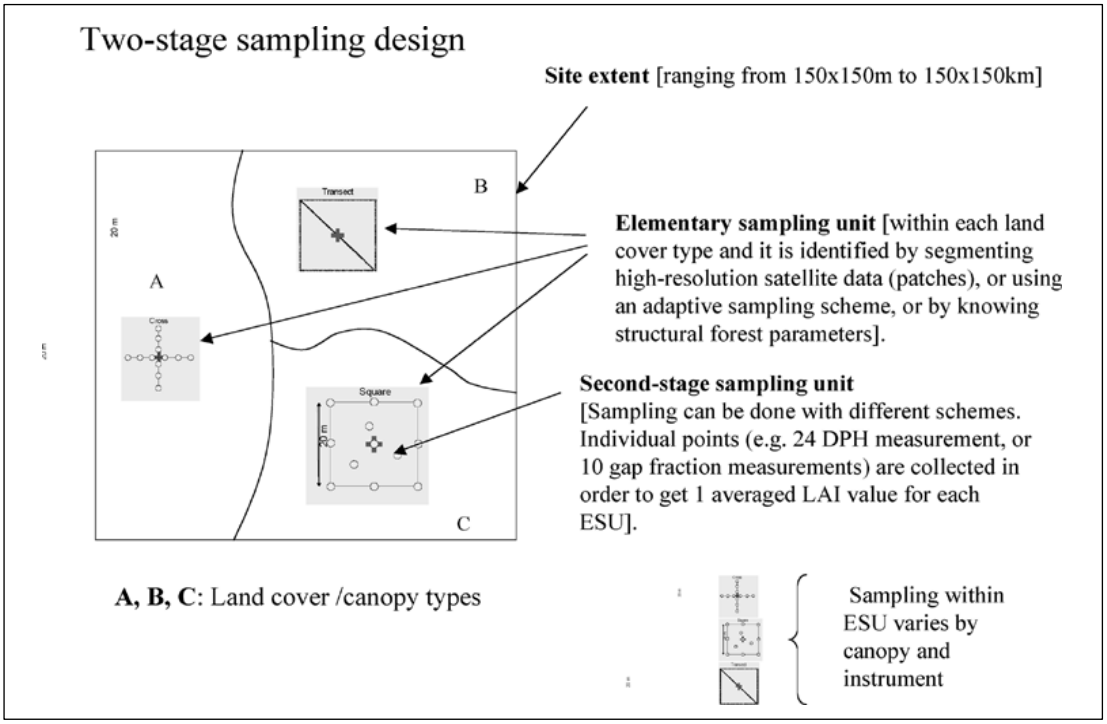

Figure 2.4 Commonly utilised two-stage sampling designs (Morisette *et al.*, 2006) consisting of an Elementary sampling unit (ESU) and Secondary sampling unit (SSU).

Differences obtained when using different ESU have been investigated by some researchers. Garrigues *et al* (2002) found the fixed pattern (cross) sample design (Figure 2.4A) and randomised design (Figure 2.4C) to be equivalent in terms of the spatial variation sampled for point-based LAI estimates. In the case of LAI measurements, a transect design was recommended (a) with a TRAC device (Morisette *et al.*, 2006) or (b) within land covers characterised by sparse or locally discontinuous vegetation (Baret *et al.*, 2006). The second approach is particularly evident in the VALERI program in which the transect sample design was associated

with destructive (as opposed to relying on indirect methods through DHP or instruments like LAI-2200) measurements of LAI (See Chapter 6 for detailed information on LAI validation).

A Global Positioning System (GPS) is usually needed to record the precise location of ESU (where all measurements are taken or at the centre of the ESU). The specification of these GPS measurements and associated positional error is a function of the project and of course the resolution of the pixel. For example, VALERI utilised non-differential GPS to locate the centre of the ESU with an error of 5 to 10 metres.

2.4.1 VALERI

For the validation of LAI products derived from medium resolution satellite sensors (Instantaneous Field of View or IFOV of 250-300m) within the VALERI project, validation sites were defined to encompass a 3km x 3km area of homogenous or constantly mixed land cover (Baret *et al*., 2006). Between 27 and 45 ESU were located (as a function of study site) within the 9 km^2 site. ESU were defined to be 20m x 20m in extent, given they are mainly using SPOT-HRV satellite images for upscaling (with a spatial resolution that ranges between 10 and 20 metres).

To guarantee a good distribution of ESU across the site, the 9 km^2 study area was subdivided into 1 km^2 tiles with three to five ESU contained in each tile. The distribution of ESU within the 1 km^2 tiles was a function of (a) land cover; (b) ESU variability; (c) access; and (d) existing ESU locations, that is, ESU were required to be well distributed within the individual 1 km^2 tile. The representativeness of this sampling design was ensured at each site via a comparison of the Normalised Difference Vegetation Index or NDVI distribution (extracted from the high resolution imagery) of the entire site to that of the sampled ESU (Baret *et al* 2006).

The spatial distribution of biophysical measurements, within each ESU of 20m x 20m, was primarily a function of the dominant vegetation and its canopy structure (Baret *et al*., 2006). If the vegetation was considered to be homogenous, estimates of LAI were made using gap fraction techniques arranged in a cross or square spatial sampling distribution (Figure 2.8*a* and *c*). Conversely, a transect sample placed diagonally across the ESU (Figure 2.8*b*) was implemented if vegetation in the ESU was considered to be heterogeneous (Baret *et al*., 2006).

2.4.2 BigFoot

To support the validation of land products derived from MODIS such as LAI, Land Cover (LC), and Net Primary Production (NPP), NASA's Terrestrial Ecology Program developed the BigFoot project (https://daac.ornl.gov/BIGFOOT_VAL/bigfoot.shtml). Sites chosen for validation typically have a 5km x 5km extent and have a flux tower in the centre (Figure 2.5) which measures water and carbon fluxes over a 1km^2 footprint to characterise NPP (Cohen *et al*., 2006). To evaluate the inter-annual validity of MODIS products, measurements of ecosystem structure and function are collected throughout the year.

Seven of the nine BigFoot sites were characterised by a sample design that included approximately 100 ESU (also termed plots), each 25m x 25m where measurements were collected (Cohen *et al*., 2006). The extent of the ESU approximates a Landsat pixel, which is the high-resolution satellite image used to up-scale ground-based measurements. To ensure the adequate characterisation of vegetation within the flux tower footprint, between 60 and 80 ESU were concentrated in the 1 km^2 cell surrounding the flux tower. The remaining ESU were located within the 5km x 5 km site (Cohen *et al*., 2006). To enable the validation of BigFoot surface products over the full site, ESU across the greater site extent were apportioned between the basic land cover components. Conversely, within the centre 1 km^2 area, the ESU were sampled using a systematic spatial-cluster design (Burrows *et al*., 2002).

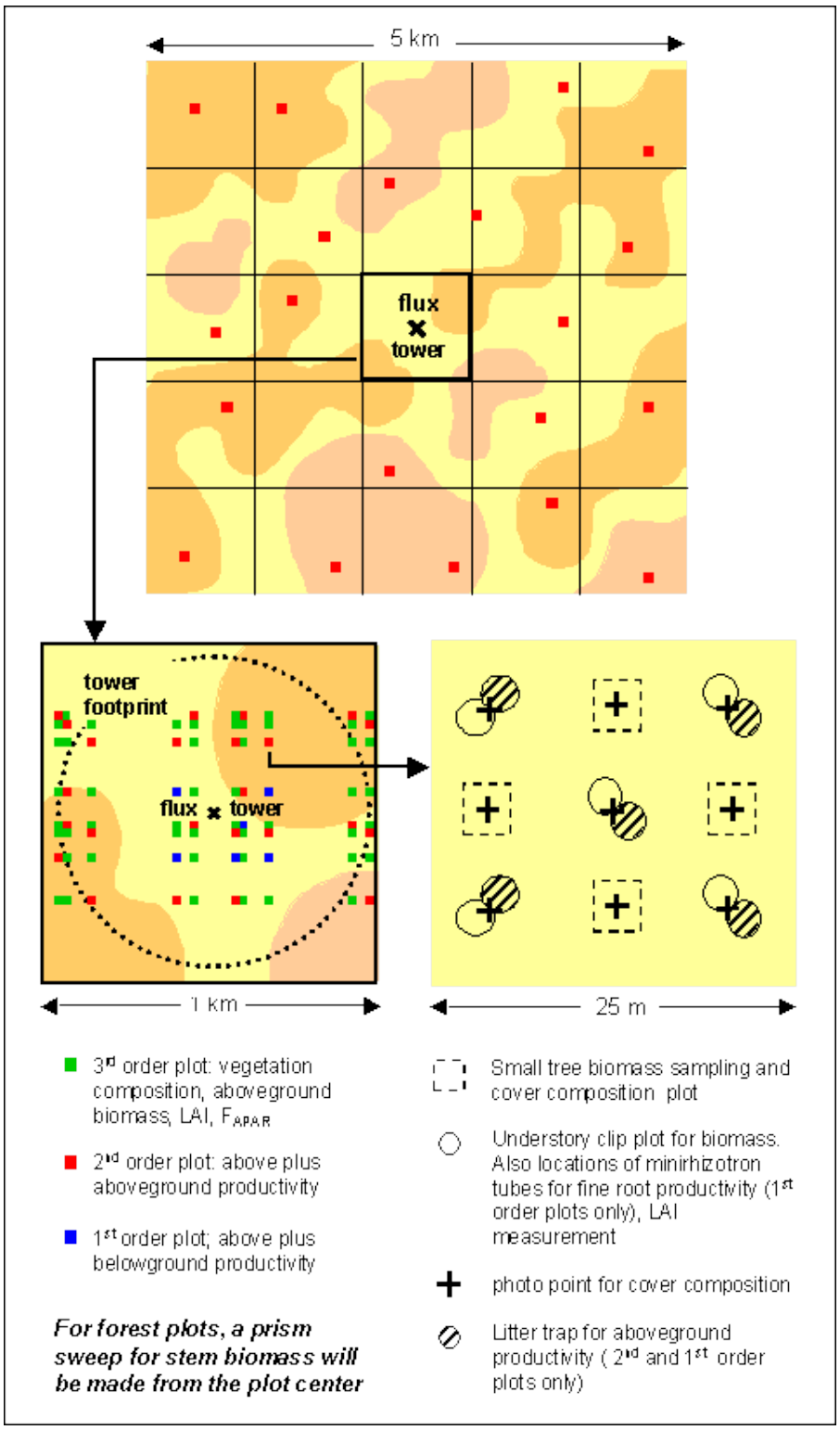

Figure 2.5 Overview of the BigFoot sample design (http://www.fsl.orst.edu/larse/bigfoot/ovr_dsgn.html).

It should be noted that a modified sampling methodology to that just outlined was developed for two BigFoot sites (Kennedy *et al.*, 2002). This modified sampling methodology was based on the use of 42 intensive ESU and 58 extensive ESU. This approach used Landsat ETM+ data to roughly characterise the range of conditions within the site in order to enable the efficient and effective allocation of samples. Within this sample design, the placement of samples was required to meet three objectives: (a) sufficiency (capture variability across the landscape); (b) efficiency (minimise field travel costs and expenses); and (c) independence of observation,

therefore avoiding replication in the field data (Kennedy *et al*., 2002). This was achieved using a constrained stochastic sampling protocol for the placement of extensive samples in the greater site area (Kennedy *et al*., 2002).

As shown in Figure 2.5, the BigFoot ESU are characterised using a multi-tiered hierarchy; that is, plots were sampled at three levels of intensity. Measurements collected within each ESU were a function of their hierarchical classification. At the lowest hierarchical level (third order plots), measurements of vegetation composition, aboveground biomass, LAI and fAPAR were taken. These measurements were repeated at second order plots with the addition of above ground productivity. In the highest first order plots, all third order measurements are collected in addition to above and below ground productivity (Figure 2.5). All ESU in the greater 5km x 5km site footprint are characterised with second order measurements. However, the proportion of each ESU or plot type is a function of the site, as exemplified by Table 2.3.

Table 2.3 Example of hierarchy of ESU in two BigFoot sites (Campbell et al.,1999). NOBS (Northern Old Black Spruce) is a boreal forest site dominated by black spruce while KONZ (Konza Prairie) is a tall grass prairie site.

Site	First Order	Second Order	Third Order	Total
NOBS	8	44	56	108
KONZ	6	38	56	100

Each ESU contains a series of sub-plots where the measurements described above are collected. Sub-plot placement was designed to ensure (a) the spatial stratification of measurements throughout the plot; (b) simple and convenient field deployment; and (c) minimal interference between the required measurements, for example, direct and indirect measurements of LAI (Campbell *et al*., 1999). The arrangement of sub-plots typically follows a regular pattern approximating the compass cardinals (Figure 2.6). However, sub-plot arrangement varies as a function of the vegetation type and site characteristics.

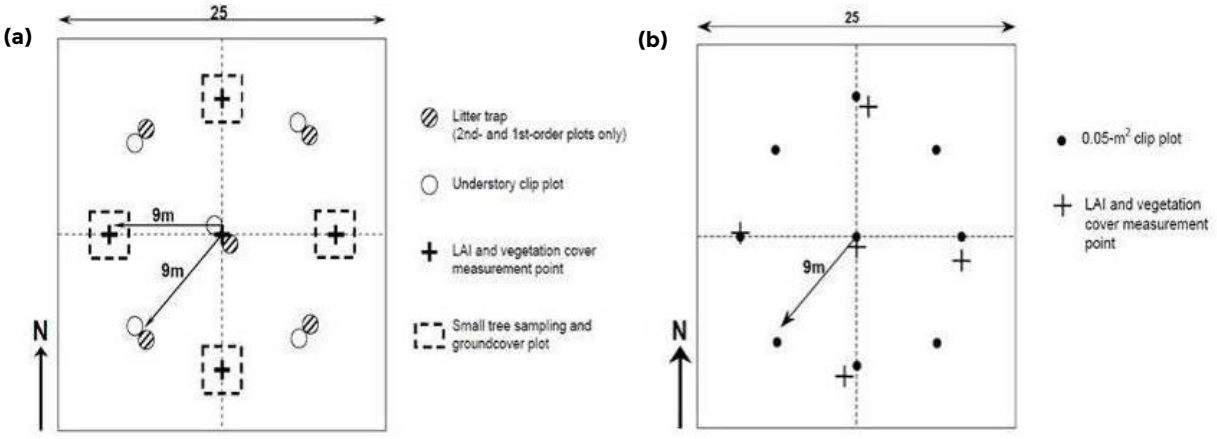

Figure 2.6 The arrangement of sub-plots and LAI measurements taken in the
(a) NOBS site
(b) KONZ BigFoot site (Campbell *et al*., 1999).

2.4.3 SLATS

In Australia, a sampling strategy widely used to collect field data for calibrating and validating fractional cover products is SLATS, which also provides information on land clearing, tree growth and regrowth (Kuhnell et al., 1998; Muir *et al.*, 2011). The SLATS sampling method has proved to be robust when using medium resolution products like Landsat for up-scaling in relatively open ecosystems across Australia. Woody vegetation mapping within the SLATS project is based on the automated and semi-automated classification of Landsat Thematic Mapper (TM) and Enhanced Thematic Mapper (ETM+) satellite imagery (Kuhnell *et al.*, 1998). According to the SLATS method, field sites are located in areas of uniform, mature vegetation communities (based on aerial photographs) and have a minimum area of approximately 100 x 100 metres (Armston *et al.*, 2009). Three line segments, each 100 m in length, are orientated at 0°, 60° and 120° from magnetic north.

Vegetation characteristics recorded in SLATS sites include FPC and stand basal area (SBA). Estimates of over-storey FPC are derived by averaging across three 100 metre point intercept transects at one metre spacings (Figure 2.7). At one metre intervals along each transect, overstorey (woody plants greater than two metres in height) and understorey (woody and herbaceous plants less than two metres in height) vegetation is recorded. Understorey herbaceous measurements are acquired using a laser pointer at zenith of zero (nadir) with intercepts classified as (a) green leaf; (b) dead leaf; (c) bare; (d) rock; (e) cryptogam; or (f) litter by the observer. Over and understorey woody measurements are done via a vertical tube method with intercepts classified as (a) green leaf; (b) dead leaf; (c) woody branch or stem; or (d) sky. Stand basal area measurements are collected at the centre point of the SLATS transect and at a 25 metre distance from the centre location along each of the line segments. Stand basal area is estimated, for each plot, as the average of seven optical wedge counts, with the transect representing the centre of a nominal one hectare plot (Figure 2.7). As described elsewhere in this handbook (e.g., Chapters 6, 7, 12, 17), the SLATS transect can also be used to collect measurements of LAI and other metrics using a variety of ground based instruments.

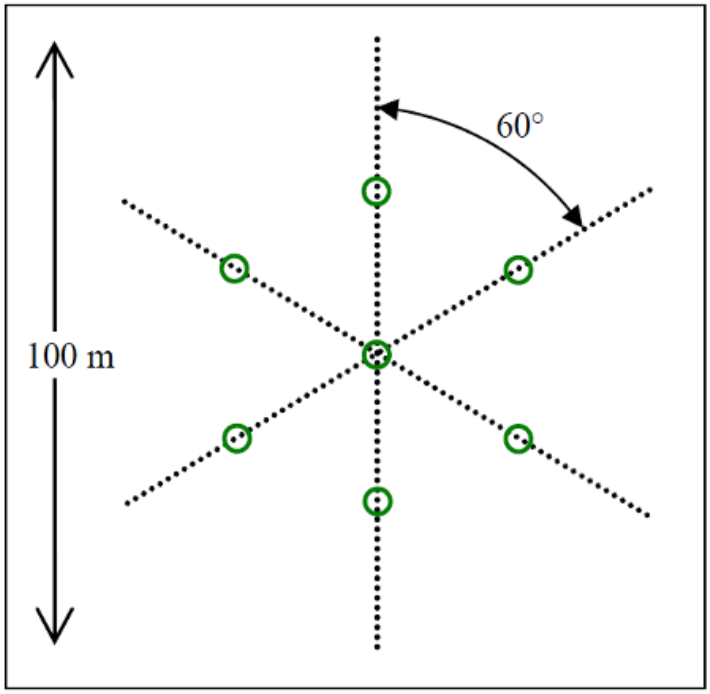

Figure 2.7 Schematic representation of the sampling design utilised in the SLATS survey (Armston et al., 2009). Green circles are located halfway between the centre location and end point (in other words, 25 metres from the central location) of each 100 m segment. Stand basal area measurements are collected in the green circles, where measurements of LAI and other metrics can also be collected.

Woodgate *et al*. (2012) recently compared plot scale LAI and FPC measurements obtained when using various sampling designs in a rainforest in Queensland (Figure 2.8). Three sampling designs were compared, namely SLATS, the VALERI cross, and a gridded one hectare plot sampled every 20 m. Their preliminary findings suggest that, in dense canopy forests, measurements obtained using various sampling designs are highly comparable and therefore the selection of the optimal sampling design should be driven by the resolution of the product that is to be validated. Nevertheless, additional factors should still be considered such as the type of forest, accessibility, and topography. For instance, when working in forests with dense canopies and understory vegetation, it may be extremely time consuming to conduct a SLATS transect. In such cases other sampling designs such as a simple transect or modification of one of the more widely used sampling designs may be more suitable (see Chapter 17, section 17.4, TERN Landscapes field and airborne campaign in the wet tropics of Far North Queensland for an example). Lawley *et al*. (2015) also review sampling methods used for site based monitoring of vegetation condition indicators while Reinke and Jones (2006) review ways for integrating EO data with field plot information.

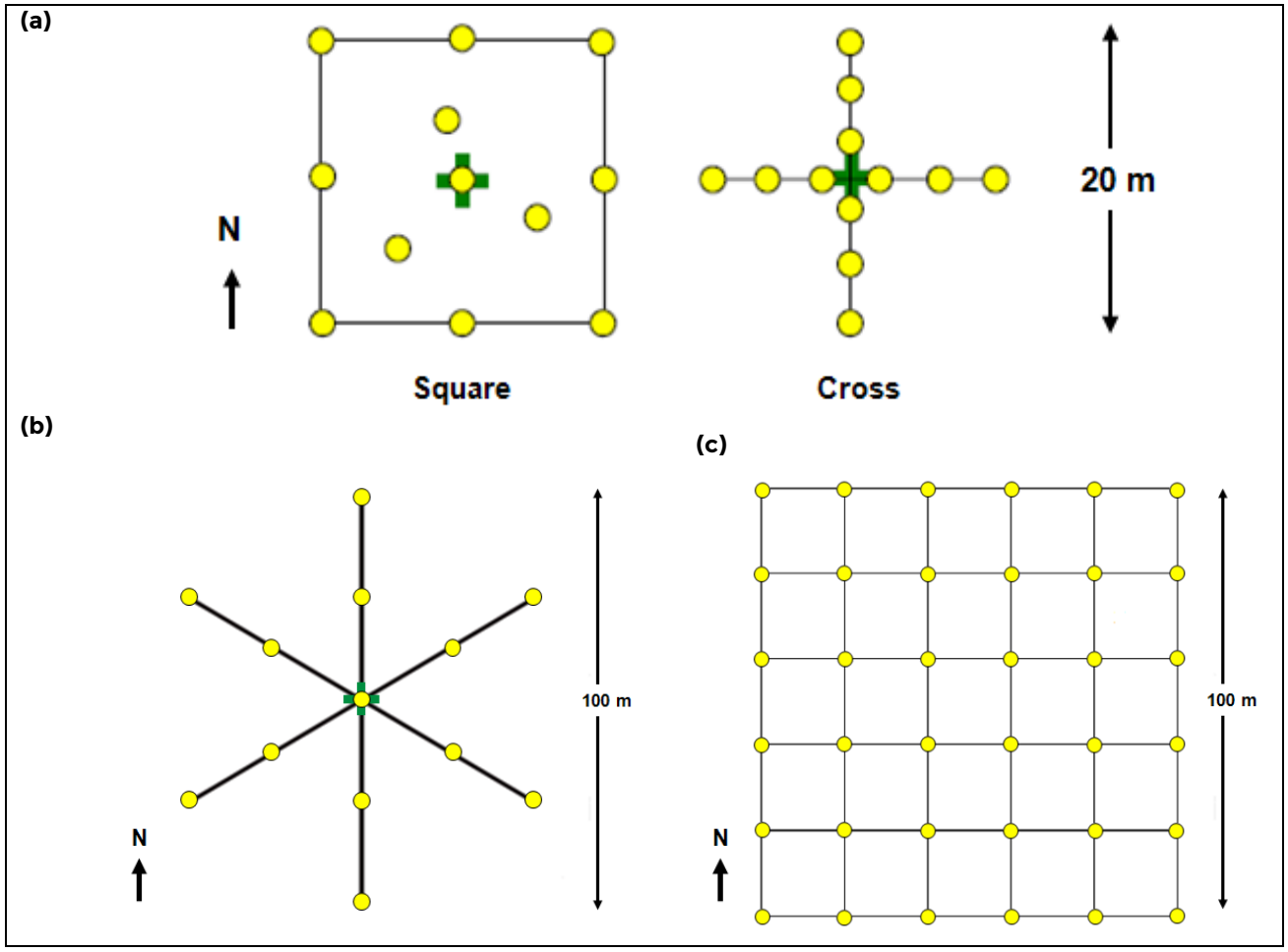

Figure 2.8 Three sampling designs investigated by Woodgate *et al*., (2012. Yellow dots indicate locations where LAI measurements were taken:
(a) VALERI cross, the green cross represents the centre of the plot which also has a GPS or known location associated with it.
(b) SLATS plot
(c) Gridded one hectare plot sampled every 20m.

2.5 Multi-stage sampling and upscaling

Validation procedures developed for moderate resolution satellite derived products emphasise the utilisation of multi-scaled approaches which integrate ground-based, airborne, and high spatial resolution satellite data collected in tandem (Morisette *et al*., 2006). Ground-based (plot scale) data can be used to validate moderate spatial resolution remote sensing models by extrapolating the field measurements to a continuous spatial area that has a compatible scale with the spatial resolution of the remotely sensed observations (Baccini *et al*., 2007). It is in this context that ground-based measurements are collected in tandem with airborne or higher spatial resolution satellite imagery, which is used as a bridging data source between the field data and land product requiring validation. Chapter 17 presents a series of Landscape Assessment validation campaigns that involved in situ ground-data collection activities concurrent with the capture of high resolution hyperspectral and LIDAR data.

Up-scaling is generally achieved through the integration of field measurements and a high-resolution image, which results in the production of a high resolution map of the parameter measured in the field (Figure 2.9). A crucial consideration when designing the sampling framework is to embed the observations in a way that allows for them to be up-scaled, from point observations to landscapes to regions to continents. Validation of the moderate-resolution product is then achieved via comparison to this high resolution product (Morisette *et al*., 2006). Chapter 7 discusses the validation of an Australian national Fractional Cover product using MODIS and Landsat.

Advanced methodological techniques capable of supporting the up-scaling of ground-based measurements to continuous high resolution maps is an area of extensive research. In the case of LAI validation for example, projects utilise a range of (a) high resolution data sources; (b) transfer functions to integrate the ground and high resolution data sources; and (c) different procedures to validate the high resolution product. A review of such methods is beyond the scope of this document (for detailed reviews see, for example, Baccini *et al*., 2007; Baret *et al*., 2006; Gupta *et al*., 1998; Hay *et al*., 1997; Hay *et al*., 2001).

Figure 2.9 Validation and up-scaling procedures (from Morisette *et al*., 2006).

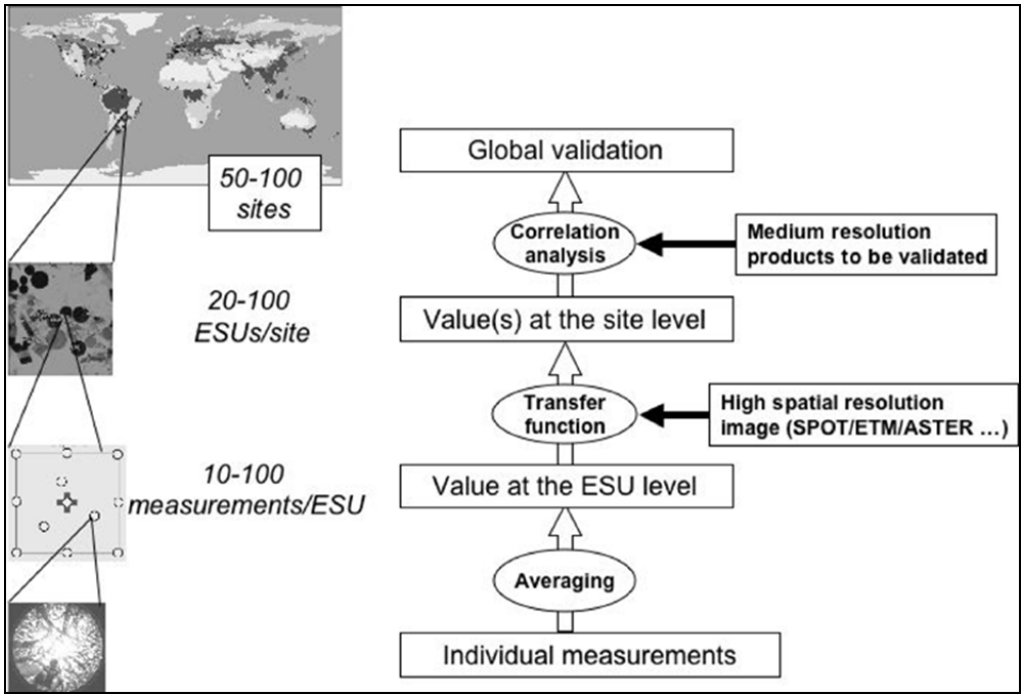

2.6 Alternative validation approaches

So far, this chapter has discussed validation activities associated with certain biophysical products (e.g. LAI) that are suited to point based sampling across intensively characterised small areas that are subsequently upscaled. There are additional sampling alternatives that may be better suited when collecting data for validating other products. This section briefly touches on some of these.

Another approach to data collection that can be used for product validation is the large-scale transect method, which biases the sampling along an environmental gradient (e.g., elevation, temperature, precipitation). The advantage of this approach is that it encompasses a large range of environmental conditions but has the disadvantage of not being representative of common ecosystem "states". An example of large-scale transects are those established by the International Geosphere-Biosphere Program (IGBP), which extend for over 1,000 kilometres and span across different biomes (Koch *et al*., 1995; Canadell *et al*., 2002). Figure 2.10a shows the distribution of IGBP terrestrial transects, scattered across four main regions (high and mid-latitudes, semi-arid tropics, and humid/sub-humid tropics). Only one of these, the NATT, falls within Australia (Sea *et al*., 2011 collected ground observations along this transect to validate the MODIS MC4 and 5 LAI products). Nevertheless, TERN has established other major transects across the Australian continent which also extend for hundreds of kilometres and traverse across bioclimatic gradients (Figure 2.10b). Plots established along these transect collect data (e.g., soil characteristics, floral composition, vegetation structure, biodiversity) that can also be used for EO product validation.

Land cover is another satellite derived product that is used by multiple stakeholders. Nowadays, multiple global and regional land cover products exist. Several authors have commented that the independent accuracy assessment of each of these products is inefficient, expensive and, due to the variety of validation procedures utilised, hinders the comparison of map accuracies (Stehman *et al*., 2010). Given these concerns there is an increasing move, within land cover mapping, towards a coordinated global land cover validation database (Stehman *et al*., 2010). Fundamental to this coordinated validation database is a rigorous probability sample of reference land cover data, which must (a) be compatible with all land cover class definitions; and (b) be based on a consistent response (sample) design protocol (Stehman *et al*., 2010).

The basic spatial unit of the proposed land cover validation dataset is a 5km x 5km block (Stehman *et al*., 2010). It is proposed that reference land cover data be derived in each sample block from a high-resolution data source. This will form the basis of map comparison and therefore land cover map validation (Stehman *et al*., 2010). The sample design in which each of these blocks will be placed is required to: (a) represent a probability based sampling design; (b) adequately sample rare land cover classes; and (c) allow flexibility to easily augment the sample, via the sampling of particular regions or strata, to tailor the available samples to the assessment of a particular land cover product (Stehman *et al*., 2010).

To fulfill these criteria Stehman *et al* (2010) propose a stratified random sampling design. To avoid sampling bias towards a particular schema, the strata within this design would not be based on a single land cover representation but utilise instead a more generalised stratification based on Koppen climatic zones and population density (Stehman *et al*., 2010). The initial sample is based on 500 blocks allocated to the 21 strata to ensure that complex, potentially ambiguous classes receive a higher proportion of samples (Stehman *et al*., 2010). The augmentation of these original samples will be based on the same probability based sample design and original strata. However, it is expected that users could increase the sampling of strata, known to contain land cover types of interest, while still maintaining a probability based sampling approach (Stehman *et al*., 2010). This sample design is flexible and allows the addition of new samples targeted to the validation of a particular land cover product. Such characteristics are particularly relevant to the current review.

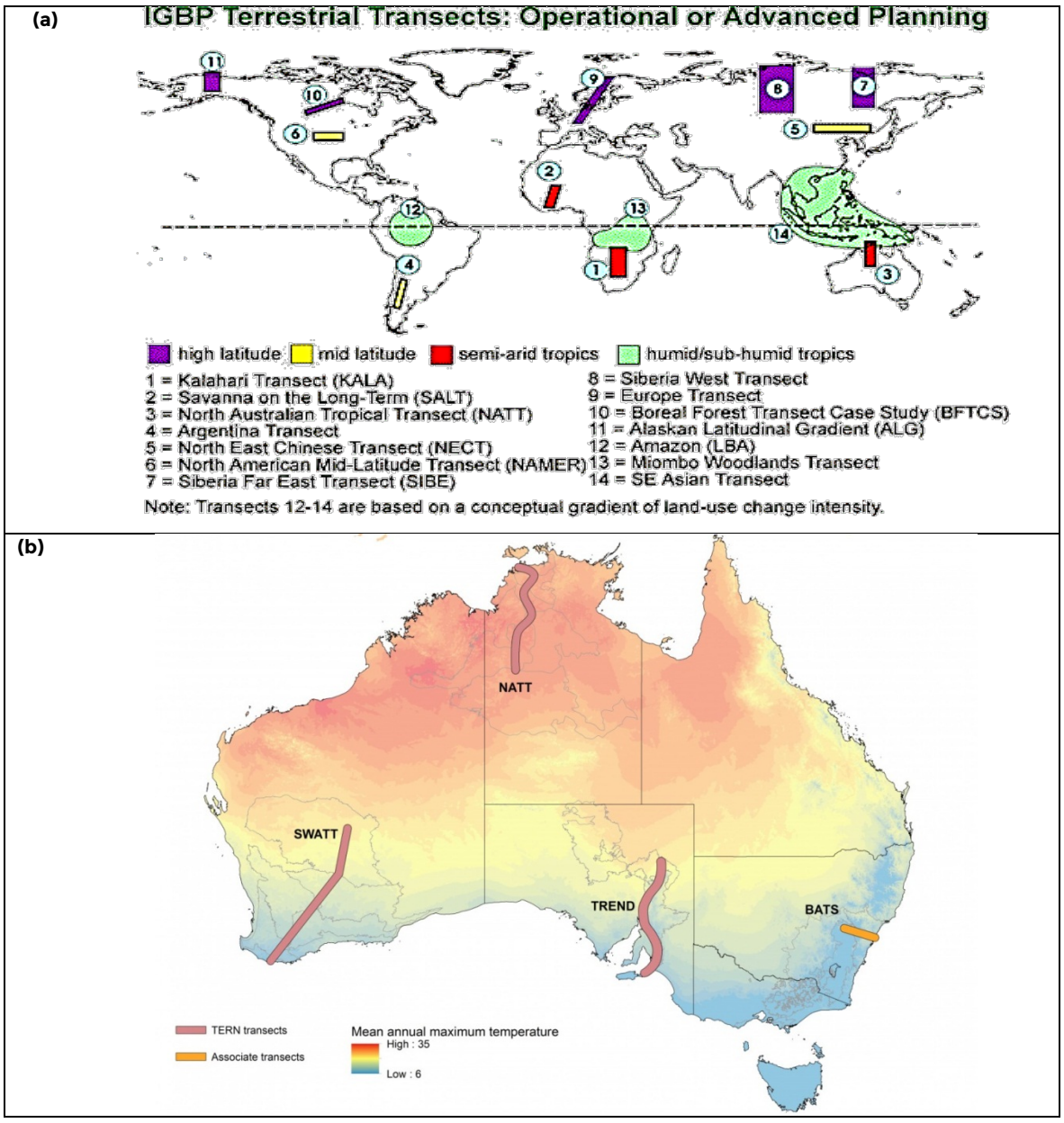

Figure 2.10 Examples of transects along environmental gradients.

(a) A set of IGBP Terrestrial transects, from Canadell *et al*., 2002 .

(b) Four of the seven major transects that make up TERN's national network of subcontinental transects which traverse major biomes, land tenures (including agricultural landscapes) and bioclimatic gradients.

2.7 Conclusion

There is a clear need for satellite remote sensing data to be validated to ensure the continued long-term provision of reliable datasets and products. Validation is a fundamentally important scientific activity. It needs to be an almost continuous component operating in tandem with EO campaigns that provides an independent check on the performance of space-based sensors and processing algorithms using high quality surface-based measurements and adhering to international guidelines and protocols. In Australia, this activity for biophysical products is being coordinated and implemented by Landscapes, who are collecting data across multiple spatial scales (ground based, airborne, and satellite data).

The successful implementation of ground based validation activities requires early and careful planning. The first consideration ought to be around exactly what is being validated and for what purpose. The sampling framework needs to be practical and consider issues like site selection (potentially selection and establishment of networks of sites), size extent, sampling framework, coordination of sampling activities, and the development and deployment of required instrumentation. This chapter has briefly discussed some of these aspects by reviewing international validation campaigns as well as by drawing on national Australian validation campaign efforts. Other chapters in this handbook provide good practice guidelines when collecting other data in the field such as LAI (Chapter 6), fCover (Chapter 7), phonological measurements (Chapter 9), biomass (Chapter 12) and vegetation spectroscopy (Chapter 13). When embarking on a field campaign, it is important to consider all the attributes that will be measured in the field and logistics associated with acquiring these.

Not reviewed in this chapter but also of utmost importance to in situ data collection is quality assurance and data quality aspects. Data quality elements such as positional and attribute accuracy, logical consistency, and completeness need to be recorded for all in situ measurements using agreed upon protocols and standards (Chapter 3). In addition, Chapter 17 (Landscape Field and Airborne Campaigns) presents several Cal/Val Landscape field/aerial acquisition campaigns as case studies, which demonstrate the logistics (e.g., number of personnel needed to record measurements of various metrics, instruments required, sampling strategy) required to undertake such work.

References

Baret, F., Morissette, J.T., Fernandes, R.A., Champeaux, J.-L., Myneni, R.B., Chen, J., *et a*l. (2006). Evaluation of the representativeness of networks of sites for the global validation and intercomparison of land biophysical products: proposition of the CEOS-BELMANIP. *IEEE Transactions on Geoscience and Remote Sensing*, 44(7), 1794–1803., available at http://ieeexplore.ieee.org/stamp/stamp.jsp?tp=&arnumber=1645280&isnumber=34482

Australian Academy of Science, Australian Academy of Technological Sciences and Engineering. (2009). An Australian Strategic Plan for Earth Observations from Space. Australian Academy of Science 2009 GPO Box 783, Canberra, ACT 2601, Australia. ISBN 085847 267 8, available at www.science.org.au/reports/index

Baccini, A., Friedl, M.A., Woodcock, C.E. & Zhu, Z. (2007). Scaling Field Data to Calibrate and Validate Moderate Spatial Resolution Remote Sensing Models, *Photogrammetric Engineering & Remote Sensing* 73(8), 945 - 954.

Campbell, J.L., Burrows, S., Gower, S.T., & Cohen, W.B. (1999). Bigfoot: Characterizing land cover, LAI, and NPP at the Landscape Scale for EOS/MODIS Validation. Field Manual 2.1. Oak Ridge National Laboratory, Environmental Science Division.

Candell, J. G., Steffen, W. L., & White, P. S. (2002). SPECIAL FEATURE IGBP / GCTE terrestrial transects: Dynamics of terrestrial ecosystems under environmental change – Introduction. Journal of Vegetation Science, 13, 297–300.

Cihlar, J., Chen, J., & Li, Z. (1997). On the validation of satellite-derived products for land applications. *Canadian journal of remote sensing*, 23(4), 381-389.

Committee on Earth Observation Satellites Working Group on Calibration and Validation (CEOS WGCV) Five-Year Work Plan 2011-2016. (2014). Version 5.5. available at http://ceos.org/document_management/Working_Groups/WGCV/WGCV_5-Year-Work-Plan-2011-2016_Feb2014.pdf.

Dowman, I. (2004). "Foreword," in International Society for Photogrammetry and Remote Sensing (ISPRS) Book Series-Post-Launch Calibration of Satellite Sensors, S. A. Morain and A. M. Buedge, Eds. Leiden, The Netherlands: A. A. Balkema.

Garrigues, S., Allard, D., Weiss, M. & Baret, F. (2002). Comparing VALERI sampling schemes to better represent high spatial resolution satellite pixel from ground measurements: How to characterise an ESU, http://w3.avignon.inra.fr/valeri/methodology/samplingschemes.pdf (accessed August 2010).

GTOS. (2008). Terrestrial Essential Climate Variables for climate change assessment, mitigation and adaptation. Rome, Italy: FAO.

Gupta, R. K., Prasad, S., & Krishna Rao, P.V. (1998). Evaluation of spatial upscaling algorithms for different land cover types. *Adv. Space Res*., 22(5), 625–628.

Hay, G. J., Niemann, K. O., & Goodenough, D. G. (1997). Spatial Thresholds, Image-Objects, and Upscaling: A Multiscale Evaluation. *Remote Sensing of Environment*, 62, 1–19.

Hay, G. J., Marceau, D. J., & Dub, P. (2001). A multiscale framework for landscape analysis: Object-specific analysis and upscaling. *Landscape Ecology*, 16, 471–490.

Hufkens, K., Bogaert, J., Dong, Q. H., Lu, L., Huang, C. L., Ma, et al. (2008). Impacts and uncertainties of upscaling of remote-sensing data validation for a semi-arid woodland. *Journal of Arid Environments*, 72(8), 1490–1505. doi:10.1016/j.jaridenv.2008.02.012.

Justice, C., Belward, A., Morisette, J., Leiws, O., Privette, J. & Baret, F. (2000). Developments in the 'validation' of satellite sensor products for the study of the land surface, *International Journal of Remote Sensing*, 21 (17), 3383 - 3390.

Koch, G. W., Vitousek, P. M., Steffen, W. L., & Walker, B. H. (1995). Terrestrial transects for global change research. Vegetatio, 121(1-2), 53–65. doi:10.1007/BF00044672

Kuhnell, C.A., Goulevitch, B.M., Danaher, T.J. & Harris, D.P. (1998). Mapping Woody Vegetation Cover over the State of Queensland using Landsat TM imagery, 9th Australian Remote Sensing and Photogrammetry Conference, Sydney, Australia.

Lawley, V., Lewis, M., Clarke, K., & Ostendorf, B. (2015). Site-based and remote sensing methods for monitoring indicators of vegetation condition: An Australian review. *Ecological Indicators*, In Press. doi:10.1016/j.ecolind.2015.03.021

Morisette, J.T., Privette, J.L. & Justice, C.O. (2002). A framework for the validation of MODIS Land products, *Remote Sensing of Environment*, 83, 77 - 96.

Morisette, J.T., Baret, F.; Privette, J.L., Myneni, R.B., Nickeson, J.E., Garrigues, S., et al. (2006). Validation of global moderate-resolution LAI products: a framework proposed within the CEOS land product validation subgroup, *IEEE Transactions on Geoscience and Remote Sensing*, 44 (7), 1804-1817, available at http://ieeexplore.ieee.org/stamp/stamp.jsp?tp=&arnumber=1645281&isnumber=34482.

Muir, J., Schmidt, M., Tindall, D., Trevithick, R., Scarth, P., & Stewart, J. (2011). Field measurement of fractional ground cover: A technical handbook supporting ground cover monitoring for Australia. prepared by DERM for ABARES. Canberra.

Reinke, K., & Jones, S. (2006). Integrating vegetation field surveys with remotely senseddata. *Ecol. Manage. Restor*. 7, 18–23.

Sea, W. B., Choler, P., Beringer, J., Weinmann, R. A., Hutley, L. B., & Leuning, R. (2011). Documenting improvement in leaf area index estimates from MODIS using hemispherical photos for Australian savannas. *Agricultural and Forest Meteorology*, 151(11), 1453–1461.

Stehman, S., Olofsson, P., Woodcock, C., Friedl, M., Sibley, A., Newell, J., *et al*. (2010). Designing a reference validation database for accuracy assessment of land cover, Accuracy 2010 Symposium, July 20-23, Leicester, UK.

Stitt, S., Dwyer, J., Dye, D., & Josberger, E. (2011). Terrestrial essential climate variables (ECVs) at a glance: U.S. Geological Survey Scientific Investigations Map 2011–3155 (1 plate; no scale).

Thackway, R. & Cresswell, I. (Eds.). 1995, An interim Biogeographic Regionalisation for Australia; A Framework for Establishing the National System of Reserves, version 4.0, Australian Nature Conservation Agency, Canberra.

Watson, D. J. (1947). Comparative physiological studies in the growth of field crops. I: Variation in net assimilation rate and leaf area between species and varieties, and within and between years. *Ann. Bot*., 11, 41-76.

Widlowski, J.L., Pinty, B., Lopatka, M., Atzberger, C., Buzica, D., Chelle, M., et al. (2013). The fourth radiation transfer model intercomparison (RAMI-IV): Proficiency testing of canopy reflectance models with ISO-13528. *Journal of Geophysical Research: Atmospheres*, 118(13), 6869-6890. doi: 10.1002/jgrd.50497.

Woodgate, W., Soto-Berelov, M., Suarez, L., Jones, S., Hill, M., Wilkes, et al. (2012). Searching for the Optimal Sampling Design for Measuring LAI in an Upland Rainforest. Proceedings of the Geospatial Science Research Symposium GSR2, Melbourne. ISBN: 978-0-9872527-1-5.

Chapter 3. Field data collection and management for Earth Observation image validation

R. Trevithick *[1]

[1] Remote Sensing Centre / Joint Remote Sensing Research Program, Department of Science, Information Technology and Innovation

*Corresponding author:
Rebecca.Trevithick@science.dsitia.qld.gov.au

Abstract

High quality field data are essential for earth observation image validation. Unfortunately, the management of these important datasets is often neglected and considered only as an afterthought following data collection. As a consequence, field data has historically suffered in quality, often becoming unusable over time.

Despite the importance of these datasets, surprisingly little has been written on the best management of this data. This chapter has evolved directly from the experience of managing the field data obtained through the various Landscapes supersite campaigns as an attempt to address this issue. It is designed as a beginner's guide, or 'traps for young players,' and attempts to be as comprehensive as possible.

The chapter covers the unique aspects of field data management for earth observation image validation within the framework of a simplified data management cycle, consisting of the following stages: planning/review, data collection, data storage, and data delivery. It offers practical advice to assist with the broad range of issues encountered at all stages of this development cycle. Additionally, the management system outlined here was developed within an open source framework and therefore the software and techniques used are available to anyone.

Key Points

- Field data are unique and complex and because of this are often inadequately managed.
- Field data should be managed within the context of a data management cycle consisting of four stages: planning/review, collection, storage, and delivery.
- Excellent open source tools exist, which can facilitate the good management of field data.

3.1 Introduction

Collecting field data is a costly exercise, both financially and in terms of human resources. Given the expense associated with data collection, it is not surprising that the current trend in field data collection is towards a model of collaboration and sharing, such as advocated by the open data community.

For data to be useful to people who were not involved in the collection, adequate documentation is essential. Field data management practices are often very risky. There are certain features of these data sets and, in particular, the environment in which these data sets are collected, that result in inconsistent data collection methods and poor records of how the data was collected. Over time, if these issues are not identified and resolved, and the data stored appropriately, they may become unusable. For these reasons, much historical field data collected has been effectively lost.

The aim of this chapter is to provide some specific guidelines to help people plan their field campaigns so that the data collected is managed sufficiently well to enable the data to be useful and as broadly applicable as possible.

3.2 Field Data

3.2.1 Field Data Attributes

There are many attributes of field data that make them unique from other data sets and require consideration when designing a field data management plan.

- **Observed in situ:** Field data are generally directly observed in situ and are not synthetically produced or simulated. Site conditions can vary considerably with unique features and limitations. In addition, the conditions in the field are often harsh and resulting observer fatigue can lead to errors.
- **Variable observers/equipment:** The equipment used to collect field data, particularly for larger campaigns, or campaigns extending over time, may vary. Even if equipment is identical in make and model, there may be differences in measurements obtained. In addition, the observers collecting the data between campaigns may vary, and there may be considerable differences in the experience levels of the individuals collecting the data. There can be inconsistencies in the data associated with subjective observer biases and differing objectives (Trevithick *et al*, 2011).
- **Variable sites:** Field data collection is normally designed around a 'typical' site with an expected set of conditions. If, however, a site is considerably different in some respect to this ideal, then the sampling strategy needs to be redesigned 'on the fly'. This results in inconsistent data formats.
- **Complex data sets:** Field data typically consists of a combination of instrument data, ancillary data ('metadata'), geographic coordinates and images. This results in complex and disjointed data sets requiring careful management so data are not misplaced.

These characteristics of field data result in highly dynamic and variable data sets. In addition, because the conditions under which the data are collected are typically less than ideal, good management is vital.

3.2.2 Terminology

Field based data sets are complicated, often consisting of several interrelated layers of data and metadata. Firstly there is the ‘raw’ data that is obtained directly in the field, via an instrument or specific measurement technique. Generally, there also exists supporting data recorded in association with the original dataset (commonly referred to as 'metadata'). Finally, depending on the use of the dataset, there may also exist high level descriptive metadata records, such as ANZLIC style metadata records. As a result, for field based data sets, the distinction between ‘data’ and ‘metadata’ is not clear and the terms are often used interchangeably. The term ‘metadata’ is often used to describe both what is referred to here as ‘ancillary data’ and 'metadata'. A clear distinction between these terms is essential as the term ‘metadata’ already has a well-defined and accepted meaning in the area of data management.

For the purposes of clarity in this document the following terminology will be adopted (examples of this terminology are provided in Table 3.1):

- **Data:** Direct quantitative measurements of the sample in question, collected via either an instrument or quantified collection method.
- **Ancillary data:** data collected in association with the primary data set, which aid in the use, but are not direct quantitative measurements of the sample. Examples include geographic coordinates, imagery and descriptive information regarding the sample, instrument or site.
- **Metadata:** Information relating to the discovery and use of the data. Examples include, scale, units, geographic and temporal scales, custodians and licensing.

Table 3.1 Examples from the Landscapes supersite data sets of the differences between 'data' and 'metadata' as defined in this document.

Data	Ancillary Data	Metadata
• Instrument Readings • Point Intercept Measurements • Raw imagery (eg. Hemispherical photography) • Leaf scans	• Instrument details • Date and time • Geographic coordinates • Comments	High level metadata records which aid in the discovery and determination of data applicability and its use. (e.g. ANZLIC).

3.3 Field Data Management Cycle/System

The concept of a data management cycle is well established and documented in the literature (DataOne, 2013), but often varies depending on the specific data type(s) being managed. For the purposes of this document a simple data management cycle is presented as a framework within which to discuss the specific issues associated with the management of field data. Each stage, consists of specific components, which are illustrated in Figure 3.1 and discussed in further detail throughout the remainder of this chapter.

The simple model described here is a cycle consisting of the following steps:

1. **Data management planning/reviewing (pre-field):** Planning for the remaining stages in the data management cycle and documenting the plan (typically in the form of data protocols) and developing necessary data recording, storage and delivery tools.
2. **Data collection and recording (in field):** Recording measurements in the field. This stage is arguably where the majority of difficulties associated with managing field data originate, typically associated with insufficient data recording and deviations from the data protocols defined in the planning stage.
3. **Data collation and storage (post-field):** Organising and storing the data for posterity. Poorly collated and stored data can result in a lack of 'future proofing' of the data. At this stage a minimal level of 'metadata' should be developed to ensure that data will remain useful for future use and for use by other users.
4. **Data delivery (post-field):** Development of methods to make the data discoverable and accessible for end users that may wish to use it. At this stage, complete metadata should exist for the product.

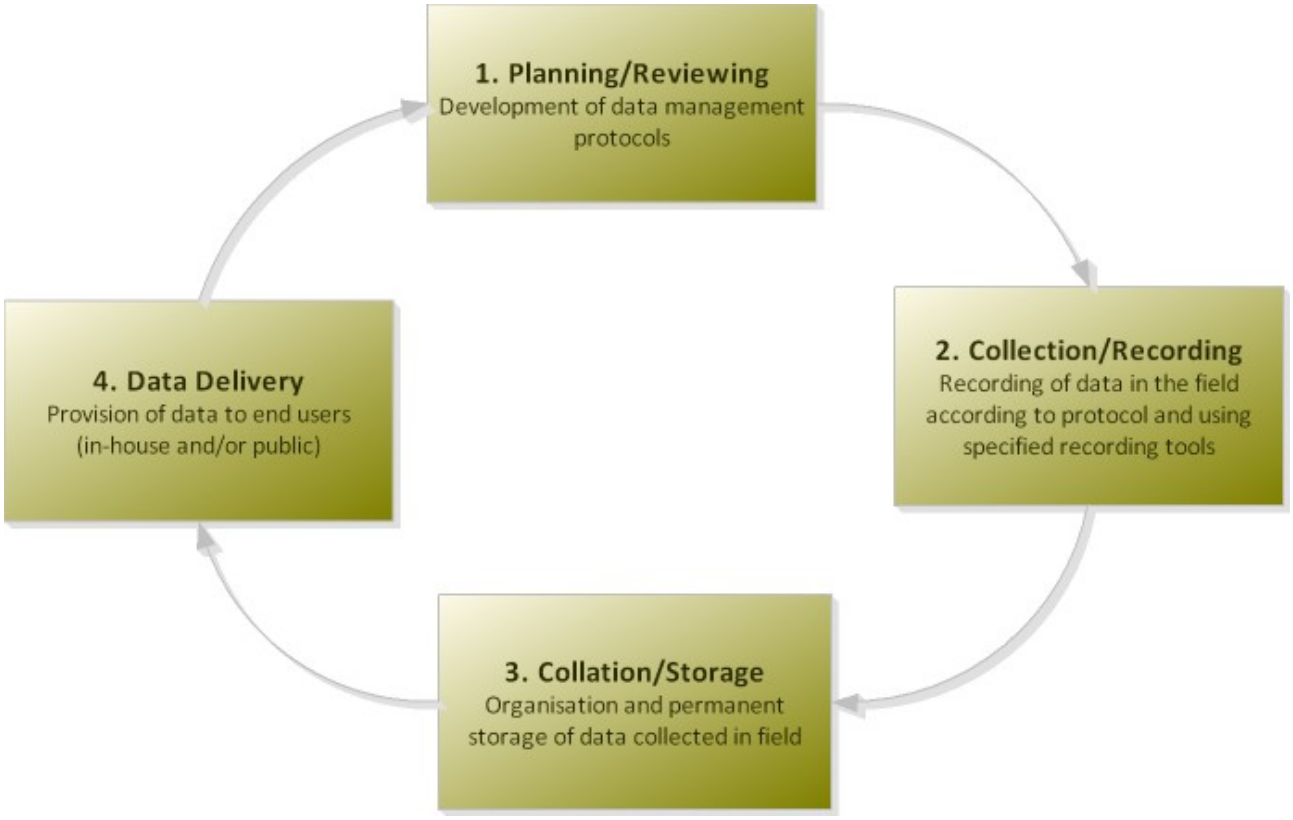

Figure 3.1 Data Management Cycle

We consider data management as a cycle, because data management systems continually evolve, and are improved on, with lessons learnt from each data acquisition cycle. This is particularly relevant with data as dynamic as field data. Regardless of the scope of the data collection campaign, this general cycle can be adapted to suit.

Eventually, the continual implementation of the full data management cycle will result in a solid field data management system, which should produce high quality, timely data and metadata. A field data management system is a form of information system, consisting of people, hardware, software, data and processes, designed to manage field data. The Landscapes field data management system is outlined in the flowchart in Figure 3.2.

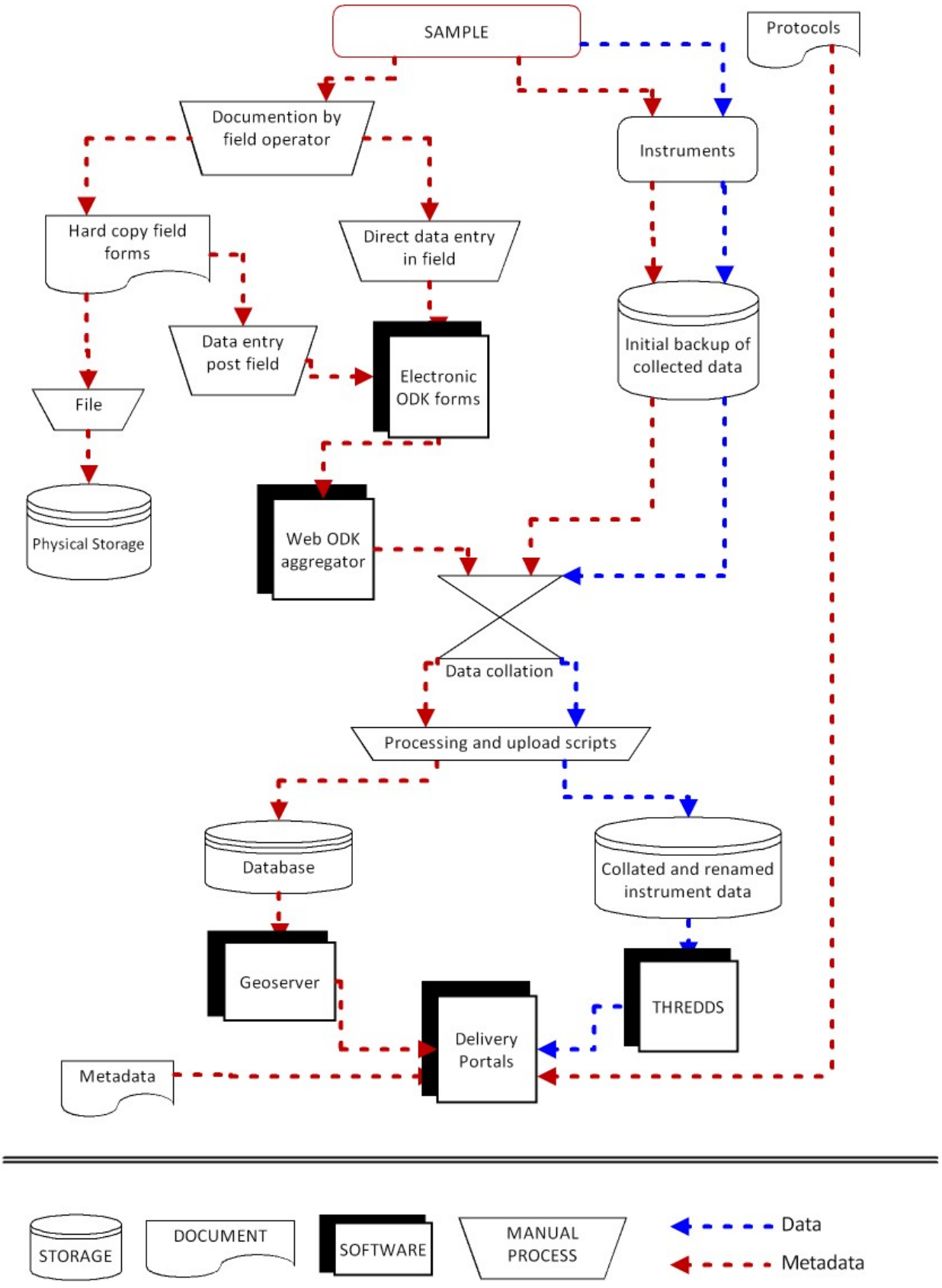

Figure 3.2 Flow chart illustrating data and metadata pathways through the Landscapes field data management system.

3.4 Data Management Planning/Review

The data management cycle begins and ends with planning and/or review. The initial planning of the collection, storage and delivery of the data should occur early in the project, prior to the commencement of any fieldwork. Careful consideration at this initial stage will help prevent major blunders occurring, such as the failure to collect essential ancillary data. Ideally, the planning process should consider all aspects of the data management cycle outlined in this document, right through to the data delivery stage. It is highly unlikely that a finalised plan will be achievable in the first iteration of the data management cycle. Therefore, at the conclusion of each campaign, the data management process should be reviewed and any necessary changes to each of the steps should be identified and implemented. If the data collection process only consists of one campaign, then adequate preparation at the planning stage is essential.

Planning for the successful management of field data takes the form of developing data collection protocols and associated tools for data recording, storage and delivery. A large component of the data planning stage is therefore documentation of the data management strategy.

3.4.1 Data Management Protocols

Data protocols outline best methods for collecting and managing data for a specific field dataset. Without a protocol, there is unlikely to be a clear plan for what data will be collected, how it will be collected, recorded and stored. This can result in variable and inconsistent data.

Protocols are often limited to details about the specific collection techniques but should also outline best management practices for recording and storing data. The primary elements of data protocols should include:

- site selection
- sampling scheme
- equipment list
- collection procedure
- data recording method

Specific considerations for each of these elements at each stage of the cycle are discussed in the following sections of this document. Protocols for the analysis of the data should also exist, but discussion of this is outside of the scope of this chapter.

Protocols, like all other elements in the data management cycle, will evolve and improve over time. An initial exploratory protocol may differ considerably from a final protocol and it may take many iterations of the data cycle before this is achieved. While this is unfortunate from a management perspective, it is naïve to expect that protocols will be perfect the first time. The appropriate approach is to consider as many issues as possible, but assume that protocols will change and incorporate as much flexibility as possible into the design of recording tools and storage methods proposed.

While protocols will evolve, any specific version of a protocol should be a clear and decisive description of the data collection process at that stage of its development. Ideally protocols will have no ambiguity and should be detailed enough and written as clearly as possible in a step by step manner. Protocols should be possible to follow by someone with limited experience, as it cannot be assumed that someone with a high level of expertise will be collecting the data. A good test is to have someone inexperienced read through the document and try to implement the method. A good example of a thorough and well developed final protocol is the ABARES technical handbook for ground cover monitoring in Australia (Muir *et al*, 2011).

Protocols should be considered a written record of how the data will be collected under ideal circumstances. Any deviation from the protocol during the actual collection process should be documented. If a protocol

proves to be unworkable in practice, then it can be adjusted in subsequent versions. After each campaign or field trip, the process of data management should be reviewed and appropriate adjustments made.

3.4.2 Data Recording, Storage and Delivery Tools

The other major outcome from the planning stage should be the consideration and design of any tools to be used in the recording, storage and delivery stages of the data management cycle. Recording tools can include hardcopy field sheets and electronic data recording tools. Knowing what software being utilised prior to data collection is particularly helpful for the development of data recording tools. Likewise, an idea of how the final data will be accessed by end users can help to determine which storage mechanism to use. The various considerations for selecting and developing these tools are discussed in greater detail in the sections on data collection and recording (Section 3.5), data collation and storage (Section 3.6) and data delivery (Section 3.7). The use of any tools should be adequately documented and this documentation should be reviewed in the planning stage of the cycle.

3.5 Data Collection and Recording

The data collection and recording stage is where the majority of problems associated with field data management occur. This is primarily a result of poor planning of the data collection process and poor design of the associated tools required to record the data. Failure of the field officers to follow correct procedure is another major cause of error. Inadequate data and metadata are then recorded, resulting in difficulty storing the data and may even lead to gross data loss. In comparison, if data are recorded carefully and with sufficient detail, most problems later in the data management cycle can be avoided. As a consequence the majority of this chapter focuses on the good design of the field data collection and recording methods.

3.5.1 Common Field Data Collection/Recording Issues

There are a number of very common errors that are made when collecting and recording field data, which can result in significant data loss or degradation of data quality. When designing a field data recording protocol these potential issues should be kept in mind.

- **Missing/incorrect essential ancillary data:** Not all ancillary data are created equally. Some data are essential, while other data are only desirable or optional. As it is not always possible to obtain this information retrospectively, it is highly recommended to try to determine all required ancillary data early, and definitely prior to commencing fieldwork, and have this clearly documented. This is particularly important if the intended users are not involved in the data collection process.
- **Deviation from protocols:** Ideally data will be collected in a manner that closely resembles that method outlined in the protocol. Unfortunately, due to the nature of field sites, some deviation from defined protocols almost invariably occurs. While the data may still be useful, data that is collected in an ad hoc manner and does not conform to the existing storage schema will either require an adjustment of the data to fit the schema or an adjustment of the schema. This can result in either errors associated with converting the data or in a weakened storage schema and reduced querying capacity of the final data. The solution is to consciously build flexibility into the collection tools and the storage schema. Any deviation from the protocol needs to be clearly documented.

- **Inadequate records/reliance on memory:** Often inadequate written records are kept on the exact details of the data collection method. Because of conditions in the field, memory is often resorted to as a recording method. However, memory is unreliable. Things can be forgotten and, even worse, remembered incorrectly. This results in data loss and data confusion, which is exacerbated if the data collection method deviated from the protocol significantly. The best method to combat this problem is well considered and well-designed data recording methods/tools that are simple to use and allow for documentation of any variations in the method.
- **Separated data:** One of the biggest issues for field data management is the separation of related data elements. This is a particularly dangerous practice, which can result in significant gross data loss. Data can easily become separated, either physically or via file organisation, with no connecting reference between the data elements. This problem largely occurs when, due to the method of collection, related data has to be recorded in two separate locations. Examples include photographs separated from handwritten data sheets and geographic coordinates separated from instrument measurements. Both these examples are due to the fact that the device used to collect each data/metadata element is necessarily different. For large campaigns such as Landscapes, where data are collected by a variety of individuals residing in different locations, this issue becomes even more significant.
- **Lack of backups:** Another extremely risky practice, which can result in gross data loss, is a lack of data backups. Generally, once the trip is completed, the data are collated and backed up. However, prior to returning to the office, backups are often not undertaken. Unfortunately, due to the remote nature of fieldwork, conditions are ideal for data to be lost. Examples of data loss include: accidental loss or destruction of hard copy field sheets, deletion or overwriting of electronic files, or loss of storage medium in transit.

3.5.2 Data Recording Tools Overview

There are a number of popular ways to record ancillary data in the field. The most common are hard copy field sheets, electronic forms and relying on the instrument itself. The main considerations when choosing are method are flexibility, convenience and consistency. Flexibility refers to how adaptable the recording method is, particularly if data were collected in an ad hoc way and do not conform to the prescribed protocol. Consistency refers to the quality of the data collected and adherence to data standards. Finally, convenience refers to how practical the recording method is to use in the field, including how reliable. Each method has advantages and disadvantages, which are identified in Table 3.2 and discussed further in the remainder of this section. Ideally, when designing a field data recording method, a balance between flexibility and consistency will be provided in the most convenient format possible.

Table 3.2 Performance of various recording devices in the field.

Recording Device	Flexibility	Consistency	Convenience
Hard-copy field sheets	High	Low	Medium
Instruments	Low	High	Medium
Specialised electronic forms	High	High	High

Hard-copy field sheets

Hard-copy field sheets are the most common way of recording ancillary data in the field due to the simplicity of implementation and low risk. While this method has some obvious benefits, there are a number of drawbacks and limitations. Given the availability of low cost alternatives, hard-copy field sheets may only serve as a backup to other methods.

- Flexibility: Hardcopy field sheets are by far the most flexible data recording method. Hard-copy field sheets allow users to entirely deviate from a given protocol and record data in any manner.
- Consistency: While field sheets allow for flexibility, the fact that they cannot enforce the collection of data in a particular format often results in inconsistent data. A well designed field sheet can increase the consistency of data obtained. Clarity in the design of the sheet is the most important factor. All data required should have a clear place in the field sheet. Measurement units and categories should be clearly stated. Sketches should be included to illustrate the collection process, including sampling design. Essential and important data elements should be made obvious. Corresponding guidelines and examples are also useful. Unfortunately, however, regardless of how exacting the designed field sheet is, inexperienced observers will invariably make mistakes or omit desirable data.
- Convenience: Hard-copy field sheets are also one of the more convenient collection methods when in the field. They are extremely reliable, with a very low rate of failure. With the exception of getting wet or torn, they largely cannot fail, and waterproof paper is an option if wet conditions are expected. Their design is largely limited only by imagination and there are numerous elements that can be incorporated to facilitate data capture. While convenient in the field, the major drawback to hard-copy sheets is that they require manual transcription. Manual transcription is time consuming, inherently prone to error and, in addition, sometimes handwritten data are illegible.

Instruments

The instruments used to collect the data often record the majority of the ancillary data required for a particular data type. For example, some spectrometers (eg. ASD) and cameras record a great deal of information within their header files, such as instrument details, date and time and, sometimes, geographic coordinates. However, despite the benefits of collecting ancillary data in this way, it is still a limited method.

- Flexibility: Depending on the specific use of the data, there is almost always additional data that needs to be recorded and these instruments are not typically customisable. Given that they are designed to be robust, with little user intervention, they are largely inflexible.
- Consistency: Instruments are designed to produce consistent output, so consistency of data and ancillary data obtained this way is typically high. The danger here is an over reliance on this method as a recording tool. If the instrument is poorly or incorrectly calibrated then data may be incorrect. So although the data collected in this manner are typically highly consistent, they can be consistently wrong. Data will either then need to be discarded or recalculated. If using the instrument to gather ancillary data, be sure the instrument is correct and note any discrepancies.
- Convenience: In some ways, ancillary data collected directly via an instrument is highly convenient; data are simply recorded for later download. Unfortunately, there is normally additional ancillary data that is not recorded by the instrument and there needs to be some way to connect the two datasets. This is the difficulty of data separation discussed in Section 3.1.1. Additionally, if an instrument fails then there may be no way of retrieving that data.

Specialised electronic forms

Historically, field data collection has largely consisted of a combination of hard copy field sheets and instrument data. However, with the advent of specialised field and mobile technology, it is possible to develop forms specifically designed to be taken into the field for the direct entry of data. In the simplest form this can consist of a basic spreadsheet such as an Excel spreadsheet. However, more recently, tools have been

developed which simplify the development of highly specialised data entry tools for devices such as mobiles and tablets. Because of the general movement towards specialised electronic data collection tools, these are discussed in greater detail in Section 3.5.3.

- Flexibility: These tools largely serve as a replacement of hard copy sheets. The flexibility of the tool is largely a question of software choice and design.
- Consistency: One of the greatest advantages to using specialised forms and applications is the ability to program various constraints into the data collection process, resulting in highly consistent data.
- Convenience: Electronic forms are highly convenient. Mobile devices are typically light and often come with additional features such as GPS technology and cameras, simplifying the data collection process. In addition, there is no manual transcription step, greatly reducing time taken collating data after collection. Major barriers to convenience are battery life and screen visibility.

3.5.3 Electronic Data Collection Tools Design

An ideal data recording system will be flexible and convenient, while maintaining high consistency in the data collected. As discussed in the previous section, one of the more promising ways to achieve this is through the development of specialised electronic data recording forms which can be used on laptops or mobile devices.

Flexibility

Electronic field devices may appear less flexible than hard-copy field sheets in regard to data capture, however in general they are typically no more restrictive. In fact, when using more modern technology such as Open Data Kit (ODK) (http://opendatakit.org/) and other customised applications, there are typically numerous ways to capture deviations in data collection. These include: annotatable photography, digital sketching and comments fields. In addition, forms can be designed so data entry fields have minimal constraints and will accept a range of inputs. Largely the loss of flexibility using these forms is a considered design choice, where input is restricted so as to increase data consistency.

Consistency

Consistency in the data obtained in the field is arguably the greatest gain obtainable using specialised electronic data collection forms. This increased consistency is mainly achieved through the introduction of constraints to the data input fields. Depending on the software being used, constraints can include, but are not restricted to:

- restrictions on data format (e.g. integer, float, text, date etc)
- restrictions to categories (via drop down lists or radio button selection)
- restrictions on required fields (fields which must be completed prior to advancing or submitting forms)
- restrictions on specific characters (e.g. no commas)
- restrictions on the range of acceptable values

Outside of constraints, there are other general practices which will improve data consistency regardless of the software being used. Do not allow for input of the same information in more than one field. This may lead to discrepancies in the final data. When populating categorical fields, be sure to include fields such as 'Not applicable' or 'Other' to avoid people using incorrect codes or leaving fields blank. Make sure the units of measurement are clearly defined.

Convenience

Ease of use is essential to facilitate people using the tools. The sequential steps in the process of collecting the data in the field should be the primary consideration when developing field recording tools. Data recording methods and tools should be designed around the sampling scheme determined:

- Do not rely on measurements being taken in a particular order. Devices should allow for data to be collected out of order and the recording methods should not depend on this. This is essential for photographs, which have no distinguishing elements in their names in the field. Having a clear record of the order they were collected in is essential.
- Make forms as modular as possible. Have one form for each database table the data corresponds to. Trying to make one universal form and load too much data at once will increase likelihood of failure.
- Hardcopy field sheets should always be developed and maintained for data that may alternatively be collected via an electronic device. The design of the hard-copy form and electronic form should be complementary, to facilitate easy entry of data. For the sake of convenience, hardcopy field sheets should ideally be one sided. Screens of field laptops and electronic recording devices should be visible in all conditions.

Readers seeking to develop their own electronic data recording forms are encouraged to investigate the Open Data Kit (ODK) (http://opendatakit.org/) as a possible solution. Landscapes has adopted the ODK framework for the development of their field data collection forms. ODK is discussed in further detail in the next section, 3.5.4.

3.5.4 Open Data Kit (ODK)

ODK is an open source package developed by Google and the University of Washington for the creation of specialised survey and field data collection forms for use with mobile devices (ODK, 2013). Mobile devices, such as phones and tablets, are in many ways the ideal field data collection device. They are portable, have an inbuilt GPS, inbuilt camera and accessible data input options. Because these devices are also web enabled, the update and backup of forms can be easily achieved.

ODK is designed to be accessible. It runs on readily available Android mobile devices and the development of the forms can be easily achieved via web based tools. Download of the data collected can be either via the internet or directly from the mobile device onto a computer. The entire package is free and very easy to implement at a basic level. All Landscapes field data are now collected with the use of specialised ODK forms.

3.5.5 Recording Common Field Data Elements

Some field data elements are largely universal, such as geographic coordinates, date/time and field photography. These data elements are often essential and often very poorly managed. Common errors associated with recording these data elements, as well as proposed good management techniques, are discussed in this section.

Geographic coordinates

It is advisable to always record geographic coordinates, even if not considered directly essential for the specific data set. Make sure to either collect geographic data in unambiguous forms (latitude/longitude) or note essential information such as the datum and zone. Often essential details are missing or recorded incorrectly, resulting in gross errors in location. Make it clear if you are using decimal degrees, degrees and decimal minutes, or degrees/minutes/seconds if using an unprojected coordinate system. If using a bearing/distance method to record geographic points, be sure to provide the geographic coordinates of the reference point. Bearing/distance measurements can be highly accurate if done correctly, and highly inaccurate if done poorly. The accuracy of the measurement can vary considerably with the instrument used to collect the coordinates, as well as the environment. If an accuracy estimate is available, record that along with the coordinates.

If coordinates are being collected for the purposes of geographic registration, as may be the case for airborne data capture, make sure that the coordinates of the reference object being used is clearly visible in any

imagery and well defined. That is the object should have a sharp corner or other clearly identifiable feature evident. These coordinates should also be collected to the highest degree of accuracy obtainable. An example for the Landscape campaigns is the use of the calibration targets, in which each corner of the target was georeferenced and shows up clearly in the imagery.

Most in situ field data collection are single point measurements, which can be recorded with a standard GPS instrument. Even transects typically consist of a series of points collected along a transect line. Some instruments can record geographic coordinates, or have the capacity to have a GPS data logger attached. If this is not the case, then how the coordinates are to be collected and recorded needs to be considered. If measurements are collected as a transect, and no data logger is available, or is not working, collect the geographic coordinates and date and time at each end of the transect, along with the measurement interval if that is appropriate. In fact, ideally that information would be collected even if a GPS logger is used in case something unfortunate occurs.

Date and time

Along with geographic coordinates, date and time should also be routinely recorded. Generally observers will record the date but, even if requested, time will largely not be recorded. It is a good idea to note the time zone. If relying on inbuilt clocks in devices, make sure the time and date are correct. Note any discrepancies between the device date/time and the actual local time.

Photos

A common practice when collecting field photos is to collect them in a standard order. However, we suggest relying on this method as little as possible. Like many data collection methods, this practice will work fine until something goes wrong, in which case it tends to fail catastrophically resulting in the photos being unusable. It is best to develop the habit, and appropriate field sheets, which allow for the recording of image numbers. As an additional measure, a series of photos taken at a site can be separated from the next site by a photograph of a field sheet, GPS reading or note. This is an excellent fail safe method of ensuring images have enough associated information to be placed with their site.

When collecting any photography of the sky ensure the imagery is consistently aligned in the same direction. Although it is largely unimportant which direction is selected, provided it is well documented, we recommend aligning the top of the camera, when the camera is laid flat, with North.

3.6 Data Collation and Storage

The data collation and storage stage of the field data management cycle consists of organising and storing data in a format that 'future proofs' the data. The main goal at this stage should be the security of the data, ensuring that it stored sensibly and with enough information, that leaving it for extended periods of time will not result in a reduction of its usefulness.

Data collation and storage can be done manually. However, depending on the scope of the data collection process, the data collation and storage stage is one area of the data management cycle that can greatly benefit from computer scripting solutions the processing of data and upload of data into storage. The greatest barrier to implementing automated processing at this stage is inconsistent input data. This is why a move towards specialised collection and data entry tools is highly recommended for ongoing projects of larger scope, as specialised electronic input forms greatly improve the consistency of data obtained. Currently the Landscape stage is managed through specialised scripts programmed in Python. The scripts are designed to work in conjunction with the specialised ODK form output, so that, if used correctly, upload is extremely efficient and accurate.

3.6.1 Data Collation

Data collation refers to the preparation of data and ancillary data obtained in the field for storage. Data should be collated as quickly as possible, ideally on the day of collection, as any problems with data are less likely to be resolved with increasing time. In some instances, data may become completely unusable if left for too long before collation. The primary goals of the collation process are:

1. **Organise data**

Data coming back from the field will be in various states of organisation. The first step in collation is to organise the data and ensure that all required data are present. This step is vital if data are to be used as input for scripts for the automatic renaming of files or uploading of data to various storage mediums.

2. **Transcribe data**

Transcribe any data in hard copy format into digital forms if necessary. Double-check any manually entered values for accuracy. Great care should be taken to ensure no errors are introduced at this stage. The original forms should ideally be scanned and stored alongside the digital data, and the original hard copy forms should be retained in a physical filing system.

3. **Identify problem data**

As part of the data collation process, any issues with the data should be identified and highlighted for management at the storage/delivery stages. Ideally data sets should be complete and acquired in a manner consistent with the method outlined in the protocol. However, there are numerous reasons this doesn't always occur and data are either collected in a different manner to that specified, or not collected at all and then estimated. Erroneous and missing observations should also be identified.

Collation of field data should not be undertaken on the original data obtained. Prior to commencing collation, all digital field data should be saved into a folder, with minimal intervention, and backed up. Using Landscapes as an example, on return from the field, all field data are stored initially in a 'dump' folder. This folder is then copied and the copied data collated and sorted. This ensures no accidental loss of data during the collation process. Once the data has been successfully collated, the original 'dump' folder can be deleted if desired, but it is suggested it be retained if storage space permits.

3.6.2 Data Storage

Once data are collated it can be uploaded into storage. Field data storage is complicated by the numerous varied elements comprising the data sets. There are three primary data storage mechanisms which all collected data will be stored in: a) physical data storage, b) digital data storage, c) database records. Some data/metadata may possibly be stored in two, or all three of these mediums. For example, some measurements may be recorded on a paper form, transcribed into an electronic document and then summarised in a database table. Each of these storage mediums is discussed in more detail below.

Physical data storage

This refers to the storage of any data with a physical presence such as original hard copy field sheets or samples. Orderly systems of managing the data are required, which enables the data to be associated with any digital records. Original hard copy sheets should always be retained if possible as information is sometimes lost through transcription and copying. These are the original source of data.

Digital data storage

Digital data, such as instrument files, associated imagery and scans as well as electronic field sheets will require storage within a computerised file system. Digital data should be stored in a logical framework. There are two primary ways to organise digital data: around site or around data type. However, any file structure may be suitable, provided it is sensible and follows a clear pattern. If a database is being used to reference the data, then the specific organisation method is largely irrelevant, provided the data are clearly referenced. For Landscapes both file structures are used, depending on the data set.

All instrument data collected in the field should be preserved in its original format, even if they undergo significant processing and there is no intention to deliver the data this way. This ensures that any problems that may arise in the remaining stages of the data management cycle can be reverted.

Database records

Certain data types and most ancillary data can be stored within a database system for querying as text, numeric, date/time or geographic fields. The most common use of a database for storage of earth observation field data is for supporting ancillary data. Instrument files and imagery are typically stored in a digital data filestore, with the location of the original files referenced in the database. However, with advanced modern databases, it is possible to store binary objects, making storage of imagery and other data possible. An example of this is the SPECCHIO database (REF), which stores both ancillary data and binary objects of the recorded spectra. However, this practice is beyond the scope of this document, and will not be discussed here.

At its simplest the 'database' structure may consist of a simple Excel sheet. While for larger or more complex projects, a fully-fledged spatial database may be the appropriate solution. For Landscapes the network of field data are captured in a PostGIS relational database. PostGIS is broadly considered the most advanced open source spatially enabled relational database. Given the availability of Excel and open source solutions like PostGIS, some design considerations for these tools are discussed in the next section (Section 3.6.2).

3.6.3 Database Design

Databases provide a searchable, electronic record of data. Typically databases are most suitable for storing ancillary data, which can be searched to locate appropriate data for use. 'Raw' instrument of measurement data can potentially also be stored, but often these are best left in the form of instrument output files, with a reference within the database. How useful a given database is for searching and locating data is dependent on how well it is designed and maintained. Databases for field data should conform to general good design principles for databases in general, but some specific considerations for field data are discussed below.

Database schema

The database storage 'schema' refers to how data are organised within the database. The more rigid and structured the schema, the greater searching power it is possible to achieve. A rigid schema also improves data quality and database functionality.

Any given field visit may consist of numerous elements that are connected in either one-to-one or many-to-one relationships, creating a complex network of data. For example, using an Landscape example, a given field location could include datasets such as point intercepts, hemispherical photography, ground lidar, ASD and LAI measurements, as well as ancillary data including geographic/temporal coordinates, site descriptions and field imagery.

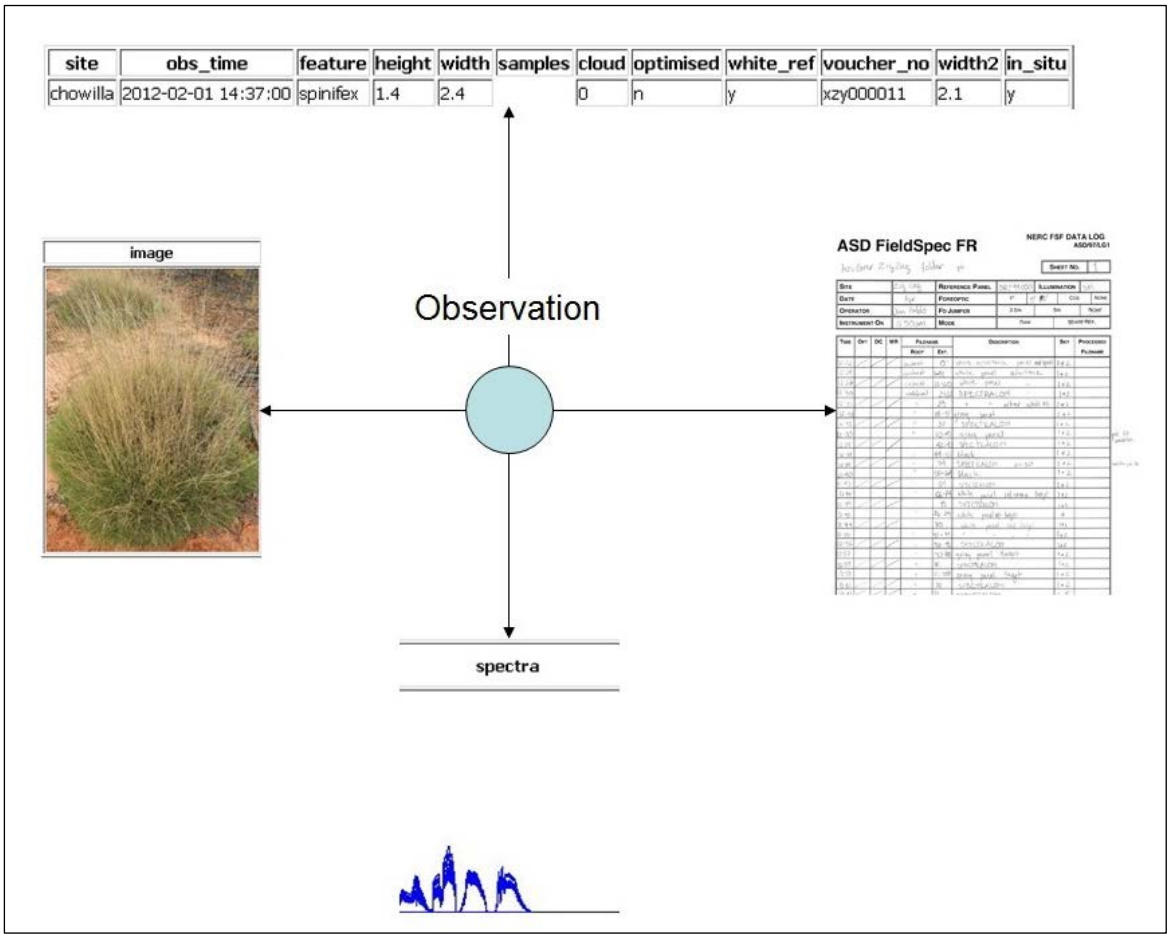

Figure 3.3 Data elements which be associated with a given field ASD observation.

If using a relational database, a primary key to connect these various datasets will need to be considered. The primary key is a unique identifier which distinguishes one record from another. For field work, one way to uniquely identify observations is to use the spatial and temporal coordinates of the sample. This is the method used by Landscapes. The obs_key is a combination of the spatial coordinates of the observation and its associated date and time. The key is of the form longitude_latitude_date_time and is unique for each sample site. All observations in the field therefore need to be associated with a geographic coordinate and a date and time. It is possible for many observations to have the same key, and if they were taken at the same approximate time in the same location, they should have the same key. For example, leaf samples and associated ASD measurements will preferably have the same key.

This approach has an added advantage of allowing for easy pairing of observations when querying the data in the database and to recall all associated data with ease. This structure works extremely well, allowing for complex SQL queries on the data.

Field data typically comes in a number of specialised formats. Attribute data are typically recorded as text, numerical data, date/time or as geographic coordinates in some form. To maximise the searching capacity of a data set, data elements in fields should be as discrete as possible and conform to these types. Additionally, codes and abbreviations should be consistent across a data field. Likewise, units used to collect the data should be consistent. If data are collected in two common units then two fields should exist, or one measurement should be converted into the other unit before storage. It is not good practice to rely on storing units as a component of a data field. This requires the value to be stored as text, making it difficult to perform numeric calculations on the data. For example, an observation containing a numerical count and associated comment should be separated into two fields, one for the number and one for the comment.

Geographic coordinates

Consider the geometry of the data being collected when designing your tables. In general, field data is point data, with observations referring back to a single point. This is the simplest method of referencing observations and is generally adequate.

Data should preferably be stored in a common geographic coordinate system. Decimal degrees with a WGS datum are proposed, regardless of the coordinate system the data was collected in. This will generally mean that some or all of the collected data will need to be re-projected prior to storage.

Spatial coordinates should be reported in decimal degrees format to at least 4 (preferably 5 or 6) significant digits past the decimal point. This does not include uncertainty introduced by a GPS instrument, which should ideally also be recorded in a separate column. Provide latitude and longitude with south latitude and west longitude recorded as negative values. Latitude and longitude are preferred over UTM coordinates, as confusion often occurs around the zones.

Date and time

Date and time formats in databases are typically recorded as a 'timestamp'. These formats are particularly useful as they have numerous associated functions enabling conversion and calculations based on date and time. Mostly this level of functionality is not required however, and simply storing the date in a yyyymmdd format is adequate. For the purposes of sorting by date, it is essential to keep this format with the year first, month second and day last, with leading zeros if necessary. Additionally, time is often not essential to record, and if not required can be omitted.

Text fields

Text is the most flexible way to store any data, as any data are acceptable to a text field. Unfortunately, text offers the least capabilities for searching and calculations. If a data element can be accommodated by a numerical field, then it is recommended that it be stored as such. Comments and explanations should not be included in a column that is meant to include numeric values only. Comments should be included in a separate column that is designed for text.

Pay particular attention to spelling and case; as well as slight variations in format, such as the use of spaces and underscores. Given the common use of Excel and CSV files for the storage and transfer of data, it is also highly recommended not to allow commas within any text field. This should also be a consideration when designing electronic field forms (see Section 3.3.3), as it is often possible to make that a constraint at the data recording stage.

Text fields are often an appropriate field for categorical data, as it allows for a descriptive record of the category to be provided. If using text fields for categorical data, however, be sure to be consistent in the wording, which will improve searching capabilities. For this reason, it may be more appropriate to use numerical codes, which relate to specific categories which are defined elsewhere.

Numeric data

Numeric field data should be stored with the same or lesser precision than it was recorded in, at a level sensible for the data type. Field data that is reported with extremely high precision should be viewed with skepticism. For example, length measurements in the field to within 1 mm are highly unlikely to have been achieved. For certain field measurements, accuracies of within 10 cm are dubious. For geographic coordinates a precision of 1 m or 1/10000 degree are recommended.

Have the storage software calculate any derived values from the raw data where possible. If using a relational database or spreadsheet, it is possible to calculate derived values 'on the fly', allowing for automatic updating when new data are inputted or data are corrected. This leads to much more consistent and accurate data than performing calculations prior to data storage.

3.6.4 File Naming

One of the most important considerations when storing digital data is the file naming convention used. Often file names have no consistent file naming convention. Alternatively, even if a convention exists it may provide very little information about the content of the files. Another error is that names of files may be highly similar or identical to data files collected separately.

Ideally file names should act as a source of metadata. File names should reflect the contents of the file and contain enough information to place the data with the associated field observation. This ensures that the data can be identified even if it's isolated from the remainder of the site data. In addition, a sensible and comprehensive file naming convention simplifies searching and can facilitate the development of automated retrieval and processing scripts if desired. File names may include, but are not limited to, references to: type of data, date of collection and site name or location. Incorporating this level of information, however, results in complicated naming conventions and it is suggested that automated renaming is undertaken to simplify the process.

A proven example of a suitable naming convention is that developed by the Queensland Remote Sensing Centre, which follows a what-when-where-processing format. This is the convention that has been adopted for the Landscapes field data sets.

Regardless of the convention adopted, make sure names contain locations to a sufficient degree of accuracy, but not unreasonably high precision. 10 m in the field may be adequate, but at some sites 1 m accuracy is achievable. At Landscapes we use 5 decimal places for field data locations. Although this is overly precise for many sites, it is appropriate for others and for the sake of consistency was chosen. For the date component, always record the year, then month, then day. This allows for easy sorting by date.

3.7 Data Discovery/Delivery

Data discovery and delivery refers to the capacity for data users to find and access the data. For many data sets, this user base may consist of only a few individuals and data delivery may not be a major component of the management cycle. However, with increased sharing of datasets and the move towards freely available public data sets, this step is potentially quite involved, entailing the hosting of data on publicly accessible databases and delivery through public portals, along with associated licensing and metadata considerations. Some of these considerations are discussed below.

3.7.1 Data Quality

Although it is recommended to retain and store all field data collected, not all of this data will be suitable for delivery. Some data may be missing essential ancillary data or metadata, or be of an insufficient quality to be used. Alternatively, data may have been collected ad hoc and not have a suitable place in the data schema. The data manager will need to make a decision about what data are of an appropriate standard for delivery. Sometimes an arbitrary call on data quality may need to be made, in this instance always err on the side of data quality, quarantining bad data or, at a minimum, clearly advising of the data's limitations.

3.7.2 Delivery mechanisms

If data are only to be delivered 'in-house' then the data storage software selected in the data storage and collation stage may be suitable for delivery. Relational databases, for example, allow for complex searches on data, and if in-house expertise exists there should be no difficulty in users finding and accessing the data. Typically, however, these storage tools are not suitable for public delivery of the data. While data files from these tools can be easily made publically available, navigating and searching the data may not be straightforward and often requires specialised skills and knowledge of the data storage schema. Free and open source options do exist for more sophisticated delivery of field data, however use of these tools requires skill in computer systems and software implementation. The Landscapes solution for web based delivery of field and airborne data is presented below as an example of one possible way to facilitate public access to this type of data.

Landscapes field and airborne data sets reside on the University of Queensland Landscapes server as instrument files within a file directory and as PostGIS database records. The PostGIS database is accessed via a GeoServer application and all possible database tables and views are available for 'publication'. GeoServer can serve this data in a variety of formats, including popular formats such as shapefiles and Google Earth KMZ files. The number of published data sets on GeoServer is potentially very large, and users finding the particular data set of interest is complicated. GeoServer, however, can be linked to other applications supporting the OpenLayers protocol, such as the Landscapes Visualisation Portal (Figure 3.4).

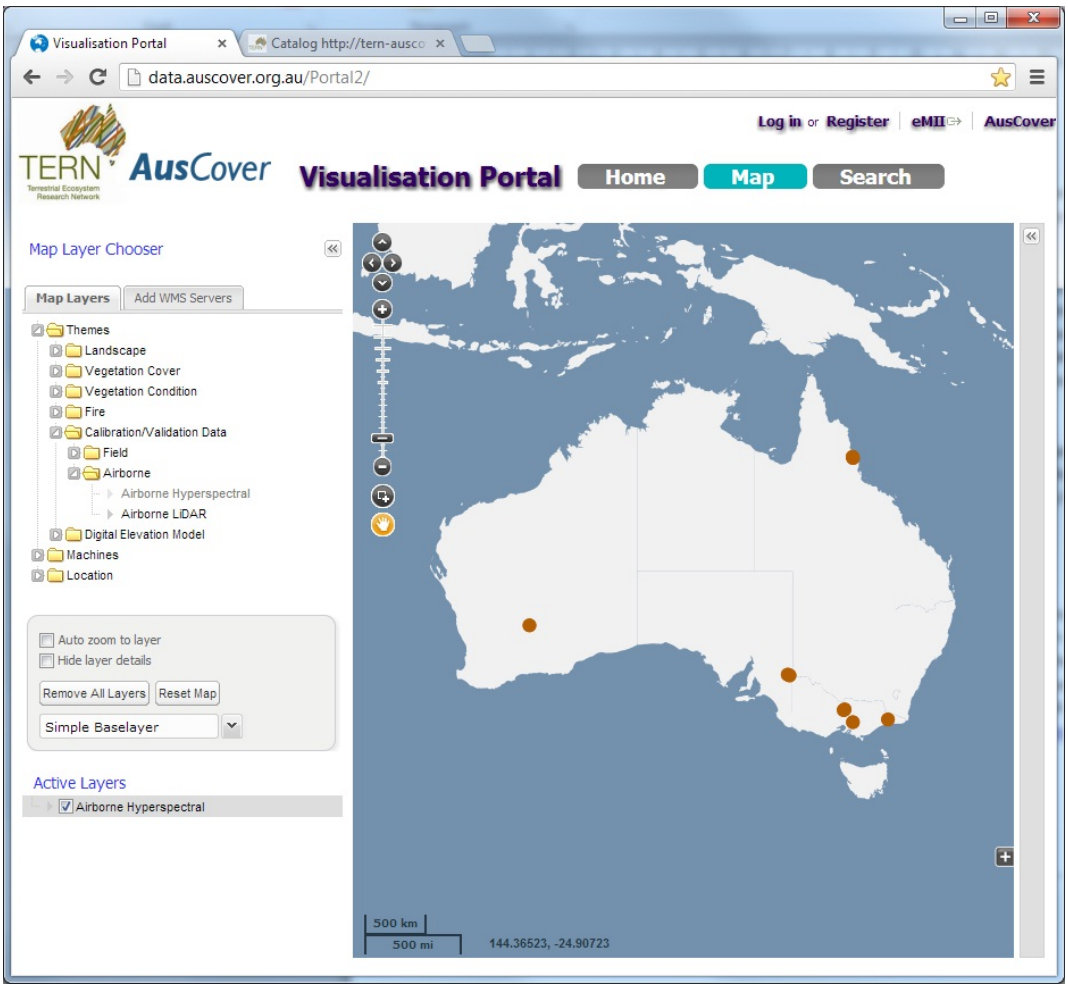

Figure 3.4 TERN Landscape Assessment's Visualisation Portal, displaying the locations of the Landscape airborne hyperspectral data collection campaigns.

Delivering the data via the visualisation portal allows for considerable control over delivery of the data. Data are contained in a logical location in a single folder. In addition, data are displayed visually with its geographic location on a map of Australia and can be explored with standard map navigation tools such as 'pan' and 'zoom', which most users are familiar with. The OpenLayers protocol also allows for the customisation of popup windows with standard HTML coding, allowing the data manager to provide the user with information relating to the data, as well as dynamic links to the data and other resources (Figure 3.5).

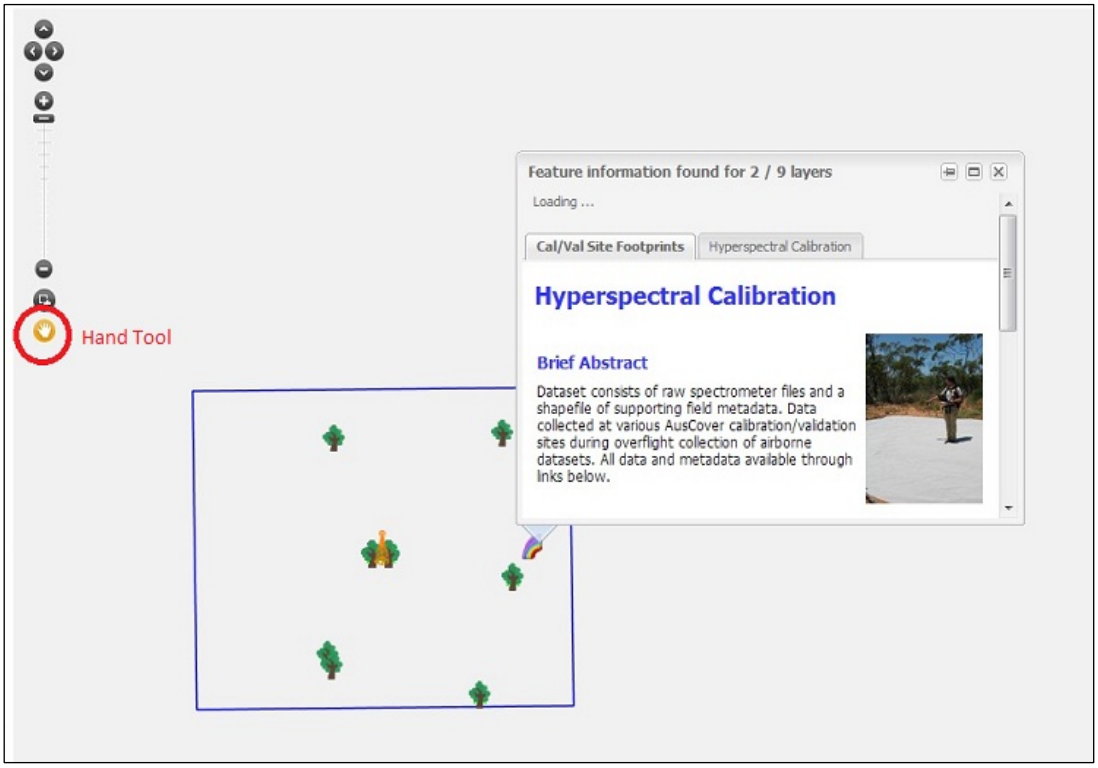

Figure 3. 5 Pop up window displaying information and links for Landscapes data sets.

3.7.3 Managing delivery of large datasets

Some data sets derived from instruments can be extremely large. This can cause difficulties for users retrieving the data, particularly via web based delivery mechanisms. At Landscapes, this posed particular difficulties delivering the airborne hyperspectral and lidar data sets via the THREDDS server, which only allows for single file download. As a consequence, due to the size of the data sets and limitations some users had with download capacity, to deliver data via this mechanism required the division of the data sets into numerous smaller zipfiles, which users downloaded separately and then pieced back together. This proved unworkable and numerous requests for delivery of the data via media prompted the introduction of an anonymous FTP server to facilitate easier access to the data.

3.7.4 Licensing and privacy

Data for public delivery and use will need an explicit licencing arrangement. For Landscapes all field and airborne data sets are released under a creative commons licence. This licencing has baseline user rights and restrictions (Creative Commons Australia, 2013), but typically allow material to be copied, distributed and reused for non-commercial purposes provided the original material is credited appropriately.

Consideration also needs to be given to whether it is legally allowable to make data publicly available. If field data was collected on private land, then explicit permission from the landholder will need to be obtained if providing that data to others. Many landholders are willing to have field data collected and used for research purposes, but may not wish details about their property made publicly available. Alternatively, they may be willing to have some information released but not all (for example quantitative data but not imagery). Data collected on public land does not typically have these restrictions.

3.7.5 Metadata

Various metadata standards exist and one should be adopted when creating descriptive metadata records. Adopting an existing metadata standard will facilitate the discovery and use of the data set.

Given the increasingly open nature of data, enabling easy referencing is becoming essential. The digital object identifier (DOI) is a digital identifier of an object which is defined under the ISO standard 26324. A DOI name is permanently assigned to an object, providing persistent network link to current information about that object. While information about an object can change over time, its DOI name will not change (International DOI Foundation, 2013). As a result, DOI's are ideal for identifying dynamic data sets which change over time, such as field data, and facilitating their referencing, in a similar way literature may be referenced.

3.7.6 Documentation

Any data management system should provide adequate documentation providing information on the use of the system. This is even more important when a system has been designed for public delivery. Documentation needs to be made as clear and user friendly as possible. At Landscapes, documentation on accessing the data, design of the system and filenaming conventions is made publically available via the Landscapes XWiki (http://data.auscover.org.au/xwiki/bin/view/Field+Sites/WebHome). Of particular note are the tutorials on accessing the data via the Landscapes spatial portal and FTP access for larger datasets. Without these tutorials, many users would require direct instruction, which is simply not feasible over the longer term.

3.8 Conclusion

Field data management is complicated by the inherent features of both the data and the collection method. But, regardless of the dataset, the issues encountered in the field data management process are surprisingly similar, with the same mistakes being repeated across unrelated projects. As a result, it is possible to provide some general management guidelines for all field data collection programs.

Field data management can be considered conceptually as a cycle consisting of four distinct stages: planning, collection, collation/storage and delivery. Each stage of the cycle depends on the stage before and so any problems associated with one stage will be exacerbated in the subsequent stages. For example, recording method and tools may be poorly considered prior to the commencement of a field campaign. As a consequence, due to a lack of quality collection protocols and tools, the data collected in the field may be poorly recorded, missing essential details or may deviate from the intended purpose of the collection. If inadequate data management systems exist then it may be too difficult to collate the data into a deliverable form. The data then sits getting 'dusty' and over time becomes unusable. Alternatively, consideration of the issues encountered at each stage of the cycle and how these will be managed should, hopefully, go some way towards resolving the reoccurring issues that arise in field data management.

References

Australian Data Service, 2012, Australian Data Service, viewed 28 February 2013, < http://www.ands.org.au/cite-data>.

Creative Commons Australia, About the Licences, viewed 28 February 2013, <http://creativecommons.org.au/learn-more/licences/>

DataOne, Best Practices, viewed 28 February 2013, <http://www.dataone.org/best-practices/>. International DOI Foundation, 2013, The DOI System, viewed 1 March 2013, <http://www.doi.org>.

Muir, J, Schmidt, M, Tindall, D, Trevithick, R, Scarth, P & Stewart, JB, 2011, Field Measurement of fractional ground cover: a technical handbook supporting ground cover monitoring for Australia, prepared by the Queensland Department of Environment and Resource Management for the Australian Bureau of Agricultural and Resource Economics and Sciences, Canberra, November.

Open Data Kit, 2013, University of Washington, viewed 28 February 2013, <http://opendatakit.org/>

Trevithick, R., Muir, J. & Denham, R, 2012, The effect of observer experience levels on the variability of fractional ground cover reference data. Proceeding of the 16th Annual ARSPC, Melbourne, Australia, August 31 - September 4th 2012.

Chapter 4. Calibration of optical satellite and airborne sensors

T. Malthus *[1], F. Li [2]

[1] Coastal Monitoring, Modelling and Informatics Group, Coastal Management and Development Program CSIRO Oceans and Atmosphere
[2] National Earth and Marine Observations Branch, Geoscience Australia

*Corresponding author:
Tim.Malthus@csiro.au

Abstract

Calibration plays a fundamental part in the acquisition and processing of all data for Earth Observation and remote sensing applications and is critical in the maintenance of the scientific value of the earth observation (EO) biophysical and geophysical data archives that are accumulating. Calibration is the process of quantitatively defining the responses of the optical system to known, controlled signal inputs and encompasses radiometric, wavelength and geometric (spatial) components. Atmospheric correction plays a fundamental role in this process and is a necessary process to reduce or remove the effects of atmospheric scattering and absorption, for target and terrain induced effects (surface bidirectional reflectance distribution function effects and topographic effects) and for the removal of sun and sky glint and air-water interface effects in imagery obtained over water.

This chapter introduces the key components in the calibration of optical remote sensing data. The intention is not to provide a practical outline of the steps to undertake calibration but to provide an overview of the concepts involved in calibration of optical data.

Key Points

- Calibration of EO data is essential if we are to reliably attribute measured spectral responses to accurate material detection or to attribute changes observed in EO-derived data over time to real environmental changes occurring at surface level.
- Calibration allows the conversion of raw electrical outputs from sensors to reliable physical-based units of radiance by determining the transfer functions and coefficients necessary to convert a sensor reading (raw data) to radiance at the top of the atmosphere (for satellite sensors).
- Calibration is applied in three ways: pre-launch calibration, in-orbit continuous calibration, and vicarious calibration.
- Vicarious calibration makes use of natural or artificial sites on the surface of the Earth for post-calibration of airborne or spaceborne sensors. Australian vicarious calibration sites include those at Lake LeFroy and the Lucinda Jetty Coastal Observatory. Artificial targets can be used for higher spatial resolution sensors including those flown from aircraft.
- “Traceability”, the process of ensuring measurements are related through an unbroken chain of comparisons to standards held by National Metrology Institutes, is critical to allowing true intercomparability between different sensors and product data sets.
- Atmospheric correction is a fundamental technique to obtain consistent and comparable measurements of surface reflectance by reducing or removing atmospheric influences, and surface bidirectional reflectance distribution function (BRDF) and terrain effects.

4.1 Introduction

The intention of the TERN Landscape Assessment facility is to provide free seamless and freely available access to earth observation derived spatio-temporal data sets related to land cover and land surface properties at national scale, to support ecosystem and earth system science research communities to do high value ecosystem research (the Integrated Marine Observing System has similar aims for the aquatic domain). To have confidence in the use of the information products delivered by Landscapes the original satellite data must be well calibrated and the products derived from it well validated. In combination, calibration and validation Cal/Val can be regarded as a process that encompasses the entire remote sensing system, from sensor to data product. Thus, both calibration and validation make key contributions to Landscapes, as they

are critical in ensuring the maintenance of the scientific value of the EO data archives (Malthus *et al*., 2010). More broadly, Earth Observing missions are important to a number of Australian Government programs (climate, hydrology, agriculture, forestry, mineral mapping, oceans and coasts etc.) and there is thus a need to ensure that earth observation data are accurately calibrated and validated to provide reliable information (AAS 2009).

Validation is covered elsewhere in this handbook (Section 4). This chapter outlines the key concepts and guidelines for calibrating mainly satellite sensor data. It is intended to outline the key concepts involved in rather than to provide a practical outline of the steps to undertake calibration. The chapter draws heavily on calibration approaches applied to the MODIS and Landsat sensors but which are typical of the approaches adopted for many other sensors. We also principally focus on calibration in a terrestrial context (as opposed to an aquatic one).

4.2 What is calibration?

The objective of calibration (and validation) Cal/Val is to develop a quantitative understanding and characterisation of the measurement system and its biases in both space and time (National Research Council, 2007). The definitions of all the common terms used here for Cal/Val are taken from the Committee of Earth Observation Satellites (CEOS, http://www.ceos.org) as follows:

1. Calibration - The process of quantitatively defining the responses of a system to known, controlled signal inputs;
2. Traceability - A property of a measurement result relating the result to a stated metrological reference through an unbroken chain of calibrations of a measuring system or comparisons, each contributing to the stated measurement uncertainty;
3. Uncertainty - A parameter that characterises the dispersion of the quantity values that are being attributed to a measured mean, based on the information used;
4. Vicarious Calibration - Vicarious calibration refers to techniques that make use of natural or artificial sites on the surface of the Earth for post (launch or flight) calibration of airborne or space-borne sensors.
5. Validation - The process of assessing, by independent means, the quality of the data products derived from the system outputs;

Radiometrically, satellite data are often provided in digital number (DN) values, but for most quantitative applications, we need DN conversion to radiometric information as an input to extract reflectance, emissivity or intensity values (in the case of optical, thermal and radar data, respectively). Accurate transfer of uncertainty from one processing stage to another is crucial. *Radiometric calibration* refers to the process of extracting physical units from the original raw spectroscopic data and assigning the channels in the sensors to a meaningful wavelength.

In essence, *geometric calibration* is the determination of the geometric, or spatial, characteristics of a sensor's imaging capabilities. Any acquired image must be an accurate representation of the 2- and 3-dimensional properties of the surface of the earth it has imaged. Corrections in spatial properties are required to account for the Earth's curvature, distortions induced by the sensor's optics and imaging system and distortions induced by the satellite platform itself (e.g. vibration, distortions in altitude). Typically, a geometric calibration is possible by means of ground control points and overlapping scenes using natural or artificial test targets on the ground surface.

4.3 Why is calibration important?

As many of the biophysical and geophysical products that we derive from EO data are preferably quantitative in nature, we need to know that the raw data from which they are derived are accurate (this holds for qualitative data as well). Calibration of EO data is essential if we are to reliably attribute measured spectral responses to accurate material detection or to attribute changes observed in EO derived data over time to real environmental changes occurring at surface level. Without proper/accurate calibration, we are unable to rule out the influence of other factors, such as instrument error or influences of the atmosphere. Accurate calibration is thus critical if we are to i) compile reliable long-term data sets for studying the effects of climate change and the fluxes of carbon and other substances to and from the oceans and land, ii) detect material objects iii) detect changes in EO data over time, iv) attribute those changes to key influences such as climate change and climate variability, and v) quantify and reduce the uncertainty in models which ingest EO and EO derived data to make accurate predictions.

Calibration is especially important when a variety of sensors and sensor datasets are used to derive bio-physical products over Australia, often to compile key time series of data encompassing different sensor generations and different sensor types. For example, long-term vegetation and related eco-hydrological products for Australia are derived from AVHRR and MODIS datasets, respectively, consisting of data from different sensors (e.g. Donohue *et al*. 2008; 2010). Furthermore, instruments may change on launch and may degrade in orbit (in radiometric, geometric and spectral characteristics). Calibration allows the traceability of sensor data to the same physical standards and hence is routinely required as sensors decay throughout their lifetime.

In summary, we need to have confidence in the reliability of data delivered by EO sensors; calibration is thus essential if we want to reliably extract information from measured radiance, to compare information acquired from different regions and different times, to compare and analyse observations with ground-based observations and incorporate satellite data into physically-based computer models.

4.4 Radiometric calibration

Calibration translates electrical output of voltages converted to counts or DN to reliable physical-based units of radiance by determining the transfer functions and coefficients necessary to convert a sensor reading (raw data) to radiance at the top of the atmosphere (for satellite sensors). The co-efficients are extracted through precise measurements in the laboratory using well-calibrated facilities and national institute of measurement traceable radiometric standards. There are a number of steps ensuring a thorough calibration approach. Radiometric and spectral responses also must be accurately monitored through the lifetime of a sensor to monitor changes in response, as it ages over time (e.g. Xiong *et a*l. 2009a).

In the case of most optical spaceborne earth observing sensors, both prelaunch and post (on-orbit) launch radiometric calibrations are undertaken (Figure 4.1). These are briefly discussed in the following sections.

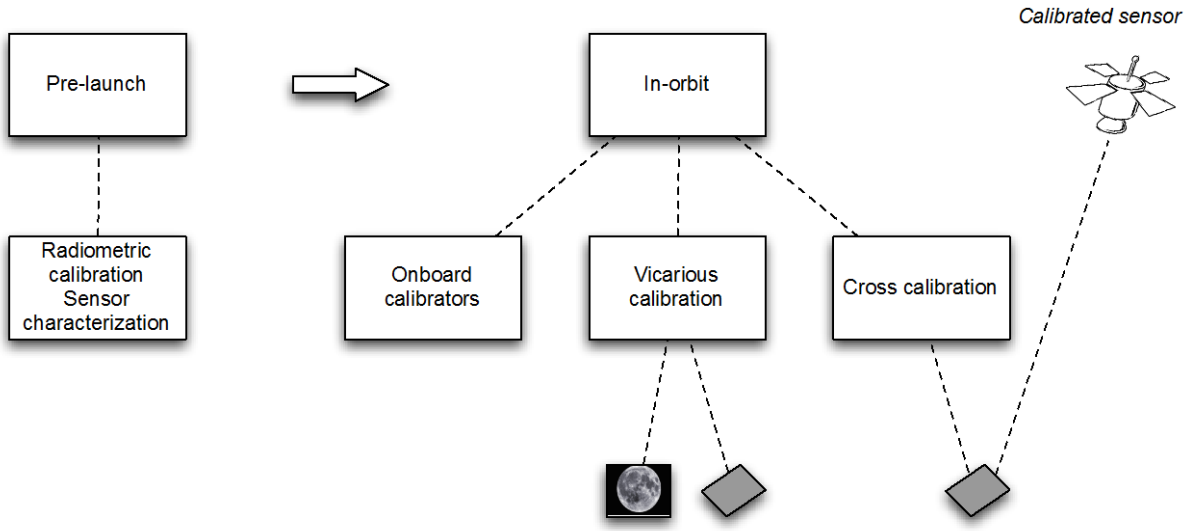

Figure 4.1 The different stages to calibration of satellite sensors.

4.4.1 Pre-launch calibration

Absolute radiometric calibration determines the relationship between sensor signals and radiance for all spectral channels. Often this involves mounting the sensor on or in a calibrated integrating sphere whose ideal spectral (ir)radiance output is homogeneous and large enough to illuminate all elements in a sensor array with the same radiance (e.g. Figure 4.2). Varying the output of the integrating sphere also allows for the study of the linearity between sensor response and radiance and the assessment of the signal to noise performance at radiance levels similar to those encountered when sensing the Earth's surface from space or airborne platforms (e.g. Ponzoni and Albuquerque 2008, Gege *et al*., 2009).

Spectral calibration is also typically undertaken and uses a monochromator or tunable laser to produce a collimated narrow beam of light that is blocked by transmission filters and is thus tuneable to different wavelengths. Measurements undertaken here allow for the determination of a range of parameters used to characterise the spectral performance of an optical sensors; these include spectral response function, centre wavelength, spectral smile, spectral sampling distance, the spectral range of pixels, and spectral resolution (e.g. Barnes *et al*. 1998, Xiong and Barnes 2006, Helder *et al*. 2012).

Figure 4.2 An integrating sphere being used to radiometrically calibrate a field spectroradiometer.

4.4.2 In-Orbit Calibration

This involves the use of in-built calibration sources and vicarious calibration or cross-calibration to other satellite sensors. The critical issue at this stage is to be able to monitor changes in sensor performance over time (Pearlman *et al*., 2003). For example, MODIS, an important sensor system for environmental monitoring first launched on the TERRA platform in 1999 and next on the AQUA platform in 2001, relies on a suite of on-board calibrators for the reflective solar bands, consisting of a solar diffuser (with a well known reflectance distribution factor) with an accompanying stability monitor and a Spectroradiometric Calibration Assembly (SRCA) which is for instrument spatial and spectral characterisation (Xiong *et al*. 2006). On each scan of the earth the sensor views the on-board calibrators. The solar diffuser calibration for the reflective solar bands is performed on a bi-weekly schedule. A Solar Diffuser Stability Monitor (SDSM) tracks the degradation in the solar diffuser itself, which is primarily caused by repeated solar exposure (Xiong and Barnes 2006). The moon and other opportunistic Earth surface targets are also used to monitor sensor performance over time (Xiong 2004, Sun *et al*. 2007).

The Landsat Data Continuity Mission (LDCM, now known and referred to here as Landsat 8), launched in February 2013, incorporates a solar view baffle and "working" diffuser panel that reflects solar illumination into the sensor. An additional "pristine" panel is used to detect changes in the working panel. Two additional lamp assemblies each consisting of six lamps inside an integrating hemisphere, are used to illuminate the full focal plane of the sensor when the shutter is closed. Instrument calibration throughout the operational life of the mission involves observation of these on-board calibration sources (observed once per week) augmented by ground based measurements. Observation of the solar diffuser requires a Landsat 8 spacecraft manoeuvre to point the solar-view baffle directly at the sun when the spacecraft is in the vicinity of the northern solar terminus (Irons et al. 2012).

4.4.3 Vicarious Calibration

Vicarious calibration refers to techniques that make use of natural or artificial sites on the surface of the Earth for post calibration of airborne or spaceborne sensors. It is used as an in-flight/in-orbit check on sensor performance (e.g. Teillet *et al*. 2001, deVries *et al*. 2007). The principle is that the relatively stable radiance from "as homogeneous as possible" earth or lunar surface (so-called "pseudo-invariant" surface) is used to estimate top-of-atmosphere radiance at the entrance aperture of a given satellite instrument to monitor performance over time and, if necessary, to update the nominal, pre-launch instrument calibration. Vicarious calibration, therefore, provides an indirect means of quality assurance of remotely sensed data and sensor performance that is independent of direct calibration methods (use of on-board radiance sources or panels). This is important as on-board illumination sources may themselves degrade over time. This has led to the establishment of a number of sites around the world on relatively large homogeneous surfaces such as salt lakes, dry lakebeds, desert sands, river deltas and ice sheets (Teillet *et al*. 2007). For oceans, the South Pacific Gyre is often used as it has the lowest concentrations and variability of optical constituents known. For higher resolution sensors artificial targets (e.g. tarps, panels and nets) have also been used (Brook and Ben-Dor, 2011).

4.4.4 The moon as a vicarious calibration target

The moon is a very stable, albeit spatially variable, reference luminous source that has been used for in-orbit vicarious calibration for a number of space-borne satellite sensors (Stone 2008). This stability makes predicting

its reflectance with illumination and viewing geometry straightforward, hence its utility for both spatial and radiometric calibration (Kieffer *et al*., 2003). Both MODIS instruments perform monthly lunar observations (e.g. Xiong 2004, Sun et al. 2007). The Operational Land Imager (OLI) sensor on Landsat 8 also views the lunar surface at monthly intervals near its full phase during the dark portion of the Landsat 8 orbit (Irons et al. 2012).

4.4.5 Earth surface vicarious calibration targets

On the earth's surface, vicarious calibration sites or targets must be well characterised, and ideally, reflected radiance should be measured at the ground surface using calibrated spectroradiometers simultaneously with sensor overflight. Key characteristics of such sites for high reflecting targets includes (Teillet *et al*. 2007):

- High spatial uniformity, relative to the pixel size;
- Surface reflectance greater than 0.3 to provide high signal-to-noise and reduce uncertainties due to the atmospheric path radiance;
- Flat, spectrally uniform reflectance properties;
- Temporally invariant surface properties (reflectance, BRDF, spectral);
- Horizontal flat surface of near Lambertian reflectance;
- Located at high altitude (to minimize aerosol loading), far from the ocean (to minimize atmospheric water vapour) and far from influence of other anthropogenic aerosols);
- Located in an arid region to minimize cloudy weather and precipitation that could change surface reflectance properties;

Australia is suited for vicarious calibration based on its geographical possession of a number of large, relatively stable, natural targets and location to provide vicarious calibration services to international satellite providers, particularly by being able to provide low latitude cloud free measurements calibration services during the northern hemisphere winter. Several well-known sites in Australia have been used, such as the (often) dry salt lakes Lake Frome and Lake Lefroy, and the aquatic targets of Lake Argyle and Bass Strait (Figure 4.3). For aquatic satellite sensors such as MODIS and MERIS significant research cruise campaigns have taken place in various locations around the Australian coast.

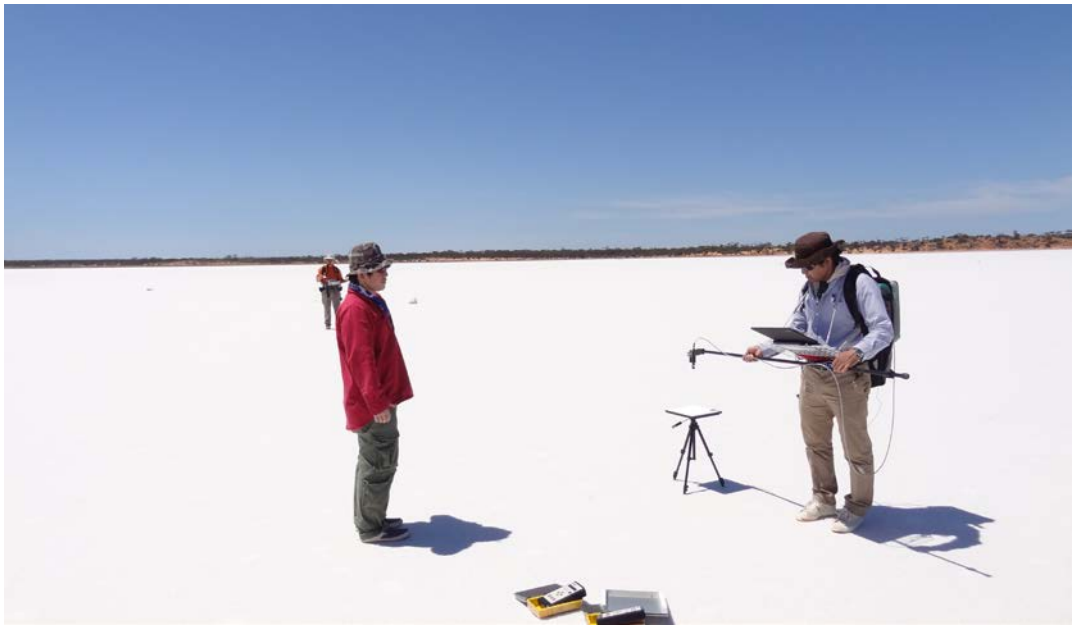

Figure 4.3
Spectral measurement campaign on Lake Lefroy, Western Australia as part of preparations for vicarious calibration of the forthcoming Hyperspectral Imager Suite (HISUI) hyperspectral sensor.

Internationally, increasingly sophisticated ground based instrumentation is being used to provide autonomous and near-continuous measurement of the characteristics at many calibration sites. In Australia, the Lucinda Jetty Coastal Observatory installation is providing the first autonomously monitored calibration data in Australia for ocean colour and coastal monitoring sensors (Brando *et al*., 2010). The dry salt Lake Lefroy in Western Australia has some autonomous and continual monitoring instruments measuring optical properties of the atmosphere and provides quantification and physical-optical characterisation of the aerosols using a CIMEL318 suntracking photometer and a weather station (Figure 4.4; Malthus *et al*. 2010).

Figure 4.4 The Cimel 318 suntracking photometer located on Beta Island at the Lake Lefroy vicarious calibration site.

To correct or validate the satellite data using vicarious calibration data involves either top-down (correction of ‘‘top-of-atmosphere” sensor data to ground-leaving reflectance using an atmospheric correction model) or bottom-up (correction of ground target reflectance to top-of-atmosphere radiance using a radiative transfer model taking into account atmospheric transmission and absorption, e.g., MODerate resolution atmospheric TRANsmission, MODTRAN). Increasingly, a combination of measurements obtained at varying scales and resolutions (e.g., in situ, airborne, and satellite) are being used to provide the basis for assessment of the on-orbit radiometric and spectral calibration characteristics of spaceborne optical sensors (Teillet *et al*. 2001, Green *et al*. 2003). “Cross-calibration” can also be employed where the well-known radiometric calibration of one satellite sensor can be transferred to another poorly calibrated sensor via near-simultaneous imaging of a common ground target (Figure 4.1; Teillet *et al*., 1990, Xiong *et al*., 2009b).

De Vries *et al*. (2007) used a vicarious calibration approach using high-reflectance, pseudo-invariant targets in western Queensland to evaluate the radiometric calibration of the Multispectral Scanner (MSS), Thematic Mapper (TM) and Enhanced Thematic Mapper+ (ETM+) sensors on Landsats 2, 5 and 7, respectively. The results confirmed the stability and accuracy of the ETM+ calibration, and the suitability of these data as a radiometric standard for cross-calibration of TM, although alternate models for some TM spectral bands were required. Updated calibration coefficients for MSS were presented using cross-calibration to the TM and ETM+ sensors. This work was further updated by Helder *et al*. (2012).

For Landsat 8, global vicarious calibration data will be used to radiometrically calibrate the OLI sensor at irregular intervals (Irons *et al*. 2012). In situ measurements of surface reflectance and atmospheric conditions will be made over terrestrial sites simultaneous to Landsat 8 over passes and used to validate OLI radiometric calibration.

The generally smaller pixel sizes of high spatial resolution satellite sensors and airborne imagery compared to daily overpass low spatial and high temporal image satellite resolutions such as MODIS, along with targeted

deployment, means that artificial vicarious calibration targets such as tarps and panels can be used (Karpouzli and Malthus 2003). In the case of airborne data, temporary targets can be rapidly deployed in advance of specific campaigns. Such targets can also help overcome the difficulties of finding sufficient natural homogeneous targets of varying brightness. Supervised vicarious calibration (SVC) (Brook and Ben-Dor, 2011) uses artificial agricultural black polyethylene nets of various densities as calibration targets, set up along the aircraft's trajectory. The different density nets, when combined with other natural bright targets, can provide full coverage of a sensor's radiometric dynamic range. The key to the successful use of any form of vicarious calibration target is the use of simultaneous field-based measurement of their reflectance properties and positions and associated data such as atmospheric condition collected with sunphotometers and weather stations; uncertainties are reduced if a number of calibration targets of varying brightness are used, a large number (30+) of reflectance measurements are made of each target, and their positions are accurately located (Secker *et al.*, 2001). It is recommended that Australia invests in permanent sites for high spatial resolution calibration, as the flood of high spatial resolution sensors will require efficient and effective sites that are permanent. An example of the use of artificial calibration vicarious calibration targets is shown in Figure 4.5.

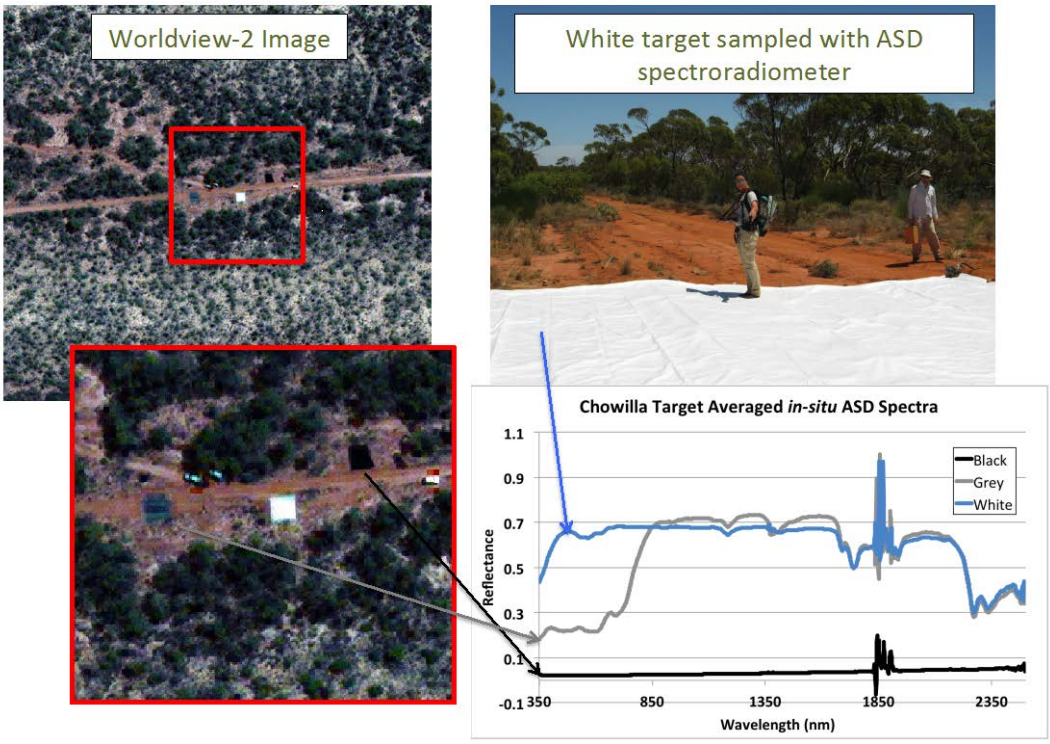

Figure 4.5 The use of white, black and grey artificial calibration targets for in-field calibration during a Landscapes campaign near Chowilla. (adapted from figure compiled by Kasper Johansen, University of Queensland).

4.4.6 Traceability

In all calibration efforts, traceability, the process of ensuring measurements are related through an unbroken chain of comparisons to standards held by National Metrology Institutes (e.g., US National Institute of Standard and Technology, NIST), is the key to allowing true intercomparability between different sensors' raw and product data sets (Fox, 2004). The "end-to-end" calibration chain is implemented via the use of ''transfer standards'' that allow traceability back to the official ''primary'' radiometric standards using internationally agreed-upon systems of units (SI) and rigorous measurement and test protocols. Integral to the establishment

of traceability is the quantification and documentation of associated uncertainties throughout the measurement chain; the fewer the number of steps in the chain, the lower the uncertainty. The advantages of maintaining traceability include a common reference base and quantitative measures of assessing the agreement of results for different sensors or measurements at different times. However, current traceability guidelines lack guidance on temporal overlap or interval length for the measurements in the unbroken chain of comparisons (Johnson *et al*. 2004).

4.5 Atmospheric correction, BRDF correction and terrain illumination correction

Radiance measured by the sensors of optical satellites from the surface includes Rayleigh and aerosol scattering, gas absorptions of the atmosphere, surface BRDF effects over the anisotropic surfaces and topographic (terrain illumination) effects for the sloping surfaces due to terrain shadows. To obtain consistent and comparable measurements of surface reflectance that characterises the surface properties from remotely sensed observations, it is necessary to process the data to reduce or remove these effects. The retrieved surface reflectance can then be used to measure land surface change through a time series. The corrections include (i) atmospheric correction for directional Rayleigh and aerosol scattering and gas absorption; (ii) surface BRDF correction to minimise the angular effects it creates and to normalize the data to nadir view and standard sun angle; (iii) terrain illumination correction to remove the terrain shading effect. In images taken over water it is important to correct for aquatic sun and sky glint caused by the water-surface refractive index and wave state.

Recently, it has become more common for these corrections to be made operationally and incorporated into standard products. This section describes the basic operational products.

Using a physics-based coupled BRDF- atmospheric correction model (e.g., Li *et al*., 2012) the three corrections can be done together as long as atmospheric, BRDF and terrain parameters are available. The following paragraphs will discuss how to obtain these parameters.

Atmospheric correction is the process to retrieve surface reflectance by removing the atmospheric effect, mainly Mie, Rayleigh and particle (aerosol) scattering and atmospheric gas (ozone, water vapour, CO_2, etc.) absorption which change with sensor view angle. There is a long history of development of atmospheric correction. With the efforts of scientists and the development of high performance computer techniques, using physics-based models to conduct atmospheric correction has become feasible and the method for visible, near and shortwave infrared wavelengths is also mature. The accessible radiative transfer models used for operational atmospheric correction range from complicated, such as the flexible MODTRAN model (Berk, et al., 1998), with spin off products such as Atmospheric CORrection Now (ACORN) and Fast Line-of-sight Atmospheric Analysis of Spectral Hypercubes (FLAASH), to simplify such as the **S**econd **S**imulation of a **S**atellite **S**ignal in the **S**olar **S**pectrum (6S) model (Vermote, *et al*., 1997a). As long as good atmospheric input data (aerosol optical depth, water vapour, ozone and CO_2 etc.) are available, MODTRAN/or 6S radiative transfer models can provide good estimates of atmospheric parameters, e.g., transmittance for sun and sensor directions, path radiance, atmospheric albedo, the ratio of diffuse to total irradiance for both sun and sensor directions. These parameters can be used for coupled atmospheric and BRDF correction model to obtain surface reflectance. Examples of these are found in the reports by the MODIS group (Vermote, *et al*., 1997b) and for Landsat correction in reports by Li *et al*. (2010), Shepherd and Dymond (2003) and Flood *et al*. (2013).

Surface BRDF minimisation is an important step to correct view and illumination angle effects and to normalise surface reflectance both in one image and between images. Due to different view and solar angles and anisotropic surfaces, observed surface reflectance is different even if the surface cover is the same. It happens for a single scene with different view and solar angles and different scenes sensed at different

seasons and geographical regions due to the solar angle variation. For BRDF correction, the most important input is the BRDF parameters; if these parameters are known, BRDF corrected surface reflectance can be retrieved using a coupled BRDF-atmosphere model. However, due to the limited availability of BRDF parameters, the correction methodology is different for different resolution imagery. For low spatial resolution data, e.g., MODIS, because of its frequent revisit (twice a day for combined Aqua and TERRA), the BRDF parameters can be obtained from the data itself (Schaaf *et al*., 2002). However, for moderate or high-resolution data, BRDF parameters have to be obtained through other data sources, e.g. from MODIS data (Li *et al*. 2010, 2012) and satellite pass overlap data (Flood *et al*., 2013).

Terrain illumination correction is an additional correction applied to inclined surfaces in areas with elevated terrain. When the surfaces are inclined, the irradiance received by optical satellite sensors is modified such that slopes facing toward the sun receive more solar irradiance and appear brighter in satellite images than those facing away from the sun. Steep terrain affects optical satellite images through both irradiance and BRDF effects; these create terrain shade. For terrain illumination correction, good Digital Surface Model (DSM) data are necessary to ensure accurate terrain parameter calculation, e.g., slope and aspect angles, incident and exiting angle as well as their relative azimuth angles, cast shadow etc. The DSM and satellite data themselves need to be very accurately georeferenced otherwise errors will be compounded. In the past, most terrain correction has been conducted using empirical models (e.g., Teillet, *et al*., 1982; Green and Craig, 1985). They are typically applied separately from atmospheric and BRDF. However, it is not convenient, especially for operational purposes. Li *et al*. (2012) proposed a physics-based model that can be applied for both flat and inclined surfaces. The model combines atmospheric correction, BRDF and terrain illumination as one. Some other models such as Atmospheric *and Topographic* Correction (ATCOR), used for the correction of airborne remote sensing data, will also do the terrain and atmospheric corrections simultaneously (e.g. Richter and Schlapfer 2002).

With atmospheric correction validation is equally as important for assessing, by independent means, the quality of the corrections applied to the satellite data. If these corrections are being carried out operationally, internal checks of product quality and consistency are a vital part of the process. Consistency is an important part of operational products. Beyond such basic checks, a goal of the products is for areas where there is no change in the land cover to have a similar optical signature over time. Thus, as with sensor calibration, vicarious calibration sites may typically be used as a check on atmospheric correction performance.

4.6 Previous Australian activity in optical sensor calibration

The often dry, clear atmospheres in Australia confer advantages for performing 'local' calibration of space instruments. The presences of several large 'natural' calibration targets (e.g. salt lakes, dunes and beaches, dense permanently vegetated forests, deep dark lakes and coastal waters) have been seen as a benefit by the international space community. Australia has benefited from these in being involved in previous calibration campaigns; this experience has been valuable in developing capability, has allowed Australian scientists to join international Earth Observation science teams at high levels and has provided early access to important satellite data streams.

A significant example of Australian involvement in international calibration activities is the activities which evaluated the performance of instruments carried on the NASA Earth Observing-1 (EO-1) platform (http://eo1.gsfc.nasa.gov), most notably the Hyperion hyperspectral sensor (Ungar *et al*. 2003, Pearlman *et al*. 2003). The Australian Cal/Val effort, involving 23 scientists, provided a key contribution to the overall scientific evaluation and validation of the sensor (Jupp and Datt 2004).

As outlined in the chapter, Australia has further invested in calibration infrastructure through the funding provided by national research infrastructure initiatives, most notably the Terrestrial Environmental Research Network (TERN), the Integrated Marine Observing System (IMOS) and AuScope (an organisation for a national earth science infrastructure program). In addition to Hyperion, satellite Cal/Val efforts have been focused on sensors including POLDER, AVHRR, MODIS, SeaWiFS, GLI, MERIS, AATSR and ADEOS-II. In all, some 17 Australian sites have been offered as primary task field sites to the international community, but the information is mixed across different international Cal/Val websites serving to reflect the ad hoc and fragmented approach that is being taken to the issue in Australia. Use of these sites has generally been as and when opportunities have arisen with specifically mounted calibration campaigns mobilised. No sites have autonomous and continual monitoring implemented. The recent (2011) formation of the Australian Satellite Calibration Working Group (ASCWG) is an attempt to better coordinate calibration and validation efforts.

4.7 Conclusion

Optical earth observation data calibration (and validation) is an essential scientific and technological activity that should be a continuous component in any earth observation program, providing an independent check on the performance of space- and airborne-based sensors and associated processing algorithms. There is a strong need for EO data to be calibrated and validated against high quality surface-based measurements following specific internationally agreed scientific criteria. Successful implementation of such activity needs careful planning of issues such as coordination of activities, selection and establishment of networks of sites, the development and deployment of instrumentation to support measurement campaigns and the adoption of common measurement and data distribution protocols. Through the benefit of geography, Australia is well poised to make a systematic contribution to the calibration of a range of international satellite missions, as long as efforts are well supported and coordinated. A network of super and ancillary vicarious calibration sites for the Australian continent could be developed to enhance this contribution.

To ensure intercomparability of measurements obtained over different sites, the instrumentation used (e.g. spectroradiometers and sunphotometers) will need to be 'fit for purpose' and properly calibrated. To this end, instrument calibration facilities are being developed at CSIRO locations in Perth and Canberra. Attention will also need to be given to the development of 'best practice' field measurement methods and of protocols for instrument quality assurance, maintenance and calibration. Such approaches can follow internationally agreed criteria (CEOS WGCV).

Use of these sites has generally been as and when opportunities have arisen with specifically mounted calibration campaigns mobilised. To date, a fragmented and uncoordinated approach to vicarious calibration in Australia has been taken. There is significant global benefit to Australia to better coordinate its approach to sensor calibration and to be in a position to offer calibration services to other satellite launching nations, not least to secure access to satellite data and to secure involvement in the planning of future missions.

In summary, successful implementation of calibration and validation of EO sensors for Australia will require coordination of activities, selection and establishment of networks of sites, the development and deployment of instrumentation to support measurement campaigns, development of laboratory calibration infrastructures, and the adoption of common measurement and data distribution protocols. There is significant benefit to Australia internationally to better coordinate its approach to sensor calibration and to be in a position to offer calibration services to other satellite launching nations, not least to secure access to satellite data and to secure involvement in the planning of future missions (Malthus 2012).

References

Australian Academy of Science/Australian Academy of Technological Sciences and Engineering (2009). An Australian strategic plan for earth observations from space. Australian Academy of Science 2009. ISBN 085847 267 8. (www.science.org.au/reports/index).

Barnes, W. Pagano, T. S., & Salomonson, V. (1998). Prelaunch characteristics of the Moderate Resolution Imaging Spectroradiometer (MODIS) on EOS-AM1. *IEEE Transactions on Geoscience and Remote Sensing*, 36, 1088-1100.

Berk, A., Bernstein, L. S., Anderson, G. P., Acharya, P. K., Robertson, D. C., Chetwynd, J. H., & Adler-Golden, S. M. (1998). MODTRAN cloud and multiple scattering upgrades with application to AVIRIS. *Remote Sensing of Environment*, 65, 367– 375.

Brando, V., Keen, R., Daniel, P., Baumeister, A., Nethery, M., Baumeister, H., Hawdon, A., Swan, G., Mitchell, R., Campbell, S., Schroeder, T., Park, Y., Edwards, R., Steven, A., Allen, S., Clementson, L., & Dekker, A. (2010). The Lucinda Jetty Coastal Observatory's role in satellite ocean colour calibration and validation for Great Barrier Reef coastal waters. In: *Proceedings of IEEE Oceans 2010*, May 2010. Sydney. (http://ieeexplore.ieee.org/xpl/login.jsp?tp=&arnumber=5603612).

Brook, A., & Ben-Dor, E. (2011). Supervised vicarious calibration (SVC) of hyperspectral remote sensing data. *Remote Sensing of Environment*, 115, 1543 – 1555.

de Vries, C., Danaher, T., Denham, R., Scarth, P., & Phinn, S. (2007). An operational radiometric calibration procedure for the Landsat sensors based on pseudo-invariant target sites. *Remote Sensing of Environment*, 107, 414-429.

Donohue, R.J., McVicar, T.R., Li, L., & Roderick, M.L. (2010). A data resource for analysing dynamics in Australian ecohydrological conditions. *Austral Ecology*, 35, 593–594.

Donohue R. J., Roderick M. L., & McVicar T. R. (2008). Deriving consistent long-term vegetation information from AVHRR reflectance data using a cover-triangle-based framework. *Remote Sensing of Environment*, 112, 2938–49.

Flood, N., Danaher, T., Gill, T., & Gillingham, S. (2013). An operational scheme for deriving standardised surface reflectance from Landsat TM/ETM+ and SPOT HRG imagery for eastern Australia. *Remote Sensing*, 5, 83-109.

Fox, N. (2004). Validated data and removal of bias through traceability to SI. In S.A. Morain, & A.M. Budge (Eds), *Post-launch Calibration of Satellite Sensors*, vol. 2, of ISPRS Book Series (pp.31-42). London: Taylor and Francis. (http://www.crcnetbase.com/doi/abs/10.1201/9780203026830.ch4).

Gege, P., Fries, J., Haschberger, P., Schotz, P., Schwarzer, H., Strobl, P., Suhr, B., Ulbrich, G., & Vreeling, W. (2009). Calibration facility for airborne imaging spectrometers. *ISPRS Journal of Photogrammetry*, 64, 387–397.

Green, A.A., & Craig, M.D. (1985). Analysis of aircraft spectrometer data, with logarithmic residuals. In G. Vane, & A. Goetz (Eds), *Airborne Imaging Spectrometer Data Analysis Workshop* (pp. 111-119). NASA JPL, Pasedena, California.

Green, R.O., Pavri, B.E., & Chrien, T.G. (2003). On-orbit radiometric and spectral calibration characteristics of EO-1 Hyperion derived with an underflight of AVIRIS and in situ measurements at Salar de Arizaro, Argentina. *IEEE Transactions on Geoscience and Remote Sensing*, 41, 1194-1203.

Helder, D.L., Karki, S., Bhatt, R., Micijevic, E., Aaron, D., & Jasinski, B., (2012). Radiometric calibration of the Landsat MSS sensor series. *IEEE Transactions on Geoscience and Remote Sensing*, 50, 2380-2399.

Irons, J.R., Dwyer, J.L., & Barsi, J.A. (2012). The next Landsat satellite: The Landsat Data Continuity Mission. *Remote Sensing of Environment*, 122, 11–21.

Johnson, C., Rice, J., & Brown, S. (2004). The establishment and verification of traceability for remote sensing radiometry, with an eye towards intercomparison of results. CEOS/IVOS Calibration Workshop, ESA/ESTEC, Noordwijk, The Netherlands. (http://earth.esa.int/workshops/ivos05/pres/17_johns.pdf).

Jupp, D.L.B. & Datt, B. (Eds) (2004). Evaluation of Hyperion performance at Australian hyperspectral calibration and validation sites. CSIRO Earth Observation Centre Report. (http://www.eoc.csiro.au/hswww/oz_pi/reports/EO1_report_final_submit.pdf)

Karpouzli, E. & Malthus, T. J. (2003). The empirical line method for the atmospheric correction of IKONOS imagery. *International Journal of Remote Sensing*, 24, 1143-1150.

Kieffer, H., Stone, T., Barnes, R., Bender, S., Eplee, R., Mendenhall, J., & Ong, L. (2003). On–orbit radiometric calibration over time and between spacecraft using the moon. *Proceedings of SPIE*, vol. 4881, pp. 287–298.

Li, F., Jupp, D. L. B., Reddy, S., Lymburner, L., Mueller, N., Tan, P. & Islam, A. (2010). An evaluation of the use of atmospheric and BRDF correction to standardize Landsat data. *IEEE Journal of Selected Topics in Applied Earth Observations and Remote Sensing*, 3, 257-270.

Li, F., Jupp, D.L.B., Thankappan, M., Lymburner, L., Mueller, N., Lewis, A., & Held, A. (2012). A physics-based atmospheric and BRDF correction for Landsat data over mountainous terrain. *Remote Sensing of Environment*, 124, 756-770.

Malthus, T., Brando, V., Jones, S., Held, A., & Dekker, A., (2010). Australian activities in calibration and validation for hyperspectral sensors. *Proceedings of ESA Hyperspectral 2010 Workshop*, Frascati, Italy, 17–19 March 2010 (ESA SP-683, May 2010).

Malthus, T.J., (2012). Frontiers in land surface observation. WIRADA (2012) Water Information Research and Development Alliance: Science Symposium Proceedings, Melbourne, Australia, 1–5 August 2011. CSIRO: Water for a Healthy Country National Research Flagship. pp. 302-314. (https://publications.csiro.au/rpr/download?pid=csiro:EP117659&dsid=DS4)

National Research Council of the National Academies (2007). Earth science and applications from space: national imperatives for the next decade and beyond. Committee on Earth Science and Applications from Space: A Community Assessment and Strategy for the Future. National Research Council, USA.

Pearlman, J.S., Barry, P.S., Segal, C.C., Shepanski, J., Beiso, D., & Carman, S.L. (2003). Hyperion, a space-based imaging spectrometer. *IEEE Transactions in Geosciences and Remote Sensing*, 41, 1160 -1173.

Ponzoni, F.J., Albuquerque, B.F.C. (2008). Pre-launch absolute calibration of CCD/CBERS-2B Sensor. *Sensors*, 8, 6557-6565.

Richter, R., & Schläpfer, D. (2002). Geo-atmospheric processing of airborne imaging spectrometry data. Part 2: Atmospheric/topo-graphic correction. *International Journal of Remote Sensing*, 23, 2631-2649.

Schaaf, C. B., Gao, F., Strahler, A.H., Lucht, W., Li, X., Tsang, T., Strugnell, N.C., Zhang, X., Jin, Y., Muller, J. – P., Lewis, P., Barnsley, M., Hobson, P., Disney, M., Roberts, G., Dunderdale, M., Doll, C., d'Entremont, R.P., Hu, B., Liang, S., Privette, J.L., & Roy, D. (2002). First operational BRDF, albedo and nadir reflectance products from MODIS. *Remote Sensing of Environment*, 83, 135-148.

Secker, J., Staenz, K., Gauthier, R., & Budkewitsch, P. (2001). Vicarious calibration of airborne hyperspectral sensors in operational environments. *Remote Sensing of Environment*, 76, 81–92.

Shepherd, J.D., & Dymond, J.R. (2003). Correcting satellite imagery for the variance of reflectance and illumination with topography. *International Journal of Remote Sensing*, 24, 3503-314.

Stone, T.C. (2008). Radiometric calibration stability and inter-calibration of solar-band instruments in orbit using the moon. In J. J. Butler, & J. Xiong (Eds), *Proceedings of SPIE*, vol. 7081, Earth Observing Systems XIII, 70810X.

Sun, J., Xiong, X., Barnes, W.L., & Guenther, B. (2007). MODIS reflective solar bands on-orbit lunar calibration. *IEEE Transactions on Geoscience Remote Sensing*, 45, 2383-2393.

Teillet, P.M, Guindon, B., & Goodenough, D.G (1982). On the slope-aspect correction of multispectral scanner data. *Canadian Journal of Remote Sensing*, 8, 84-106.

Teillet, P.M., Slater, P.N., Ding, Y., Santer, R.P., Jackson, R.D., & Moran, M.S. (1990). Three methods for the absolute calibration of the NOAA AVHRR sensors in-flight. *Remote Sensing of Environment*, 31, 105–120.

Teillet, P.M., Fedosejevs, G., Gauthier, R.P., O'Neill, N.T., Thome, K.J., Biggar, S.F., Ripley, H., & Meygret, A. (2001). A generalized approach to the vicarious calibration of multiple Earth Observation sensors using hyperspectral data. *Remote Sensing of Environment*, 77, 304-327.

Teillet, P.M., Barsi, J. A., Chander, G., & Thome, K.J. (2007). Prime candidate earth targets for the post-launch radiometric calibration of space-based optical imaging instruments. In J. J. Butler, & J. Xiong (Eds), Proceedings of SPIE, vol. 6677. *Earth Observing Systems* XII, 66770S.

Ungar, S. G., Pearlman, J.S., Mendenhall, J.A., & Reuter, D. (2003). Overview of the Earth Observing One (EO-1) Mission. *IEEE Transactions on Geoscience and Remote Sensing*, 41, 1149-1159.

Vermote, E.F., Tanré, D., Deuzé, J.L, Herman, M., & Morcrette, J.J. (1997a). Second simulation of the satellite signal in the solar spectrum, 6S: an overview. *IEEE Transactions on Geoscience and Remote Sensing*, 35, 675–686.

Vermote, E.F., El Saleous, N., Justice, C.O., Kaufman, Y.J., Privette, J.L., Remer, L., Roger, J.C., & Tanre, D. (1997b). Atmospheric correction of visible to middle-infrared EOS-MODIS data over land surfaces: Background, operational algorithm and validation. *Journal of Geophysical Research*, 102, D14, 17131-17141.

Xiong, X., Sun, J., Xiong, S., & Barnes, W.L. (2004). Using the moon for MODIS on-orbit spatial characterisation. *Proceedings of SPIE* Vol. 5234, Sensors, Systems, and Next-Generation Satellites VII, R. Meynart, S. P. Neeck, H. Shimoda, J. B. Lurie, M. L. Aten, Editors. 0277-786X. (http://oceancolor.gsfc.nasa.gov/MODIS/Aqua/L1B/publications/moon_jack.pdf).

Xiong, X., Che, N., & Barnes, W. (2006). Terra MODIS on-orbit spectral characterisation and performance. *IEEE Transactions on Geoscience and Remote Sensing*, 44, 2198-2206.

Xiong, X., & Barnes, W. (2006). An overview of MODIS radiometric calibration and characterisation. *Advances in Atmospheric Sciences*, 23, 69-79.

Xiong, X., Wenny, B., & Barnes, W.L. (2009a). Overview of NASA Earth Observing Systems Terra and Aqua moderate resolution imaging spectroradiometer instrument calibration algorithms and on-orbit performance. *Journal of Applied Remote Sensing*, 3, 032501.

Xiong, X., Wu, A., Angal, A., & Wenny, B. (2009b). Recent progress on cross-comparison of Terra and Aqua MODIS calibration using Dome C. *SPIE Proceedings* Vol. 7474 Sensors, Systems, and Next-Generation Satellites XIII, R. Meynart; S. P. Neeck; H. Shimoda, Editors. 74711. (http://proceedings.spiedigitallibrary.org/proceeding.aspx?articleid=788949).

Acronyms

ASCWG	Australian Satellite Calibration Working Group
BRDF	Bidirectional reflectance distribution function
CEOS WGCV	Committee on Earth Observing Satellites Working Group on Calibration and Validation
DN	Digital Number
DSM	Digital Surface Model
MODTRAN	MODerate resolution atmospheric TRANsmission (for radiative transfer through the atmosphere)
NIST	National Institute of Standards and Technology (USA)
SDSM	Solar Diffuser Stability Monitor
SRCA	SpectroRadiometric Calibration Assembly
SVC	Supervised Vicarious Calibration

Satellites/Sensors

AVHRR	Advanced Very High Resolution Radiometer (NOAA)
AATSR	Advanced Along Track Scanning Radiometer (ESA)
ADEOS-II	Advanced Earth Observing Satellite 2
ETM+	Enhanced Thematic Mapper (Landsat 7)
GLI	Global Imager
LDCM	Landsat Data Continuity Mission (Landsat 8, NASA)
MERIS	MEdium Resolution Imaging Spectrometer

MODIS	Moderate Resolution Imaging Spectrometer (on TERRA and AQUA satellites, NASA)
POLDER	Polarization and Directionality of the Earth's Reflectances
SeaWIFS	Sea-Viewing Wide Field-of-View Sensor
TM	Thematic Mapper (Landsat 5)

ACORN, ATCOR, FLAASH – different atmospheric correction software tools

Chapter 5. Effective guidelines for calibration and validation of SAR data and derived biophysical products

A. Mitchell[*1], M. Thankappan[2]

[1] School of Biological, Earth and Environmental Sciences, The University of New South Wales
[2] National Earth and Marine Observations Branch, Environmental Geoscience Division, Geoscience Australia

*Corresponding author:
A.Mitchell@unsw.edu.au

Abstract

Drawing on the unique strengths of Synthetic Aperture Radar (SAR), data have been used extensively to map forest extent and land cover, e.g., Hoekman *et al*. (2010), Walker *et al*. (2010), detect change arising from deforestation or regrowth, e.g., Almeida-Filho *et al*. (2007), Santoro *et al*. (2010), and estimate forest structural parameters and total above ground biomass (AGB), e.g., Cartus *et al*. (2012), Lucas *et al*. (2010), Santoro *et al*. (2011). In the first instance, the processing of suitably calibrated imagery is required. This chapter addresses data calibration and standard processing methods for geometric and radiometric calibration of SAR data, and external calibration using corner reflectors to verify SAR system performance. Subsequent analysis requires the collection of field or other data to support the development of algorithms to retrieve forest structure or biomass and validate SAR derived forest type, land cover and change maps. Strategies for calibration and validation of SAR derived biophysical products such as forest and land cover are outlined. The methods are available should TERN acquire SAR data and provide pre-processed and/or value-added products to users in future.

Key points

- SAR system performance needs to be verified by internal and/or external calibration to achieve high radiometric accuracies.
- Geoscience Australia is in the process of establishing a network of corner reflectors for external calibration of SAR data.
- Ideally, SAR images acquired under like conditions (e.g., minimal soil moisture) should be used to create wide-area, seamless mosaics, from which land cover and other biophysical parameters are retrieved.
- A combination of frequencies and polarisations may improve the separation of land cover and forest types.

5.1 Geometric and radiometric calibration of SAR data

Rigorous orthorectification and radiometric correction of data are fundamental steps in the SAR processing chain. The corrections are necessary prior to comparison of images and direct or model-based retrieval of biophysical parameters. The impact of terrain, canopy and soil moisture and timing of image acquisition need be considered when producing suitably calibrated data for quantitative analysis. Together with the specific SAR imaging geometry (i.e., frequency, polarisation and view angle), these factors affect the interpretation and application of the data.

Orthorectification or geocoding typically uses a Digital Elevation Model (DEM) to associate pixel coordinates with map coordinates. Radiometric calibration is applied to counter systematic noise and normalise intensity data to facilitate comparison between images acquired at different times. Terrain Illumination Correction (TIC) is additionally applied to correct the brightness variations resulting from topography and SAR side-viewing geometry. Wide-area mosaics can be produced from suitably orthorectified, radiometrically calibrated, terrain illumination corrected intensity data. Rigorous and consistent processing of SAR data is required for subsequent quantitative and time-series analysis, direct retrieval of biophysical parameters such as above ground biomass, and may improve the results of land cover classification, Loew and Mauser (2007).

5.1.1 Orthorectification

Orthorectification or *geocoding* is the process by which SAR data are converted from slant range to ground range geometry and in a defined cartographic system. A rigorous Range-Doppler approach with a DEM (terrain geocoding) or without (ellipsoidal geocoding) may be considered. The DEM or ellipsoid height provides the starting point for calculating the position of each backscatter element with respect to sensor position, velocity vectors and Doppler frequencies, into slant range coordinates. Given precise orbital information, sub-pixel accuracy can be achieved when geocoding using nominal sensor parameters without the need for Ground Control Points (GCPs). A resampling step ensures regular pixel spacing in ground range across the image swath. Topographic features appear flattened in the orthorectified image as distortions due to relief have been removed.

The results of terrain geocoding are more precise as the use of a DEM means that local terrain height is taken into account when calculating the actual scattering area. The lack of DEM information typically leads to significant inaccuracies in the position of features compared to a terrain geocoded equivalent. The highest quality DEM available should be used in orthorectification to minimise geo-location errors and stretching effects and generate reliable local incidence angle (LIA) information. DEMs and derivates derived from the Shuttle Radar Topography Mission (SRTM) are available through TERN at a resolution of 1 and 3 arc seconds. A high quality DEM has a continuous (void-free) surface and smooth height profile. Low quality DEMs are blocky in appearance, lack fine detail and will likely induce artefacts in the geocoded image. When geocoding using a poor quality DEM, feathering or stretching effects are observed where the process attempts to restore the position and brightness of backscattering elements.

Geo-location accuracy is assessed by comparing the position of features with that sourced from data of known higher positional accuracy. Geocoded images can be resampled to match other image data and spatially linked for quick assessment of co-registration accuracy. The position of accurately located GCPs measured using differential GPS in the field or through automated feature detection approaches can be compared. Calculation of the Root Mean Square Error (RMSE) provides an indication of registration accuracy with respect to the coordinate transformation method. Low values of RMSE are indicative of high registration accuracy. With knowledge of the displacement error and direction, additional GCPs can be sourced to counter the observed (whether consistent or random) shifts between image.

5.1.2 Radiometric calibration

Radiometric calibration of the backscatter coefficient is essential for subsequent comparison of images acquired by different sensors, or using different observation modes, or at different times of year. Standard radar equations are applied to correct for systematic errors and brightness variations due to terrain. Steep terrain induces brightness variations due to changes in the local scattering area and alteration of scattering mechanisms through changes in SAR viewing angle, Loew and Mauser (2007). Those slopes facing towards the radar receive a greater proportion of the incident radiation compared to those slopes facing away from the radar sensor.

Radiometric corrections take into account the (i) scattering area, the real illuminated area of each pixel as a result of topography and incidence angle, (ii) antenna gain pattern, the variation in range direction of the ratio of the signal received or transmitted compared to an isotropic antenna, and (iii) range spread loss, the variation in backscatter with sensor-to-ground distance variation from near to far range. Radiometric normalisation is then applied to correct for the effects of incidence angle on backscatter intensity. Visual assessment of the results should reveal a more homogeneous brightness from near to far range across the normalised image.

5.1.3 Terrain Illumination Correction (TIC)

Corrections for geometric distortion are more widely available in commercial software packages, but robust correction of radiometric distortions are either not available or use simplistic methods. As SAR backscatter is strongly dependent on the slope and aspect of the terrain, Terrain Illumination Correction (TIC) procedures use an input DEM and imaging geometry model to better define the ground surface area contributing to the backscatter of each pixel. Numerous theoretical and experimental studies have led to the development of 3 types of published models to account for terrain induced radiometric variations over rough (largely vegetated) surfaces: (i) Semi-empirical methods, e.g., Ulaby *et al*. (1986), (ii) Statistical models, e.g., Teillet *et al*. (1985), and (iii) Geometric models, e.g. van Zyl (1993), Kellndorfer *et al*. (1998), Zhou *et al*. (2011).

The effect of TIC on images is evident in the smoother appearance of the surface where the terrain is seemingly flattened (illustrated in Figure 5.1). Prior to TIC, illuminated forward slopes appear quite bright and backward slopes appear quite dark. TIC smooths out the overall backscatter response by reducing the backscatter on forward slopes and increasing the backscatter on backward slopes. Evidence of topography still exists in the TIC images (Figure 5.1b), but for the most part has been flattened, inducing a smaller dynamic range. Backscatter remains largely unchanged in flat areas, indicative of successful implementation of TIC.

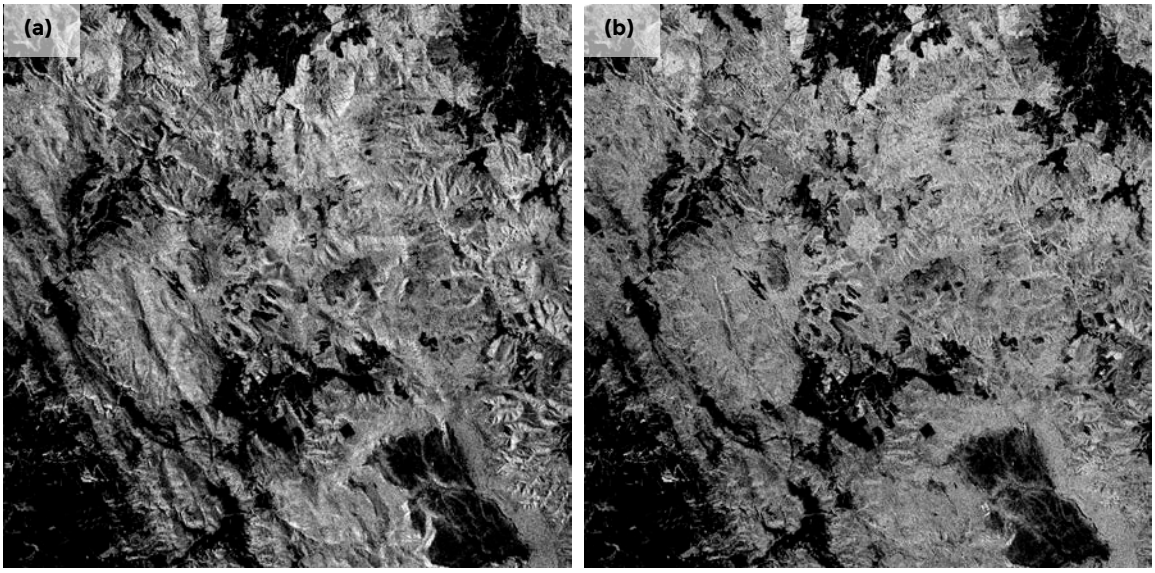

Figure 5.1 ALOS PALSAR HV backscatter data illustrating
(a) Radiometrically calibrated data prior to correction, and
(b) Terrain Illumination Corrected (TIC) data.

Even after rigorous radiometric and terrain illumination correction of data, noticeable artefacts may be observed in the data. The side-viewing imaging geometry of SAR results in inherent distortions in the data, particularly in the presence of steep terrain. These distortions are most severe in the range direction and at near range, and mask or reduce the useful backscatter information related to land cover or biophysical parameters. The projection of ground targets onto the radar image plane, i.e., slant range, results in non-linear compression of imaged data. In the presence of topography, these distortions are manifest as foreshortening, layover and shadow.

Foreshortening occurs when terrain slopes illuminated by side-viewing radar appear compressed in scale, the effect of which is more pronounced for steeper slopes when observed at steeper incidence angles. Layover is an extreme form of foreshortening or elevation displacement, and occurs when the top of an object is closer to the radar and is imaged before its base. In imagery, it appears as though the feature has collapsed over

towards the radar. Radar shadow occurs in the absence of incident radar illumination. The occurrence and amount of radar shadow is dependent on imaging parameters including radar look direction, incidence angle and satellite altitude, and terrain features such as orientation and slope. Shadow predominates in terrain viewed at large incidence angles, and the lack of signal return means a loss of thematic information.

Masking of layover and shadow areas, where there is limited to no useful backscatter information, is recommended prior to classification, either as part of the training process whereby samples are identified in areas of layover or shadow and included as one of several classes to be mapped, or in a post-classification or filtering step where infilling of thematic information occurs using neighbourhood values and local context.

5.2 Corner reflectors for radiometric calibration of SARs

Radiometric calibration is the process of characterising the end-to-end performance of the SAR system's ability to measure the amplitude and phase of the backscattered signal. The performance of SAR instruments needs to be verified by internal and/or external calibration to achieve high radiometric accuracies. Internal calibration involves characterisation of the radar system performance using signals from devices built into the sensor system; external calibration involves the use of ground based point or distributed targets, Curlander and McDonough (1991). In this Section, external SAR radiometric calibration is covered, with special reference to the recent use of point targets in an Australian context.

For external radiometric calibration, the performance of the SAR instrument is related to a known measurement standard; point targets such as corner reflectors or active transponders can be used for radiometric calibration. Alternatively, distributed targets of known radar cross section (RCS) such as agricultural fields, tropical rain forests, or boreal forests, could also be used, provided the area is uniform, and the average RCS for a particular radar frequency, polarisation, viewing geometry and time of year is known. Corner reflectors are routinely used, as they have low maintenance and are of low cost compared to active devices such as transponders, which also need power for operation. Corner reflectors also exhibit a RCS relative to their small size, and maintained over a wide range of incidence angles, ensuring their proper identification in the SAR image.

Geoscience Australia has implemented the geospatial component of the Australian Geophysical Observing System (AGOS). AGOS infrastructure includes a network of corner reflectors. The corner reflectors have been installed in areas specific to AGOS research interests, and designed such that they can be used to monitor crustal deformation and to perform ongoing radiometric, geometric, and impulse response measurements for calibration of SAR instruments on space borne or airborne platforms, Garthwaite *et al*. (2013, 2015).

Geoscience Australia manufactured 18 corner reflector prototypes with different sizes and material finishes to identify optimal prototypes for calibration applications. A triangular trihedral design was chosen for the corner reflectors because of the simplicity of manufacture, long-term structural rigidity and relative stability for large RCS. The corner reflector prototypes were characterised at the Defence Science and Technology Organisation ground reflection range facility in Adelaide, by comparing actual RCS measurements with the expected theoretical values and quantifying the change in RCS at different azimuth and elevation angles. Results from the characterisation of the corner reflectors have shown that the RCS performance of the prototypes is comparable to theoretical values, Thankappan *et al*. (2013).

The corner reflector prototypes were temporarily deployed at a test site north of Canberra for field performance evaluation over a 5-month period. Performance testing involved data acquisitions using SAR satellites at X and C-band to verify that the observed RCS of the corner reflectors are comparable to theoretical

values for calibration of the SAR instruments. Following the performance evaluation, a total of 40 corner reflectors have been deployed permanently in Queensland, Australia. Details of the location and orientation of the corner reflectors are available from Geoscience Australia.

It is anticipated that the corner reflector infrastructure will be exploited by international satellite operators for independent verification of SAR instrument performance, and will count towards Australia's valuable contribution to international efforts on calibration of satellite borne SAR instruments.

5.3 Importance of data selection

It would be remiss to not include some discussion on the importance of initial data selection when processing SAR imagery. SAR data is heavily influenced by dielectric properties and variations in backscatter may be evident within and between strip data or single scene products acquired during or after rainfall events. This banding is problematic when generating regional mosaics and for those studies reliant on consistent backscatter relationships, e.g., land cover mapping and retrieval of biophysical attributes such as AGB. Increased soil and/or canopy moisture can enhance the backscatter signal by a few decibels (dB). As such, only those images acquired under dry or like conditions should be used to create a seamless mosaic.

A case study from Queensland, Australia, published by Lucas *et al*. (2010), highlights the importance of data selection with reference to environmental conditions for the compilation of wide-area mosaics. Strip data acquired by the Advanced Land Observing Satellite Phased Array L-band SAR (ALOS PALSAR) as part of the Kyoto and Carbon (K&C) Initiative have been used to generate relatively seamless mosaics for many areas worldwide, but several strips acquired over northern Australia had noticeably higher backscatter values compared to neighbouring strips despite implementation of appropriate across track correction routines (Figure 5.2a). Reference to meteorological records and satellite measurements of soil moisture and vegetation water content suggested that rainfall during or several days prior to image acquisition and subsequent rates of evapotranspiration were primarily responsible.

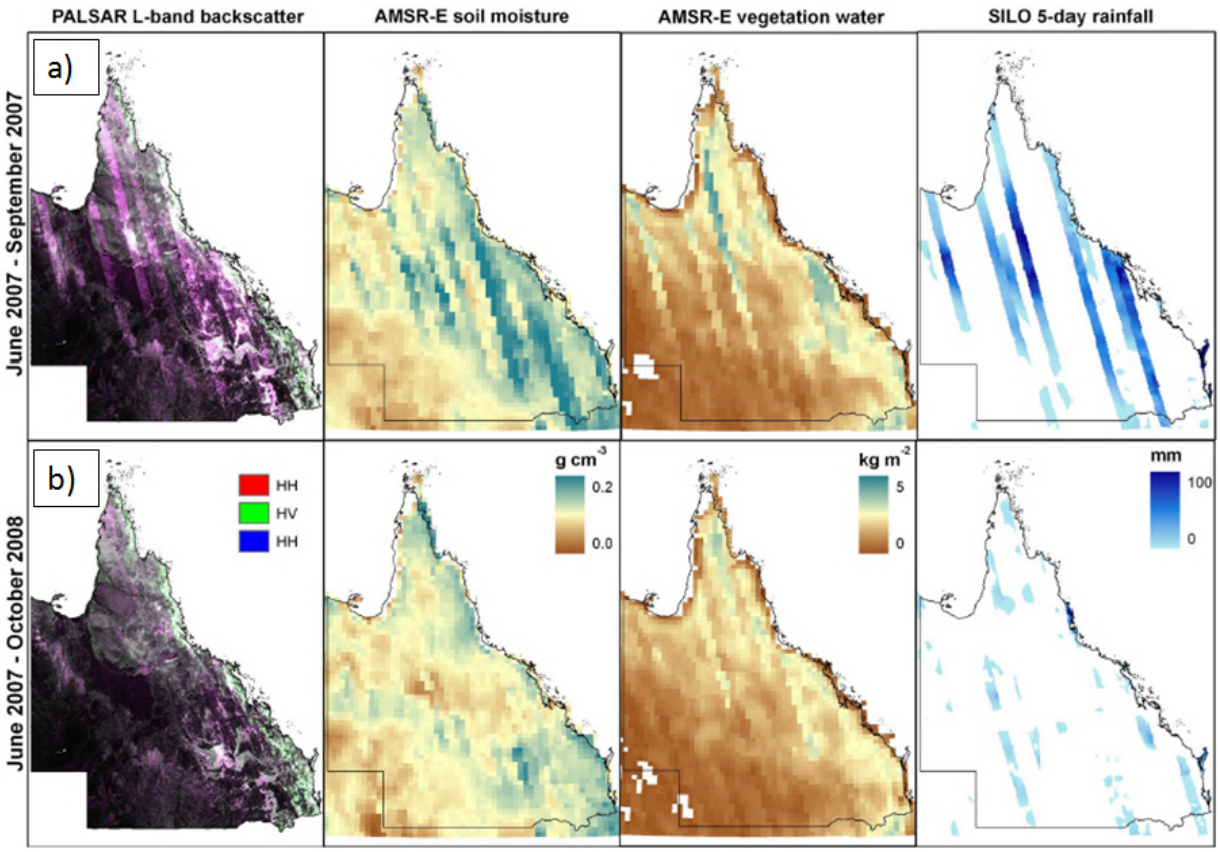

Figure 5.2 The impact of surface moisture on radar backscatter: ALOS PALSAR mosaics generated for Queensland using a) strips acquired on random dates of acquisition in 2007, and b) following periods where surface moisture was at a relative minimum (bottom). Soil moisture and effective vegetation water content derived from AMSR-E and rainfall over the timeframe of PALSAR acquisitions are also illustrated, Lucas *et al*. (2010).

It was not possible to correct the backscattering coefficient because of the high variability in these meteorological parameters. Their solution involved using data from dry periods only, either from 1 year or several, and resulted in a mosaic with relative consistency in data values (Figure 5.2b). The results demonstrate the importance of consulting meteorological data acquired at ground stations (e.g., SILO climate database) or as measured by spaceborne sensors (e.g., the Advanced Microwave Scanning Radiometer - Earth Observing System, AMSR-E) prior to scene selection, particularly in areas with irregular rainfall and evapotranspiration.

Another important consideration when mosaicking is that images may have been acquired several weeks apart, depending on the revisit time of the sensor. The ALOS PALSAR, for example, has a 46-day repeat cycle and it is therefore possible that real on-ground change could have occurred in the overlapping area of adjacent images acquired on different dates. The change may be in the form of, for example, increased soil moisture due to rainfall or a flood event, or a change in spectral or textural properties due to crop/canopy growth or a change in land cover, e.g., clear felling of timber. It may be necessary to exclude the area of overlap or use averaging techniques when creating a mosaic.

5.4 Key considerations when using SAR to map land cover

SAR backscatter is highly dependent on target properties, including structure, roughness and dielectric (moisture content), and imaging parameters such as frequency, polarisation and view angle. Slope and terrain induced artefacts such as layover and shadow also affect our interpretation of features. When imaging the forest canopy using SAR, a saturation point is eventually reached, whereby the forest biomass may increase but radar backscatter does not, Williams *et al*. (2011). This point varies with frequency with early onset at X- and C-bands, and at around 50 - 100 t/ha for L-band and around 150 t/ha for P-band. Typically, data acquired at different wavelengths and polarisations is required for optimal understanding of the target being imaged. Higher resolution and polarimetric and interferometric capability provides additional information that can be exploited, Williams *et a*l. (2011).

Some key observations from the literature when using SAR to map land cover types are summarised below.

- **Forest and non-forest is more easily separated using longer wavelength SAR data**

The separation arises from distinct differences in backscatter observed in L-band data acquired over forest and non-forest areas, Leckie and Ranson (1998). Longer wavelength L-band (~24 cm wavelength) has an increased capacity for penetration of the vegetation canopy and greater opportunities for interaction with underlying woody structures and the ground surface. The cross-polarisation (HV) is preferred over the co-polarisation (HH) for better separation of forest and non-forest. The L-band HH:HV ratio provides a useful indicator of forest cover. Shorter wavelength C- (~5.8 cm) and X-band (~3 cm) have reduced capacity for penetration and largely interact with surface structures of comparable size to the wavelength (e.g., leaves and small branches).

- **Longer wavelength SAR improves the separation of forest and land cover types**

Longer wavelength SAR demonstrates improved separation of structurally distinct vegetation types, largely attributed to the capacity for penetration and greater opportunities for ground-volume interactions, Balzter *et al*. (2003). The lack of penetration of the canopy at C-band and predominance of volume scattering between similarly sized vegetation components reduces the ability to discriminate between cover types. Improved separation of certain cover types might be achieved through the integration of C- and L-band data, e.g., Haarpaintner *et al*. (2009), Hoekman (2012). DEM derived topographic information and texture metrics may also assist in discriminating forest types, Otukei *et al*. (2011), Wang *et al*. (2012), e.g., rainforest in gullies and dry eucalypt forest along ridgelines.

- **L-band is more sensitive to changes in forest structure compared to C- or X-band**

The sensitivity of SAR backscatter to forest structure increases with increasing wavelength, Tanase *et al*. (2011). Shorter wavelength C- and X-band is less sensitive to changes in forest structure due to rapid saturation of the signal at these wavelengths. In Tasmania, the mapped forest/non-forest distribution varied as a function of C- and L-band capacity to discriminate bare (harvested) ground, young regrowth and mature plantation, Mitchell *et al*. (2014). Young eucalypt regrowth was more easily discriminated using ALOS PALSAR (L-HH and HV) data compared to RADARSAT-2 (C-VV and VH) data. Young plantation exhibited similar high C-band backscatter to native forest. L-HV was found to be the best discriminator of cover types. Both the frequency and polarisation influence the type of information that is observed or extracted.

- **Time-series L-band data facilitates mapping of successive stages of regrowth**

Longer wavelength cross-polarised data (L-HV) facilitates the discrimination of successive stages of regrowth. Time-series ALOS PALSAR L-HV spectra were extracted over eucalypt plantations in NE Tasmania to assess the change in backscatter response with growth over a 4-year period, Mitchell *et al*. (2014). L-HV backscatter dominates the response from mature plantation due largely to volume scattering between canopy

components. An abrupt change in backscatter of up to 3 dB is observed following clearing of forest. As trees are cut, the contribution to backscatter from volume scattering decreases, and greater surface scattering at L-HH is observed. Thereafter, a gradual increase in backscatter is observed, with L-band interactions with seedlings and on-ground debris. As the saplings grow, L-band responds to the structural changes and increase in canopy volume and woody (branch and trunk) biomass. A positive change or increase in backscatter between dates is indicative of regeneration. The backscatter response is more variable in these growing plantations compared to mature plantation. The integration of L-band SAR with variables such as foliage projective cover (FPC) derived from optical remote sensing data also provide greater capacity for mapping regrowth and degradation stages, Lucas et al. (2014).

- **Woody debris left on ground following harvesting can be misinterpreted as forest cover**

Tree trunks and other woody debris left on ground following harvesting can elevate the L-band backscatter response. These areas are easily misinterpreted or misclassified as forest. Texture metrics may be useful for discrimination as distinct rows and light-dark striping is often observed in plantation forest.

- **L-band is particularly useful for separating flooded and non-flooded forest**

This is largely due to strong double bounce interactions between large woody components (trunks and branches) and the flooded surface which enhances the backscatter signal by a few dB. Lower backscatter is observed over non-flooded forest as a result of the predominance of volume and multiple scattering mechanisms, Evans *et al*. (2010).

- **The integration of short and longer wavelength SAR data can improve the separation of bare ground and grassland**

At L-band, bare ground and grassland are often confused. Short stature vegetation, such as shrub or grassland is largely invisible at long wavelengths. Shorter wavelength C- or X-band SAR data can improve the separation in these areas as the size of features is more comparable with the radar wavelength, Milne *et al*. (2008).

- **High resolution SAR data facilitates mapping of forest degradation**

High resolution TerraSAR-X data (1 – 2 m spatial resolution) can be used to identify degraded forests or instances of selective logging. Detection relies on the loss of or damage to individual tree crowns, ensuing gaps in the canopy, and their identification in high resolution imagery. Such fine-scale change may be difficult to detect using coarser resolution data such as ALOS PALSAR with a spatial resolution of 12.5 m. The high frequency of observations also assists in detecting rapid changes in forest cover.

- **Terrain induced geometric and radiometric distortions alter our perception of land cover**

The combination of look angle, slope and topography affects our visualisation of features. In steep terrain, SAR images are distorted both geometrically and radiometrically. The effects are worse with smaller radar look angles. From a radiometric perspective, slopes facing towards the radar are very bright, and those facing away, i.e., not illuminated by the radar appear dark. Layover and shadow are easily identified (with use of a high resolution DEM), but not so easily corrected for. Where the backscatter is unreliable, these areas should be masked out and labelled in a post-classification step using local data.

- **Boundary effects are evident at the edge of forest and clearings**

Boundary effects occur at the edge of intact forest and clearings or secondary forest, resulting in increased backscatter at the near boundary and radar shadows at the far boundary, Leckie and Ranson (1998). These effects should be identified by association and subsequently removed or re-classified.

5.5 Cal/Val sampling strategy

There is no substitute for direct measurement through field inventory for Cal/Val of biophysical products. Field assessments are necessarily undertaken in several stages over the lifetime of a project. An initial reconnaissance is useful to scope out access to areas and familiarise with the terrain and spatial distribution and diversity of vegetation communities. A dedicated field campaign(s) is required to collect essential land cover and structural data to assist in analysing satellite imagery, calibrate algorithms, e.g., for biomass retrieval, and provide training and testing data for classification of land cover. The types of measurements that are required include, but are not limited to, those that relate to the woody vegetation components, such as tree height, trunk diameter, basal area and stem density. Lastly, a validation campaign is needed for acquiring additional validation data and interpreting classifications and other derived biophysical data for continuous improvement. Readers are referred back to Chapter 3 for discussion on field data collection and management for validation of remotely sensed imagery.

Although an essential step in the process, field survey can be time-consuming, labour-intensive, costly and constrained by access. A key assumption is that field or other data (e.g., high resolution airborne or satellite data) of presumed higher accuracy is collected to support algorithm development or validation. Measurements acquired by airborne sensors can be used in model predictions, simulation studies and validation of satellite derived image products. The sampled area should be homogeneous and large enough in area to be representative of the target relative to the spatial resolution of the observing sensor. In other words, the SAR backscatter extracted from the sampled area should represent the average backscatter for that target, Patel and Srivastava (2013).

Given the high sensitivity of SAR backscatter to dielectric and geometric properties, a large number of target properties are required to support the interpretation of imagery. This ground truth should necessarily be acquired coincident with or as near to the time of image acquisition for best correlation between image and ground data. The use of ill-timed ground truth will introduce errors arising from seasonality, meteorological conditions, and occurrence of on-ground change (e.g., land clearing). Good quality control will ensure that measurement error due to technique or instrumentation, both random and systematic in form, does not introduce bias into the Cal/Val activity. Sampling design, scaling, temporal frequency, class definitions and a myriad of issues must be dealt with, and often these are considered at project-scale due to the lack of standardised methods.

Sampling strategy is a well debated theme in the scientific community. Random sampling minimises the risk of bias and can be implemented by randomly locating sample points or plots within an area or randomly positioned grid, IPCC (2003). It is often difficult to achieve a sufficient sampling density and one that adequately represents different biogeographic regions, landforms, vegetation, land cover and soil types. Sampling with too low a density will likely incur a loss in spatial variation. Compromises are made and the theoretical approach is often not practical in the field. Random stratified sampling is widely regarded as an efficient approach, whereby the population is first subdivided using ancillary data, e.g., based on elevation, soil type or administrative boundary, and sampling undertaken within each stratum, IPCC (2003). Following stratification, sampling statistics are applied to determine the number of plots that will satisfy accuracy requirements, Fox *et al*. (2011). In this way, the variability in the landscape is compartmentalised and fewer samples are required to adequately capture each subdivision. Alternatively, systematic sampling distributes sample points evenly across the sample area, IPCC (2003), for more efficient sampling over large areas.

Scaling becomes an issue when, for example, forest inventory plots of a defined size are used to validate image derived products. Assumptions are made as to the homogeneity of the land cover in the landscape. Clustering of plots might be necessary or further development of methods for upscaling forest inventory plots to the appropriate scale, Lowell *et al*. (2012).

Land cover/land-use definitions tend to vary between countries, with different interpretations of, for example, the height and cover thresholds to define forest. Local context should be taken into consideration when defining the cover classes to be mapped, and a consistent approach to their identification realised. Validation of land cover/land-use change or change in carbon stocks requires either repeat sampling using temporary or permanent inventory plots or use of time-series data, IPCC (2003). The measurement interval is determined by the frequency and scale of the disturbance and reporting requirements. Consistent measurement of vegetation type and structural change through time is required.

Recommendations for 'ground truthing' SAR derived forest/land cover information:

- **Identify calibration sites in distinct biogeographic regions**

To maximise sampling effort, calibration sites are identified in distinct biogeographic regions with variable forest cover and land use history. The sites provide a test-bed for SAR processing strategies prior to wide-scale implementation.

- **Interrogate imagery for visual differences between cover classes**

Interrogation of SAR imagery will likely reveal many areas of distinct texture, visual boundaries between cover types, some obvious (e.g., cropland adjacent to forest), some more subtle (e.g., plantation of varying age) and variations in spatial patterns and radar response (e.g., rainforest and dry eucalypt forest). Field sites may be selected on the basis of these observations, with the intent on visiting as many sites as possible in the allocated time.

- **Stratify sampling according to terrain, vegetation or other bio-geo-physical attribute**

Stratify the landscape to ensure the full range of terrain type and class habitat is captured. DEMs and topographic modelling provide useful inputs for stratification. Locate training and validation sites in areas of like vegetation cover across the variable range in distribution. Identify sites on both leading and trailing slopes and flat ground. Also include sites that fall in areas of radar shadow.

- **Collect descriptive and structural data**

All sites should be GPS located. General descriptions of the land cover and vegetation (e.g., species, number of strata, and presence of understorey) and oblique photographs in all compass directions are taken. Hemispherical photography is useful when investigating canopy geometry and Leaf Area Index (LAI). Plot based measurements may include (but are not limited to) tree height, Diameter at Breast Height (DBH), basal area, crown diameter and stem density. Radar backscatter is calibrated to *in situ* (plot based) measurements of Above Ground Biomass (AGB), estimated using allometry. More studies are needed on the requirements, in terms of sample sizes and spatial extents, for field based calibration and validation of AGB models, Goetz *et al*. (2009).

Field survey data are used as training for classification of vegetation and land cover, estimation of biophysical parameters and subsequent validation. Large-scale prints of SAR imagery and change analysis are useful in the field. The change images identify mapped areas of deforestation and regeneration and can be verified by on-site visit.

- **Image analysis guided by field data**

Radar spectra extracted over field sites are used to observe the multi-date variation in backscatter response and assess the potential of SAR for discrimination of land cover classes. Separability metrics are calculated to determine ranked separability between classes. Where only limited ground truth is available, a certain proportion of field points, e.g., 30 % is set aside for validation, or assessing the accuracy of the derived classification.

References

Almeida-Filho, R., Rosenqvist, A., Shimabukuro, E. & Silva-Gomez. (2007). Detecting deforestation with multitemporal L-band SAR imagery: a case study in western Brazilian Amazonia. International Journal of Remote sensing, 28, 6, 1383-1390.

Balzter, H., Skinner, L., Luckman, A. & Brooke, R. (2003). Estimation of tree growth in a conifer plantation over 19 years from multi-satellite L-band SAR. Remote Sensing of Environment, 84, 184-191.

Cartus, O., Santoro, M. & Kellndorfer, J. (2012). Mapping forest aboveground biomass in the Northeastern United States with ALOS PALSAR dual-polarisation L-band. Remote Sensing of Environment, 124, 466-478.

Curlander J.C. & MacDonough R.N. (1991). Synthetic Aperture Radar: Systems and Signal Processing. New Jersey: John Wiley and Sons.

Evans, T.L., Costa, M., Telmer, K. & Silva, T.S.F. (2010). Using ALOS/PALSAR and RADARSAT-2 to map land cover and seasonal inundation in the Brazilian Pantanal. IEEE Journal of Selected Topics in Applied Earth Observations and Remote Sensing, 3, 4, 560-575.

Fox, J.C., Yosi, C.K. & Keenan, R.J. (2011). Assessment of timber and carbon stocks for community forest management. In Fox, J.C., Keenan, R.J. & Saulei, S. (Eds.), Native forest management in Papua New Guinea: advances in assessment, modelling and decision-making, ACIAR Proceedings No. 135 (201 pp). Canberra: Australian Centre for International Agricultural Research.

Garthwaite, M.C., Thankappan, M., Williams, M.L., Nancarrow, S., Hislop, A. & Dawson J. (2013). Corner Reflectors for the Australian Geophysical Observing System and Support for Calibration of Satellite-borne Synthetic Aperture Radars. Proceedings of the Geoscience and Remote Sensing Symposium (IGARSS), Melbourne, Australia, 21-26 July, IEEE International, pp. 266-269.

Garthwaite, M. C., Nancarrow, S., Hislop, A., Thankappan, M., Dawson, J. H., Lawrie, S. (2015). The Design of Radar Corner Reflectors for the Australian Geophysical Observing System: a single design suitable for InSAR deformation monitoring and SAR calibration at multiple microwave frequency bands. Record 2015/03. Geoscience Australia, Canberra. http://dx.doi.org/10.11636/Record.2015.003Goetz, S.J., Baccini, A., Laporte, N.T., Johns, T., Walker, W., Kellndorfer, J., Houghton, R.A. and Sun, M. (2009). Mapping and monitoring carbon stocks with satellite observations: a comparison of methods. Carbon Balance and Management, 4, 2.

Haarpaintner, J., Almeida-Filho, R., Shimabukuro, Y.E., Malnes, E. & Lauknes, I. (2009). Comparison of ENVISAT ASAR deforestation monitoring in Amazonia with Landsat-TM and ALOS PALSAR images. Proceedings of Anais XIV Simposio Brasileiro de Sensoriamento Remoto, INPE, Natal, Brazil, April 25-30, pp. 5857-5864.

Hoekman, D., Vissers, M.A.M. & Wielaard, N. (2010). PALSAR wide-area mapping of Borneo: methodology and map validation. IEEE Journal of Selected Topics in Applied Earth Observations and Remote Sensing, 3, 4, 605-617.

Hoekman, D. (2012). Key Science Questions: Optimising information extraction from C-band SAR. GEO FCT Science and Data Summit #3, Arusha, Tanzania, February 6-10.

Intergovernmental Panel on Climate Change (IPCC). (2003). Good Practice Guidance for Land Use, Land-Use Change and Forestry. Penman, J., Gytarsky, M., Hiraishi, T., Krug, T., Kruger, D., Pipatti, R., Buendia, L., Miwa, K., Ngara, T., Tanabe, K. & Wagner, F. (Eds.), Institute for Global Environmental Strategies (IGES), IPCC.

Kellndorfer J., Pierce, L. E., Dobson, M.C. & Ulaby, F.T. (1998). Toward consistent regional-to-global-scale vegetation characterization using orbital SAR systems. IEEE Transactions on Geoscience and Remote Sensing, 36, 5, 1396– 1411.

Leckie, D.G. & Ranson, K.J. (1998). Forestry applications using imaging radar. In Henderson, F.M. & Lewis, A.J. (Eds.), Principles and Applications of Imaging Radar, Manual of Remote Sensing (Vol 2, 3rd ed., pp.435-509). New Jersey: John Wiley & Sons.

Loew, A. & Mauser, W. (2007). Generation of geometrically and radiometrically terrain corrected SAR image products. Remote Sensing of Environment, 106, 337-349.

Lowell, K., Mitchell, A.L., Milne, A.K., Tapley, I., Held, A., Caccetta, P., Lehmann, E. & Zhou, Z-S. (2012). GEO Forest Carbon Tracking Task, Tasmania National Demonstrator: Verification, continuous improvement and reporting methods for national demonstrators, Vol. 4, Sept 2012. Technical report prepared for the Department of Climate Change and Energy Efficiency (DCCEE).

Lucas, R., Armston, J., Fairfax, R., Fensham, R., Accad, A., Carreiras, J., Kelley, J., Bunting, P., Clewley, D., Bray, S., Metcalfe, D., Dwyer, J., Bowen, M., Eyre, T., Laidlaw, M. & Shimada, M. (2010). An evaluation of the ALOS PALSAR L-band backscatter – above ground biomass relationship Queensland, Australia: Impacts of surface moisture condition and vegetation structure. IEEE Journal of Selected Topics in Applied Earth Observations and Remote Sensing, 3, 4, 576-593.

Lucas, R.M., Clewley, D., Accad, A., Butler, D., Armston, J., Bowen, M., Bunting, P., Carreiras, J., Dwyer, J., Eyre, T., Kelly, A., McAlpine, C., Pollock, S. & Seabrook, L. (2014). Mapping forest growth and degradation stage in the Brigalow Belt Bioregion of Australia through integration of ALOS PALSASR and Landsat-derived foliage projective cover data. Remote Sensing of Environment, 155, 42-57.

Milne, A.K., Tapley, I., Mitchell, A.L. & Powell, M. (2008). Trial of L-band radar for mapping inundation patterns in the Macquarie Marshes. Stage III Consultancy Report submitted to the NSW Department of Environment and Climate Change (formerly DECC; now OEH), Dec 2008.

Mitchell, A.L., Tapley, I., Milne, AK., Williams, M.L., Zhou, Z-S., Lehmann, E., Caccetta, P., Lowell, K. & Held, A. 2014. C- and L-band SAR interoperability: Filling the gaps in continuous forest cover mapping in Tasmania. Remote Sensing of Environment, 155, 58-68.

Otukei, J.R., Blaschke, T., Collins, M. & Maghsoudi, Y. (2011). Analysis of ALOS PALSAR and TerraSAR-X data for protected area mapping: a case of the Bwindi Impenetrable National Park - Uganda. Proceedings of the IEEE International Geoscience and Remote Sensing Symposium (IGARSS), 24-29 July, Vancouver, Canada, pp. 348-351.

Patel, P. & Srivastava, H.S. (2013). Ground truth planning for synthetic aperture radar (SAR): Addressing various challenges using statistical approach. International Journal of Advancement in Remote Sensing, GIS and Geography, 1, 2, 1-17.

Santoro, M., Fransson, J.E.S., Eriksson, L.E.B. & Ulander, L.M.H. (2010). Clear-cut detection in Swedish boreal forest using multi-temporal ALOS PALSAR backscatter data. IEEE Journal of Selected Topics in Applied Earth Observations and Remote Sensing, 3, 4, 618-631.

Santoro, M., Beer, C., Cartus, O., Schmullius, C.C., Shvidenko, A. & McCallum, L. (2011). Retrieval of growing stock volume in boreal forest using hyper-temporal series of Envisat ASAR ScanSAR backscatter measurements. Remote Sensing of Environment, 115, 2, 490-507.

Tanase, M., Riva, J.D.L., Santoro, M., Perez-Cabello, F. & Kasischke, E. (2011). Sensitivity of SAR data to post-fire forest regrowth in Mediterranean and boreal forests. Remote Sensing of Environment, 115, 2075-2085.

Teillet, P.M., Guindon, B., Meunier, J.F. & Goodenough, D.G. (1985). Slope-aspect effects in Synthetic Aperture Radar imagery. Canadian Journal of Remote Sensing, 11, 1, 39-50.

Thankappan, M., Garthwaite, M.C., Williams, M.L., Nancarrow, S., Hislop, A. & Dawson J. (2013). Characterisation of Corner Reflectors for the Australian Geophysical Observing System to Support SAR Calibration. Proceedings of the ESA Living Planet Symposium, Edinburgh, UK, 9-13 September.

Ulaby, F.T., Moore, R.K. & Fung, A.K. (1986). Microwave Remote Sensing, Active and Passive. (vol III). Norwood, MA: Artech House.

Walker, W.S., Stickler, C.M., Kellndorfer, J.M., Kirsch, K.M. & Nepstad, D.C. (2010). Large-area classification and mapping of forest and land cover in the Brazilian Amazon: a comparative analysis of ALOS/PALSAR and Landsat data sources. IEEE Journal of Selected Topics in Applied Earth Observations and Remote Sensing, 3, 4, 594-604.

Wang, Y-C., Feng, C-C. & Vu Duc, H. (2012). Integrating multi-612 sensor remote sensing data for land use/land cover mapping in a tropical mountainous area in northern Thailand. Geographical Research, 50, 3, 320-331.

Williams, M.L., Yohannan, A.I., Milne, A.K. & Tapley, I. (2011). The information content of synthetic aperture radar imagery of tropical forests. In Fox, J.C., Keenan, R.J. & Saulei, S. (Eds.), Native forest management in Papua New Guinea: advances in assessment, modelling and decision-making. ACIAR Proceedings No. 135 (201 pp). Canberra: Australian Centre for International Agricultural Research.

van Zyl J.J. (1993). The effect of topography on radar scattering from vegetated areas. IEEE Transactions on Geoscience and Remote Sensing, 31, 1, 153–160.

Zhou, Z-S., Lehmann, E., Wu, X., Caccetta, P., McNeill, S., Mitchell, A. Milne, A., Tapley, I. & Lowell, K. (2011). Terrain slope correction and precise registration of SAR data for forest mapping and monitoring. Proceedings of the 34th International Symposium on Remote Sensing of Environment (ISRSE), 11-15 April, Sydney.

Chapter 6. Overview of ground based techniques for estimating LAI

M.T. Schaefer [1], E. Farmer[2], M. Soto-Berelov[2,4], W. Woodgate[2,3], S. Jones[2,3]

[1] Precision Agriculture Research Group. School of Science and Technology, University of New England
[2] Remote Sensing Centre, School of Mathematical and Geospatial Sciences, RMIT University
[3] Cooperative Research Centre for Spatial Information

*Corresponding author:
Michael.Schaefer@csiro.au

Abstract

Leaf Area Index (LAI) is typically defined as the total one-sided area of leaf tissues per unit of ground surface area. Utilising this definition, LAI is a dimensionless unit which characterises the canopy of a given ecosystem (Breda, 2003). LAI and the fraction of absorbed photosynthetically active radiation (fAPAR) are two biophysical parameters that are closely related and often measured and validated in parallel in the field. fAPAR is defined as the fraction of photosynthetically active radiation (PAR) in the 400-700 nm wavelengths that is absorbed by a canopy and it can include over-storey, understory and ground cover elements (Gower et al., 1999; Fensholt et al., 2004). This chapter provides a basic review of LAI product validation, supplemented with information on the allied metric fAPAR. After presenting a brief introduction of these concepts (LAI and fAPAR), some of the major global LAI product validation programs are reviewed. This is followed by a discussion of different validation methods that can be used in the field and in situ sensors used to collect LAI and fAPAR measurements (e.g., Li-Cor LAI-2200, TRAC, AccuPar Ceptometer, Digital Hemispherical Photography or DHP and the Plant Canopy Imager CI-110). The chapter finishes by presenting a methodology that illustrates MODIS collection 5 LAI validation efforts in Australian vegetated ecosystems. Additional guidance on sampling designs that can be used for LAI validation can be found in Chapter 2.

Key points

- Validation can be achieved by comparing product values against reference data or by up-scaling observations gathered in the field using intermediate to large resolution imagery.
- Ground based measurements of LAI can be obtained directly when leaf area is physically measured or indirectly, by inferring LAI from other variables through observation (indirect non-contact techniques) or through the application of allometric equations (indirect contact techniques).
- Direct validation methods produce more accurate results given they avoid issues associated with foliage clumping and leaf angle distribution, however they are more labour intensive and time consuming than indirect methods. Accordingly, ground-based estimates of LAI are primarily acquired using indirect techniques.
- Allometric techniques establish a relationship between leaf area and another more easily obtainable variable such as DBH. However, allometric relationships tend to be site and time specific. The application of general allometric relationships as opposed to stand-specific ones can potentially result in moderate to large errors of estimated LAI values.
- Indirect, non-contact techniques to estimate LAI frequently rely on optical instruments that make use of radiative transfer theory to infer LAI from measurements of radiation transmission through the canopy. Optical instruments typically used to estimate LAI on the ground using indirect techniques include the LAI-2200 plant canopy analyser, the AccuPAR ceptometer, digital hemispherical photography (DHP), and the Tracing Radiation and Architecture of Canopies (TRAC) instrument.
- Indirect LAI estimates taken from indirect optical methods can be biased depending on the leaf inclination, canopy element clumping, and canopy cover characteristics, so they may require calibration via direct LAI measurements. Therefore, you cannot assume ground-based estimates are without error.
- Given the variety of techniques and instruments available for measuring LAI, the most appropriate instrument is likely to be a function of the canopy structure and study area characteristics. However, hemispherical gap measurement devices are typically suited to most environments.
- LAI measurements using hemispherical photography and plant canopy analysers are best captured under completely diffuse lighting conditions such as dawn/dusk.
- LAI and fAPAR are associated metrics are frequently validated coincidentally.

6.1 Introduction

6.1.1 LAI

Leaf area index or LAI, typically defined as the total one-sided area of leaf tissues per unit of ground surface area (Breda, 2003)[1], is a key biophysical parameter influencing vegetation photosynthesis, transpiration and energy balance at the land surface (Tian et al., 2002). LAI significantly influences the within and below canopy microclimate of a given vegetation stand controlling water interception, radiation transfer, water and carbon gas exchange (Breda, 2003). Consequently, LAI is an important driver in ecosystem productivity models, operating at local to global scales, and global models of climate, hydrology and biogeochemistry (Morisette et al., 2006) and is considered an Essential Climate Variable (ECV). There are several satellite derived LAI products (and a number of regional LAI mapping projects) that are available to the science community (Table 6.1).

Table 6.1
Exemplar global LAI mapping projects.

Project	Agency	Sensor(s)	Website
MODIS (Moderate Resolution Imaging Spectrometer)	MODIS Land Team NASA	MODIS	http://modis-land.gsfc.nasa.gov
POLDER (Polarisation and directionality of the Earth's reflectance)	CESBIO/ CNES	POLDER-2	http://smsc.cnes.fr/POLDER/
GLOBCARBON	ESA	AVHRR VEGETATION POLDER MERIS	http://dup.esrin.esa.it/prjs/prjs43.php
CYCLOPES (Carbon Cycle in Land Observational Products from an Ensemble of Satellite)	European Union (FP5 project)	VEGETATION MERIS AATSR AVHRR	http://toyo.mediasfrance.org/?CYCLOPES-Project

6.1.2 fAPAR

The parameter fAPAR is defined as the fraction of photosynthetically active radiation (PAR) in the 400-700 nm wavelength range that is absorbed by a canopy. However, this can include over-storey, understory and ground cover elements (Gower et al., 1999; Fensholt et al., 2004). It can be said then that fAPAR expresses the energy absorption capacity of a vegetation canopy (Fensholt et al., 2004) and is a key input to a number of primary productivity models based on simple efficiency considerations from local to global scales (Prince,1991).

fAPAR is influenced by illumination conditions within a vegetation canopy. It varies with both sun position (solar zenith and azimuth angles) as well as atmospheric conditions (Weiss and Baret, 2011). Due to this, it is

[1] Utilizing this definition, LAI is a dimensionless unit which characterises the canopy of a given ecosystem (Breda, 2003). Multiple authors have identified issues regarding the application of this simplistic LAI definition (Hill et al., 2006; Zheng & Moskal, 2009, amongst others). Issues identified include the inability of this definition to accommodate needle-leaf canopies and those canopies characterised by vertical (erectophile) leaf angle distributions (Hill et al., 2006). This is particularly relevant to Australia, given the needle-leaf forms of frequently occurring species like Callitris, Casuarina and Acacia as well as the vertical leaf structure typical of Eucalyptus species (Hill et al., 2006). Such issues have resulted in a variability of LAI definition (see Zheng & Moskal, 2009 for a review). Consequently, there is a need to ensure the standardised definition, and appropriate documentation of all field based LAI measurements.

imperative that field validation of fAPAR is undertaken throughout the day under a variety of illumination conditions.

Similar to LAI, there are multiple satellite derived fAPAR products that are available to the science community including MODIS, POLDER, GLOBCARBON and CYCLOPES (Table 6.2). Such global products are supplemented by a number of regional fAPAR mapping projects that usually overlap/coincide with LAI mapping projects as the two products are closely related.

Table 6.2
Exemplar global fAPAR mapping projects available to the community (adapted from Weiss et al., 2007).

Project	Agency	Sensor(s)	Website
NASA	MODIS	MODIS	http://modis-land.gsfc.nasa.gov
MGVI	ESA	MERIS	http://ntrs.nasa.gov/search.jsp?R=20010106090
POLDER	CNES	POLDER	http://smsc.cnes.fr/POLDER/A_produits_scie.htm
MERIS	ESA	MERIS	http://www.brockmann-consult.de/cms/web/beam/
CYCLOPES	European Union (FP5 project)	VGT	http://toyo.mediasfrance.org/?Projet-CYCLOPES,18

6.2 LAI Validation

LAI products are validated by collecting LAI measurements across a range of scales, the largest of which consists of ground-based measurements. These can be compared directly against the coarse resolution LAI product values, as has been done to validate MODIS collection 4 LAI in Australia using hemispherical cameras to derive ground-based measurements of LAI (Hill et al., 2006; Sea et al., 2011). Validation can also be achieved by up-scaling observations to the coarse resolution satellite product. As will be described in the next section, ground based measurements can be obtained directly when leaf area is physically measured or indirectly, by inferring from other variables through observation or through the application of allometric equations as will be described below. Although direct methods are believed to be more accurate since they avoid issues associated with foliage clumping and leaf angle distribution, they are much more labour intensive and infeasible in many cases (Breda, 2003; Jonckheere et al., 2004). Chapter 2 has reviewed several sampling designs that can be used for indirect LAI validation.

On a global scale, multiple agencies that are brought together under the CEOS WGCV - LPV subgroup have been working together to validate moderate resolution LAI products (Table 6.3). A thorough review of these projects is provided by Morisette et al., (2006) with a summary given below:

- Boston University is responsible for the development of the NASA Earth Observing System (EOS) LAI products. Validation activities focus on the refinement and validation of LAI products and the algorithms driving the development of these products.
- The Validation of Land European Remote sensing Instruments (VALERI) program, primarily supported by CNES and INRA, focuses on the development of methodological approaches to support (a) the up-scaling of field measurements to generate high-spatial resolution maps of biophysical variables; and (b) the subsequent utilisation of these products to validate moderate resolution global products (Baret et al., 2005).
- The BigFoot program (1999 – 2003) grew out of projects that aimed to characterise Long Term Ecological Research (LTER) sites across the United States. The BigFoot project focuses on the validation of the MODIS derived LAI, land cover and net primary productivity land products (Cohen et al., 2006).

- The Canadian Centre for Remote Sensing (CCRS) produced LAI maps for Canada which have been validated across over 250 forest and shrubland dominated LAI plots. These 250 LAI plots were located in 10 study areas and aimed to sample a variety of Canadian forest types.
- The University of Alberta LAI studies focus on tropical forest regions. Satellite imagery, for both dry and moist tropical forest sites are used to study the relationship between field derived LAI and high-resolution satellite products.
- The United States Environmental Protection Authority (EPA) has conducted research to quantify error in the MODIS LAI product. The EPA has measured LAI (between 2001 and 2005) at six forested sites in North Carolina and Virginia in the United States of America.
- Research for the CARBOEUROPE project is conducted in Italy by the University of Milano-Bicocca. LAI measurements, sampled at 13 sites, have been collected with the aim of (a) developing localised relationships between canopy properties and carbon exchanges; and (b) validating moderate resolution, satellite derived LAI map products.
- The University of Helsinki, Finland, is working to develop more accurate LAI estimation methodologies within boreal conifer dominated regions.
- Penn State University's research focuses on the MODIS LAI products and their integration into crop models. The validation components of this research focus on the quantification of LAI uncertainty in products derived on corn, soybean and rice fields.

In addition, the CEOS WGCV - LPV has produced a global LAI product validation protocol (CEOS. 2014). This is a comprehensive review of current global LAI product validation methods and measurement techniques that also includes recommendations aimed at LAI product producers, LAI validation groups, the wider Science community, and CEOS. This is a valuable resource that includes definitions of key terms and good practice knowledge around validation procedures of satellite products. It is available to the wider community through the CEOS WGCV LPV website (http://lpvs.gsfc.nasa.gov/LAI_home.html).

There is also an On Line Interactive Validation Exercise (OLIVE) that allows the user community to quantify the performances of Earth observation land products (LAI, fAPAR, and FCOVER). It provides reliable and consistent information on the accuracy and associated uncertainty of EO products using standards defined by the CEOS - LPV subgroup (Weiss et al., 2014). OLIVE *(http://calvalportal.ceos.org/olive)* is fully supported by the CEOS/LPV subgroup and allows users to reach Stages 2 and 3 of the validation process. In other words, it allows estimates of product accuracy over a significant set of locations and time through an inter-comparison exercise between existing products. Product uncertainty is quantified using reference in situ data over multiple locations representative of the Earth's surface. OLIVE is expected to eventually reach Stage 4 of the validation process following regular updates and an increasing participation of the scientific community.

Currently, OLIVE is running in beta mode. The scientific community can access it to validate and inter-compare new products to existing ones. A validation exercise can be achieved in a private (results only accessible to user) or public mode (access to the whole OLIVE community).

Table 6.3 Exemplar LAI validation campaigns, as outlined by Morisette et al., 2006.

Group	Field Instruments	Conversion of PAI to LAI	Understorey correction	Site extent	Sampling scheme	High resolution imagery	Transfer function	Accuracy of high-resolution LAI map	Sensor used
Boston University	LAI-2000	No	Yes	Various: from 5x5 km to 10x10 km	Two-stage	Landsat ETM+ (future: ASTER)	Parametric regression Fine-resolution MODIS algorithm	Derived from regression equations	MODIS
VALERI	LAI-2000 DHP	No	Yes	3x3 km	Two-stage	Landsat ETM+ SPOT HRVIR/HRG (future: ASTER)	Parametric regression Kriging	Cross validation and kriging variance	MODIS VEGETATION MERIS POLDER AVHRR
BigFoot	LAI-2000 Allometry Destructive harvest	No	No	5x5 km	Two-stage	Landsat ETM+ (future: ASTER)	Reduced major axis regression	Cross validation	MODIS
CCRS	LAI-2000 TRAC DHP	Species-based conversion factors	No	10x10km 150x150km	Two-stage	Landsat TM/ETM+	Parametric regression	Derived from regression equations	VEGETATION MODIS POLDER
University of Alberta	LAI-2000 DHP Litter traps	Using DHP from dry season and calibration from leaf litter and specific leaf area data	No	10x10km	Two-stage	Landsat ETM+ Hyperion IKONOS/Quickbird	Parametric & non-parametric regression, Bayesian network and Neural network	Calibration for dry forest	MODIS
US EPA	DHP TRAC	No	Yes (on two sites)	1x1km to 2x2km	Two-stage	Landsat ETM+ IKONOS	NA	NA	MODIS
Italy	LAI-2000 DHP Destructive harvest	No	Yes	From 250x250m to 1x1 km	Two-stage	Landsat ETM+ Hyper-spectral airborne	Parametric regression	Derived from regression equations	MODIS
Finland	LAI-2000	No	No	1x1 km (two sites) 3x3 km (two sites)	One-stage Two-stage	Landsat ETM+ SPOT HRVIR	Parametric regression	Derived from regression equations	MODIS
Penn State	LAI-2000 AccuPAR	No	No	1.6x1.6 km	One-stage	ASTER	In progress	NA	MODIS

6.2.1 Direct field measurement of LAI

Direct measurements of LAI are based on the measurement of leaf area where leaves are collected via techniques such as harvesting and litter collection. Area harvesting techniques require the periodic, destructive sampling of all vegetation within the sample plot during the growing season (Gower et al., 1999). Such destructive harvesting of a sample plot is based on the up-scaling of measurements to the vegetation patch or stand and, as a consequence, assumes lateral homogeneity. In other words, it is assumed that the plot is representative of the stand (Jonckheere et al., 2004).

In deciduous stands, an additional measure of leaf area can be estimated from litter traps. The advantage of this approach is that it is non-destructive. Litter traps are based on the collection of leaf litter from a specified ground area. Multiple collections are made over the leaf fall period to prevent the loss of leaf material due to decomposition processes (Breda, 2003). LAI is estimated from the accumulated leaf area over all leaf fall collections and thus represents an integrated measure of LAI over the measurement time period. However, authors note that the litter trap collection cannot provide estimates of LAI (a) at a single moment in the growing season nor (b) within temporal or vertical profiles (Jonckheere et al., 2004). At the same time, there is no consensus on the location or sample design of litter traps (Jonckheere et al., 2004), therefore extensive experimental documentation is essential.

Subsequent to leaf collection via harvesting or litter collection, leaf area is calculated within planimetric or gravimetric approaches. The first are based on a contour assessment, and subsequent area calculation, of the leaf in a horizontal plane (Jonckheere et al., 2004). Various planimeters are available for this purpose. Conversely, gravimetric methods correlate the dry weight of the leaves to leaf area. Such measurements are typically applied to a sub-sample of leaves in order to develop a relationship between area and dry mass, that is, the specific leaf area (SLA, $cm^2\ g^{-1}$).This leaf area (SLA) to mass ratio is variable as a function of both species and site characteristics (Breda, 2003).

The harvesting of all vegetation, within a predefined sample plot, is widely utilised when measuring the leaf mass of crop or pasture areas (Breda, 2003). However, the exhaustive, potentially time consuming (Jonckheere et al., 2004) and destructive characteristics of this technique limit its applicability to forest canopies (Breda, 2003). Consequently, allometric measurements are more frequently used within forested canopies.

6.2.2 Indirect field measurement of LAI

Indirect techniques typically infer leaf area from observations of another variable. Such techniques are generally less destructive and time consuming than the previously outlined direct approaches. Jonckheere et al. (2004) classify indirect, ground-based LAI measurement techniques into two categories (a) indirect contact LAI measurements; and (b) indirect non-contact LAI measurements. Such a categorisation will be utilised in the following discussion.

Indirect contact LAI measurements

Allometric techniques establish a relationship between leaf area and the dimension of woody elements within a tree. For example, established allometric equations can relate leaf area (determined via destructive harvest), to the sapwood area at tree breast height or the crown base (Jonckheere et al., 2004). Such equations are based on the assumption that leaf area is in balance to the amount of connective tissue

within the tree (Breda, 2003). Proposed modifications to this relationship include the inclusion of sapwood permeability (Jonckheere et al., 2004). The complexity of quantifying sapwood diameter and permeability (Breda, 2003; Jonckheere et al., 2004) has led to the development of multiple allometric equations which are not reliant upon this measure. Frequently utilised woody measurements include stem diameter, stem density, tree height and crown base height (Jonckheere et al., 2004; Jupp et al., 2008).

Allometric relationships have been demonstrated to be site and time specific (Breda, 2003; Jonckheere et al., 2004). Equally, sapwood area/leaf area relationships have been shown to be dependent upon tree size, season, nutrient

availability, soil water availability, local climate and canopy structure (Gower et al., 1999; Jonckheere et al., 2004). Such abiotic and biotic factors can result in moderate to large errors in LAI derivation for a stand when general allometric relations, as opposed to stand-specific ones, are implemented (Gower et al., 1999).

There are additional techniques capable of providing indirect measures of leaf area. One of these is the line-intercept method, which involves conducting a vertical transect through the canopy under known elevation and azimuth angles (Jonckheere et al., 2004).

Indirect non-contact LAI measurements

Indirect, non-contact techniques frequently rely on optical instruments that make use of radiative transfer theory to infer LAI from measurements of radiation transmission through the canopy (Breda, 2003; Jonckheere et al., 2004). Such techniques are advantageous in that they are non-destructive. Indirect measurements do not, typically, estimate LAI given they usually consider all canopy elements (woody and non-woody) within their field-of-view; as opposed to measuring only the green leaf area. Consequently, the terms Plant Area Index (PAI) or Surface Area Index (SAI) are commonly utilised when estimating LAI via indirect measurement techniques (Breda, 2003).

Multiple optical instruments indirectly estimate LAI from measurements of the canopy gap fraction, where canopy gap fraction is derived from measurements of radiation transmission through the canopy. LAI is calculated by inversion of the exponential expression of the gap fraction. Gap fraction or gap probability '*Pgap*' may be defined as the proportion of canopy gaps visible in a given viewing direction. LAI is a function of several structural attributes that affect the extinction of light within plant canopies and consequently the remote sensing signal, namely the; (i) proportion and density of leaf and non-leaf components (these attributes combine to give the metric PAI (ii) canopy element angle distribution, and (iii) degree of canopy element clumping. Each of these structural attributes can vary substantially with viewing angle, scale, and environment, even amongst stands of the same species. The physical formulation of LAI and canopy gaps is based on the Beer-Lambert law, relating the attenuation of light to the properties of the material through which the light is travelling (Lambert, 1760). Nilson (1971) demonstrated how the directional gap probability $Pgap(\Phi, \theta)$ (Φ = azimuth angle, θ = zenith angle) of an incident beam of radiation will pass through a clumped canopy to reach a given point inside or below the canopy using the modified Beer-lambert law of light extinction. Chen et al., (1996) modified Nilson's formulation to account for the proportion of woody elements 'α', which was subsequently modified by Woodgate et al., (under review, AFM) to account for the angular nature of woody elements:

$$LAI = \frac{-\log P_{gap\,T}(\theta)\cos(\theta)(1-\alpha)}{G_T(\theta)\Omega_T(\theta)} \qquad \textit{(equation 6.1)}$$

Where $Pgap_T(\theta)$ is the gap probability of all canopy elements (i.e. leaf and wood), $G_T(\theta)$ is the combined projection coefficient of wood and leaf elements, $\Omega_T(\theta)$ is the total clumping factor of all canopy elements, and α is the woody-to-total-area ratio. $\cos(\theta)$ is the correction for path length through the canopy, which increases with higher zenith angles. α relates the woody projection function 'G_W' and leaf projection function 'G_L' coefficients to the total element projection function 'G_T' by:

$$G_T(\theta) = (1- \alpha)G_L(\theta) + \alpha.G_W(\theta) \qquad \textit{(equation 6.2)}$$

Eqn. 6.1 assumes a random orientation in azimuth angle for both woody and leaf components. In many cases this would be a valid assumption for woody components since; (i) for typically cylindrical vertical tree stems, a large proportion of the woody surface area is in the stem, and (ii) most stem and branch components in the trunk are circular in nature, and typically spread radially throughout the branching orders, thus leading to a more equal probability of occurrence in all azimuth directions. Therefore, the projected area of leaf and woody canopy elements becomes a function of only zenith view angle when this assumption is satisfied.

Most plant canopies are typically clumped to some degree, which is scale dependent. Chen et al. (1997) proposed that without correction for non-random canopy element distribution, the result is the effective LAI (LAI_e) or effective PAI (PAI_e), depending on whether a correction for α was made or not. $\Omega(\theta) = 1$ occurs when the spatial distribution of elements are random, $\Omega(\theta) < 1$ implies a clumped or aggregated canopy, and $\Omega(\theta) > 1$ implies a regularly distributed canopy, where less gaps are visible than a theoretically random canopy with the same PAI and $G(\theta)$. The authors state that with multiple angle measurements of $Pgap(\theta)$ and $G(\theta)$, the PAI_e can be calculated simultaneously. Additionally, single narrow angular gap fraction of approximating single view zenith angles has also been used to estimate PAI_e

(Neumann et al., 1989; Leblanc & Chen, 2001). However, without knowledge of the spatial distribution of leaves within the canopy (Ω) only the product of Ω and PAI can be calculated. Chen et al. (1997) utilise PAI_e for the derivation of LAI in clumped canopy comprising both leaf and wood elements following the equation:

$$LAI = (1 - \alpha)\frac{PAI_e}{\Omega} \qquad \textit{(equation 6.3)}$$

where α is the woody-to-total plant area ratio and Ω is a parameter determined by the spatial distribution of leaves within the canopy. PAI_e is typically measured at the ground surface and includes the contribution of dead leaves, woody branches and trunks. As such, measurements represent SAI or PAI. A factor (1 - α) is used to remove the contribution of non-leafy surfaces from the PAI_e measurement (Chen et al., 1997). Note that PAI_e in Eqn. 6.3 is equivalent to $-\log(Pgap_T(\theta)).\cos(\theta) / G(\theta)$. Also note that $(1 - \alpha).PAI_e = LAI_e$.

An important element of equation (6.3) is the fact that PAI_e can be calculated without prior knowledge of the foliage angle distribution if the gap fraction is estimated at multiple zenith angles (Chen et al., 1997) using a modified version of Miller's formula Miller (1967):

$$PAIe = 2\int_0^{\pi/2} -\ln\left(P_{gap}(\theta_v)\right)\cos\theta_v \sin\theta_v \, d\theta_v \qquad \textit{(equation 6.4)}$$

$$W_i = d\theta_i.\sin\theta_i \; / \sum_{i=1}^{i=n} d\theta_i.\sin\theta_i \qquad \textit{(equation 6.5)}$$

where *Pgap* denotes the gap fraction and ϑ_v denotes the view zenith angle. $Pgap(\theta_v)$ is averaged per zenith ring, where each ring has a ring centre angle ϑ_i and angular width $d\vartheta_i$. *i* denotes the zenith ring number, *n* is the number of zenith rings. Utilising zenith rings allows discretisation of the instrument field-of-view into smaller zenith segments in order to compute multiple *Pgap* estimates for input into Eqn. 6.4. The sum of W_i, the zenith ring weighting function (Eqn. 6.5), for all *n* is equal to unity. LAI_e can be calculated from Eqn. 6.4 using angular *Pgap* measurements. The correct method for estimating LAI_e from multiple measurement locations, such as a plot, is to first average the angular *Pgap* over all measurement locations, and then apply Eqn. 6.4 (Ryu et al., 2010). This ensures no correction for non-random distribution of clumping at scales larger than the measurement location, caused by the potential logarithmic averaging of LAI_e that may occur at multiple measurement locations (Kucharik et al., 1997; Ryu et al., 2010).

The extinction coefficient *k*

Monsi and Saeki (1965) provided a theoretical relationship of light extinction coefficient *'k'* to LAI in a plant community based on a form of the Beer-Lambert law (Lambert, 1970). Their model provided a basis for many subsequent studies, both experimental and theoretical, and continues to be used to this day:

$$\frac{I}{I_o} = \mathrm{e}^{-k.LAI} \qquad \textit{(equation 6.6)}$$

where *I* is the light intensity under the LAI layer, I_o is the light intensity above the LAI layer, and *k* is the extinction coefficient. The ratio $I:I_o$ is equivalent to light transmittance or *Pgap* at the point of measurement.

k is essentially a function of leaf clumping, leaf angle projection and view zenith angle when the assumption of a horizontally continuous canopy with no woody elements is met. However, this model has been further expanded to account for the impact of woody components on the element projection function and clumping (Woodgate et al., under review, AFM). A parameterisation of *k* is as follows for a canopy with foliage and woody elements:

$$k(\theta) = G_T(\theta)\Omega_T(\theta)/\cos(\theta)(1 - \alpha) \qquad \textit{(equation 6.7)}$$

Eqn. 6.7 can be modified for the case of an individual tree encompassed by a geometric volume or object, such as a cylinder, as follows:

$$k(\theta) = G_T(\theta)\Omega_T(\theta)/l_{ave}(\theta)\,(1 - \alpha) \qquad \textit{(equation 6.8)}$$

where l_{ave} is the average path length through the geometric volume encompassing the tree. Eqn 6.7 incorporates clumping at all scales, e.g. between crown and within crown. Eqn. 6.8 incorporates within-crown clumping only for crowns encased in a geometric shape.

We know that *k* is a function of G and Ω, which are both independently measureable quantities. Therefore, Woodgate et al., (*under review, AFM*) recommended splitting *k* into its measureable sub-components so that assumptions and its derivation are explicit. This makes *k* more comparable for other studies, and also enables uncertainty estimates to be placed on the metric. A general outline of independent methods to estimate each parameter of *k* (Eqn. 6.7, 6.8) and LAI (Eqn. 6.1) are presented.

Canopy gap fraction '*Pgap*'

Multiple canopy analysers, based on the above principles, measure the transmittance of radiation through the canopy. These instruments include, but are not limited to, the (a) SunSCAN (Delta-T Device Ltd, Cambridge, UK); (b) AccuPAR ceptometer (Decagon Devices, Pullman, USA); (c) LAI-2200 plant canopy analyser (Li-Cor Inc., Lincoln, Nebraska, USA); (d) DEMON instrument (CSIRO); and (e) Terrestrial Laser Scanning (TLS) (Table 6.4). Such devices differ in their measurement characteristics. For example, the SunSCAN and AccuPAR devices measure the incident and transmitted photosynthetically active radiation (PAR) while the LAI-2200 measures the canopy gap fraction from multiple zenith angles (Table 6.4). Transmittance is analogous to *Pgap*. When optimal instrument lighting conditions are met, the difference between transmittance and *Pgap* are negligible; such as uniform diffuse lighting with a uniform sky background or conversely direct lighting conditions (Table 6.4). In both instances, the optimal lighting conditions are stable; and the foliage is assumed to be black with no multiple scattering of radiation, which is more prevalent in direct sunlit conditions.

Table 6.4
LAI/PAI canopy analysers (adapted from Breda, 2003). Ordered from left to right in popularity for frequency of use.

	DHP	LAI-2200	AccuPAR	SunScan	TRAC	TLS	DEMON
Company	Many specialised and non-specialised	LI-COR, Lincoln, Nebraska, USA	Decagon Devices, Pullman, ISA	Delta-T Devices Ltd, Cambridge, UK	3rd Wave Engineering, Ontario, Canada	Many commercial and some non-commercial	CSIRO
Principle	Gap fraction for each zenith angle acquired simultaneously	Gap fraction for each zenith angle acquired simultaneously	Gap fraction or sunflecks	Gap fraction or sunflecks	Gap size distribution from transects at one zenith angle	Gap fraction for each azimuth and zenith angle with range to target recorded	Gap fraction zenith angles from the sun at different angles to the vertical
Waveband	400-700nm typical	320-490 nm	400-700 nm	400-700 nm	400-700nm	900nm, 1550 nm typical	430 nm
Illumination conditions	Uniform overcast sky or clear sky at sunset or sunrise	Uniform overcast sky or clear sky at sunset or sunrise	Wide range of daylight condition. Best in bright sunlight	Wide range of daylight condition. Best in bright sunlight	Direct sunlight conditions on a clear day	Day or night	Clear bright day from early morning until noon
Wood-leaf separation	Yes	No	No	No	No	Yes	No

Correction for the proportion of woody material '*α*'

Frequently, it is hard to distinguish foliage from woody elements such as branches and trunks using indirect methods such as DHP and TLS. Because of this, PAI is derived instead of LAI. An area under current investigation is the separation of woody from non-woody elements from indirect techniques. The separation of leaf and wood can be used to estimate the proportion of woody to total plant area 'α'. Techniques used to estimate alpha include: destructive harvesting (Gower

et al., 1999), classification of woody and non-woody canopy elements with RGB DHP (Sea et al., 2011) or near-infrared cameras (Fig. 6.2, Kucharik et al., 1998), and Terrestrial Laser Scanning (Béland et al., 2014; Danson et al., 2014).

Foliage and Wood angle distribution and projection functions 'G_L' and 'G_W'

The leaf and non-leaf (wood) element angle distributions are used to characterise the projected leaf area (G_L) and wood area (G_w) as a function of viewing angle. A number of direct and indirect techniques to measure leaf inclination angles exist (e.g. directly with a plumb-bob and protractor or indirectly from levelled photos, Ryu et al., 2010). Replicating leaf angle measurement techniques on woody components may be challenging. However, due to recent advances in semi-automated tree reconstruction methodologies (Côté et al., 2009; Raumonen et al., 2013), 3D computer reconstruction models can be efficiently queried to determine the element distribution functions and subsequently to derive G_W and G_L precisely. Conversely, LAI_e and PAI_e can also be estimated without prior knowledge of the foliage and wood angle distribution at the narrow zenith angle range centered on $\Theta \approx 57.3$ degrees, where foliage angle projection functions (Wilson 1963; de Wit, 1965) and wood angle projection functions (Woodgate et al., under review, AFM) have been shown to converge. Therefore, both G_L and G_W may not need to be measured in the field if inverting over a narrow gap fraction range ($\pm \approx 2.5$ degrees) centered on the 57.3 degree zenith angle.

Figure 6.2 Infrared camera (Canon EOS 450D with the Sigma 8mm EX fisheye lens) used in the Robson Creek rainforest in Far North Queensland. The use of infrared cameras can assist distinguishing woody versus non-woody elements in a canopy.

Canopy element clumping 'Ω'

A number of instruments employ clumping retrieval methodologies, which are typically based on logarithmic averaging of *Pgap* or gap size distribution information (Leblanc et al., 2014). DHP can be utilised to estimate various clumping retrieval methods such as the: 'LX' (Lang and Xiang, 1986), 'CCL' (Chen & Cihlar, 1995) later modified by Leblanc (2002a), 'CLX' (Leblanc et al., 2005), and 'CMN' methods (Pisek et al., 2011), all following nomenclature by Leblanc et al., (2014). The LAI-2000/2200 instruments employ the LX method, and the TRAC instrument employs the CCL method. Other methodologies such as Jupp et al., (2008), which was developed for TLS, may subsume clumping values into their final PAI estimate. An exemplar procedure for estimating clumping from DHP is provided in **section 6.4.1.**

Some typical indirect non-contact instruments that are used to estimate LAI in the field are outlined below.

- **Digital Hemispherical photography (DHP)**

Hemispherical photography is a technique for quantifying plant canopies via photographs captured through a hemispherical or fisheye lens (Figure 6.1). Such photographs can be captured from beneath the canopy, looking upwards, (orientated towards zenith) or above the canopy looking downwards (Jonckheere et al., 2004). Hemispherical photographs produce a projection of the hemisphere onto a plane. The nature of this projection is a function of the lens utilised. However, the simplest and most common hemispherical lens geometry is the polar or equi-angular projection (Jonckheere et al., 2004).

With increases in the availability of digital cameras and image processing software digital hemispherical photography (DHP) is increasingly being used in addition to or as a replacement for other canopy analysers (Breda, 2003). DHP represents a rapid, low-cost and non-destructive methodology for the (a) estimation of LAI (Jupp et al., 2008); and (b) creation of a permanent canopy structure records. Such records include species, site and age-related differences in canopy architecture (Jonckheere et al., 2004).

Multiple software packages are available to support the derivation of canopy gap fraction, and its subsequent conversion to LAI, from DHP. For example, CAN-EYE was developed as part of VALERI (Baret et al., 2005). This dedicated image processing software is required to separate sky (or soil for downward looking) and plant canopy elements in the photographs, derive the canopy gap and subsequently convert the gap fraction to LAI. Determination of an appropriate threshold to separate these elements is fundamental to the accurate estimation of canopy gap fraction and LAI via these techniques (White et al., 2000).

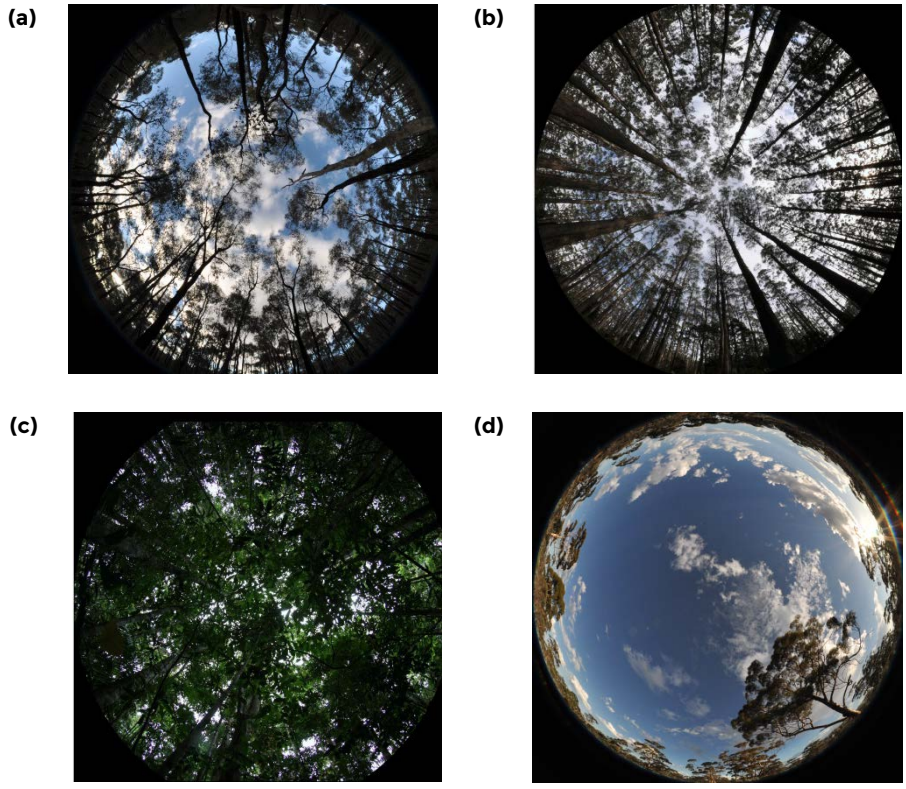

Figure 6.3 Examples of DHP in various forest environments:
(a) Dry sclerophyll forest near Nagambie, Victoria^;
(b) Mountain Ash forest near Watts Creek, Victoria^;
(c) Wet tropics rainforest in Robson Creek, Far North Queensland (EOS 50D with a Sigma 8mm EX fisheye lens);
(d) Great western woodlands near Kalgoorlie, Western Australia^. ^ denotes the Nikon D90 with a Sigma EX 4.5mm circular fisheye lens.

Hemispherical cameras also have the advantage of (a) enabling efficient estimates of canopy clumping through various gap size inversion techniques (Leblanc et al., 2014); (b) being applicable in low and high canopies (by taking downward and upward looking photographs); (c) less sensitive to variable illumination conditions; and (d) are a permanent record

of canopy structure, when compared to the LAI-2200. Such advantages have led to the progressive replacement of LAI-2200 measurements with DHP within the VALERI project (Baret et al., 2005).

- **LI-COR LAI-2000 and LAI-2200**

The LAI-2200 Plant Canopy Analyser (and its predecessor LAI-2000) calculates the effective PAI from radiation measurements collected below 490 nm with a fisheye optical sensor (148° field-of-view) (LI-COR, 2009). Measurements collected above and below the canopy are used to determine the transmission of light, through the canopy, at five view angles simultaneously (LI-COR, 2009). PAI estimates derived via the LAI-2200 are based on four assumptions (a) the foliage is black, that is, no radiation is transmitted or reflected by the vegetation; (b) the foliage elements are small in comparison to the area of view of each sensor ring; (c) the foliage is randomly distributed; and (d) the foliage is azimuthally randomly orientated, that is, the leaves face in all compass directions (LI-COR, 2009). The LAI-2200 also computes an effective clumping factor (Ryu et al., 2010) of the canopy, which is an upper limit to the 'true' clumping factor indicating how much the canopy appears to depart from random distribution. Recently, a methodology was presented by (Chianucci et al., 2014), which improves the LAI-2200's ability to estimate clumping based on restricting the field-of-view with azimuth view caps to measure multiple angular segments at each location. Increasingly large corrections for foliage clumping are made as more restrictive view caps are utilised, based on the logarithm averaging that occurs at the scale larger than the sensors field-of-view (Ryu et al., 2010; Chianucci et al., 2014). Although the authors believe DHP methods comparatively offer greater efficiency for this method, only requiring one measurement per location, with the added advantage of applying multiple clumping retrieval methods (Leblanc et al., 2014).

The LAI-2200 configuration enables measurements in a range of canopies with methodological approaches utilising one or two LAI-2200 sensors attached to a single data logger (LI-COR, 2009). Measurements can be collected under a variety of sky conditions. However, diffuse lighting conditions such as those present at dawn and dusk as well as when the sky is uniformly overcast, represent the optimal operational conditions (LI-COR, 2009). If measurements are taken under non-diffuse conditions then an underestimation of the measured effective LAI of up to 20% can result from multiple scatterings of light radiation as it passes through the plant canopy. Even though multiple scattering effects can be corrected (see Leblanc and Chen, 2001, who were able to reduce the error in LAI_e measurements to within 2% and recommend the adoption of their methodology when collecting LAI measurements under non-diffuse conditions), it can be time consuming and require extensive calibration efforts therefore diffuse lighting conditions are recommended.

- **AccuPAR ceptometer**

The AccuPAR ceptometer measures the incident and transmitted photosynthetically active radiation (PAR). The device is optimal for low and regular canopies (Breda, 2003). The ceptometer integrates instantaneous fluxes of PAR radiation along a probe or wand which consists of a series of sensors sensitive to wavelengths in the region of 400-700 nm (White et al., 2000; Breda, 2003). Measurements are repeated both above and below the canopy in order to characterise incident and transmitted PAR. Ceptometer measurements should, ideally, be collected in bright sunny conditions within one hour of solar noon (White et al., 2000).

- **Tracing Radiation and Architecture of Canopies (TRAC and TRAC II)**

The TRAC instrument (3rd Wave Engineering, Ontario, Canada) differs from those instruments outlined above in that it measures both the canopy gap fraction and canopy gap size distribution. Gap fraction, as previously outlined, is the proportion of gaps within a canopy at a given solar angle. Conversely, gap size is the physical dimension of the gaps between individual elements (Gower et al., 1999; LeBlanc et al., 2002).

As stated previously, the spatial distribution of leaves within a canopy cannot be assumed to be random. This is a direct consequence of foliage clumping. As a result, measurements based on an assumption of a random spatial distribution can underestimate LAI (Chen et al., 1997). Chen et al. (1997) demonstrate that gap size information can be related to the clumping index of a canopy hence the inclusion of this parameter within the TRAC device.

The TRAC device is based on the assumption that, as a consequence of non-random elements, the gap size distribution of a canopy contains multiple gaps. As the gap size distribution of a random canopy is known, gaps resulting from non-randomness can be identified and excluded from the total gap fraction accumulation; the gap fraction usually measured from radiation transmittance (LeBlanc et al., 2002). The difference between the measured gap fraction and gap fraction

derived subsequent to non-random gap removal is subsequently utilised to quantify foliage clumping within the canopy (LeBlanc et al., 2002). This clumping index then enables conversion of the effective PAI to PAI (Chen et al., 1997).

- **Plant Canopy Imager CI-110**

The CI-110 (CID Bio-Science, Camas, WA USA) is a similar instrument to DHP, but with lower resolution and an interface that enables the user to simultaneously capture wide-angle (hemispherical) plant canopy images and estimate PAI and PAR levels from a single canopy scan (Figure 6.3).

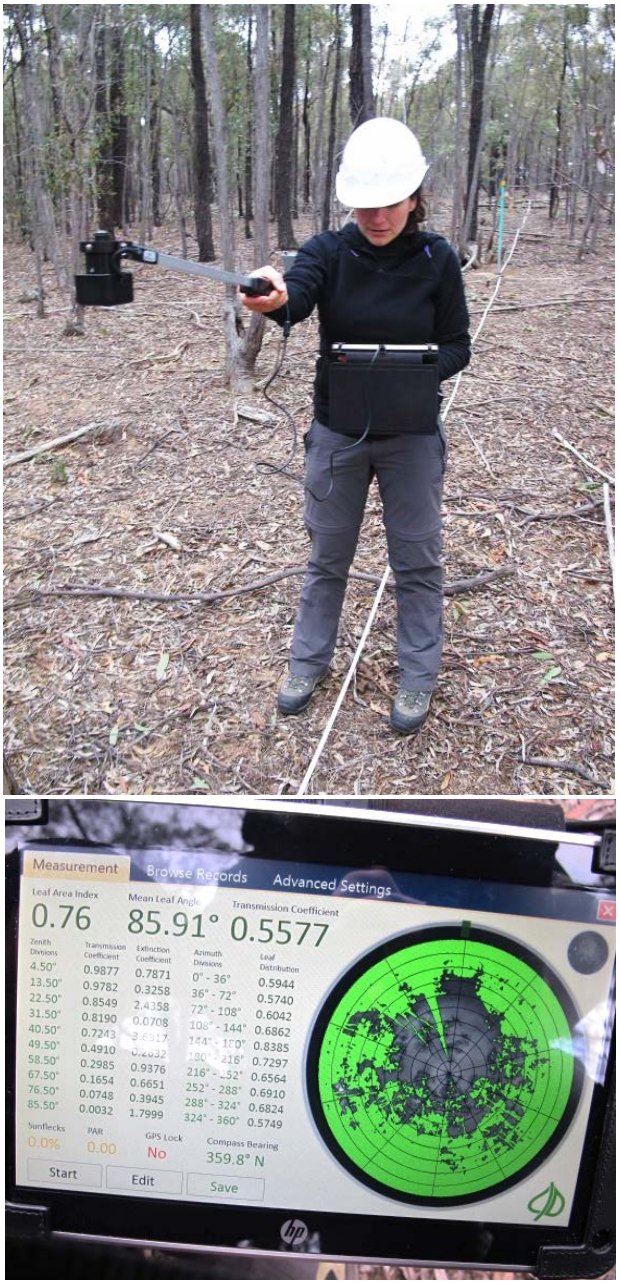

Figure 6.3 CI-110 canopy analyser. Photo on top shows measurements being acquired along a SLATS transect while photo below shows the graphical user interface of the instrument (note LAI measurement given on top left).

The CI-110 is a passive self-levelling imaging sensor. It has a 180^{o} FOV (field of view) and a 24 sensor PAR wand used to measure the amount of incident solar radiation in the visible spectrum. The sensor is GPS enabled and can be used under any sky conditions (even varying lighting conditions) due to the integrated optical filter that ensures that scattered radiation does not affect the sensor by restricting radiation above 490 nm. This minimises the effect of light scattered by foliage and allows measurements to be conducted from below or within the canopy under varied light conditions (CID Bio-Science Inc., 2012).

PAI, canopy transmission coefficients and mean leaf angle are calculated by the external CI-110 computer software from the gap fraction inversion procedure (Norman and Campbell, 1989). Although, inversion techniques where more than one variable is unknown should be treated with caution, such as in the previous example with both PAI and leaf inclination unknown. It is possible to calculate the PAI from a single image, however it has been found that a more accurate result is obtained for a field site when several readings and an average is taken. A recent comparison with high-resolution DHP methods was undertaken by Woodgate et al., (2015), which suggested that instruments unable to standardise exposure could cause issues for accurate *Pgap* from classified images in a range of forest environments and optimal lighting conditions. Advantages of high-resolution DHP cameras utilising RAW imagery have also been highlighted for more accurate classification of images (Jonkheere et al., 2005; Macfarlane et al., 2014).

- **Alternative approaches – Terrestrial Laser Scanning (TLS)**

In addition to the instruments outlined above, there is an increasing utilisation of active measurement techniques to estimate LAI. Such approaches are exemplified by the ground-based laser system, Echidna (Jupp et al., 2008) and many other similar commercial terrestrial laser scanners (such as the FARO Focus 3D 120, the Leica C10, Leica HDS7000 and the Riegl VZ1000). An advantage of active sensors such as terrestrial laser scanners is their relative insensitivity to lighting conditions, and additional measurement of range (Newnham et al., 2012). To compute the PAI from a ground-based laser scan, knowledge of the gap probability is required. The gap probability is defined as the probability of a gap appearing between the exit point of the sensor and the 'target' as a function of zenith angle (θ) and height above ground level (*z*) (Jupp et al., 2008). This can be computed from the laser scan itself. The gap probability is then expressed as:

$$Pgap(z,\theta) = e^{-G(\theta)PAI(z)/cos(\theta)} \quad \text{(equation 6.9)}$$

equation 5 is similar to equation 1, however in this case, $LAI(z)$ is the best estimate based on measurements of $P_{gap}(z,\theta)$ from multiple zenith rings, where $G(\theta)$ is the fraction of the leaf area projected on a plane normal to the zenith angle θ (Ross *G* function; Ross, 1981). This allows no separation of foliage and woody vegetation, so it is assumed that plant area index (PAI) is equal to the LAI. Although a correction for the proportion of woody material can be conducted post-hoc. To calculate the PAI from equation 5, the equation is simply inverted (Strahler et al., 2008):

$$PAI(z) = \frac{-ln\, Pgap(z,\theta)\, cos(\theta)}{G(\theta)} \quad \text{(equation 6.10)}$$

A number of alternative methods to derive PAI have been suggested. These are primarily based on gap probability theory (e.g. Hosoi et al., 2007; Béland et al., 2014; Moorthy et al., 2008; Huang & Pretzsch 2010). However, TLS remains challenging for large-area PAI characterisation due to (i) the high cost of commercial instruments, (ii) the limited scanning efficiency (caused by environmental factors combined with size and weight of instruments, and limited instrument capabilities of data processing, storage and battery life), and (iii) the ill-posed nature of the lidar beam interaction with canopy elements (Béland et al., 2014; Hancock et al., 2014).

TLS limitations are progressively being overcome with the development of new scanners and collaboration between researchers, both in the research and commercial domains. For example, the latest ECHIDNA design (Dual-Wavelength ECHIDNA Lidar – DWEL) incorporates two lasers of different wavelength that produce a vegetation index from the intensity of the reflected laser energies. This allows the vegetation to be both structurally and functionally assessed. This design also enables the separation of woody and non-woody vegetation material thus allowing the true LAI value to be calculated.

Furthermore, collaborative research groups such as the Terrestrial Laser Scanner International Interest Group (TLSIIG) are undertaking activities to further the understanding and application of TLS for assessment and monitoring of vegetation dynamics and parameters (TLSIIG, 2014).

Canopy-analysers comparison: LAI Estimation

The footprint of each of the outlined canopy analysers varies as a function of (a) the device utilised; and (b) the canopy sampled. For example, when utilising the LAI-2200 and DHP, with observations between 60 and 70 degrees from the zenith, the footprint of the instruments will correspond to a 150 metre diameter disk in forests (up to 40 metres in height). Conversely, in very short canopies the footprint is reduced to less than 2 metres (Morisette et al., 2006). For the AccuPAR and TRAC devices, the footprint is dependent upon the sun zenith angle and tree height (Morisette et al., 2006). Equally,

in comparison to other instruments, the TRAC device is based on a measurement transect and will therefore result in a rectangular footprint. The length of this footprint is determined by the transect length, the width by the solar angle and canopy height (Morisette et al., 2006).

Several authors report the underestimation of PAI via indirect measurement techniques, a consequence of the non-random distribution of foliar elements within the canopy and therefore violation of the assumptions supporting PAI estimation (Chen et al., 1997; Breda, 2003). As stated previously estimates of spatial clumping, inferred from the gap size distribution, can be utilised in the conversion of effective PAI to PAI as demonstrated by the TRAC instrument (Chen et al., 1997). However, given the complexity of measuring canopy gap size distribution (and its reliance on a TRAC instrument) simplified measures of clumping index have been derived based on (a) the ratio of the crown depth to crown diameter (Gower et al., 1999); and (b) an estimate of gap size distribution as derived from DHP (cf. Leblanc et al., 2014).

A further discrepancy between direct and indirect LAI estimates, specific to woody vegetation types, is the result of indirect methods calculating PAI as opposed to LAI. This is a direct consequence of optical techniques including non-green elements, that is, woody branches and stems in LAI measurements. The accurate measurement of LAI therefore requires the calculation of contributions from woody vegetation elements (Chen et al., 1997; Breda, 2003). Multiple methodologies for the derivation of LAI from PAI are proposed in the research literature (see section 6.2.2 *Correction for the proportion of woody material 'α'* and Breda (2003) for a comprehensive review).

The spatial and temporal relevance of ground-based LAI measurements is an important consideration (Breda, 2003). For example, the timing of sampling should consider seasonal (natural and incident) variation in LAI (Breda, 2003). Equally, the spatial variability of the canopy will influence the required number and spatial arrangement of LAI measurements. When LAI is estimated indirectly from gap fraction or radiation attenuation measurements, the number of measurements required to estimate LAI with a given accuracy is a function of canopy heterogeneity (Gower et al., 1999). Another key consideration is which zenith angles are to be used for analysis from indirect instruments. As previously discussed, PAI can be inverted over a range of zenith angles, or a single zenith angle, which in turn affects the sampled canopy proportion, with higher zenith angles (60 degrees) sampling a larger area than near zenith.

Multiple studies compare LAI as derived from direct and indirect measurement techniques (Whitford et al., 1995; Gower et al., 1999; White et al., 2000; Breda, 2003; Coops et al., 2004). Gower et al. (1999) concluded that overall, direct and indirect estimates of LAI were within 25 to 30% for most canopies. Although, it should be noted that improvements to indirect LAI retrieval techniques and methodologies have been made since. However, the authors note that indirect estimates of LAI reach asymptote at approximately five or six. This is in comparison to direct measurements which reached a LAI of nine in the study area. The authors conclude that the saturation of gap fraction techniques at LAI values approaching five or six necessitates the direct measurement of LAI for canopies expected to have LAI values greater than this threshold (Gower et al., 1999). This finding warrants further research utilising the latest independent structural parameters retrieval methods.

6.2.3 Recommendations and areas for improvement

A comparison of current LAI validation programs as shown in Table 6.3 suggests that indirect techniques are primarily used for the ground-based estimation of LAI. This is because indirect techniques can measure large areas of land more efficiently than direct techniques. LAI is typically estimated via four optical instruments (a) the LAI-2200 plant canopy analyser; (b) the AccuPAR ceptometer; (c) digital hemispherical photography (DHP) and (d) the Tracing Radiation and Architecture of Canopies (TRAC) instrument (Table 6.3).

Although utilised, the inclusion of destructive (direct) LAI measurements is limited. Equally, it should be noted that multiple validation programs include more than one LAI estimation technique (Table 6.3). Such a trend was reflected in the BigFoot project which utilised (a) direct measurements including periodic harvest for non-forest sites and the application of allometric relationships at forested sites and (b) indirect LAI estimation techniques, LI-COR LAI-2000 as a function of vegetation type and date (Morisette et al., 2006). In an Australian context, Hill et al. (2006) estimated LAI, via ground-based measurements, using (a) hemispherical photography at a tropical rainforest site in North Queensland; (b) LI-COR measurements in remnant forests within New South Wales; and (c) tree and understory hemispherical photography in both central Queensland and North East Victoria.

Given the variety of techniques and instruments available for measuring LAI, the most appropriate instrument is likely to be a function of the canopy structure and study area characteristics (White et al., 2000). Jonckheere et al. (2004) conclude that an ideal device for measuring LAI should (a) be a hemispherical sensor that simultaneously measures the canopy gap fraction at a range of zenith angles, thus ensuring a more efficient sample than can be achieved with linear sensors; (b) permit the derivation of gap size distribution in order to provide information on leaf clumping; (c) enable the identification of green and non-green canopy elements; and (d) permit a characterisation of LAI over low vegetation canopies by looking downwards. The authors conclude that such characteristics can be achieved using a hemispherical camera based approach.

Areas for continued research are the standardisation of (a) field approaches for DHP data collection; (b) segmentation/classification into green and non-green elements; (c) the computation of the woody projection function (Woodgate et al., under review AFM), and (d) the definition of appropriate exposure, spectral, radiometric and spatial resolution settings required to ensure rigorous data collection (Jonckheere et al., 2004; Macfarlane et al., 2014).

6.2.4 Australian canopies and LAI

Hill et al. (2006) state that in Australia all satellite, airborne, or ground-based measurements of LAI are influenced by the leaf inclination of the *Eucalyptus* species which tend to range between 60 and 80 degrees. As a result, ground-based measurements of LAI derived from gap fraction, plant canopy analysers, camera-based point quadrats and hemispherical photographic techniques all produce biased estimates (Coops et al., 2004). Research has demonstrated that such biases are potentially larger in sparse canopies (Whitford et al., 1995). This is an important consideration given 78% of native forests in Australia (which represent an estimated 147.4 million hectares) are Eucalypt species (ABARES, 2012).Consequently, the authors suggest that indirect (optical) methods of LAI estimation require calibration, via direct LAI measurement, to produce accurate estimates of canopy LAI within Australian ecosystems (Coops et al., 2004).

Equally, as a consequence of this vertical leaf inclination and a higher proportion of radiation transmittance to the forest floor, Hill et al. (2006) conclude that projected foliage cover, when adjusted for woody canopy elements, may provide a better correlation with satellite based LAI products.

6.3 fAPAR Validation

A review of LAI validation programs demonstrates that *fAPAR* and LAI are associated metrics which are frequently validated coincidentally. This is exemplified by the VALERI and BigFoot projects which both estimate *fAPAR* and LAI in conjunction.

6.3.1 In situ fAPAR Measurements

Weiss and Baret (2011) suggest that there are four in situ methods of quantifying the *fAPAR* at the local scale: the use of quantum sensors that measure all the terms of the radiation balance; instantaneous PAR transmittance measurements; directional measurements using LAI-2200, DHP or LiDAR; and finally describing the 3D optical elements of the canopy as realistically as possible and then simulating the *fAPAR*. However, the most common in situ *fAPAR* measurements that are used are calculated from the difference in photosynthetically active radiation (PAR) entering and leaving the canopy, that is, PAR absorption, divided by the incoming PAR (f_{IPAR}).

Many in situ sensors such as the LAI-2200, lidar, DHP, AccuPAR ceptometer and other ceptometers can be used to calculate the f_{IPAR}. However, care must be taken when using such measurement devices. Asner et al. (1998) mentioned that f_{IPAR} underestimates *fAPAR* by about 3-10 % for canopies containing dense green materials while these underestimations rise to levels of around 10-40% when considering shrublands and woodlands with LAI < 3.0.

The BigFoot project estimates *fAPAR* via two techniques, firstly, from the DIFFN variable provided by the LI-COR LAI-2200 and, secondly, from a continuous PAR tram system (http://daac.ornl.gov/BIGFOOT_VAL/bigfoot.shtml). The PAR

tram system measures incident and transmitted PAR both above and below the canopy at increments along a 30 metres track (BigFoot Website).
Fensholt et al. (2004) collected ground-based measurements of *fAPAR* (and LAI) at a series of grassland savannah sites in order to validate MODIS derived *fAPAR* data products. *fAPAR* is measured with a SKYE PAR Quantum sensor (Fensholt et al., 2004). Fensholt et al. (2004) derived daily averages of *fAPAR* by repeating measurements at 10 minute intervals between 9am and 3pm. The authors utilised repeated measurements over a large range of solar zenith angles, so to minimise errors introduced by the correction factor *G*, a function introduced into *fAPAR* derivation to account for non-random leaf angle distributions (Fensholt et al., 2004). Sensitivity analysis demonstrated that measurements averaged over this time period were representative of 10.30am and 10.30pm values and therefore compatible with MODIS derived *fAPAR* measurements (Fensholt et al., 2004).

The ratio of the incident PAR recorded above and below the canopy is closely related to canopy gap fraction. This measure is therefore influenced by sun zenith angle, the amount of diffuse radiation and canopy clumping (Gower et al., 1999). Other error sources in the ground-based estimation of PAR include: (a) variation in the soil albedo; (b) the *fAPAR* model assumptions; and (c) uncertainty in LAI measurements. The last is relevant only if PAR is being derived from LAI as opposed to being directly measured (Fensholt et al., 2004).

6.4 Exemplar methodology for the validation of satellite LAI products in Australia using an up-scaling approach

The validation of specific satellite remote sensing products has been the focus of many research groups and programs in the past (Table 6.3). TERN's Landscape Assessment platform is currently validating the MODIS Collection 5 LAI product for the Australian continent. The validation of this product is a multi-step process involving current in situ field measurements, historical LAI data, and intermediate resolution measurements (such as airborne laser scanning or ALS). This is followed by the up-scaling of in situ measurements to moderate resolution (on the order of $1km^2$) using intermediate measurements (e.g., Landsat imagery).

Due to the enormity of Australia, it is imperative that reference data used to validate the MODIS LAI product is collected from multiple locations and ecosystems across the continent. Accordingly, TERN's Landscape Assessment platform utilises data collected from TERN calibration/validation supersites around Australia in conjunction with data collected by other TERN observatory platforms, including TERN Ecosystem Surveillance, as well as historical LAI records, such as those contained in Hill et al. (2006).

In situ LAI measurement techniques that are most commonly used by TERN field teams at the calibration/validation sites include digital hemispherical photography and plant canopy analysers (such as LAI-2200 and CI-110). At each of these calibration/validation supersites, ALS has been flown, from which the effective LAI can be derived using a Beers Law inversion of the gap fraction. This provides a means of up-scaling the in-situ measurements (via a transfer function) to a moderate resolution, similar to that achieved using MODIS.

At TERN's calibration/validation SuperSites, ground-based LAI measurements are typically collected along the SLATS Star transect at 25 m intervals (Figure 6.4). Typically there are about five to seven SLATS transects per 5km by 5km supersite.

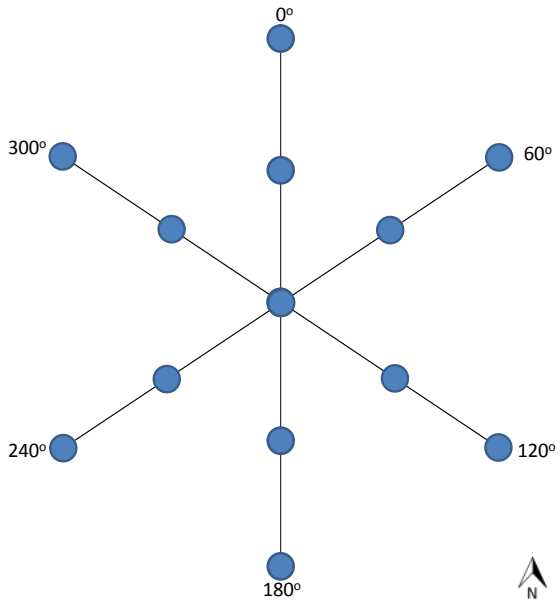

Figure 6.4 SLATS Star Transect representing a single validation field site or plot. Each transect segment is 100 m in length with the blue representing locations where hemispherical photos were taken. http://data.auscover.org.au/xwiki/bin/view/Field+Sites/Star+Transect+Protocol+Web+Page

LAI measurements using hemispherical photography and plant canopy analysers are best captured under completely diffuse lighting conditions such as uniform overcast skies or at dawn/dusk. Steps followed by TERN Landscape Assessment field teams to measure and validate LAI are described below. These are recommended to be taken under diffuse lighting conditions.

6.4.1 Digital Hemispherical Photography (DHP)

1. **Sampling Design:** At each SLATS site or plot, DHP are taken at 13 locations: 1 in the centre of the star transect, 6 half way along each arm (at 25 m from centre), and 6 at the ends of each transect (indicated by the blue dots in Figure 6.4).
2. **Image Capture:** Ensure that the camera is near level for each of the photographs and that the top of the photograph (top of the camera) faces magnetic north to simplify post processing of the images.
3. Typically images are taken at breast height (1.30 m above the ground surface). However, if understory is present, it is good practise to take photographs from above and below the understory. For grassy ecosystems, if possible it is encouraged to take photographs from ground level as well as above the ground looking down. Note: images are recommended to be taken at least ±1m away from large tree stems, as a distance less than this threshold may bias the gap fraction, clumping, and PAI from unrepresentative images. If the measurement locations will be used for monitoring purposes, then permanent markers are recommended to be placed at each of the measurement locations. For the full TERN Landscape Assessment digital hemispherical photography protocol, refer to the TERN Landscape Assessment wiki (http://data.auscover.org.au/xwiki/bin/view/Field+Sites/Hemispheric_Protocol).
4. Ensure the camera is taking high quality format jpeg images in addition to storing RAW format. The choice of RAW or in-camera jpeg image format is important for the post-processing stage of image classification. Enable the camera bracketing function and set to ± 1 f-stop. This ensures that three differently exposed images can be captured efficiently. Set the exposure metering to matrix metering, which utilises the entire camera scene within the viewfinder to assess the appropriate metering. Set the exposure program of the camera to Aperture Priority. The choice of exposure level is a manual and iterative approach, following the guidelines of Beckschäfer et al.,

(2013). At each location, take a photo (automatic exposure is good starting point) and (i) in preview mode look at the image for overexposure (most likely at zenith if diffuse lighting) and for clear separation of foliage and sky in the bright parts of the image, and (ii) check the histogram of the image to ensure there are few pixels with maximum digital number value (indicating overexposure). Ideally, the sky pixels peak is located just below the maximum histogram value. If the image is overexposed, reduce the shutter speed and vice versa. Repeat the process until this criteria has been satisfied. This will create measurement redundancy in the image capture process. If the RAW format is used for post-processing, then additional firmware can be installed on some cameras that enable the preview of the RAW histogram, such as Magic Lantern (ref http://www.magiclantern.fm/) or the Canon Hack Development Kit (WWW ref - http://chdk.wikia.com/wiki/CHDK). Although the RAW image format is less sensitive to camera exposure level due to greater dynamic range (or bit-depth), it is still important to ensure the images are not over- or under-exposed as the lost detail cannot be recovered in post-processing stages. Otherwise shooting the camera 1 stop under automatic exposure is recommended (Macfarlane et al., 2014).

5. ISO is essentially the camera's sensitivity to light. Low ISO values tend to be preferred given they increase the signal to noise ratio. For camera stability, it is highly recommended to use low ISO values (100-400) in conjunction with a tripod (and remote trigger). This will lead to a reduction in mixed pixels and a more accurate image classification. The ISO value should only be increased if the shutter speed is very long (e.g. > 0.5 seconds) – as wind and camera movement can cause blurring in the image.

6. **Post Processing:** There are a number of post-processing methods to classify the images and subsequently derive canopy structural metrics. Two exemplar processes are outlined below; one for the RAW image format, and one for the in-camera jpeg format. The advantage of the RAW image processing method is that it was shown to be almost insensitive to camera exposure (Macfarlane et al., 2014). Whereas in-camera jpeg format image classification is very sensitive to camera exposure, thus leading to significantly different structural metric estimations. It is important to note that camera and lens calibration parameters (i.e. the lens projection centre or 'offset' and lens projection function or 'radial distortion') need to be known to for the post-processing stages.

Method 1 (RAW): The RAW imagery can be processed in a number of stages, combining three software packages to produce canopy openness, gap fraction, PAI and canopy element clumping metrics. The stages are as follows:

1. **Image format conversion:** Convert the RAW imagery into 8 bit jpeg format for further analysis, using an updated method outlined in Macfarlane et al., (2014). This stage involves an automated process utilising the open source software functionality of dcraw (WWW ref: https://www.cybercom.net/~dcoffin/dcraw/); please contact Craig Macfarlane (craig.macfarlane@csiro.au) for a compilation.

2. **Image classification:** The subsequent steps are applicable to both in-camera jpegs and the converted RAW to jpeg formats. The DCP toolbox v3.14 (Macfarlane 2011; Macfarlane et al., 2014, craig.macfarlane@csiro.au), has in-built functionality to automate the image classification process. Key outputs of this step include a binary classified image, and a report of canopy openness and proportions of mixed pixels. The lens projection centre (coordinates) and image diameter are required input settings.

3. **Intermediate step to compute canopy element clumping:** Utilising the classified images from Step 2, input them into DHP.exe to compute TRAC instrument-like profiles for input into the TRACWin.exe software (contact Sylvain Leblanc for a copy of both DHP.exe and TRACWin.exe; sylvain.leblanc@nrcan-rncan.gc.ca). It is recommended to compute a single TRAC-like profile per plot of images.

4. **Canopy element clumping, PAI_e, PAI, and LAI:** Use the TRAC-like profiles created in DHP.exe as input into TRACWin.exe to compute canopy element clumping and PAI. Batch mode can be utilised for efficient processing of plots. The in-built CLX clumping method with a segment size of 15 or 45 degrees is recommended, please refer to Leblanc et al. (2014) for further information. Note: a post-hoc correction for the lens projection function may be required, due to the default linear projection function assumed in DHP.exe and TRACWin.exe. If the scene G function is unknown, i.e. the angular distribution of wood or leaf elements have not been quantified, then the 55-60 degree zenith angle range is recommended to use for the clumping metric, due to the G projection function of leaf and wood converging to be equal 0.5 at that angle. Clumping at $\Theta \approx 57.3$ degrees can combined with the known G (≈0.5), and PAI_e estimated from the average P_{gap} at the same zenith angle range using Eqn. 6.4 to compute PAI. A correction for the proportion of woody material to plant material 'α' can also be made if available to convert PAI into LAI (Eqn. 6.3).

Method 2 (in-camera jpeg): Photographs from each site are post processed using CAN-EYE imaging software (Weiss and Baret, 2010). CAN-EYE is used to extract LAI, average leaf inclination angle (ALA), fraction of absorbed photosynthetically active radiation (fAPAR), vegetation cover fraction (FCOVER) and bidirectional gap fraction. It is also possible to use CAN-EYE with pre-classified images from the RAW format, which have been re-formatted to jpeg.

The exact process used to calculate the effective LAI and true LAI from the DHP images using the CAN-EYE software is set out step-by-step in the CAN-EYE user manual (Weiss and Baret, 2010). However, a schematic diagram of the general classification process is provided in Figure 6.5.

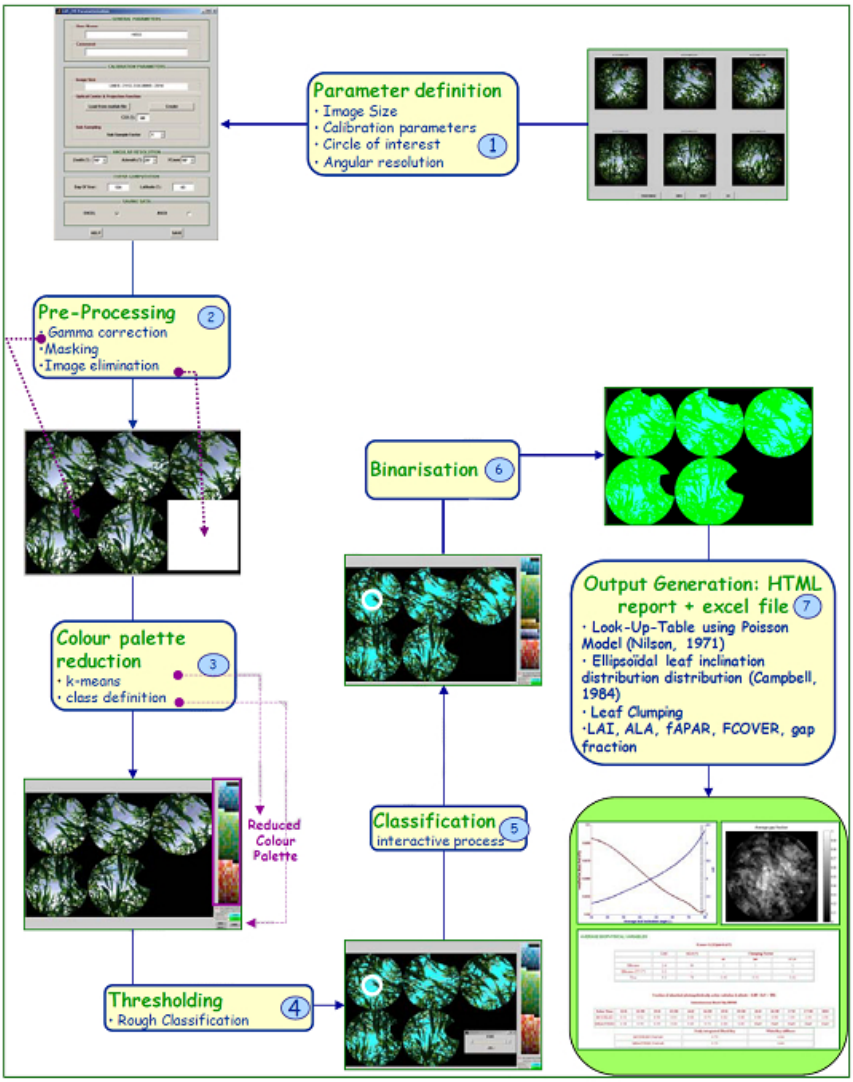

Figure 6.5 Schematic diagram representing the general process where-by images are processed and LAI is calculated using the CAN-EYE imaging software (image extracted from Weiss and Baret, 2010).

6.4.2 Plant Canopy Analyser – LAI-2200

1. Upon commencing measurements, be sure to record an 'above canopy' reference measurement in a clearing. The sensor wand is then switched into 'below canopy' mode so that the LAI measurements can be made. LAI-2200 measurements are to be taken at the same positions as the DHP measurements at regular intervals along each of the 100 m transects, ideally with a GPS logger attached to the LAI-2200 console to record the position. If a GPS logger is not available then the correct procedure is as follows.
2. Measurements are to be taken along each transect arm in the same order and direction as the star transect point intercept measurements were taken.
3. Take measurements at regular specified intervals.
4. Record each transect as a separate file with the transect name and measurement interval (e.g. chow01_transect1_5m). For the full TERN Landscape Assessment LAI-2200 protocol, refer to the LAI-2200 user manual which outlines the full methods to be used in different vegetation types and the TERN Landscape Assessment wiki (Licor, 2009 and http://data.auscover.org.au/xwiki/bin/view/Field+Sites/LAI2200+Protocol).

6.4.3 Terrestrial Laser Scanning (TLS)

5. At each of the TERN calibration/validation field sites, TLS measurements are also recorded (Figure 6.6) along each SLATS plot. As each TLS produces a 360° FOV point cloud of the immediate area of ground and canopy, a modified SLATS star transect is used.

Figure 6.6 Recording TLS measurements and metadata in the field using a Riegl Laser Scanner.

6. A total of five TLS scans are taken per SLATS plot (Figure 6.7): 1 scan taken at the centre followed by 4 scans taken approximately 35 m from the centre along each of the NE, SE, SW and NW transect arms. By using this spatial configuration of scans, a complete characterisation of the structural properties of the vegetation can be made.

Figure 6.7 Modified SLATS Star Transect representing a single validation field plot. Each of the blue dots indicates a TLS measurement position, allowing for a complete site characterisation of the vegetation structure to be made using this spatial configuration.

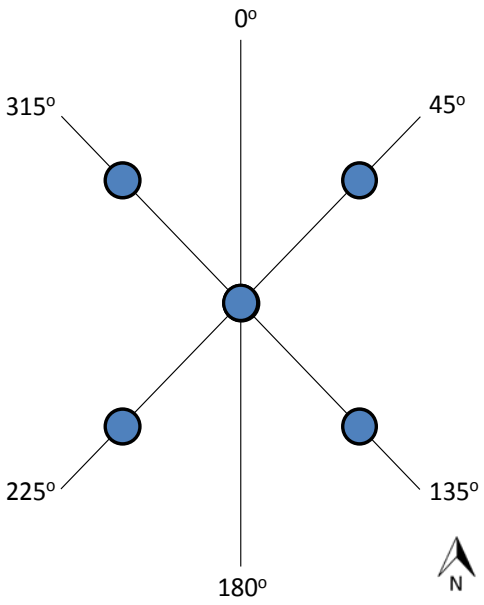

7. Once all the in situ vegetation measurements (DHP, TLS and plant canopy analyser) at each plot site have been recorded, post processing and collation of the data is carried out.

6.4.4 Up-scaling of the in situ LAI measurements

To compare with or validate a moderate resolution satellite product (such as the MODIS Collection 5 LAI product), in situ measurements must be up-scaled via the use of high resolution satellite imagery or airborne Lidar data (Morisette et al., 2006). TERN Landscape Assessment will primarily use Landsat imagery to up-scale the in situ measurements, however both up-scaling methods will be assessed where airborne lidar (ALS) is available. The process implemented to up-scale in situ measurements is set out below:

When Using Satellite Imagery

8. The direct validation approach (Morisette et al., 2006) consists in using high spatial resolution imagery (on the order of 20 - 30 m) to scale the ground LAI measurements up to a moderate resolution pixel size (approximately 1km x 1 km). For this, a ‘‘transfer function’’ between high spatial resolution surface reflectance and LAI measurements is established.
9. The transfer function is applied to an appropriate extent of the high spatial resolution image (for the TERN Ecosystem Processes SuperSites, a 100 m x 100 m tile size is used).
10. The resulting high spatial resolution LAI map is aggregated up to a coarser pixel size for comparison with moderate resolution products such as MODIS.

Using Airborne Laser Scanning (ALS)

11. The ALS LAI is calculated using the intensity model described by Hopkinson and Chasmer (2007). This involves calculating gap fraction grids for the field site area with the same resolution as the satellite imagery that is used (namely Landsat imagery with 30 m pixel size).
12. Gap fraction grids are calculated in their simplest form by taking a ratio of the below canopy returns to the total number of ALS returns for a given grid cell size. This results in an index of canopy gaps (P).
13. A simple Beers Law inversion is then applied to obtain the effective LAI;

$$LAI_e = \frac{-\ln Pgap}{k} \qquad \textbf{(equation 6.11)}$$

Where *Pgap* is the gap fraction and *k* is the site dependent extinction coefficient.

14. The resulting LAI_e grid can then be used in the same manner as the satellite imagery to up-scale the in situ LAI measurements. A transfer function between the in situ and ALS measurements is applied, and the resulting high resolution LAI map is aggregated up to a coarser pixel size to be compared directly with moderate resolution products (e.g. Figure 6.8).

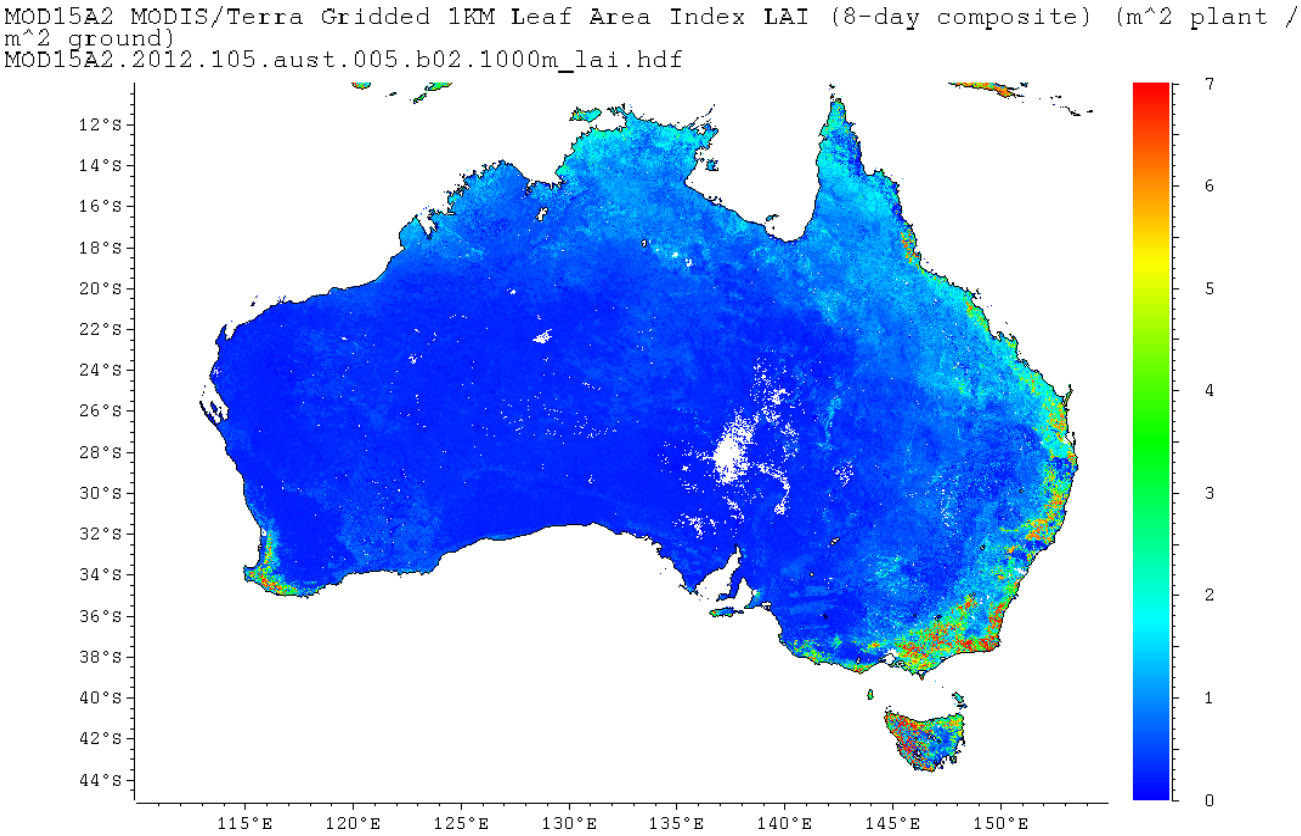

Figure 6.8 MODIS Collection 5 LAI product. Gridded 1 km x 1 km, 8-day composite product for Australia, acquired using the MODIS Terra sensor.

The use of these two up-scaling methods (satellite imagery and ALS) in conjunction with a suite of in situ measurements and historical data will allow TERN Landscape Assessment to validate the MODIS Collection 5 LAI product on a continental scale.

References

ABARES, 2012. Australia's forests at a glance 2012, ABARES, Canberra, August. Availlable at http://adl.brs.gov.au/data/warehouse/9aaf/9aafe003/fag12d9aafe003201208/ForestsAtGlance_2012_v1.0.0.pdf.

Asner, G. P., Wessman, C. A. & Archer, S. (1998) Scale dependence of absorption of photosynthetically active radiation in terrestrial ecosystems. *Ecological Applications* **8** 1003-1021.

TERN Landscape Assessment Wiki (2013). http://data.auscover.org.au/xwiki/bin/view/Main/

Baret, F., Weiss, M., Allard, D., Garrigues, S., Leroy, M., JeanJean, H., et al., (2005) VALERI: a network of sites and a methodology for the validation of medium spatial resolution land satellite products, *Remote Sensing Environment* (Accessed at http://w3.avignon.inra.fr/valeri/documents/VALERI-RSESubmitted.pdf - August 2010).

Beckschäfer, P, Seidel, D, Kleinn, C, & Xu, J. (2013). On the exposure of hemispherical photographs in forests. [On the exposure of hemispherical photographs in forests]. *iForest - Biogeosciences and Forestry*, 6(4), p. 228-237. doi: 10.3832ifor0957-006

Béland, M., Baldocchi, D. D., Widlowski, J-L., Fournier, R A., & Verstraete, M. M. (2014). On seeing the wood from the leaves and the role of voxel size in determining leaf area distribution of forests with terrestrial LiDAR. *Agricultural and Forest Meteorology, 184*(0), p. 82-97. doi: http://dx.doi.org/10.1016/j.agrformet.2013.09.005

BigFoot Website: http://www.fsl.orst.edu/larse/bigfoot/overview.html (Accessed August 2010)

Breda, N.J.J. (2003). Ground-based measurements of leaf area index: a review of methods, instruments and current controversies, *Journal of Experimental Botany*, 54(392) p.2403 - 2417.

CEOS. (2014). Global LAI Product Validation Good Practices v2.0. In R. Fernandes, S. Plummer & J. Nightingale (Eds.).

Chen, J.M., & Cihlar, J. (1995). Quantifying the effect of canopy architecture on optical measurements of leaf area index using two gap size analysis methods. *Geoscience and Remote Sensing, IEEE Transactions on, 33*(3), 777-787. doi: 10.1109/36.387593

Chen, J.M., Rich, P.M., Gower, S.T., Norman, J.M. & Plummer S. (1997). Leaf area index of boreal forests: theory, techniques and measurements, *Journal of Geophysical Research*, 142 (D24), p. 29,429-29,443.

Chianucci, F., Macfarlane, C., Pisek, J., Cutini, A., & Casa, R. (2014). Estimation of foliage clumping from the LAI-2000 Plant Canopy Analyzer: effect of view caps. Trees, 1-12.

CID Bio-Science Inc. (2012). *Plant Canopy Imager CI-110 Instruction Manual, Version 5.0.3*, CID Bio-Science Inc., Camas, WA USA.

Coops, N.C., Smith, M.L., Jacobsen, K.L., Martin M. & Ollinger, S. (2004). Estimation of plant and leaf area index using three techniques in a mature eucalypt canopy, *Austral Ecology*, 29 p. 332 - 341.

Cohen, W.B., Maiersperger T.K., Turner, D.P., Ritts, W.D., Pflugmacher, D., Kennedt, R.E., Kirschbaum, A., Running, S.W., Costa, M. & Gower, S.T. (2006). MODIS Land Cover and LAI Colelction 4 Product Quality Across Nine Sites in the Western Hemisphere, *IEEE Transactions on Geoscience and Remote Sensing*, 44 (7) p.1843 - 1857.

Côté, J.-F., Widlowski, J.-L., Fournier, R.A., & Verstraete, M.M. (2009). The structural and radiative consistency of three-dimensional tree reconstructions from terrestrial lidar. *Remote Sensing of Environment, 113*(5), 1067-1081. doi: http://dx.doi.org/10.1016/j.rse.2009.01.017

Danson, F.M., Gaulton, R., Armitage, R.P., Disney, M., Gunawan, O., Lewis, P., Pearson, G., & Ramirez, A.F. (2014). Developing a dual-wavelength full-waveform terrestrial laser scanner to characterize forest canopy structure. *Agricultural and Forest Meteorology, 198–199*(0), 7-14. doi: http://dx.doi.org/10.1016/j.agrformet.2014.07.007

de Wit, C.T. (1965). *Photosynthesis of leaf canopies*: Centre for Agricultural Publications and Documentation.

Fensholt, R., Sandholt, I & Rasmussen, M.S. (2004). Evaluation of LAI, fAPAR and the relation between fAPAR and NDVI in semi-arid environments using in-situ measurements, *Remote Sensing of Environment*, 91 p. 490 - 507.

Gower, S.T., Kucharik, C.J. & Norman, J.M. (1999). Direct and Indirect Estimation of Leaf Area Index, fAPAR and Net Primary Production of Terrestrial Ecosystems, *Remote Sensing of Environment*, 70 p. 29 - 51.

Hancock, S., Essery, R., Reid, T., Carle, J., Baxter, R., Rutter, R., & Huntley, B. (2014). Characterising forest gap fraction with terrestrial lidar and photography: An examination of relative limitations. *Agricultural and Forest Meteorology*, 189–190(0), p. 105-114. doi: http://dx.doi.org/10.1016/j.agrformet.2014.01.012

Hill, M.J., Senarath, U., Lee, A., Zeppel, M., Nightingale, J.M., Williams, R. & McVicar, T.R. (2006). Assessment of the MODIS LAI product for Australian ecosystems, *Remote Sensing of Environment*, 101 p. 495 - 518.

Hopkinson, C. & Chasmer, L. (2007). Using discrete laser pulse return intensity to model canopy transmittance. *Photogrammetric Journal of Finland*, 20 (2) p. 16 – 26.

Hosoi, Fumiki, & Omasa, Kenji. (2007). Factors contributing to accuracy in the estimation of the woody canopy leaf area density profile using 3D portable lidar imaging. *Journal of Experimental Botany*, 58(12), p. 3463-3473. doi: 10.1093/jxb/erm203

Huang, P., & Pretzsch, H. (2010). Using terrestrial laser scanner for estimating leaf areas of individual trees in a conifer forest. *Trees - Structure and Function*, 24(4), p. 609-619.

Jonckheere, I., Fleck, S., Nackaerts, K., Muys, B., Coppin, P., Weiss, M. & Baret, F. (2004). Review of methods for in situ leaf area index determination Part I. Theories, sensors and hemispherical photography, *Agricultural and Forest Meteorology*, 121 p. 19 - 35.

Jupp, D.L.B, Culvenor, D.S., Lovell, J.L., Newsham, G.L., Strahler, A.H. & Woodcock, C.E. (2008). Estimating forest LAI profiles and structural parameters using a ground-based laser called Echidna, *Tree Physiology* 29 p. 171 - 181.

Kucharik, C.J., Norman, J.M., Murdock, L.M., & Gower, S.T. (1997). Characterizing canopy nonrandomness with a multiband vegetation imager (MVI). *Journal of Geophysical Research: Atmospheres, 102*(D24), 29455-29473. doi: 10.1029/97JD01175

Lambert, J. (1760). Photometria, sive de Mensura et gradibus luminis, colorum et umbrae (Augsberg: Eberhard Klett).

Lang, A.R.G., & Xiang, Y. (1986). Estimation of leaf area index from transmission of direct sunlight in discontinuous canopies. *Agricultural and Forest Meteorology, 37*(3), 229-243. doi: 10.1016/0168-1923(86)90033-x

Leblanc, S.G. & Chen, J.M. (2001). A practical scheme for correcting multiple scattering effects on optical LAI measurements, *Agricultural and Forest Meteorology*, 110 p. 125 - 139.

Leblanc, S.G. (2002). Correction to the plant canopy gap-size analysis theory used by the Tracing Radiation and Architecture of Canopies instrument. *Applied Optics, 41*(36), 7667-7670.

Leblanc, S.G., Chen, J.M., Fernandes, R., Deering, D.W., & Conley, A. (2005). Methodology comparison for canopy structure parameters extraction from digital hemispherical photography in boreal forests. *Agricultural and Forest Meteorology, 129*(3–4), 187-207. doi: 10.1016/j.agrformet.2004.09.006

Leblanc, S.G., Chen, J.M. & Kwong, K. (2002). *Tracing Radiation and Architecture of Canopies: TRAC manual (Version 2.1.3)*, Natural Resources Canada.

Leblanc, S.G., & Fournier, R.A. (2014). Hemispherical photography simulations with an architectural model to assess retrieval of leaf area index. *Agricultural and Forest Meteorology*, 194(0), 64-76. doi: http://dx.doi.org/10.1016/j.agrformet.2014.03.016

LI-COR (2009). *LAI-2200 Plant canopy Analyser: Instruction Manual*, LI-COR Inc., Lincoln Nebraska, USA.

Miller, J.B. (1967). A formula for average foliage density. *Australian Journal of Botany*, 15, 141-144.

Moorthy, I., Miller, J R., Hu, B., Chen, J., & Li, Q. (2008). Retrieving crown leaf area index from an individual tree using ground-based lidar data. *Canadian Journal of Remote Sensing, 34*(3), 320-332. doi: 10.5589/m08-027

Morisette, J.T., Baret, F., Privette, J.L., Myneni, R.B., Nickeson, J., Garrigues, S., et al., (2006). Validation of global moderate-resolution LAI Products: a framework proposed within the CEOS Land Product Validation subgroup, *IEEE Transactions on Geoscience and Remote Sensing*, 44 (7) p.1804 - 1817.

Neumann, H.H., Den Hartog, G., Shaw, R.H. 1989. Leaf area measurements based onhemispheric photographs and leaf-littercollection in a deciduous forest duringautumn leaf-fall. Agricultural and Forest Meteorology. 45, 325-245.

Newnham, G., Armston, J., Muir, J., Goodwin, N., Tindall, D., Culvenor, D., Püschel, P., Nyström, M., & Johansen, K. (2012). Evaluation of Terrestrial Laser Scanners for Measuring Vegetation Structure. In C. S. A. Flagship (Ed.): CSIRO.

Norman, J.M. & Campbell, G.S. (1989). Plant Physiological Ecology: Field Methods and Instrumentation. Eds., Pearcy, R.W., Ehleringer, J.R., Mooney, H.A. & Rundel, P.W. (London: Chapman and Hall) p. 301-325.

Pisek, J., Lang, M., Nilson, T., Korhonen, L., & Karu, H. (2011). Comparison of methods for measuring gap size distribution and canopy nonrandomness at Järvselja RAMI (RAdiation transfer Model Intercomparison) test sites. *Agricultural and Forest Meteorology, 151*(3), 365-377. doi: http://dx.doi.org/10.1016/j.agrformet.2010.11.009

Prince, S.D. (1991) A model of regional primary production for use with coarse resolution satellite data. *International Journal of Remote Sensing* 12 (6) 1313-1330.

Raumonen, P., Kaasalainen, M., Åkerblom, M., Kaasalainen, S., Kaartinen, H., Vastaranta, M., Holopainen, M., Disney, M., & Lewis, P. (2013). Fast automatic precision tree models from terrestrial laser scanner data. *Remote Sensing, 5*(2), 491-520.

Ross, J. (1981) The radiation regime and architecture of plant stands. *Dr. W. Junk Publishers*, The Hague, Netherlands. pp 392.

Ryu, Y., Nilson, T., Kobayashi, H., Sonnentag, O., Law, B.E. & Baldocchi, D.D. (2010). On the correct estimation of effective leaf area index: Does it reveal information on clumping effects? *Agricultural and Forest Meteorology*, 150 (3) p. 463 - 472.

Sea, WB, P Choler, J Beringer, RA Weinmann, LB Hutley and R Leuning (2011). Documenting improvement in leaf area index estimates from MODIS using hemispherical photos for Australian savannas. Agricultural and Forest Meteorology 151: 1453–1461.

Strahler, A. H., Jupp, D. L. B., Woodcock, C. E., Schaaf, C. B., Yau, T., Zhau, F., Yang, X., Lovell, J., Culvenor, D., Newnham, G., Ni-Miester, W. & Boykin-Morris, W. (2008) Retrieval of forest structural parameters using a ground-based lidar instrument (Echidna®). *Canadian Journal of Remote Sensing* **34** (2) S426-S440.

Tian, Y., Woodcock, C.E., Wang, Y., Privette, J.L., Shabanov, N.V, Zhou, L. et al., (2002). Multiscale analysis and validation of the MODIS LAI product I. Uncertainty assessment, *Remote Sensing of Environment*, 83 p. 414 - 430.

Weiss, M., Baret, F., Garrigues, S. & Lacaze, R. (2007) LAI and fAPAR CYCLOPES global products derived from VEGETATION. Part 2: validation and comparison with MODIS collection 4 products. *Remote Sensing of Environment* **110** 317-331.

TLSIIG. (2014). Terrestrial Laser Scanning International Interest Group. http://128.197.168.195/?page_id=37, Retrieved 21/02/2014.

Weiss, M. & Faret, F. (2010). CAN-EYE v6.1 User Manual. French National Institute of Agronomical Research (INRA). https://www4.paca.inra.fr/can-eye

Weiss, M. & Baret, F. (2011). fAPAR (fraction of Absorbed Photosynthetically Active Radiation) estimates at various scale. *34th International Symposium on Remote Sensing of Environment.*

Weiss, M., Baret, F., Block, T., Koetz, B., Burini, A., Scholze, B., et al., (2014). On line validation exercise (OLIVE): A web based service for the validation of medium resolution land products. application to FAPAR products. *Remote Sensing*, *6* (5), 4190–4216. doi:10.3390/rs6054190

White, M.A., Asher, G.P., Nemain, R.R., Privette, J.L. & Running, S.W. (2000). Measuring Fractional cover and Leaf Area Index in Arid Ecosystems: Digital Camera, Radiation Transmittance and Laser Altimetry Methods, *Remote Sensing of Environment*, 74 p. 45 – 57

Whitford, K.R., Colquhoun, I.J., Lang, A.R.G. & Harper B.M. (1995). Measuring leaf area index in a sparse eucalypt forest: a comparison of estimates from direct measurement, hemispherical photography, sunlight transmittance and allometric regression, *Agricultural and Forest Meteorology*, 74 p. 237 - 249.

Wilson, J. (1963). Estimation of foliage denseness and foliage angle by inclined point quadrats. *Australian Journal of Botany, 11*(1), 95-105. doi: http://dx.doi.org/10.1071/BT9630095

Woodgate, W., Disney, M., Armston, J.D., Jones, S.D., Suarez, L., Hill, M.J., Wilkes, P., Soto-Berelov, M., Haywood, A., & Mellor, A. (*under review*). Quantifying the impact of ignoring woody material in estimating canopy gap fraction and Leaf Area Index in woody ecosystems. *Agricultural and Forest Meteorology*.

Woodgate, W., Jones, S.D., Suarez, L., Hill, M.J., Armston, J.D., Wilkes, P., Soto-Berelov, M., Haywood, A., & Mellor, A. (2015). Understanding the variability in ground-based methods for retrieving canopy openness, gap fraction, and leaf area index in diverse forest systems. *Agricultural and Forest Meteorology, 205*(0), 83-95. doi: http://dx.doi.org/10.1016/j.agrformet.2015.02.012

Zheng, G. & Moskal, L.M. (2009). Retrieving Leaf Area Index (LAI) Using Remote Sensing: Theories, Methods and Sensors, *Sensors*, 9, p. 2719 - 2745.

Chapter 7. Validation of Australian Fractional Cover Products from MODIS and Landsat Data

P. Scarth*[1,4], J.P. Guerschman [2], K. Clarke[3], S. Phinn,[1,4,]

[1]Joint Remote Sensing Research Program, The University of Queensland

[2]CSIRO Land and Water

[3]Spatial Information Group, Biological Sciences, The University of Adelaide

[4]Biophysical Remote Sensing Group, The University of Queensland

*Corresponding author:

P.Scarth@uq.edu.au

Abstract

The area of ground covered by live or photosynthetic green vegetation, senescent or non-photosynthetic vegetation and bare ground is a fundamental measurement and a regularly updated map product that is required from catchment to continental scales in Australia and other areas around the world. This chapter outlines the four most common fractional cover mapping approaches used for delivering national products (kept on the TERN Landscape Assessment Data Portal) of vegetation and bare ground cover fractions in Australia, along with work undertaken to validate these. It specifically includes: the approach of Guerschman *et al*. (2009) derived from MODIS data; the relative spectral mixture analysis (RSMA) approach of Okin *et al*. (2007), the Spectral Mixture Analysis Time Series (SMATS), as implemented by Okin *et al*. (2013) for MODIS data; the land condition index (LCI) approach of Clarke *et al*. (2011); and Landsat seasonal fractional cover approach, implemented by Scarth *et al*. (2010) and applied to Landsat TM and ETM; and to MODIS data (by Guerschman *et al*., 2015). Chapter 18 describes how a national network of reference sites was established and used to improve the MODIS (Guerschman *et al*., 2009) and Landsat (Scarth *et al*., 2010) derived fractional cover products for Australia.

Key Points

- Fractional cover is a fundamental site and landscape scale measurement required by landholders, non-government organisations and state and federal government departments.
- In Australia, remotely sensed fractional cover products are routinely produced using both MODIS and Landsat satellites.
- The validation of these products has been undertaken using field data collected across representative sites.
- The validated MODIS and Landsat derived fractional cover products are now used as key indicators for a range of environmental monitoring and management activities.

7.1 Introduction

A fundamental measurement and regularly updated map product required from catchment to continental scales in Australia and other areas around the world is the area of ground covered by live or photosynthetic green vegetation, senescent or non-photosynthetic vegetation and bare ground. These measurements have traditionally been made from on-ground measurements using a variety of qualitative and quantitative approaches centred on plots or transects, where the locations have been chosen to be representative of vegetation communities, ecosystem types or management practices. This is one of the measurements that can be made accurately and reliably from satellite image data based on spectral un-mixing algorithms which have been extensively tested at both Landsat TM/ETM/OLI (30 m pixels) and MODIS (500 m pixels) scales since the late 1990's. These methods deliver a percentage cover estimate in each pixel, which sums to 100%, e.g. 50% green vegetation, 30% non-photosynthetic vegetation and 20% bare ground, plus a residual error term. This chapter outlines the four most common fractional cover mapping approaches for delivering national products (kept on the TERN Landscape Assessment Data Portal) for vegetation and bare ground cover fractions in Australia, along with their validation. The text uses material already presented in published papers and the TERN Landscape Assessment Data Portal:

- the approach of Guerschman *et al*. (2009) for MODIS data;
- the relative spectral mixture analysis (RSMA) approach of Okin *et al*. (2007), now the Spectral Mixture Analysis Time Series (SMATS), as implemented by Okin *et al*. (2013) for MODIS data;
- the land condition index (LCI) approach of Clarke *et al*. (2011); and

- the Landsat seasonal fractional cover approach, implemented by Scarth *et al*. (2010) and applied to Landsat TM and ETM data.
- the approach of Guerschman *et al*. (2015) who implemented the same algorithm as Scarth *et al*. (2010) for MODIS data

For each approach the methods used are first outlined, followed by a description of the validation that has been applied to them to date and the validation results. This chapter should be read in association chapter 18 "A Calibration and Validation Framework To Support Ground Cover Monitoring For Australia" as it outlines the extensive field programs used to both calibrate and validate two of the fractional cover mapping algorithms.

7.2 Examples of Fractional Cover Use in Australia

Fractional cover data are used for a range of regional (10^2 km^2) to continental (10^6 km^2) government monitoring programs, as well as providing direct input into a range of ecosystem and hydrologic models. The Queensland state government uses fractional cover in its annual reef reporting framework. Water quality modellers in the Paddock to Reef Monitoring and Modelling program use it to assess cover factor of catchments and prioritise at-risk areas. The Northern Territory government uses ground cover deciles to report on the condition of its pastoral estate in its Pastoral Land Board Annual Report and the New South Wales and Victorian state governments are exploring the use of fractional cover data to assess the impact of funded works on cover maintenance to prevent wind erosion. The NRM Hub project that provides land managers with systems, tools, data, and skills needed to improve access to property-scale information and knowledge is also a user of these products.

The Dustwatch program funded by the NSW Office of Environment & Heritage uses MODIS-based ground cover to determine areas that are susceptible to wind erosion. The program produces a monthly report tracking dust activity, wind and rainfall and ground cover trends in the southern portion of the Australian continent.

The MODIS CSIRO fractional cover product was used in South Australia to develop insight into the patterns and trends in regional soil exposure dynamics, as a key indicator of landscape condition (Clarke *et. al*, 2014). Several indicators were created, each aiming to reveal information on soil exposure dynamics to assist understanding and management of soil exposure and soil erosion risk. This information is being utilised by the South Australian Arid Lands NRM in developing their Climate Change Action Plan.

7.3 Australian Fractional Cover Algorithms

The fractional cover methods described here were initially developed to assess groundcover in rangeland environments. Fractional cover is a critical variable for rangelands management. It is highly variable in space and time, changing in response to both climatic variation and local pressure from grazing animals and anthropogenic influence such as cropping cycles, vegetation management and fire. In most natural systems, groundcover can be classified into green, non-green or bare cover. This classification problem requires a remote sensing mixture modelling approach to be used, where the pixel reflectance is assumed to be a linear combination of the fractional area of each cover type.

Spectral unmixing of cover fraction relies on having a good spectral reflectance library of pure or homogenous spectral examples (endmembers) of key cover types (green vegetation, non-green vegetation, bare ground), where the reflectance spectra were collected either in the field from a spectrometer or from the image itself. As it is rare to find a pure 30m x 30m Landsat or 500m x 500m MODIS pixel in heterogeneous rangeland

environment, it is necessary to develop methods to derive synthetic endmembers from field data representing impure pixels. It has been shown that a linear unmixing process is mathematically equivalent to multiple regression when an image index is derived by regressing the individual bands against field data. These methods use multiple regression of the field data against the image data to derive endmembers that can then be used within a constrained unmixing approach. Since the regression estimates represent an optimal estimator only in the training sites, we can use these endmember estimates within a constrained unmixing algorithm to provide a better estimate of the cover fractions outside the training regions. Each of the three algorithms discussed in this chapter implements the algorithm differently, but all provide the same output fractions. All data are available from the TERN Landscape Assessment data portal and the Landsat based product will soon be available from Google's Earth Engine.

7.3.1 MODIS – CSIRO by J.Guerschman after Guerschman et al. (2009)

Fractional cover was derived using a linear unmixing methodology. The method, which was documented in a journal paper published in Remote Sensing of Environment (Guerschman *et al*., 2009), uses the NDVI and the ratio of MODIS bands 7 and 6 (2100 and 1600 nm respectively). A basic assumption of this method is that areas with high fractions of bare soil (BS) have a flat spectral feature in the shortwave infrared (SWIR) and therefore a relative high (close to 1) ratio of MODIS bands 7 and 6. Areas with high proportion of non-photosynthetic vegetation (NPV) have a lower reflectance in the 2100 nm region compared to the 1600 nm region and therefore a lower (around 0.6) ratio of MODIS bands 7 to 6. The methodology was originally developed for the Australian tropical savannas and evaluated using field measurements of grass curing in 10 sites, six of which are located in tropical savannas while four are located in grasslands in the west and south east of Australia. The resulting method was applied to the whole Australian Continent.

The dataset consists of the estimated fraction of photosynthetic vegetation, non-photosynthetic vegetation and bare ground for the Australian continent, at 500 meters spatial resolution, for 16-day composites from February 2000 to current. The data are freely available and can be accessed and downloaded from the National Computing Infrastructure (NCI):

https://remote-sensing.nci.org.au/u39/public/html/modis/fractionalcover-clw/

7.3.2 MODIS – LCI by K. Clarke after Clarke et al. (2011)

The Land Condition Index Product (LCI) is a normalised difference index based on MODIS band 6 (1.63 - 1.65 µm) and band 7 (2.11 - 2.16 µm), with the specific formulation detailed in Clarke *et al*. (2011). The theoretical basis for the index is that the ratio of MODIS band 6 and 7 reflectance is similar for photosynthetic vegetation (PV) and non-photosynthetic vegetation (NPV), but this ratio is different for soil. PV and NPV both absorb more strongly in MODIS band 7 than in band 6, whereas soils tend to reflect similarly in both bands. The formulation of the index results in relatively high values (0.3) for PV and NPV, and relatively low values (close to 0) for bare soil.

7.3.3 MODIS – RSMA by K. Clarke after Okin et al. (2007, 2013)

This method was developed in South Australia collaboratively by Greg Okin (University of California), Ken Clarke and Megan Lewis (both University of Adelaide) (Okin *et al.*, 2013). The Relative Spectral Mixture Analysis (RSMA) approach measures change in fractional cover of bare, green and non-green vegetation over time, relative to a baseline date. This index is produced from 500-m MODIS nadir BRDF-adjusted reflectance (NBAR) data, and was introduced in Okin (2007). An evaluation of the RSMA and two other spectral mixture analysis (SMA) techniques against *in situ* fractional cover data collected at a MODIS appropriate scale was performed in South Australia in Okin *et al*. (2013). The study found that while RSMA did not always provide the best fractional cover estimates, it was consistently very accurate for all cover types.

7.3.4 Landsat Seasonal - Joint Remote Sensing Research Program - after Scarth et al. (2010)

Landcover fractions representing the proportions of green, non-green and bare cover were retrieved by inverting multiple linear regression estimates and using synthetic endmembers in a constrained non-negative least squares unmixing model. The bare soil, green vegetation and non-green vegetation endmembers are calculated using models linked to an intensive field sampling program whereby more than 600 sites covering a wide variety of vegetation, soil and climate types were sampled to measure overstorey and ground cover following the procedure outlined in Muir *et al*. (2011). A constrained linear spectral unmixing using the derived endmembers has an overall model Root Mean Squared Error (RMSE) of 11.8%. Values are reported as percentages of cover plus 100. The fractions stored in the 4 image layers are: Band1 - bare (bare ground, rock, disturbed), Band2 - green vegetation, Band3 - non green vegetation (litter, dead leaf and branches), Band4 - Mask Layer encoding cloud, cloud shadow, water and areas with topographic shadow. A value of 1 indicates good data. Value of 0 indicates no-data. Value of 2 indicates unmixing error was excessive, Value of 3 indicates water was detected in the pixel. Value of 4 indicates the pixel had cast shadow. Value of 5 indicates the pixel incidence or exidence angle exceeded 80 degrees. Value of 6 indicates a cloud shadow was detected. Value of 7 indicates a cloud was detected.

7.3.5 MODIS – CSIRO by J.Guerschman after Guerschman et al. (2015)

Guerschman *et al*. (2015) adopted a similar approach as the one developed by Scarth *et al*. (2010) and tested it in Landsat and MODIS data using the same calibration and validation points. They used 1171 fractional cover observations made between 2002 and 2013 following the procedure outlined in Muir *et al*. (2011). For each observation surface reflectance was obtained from Landsat (TM or ETM) and from two MODIS products (MODIS NBAR, MCD43A4 and MODIS 8-day surface reflectance, MOD09A1). The endmembers for the three fractions were derived by linear inversion of the field data and spectral arrays in a similar way as described in for the Landsat Seasonal product. Then estimates of the three fractions are obtained by linear unmixing in a constrained non-negative least squares unmixing model, also similar to the Landsat product.

7.4 Australian Fractional Cover – Validation Approaches

7.4.1 MODIS – CSIRO by J.Guerschman after Guerschman et al. (2009)

In 2011 a validation exercise was performed, using field measurements taken following the SLATS transect protocol (Muir *et al*., 2011, also described in Chapter 18 of this text). A total of 567 field observations were available at the time and were used for comparing with the model-derived fractions. The validation is summarised in a science report (Guerschman *et al*., 2012) that is available from: https://publications.csiro.au/rpr/pub?pid=csiro:EP116314 .

7.4.2 MODIS – LCI by K. Clarke after Clarke et al. (2011) and RSMA by K. Clarke after Okin et al. (2007, 2013)

In 2010 an evaluation of the LCI and RSMA was performed, using field validation data collected in in the Mid-north region of South Australia. This is a rain-fed cropping region that with a Mediterranean climate and receives an average annual rainfall of approximately 500 mm. Summers are hot and dry (from December to February), and winters are mild and wet winters (July to August). Agriculture in the region is predominantly cereal (wheat and barley) cropping, with some legume and canola (*Brassica napu*).

Cover during the summer is typically post-cropping residue, and is dry and sparse. However, out of season rainfall can cause summer weed and pasture growth and produce significant green vegetation cover. Autumn rainfall (March to May) results in weed and pasture growth and an increase in green vegetation cover until herbicide spraying of weeds followed by seeding, or direct-drill seeding, which reduce cover levels to an annual minimum in May or June, depending on the particular seasonal conditions. After seeding, crops germinate and grow, resulting in a peak in green vegetation cover in September. Crops ripen and then senesce, resulting in a transition to maximum non-photosynthetic vegetation cover between October and November, until harvest in November or December. Crop residues, non-photosynthetic vegetation cover then slowly declines throughout summer due to natural decay and grazing by stock.

Collection of field (*in situ*) fractional cover data: Field (*in situ*) fractional cover data was collected on three dates at a MODIS appropriate scale using two survey methods, one step-point and the other photographic (results not reproduced here). The three dates, April, June and October, were chosen to ensure that a wide range of variation in fractional green vegetation (*f*GV), dead or non-photosynthetic vegetation (*f*NPV) and soil exposure (*f*Soil) were sampled. The April and June surveys recorded a range of *f*NPV and *f*Soil, while the October survey captured maximum *f*GV cover.

The step-point method entailed walking large distances through fields, and therefore to avoid damage to crops was only used on the first two survey dates (April and June) when crops were either not present, or very new. The photographic method was used on the last survey date to minimise crop disturbance.

Step-point method: A step point transect was conducted by surveyors crossing the field from fence to fence in a "W" pattern. Surveyors travelled from a road-side field corner to the opposite fence at the 1/3rd point, back to the middle of the road-side fence, crossed again to the opposite fence at the 2/3rd point, then finished

at the other road-side field corner. The surveyors recorded the cover type (green vegetation (GV), non-photosynthetic vegetation (NPV), or soil) every second step under a thin line drawn on the end of their shoe.

The total number of step-point recordings taken within each field was dependent on field size and geometry, and ranged from 560 to 2500 (equating to approximate transect distances of 900 m to 4000 m). Fractional cover was calculated for each field as the proportion of each cover type in the step-point tally.

Photographic method: To minimise crop disturbance on the October survey date, when the crops were fully developed, a minimally invasive photographic method was used. In each field between six and thirty nadir-oriented colour digital photographs were taken from approximately one meter above the canopy, and fractional GV, NPV, soil and shadow was quantified (Figure 7.1). Photographs were taken within two hours of local solar noon.

To quantify fractional cover, a regular 10 x 10 grid was overlain on each photograph, and each grid point was visually classified as either GV, NPV, soil or shadow. These counts were then tallied for each field, and fractional cover of each component was calculated as the proportion of each cover type (excluding shadow).

Photographs were taken along short transects near the corners of fields, far enough into the field to minimise edge effects. While more photographs were taken in fields with more perceived cover variation, analysis revealed little variation in cover levels between photographs within fields.

Figure 7.1 Example nadir-oriented field cover assessment photograph taken from 1 m above canopy, with 10 x 10 sample grid overlain (red + symbols).

Comparison of step-point and photographic method: The superficial differences between the step-point and photographic methods should not differentially influence the measured fractional covers. Both methods were designed to minimise human error and bias, and both relied on visual interpretation of cover type at points.

Comparison of remotely sensed and *in situ* data: Linear regression relationships between remotely-sensed and field fractional cover values were calculated, with the remotely sensed values treated as the independent

variable, and the field values treated as the dependent variable. For RSMA, Root-mean-square error (RMSE) and mean absolute error (MAE) were calculated to quantify the error in the remote sensing estimates of fractional cover. These results are presented in Okin *et al*. (2013). For LCI, correlation coefficients were calculated and are presented in Clarke et al. (2011).

7.4.3 Landsat Seasonal – Joint Remote Sensing Research Program – after Scarth et al. (2010)

Fractional cover field data were collected over several campaigns lasting from January 2000 until September 2012. Sites were selected based on an analysis of land types across Australia, coupled with the expert knowledge of local field officers who pinpointed appropriate target sites. These sites were located in both homogeneous and heterogeneous environments across both grazing and cropping lands, and also sampled a range of overstorey tree canopies so that algorithms to remove the effect of tree canopies could be developed at a later stage. A map of field site location is shown in Figure 7.2. The field survey method and the attributes collected are described in Muir et al. (2011).

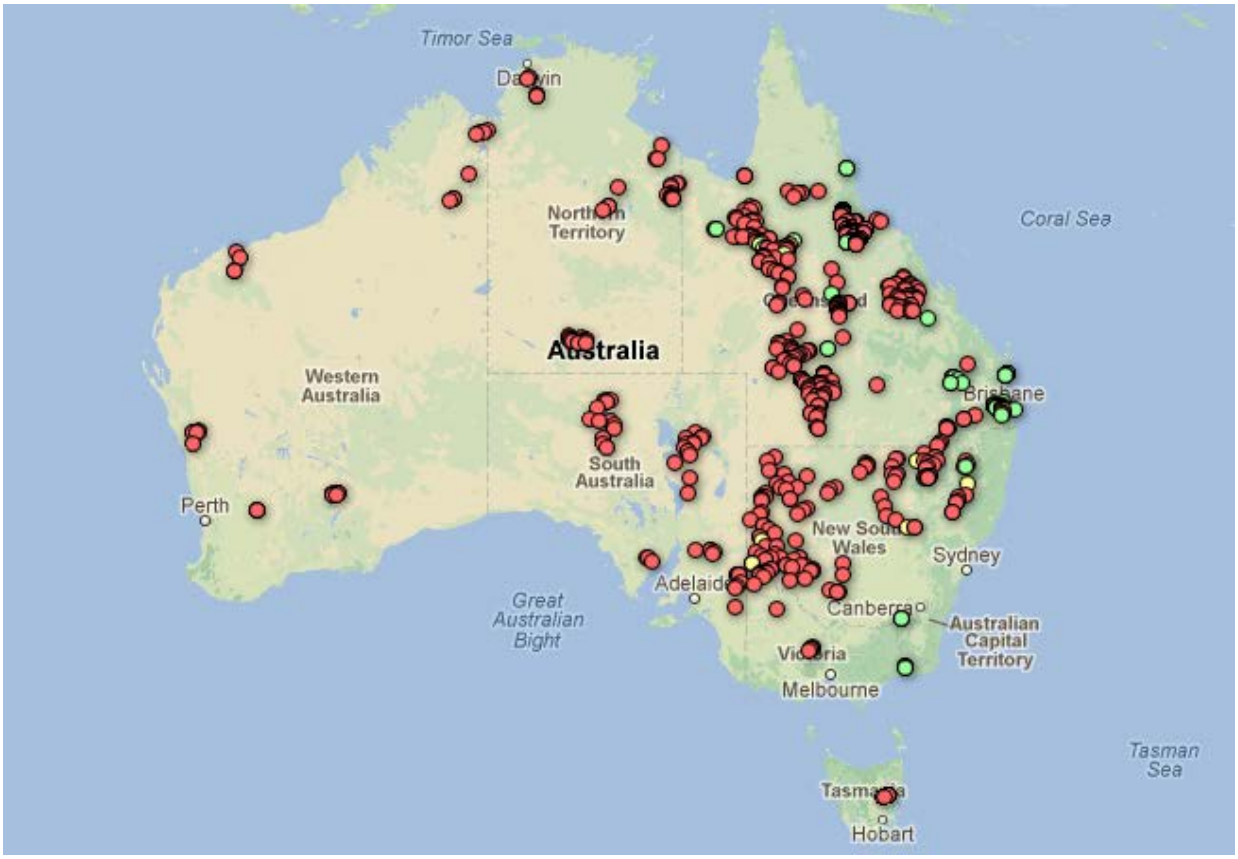

Figure 7.2 Map of Australia showing the location of field sample plots (red dots)

7.5 Australian Fractional Cover – Validation Results

7.5.1 MODIS – CSIRO by J.Guerschman after Guerschman et al. (2009)

The distribution of the land pixels in Australia suggest that the data used by Guerschman *et al*. (2009) to calibrate the current model (taken in the northern part of Northern Territory [NT]) is not representative of all the possible conditions found in the Australian rangelands. While expected, this result emphasises the need for a more comprehensive collection of field data to better represent fractional cover in the rangelands.

Concurrent vegetation and spectral measurements taken at 14 sites in the Murrumbidgee catchment, selected a priori for having an homogeneous land cover at the MODIS scale, suggested that:

- The hyperspectral model proposed by Guerschman *et al*. (2009) can accurately resolve the vegetation cover fractions (root mean squared error [RMSE] between 10 and 12%).
- When aggregated to MODIS spectral bands or convoluted, the spectral measurements can also estimate vegetation fractional cover without an important loss in accuracy (RMSE between 12 and 14%).
- When actual MODIS data are used the model can also reproduce vegetation cover with RMSE between 13 and 16%.
- When considered simultaneously, data from 556 field observations (over space and/or time) show an overall error (RMSE) of the model of 17.2% in the photosynthetic vegetation (PV), 25% in the non-photosynthetic vegetation (NPV) and 26% in the bare soil (BS) fractions. The NPV and BS estimations have considerable bias (NPV is underestimated and BS overestimated).

An attempt to quantify the effects of site heterogeneity on the model performance using a single Landsat epoch of the dry season of 2004 did not provide conclusive results. There was a very weak relationship between the heterogeneity metrics calculated and model performance.

This may be due to:

- using a single Landsat image not coincident with the date when the field measurement occurred failing to properly capture the actual heterogeneity at the time of the visit
- the metrics calculated being inappropriate for the purpose
- a weak relationship between site heterogeneity and model performance. It is recommended that a better assessment of the site heterogeneity is performed using Landsat imagery acquired close to the date the site was visited.

An analysis of the effects of soil surface colour on the model performance suggested that bright soils were associated with poor model performance. However, these results should be taken with caution as the scale of the soil map used is likely not appropriate for characterising the soil colour of a specific site. Recent progress in proximal soil sensing techniques could provide a better way to assess these effects.

An analysis of soil moisture content of the upper layer on model performance showed that soil moisture does have a significant effect. Model estimates in wet soils tend to be confounded with NPV. An analysis of the duration of wet conditions in the upper soil layer (which affects the spectral properties observed by the satellites) in space and in time would be beneficial to understand its effect on the estimates at a continental scale.

A recalibration of the model in its current configuration using all the available field observations decreased the RMSE of the three cover fractions from 17% to 14.7% (PV), 25% to 20.6% (NPV) and from 26% to 17% (BS).

The new parameters eliminated the bias in the three fractions. A new dataset with the new parameter values has been produced and was made available through the TERN Landscape Assessment website.

7.5.2 MODIS – LCI by K. Clarke after Clarke et al. (2011)

Linear regression relationships were calculated between LCI and NDVI and field fractional cover, with LCI and NDVI treated as the independent variable, and the field values treated as the dependent variable. The results are presented in Clarke et al. (2011), and the regressions are shown in Figure 7.3 below.

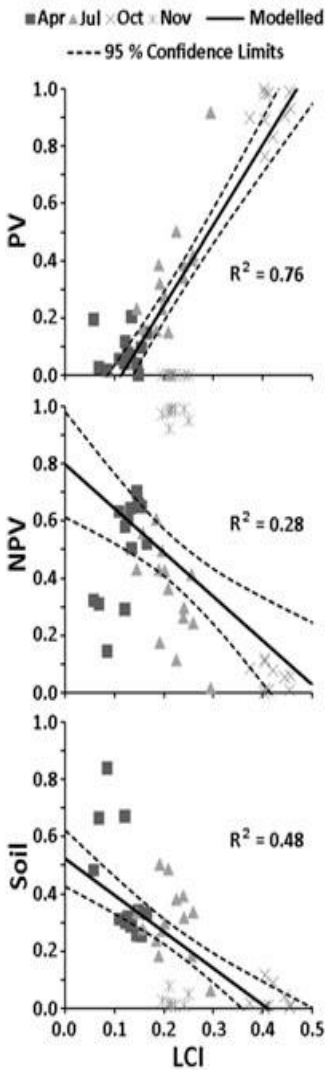

Figure 7.3 Remotely sensed LCI values plotted against in situ values for Soil, PV and NPV (from Clarke et al., 2011).

7.5.3 MODIS – RSMA by K. Clarke after Okin et al. (2007, 2013)

Linear regression relationships between remotely-sensed and field fractional cover values were calculated, with the remotely sensed values treated as the independent variable, and the field values treated as the dependent variable. Root-mean-square error (RMSE) and mean absolute error (MAE) were calculated to quantify the error in the remote sensing estimates of fractional cover. These results are presented in Okin *et al*. (2013) and a sample is shown in Figure 7.4 below.

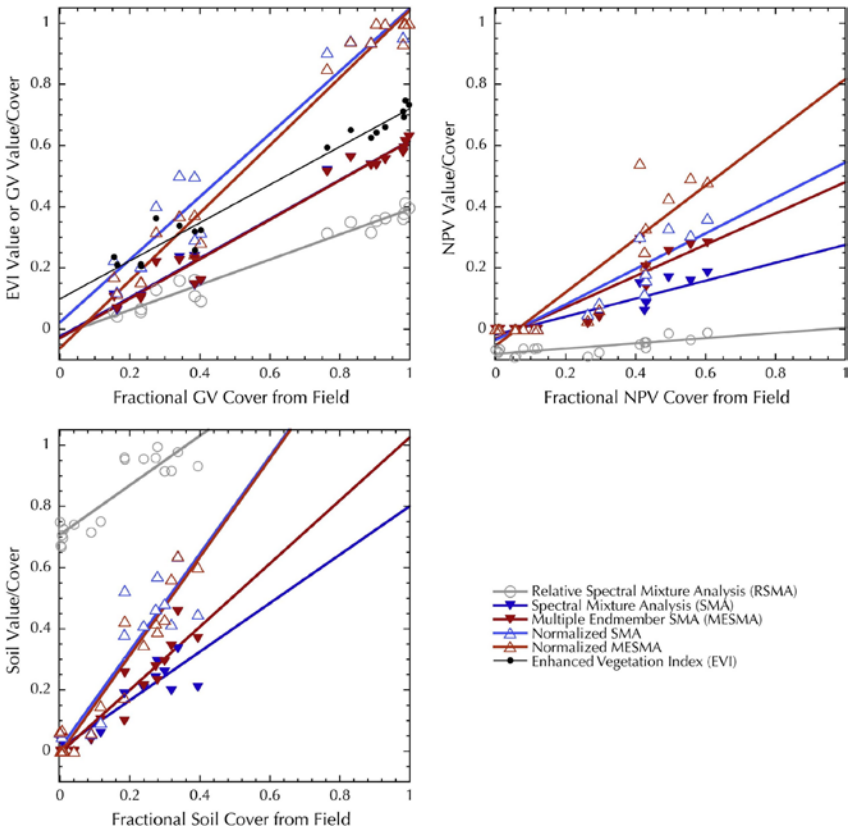

Figure 7.4 Remotely-sensed index/cover values for GV, NPV, and soil plotted against in situ values. Lines are best-fit linear regressions (from Okin *et al*., 2013: Figure 4).

7.5.4 Landsat Seasonal - Joint Remote Sensing Research Program - after Scarth et al. (2010)

The field data derived endmembers were initially visually checked from anomalies and then assessed against the field data for their modelling performance. The final model fit is shown in Figure 7.5. This final model has a root mean square error of 9.5% for Green cover, 12.3% for non-green cover and 11.2% for bare cover.

Figure 7.5 From left to right. Unmixing results for the green, non-green and bare fractions, showing the model predicted result against the field determined cover amount.

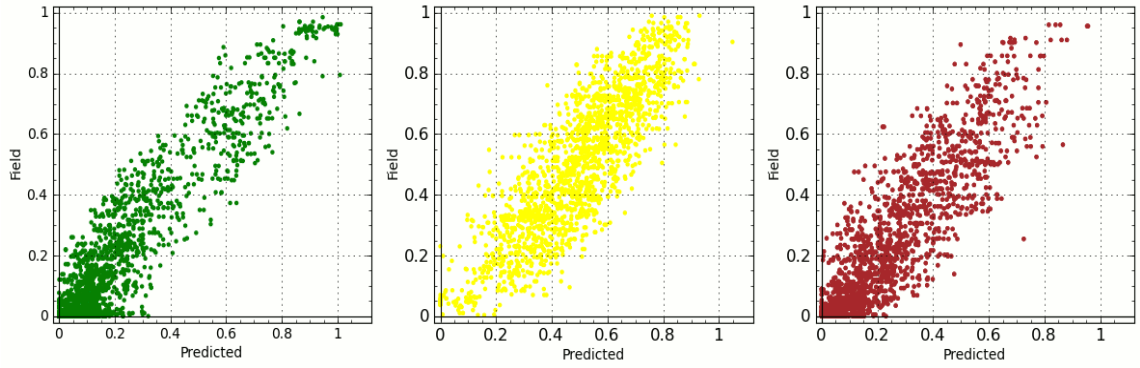

The final model was applied to 60,000 Landsat images across Australia and the results were visually interpreted by operators with knowledge over these landscapes. The subset in Figure 7.6 shows a heterogeneous rangeland landscape where there are dark downs soils, a significant drainage system across the image with associated lighter clay soils and some sparse woodland in the south. The fraction image accurately maps the variation between the bare, green and non-green components within the imagery, captures the connectivity of the riparian system and shows clear fenceline differences in the cover amounts in various paddocks on the image.

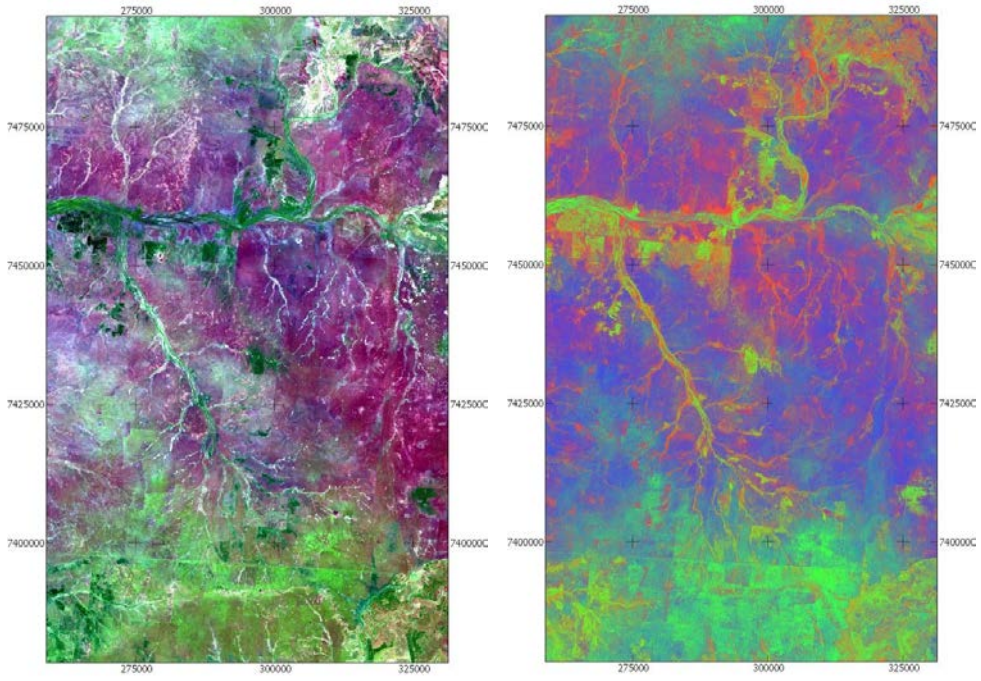

Figure 7.6
Left panel shows a portion of Landsat ETM+ data captured on 3rd June 1999 over Path 95, Row 76 with Bands 543 displayed as RGB. Right panel shows the fraction image with bare, green and non-green fractions displayed as RGB. Gridlines indicate coordinates on the EPSG:32754 grid.

7.5.5 MODIS – CSIRO by J.Guerschman after Guerschman et al. (2015)

Estimates of the errors in the fractions retrieved by the algorithm was obtained by comparing the observed and estimated fractions for the 1171 observations. A cross-validation step was included during model calibration to select the optimal number of singular values to avoid over-fitting. Figure 7.7 shows the results of the validation. The unmixing performed using Landsat (taking a window of 3 × 3 pixels for each site) most closely matched the field site estimates that were collected at the same spatial support. The goodness of fit decreased when the Landsat reflectance was aggregated to an area similar to the MODIS pixel. The unmixing of the two MODIS products (MCD43A4 and MOD09A1) had a lower goodness of fit (i.e., lower correlation and higher RMSE) to the obtained using the $L_{17\times17}$. Amongst the MODIS products, MOD09A1 had a slightly better goodness of fit than MCD43A4.

Overall, for MODIS data, the estimates had a RMSE of 13% for the green fraction, 18% for the NPV fraction and 16.5% for the bare fraction. These results are an improvement over the method of Guerschman et al. (2012) who had reported RMSEs of 17.2% (PV), 25% (NPV) and 26% (BS).

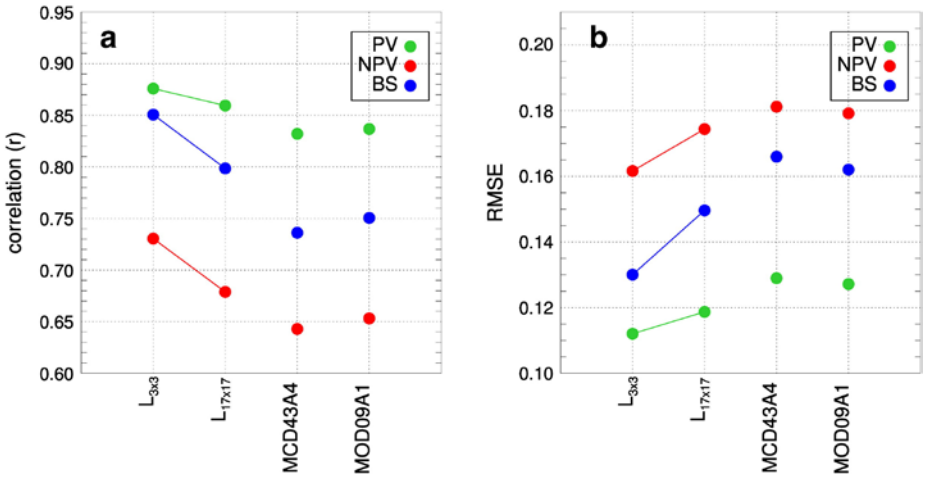

Figure 7.7. Summary metrics for the spectral unmixing using alternative surface reflectance sources. (a) Pearson's correlation coefficient and (b) root mean square error. $L_{3\times3}$ and $L_{17\times17}$ correspond to the Landsat surface reflectance aggregated to alternative window sizes, MCD43A4 and MOD09A1 correspond to the two MODIS products tested

Similarly to the approach of Guerschman et al. (2009) this method was applied to the full collection of MODIS data for Australia. The resulting product have the spatial patterns as shown in Figure 7.8.

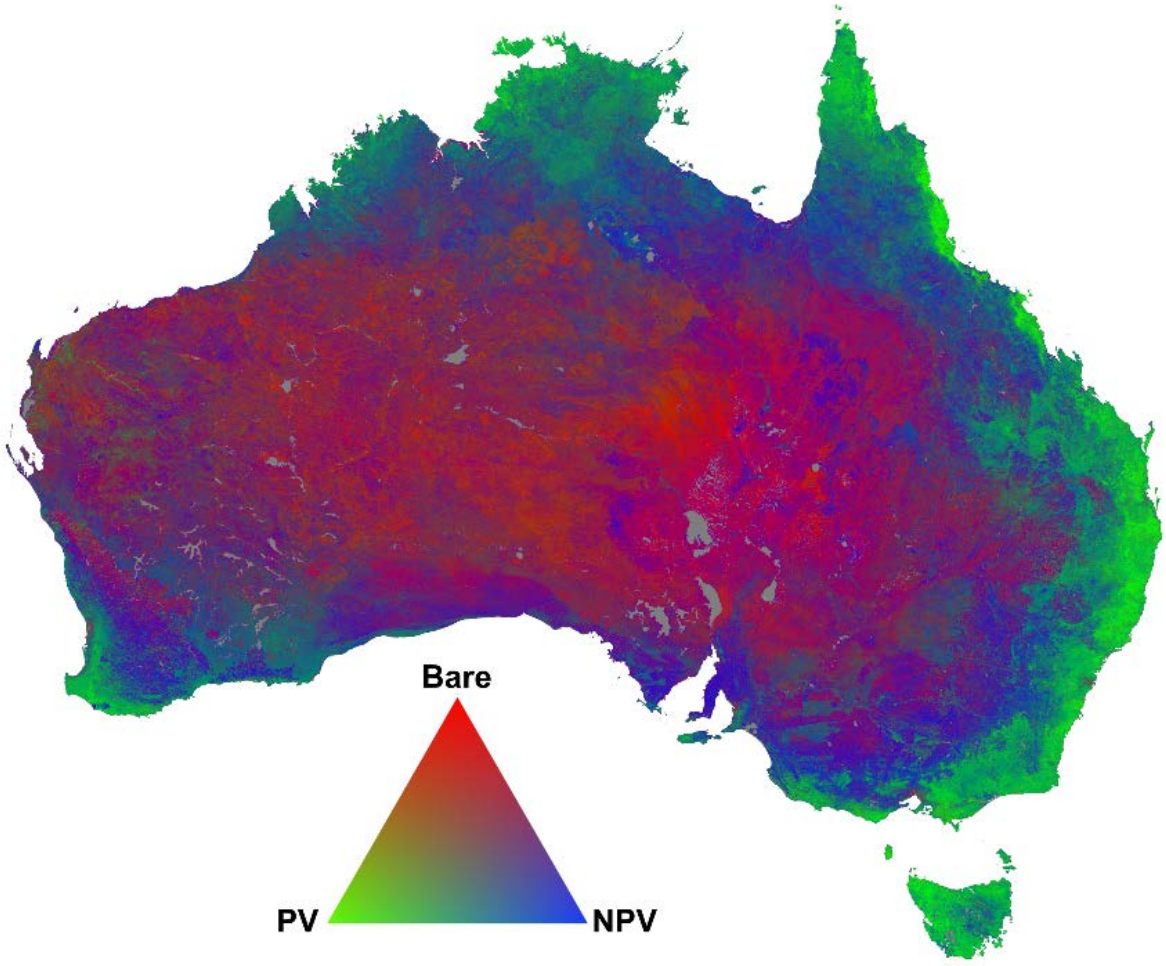

Figure 7.8. Fractional Cover image for Australia for April 2015.

7.6 Future Fractional Cover Mapping and Validation

The three approaches presented in this chapter demonstrate how a network of field sites and imagery can be used to develop robust national scale fractional cover models that successfully retrieve estimates of green, dead and bare ground fractions. The MODIS based approaches of Guerschman and Clarke produced moderate to high levels of accuracy over most of the cover types validated across Australia. In the Landsat based approach of Scarth, the use of synthetic endmembers in a constrained non-negative least squares unmixing model enabled the successful retrieval of the groundcover fractions over a large number of scenes across Australia. To further improve these products, future work will concentrate on collecting additional field data over a variety of different environments along with coincident imagery. By using extensive field data sets to drive the MODIS and Landsat derived fractional cover time series products, these can serve as key indicators used for a range of environmental monitoring and management activities from catchment to state and continental scales.

References

Clarke, K., Lewis, M., Dutkiewicz, A., Forward, G., & Ostendorf, B. (2011). Spatial and temporal monitoring of soil erosion risk with satellite imagery. Land Condition Monitoring Reports, Report 4. Adelaide, The University of Adelaide, report for the South Australian Department for Environment and Natural Resources.

Clarke, K., Lawley, E., Raja Segaran, R., & Lewis, M. (2014) Spatially-explicit environmental indicators for regional NRM planning for climate change. Adelaide, The University of Adelaide, Report for Natural Resources SA Arid Lands.

Guerschman, J. P., Hill, M.J., Renzullo, L. J., Barrett, D. J., Marks, A. S., & Botha, E. J. (2009). Estimating fractional cover of photosynthetic vegetation, non-photosynthetic vegetation and bare soil in the Australian tropical savanna region upscaling the EO-1 Hyperion and MODIS sensors, *Remote Sensing of Environment*, 113(5), 928–945, doi:10.1016/j.rse.2009.01.006.

Guerschman, J. P., Oyarzábal, M., Malthus, T. McVicar, T. R., Byrne, G. , Randall, L. & Stewart, J. (2012)/ Evaluation of the MODIS-based vegetation fractional cover product, CSIRO Land and Water, Canberra, Australia, Canberra. [online] Available from: http://www.clw.csiro.au/publications/science/2012/SAF-MODIS-fractional-cover.pdf

Guerschman, J. P., Scarth, P. F., McVicar, T. R., Renzullo, L. J., Malthus, T. J., Stewart, J. B., Rickards, J.E. & Trevithick, R. (2015). Assessing the effects of site heterogeneity and soil properties when unmixing photosynthetic vegetation, non-photosynthetic vegetation and bare soil fractions from Landsat and MODIS data. *Remote Sensing of Environment*, 161, 12–26. doi:10.1016/j.rse.2015.01.021

Muir, J., Schmidt, M., Tindall, D., Trevithick, R., Scarth, P., & Stewart, J., (2011). Guidelines for Field measurement of fractional ground cover: a technical handbook supporting the Australian collaborative land use and management program. Tech. rep., Queensland Department of Environment and Resource Management for the Australian Bureau of Agricultural and Resource Economics and Sciences, Canberra. Retrieved from http://data.daff.gov.au/data/warehouse/pe_hbgcm9abll07701/HndbkGrndCovMontring2011_1.0.0_HR.pdf

Okin, G. S. (2007). Relative spectral mixture analysis — A multitemporal index of total vegetation cover. *Remote Sensing of Environment*, 106(4), 467–479. doi:10.1016/j.rse.2006.09.018

Okin, G.S., Clarke, K.D., & Lewis, M.M. (2013), Comparison of methods for estimation of absolute vegetation and soil fractional cover using MODIS Normalized BRDF-Adjusted Reflectance Data. *Remote Sensing of Environment*, v. 130, 266-279, doi:10.1016/j.rse.2012.11.021.

Scarth, P., Röder, A., & Schmidt, M. (2010). Tracking grazing pressure and climate interaction - the role of Landsat fractional cover in time series analysis. In: Proceedings of the 15th Australasian Remote Sensing and Photogrammetry Conference (ARSPC), 13-17 September, Alice Springs, Australia. Alice Springs, NT. doi:10.6084/m9.figshare.94250.

Chapter 8. Persistent Green Vegetation Fraction

T. Gill[1], K. Johansen[2], P. Scarth[3], J. Armston[3], R. Trevithick[3], N. Flood[3]

[1]Science Division, NSW Office of Environment and Heritage
[2] King Abdullah University of Science and Technology, Saudi Arabia
[3] Remote Sensing Centre / Joint Remote Sensing Research Program, Department of Science, Information Technology and Innovation

*Corresponding author:
Tony.Gill@environment.nsw.gov.au

Abstract

The Landsat based Persistent Green Vegetation Fraction product was produced using a time-series of annual images covering the whole of Australia between 2000 and 2010. Persistent Green Vegetation is nominally woody vegetation. The production of the map included initial image pre-processing and masking before a time-series of images of green, non-green and bare ground fractions were produced. The green fraction was further divided into persistent and non-persistent green vegetation to derive the fraction of persistent green vegetation persisting between 2000 and 2010 in Australia. Initial comparison of Landsat Persistent Green Vegetation Fractions with airborne Light Detection and Ranging (LiDAR) derived woody foliage projective cover fractions showed differences that were vegetation type specific (Root Mean Square Error (RMSE) 0.131±0.076). It is anticipated that the Persistent Green Vegetation Fraction product will support the evaluation of management activities and various vegetation structure and land cover change mapping applications.

Key points

- The Persistent Green Vegetation Fraction product is a consistently processed and validated Landsat based map of vegetation appearing persistently green (i.e. mainly woody vegetation) over an 11 year period between 2000 and 2010;
- The Persistent Green Vegetation Fraction product is the first Australia-wide map (nominally) showing the fraction and extent of woody vegetation at the Landsat scale; and
- The Persistent Green Vegetation Fraction product may support management activities, vegetation structure assessment, carbon applications, landscape ecology research and land cover mapping applications in various environments across Australia.

8.1 Introduction and Background Information

The Persistent Green Vegetation Fraction product provides an estimate of the vertically-projected green-vegetation fraction, where vegetation is deemed to persist over time. These areas are nominally woody vegetation. The product also shows those areas where green vegetation does not persist over time. These areas are nominally bare ground or consist of understorey species that green-up in response to rain. It is intended that this product will facilitate the assessment of environmental management programs, carbon accounting and land-cover change assessment in Australia. Measurements of persistent green vegetation will also provide an essential variable for ecological and ecosystem models of vegetation structure and dynamics in Australia.

The Persistent Green Vegetation Fraction product is a Landsat based product produced on 30 m x 30 m pixels for the entire Australian mainland and Tasmania. The product is based on an inter-annual time-series of Landsat-5 Thematic Mapper (TM) and Landsat-7 Enhanced Thematic Mapper Plus (ETM+) image data. One dry season image is collected per year in the period from 2000 to 2010. As such it represents the best estimate of persistent green cover within this 11 year period. As part of the product, three derivatives are delivered: (1) masks; (2) statistics; and (3) the Persistent Green Vegetation Fraction product. The Landsat based Fractional Cover product, described in Chapter 7, is one of the inputs used to create the Persistent Green Vegetation Fraction product.

The Persistent Green Vegetation Fraction product was developed as part of a Terrestrial Ecosystem Research Network (TERN) Labndscapes Brisbane node deliverable. The objective was to produce a well calibrated and validated Landsat based map of the Persistent Green Vegetation Fraction based on a 2000 to 2010 time-series for the whole of Australia. The product has been based on the successful development and application of the Foliage Projective Cover (FPC) product developed by the Queensland Government's Remote Sensing Centre at part of the Statewide Landcover and Trees Study (SLATS). FPC is defined as the vertically projected cover of photosynthetic foliage of all strata, or equivalently, the fraction of the vertical view that is occluded by foliage stemming from woody vegetation (Armston *et al.*, 2009). The production of the FPC product for Queensland requires the application of masks produced from land-cover and land-use maps to omit agricultural areas as well as manual steps to refine the cloud masking and the final FPC map. As land-cover and land-use maps were not available for the whole of Australia, this step could not be implemented at a continental scale. Also, the manual steps use to refine the final FPC maps are labour-intensive and hence prohibitively time-consuming at the continental scale. Hence, it was decided to develop a fully automated approach and rename the FPC product to Persistent Green Vegetation Fraction, as it could not be guaranteed that persistently green pastures would be discriminated from woody vegetation. An example of this includes the Atherton Tablelands in Far North Queensland with consistently green fields.

8.2 Data Collection

Approximately 4000 Landsat-5 TM and Landsat-7 ETM+ images were downloaded from the United States Geological Survey (USGS) Earth Explorer website. A total of 374 worldwide reference system 2 (wrs2) scenes were required per year for continental coverage. A number of criteria were developed to identify the most suitable images. The first criterion was to use Landsat-5 TM and Landsat-7 ETM+ Scan Line Corrector (SLC)-on data with no or as small a proportion of cloud cover as possible. The second criterion was to identify suitable image data on anniversary dates to reduce seasonal effects of woody vegetation. Hence, the search for images focussed on the dry season of any particular area of Australia, as this increased the chances of identifying cloud free images collected at the same time of the year for the time period between 2000 and 2010. The dry season images also enhanced the spectral contrast between evergreen tree and shrub canopies and the predominantly senescent ground cover.

8.3 Processing Workflow

All processing steps in the workflow (Figure 8.1) for producing the Persistent Green Vegetation Fraction product were automated. The initial step involved the pre-processing of the downloaded Landsat images to convert the images to Bidirectional Reflectance Distribution Function (BRDF) corrected reflectance. The method combines a simple top-of-atmosphere reflectance adjustment with an empirical BRDF model. The model parameters were derived from an overlapping sequence of Landsat images and were applied to produce spatially matched mosaics of Landsat ETM+ and TM imagery (Figure 8.2) (Danaher, 2002). The next step involved a number of masking routines to omit areas with cloud, cloud shadow, snow, topographic shadow, high incidence and exitance angles and water. Following the masking process, an unmixing algorithm and field data were used to create fractional cover images of green, non-green and bare ground fractions. A time-series algorithm combined with statistics and field data was used to classify persistent green vegetation and its fractional cover. Finally LiDAR data were used to validate the Persistent Green Vegetation Fraction product of Australia.

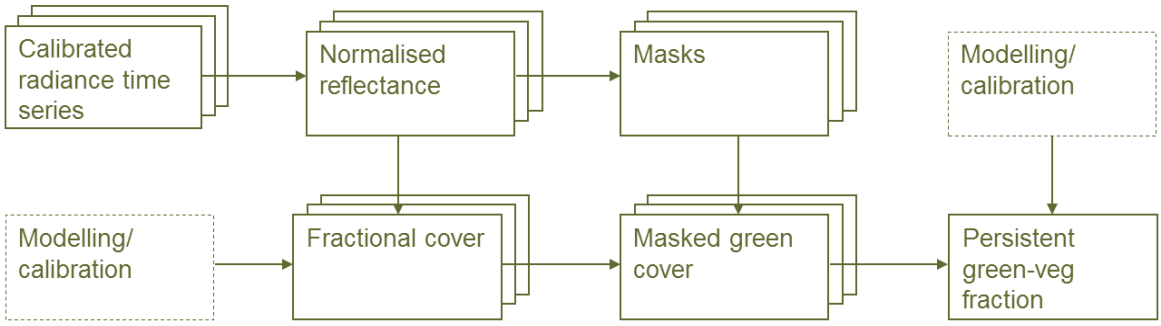

Figure 8.1 Flowchart showing the processing flow for producing the Landsat based Persistent Green Vegetation Fraction product of Australia.

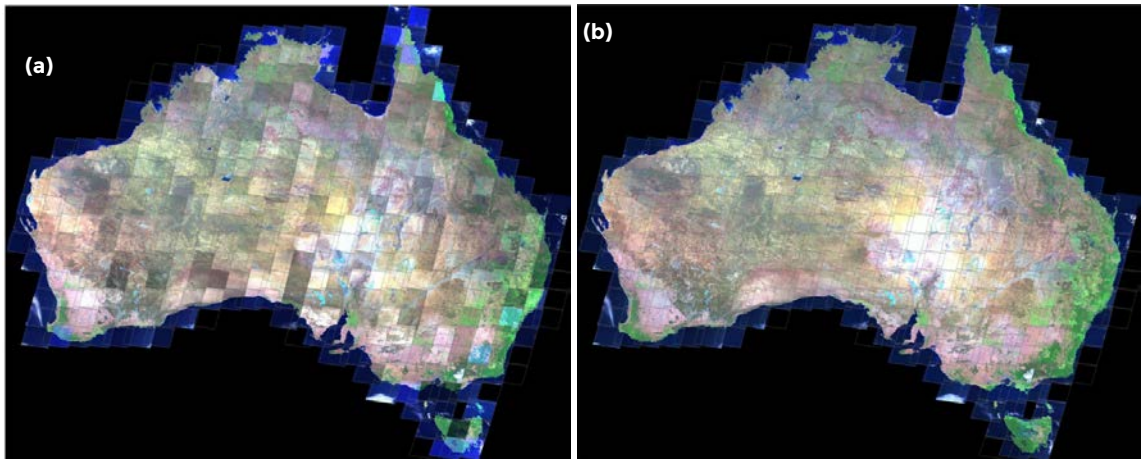

Figure 8.2
(a) Landsat images at-sensor radiance converted to
(b) BRDF corrected reflectance

8.3.1 Masking

A number of different masks were applied to omit areas with cloud, cloud shadow, snow, water, topographic shadow, and incidence and exitance angles greater than 80°. This process produced one composite mask image for each of the images in the time-series and these are provided as part of the Persistent Green Vegetation Fraction product, where the pixel values in the mask are:

0 = no data
1 = no mask
2 = large incidence or exitance angle (> 80°)
3 = topographically cast shadow
4 = cloud
5 = cloud shadow
6 = water
7 = snow.

If more than one mask could be applied to a pixel, then the above list of pixel values determines precedence with lower values having a higher precedence. For example cloud, with a code of 4 takes precedence over water, with a code of 6. In addition, if the fraction of pixels in the time-series classified as water is greater than 0.3, then the pixel is masked as water in the composited mask.

The cloud and cloud shadow mask was based on the Fmask (Zhu and Woodcock, 2012), which is an object-based cloud and shadow detection approach designed for Landsat image data. The reflectance image and the brightness temperature band are used to produce a temperature, spectral variability and brightness probability to identify the probability of being a cloud. Once the cloud layer is produced the corresponding cloud shadows are identified using the near infrared band together with information on sensor viewing angle and solar angle to predict the cloud shadow location and extent. This Fmask also included a snow mask.

A water mask based on discriminant analysis was applied to the images to omit all water bodies (Danaher and Collett, 2006). The water index was developed using Canonical Variates Analysis of visually identified water and non-water signatures in radiometrically calibrated Queensland wide Landsat image data. The index is a linear combination of bands, log transformations of bands and interactive band terms, which were used to set a threshold to mask water bodies.

Topographically shaded areas include areas that lie in shadows cast from the surrounding topography. The topographic shadow mask was created by a ray casting technique (Robertson, 1989). It was assumed that the light source was at infinity – i.e. all light is parallel and therefore the adjustment for perspective was not required. The satellite and sun azimuth and zenith angles were calculated per pixel directly from the orbital geometry. This mask allowed omission of areas within deep shadows cast by the surrounding terrain.

Incidence, exitance and relative azimuth angles are the satellite and sun angles, but transformed so that they are relative to the plane of the surface terrain. The incidence angle is the angle between the sun and the normal to the surface. The exitance angle is the angle between the satellite and the normal to the surface. The relative azimuth is the angle lying in the plane of the surface, between the projections into that plane of the lines to the sun and satellite. This information was used to produce a high sun incidence angle, i.e. the angle at which the Sun's rays strike the Earth's surface, and exitance angle mask to omit areas with an angle >80°.

8.3.2 Fractional Cover Product

The pre-processed and masked Landsat images were then used to produce fractional cover images of green, non-green and bare ground. A constrained (fractions have to add up to 100%) non-negative least squares unmixing model was applied based on endmembers selected from a collection of over 800 field sites (Figure 7.2). The overall model RMSE was 11.8% (Figure 7.5) with fractions stored in three image layers: Band1 – bare (bare ground, rock, disturbed), Band2 – green vegetation, Band3 – non green vegetation (litter, dead leaf and branches). Further details on the Landsat based Fractional Cover product (Figure 8.3) can be found in Chapter 7 of this book.

Figure 8.3
Landsat based Fractional Cover image.

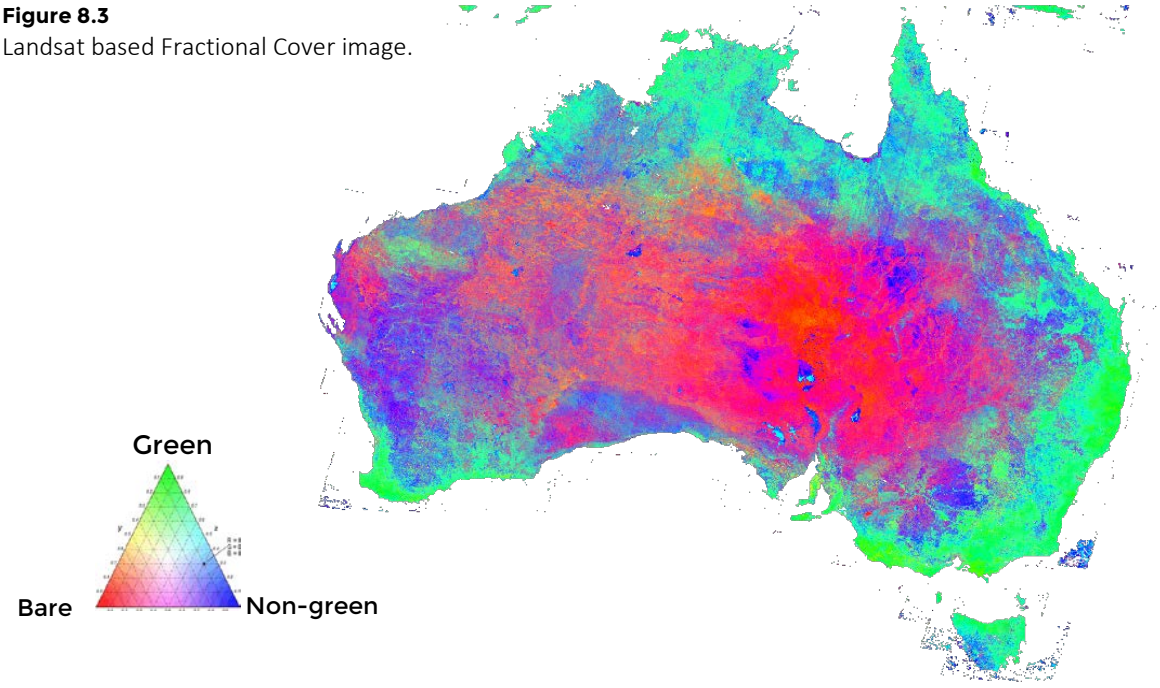

8.3.3 Classification of Persistent and Non-Persistent Green Vegetation

The Persistent Green Vegetation Fraction product shows those areas classified as persistent green and non-persistent green. A fractional cover estimate is provided for the persistent-green pixels. One image per WRS-2 scene is produced for the 11 year time-series. Pixel values are in the range 100-200, the null pixel is 0. Pixel values of 100 correspond to areas classified as non-persistent. Pixel values greater than 100 correspond to areas classified as persistent green. The fractional cover can be obtained from the pixel value using equation

1.

$$\text{Fraction} = \text{Digital Number (DN)} * 0.01 - 1 \qquad \textbf{(equation 1)}$$

The Persistent Green Vegetation Fraction product is derived from an inter-annual time-series of the green layer of the Landsat based Fractional Cover product described in Chapter 7. The Landsat based Fractional Cover product provides an estimate of the vertically-projected fraction of green vegetation, non-green vegetation and bare ground for each pixel. A robust regression of the form Y~b0 + b1*X, where Y is the green fraction and X is time, was fit to the masked time-series of green vegetation fractions to produce statistics that could be used to separate persistent from non-persistent green vegetation. The following seven statistics were derived from the regression modelling for each pixel:

1. Fitted fraction from the model at 30 June 2005 (the centre of the time-series);
2. Number of observations in the time series;
3. Minimum green fraction in the time series once outliers are removed, where an outlier is defined as a point whose residual (observed-fitted) is greater than MAD/0.6745 where MAD is the median absolute deviation of observations from the fitted line;
4. A measure of the standard error of the robust regression fit calculated using equation 2:

sqrt(chisqd/(N-2)) **(equation 2)**

where N is the number of observations in the time-series and chisqd is the weighted sum of squares of residuals;

5. A measure of the normalised standard error of the robust regression fit calculated as standard error divided by the minimum;

6. The slope of the regression line in units of percent green fraction per day; and

7. The standard deviation of negative residuals, i.e. those observations below the fitted line.

A training data set was obtained from field and image-interpreted observations of woody and non-woody locations in Australia, including a total of approximately 5100 point based sites of persistent and non-persistent green vegetation (Figure 8.4). The field based observations were derived from fractional cover field sites (SLATS star transects) across Australia, Diameter at Breast Height (DBH) field sites in the Northern Territory, low-foliage scrub sites within rangelands, woody vegetation sampling sites in Western Australia and biomass field sites in Queensland. The image based observations were derived mainly from SPOT-5 imagery and Google Earth to identify woody and non-woody vegetation.

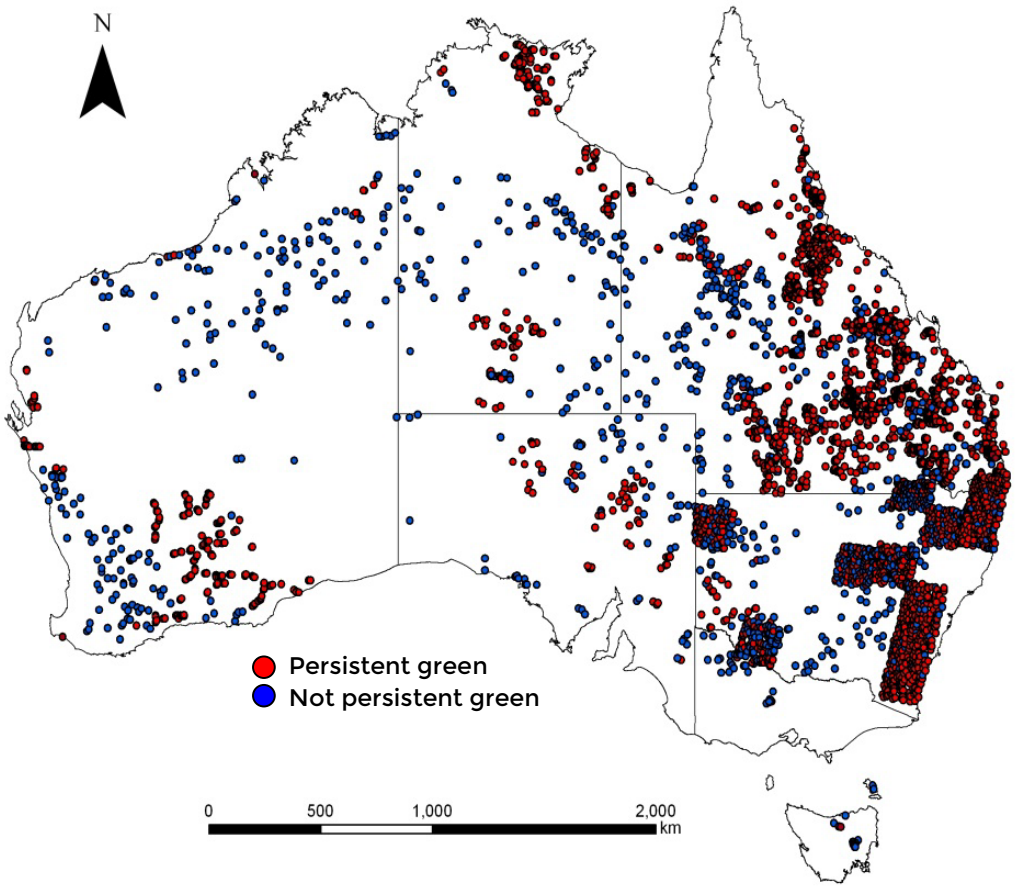

Figure 8.4 Field and image-interpreted observations (approximately 5100) of woody and non-woody locations.

A decision tree classifier implemented in R was calibrated based on the training data to classify pixels as persistent-green or non-persistent green using the produced robust regression statistics. The calibrated decision tree used to classify each pixel had the structure outlined in Figure 8.5.

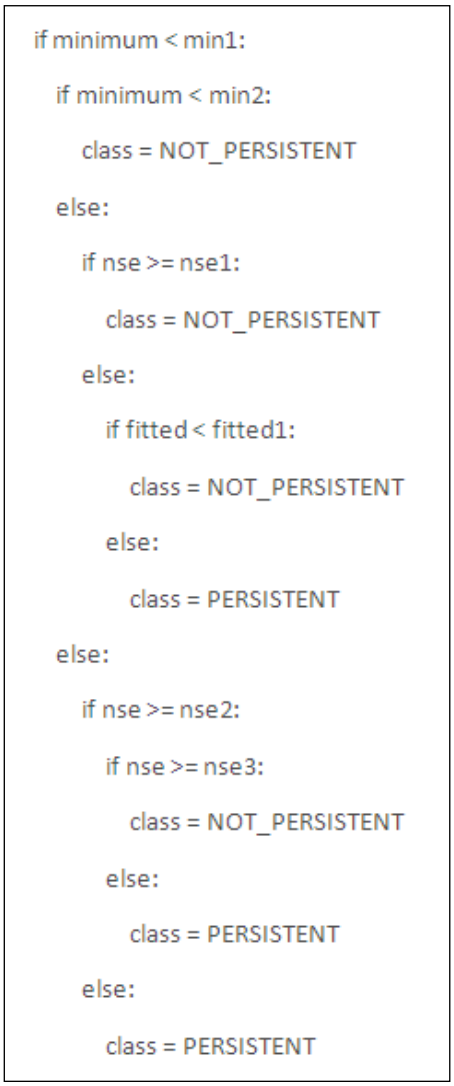

Figure 8.5 Decision tree used to classify each pixel as persistent-green or non-persistent green. minimum, nse and fitted are the minimum, normalised standard error and fitted fraction at 30 June 2005 for the time series. min1, min2, nse1, nse2, nse3 and fitted1 are the calibrated decision tree thresholds and take the values of 107.741297*, 104.540152*, 0.155654079, 0.101371804, 0.142790501, and 113.387517*, respectively. Those values marked with an asterisk are scaled DN values and the fraction is calculated as fraction=DN*0.01-1.

Figure 8.6 shows the variation in fractional cover for persistent and non-persistent green vegetation. Figure 8.7 shows how the variation over time and the minimum fraction of green vegetation within the time-series enable discrimination of persistent and non-persistent green vegetation.

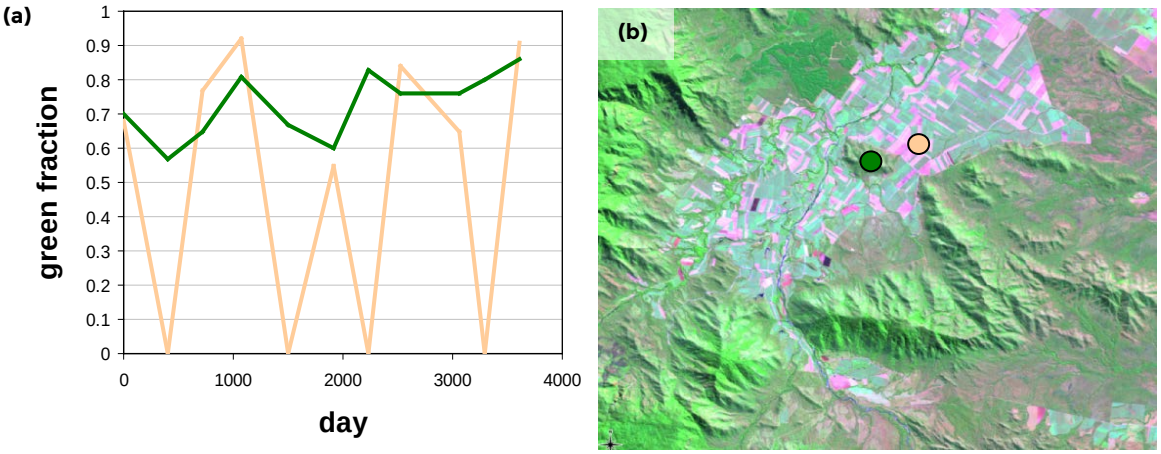

Figure 8.6
(a) Variation over the 11 year time-series (presented in a unit of days) of fractional cover of a persistent (green dot and line) and non-persistent (orange dot and line) green vegetation site, representing
(b) remnant woody vegetation and agricultural fields, respectively.

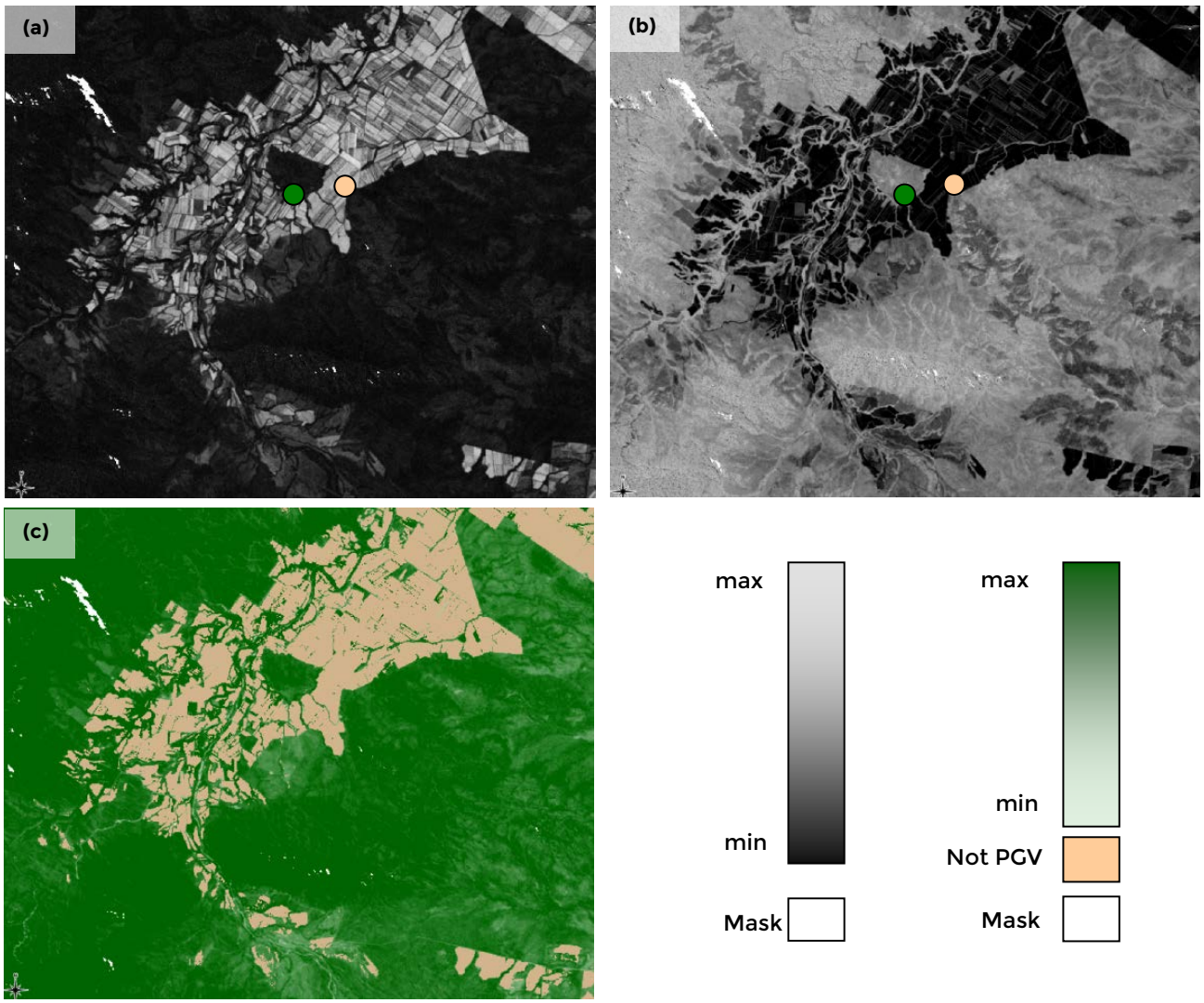

Figure 8.7 **(a)** Fractional cover variation in time-series,
(b) Minimum fraction in time-series, and
(c) Persistent green fraction.

The fractional cover for each pixel classified as persistent green vegetation was predicted using equation 3:

$$\text{Predicted} = \text{fitted} - 3 * \text{stdBelow} * (1 - \text{fitted})^2 \qquad \textbf{(equation 3)}$$

Where fitted is the green fraction from the regression model and stdBelow is the standard deviation of the negative residuals. This equation predicts the green fraction as the fitted fraction minus a correction factor. The correction factor decreases the fitted value. The amount is decreased by the standard deviation of the negative residuals. These residuals are a result of the variation in abundance of understory vegetation over time. As the canopy cover increases less of the understorey vegetation is observed and so the correction factor is reduced by the (1-fitted)^2 term. The multiplier of 3, is a parameter, and was derived by optimisation. The root mean squared error of a regression model that relates the predicted fraction to field-measured overstorey foliage projective cover was minimised.

Figures 8.8, 8.9, 8.10, 8.11, and 8.12 provide examples of the final Persistent Green Vegetation Fraction product.

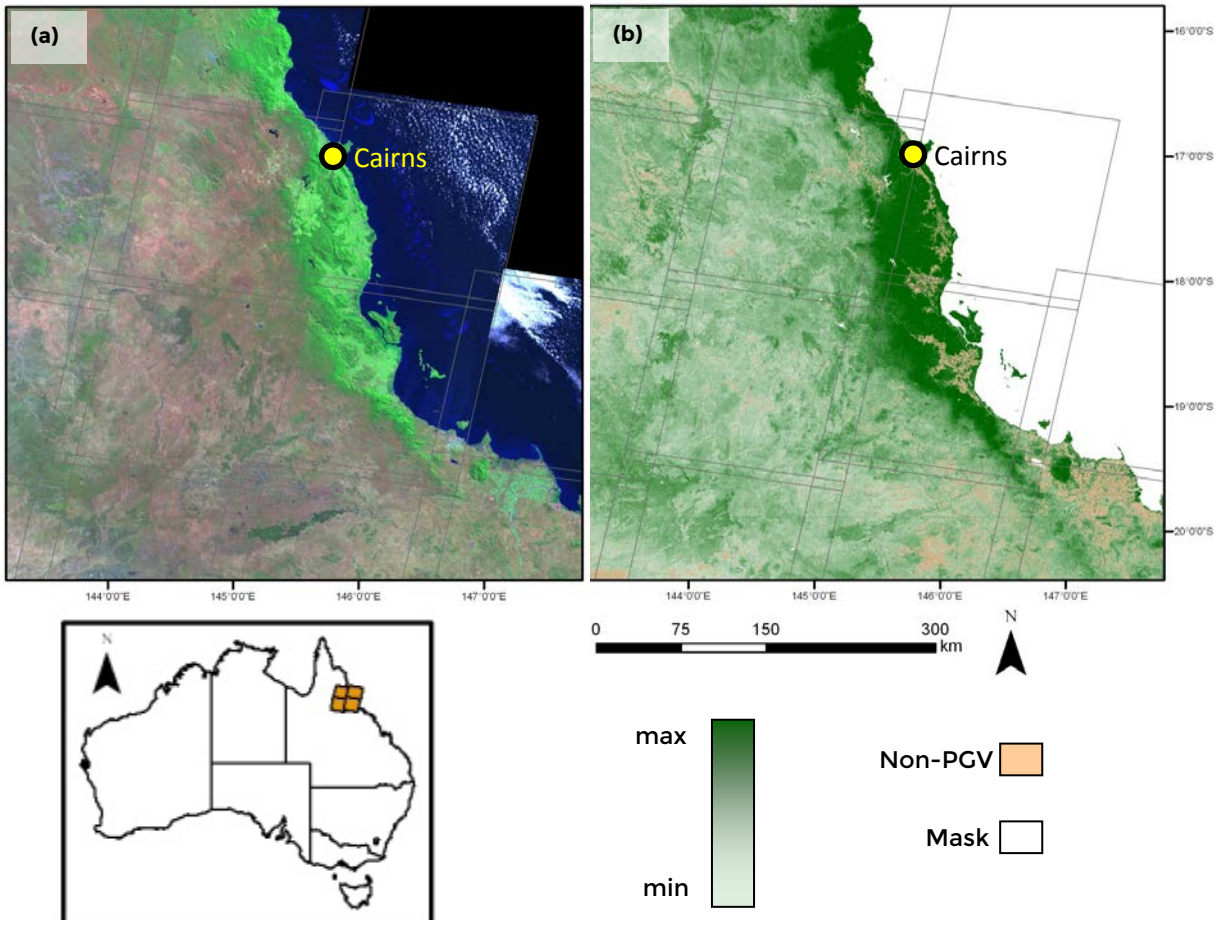

Figure 8.8 Landsat based:

(a) Reflectance image and

(b) Persistent Green Vegetation Fraction of the Cairns region of Far North Queensland. The footprints of each Landsat scene are outlined.

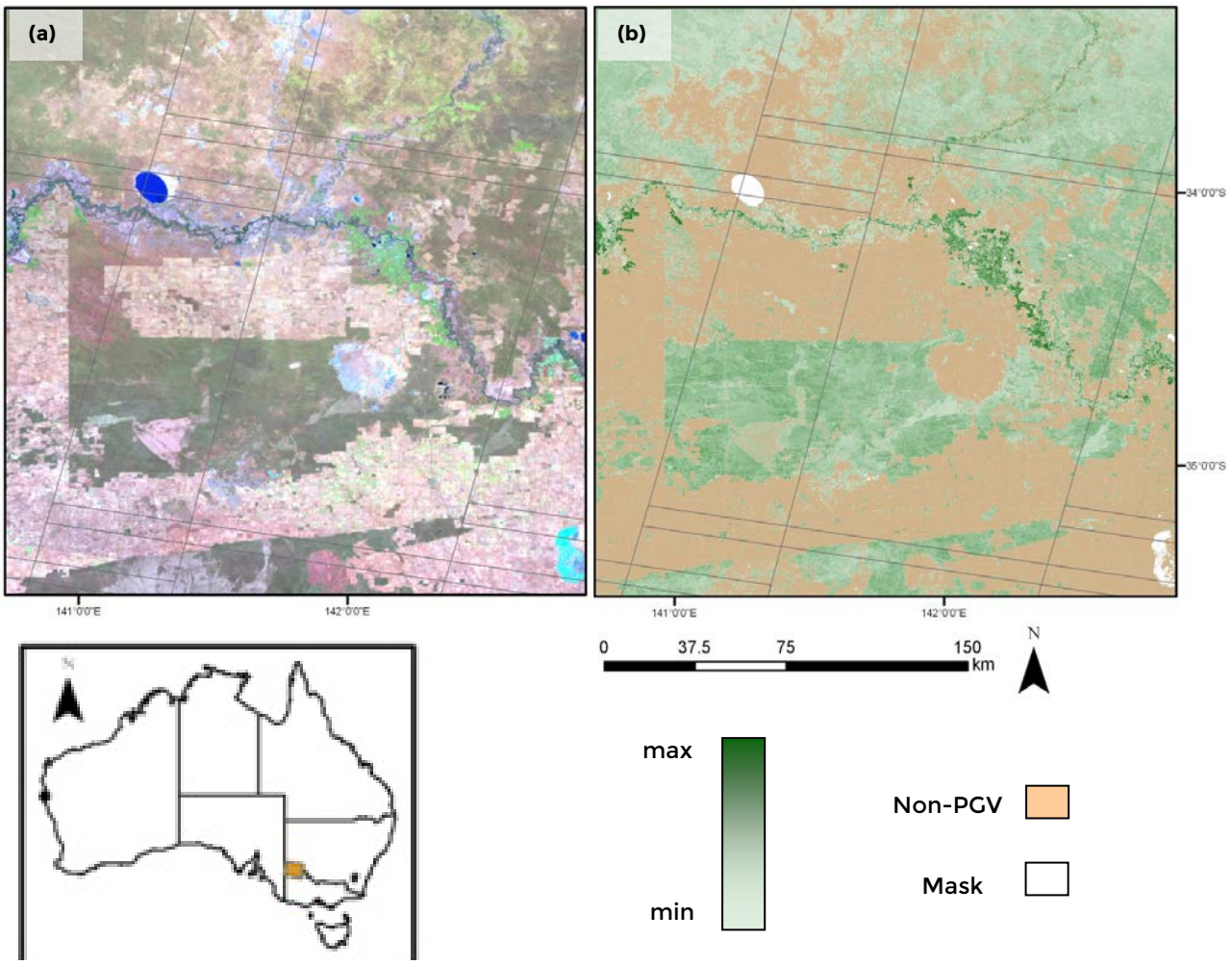

Figure 8.9 Landsat based:

(a) Reflectance image and

(b) Persistent Green Vegetation Fraction of the area between the South Australia, Victoria and New South Wales borders. The footprints of each Landsat scene are outlined.

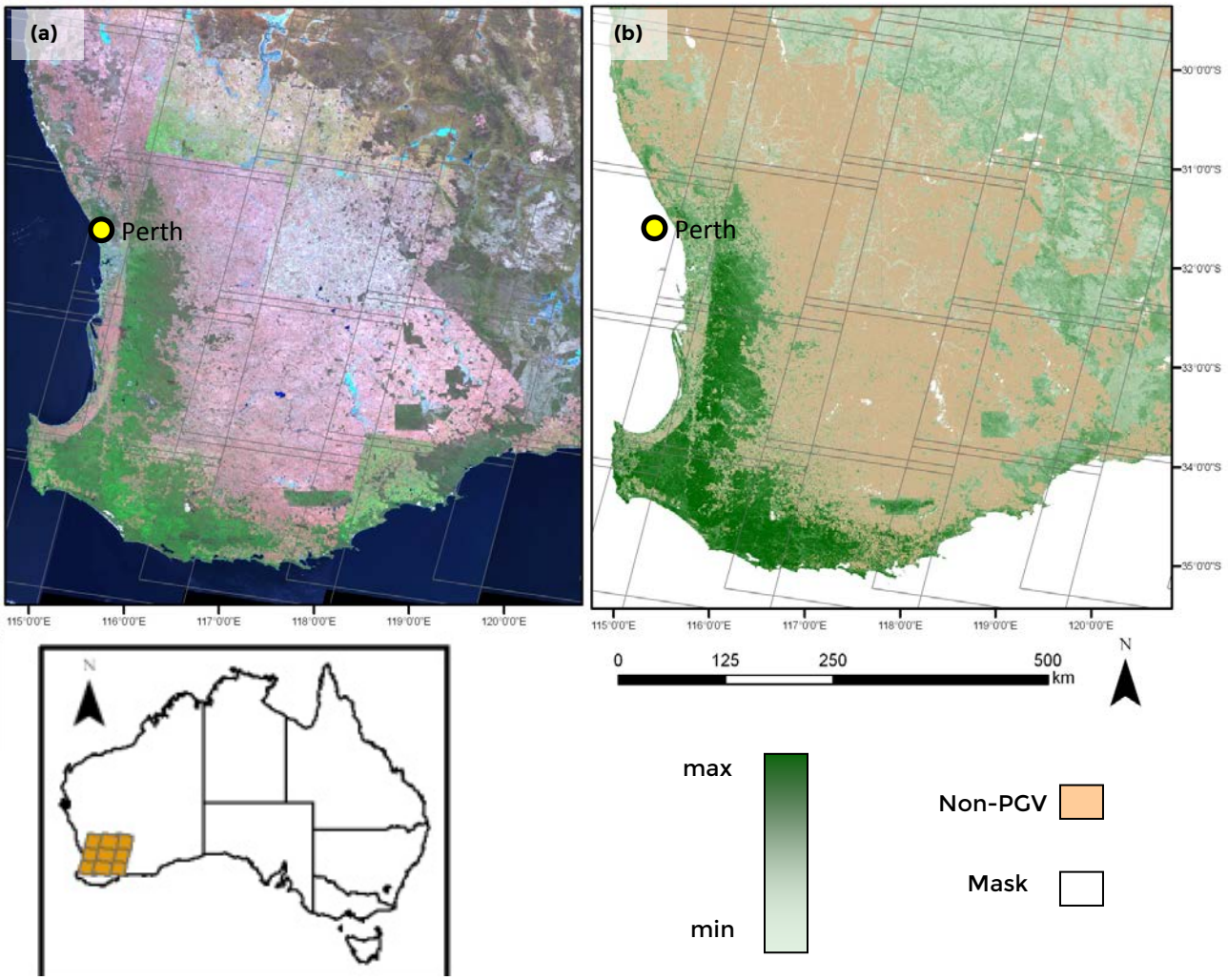

Figure 8.10 Landsat based:

(a) Reflectance image and

(b) Persistent Green Vegetation Fraction of the Perth region of Western Australia. The footprints of each Landsat scene are outlined.

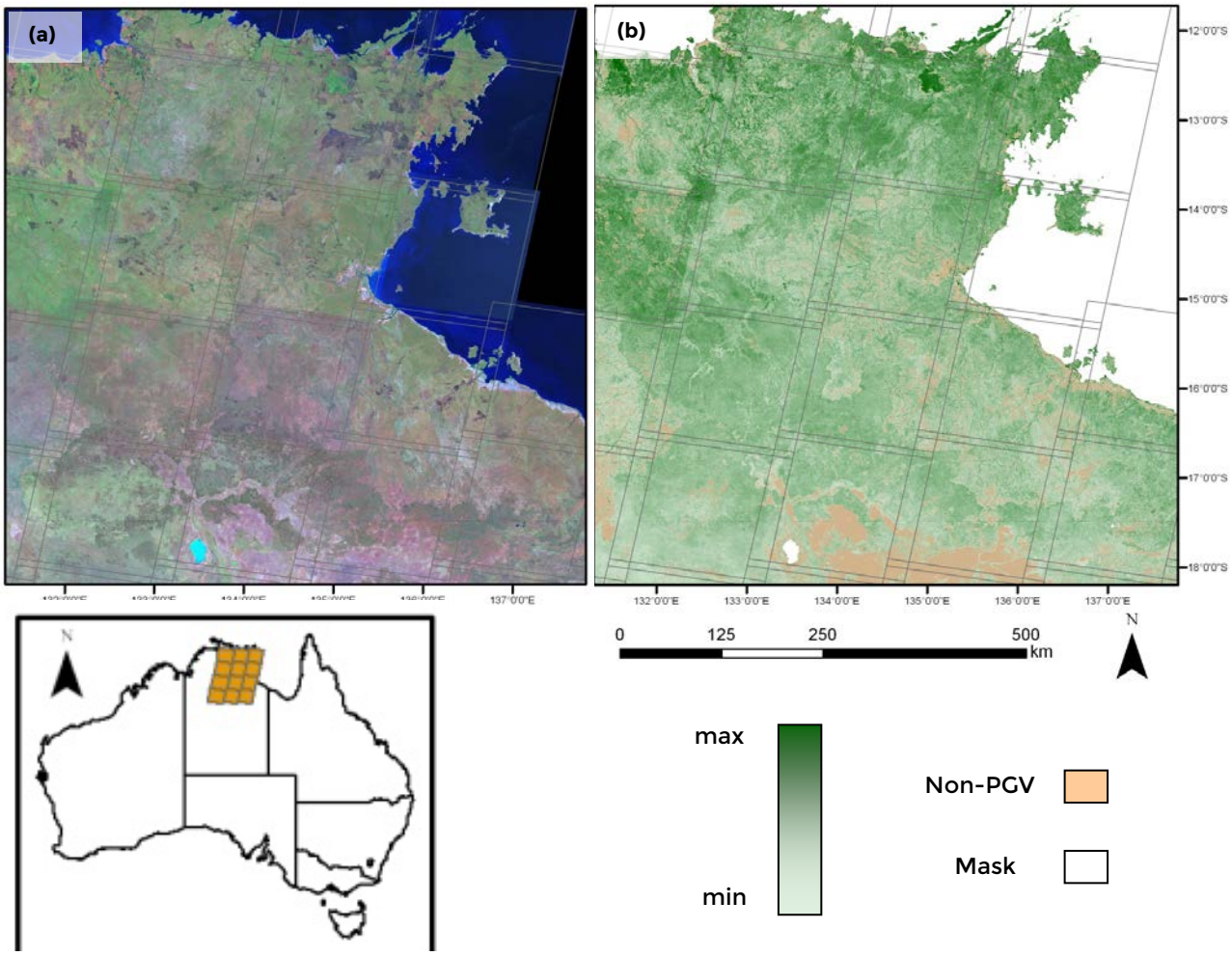

Figure 8.11 Landsat based:
(a) Reflectance image and
(b) Persistent Green Vegetation Fraction of the north-eastern parts of the Northern Territory. The footprints of each Landsat scene are outlined.

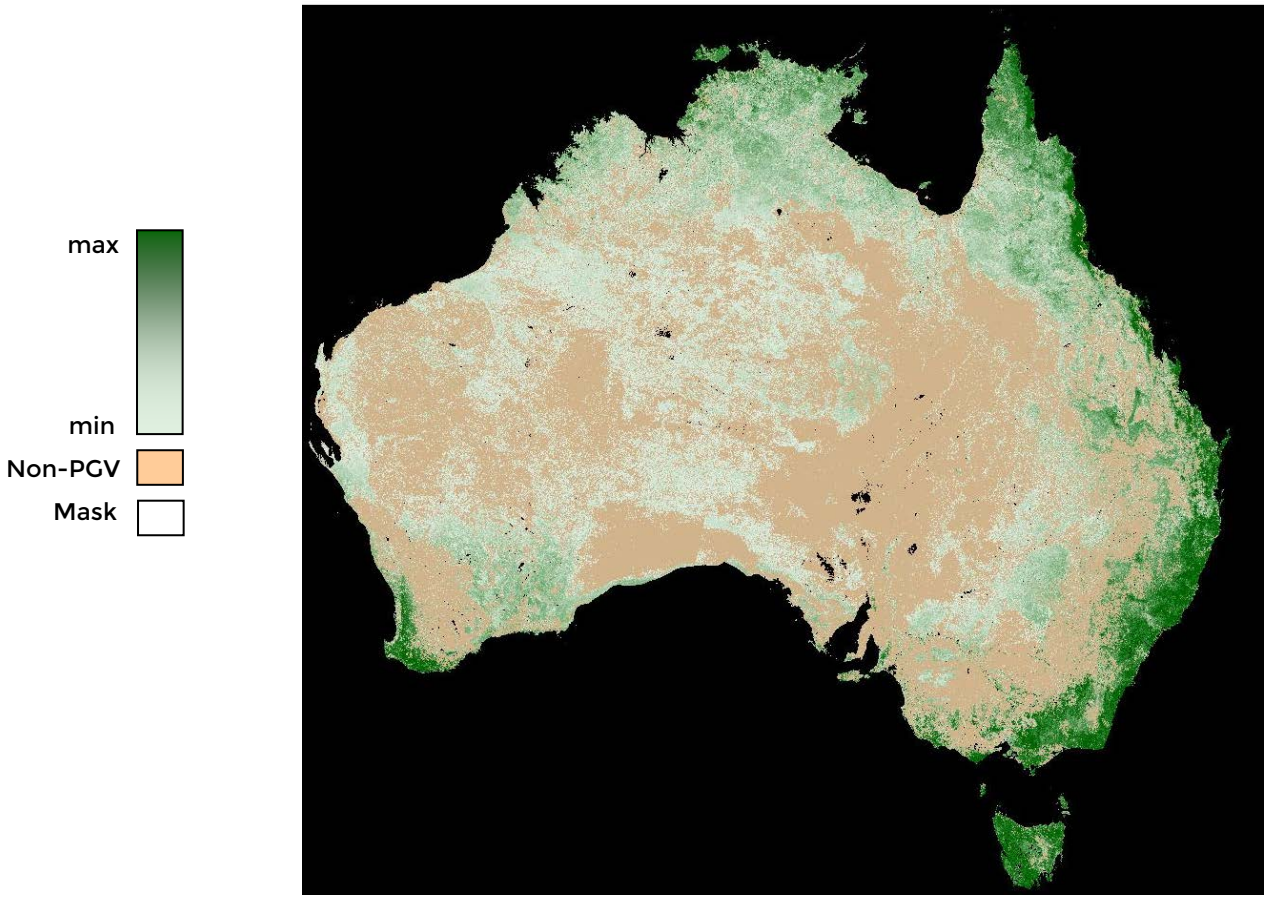

Figure 8.12 Persistent Green Vegetation Fraction of Australia based on a 2000-2010 time-series of Landsat image data.

8.4 Validation

Three validation stages were included in the production of the Persistent Green Vegetation Fraction product. These included:

1. Validation of Fractional Cover product – already described in chapter 7 "Validation of Australian Fractional Cover Products from MODIS and Landsat Data";
2. Validation of woody/non-woody vegetation; and
3. Validation of final product using airborne LiDAR derived estimates of vertically projected cover.

This section will present initial validation results of points 2 and 3. The classification accuracy of persistent and non-persistent green vegetation was determined by comparison to field and image-interpreted reference data of woody and non-woody vegetation. The overall accuracy achieved was 82.6% (kappa statistics of 0.678) (Table 8.1).

Table 8.1 Error matrix showing the producer's and user's accuracies for mapping persistent and non-persistent green vegetation.

		Reference data			
		Non- persistent green	**Persistent green**	Total	User's accuracies (%)
Mapped data	**Non- persistent green**	878	440	1318	66.61
	Persistent green	457	3366	3823	88.05
	Total	1335	3806	5141	
	Producer's accuracies (%)	65.77	88.44		

An accuracy assessment of the Persistent Green Vegetation Fraction product was produced by comparison to field measured woody foliage projective cover (AusCover Xwiki, 2014). A linear regression analysis showed an r^2 value of 0.859, slope of 0.928 and intercept of 0.005 (Figure 8.13).

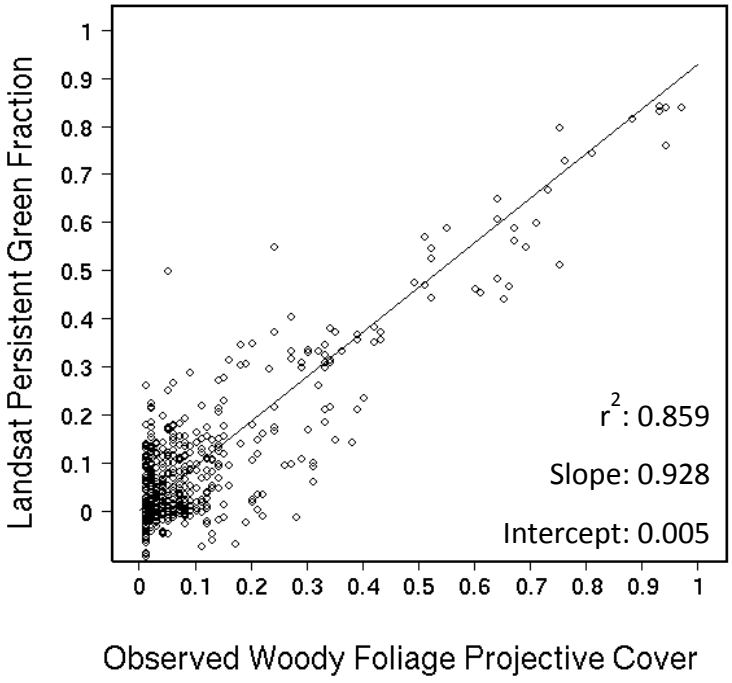

Figure 8.13 Regression of field observed woody foliage projective cover and Landsat derived Persistent Green Vegetation Fraction.

A large amount of airborne waveform LiDAR data collected within the 2000-2010 time period were collated (Figure 8.14). All these LiDAR data sets were captured by Airborne Research Australia (ARA), Flinders University, using a Riegl LMS-Q560 laser scanner and had similar scanner and survey properties. Airborne LiDAR data over TERN Landscape Assessment sites (Figure 8.14) were acquired outside the 2000-2010 time period and therefore not used for validation of the Landsat product. Coincident LiDAR and star transect data available from these sites were still used for the calibration of LiDAR gap probability to woody foliage projective cover.

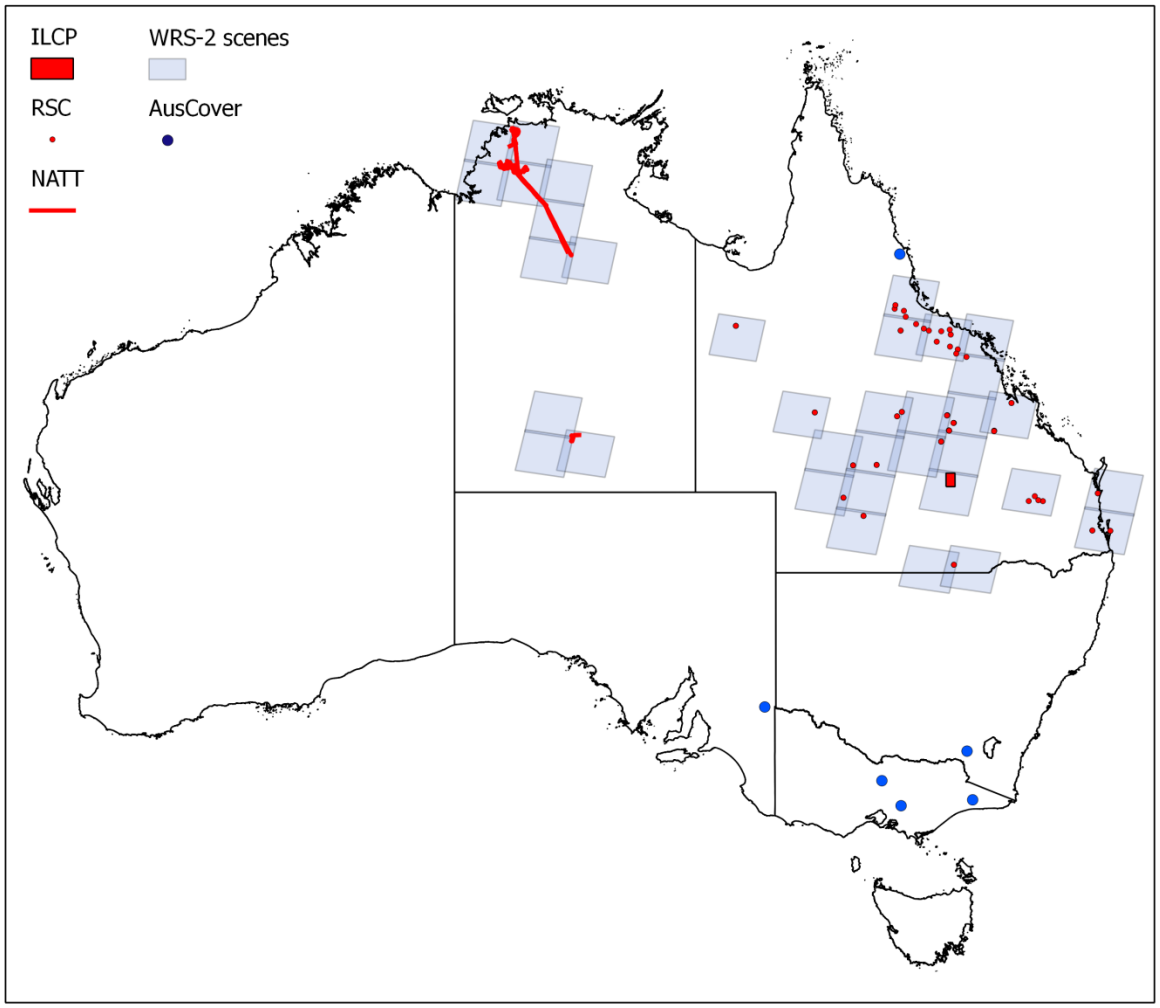

Figure 8.14 The Landsat WRS-2 scenes and LiDAR data sets used for the validation of the Persistent Green Vegetation Fraction product. LiDAR data sets included the North Australian Tropical Transect (NATT), the Queensland Government's Remote Sensing Centre (RSC) sites, and the Injune Landscape Collaborative Project (ILCP) site. The TERN Landscape Assessment LiDAR sites were included in the calibration of LiDAR gap probability to woody foliage projective cover only, since they were captured outside the 2000-2010 period.

For this initial validation, the approach described by Armston *et al.* (2009) was followed. Waveform LiDAR data were post-processed to discrete returns by the ARA. LiDAR fractional cover, equivalent to 1 - gap probability (P_{gap}), was calculated as the number of first returns above height *z* divided by the number of pulses within each 30 m pixel. The height threshold z was set to 0.5 m to ensure near-ground objects (e.g. litter, termite mounds, grass) did not contribute to the cover estimates. LiDAR fractional cover was calibrated to woody foliage projective cover using SLATS star transect measurements (Figure 8.15). The form of the calibration model was $1-(P_{gap})^{\alpha}$, where α is the calibration parameter to be optimised and is related to bias caused by non-green plant area and LiDAR system characteristics.

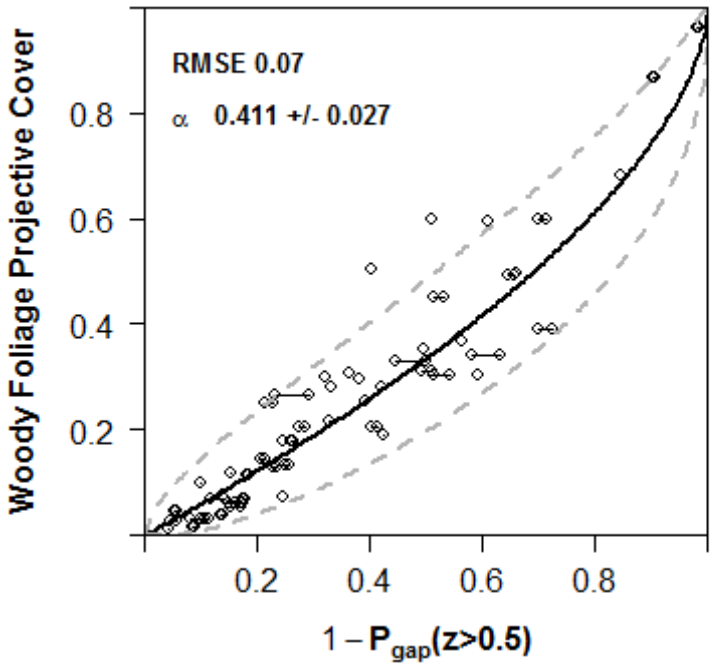

Figure 8.15 Relationship between field derived woody foliage projective cover (using the SLATS star transect approach) and LiDAR derived fractional cover (1 – gap probability) at a height of > 0.5 m above the ground. The dashed lines show 95% credible intervals.

The fitted Landsat model was used to calculate the Persistent Green Vegetation Fraction for the date of LiDAR data capture. Flight paths and the National Vegetation Information System (NVIS) national map of Major Vegetation Subgroups (Version 4.1; DSEWPaC, 2012) were used to stratify the coincident Landsat and LiDAR data for comparison by vegetation type. Comparisons were at the 30 m pixel level and only pixels classified as persistent green were included.

The mean Root Mean Square Error (RMSE) and Pearson correlation coefficient across all flight paths were 0.13±0.076 and 0.71±0.15, respectively. The RMSE varied substantially by flight path (RMSE 0.053 – 0.46) and NVIS Major Vegetation Subgroup (RMSE 0.057 – 0.64). Figure 8.16 shows examples of comparisons for NVIS Major Vegetation Subgroups.

Landsat estimates of Persistent Green Vegetation Fraction were unbiased at high cover values (> 0.75; e.g. Figure 8.16c), which is an improvement on previous Foliage Projective Cover products in Queensland (Kitchen et al., 2010). However, estimates of Landsat Persistent Green Vegetation Fraction were often higher than LiDAR estimates at lower cover levels (< 0.75). This was interpreted as persistent green vegetation cover from herbaceous and woody understorey (z < 0.5) being included in the Landsat Persistent Green Vegetation Fraction but not the LiDAR woody foliage projective cover (e.g. Figure 8.16d). A clear example is provided in Figure 8.17, where the LiDAR derived estimates of Persistent Green Vegetation Fraction were significantly lower than those derived from the Landsat product. This was because of the presence of a low but dense shrub layer, which was not included in the LiDAR processing because of the 0.5 m height threshold. The 20 km transect displayed in Figure 8.17 finished within an area of rainforest, where the estimates of the Landsat and LiDAR derived Persistent Green Vegetation Fraction were very similar because most of the vegetation appeared about the set 0.5 m LiDAR height threshold.

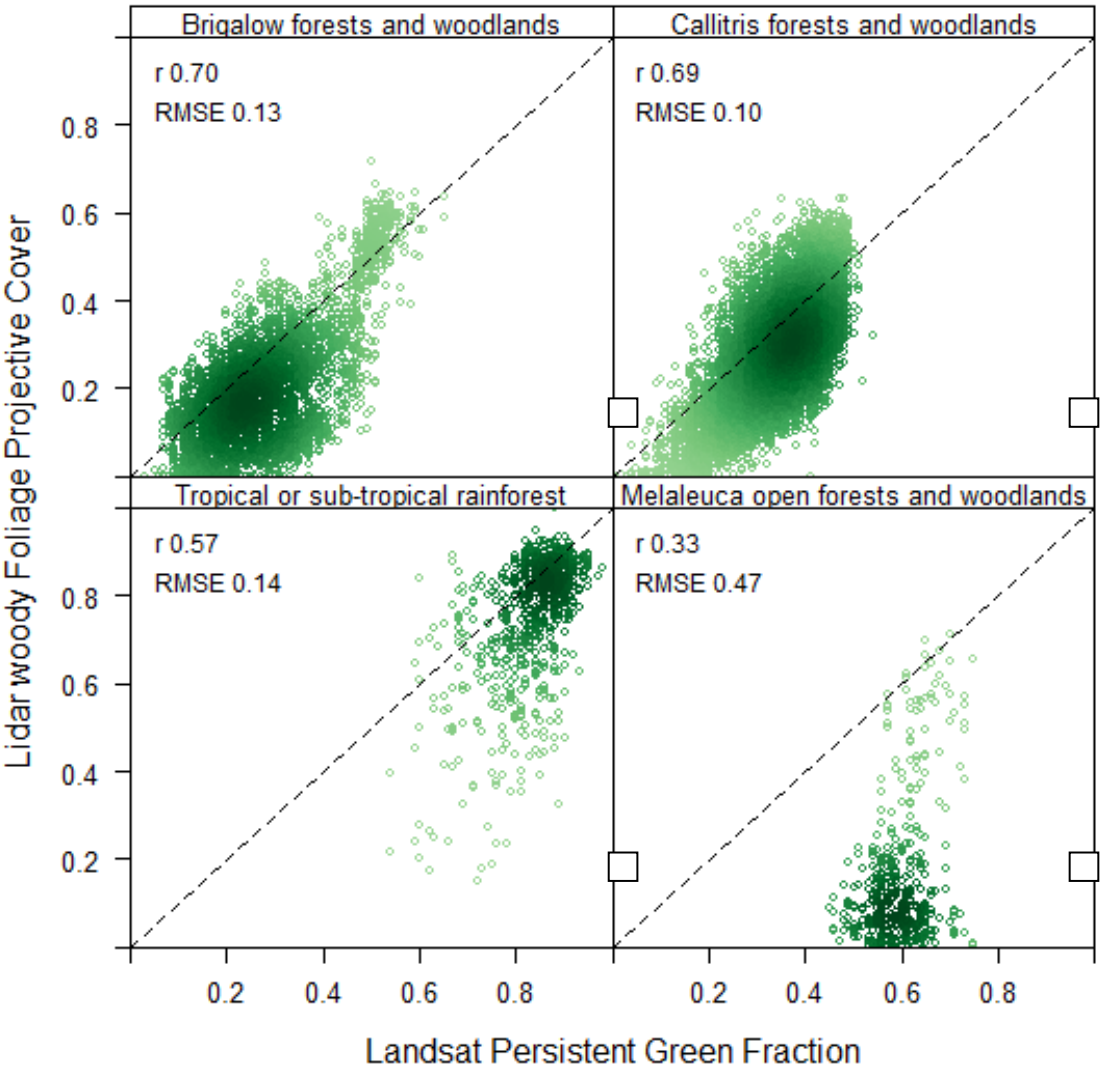

Figure 8.16 Example comparisons of LiDAR woody foliage projective cover and Landsat derived Persistent Green Vegetation Fraction for NVIS Major Vegetation Subgroups including (a) Brigalow (*Acacia harpophylla*) forest and woodlands, (b) Callitris forests and woodlands, (c) Tropical or sub-tropical rainforest, and (d) Melaleuca open forests and woodlands.

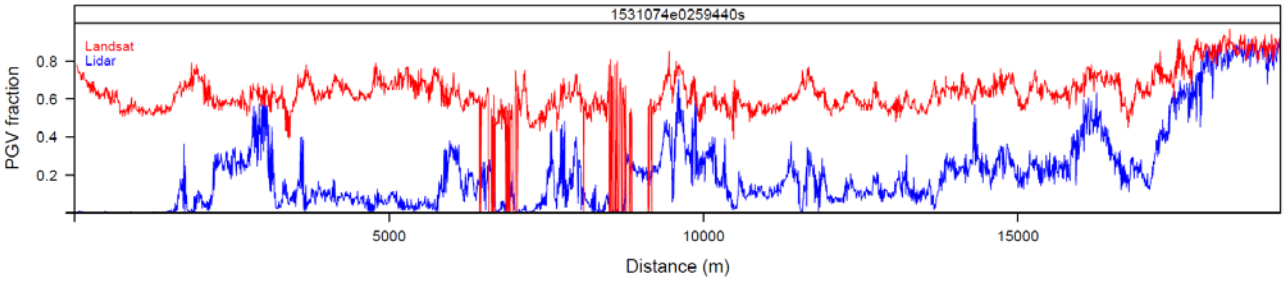

Figure 8.17 Estimated Persistent Green Vegetation Fraction from Landsat and LiDAR data along a 20 km transect.

8.5 Quality and Limitations

The input fractional cover product produces uncertain and often over-predicted estimates for the green fraction in the Simpson Desert Dunefields. These areas correspond to spinifex species. The persistent vegetation fraction in these regions is likely to be misclassified. These problems are in and around the WRS-2 scenes (path/row): 099/077, 100/077, 100/078, 101/078. Systematic striations can be seen in some scenes due to Landsat 7 SLC-off gaps. While all effort was made to produce the product using Landsat 7 SLC-on and Landsat 5 data, the SLC-off product had to be used where cloud-free, dry season imagery could not be obtained from the preferred sensors. These are most evident in cloudy regions of Cape York Peninsula and Tasmania. Striations caused by saturation in the Landsat image bands result in potential misclassification of persistent-green areas as non-persistent green.

8.6 Conclusions and Future Work

A nationally consistent calibrated and validated map of Persistent Green Vegetation Fraction at the Landsat scale was produced in collaboration with state and federal government agencies and researchers associated with TERN Landscape Assessment. The Persistent Green Vegetation Fraction product and associated metadata are freely accessible through the TERN Data Discovery Portal. It is anticipated that the main uses of the product will include:

- Determining (1) wooded extent; (2) forest extent; (3) forest density/forest crown cover/foliage cover; and (4) rangeland extent;
- Correcting fractional cover to ground cover; and
- Evaluating the effectiveness of management activities.

More experimental use of the product may include:

- Carbon applications and basal area mapping;
- Supporting land-cover/land use/biodiversity/carbon mapping;
- Assessing greenness trends in regions;
- Mapping water bodies across the landscape; and
- Mapping vegetation connectivity across the landscape.

There are a number of options for improving the current Persistent Green Vegetation Fraction product, which future work may focus on. Additional Landsat image data dating back to the launch of Landsat-4 TM will allow a longer time-series to be used and would likely improve the mapping accuracies of the Persistent Green Vegetation Fraction. The use of all Landsat images (up to 23 images per year per Landsat sensor) in the time-series will allow better discrimination of the Persistent Green Vegetation Fraction and may enable detection of woody thinning and thickening. Further validation with waveform LiDAR data in additional States and Territories will increase user confidence in the product.

The data are available to the public from TERN's Landscape Assessment platform (www.auscover.org.au). Land managers, ecologists, and researchers will find the information useful. It's suited to a range of activities including property planning, government planning, fire risk assessment, native vegetation mapping, and habitat identification. There are currently two applications examples. Firstly, the dustwatch program (www.dustwatch.edu.au) uses the products to identify woody areas that are not susceptible to wind erosion. Secondly, current research is using the product with L-Band RADAR and space-borne LiDAR to create a vegetation structure class map for Australia.

References

Armston, J., Denham, R., Danaher, T., Scarth, P. & Moffiet, T. (2009). Prediction and validation of foliage projective cover from Landsat-5 TM and Landsat-7 ETM+ imagery. *Journal of Applied Remote Sensing*, 3, 033540.

AusCover Xwiki (2014). SLATS Star Transect Protocol. URL: http://data.auscover.org.au/xwiki/bin/view/Field+Sites/Star+Transect+Protocol+Web+Page [last accessed 16 April 2015].

Breiman, L., Friedman, J., Stone, C.J. and Olshen, R.A. (1984). *Classification and regression trees*. Chapman & Hall/CRC.

Danaher, T. (2002). An empirical BRDF correction for Landsat TM and ETM+ imagery. *Proceedings of the 11th Australasian Remote Sensing and Photogrammetry Conference*, Brisbane.

Danaher, T. and Collett, L. (2006). Development, optimisation, and multi-temporal application of a simple Landsat based water index. *Proceedings of the 13th Australasian Remote Sensing and Photogrammetry Conference*, Canberra.

Department of Environment, Water, Population and Communities (DSEWPaC), Australian Government. (2012). Australia - Estimated Pre-1750 Major Vegetation Subgroups - NVIS Version 4.1 (Albers 100m analysis product): http://www.environment.gov.au/erin/nvis/data-products.html [last accessed 16 April 2015].

Draper, N. & Smith, H. (1998). Applied Regression Analysis, 3rd Ed., New York, John Wiley & Sons, Inc.

Johansen, K., Gill, T., Trevithick, R., Armston, J., Scarth, P., Flood, N. and Phinn, S. (2012). Landsat based Persistent Green-Vegetation Fraction for Australia. *Proceedings of the 16th Australasian Remote Sensing and Photogrammery Conference*. Melbourne.

Robertson, K. (1989). Spatial transformation for rapid scan-line surface shadowing. *IEEE Computer Graphics and Applications*, 9(2), 30-38.

Scarth, P., Roder, A. & Schmidt, M. (2010), Tracking grazing pressure and climate interaction–the role of Landsat fractional cover in time series analysis. *Proceedings of the 15th Australasian Remote Sensing and Photogrammetry Conference*, Alice Springs.

USGS World Wide Reference System: http://landsat.usgs.gov/worldwide_reference_system_WRS.php [last accessed 16 April 2015].

Zhu, Z. & Woodcock, C.E. (2012). Object-based cloud and cloud shadow detection in Landsat imagery. *Remote Sensing of Environment*, 118, 83-94.

Acknowledgements

A large number of people and government agencies and non-government organisations have contributed to the production of the Persistent Green Vegetation Fraction product. Particularly, the following people and institutions are thanked for input and provision of data sets: Jasmine Rickards (ABARES), Andrew Edwards (NT Bushfires), Nick Cuff (NT NRETAS), Gary Bastin (ACRIS / CSIRO), Graeme Behn (WA DEC), Jorg Hacker (ARA), Jason Beringer (Monash University), Stefan Maier (CDU), Tim Danaher (NSW OEH), QLD Herbarium and the Murray-Darling Basin Authority.

Chapter 9. Satellite Phenology Validation

N. Restrepo-Coupe [*1], A. Huete[1], and K. Davies[1]
[1] Plant Functional Biology and Climate Change Cluster, University of Technology, Sydney

*Corresponding author:
nataliacoupe@gmail.com

Abstract

Phenology is the study of the timing of recurring climate or weather-driven biological events, the causes of their periodicity, their relationship with biotic (e.g. fruit availability) and abiotic (e.g. rain) drivers and the interrelations between the seasonal cycle of the same or different species. Regional and continental scale phenology are often characterised with the use of different Remote Sensing (RS) products (e.g. vegetation indices) obtained from coarse resolution, high-temporal frequency satellites such as the Moderate Resolution Imaging Spectroradiometer (MODIS). The Australian phenology product (derived from the MODIS Enhanced Vegetation Index, EVI) depicts the vegetation status of a complex array of ecosystems ranging from arid and semi-arid savannas and grasslands to sclerophyll and tropical forests. These ecosystems respond differently to climate drivers presenting technical challenges when interpreting and deriving satellite and in-situ phenology. Here we present a literature review of the different methods used to study in-situ phenology: eddy covariance flux tower measurements (EC), digital repeat photography (phenocams), Leaf Area Index, and citizen science, to name a few. We document our approach to data processing of EC and optical indices, with an emphasis (instrument set-up and data collection) on the use of phenocams and the challenges imposed by Australian ecosystems. We demonstrate how in-situ measurements can be used for the validation and the interpretation of satellite-derived phenology, and how they contribute to the understanding of water and carbon flux seasonal cycles.

Key points

- Explanation of common phenology metrics with a focus on those most appropriate for Australian ecosystems.
- Review of the various methods used for validating satellite derived phenology products, particularly those applicable in Australia.
- Multi-scale integration of satellite data with in-situ observations of eddy covariance fluxes, pheno-camera derived greenness indices, and other field observations of vegetation phenology.
- Advantages and challenges in using time-lapse camera (phenocams) and data analysis strategies.

9.1 Introduction

Phenology is defined as the study of the timing of recurring climate or weather-driven biological events, the causes of their periodicity, their relationship with biotic (e.g. fruit availability) and abiotic (e.g. rain) drivers and the interrelations between the seasonal cycle of the same or different species. A better knowledge of the relationships of phenological responses to climate drivers (temperature, precipitation, length of the dry season, etc.) will advance our understanding of ecological responses to climate change.

Regional and continental scale phenology are often characterised with the use of different Remote Sensing (RS) products (e.g. vegetation indices) obtained from coarse resolution, high-temporal frequency satellites such as the Advanced Very High Resolution Radiometer (AVHRR) and the Moderate Resolution Imaging Spectroradiometers (MODIS) (Zhang *et al.*, 2003). The length of the time series (from 10 to 30 years), the high temporal frequency (from twice daily to 2 days), internal consistency, and quantitative nature of the satellite measurements are highly desirable qualities when extrapolating future ecosystem responses to climate. In this chapter, we focus on the validation of vegetation phenology acquired by satellite sensors with particular emphasis on MODIS derived phenologic metrics. We present a review of what phenology metrics that need to be validated, why do it, and finally, we explore some of the common methods used for RS-derived phenology validation with an emphasis on the challenges posed by Australian ecosystems (instrument set-up and data collection).

9.1.1 What phenology metrics in TERN Landscape Assessment products need to be validated?

Satellite based vegetation phenology concerns the timing and measuring the magnitude of seasonal changes in RS products. The most commonly used products are: (1) Enhanced Vegetation Index (EVI), (2) Normalised Difference Vegetation Index (NDVI), (3) MODIS and AVHHR Fraction of Absorbed Photosynthetic Active Radiation (fPAR) and (4) MODIS Leaf Area Index (LAI).

Phenology metrics are quantitative expressions of seasonal vegetation dynamics that are consistently applied in space and time and facilitate inter-annual and long-term quantitative trends and analyses. Commonly used satellite phenology metrics are graphically presented in Figure 9.1 and can be separated according to (a) time and event-based metrics of greenness and (2) amplitude or greenness value metrics. Time and event-based metrics include start of active growing season (*SGS*), end of growing season (*EGS*), length of active growth season (*LGS*), and peak period of the growing season (*PGS*), i.e. the point in time of maximum vegetation activity. Amplitude or greenness value metrics include the base value of zero vegetation activity, maximum or peak greenness value, minimum greenness value, annual mean greenness value, amplitude of maximum minus minimum greenness, rate of greenup, rate of senescence or drying, absolute integral over the growing season (area), scaled integral over season (absolute - base value), and the root-mean-square-error (RMSE) of fitting an appropriate function (e.g. Fourier transform) to the observations.

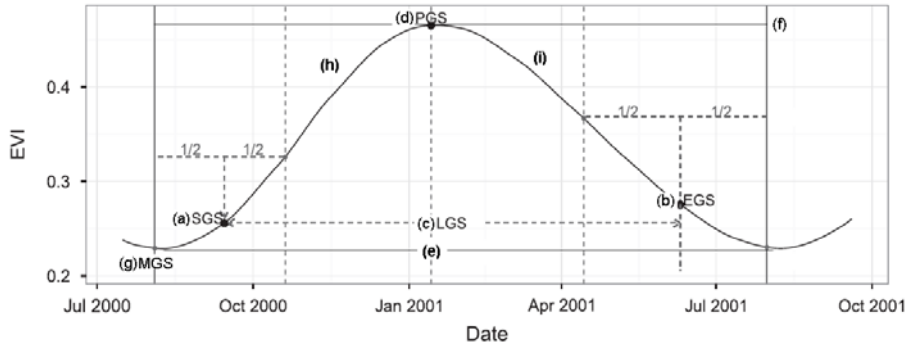

Figure 9.1 Common phenology metrics shown on a seasonal profile derived from the MODIS EVI. Where (a) start of growing season, *SGS*; (b) end of growing season, *EGS;* (c) length of growing season, *LGS*; (d) peak of growing season time, *PGS*; (e) base value; (f) peak value at *PGS*; (g) minimum greenness value, *MGS*; (h) rate of greening; and (i) rate of senescence. Modified from Ma et al. (2013).

The need for a dedicated Australian phenology product is based on the challenges imposed by Australian vegetation dynamics, for example, savannas are made up of a complex array of understory and overstory components where the time-area integral is typically decomposed into its tree and grass components. Rainfall driven ecosystems in the semi-arid interior may not exhibit an annually reoccurring phenological trajectory. Sclerophyll forests are dominated by Eucalyptus whose leaf-angle distribution is generally erectophile, and differences in their adaxial and abaxial spectral properties offer thermal protection to the trees but may complicate spectral analysis. Northern tropical sites are described as dominated by evergreen planophile and semi-evergreen tree species, leafing out at different times of the year.

In this section we summarise how the different metrics are calculated and give some examples of their application for ecological studies.

Time metrics for persistent and recurrent vegetation functional classes

The three most important time metrics are *SGS*, *EGS* and *PGS*. Given the spatial resolution of each pixel (e.g. MODIS VIs from MOD13Q1 are 250 x 250m) these metrics correspond to the combined effect of a mixture of plants, and include the structure and spectral characteristics of all ecosystem components. In general, the *SGS* is determined as the midpoint between of time of minimum VI and the time where the fastest growth rate during green-up occurs (see next section). *SGS* can also be determined as the time when the VI reaches a set value between a pre-determined baseline VI value and the maximum VI (e.g. 10 %). Similarly, the *EGS* is determined as the midway point between the fastest browning time and the minimum VI. *PGS* corresponds to the time when the VI reaches its maximum value during the growing season.

The application of *SGS, EGS* and *PGS* includes habitat classification schemes (e.g. forest types as in Clerici *et al.* (2012), and cross-site comparisons of inter-annual variability as a base to determine ecosystem productivity sensitivity to phenology and climate change (Ma et al., 2013; A. D. Richardson *et al*., 2010).

First derivative: Rate of greenup and rate of drying

The rate of green-up is theoretically related to the structure of the vegetation (Jönsson & Eklundh, 2003). It is estimated as the ratio between the amplitude of the time series and the time difference between the season start and the midpoint of the seasonality and vice versa, for the calculation of the rate of senescence. The asymmetry between the rate of green-up and rate of senescence can be used to characterise different ecosystem types (e.g. a typical agricultural pattern would show a slow greenup and rapid senescence). Changes to the rates when compared to the mean annual rate (composite) can also be interpreted as an indicator of stress or healthy conditions.

Small and large annual integrals for persistent and recurrent vegetation functional classes

Variations of the area under the VI curve have been used as measure of ecosystems productivity. For example, the early growing season NDVI integral has been shown to be strongly correlated to ground-based forest measurements of diameter increase and seed production and standardised tree ring width at the U.S. central Great Plains (Wang, Rich, Price, & Kettle, 2004). Interestingly, Wang (2004) reports that the increase in tree height growth showed higher correlation to the integrated NDVI from the previous year. Meanwhile, changes in foliage production (LAI measured by litter-traps) only showed a relatively weak correlation to NDVI integrated over the entire growing season, demonstrating the difficulties in understanding the physical mechanisms present in the different phenology products and the need for their validation.

Peak of season amplitude and minimum dry season baseline value

The minimum dry season baseline value of the MODIS or AVHRR fPAR and MODIS LAI products are considered to be a good estimate of the evergreen/ tree/shrub cover fraction and proxy for productivity of the persistent, non-deciduous perennial vegetation (e.g. vascular plants with deep roots and slow biomass growth and decay) (Donohue, McVICAR, & Roderick, 2009). By contrast, the peak of season amplitude (*PGS* value minus baseline) has been associated with the fraction of cover and photosynthetic activity of the recurrent, deciduous, annual, and ephemeral vegetation (e.g. shallow roots, grasses, and low plants) (Opie, Newnham, & Guerschman, 2011).

9.1.2 Validation objectives (why do it?)

As we have seen among the many applications, phenology is a key tool in the study of food web interactions (Straile, 2002), changes in ecosystem productivity (Myneni et al., 2007), land surface modelling (A. D. Richardson *et al.*, 2012), biosphere-atmosphere feedbacks (Flanagan, 2009), health applications such as allergens and infectious diseases (Luvall *et al.*, 2011), and agriculture (planting and harvest times, pest control) (Chmielewski, 2003). Phenology has also been defined as an adaptive trait in shaping plant species distribution (Chuine, 2010). Moreover, the Intergovernmental Panel on Climate Change (IPCC) relies on phenology studies as compelling evidence that species and ecosystems respond to changes in climate (Rosenzweig *et al.*, 2007). Validating satellite phenology is important and necessary for proper interpretation of climate variability and the consequent shifts in seasonal and inter-annual biome responses.

9.1.3 Methods to validate satellite phenology

Methods commonly used to validate satellite phenology are: airborne hyperspectral/multi-spectral measurements, measurement of carbon, water, energy fluxes by Eddy Covariance (EC) methods, measurements of LAI (e.g. litter-traps or LI-2000 transects), biomass inventories, sampling of leaf pigments (e.g. chlorophyll and carotenoids), automated RGB and multi-spectral cameras, and hemispherical photography. Table 9.1 presents a summary of the different phenology validation methods and their advantages and disadvantages.

Table 9.1 Information regarding some of the most used field validation methods for satellite phenology products.

Validation Tool	Temporal	Scale	Objective	Cons	Pros
Cameras	Continuous	Sub-canopy and canopy (more than 1 tree or patch of grass)	Continuous observation of canopy and understory images. Identify visual changes in canopy or sub-canopy greenness, flowering, etc. Obtain indices from different combinations of the RGB (red-green-blue) bands	Non uniform protocols / Used qualitatively	Inexpensive
Eddy covariance data	Continuous	Ecosystem	Ecosystem photosynthetic capacity (C-flux)	Cost and required technical knowledge. Not able to discern if changes in ecosystem capacity are due to changes in LAI, leaf capacity or a combination of the two	Continuous / Other physical variables being measured / Long term
Tower radiation sensors	Continuous	Sub-canopy and canopy	NDVI, albedo Photosynthetic Active Radiation (PAR) and albedo Short Wave (SW)	Expensive: requires a datalogger, technical personnel (clean and maintain), and the cost of the instruments.	Required for a myriad of applications: driver land surface models, EC gap-filling and data analysis
Optical sensors	Continuous	Sub-canopy and canopy	NDVI, PRI, reflectance in individual bands	High cost. At heterogeneous ecosystems, it may be difficult interpretation (it is unknown where most of the signal is coming.	Specific bands and indices can be measured. Continuous
Leaf and canopy scale field measures	Seasonal	Individual	Leaf spectral properties, chlorophyll, etc). Forest inventories (litter, soil carbon, understory and overstory biomass and LAI).	Low spatial resolution / Labor and time intensive	High spectral resolution. Under a controlled light environment. Can be associated to leaf trait data. Treats independently the different ecosystem components
Airborn campaings and finer-resolution satellite data	Seasonal	Landscape	Leaf spectral properties as a measure of photosynthetic capacity (chemistry, pigments, etc). LIDAR (LAI, basal area, structure of the ecosystem)	Cost / Low temporal resolution	High spectral and spatial resolution
Citizen/Research Observations	Continuous	Species	Record main phenological events in key species	Qualitative / Subjective / Species specific	Public involvement / Inexpensive

Tower flux observations

The eddy covariance (EC) method is a commonly used technique to study ecosystem seasonality and inter-annual variability of Net Ecosystem Exchange (*NEE*), sensible (*H* in W m^{-2}) and latent heat (*LE* in W m^{-2}*),* and momentum fluxes (τ in kg $m^{-1}s^{-2}$). The above-mentioned fluxes represent climatic/weather and biotic controls (vegetation status), thus the timing and magnitude of the vegetation signal can be related to RS phenology (See section 8.1 and 8.2). For a complete description of the method, standardisation and sensors please refer to the works of Papale et al., (2006); Richardson and Hollinger, (2007) and (2001), among others. Section 8.2 presents the proposed method of phenology validation using eddy-flux data.

Automated camera systems: Digital 3-band (Red Green Blue, RGB), multi-spectral (Green, Red and NIR), and hyperspectral cameras

Automated time-lapse digital photography (phenocams) offer a unique opportunity as the images can be sub-sampled and the spectral characteristics of different ecosystem components (e.g. individual trees, grasses, etc.) can be determined. However, they can also be misused as their output values are difficult to interpret and their values are not straightforward measures of reflectance. We present some key issues encountered while setting up and using phenocams in Section 9.3.

Tower radiation sensors (Photosynthetic Active Radiation, PAR and Short Wave Radiation, SW)

The combination of tower mounted radiation sensors has been used in order to track in-situ NDVI and fPAR, both useful validation tools for phenology and the understanding of ecosystem functioning. Section 9.4 reviews some of the basic equations and methods.

Tower-mounted optical sensors

Similar to tower radiation sensors, the objective of optical sensors is to partially bypass the effects of atmospheric conditions (e.g. clouds and aerosols) and changes in the observation angle and measure incoming and reflected radiation in given spectral bandwidths (e.g. Red, Green, NIR) at high frequency (e.g. 30 minutes). Important issues should be considered, before the installation of these sensors. These issues include determination of the required field-of-view (FOV), radiometric and spectral resolution, spatial footprint, orientation, and definition of instrument recalibration requirements (some of these issues are addressed in Section 9.3: Phenocams).

Using the existing network of flux towers, arrays of optical sensors have been installed in Scandinavia (Sweden and Finland), and Central Europe (see Eklundh *et al*. (2011) and Balzarolo *et al*. (2011) respectively). Observed indices such as the EVI, NDVI, Photochemical Reflectance Index (PRI), and Water Band Index (WBI) are an important satellite phenology validation tool and provide in-situ information about plant development, chlorophyll and nitrogen content, and variations in reflectance due to snow cover and vegetation. However, there is a growing need for standardisation and development of common protocols as their deployment can be costly and, in some cases (e.g. for hyperspectral sensors), they require high energy inputs for maintaining constant temperature levels. Balzarolo *et al*. (2011) suggests the implementation of a common language following Schaepman-Strub *et al*. (2006) that facilitates the interpretation and reproducibility of any results.

Leaf and canopy scale field measures for discrete phenophase periods

Seasonal field campaigns to record leaf chemistry/spectra, LAI, fraction of cover and other ecosystem properties, can be used as a validation tool. Some common measures of canopy and leaf status are: leaf chlorophyll content, specific leaf area (*SLA*), LAI, and fraction of vegetation (*Fveg*). Changes in LAI/vegetation fraction will inform us on one of the two main co-varying phenological changes in vegetation foliage: quantity. Changes in leaf chemistry and pigments will be representative of the foliage quality. The reader is invited to see works by Doughty and Goulden (2008) and Hutyra *et al*. (2007) on tropical forests for seasonal inventories of LAI and their link to seasonal changes in VIs. For a complete explanation of LAI sampling, leaf chemistry and fraction of vegetation see their respective chapter in this Greenbook.

Snapshot airborne campaigns and finer-resolution satellite data (e.g. SPOT, Landsat)

Hyperspectral flight campaigns are a powerful tool when scaling up leaf spectral properties (related age and traits) from individuals to ecosystem scale. In particular, concurrent leaf spectral measurements linked to CO_2 exchange measurements (LI6400) is a first test to relate leaf-landscape optical properties to photosynthetic capacity. The use of airborne campaigns in phenology validation (MODIS) is restricted due to their high cost. High spatial resolution imagery has "replaced" hyperspectral data, as in Fisher and Mustard (2007), where 30 m pixel Landsat TM and ETM+ derived phenologies over deciduous forests display significant spatial heterogeneity (<2 weeks in less than 500 m) compared to the MODIS VIs derived regional scale variability. In this example, Fisher and Mustard (2007) found that the cross-sensor comparison is better than MODIS uncertainty (error of ~3.25 days).

Citizen science

Cherry blossom records going back to the 9th century in Japan (Primack, Higuchi, & Miller-Rushing, 2009) constitute one of the longest phenological time series. New, well-organised observation networks and open-access databases of citizen scientists have been established in North America (the US phenological network; (Betancourt *et al.*, 2007) and Europe (the International Phenological Gardens and the European Phenology Network; Scheifinger et al. 2002; van Vliet *et al*. 2003). Observations include flower tracking, long-term research plots, first ripe fruits, and bud-burst, among many others.

Most field validation of phenology is based on heavily monitored sites where observations of bud-burst, leaf development, leaf-colour and leaf drop are recorded at 3 to 7-day intervals (e.g. Harvard Forest as in Fisher and Mustard (2007). However, species-level phenology does not always translate directly to whole ecosystem phenology. There is a need to establish well-defined thresholds (i.e. start of greenup defined in-situ as bud-burst for 50% of the canopy). Spatially there are also difficulties in obtaining the exact location of the validation sites. It is difficult to precisely co-locate the validation site with MODIS pixels because ground data has generally been collected over a large area overlapping several pixels. Temporarily MODIS retrievals can differ from in-situ data by about 3 or more days.

Phenology validation by phenology networks (citizens and research station) could be impractical as a great percentage of Australia is uninhabited. However, recent efforts by the TERN lead project "Transects for Environmental Monitoring and Decision Making" to implement a citizen science mobile phone application would be a first step in involving citizens in the surveillance and record of how sites change over time (see http://www.trendsa.org.au/).

9.1.4 How to capture green-up and other metrics at landscape scales

When scaling up in-situ phenological measurements, two objectives one wishes to achieve are: (1) to validate the phenology product through independent means; and (2) determine accuracy, precision or uncertainty for the RS product. Ideally, one would want an array of cameras or sensors to capture site heterogeneity and match the satellite footprint (e.g. cover at least one square kilometre scale). Basic questions in order to address a scaling problem would be: number of replicates (as in number of pixels or footprint of an optical sensor), site heterogeneity and what we define as greenup. For this last item, most of phenology metrics derived from satellite-derived VIs rely on the assumption that observations are highly correlated to chlorophyll concentration (greenness) and the spatial coverage of the leaves (opacity) (Fisher & Mustard, 2007). These assumptions can be simplified in deciduous systems. However, at savannas and more complex forests, there is a combination of factors that increase the difficulty of the interpretation of the greenness time series requiring a more intensive or higher replication of in-situ sampling. Moreover, few studies have addressed the question of whether the quantity or the quality of leaves are the drivers of changes in VIs and reflectances as they require a complicated array of measurements (leaf gas exchange or eddy covariance C-fluxes, fPAR, and

LAI). At an Amazonian forest site, Doughty and Goulden (2008) showed that only the combined effect of seasonal changes in LAI (in-situ) and seasonal changes in leaf age and leaf photosynthesis was able to explain the seasonality of eddy flux measurements of Gross Ecosystem Productivity (GEP). Moreover, at the leaf level, not all leaf components are green constituents (e.g. chloroplast). Vein and cell walls can contribute 20 - 50 % of the spectral signal depending on species, leaf morphology, and growth history (Hanan, Kabat, Dolman, & Elbers, 1998). In particular, changes on VIs, reflectances and other spectral properties will change as the leaf ages (Figure 9.2).

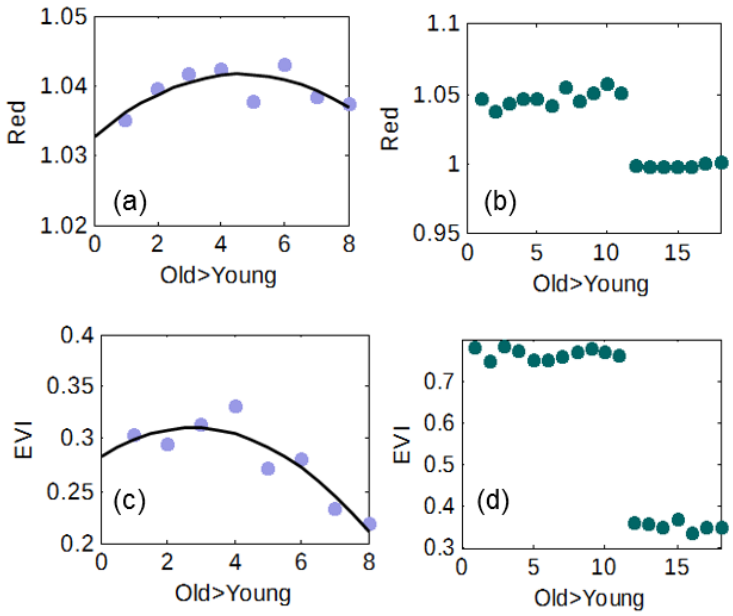

Figure 9.2 Relationships between relative leaf age (old to young along a branch), red reflectance (top panels), and the EVI (lower panels). Leaf spectra obtained using an ASD portable spectroradiometer and a LI-1800 integrating sphere. Each point correspond to the mean of 6 measurements (each a 30 sample average) for
(a) EVI Eucalyptus
(b) EVI Tropical plant
(c) Red Eucalyptus
(d) Red Tropical plant.

9.2 Eddy covariance towers

Measures of ecosystem photosynthetic capacity obtained by the eddy covariance method (C-flux) such as ecosystem light use efficiency (*LUE*), *GEP* at saturation (GEP_{sat}) and photosynthetic capacity (*Pc*) (rather than *GEP*) have been shown to be a good tool for satellite phenology validation (Figure 9.3). Thus as Australian satellite observations of landscape phenology, in particular at arid and semi-arid ecosystems are challenging due to the extensive prevalence of tree-shrub-grass assemblages in which each vegetation functional class exhibits a unique phenological profile, the productivity of the tree layer may increase simultaneously with decreases in grass layer productivity potentially resulting in a misdiagnosed satellite phenology (e.g. EVI inversely related to *GEP*, Figure 9.3).

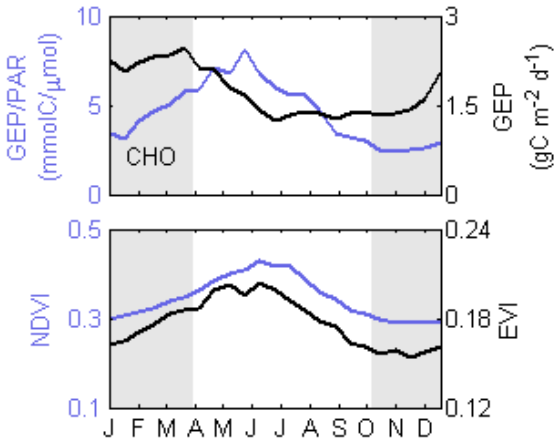

Figure 9.3 Calperum-Chowilla flux site. Top: tower measured Gross Ecosystem Productivity (GEP; black line) and ratio between GEP and incoming Short Wave Radiation (SW_{in}; blue line). Bottom: MODIS EVI (black line) and NDVI (blue line). Special thanks to Prof D. Chittleborough, Prof W. Meyer, Dr. G. Whiteman and T. Luckbe.

We obtain *LUE, GEP*$_{sat}$ and *Pc* using the relationship between *GEP* and incoming short wave radiation measured at the tower (SW_{in}) or photosynthetic active radiation (*PAR*) (calculated as *PAR*= SW_{in} when unavailable) (Figure 9.4). Thanks to the efforts from the OzFlux network one can evaluate the synchronicity between C-flux derived photosynthetic capacity (combination of LAI and leaf capacity) and satellite products.

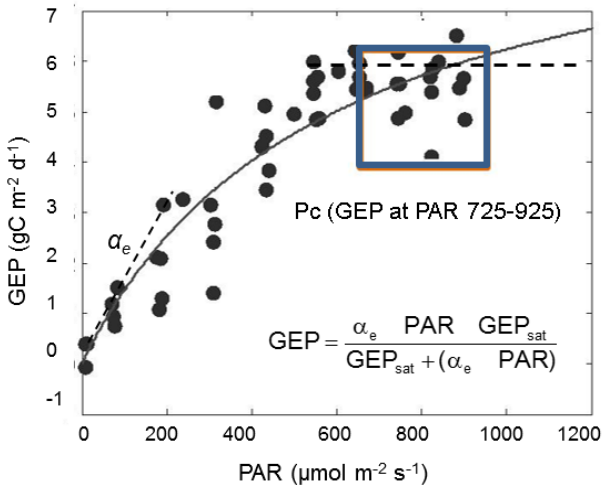

Figure 9.4 Rectangular hyperbola fitted to 8-day worth of Gross Ecosystem Productivity (GEP) and incoming photosynthetic active radiation (PAR) data measured at Calperum-Chowilla OzFlux site (June, 2012). Photosynthetic Capacity (Pc), Light Use Efficiency (LUE) and GEP at saturation (GEP_{sat}) are calculated, as shown.

9.3 Phenocams

Automated cameras can be installed at different TERN Ecosystem Surveillance and TERN Ecosystem Processes sites with the aim of recording hourly and daily changes in vegetation. The cameras are permanently placed and will provide hourly daytime near-surface remote sensing data of the forest canopy (from the top of an eddy flux or fire observation tower) and/or understory phenology (3 cameras at each study site).

The computation of reflectance values from digital image numbers (DNs) is problematic because issues related to sun angle: stray light over the canopy, differences in canopy illumination across a single image, and shadows. There is disagreement regarding the optimal conditions for image capture with less than 100% diffuse radiation or under a 100% cloudless sky. Moreover, it is not always possible to have one or the other light environment and in many cases the camera time series will needed to be gap filled. As stated by Hufkens *et al*. (2010) the high variability of the image data and its quality can impede the full automation of its processing.

9.3.1 RGB and spectral cameras

In Australia, efforts to instrument flux tower sites with RGB cameras for phenology validation started in early 2000. Their value as a recording tool of the different phenological changes (visual or more complex analysis) has been proved in different applications (Crimmins and Crimmins 2008; Huemmrich *et al*. 1999; Richardson *et al*. 2007). The selection between multispectral, hyperspectral and RGB cameras is generally made based on the cost and available technical resources. Characteristics of some of the cameras used in phenology validation are presented in Table 9.2.

Table 9.2 Some of the cameras used in phenology validation.

Camera	Type	Interface	Software	Users
Nikon	RGB	Computer	photopc or gphoto (Linux)	Phenological Eyes Network
Wingscapes®	RGB	SD card	Programmable camera	AusCover
Campbell Sc CC5MPX and CC640	RGB	Datalogger (e.g. CR1000)	Eddlog	Fluxnet
StarDot NetCam SC IR	RGB	Computer (IP address)	N/A	US phenology network – Ameriflux
Tetracam® (Chatsworth, CA) 6-band or ASM	Multispectral	SD card	Programmable camera	
SOC®	Hyperspectral	Computer	Camera Proprietary	

9.3.2 Camera inclination and azimuth

The positioning of the camera may have direct consequences on the data analysis. A combination of oblique and nadir cameras can therefore be used. The nadir looking (straight down) cameras capture an image where issues related to backscatter (sun behind observer) and forward-scatter (sun opposite observer) can be minimised. An oblique camera will capture a wider portion of the ecosystem and specifically focus on some key elements of the site. However, given that specular reflection of leaves can occur for camera inclination angles >30 degrees from the vertical, it is suggested to work at <30 degree angles.

In the southern hemisphere, primarily in summer months (Figure 9.5), orienting the camera to face towards the south results in backscattering, and the image will show a bright region where all shadows are hidden (hotspot; see Figure 9.5). By contrast, forwardscattering (sun opposite to the observer) will result in mirror-like reflection from the leaves and bright object edges. Interesting, at many sites it is common to have both scenarios (forwardscattering / backscattering) as the solar azimuth will change during the year from N to S and vice versa.

It is preferred to seasonally maintain backscatter conditions, and limit the analysis to images collected when the sun is close to local noon (11:00-12:00 am), even if this configuration results in the greatest variation in the solar zenith angle (SZA). Having the sun facing into the camera is less desirable as it is difficult to separate the different vegetation components (wood, leaves, and shadows among others) (B Nelson personal communication). In summary, the camera azimuth position is a compromise for each individual flux-tower site as it is necessary to balance the needs of the cameras with the EC, which usually has priority.

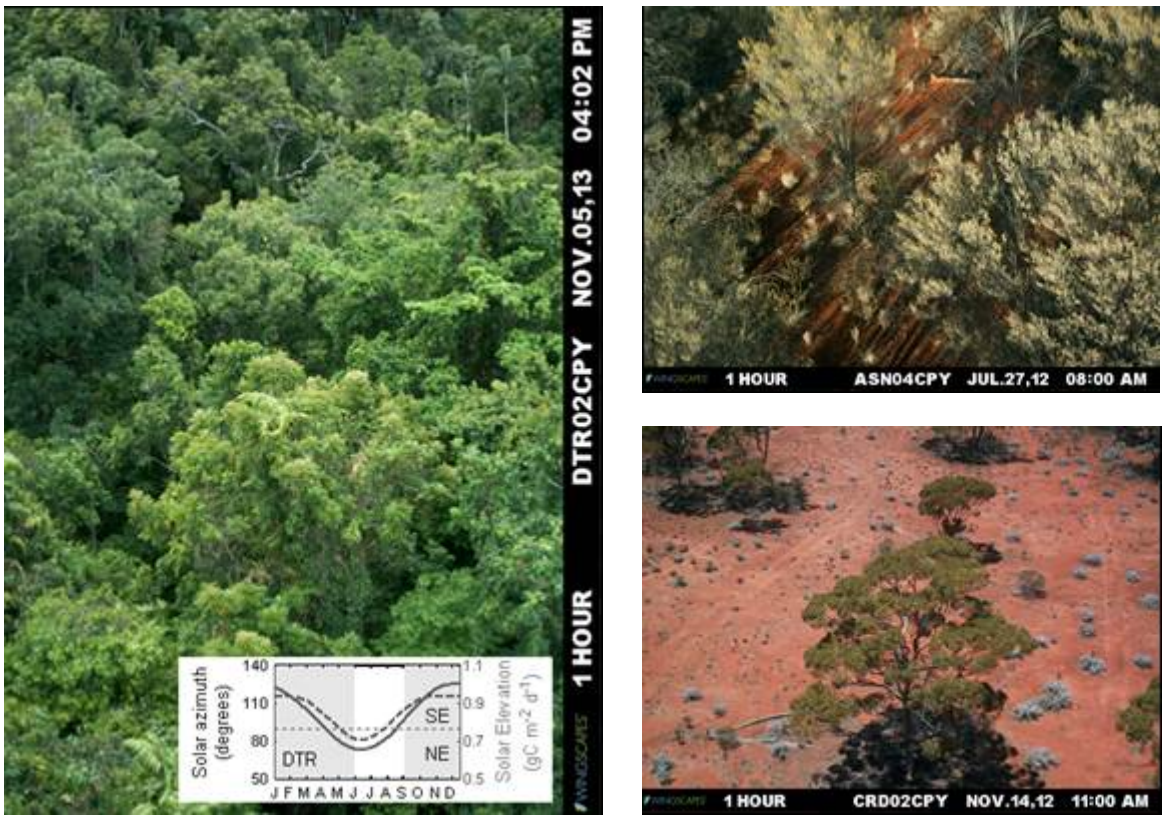

Figure 9.5 Camera azimuth and inclination:
Left panel: Daintree/Cape Tribulation flux tower phenocam, sun behind the observer (backscatter) and the presence of a hot spot at the center of the image (special thanks to Prof. M. Liddell and N. Weigand).
Left side inset: seasonal cycle solar elevation at 11:00 am (right axis, grey), and azimuth (left axis, black), azimuth values >90 indicate sun at the southeast (SE) and <90 at the northeast (NE).
Right top panel: Sun at low angle and mirror like effect on leaves. Sun behind the observer at the Alice Springs Mulga flux tower phenocam (special thanks to Prof. D. Eamus and J. Cleverly).
Right low panel: Credo flux tower site phenocams images showing fowardscatter (Special thanks to C Macfarlane). Both right panels show issues posed by the shadows at arid and semi-arid environments.

For all camera orientations, shadows from the vegetation and existing structures (e.g. from the flux tower) can increase the difficulty of processing the images. Using Green/Red band ratio and other ratios will decrease, but not completely remove, the influence of dark or bright areas across the image (see section on the computation of Red/Green (RGB) and NIR/Red ratios).

9.3.3 Over- and understory

For Australian multi-functional and multi-strata canopy types, two sets of cameras are needed to adequately characterise landscape phenologies, including an overstory and understory camera (or herbaceous and woody layer camera).

The tree layer needs an oblique view (30-60 from zenith) to capture sufficient number of trees and sampling of landscape cover while the understory should be nadir view or slightly oblique (0-30 degree). Azimuthal orientation should be as described in section above (camera inclination and azimuth). For the understory cameras, key species or the location of the soil moisture/temperature array will dictate the location of the camera.

9.3.4 Diurnal, daily, and seasonal settings, including frequency of observations

Most phenocams record images every 30 – 60 minutes. Our experience in very wet environments (e.g. Amazon basin, see Figure 9.6) shows that a high frequency of images captures allows us to choose a time of day to be used when calculating the time series and to avoid using a "fixed" capture time where rain or fog may affect the quality of the images. Some researchers do select images captured during cloudy periods (under diffuse radiation) in order to avoid saturation, stray light or to correct for a seasonal changing SZA, in particular at those locations where the camera alternative captures images in fowardscatter and backscatter conditions (see the works of B. Nelson and previous section "Camera inclination and azimuth"). This approach, however, is known to introduce significant noise, thereby increasing the uncertainty of the observations, as the light environment is difficult to characterise. Arid and semi-arid sites (~75% of Australia) are cloudless for long periods of time (weeks to months), and this may translate into an incomplete time series if only images during diffuse radiation periods are used, although they will correspond to the dry/dormant season.

Some ecosystem components like the soil biological crusts respond after rain (greenup) at a faster rate (<30 minutes). Even if the satellite will not capture these biological pulses, the phenocam can inform the flux tower measured C-fluxes about the length and spatial extent of the response - an interesting result by itself.

9.3.5 Camera settings, integration times, F-stop, etc.

Some hyperspectral cameras (e.g. SOC710 Surface Optics) allow the user to change the camera settings to obtain good quality images (spectral range, no saturation, etc.) under different light environments (e.g. outdoor or indoor locations). The f-stop regulates the aperture of the lens, a value of 2.8 or 5.6 means more light inside the camera compared to 11 or 22. Closing the lens (move the f-stop to higher values) translates in improving the depth of field and focus at the extremes of the spectrum and it can help in outdoor conditions by avoiding saturation. However, it is best to try to fix the f-stop and get more or less light into the camera via changing other parameters. Similar results can be obtained by modifying the integration time. In general, radiance and spectral factory calibrations are done using a fixed f-stop (e.g. 5.6) as it provides a good trade-off between speed and quality. If we assume that each increment in the f-stop (e.g. 5.6 to 8), cuts the illumination in half, the integration time can be doubled in order to obtain similar results (e.g. 10 milliseconds integration time at f5.6 vs. 20 milliseconds at f-stop 8). It is always good practice to obtain the highest number of digital counts as possible.

Some cameras offer the possibility to modify the electronic gain as an alternative to integration times, as increasing integration times in windy conditions can be problematic. However, since the gain is electronic, noise in the image will also increase correspondingly. It is suggested to use a gain value of '1' or unity (no gain).

Very simple cameras (e.g. Wingscapes®) do not offer any of the above- mentioned settings. However, light settings can be set to auto, sunshine, fluorescent and other light environments. As we want to capture each object reflective properties rather than changes to the camera settings, we fixed the light setting to sunshine (outdoor conditions). Moreover, if the camera allows the user to obtain RAW files rather than JPEG, it is recommended the use of RAW as Gamma correction and other image enhancement filters are usually applied to the RAW data in order to generate JPG extension files.

9.3.6 Use of White/Grey references

In order to calculate reflectance, measures of incoming light are necessary. For this purpose, a reference plate (TEFLON or Spectralon) is installed in front of the camera so the image captures all or part of the plate. If the plate is going to be used as a reference it needs to be installed horizontally (see Figure 9.6b). Our experience has shown us that the plate can be under a different light environment than the rest of the canopy (e.g. patchy clouds) and not represent the light environment of the canopy (Figure 9.6a). The area immediately around the plate should not be included on the analysis. Moreover, the spectral range of the camera is generally stretched. For example, vegetation is "dark" on the red region of the spectra (0.63-0.69 nm) and the plate will be highly reflective. Thus to avoid saturation, the aperture will need to be closed. However, this would not be able to capture subtle changes in the canopy due to the strong absorption in the red region by vegetation (see Figure 9.6c). Grey standards have been suggested to bypass issues related to spectral range and saturation but they can easily degrade (e.g. due to dirt) in outdoor conditions. References therefore seem impractical and not required if working with ratios.

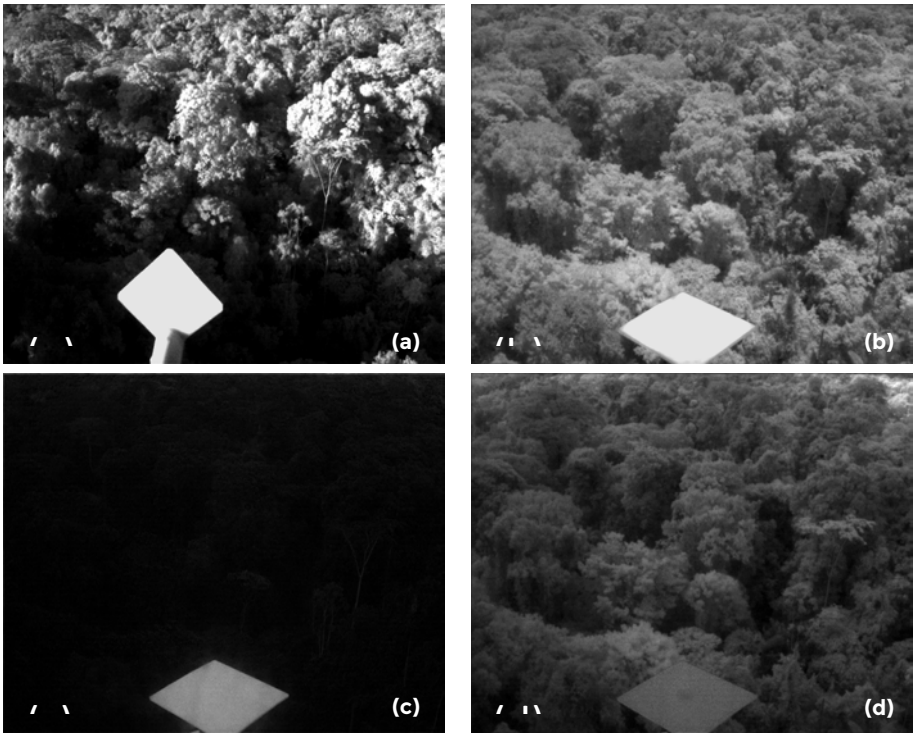

Figure 9.6 TETRACAM 3-band camera (NIR, Red, and Green) installed at the Amazon basin K67 eddy flux tower. With
(a) NIR band showing the TEFLON panel set vertically (check camera consistency, no use as reference);
(b) NIR band showing the TEFLON plate set horizontally to be used as reference standard (note observable glare around the plate);
(c) Red band; and
(d) Green band.
All images as Digital Counts 0-255. Acknowledgments to Prof. Scott Saleska and Prof. Alfredo Huete

9.3.7 Computation Red/Green (RGB) and NIR/Red ratios (spectral) with and without use of reference

Preliminary work trying to analyse and isolate different components of the canopy (i.e. species, over-story - understory), and sub-canopy (e.g. soil crust) by calculating different indices (Region of Interest or RIO). These indices included: (1) excess green index (VEG1= 2*Green-Blue-Red); (2) Red Green Ratio Index (Red/Green or RGRI) (see Figure 9.7); (3) Green Chromatic Coordinate GCC=Green/(Red+Green+Blue); RGB greenness = (Green-Red) + (Green-Blue) and (5) excess green (ExG=2G-R-B) (Coops *et al.*, 2012; Hufkens *et al.*, 2010; Sonnentag *et al.*, 2012). Recent effort has gone to use other the cameras to collect measures of ecosystem status such as LAI (Ryu *et al.*, 2012), crown cover (Pekin & Macfarlane, 2009) and texture (Parrott, Proulx, & Thibert-Plante, 2008). The final objective would be to relate the above-mentioned indices to different measures of photosynthetic capacity and use them to validate MODIS derived phenologies. Moreover, the camera derived images and ratios constitute a spectral and a visual archive that can be later accessed and re-interpreted in a similar fashion to RS images and products (Coops et al., 2012).

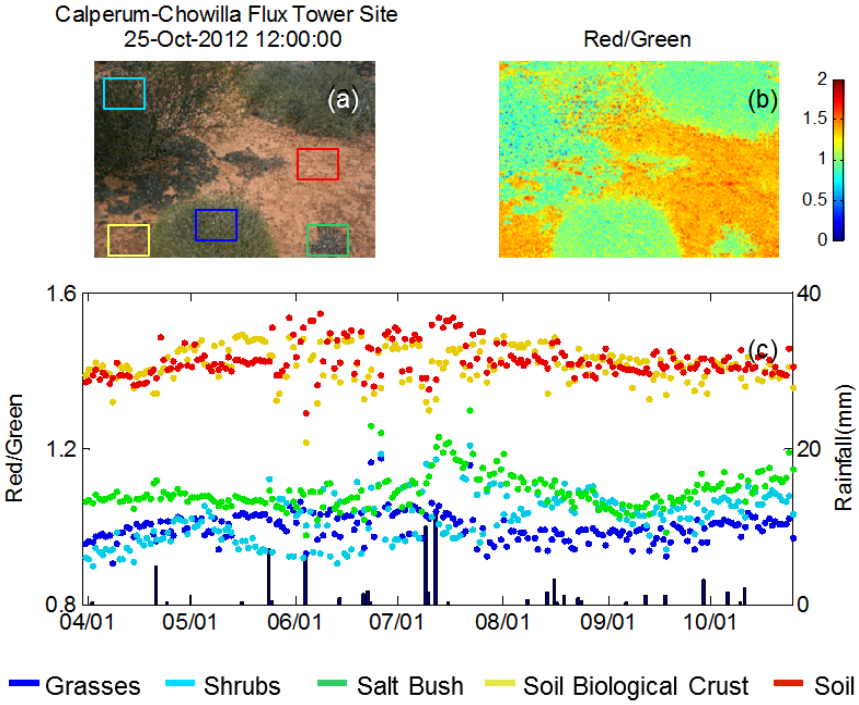

Figure 9.7 Phenocam RGB camera (wingscapes®) installed at Calperum-Chowilla eddy flux tower. With (a) an RGB image of the understory (squares indicate sub-sampling of different image component); (b) Red/Green ratio from the understory camera; (c) Red/Green ratio time series for different components including grasses, shrubs, salt bush, biological crust and soil with daily precipitation (black bars).

9.4 Other methods for validation

Here we present some of the equations and considerations used to calculate and measure in-situ fPAR and NDVI that rely on radiation sensors. Even though they offer promise for future validation and are appropriate given sufficient resources, up-to-date no OzFlux site has a suitable array of PAR sensors installed to generate a year-round PAR time series.

9.4.1 Radiation sensor NDVI

As in Doughty and Goulden (2008) and Huemmrich *et al*. (1999) it is possible to derive in-situ NDVI using a pair (upward and downward facing) of PAR sensors (wavelength: 400 to 700 nm) combined with a set of shortwave (SW) radiation sensors (wavelength: 310 to 2800 nm) The following steps are required: First, PAR units of µmol m^{-2} s^{-1} need to be converted to W m^{-2} (SW) by multiplying PAR by 0.25 J $mmol^{-1}$ (energy of photons in green light) (Huemmrich *et al*., 1999). Assuming NIR = SW – PAR, albedo NIR (NIRα) is calculated as:

$$NIR\alpha = NIR_{up} / NIR_{down} \quad \text{(equation 9.1)}$$

where NIR_{down} is the incident NIR obtained by the SW and PAR sensors facing upwards ($NIR_{down} = SW_{in} - PAR_{in}$) and viceversa for NIR_{up} ($NIR_{up} = SW_{up} - PAR_{up}$).

Subsequently, albedo PAR (PARα) is calculated as PAR_{up} / PAR_{down} and the tower measured NDVI ($NDVI_{tower}$) is defined as:

$$NDVI_{tower} = (NIR\alpha - PAR\alpha) / (NIR\alpha + PAR\alpha) \quad \text{(equation 9.2)}$$

The $NDVI_{tower}$ has shown to correlate well with satellite NDVI and more importantly, to be insensitive to seasonal changes in solar zenith angle (Huemmrich *et al*., 1999).

Whilst most radiation sensors are advertised as having a 180-degrees field of view (FOV), the actual FOV will be closer to fully hemispherical, but not quite. Moreover, radiation sensors are more sensitive towards the centre of their FOV and some instrument user manuals (depending on manufacturer) will list their half angle (HA) that is often defined as the angle at which 95% of the detected signal is obtained from.

In order to calculate the footprint of the sensor one can use 178 degrees as FOV, a value of 89 as HA and the mounting height of the sensor (h):

$$footprint = 2 \, x \, a, \quad \text{(equation 9.3)}$$

where, a = (height x sin(HA)) / sin(1). For this example, let us use h=10 m. Therefore, a = (10 x sin(89)) / sin(1) = 572.9 m, and the footprint = 1145.8 m.

9.4.2 fPAR

The fraction of absorbed PAR (fAPAR or fPAR) is defined as the fraction of incoming solar radiation in the PAR spectral region (0.4 nm to 0.7 nm) that is absorbed by vegetation. It is tightly coupled to productivity and photosynthesis. GEP is commonly modelled as: GEP = LUE * fPAR * PAR where LUE is the Ecosystem Light Use Efficiency, a measure of the ecosystem capacity (leaf chlorophyll, N, LAI) for production. Therefore, the phenology and seasonality of fPAR constitutes a key parameter in ecosystem characterisation.

Interestingly, fPAR is the result of the combined effects of the photosynthetically active vegetation (PAV, mostly chloroplast), non-photosynthetic vegetation (NPV, mostly senescent foliage, branches, stems) and leaf non-photosynthetic components inside the leaf (e.g. veins and cell walls) (Xiao *et al*., 2004). At savannas, shrublands and ecosystems with low LAI (0-3), the non-green fraction (NPV) has a significant effect on fPAR, artificially increasing its values 10 – 40% at the canopy level (Asner, Wessman, & Archer, 1998) and the non-photosynthetic components can range between 20 % to 50 % depending on species, leaf morphology, leaf age and growth history (Hanan *et al*., 1998). Having in mind that fPAR = $fPAR_{PAV}$ + $fPAR_{NPV}$, total fPAR can be directly calculated by measure radiation at different heights, as:

$$fPAR = \frac{PAR_{in_top} - PAR_{out_top} - PAR_{in_canopy}}{PAR_{in_top}} \qquad \textbf{(equation 9.4)}$$

where PAR_{in_top} is incoming PAR measured at the top of the tower, PAR_{in_canopy} incoming light inside the canopy (height/2, or 3 x height/4) or at ground level and PAR_{out_top} reflected PAR at the top of the tower. Equation 5 is used in forest sites where most of the absorption occurs on the top layers of the canopy. At more sparse vegetation sites fPAR is calculated as:

$$fPAR = \frac{PAR_{in_top} - PAR_{out_top} - PAR_{in_soil} + PAR_{out_soil}}{PAR_{in_top}} \qquad \textbf{(equation 9.5)}$$

where PAR_{out_soil} is the soil reflected PAR and PAR_{in_soil} is the PAR incident to the soil surface. Moreover, fPAR has been also calculated using the mean in-situ LAI, and a light extinction coefficient (k) as in Ruimy et al. (1999):

$$fPAR = 0.95(1 - exp^{-k\,LAI}) \qquad \textbf{(equation 9.6)}$$

where k is a site-specific extinction (e.g. ~0.5 for grasslands).

9.5 Conclusions

Validation of satellite derived phenology is important and offers two essential benefits: (1) It increases the confidence on the time and magnitude metrics, as well as provide the ability to introduce confidence intervals – to evaluate the uncertainty of the datasets (e.g. SGS ± 3 days), and (2) the combination of phenology and seasonality derived from satellite sensors, flux tower gas exchange measurements, optical sensors and phenocam imagery can contribute to our understanding of the mechanisms driving the carbon and water cycle, scaling factors at play, and provide an ecological basis for interpretation for the phenology satellite products. The selection of the validation tool of choice would depend upon the question in mind (e.g. understory/overstory vegetation response to rainfall events), the pre-existing infrastructure, and the cost associated with equipment purchase and technical personnel.

Acknowledgements

This work was supported by the Australian Government's Terrestrial Ecosystems Research Network (www.tern.gov.au), a research infrastructure facility established under the National Collaborative Research Infrastructure Strategy and Education Infrastructure Fund (Super Science Initiative) through the Department of Industry, Innovation, Science, Research and Tertiary Education. The authors would like to thank the University of Technology,Sydney and our collaborators: Dr. R Silbersteinand, Dr. C. MacFarlane, Dr. D. Chittleborough, Prof W. Meyer, Dr. G. Whiteman, T. Luckbe, Dr. J. Cleverly, Dr. N Boulain, R Faux, Dr. N. Grant, Prof. Derek Eamus, and Prof. S. Saleska.

References

Asner, G. P., Wessman, C. A., & Archer, S. (1998). Scale Dependence of Absorption of Photosynthetically Active Radiation in Terrestrial Ecosystems. *Ecological Applications*, *8*(4), 1003–1021. http://doi.org/10.1890/1051-0761(1998)008[1003:SDOAOP]2.0.CO;2

Balzarolo, M., Anderson, K., Nichol, C., Rossini, M., Vescovo, L., Arriga, N., … Martín, M. P. (2011). Ground-Based Optical Measurements at European Flux Sites: A Review of Methods, Instruments and Current Controversies. *Sensors*, *11*(9), 7954–7981. http://doi.org/10.3390/s110807954

Betancourt, J. L., Schwartz, M. D., Breshears, D. D., Brewer, C. A., Frazer, G., Gross, J. E., … Wilson, B. E. (2007). Evolving plans for the USA National Phenology Network. *Eos Transactions AGU*, *88*(19), 211.

Chmielewski, F.-M. (2003). Phenology and Agriculture. In M. D. Schwartz (Ed.), *Phenology: An Integrative Environmental Science* (pp. 505–522). Springer Netherlands. Retrieved from http://link.springer.com/chapter/10.1007/978-94-007-0632-3_31

Chuine, I. (2010). Why does phenology drive species distribution? *Philosophical Transactions of the Royal Society B: Biological Sciences*, *365*(1555), 3149–3160. http://doi.org/10.1098/rstb.2010.0142

Clerici, N., Weissteiner, C. J., & Gerard, F. (2012). Exploring the Use of MODIS NDVI-Based Phenology Indicators for Classifying Forest General Habitat Categories. *Remote Sensing*, *4*(6), 1781–1803. http://doi.org/10.3390/rs4061781

Coops, N. C., Hilker, T., Bater, C. W., Wulder, M. A., Nielsen, S. E., McDermid, G., & Stenhouse, G. (2012). Linking ground-based to satellite-derived phenological metrics in support of habitat assessment. *Remote Sensing Letters*, *3*(3), 191–200. http://doi.org/10.1080/01431161.2010.550330

Crimmins, M. A., & Crimmins, T. M. (2008). Monitoring plant phenology using digital repeat photography. *Environmental Management*, *41*(6), 949–958. http://doi.org/10.1007/s00267-008-9086-6

Donohue, R. J., McVICAR, T. R., & Roderick, M. L. (2009). Climate-related trends in Australian vegetation cover as inferred from satellite observations, 1981–2006. *Global Change Biology*, *15*(4), 1025–1039. http://doi.org/10.1111/j.1365-2486.2008.01746.x

Doughty, C. E., & Goulden, M. L. (2008). Seasonal patterns of tropical forest leaf area index and CO2 exchange. *Journal of Geophysical Research*, *113*, 12 PP. http://doi.org/200810.1029/2007JG000590

Eklundh, L., Jin, H., Schubert, P., Guzinski, R., & Heliasz, M. (2011). An Optical Sensor Network for Vegetation Phenology Monitoring and Satellite Data Calibration. *Sensors*, *11*(8), 7678–7709. http://doi.org/10.3390/s110807678

Falge, E., Baldocchi, D., Olson, R., Anthoni, P., Aubinet, M., Bernhofer, C., … Wofsy, S. (2001). Gap filling strategies for long term energy flux data sets. *Agricultural and Forest Meteorology*, *107*(1), 71–77. http://doi.org/10.1016/S0168-1923(00)00235-5

Fisher, J. I., & Mustard, J. F. (2007). Cross-scalar satellite phenology from ground, Landsat, and MODIS data. *Remote Sensing of Environment*, *109*(3), 261–273. http://doi.org/10.1016/j.rse.2007.01.004

Flanagan, L. B. (2009). Phenology of Plant Production in the Northwestern Great Plains: Relationships with Carbon Isotope Discrimination, Net Ecosystem Productivity and Ecosystem Respiration. In *Phenology of Ecosystem Processes: Applications in Global Change Research* (p. 275). New York, USA: Springer.

Hanan, N. P., Kabat, P., Dolman, A. J., & Elbers, J. A. (1998). Photosynthesis and carbon balance of a Sahelian fallow savanna. *Global Change Biology*, *4*(5), 523–538. http://doi.org/10.1046/j.1365-2486.1998.t01-1-00126.x

Huemmrich, K. F., Black, T. A., Jarvis, P. G., McCaughey, J. H., & Hall, F. G. (1999). High temporal resolution NDVI phenology from micrometeorological radiation sensors. *Journal of Geophysical Research*, *104*(D22), 27935–27,944. http://doi.org/10.1029/1999JD900164

Hufkens, K., Friedl, M. A., Richardson, A., Milliman, T., & Migliavacca, M. (2010). Vegetation Phenology from MODIS / AVHRR / PhenoCam: scaling and validation possibilities. Presented at the NASA Terrestrial Ecology Science Team Meeting, La Jolla, CA, USA: NASA.

Hutyra, L. R., Munger, J. W., Saleska, S. R., Gottlieb, E., Daube, B. C., Dunn, A. L., … Wofsy, S. C. (2007). Seasonal controls on the exchange of carbon and water in an Amazonian rain forest. *Journal of Geophysical Research: Biogeosciences*, *112*(G3), n/a–n/a. http://doi.org/10.1029/2006JG000365

Jönsson, P., & Eklundh, L. (2003). Seasonality extraction from satellite sensor data. In *Frontiers of Remote Sensing Information Processing* (pp. 487–500). Singapore: World Scientific Publishing.

Luvall, J. C., Sprigg, W. A., Levetin, E., Huete, A., Nickovic, S., Pejanovic, G. A., … Crimmins, T. M. (2011). Use of MODIS satellite images and an atmospheric dust transport model to evaluate Juniperus spp. pollen phenology and dispersal (Vol. Volume XXXVIII-8/C23, p. 54). Presented at the WG VIII/2: Advances in Geospatial Technologies for Health, Santa Fe, New Mexico, USA: ISPRS.

Ma, X., Huete, A., Yu, Q., Coupe, N. R., Davies, K., Broich, M., … Eamus, D. (2013). Spatial patterns and temporal dynamics in savanna vegetation phenology across the North Australian Tropical Transect. *Remote Sensing of Environment*, *139*(0), 97–115. http://doi.org/10.1016/j.rse.2013.07.030

Myneni, R. B., Yang, W., Nemani, R. R., Huete, A. R., Dickinson, R. E., Knyazikhin, Y., … Salomonson, V. V. (2007). Large seasonal swings in leaf area of Amazon rainforests. *Proceedings of the National Academy of Sciences*, *104*(12), 4820 –4823. http://doi.org/10.1073/pnas.0611338104

Opie, K., Newnham, G., & Guerschman, J. P. (2011). *Comparison of land cover data products and their impact on continental water assessments* (p. 20). CSIRO.

Papale, D., Reichstein, M., Aubinet, M., Canfora, E., Bernhofer, C., Kutsch, W., … Yakir, D. (2006). Towards a standardized processing of Net Ecosystem Exchange measured with eddy covariance technique: Algorithms and uncertainty estimation. *Biogeosciences*, *3*(4), 571–583.

Parrott, L., Proulx, R., & Thibert-Plante, X. (2008). Three-dimensional metrics for the analysis of spatiotemporal data in ecology. *Ecological Informatics*, *3*(6), 343–353. http://doi.org/10.1016/j.ecoinf.2008.07.001

Pekin, B., & Macfarlane, C. (2009). Measurement of Crown Cover and Leaf Area Index Using Digital Cover Photography and Its Application to. *Remote Sensing*, *1*(4), 1298–1320. http://doi.org/10.3390/rs1041298

Primack, R. B., Higuchi, H., & Miller-Rushing, A. J. (2009). The impact of climate change on cherry trees and other species in Japan. *Biological Conservation*, *142*(9), 1943–1949. http://doi.org/10.1016/j.biocon.2009.03.016

Richardson, A. D., Anderson, R. S., Arain, M. A., Barr, A. G., Bohrer, G., Chen, G., … Xue, Y. (2012). Terrestrial biosphere models need better representation of vegetation phenology: results from the North American Carbon Program Site Synthesis. *Global Change Biology*, *18*(2), 566–584. http://doi.org/10.1111/j.1365-2486.2011.02562.x

Richardson, A. D., Black, T. A., Ciais, P., Delbart, N., Friedl, M. A., Gobron, N., … Varlagin, A. (2010). Influence of spring and autumn phenological transitions on forest ecosystem productivity. *Philosophical Transactions of the Royal Society B: Biological Sciences*, *365*(1555), 3227–3246. http://doi.org/10.1098/rstb.2010.0102

Richardson, A. D., Jenkins, J. P., Braswell, B. H., Hollinger, D. Y., Ollinger, S. V., & Smith, M.-L. (2007). Use of digital webcam images to track spring green-up in a deciduous broadleaf forest. *Oecologia*, *152*(2), 323–334. http://doi.org/10.1007/s00442-006-0657-z

Richardson, A., & Hollinger, D. Y. (2007). A method to estimate the additional uncertainty in gap-filled NEE resulting from long gaps in the CO2 flux record. *Agricultural and Forest Meteorology*, *147*, 199–208.

Rosenzweig, C., Casassa, G., Karoly, D. J., Imeson, A., Liu, C., Menzel, A., … Tryjanowski, P. (2007). Assessment of Observed Changes and Responses in Natural and Managed Systems. In *Climate Change 2007: Impacts, Adaptation and Vulnerability. Contribution of Working Group II to the Fourth Assessment Report of the Intergovernmental Panel on Climate* (pp. 79–131). Cambridge, UK: Cambridge University Press. Retrieved from http://www.ipcc.ch/pdf/assessment-report/ar4/wg2/ar4-wg2-chapter1.pdf

Ruimy, A., Kergoat, L., Bondeau, A., & Intercomparison, T. P. O. T. P. N. M. (1999). Comparing global models of terrestrial net primary productivity (NPP): analysis of differences in light absorption and light-use efficiency. *Global Change Biology*, *5*(S1), 56–64. http://doi.org/10.1046/j.1365-2486.1999.00007.x

Ryu, Y., Verfaillie, J., Macfarlane, C., Kobayashi, H., Sonnentag, O., Vargas, R., … Baldocchi, D. D. (2012). Continuous observation of tree leaf area index at ecosystem scale using upward-pointing digital cameras. *Remote Sensing of Environment*, *126*(0), 116–125. http://doi.org/10.1016/j.rse.2012.08.027

Schaepman-Strub, G., Schaepman, M. E., Painter, T. H., Dangel, S., & Martonchik, J. V. (2006). Reflectance quantities in optical remote sensing—definitions and case studies. *Remote Sensing of Environment*, *103*(1), 27–42. http://doi.org/10.1016/j.rse.2006.03.002

Scheifinger, H., Menzel, A., Koch, E., Peter, C., & Ahas, R. (2002). Atmospheric mechanisms governing the spatial and temporal variability of phenological phases in central Europe. *International Journal of Climatology*, *22*(14), 1739–1755. http://doi.org/10.1002/joc.817

Sonnentag, O., Hufkens, K., Teshera-Sterne, C., Young, A. M., Friedl, M., Braswell, B. H., … Richardson, A. D. (2012). Digital repeat photography for phenological research in forest ecosystems. *Agricultural and Forest Meteorology*, *152*(0), 159–177. http://doi.org/10.1016/j.agrformet.2011.09.009

Straile, D. (2002). North Atlantic Oscillation synchronizes food-web interactions in central European lakes. *Proceedings of the Royal Society of London. Series B: Biological Sciences*, *269*(1489), 391–395. http://doi.org/10.1098/rspb.2001.1907

Van Vliet, A. J. H., de Groot, R. S., Bellens, Y., Braun, P., Bruegger, R., Bruns, E., … Sparks, T. (2003). The European phenology network. *International Journal of Biometeorology*, *47*(4), 202–212. http://doi.org/10.1007/s00484-003-0174-2

Wang, J., Rich, P. M., Price, K. P., & Kettle, W. D. (2004). Relations between NDVI and tree productivity in the central Great Plains. *International Journal of Remote Sensing*, *25*(16), 3127–3138. http://doi.org/10.1080/0143116032000160499

Xiao, X., Zhang, Q., Braswell, B., Urbanski, S., Boles, S., Wofsy, S., … Ojima, D. (2004). Modeling gross primary production of temperate deciduous broadleaf forest using satellite images and climate data. *Remote Sensing of Environment*, *91*(2), 256–270. http://doi.org/10.1016/j.rse.2004.03.010

Zhang, X., Friedl, M. A., Schaaf, C. B., Strahler, A. H., Hodges, J. C. F., Gao, F., … Huete, A. (2003). Monitoring vegetation phenology using MODIS. *Remote Sensing of Environment*, *84*(3), 471–475. http://doi.org/10.1016/S0034-4257(02)00135-9

Chapter 10. Estimating foliar chemistry of individual tree crowns with imaging spectroscopy

K. N. Youngentob *[1]
[1] Australian National University

*Corresponding author:
Kara.Youngentob@anu.edu.au

Abstract

Recent advances in remote sensing are making it possible to measure variations in foliar chemistry and plant productivity across landscapes. The patterns of chemical and energy distributions revealed with imaging spectroscopy can be used to investigate the processes responsible for the function, composition and health of ecosystems, identify areas of stressed or diseased foliage for targeted treatment, estimate forage quality for herbivorous species, and identify some plant species through their unique chemical signatures. The following chapter outlines a method for estimating foliar nutrients and plant secondary metabolites at an individual tree-crown level with imaging spectroscopy data. These are the methods that will be used to create open-source foliar chemistry maps for selected Terrestrial Ecosystem Research Network (TERN) sites.

Key Points

- Remote sensing biochemical properties of individual tree canopies can provide valuable information for forest and wildlife management and ecosystem studies.
- We describe a procedure for modelling foliar chemistry from high spectral and high spatial resolution airborne remote sensing data.
- The model development involves collecting training and testing datasets from identifiable tree crowns within the imagery, laboratory chemical analyses, pixel selection, and spectral pre-treatment routines.

10.1 Introduction

Until recently, assessing plant chemistry on a landscape-scale has been impractical because it required collecting thousands of samples in the field for lengthy laboratory analyses. Recent technological advances in infrared spectroscopy and hyperspectral remotes sensing are opening the door to the rapid assessment of leaf chemical composition in the lab and across whole forest canopies (for reviews see Majeke *et al*. 2008 and Kokaly *et al*. 2009). Imaging spectroscopy builds upon the extensive laboratory spectroscopy research that has identified strong relationships between the absorption of electromagnetic radiation and various chemical constituents (Curran 1989, Kokaly and Clark 1999, and Ebbers *et al*. 2002). Molecular vibrations resulting from the rotation, bending and stretching of chemical bonds absorb electromagnetic radiation at frequencies that correspond to their energy state and create harmonics and overtones in the near-infrared (NIR) and shortwave infrared (SWIR) regions of the electromagnetic spectrum. Variations in reflectance at wavelengths that correspond to specific molecular interactions can be used to identify and quantify the chemical composition of materials based on high resolution spectral data (Table 10.1).

Laboratory spectroscopy methods for estimating foliar chemicals based on visible and infrared portions of the electromagnetic spectrum typically use a combination of spectral feature enhancement and noise reduction techniques along with regression or principle component based modelling. These methods rely on training and testing datasets for model calibration and accuracy assessment. The techniques described in this chapter are based on those laboratory techniques, which are then applied to the airborne spectra collected with an imaging spectrometer, rather than spectra collected by a laboratory or field spectrometer. Several imagery processing steps are required to select relatively pure canopy leaf spectra from an airborne remote sensing image for training and testing data. Similarly, applying the resulting prediction algorithm to an entire image requires careful masking of non-canopy pixels and crown delineation to isolate individual tree crowns within the scene.

Table 10.1 Recognised absorption features for various foliar chemical components adapted from "Using imaging spectroscopy to estimate integrated measures of foliage nutritional quality" by K. N. Youngentob *et al*., 2012, *Methods in Ecology and Evolution*, 3, p. 423.

Known absorption feature (nm) and related biochemical (s)	Absorption mechanism and reference
460 Chlorophyll b	Electron transition (Curran 1989)
570 Chlorophyll and nitrogen	Electron transition (Penuelas *et al.* 1994)
640 Chlorophyll b	Electron transition (Curran 1989)
Chlorophyll a	Electron transition (Curran 1989)
Red-edge (680–800)	Shift from photo absorption by chlorophyll to photon reflectance by mesophyll (Curran 1989; Filella & Penuelas 1994; Soukupova, Rock, & Albrechtova 2002; Ferwerda, Skidmore, & Stein 2006)
800 Tannin	
910 Nitrogen, protein	C-H stretch, 3rd overtone (Curran 1989)
930 Oil	C-H stretch, 3rd overtone (Curran 1989; Ferwerda, Skidmore, & Stein 2006)
948 Tannin	
970 Water, starch	O-H bend, 1st overtone (Curran 1989)
1420 Lignin	C-H stretch, C-H deformation, O-H stretch, 1st overtone (Curran 1989)
1450 Sugar, starch, water, lignin	C-H stretch, C-H deformation, O-H stretch, 1st overtone (Curran 1989; Soukupova, Rock, & Albrechtova 2002)
1456 Tannin	
1470 Lignin, tannin	C-H stretch, O-H stretch, 1st overtone (Curran 1989; Soukupova, Rock, & Albrechtova 2002; Ferwerda, Skidmore, & Stein 2006)
480 Cellulose, lignin	
1490 Cellulose, sugar	
1560 Cellulose, lignin	O-H stretch, 1st overtone (Elvidge 1990)
1640 Nitrogen, tannin	N-H stretch, 1st overtone, NH3+ NH deformation, 3rd overtone, C-H stretch, 1st overtone (Murray & Williams 1987; Curran 1989; Ferwerda, Skidmore, & Stein 2006)
1645 Nitrogen	NH3 + NH deformation, 3rd overtone (Murray & Williams 1987)
1675 Tannin	C-H stretch, 1st overtone (Curran 1989; Soukupova, Rock, & Albrechtova 2002)
1690 Lignin, starch, protein	
1780 Cellulose, sugar, starch	C-H stretch, 1st overtone, O-H stretch, H-O-H deformation (Curran 1989)
1960 Starch, sugar	O-H stretch, O-H rotation, N-H asymmetry (Curran 1989)
1980 Protein	
2172 & 2180 Protein, nitrogen	N-H rotation, C-H stretch, C = O stretch, Aromatic C = C bond, 3rd overtone (Curran 1989; Kokaly 2001; Soukupova, Rock, & Albrechtova 2002; Ferwerda, Skidmore, & Stein 2006)
2175 Tannin	
2179 Phenolic compounds	
2280 Starch, cellulose	C-H stretch, CH2 deformation, C-H rotation, C = O stretch, N-H stretch (Curran 1989; Soukupova, Rock, & Albrechtova 2002)
2287 Lignin	
2300 Protein, nitrogen	

This chapter is divided into subsections that will cover the various components of the methodology for estimating foliar chemistry at an individual tree crown level with airborne remote sensing data. These are the methods that will be used to create open-source foliar chemistry maps (chlorophyll a and b, total carotenoids, anthocyanins, carbon, nitrogen, dry matter digestibility and available nitrogen) for selected TERN sites. An important caveat is that imaging spectroscopy is a relatively new and rapidly developing tool for measuring and monitoring landscape characteristics. The methods presented here for estimating and mapping variations in foliar chemicals across tree canopies with airborne hyperspectral remote sensing data are intended for research purposes. Further refinement and improvements of these methods are expected as the technology and our capabilities continue to develop and evolve.

10.2 Leaf sample collection and analysis

Leaf sampling from selected trees in the imagery is conducted to provide model training and testing datasets of trees with known foliar chemical compositions. The foliar chemical concentration of each sampled tree is combined with the corresponding canopy spectral information from the remote sensing data to develop equations to predict foliar chemistry in unmeasured tree canopies based on spectral signatures from the remote sensing data. There are a number of considerations when selecting trees from which to develop your models. Selected trees should have more than fifty-percent canopy leaf cover and their canopies should be easily identifiable in the imagery. Sparsely leafed trees, understory trees, and trees with overlapping canopies with other trees should be avoided for training and testing datasets.

If LiDAR data are available, and both the LiDAR and hyperspectral data are geo-corrected to at least one-meter accuracy, then trees can be selected that are clearly visible from above the forest canopy (not overlapping) or emergent from the canopy. If LiDAR data are unavailable, and the hyperspectral imagery is collected from a closed-canopy forest, then it is recommended that you collect some additional remote sensing flight-lines over nearby areas where the trees are isolated or semi-isolated, such as paddocks or partially cleared forest (Youngentob *et al*. 2012). However, it is important that the samples trees are the same species as found in the contiguous forest in the imagery. It should be noted that due to differing environmental conditions, it is possible that trees sampled from open areas will have significantly different spectral and chemical profiles from trees of the same species that are found in forested areas. It is acceptable for the sampled trees to differ as a population from trees within the forest, on average, as long as they capture the range of spectral and chemical values of the forest trees. If the variability of spectral and chemical values in your forest is not captured by your sample, then the model will not be able to accurately predict foliar chemistry in canopies that fall outside the sampled spectral and chemical range. Increasing the sample size will help to improve the odds of incorporating the spectral and chemical variability that you are likely to encounter in tree canopies within the imagery.

The total number of trees that need to be sampled is a matter of considerable uncertainty and may be influenced by the forest type and diversity of tree species. If you are able to collect fresh leaf spectra or canopy spectra with a field spectrometer in advance of the airborne remote sensing flight, the Mahalanobis distance calculations of spectral variation (Equation 1) can be used to estimate the spectral variability of the population.

Let be the p x 1 vector corresponding to the k-th sample spectrum, where p is the number of wavebands, and the 't' superscript denotes the vector transpose. The Mahalanobis distance is defined as:

$$d(\mathbf{x}_k,\ \mathbf{m}) = (\mathbf{x}_k - \mathbf{m})^t \sum^{-1} (\mathbf{x}_k - \mathbf{m}), \qquad \text{(equation 10.1)}$$

where $\mathbf{m}$ is the mean vector (spectrum) of the samples,

$$\mathbf{m} = \frac{1}{K} \sum_{k=1}^{K} \mathbf{x}_k,$$

and Σ is the *p* x *p* covariance matrix, defined as

$$\Sigma = \frac{1}{K-1} \sum_{k=1}^{K} (\mathbf{x}_k - \mathbf{m})(\mathbf{x}_k - \mathbf{m})^t,$$

Software, such as WinISI (InfraSoft International, Port Matilda, PA), can be used to calculate spectral variability based on Mahalanobis distance and provide an indication of the number of samples that should be collected to account for this variability, if a representative sample of the population is provided. This information can also be used to determine whether the spectral variability of one population (i.e., a contiguous forest) can be captured by another (i.e., trees in a paddock).

Previous experience from calculating spectral variability in eucalypt forests suggests that the total number of trees that need to be sampled for model training and testing is between 100-300 individuals, depending on the spectral and chemical variability of a forest. However, canopy chemistry of eucalypt woodlands dominated by one species has been modelled with a training and testing dataset of 60 trees (Huang *et al*. 2004). Conversely, highly diverse tropical forest may require over a thousand samples to develop accurate prediction equations (Asner *et al*. 2011). If you are unable to estimate spectral variability in advance, we recommend that you sample at least ten individuals of each canopy tree species, and if there are fewer than 10 canopy species, then a minimum of 100 individuals.

Leaf-age can influence the concentrations of foliar chemicals in eucalypts (Kavanagh & Lambert, 1990). Although Eucalyptus and many other Australian tree genera can produce new foliage throughout the year when conditions are favourable (Williams & Woinarski, 1997), it is strongly recommended to time your data acquisition to correspond with peak leaf maturity at the end of the growing season. Tree chemistry can also change over time due to environmental factors. For this reason, leaf samples should be collected as close to the time of the over flight as possible, preferably within the same week. Models based on foliar chemistry assessed from samples collected more than a couple of weeks before or after the imagery acquisition, or mixed with samples collected over different time periods of longer than a few weeks, may not work.

Collect the leaf samples from the top third of the canopy (i.e., visible to the sensor) and from an area in the canopy that is exposed to sunlight (i.e., top portion of branches). Leaf samples can be obtained with the aid of a sharp-shooter, arborist sling-shot, or cutting pole depending on the height of the tree. The arborist sling-shot method involves shooting a weighted bag with an attached thin nylon rope over a branch in the top third of the canopy. A flexible wire saw can then be pulled over the branch with the rope, or the branch can be pulled down with force using a sharp tug of the rope. Regardless of the method used, falling tree branches are dangerous and appropriate safety equipment, including a hard-hat and safety glasses must be worn at all times.

As soon as the branch is obtained, collect approximately 50 grams of fully-expanded adult foliage. Carefully pick the leaves from the branch so that the leaves are not broken or crushed as they are removed. Place the sample(s) into a paper sandwich bag. Collect an additional six adult leaf samples and place in a small plastic sandwich bag. Label both bags with the tree ID number. We also recommend writing the tree ID number on water proof paper with a pencil or waterproof pen and placing this paper in the bags with the leaves in the event that the writing on the outside of the bags is somehow rendered illegible. Place both bags in a portable cooler with dry ice (solid carbon dioxide). Keep leaf samples frozen, preferably at least -80 degrees, until chemical analyses can be performed.

Record the location of the tree with a differentially corrected GPS unit. Measure the diameter at breast height (DBH) and the height of the tree. Record the tree species and any notable features (e.g., florescence status, signs of herbivory). We also recommend marking the tree with an aluminium tree tag and an aluminium or galvanised nail to aid in relocating the tree.

An important caveat is that leaf samples collected from a few branches may not represent the foliar chemistry of an entire tree canopy. It is also possible that the concentrations of foliar chemicals may change between the time of the over-flight and the time when the leaf samples are collected. These factors could contribute to model error. You can minimise these potential sources of error by collecting mature leaves from the top-third of the canopy (visible to the sensor) and through conscientious timing of leaf sample collection. The complicated logistics of remote sensing data acquisition in combination with concurrent field campaigns and the realistic limitations of canopy-leaf sampling, mean that these potential sources of error cannot be entirely eliminated.

Protocols for foliar chemical assays are publically available online through CSIRO Publishing's Prometheus Wiki (protocols in ecological and environmental plant physiology: http://prometheuswiki.publish.csiro.au/tiki-custom_home.php).

10.3 Hyperspectral data pre-processing and collection of tree canopy spectra from the imagery for model calibration

The image analyses described below can be performed using ENVI (Research Systems, Inc., Boulder, Colorado); or other appropriate imagery software. Following atmospheric correction and georeferencing of the image (see chapters 4 and 15), apply a normalised difference vegetation index (NDVI)-based mask to remove pixels dominated by non-photosynthetic vegetation, soil, roads, and buildings (Xiao et al. 2004). NDVI is the ratio of reflectance (ρ) in two spectral bands located in the red (0.63-0.69 µm) and near-infrared (NIR, 0.76-1.4 µm) regions of the electromagnetic spectrum (Equation 10.2).

$$\text{NDVI} = (\rho_{NIR} - \rho_{RED})/(\rho_{NIR} + \rho_{RED}) \qquad \textbf{(equation 10.2)}$$

This ratio takes advantage of the spectral properties of chlorophyll, which absorbs electromagnetic radiation in the "red" wavelengths, and mesophyll (a plant structural component) that reflects radiation in the NIR wavelengths.

Next, apply continuum removal to the whole spectrum of every pixel in the masked imagery in order to normalise reflectance values and emphasise absorption features in the data (Clark and Roush 1984). In continuum-removal (Equation 3), a convex hull is fitted over a spectrum to connect the points of maximum reflectance with a straight line. The reflectance value (ρ) of a specific wavelength (λ) is then divided by the reflectance value of the continuum-line ($\rho_{c\lambda}$) at the corresponding wavelength:

$$\text{CR} = \frac{\rho_{\lambda}}{\rho_{c\lambda}} \qquad \textbf{(equation 10.3)}$$

The peak reflectance points where the continuum-line meets the actual spectrum are standardised to unity, and CR values decrease towards zero as the distance between the continuum-line and the original spectrum increases (Figure 10.1).

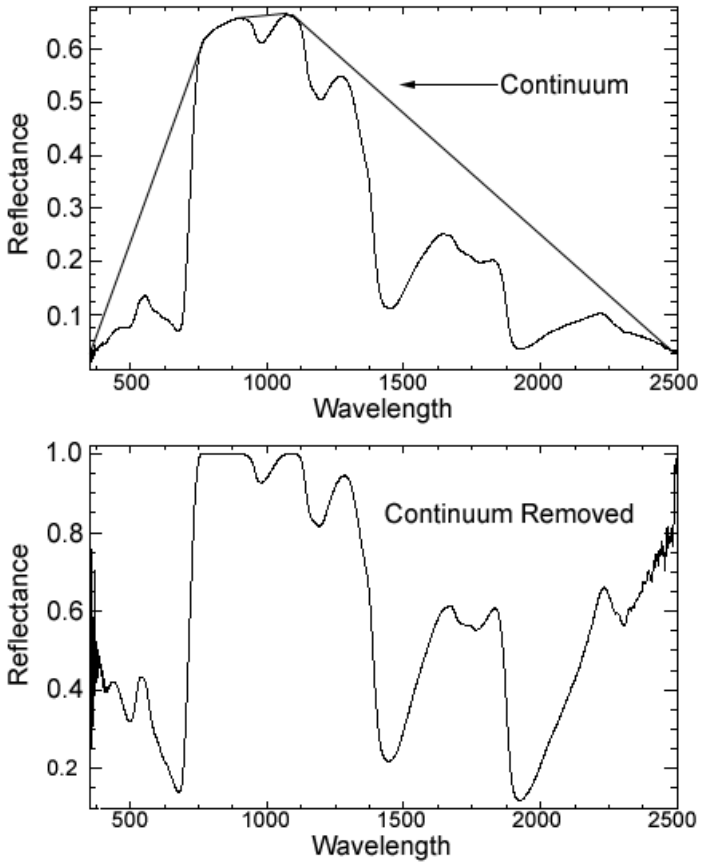

Figure 10.1 A continuum line fit over a Eucalyptus leaf reflectance spectrum (upper) and the resulting continuum-removed spectrum (lower). Reprinted from "Mapping two *Eucalyptus* subgenera using multiple endmember spectral mixture analysis and continuum-removed imaging spectrometry data," by K.N. Youngentob et al., 2011, *Remote Sensing of Environment*, 115, p. 1117.

Many native Australian trees, and particularly eucalypts, have an open-canopy architecture and pendulous leaves, which can result in mixed-pixels containing elements of leaves, bark and the ground beneath the tree. The selection of relatively pure canopy foliage pixels from the imagery is important for scaling reference values based on leaf chemistry to canopy-level spectra (Huang *et al*. 2007). To do this, first locate the tree crowns in the image from which the canopy-leaf samples have been collected. This may require revisiting the fieldsite with print-outs of the imagery. Once the tree crowns are positively identified, display the reflectance data in three wavebands from the SWIR (1.65 μm), NIR (0.84 μm) and VIS red-edge (0.67 μm) regions of the electromagnetic spectrum (red, green and blue, respectively). Viewed in this combination, green pixels indicate high concentrations of chlorophyll containing vegetation (e.g., canopy leaves) and purple, blue, yellow and white pixels are either not as photosynthetically active (e.g., bark and branches) or highly shaded (Figure 10.2). Following the methods of Huang *et al*. (2004) select only those tree canopies from which at least 4 "good" (green) pixels can be collected from each tree for model training and testing data-sets. Make sure to remove duplicate pixels that can result from the nearest-neighbour resampling of image pixels during some geocorrecting procedures. Obtain a mean, median and maximum spectral value for each tree canopy based on the pixels collected from that canopy.

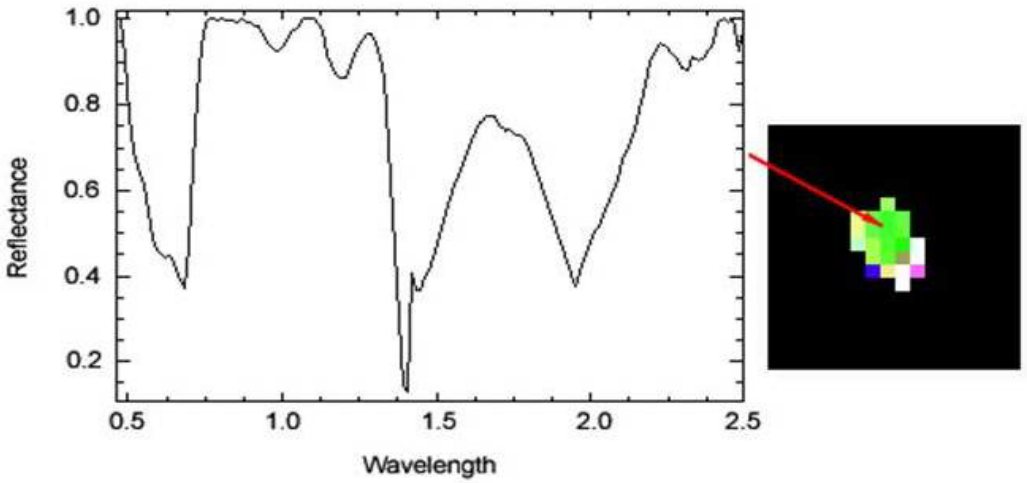

Figure 10.2 A continuum-removed reflectance spectra from a selected tree canopy pixel. The imagery data has been displayed in three wavelengths (1.65 µm, 0.84 µm, and 0.67 µm). White, blue, brown, yellow and purple pixels are not as photosynthetically active as green pixels. Adapted from "Mapping two *Eucalyptus* subgenera using multiple endmember spectral mixture analysis and continuum-removed imaging spectrometry data," by K.N. Youngentob et al., 2011, *Remote Sensing of Environment*, 115, p. 1120.

10.4 Spectral transformations and modeling

The effects of field-of-view and photon-scattering can influence the amount of radiance that reaches a sensor and negatively affect the signal-to-noise ratio of spectra collected with imaging spectrometers (Tsai & Philpot, 1998; Richards & Jia, 2006). Several methods, including scatter-corrections, smoothing transformations, and derivative analysis have been developed to enhance signal components and reduce background effects in spectral data (Dhanoa *et al*., 1994; Tsai & Philpot, 1998; Figure 10.3). We use WinISI software (Win ISI, Port Matilda, PA) for the transformation procedures described below.

Transform the mean, medium and max continuum-removed reflectance values into pseudo-absorption by calculating (log(1/CR) (Huang *et al*. 2004). To remove the effects of curvi-linearity and baseline shift, detrend the log(1/CR) spectra by subtracting an individually fitted second-degree polynomial from each spectra. Then apply a standard normal variate (SNV) scatter correction to remove unnecessary signal components (Barnes et al. 1989). We recommend testing various combinations of Savitzy-Golay derivative-based spectral smoothing functions provided by the WinISI software (Win ISI; Port Matilda, PA), which also has been demonstrated to improve model fit by emphasising absorption features whilst reducing noise (Tsai and Philpot 1998). Variability in optimal derivative and smoothing treatments among models is common in studies that used similar spectrometry methods with laboratory or imaging spectra (e.g., Youngentob et al. 2012, Huang *et al*., 2004, Ebbers *et al*. 2002). This is because the reflectance characteristics that correspond to particular foliar constituents have unique signatures that will interact differently with the various derivative and smoothing treatments according to their band-depth, location and width.

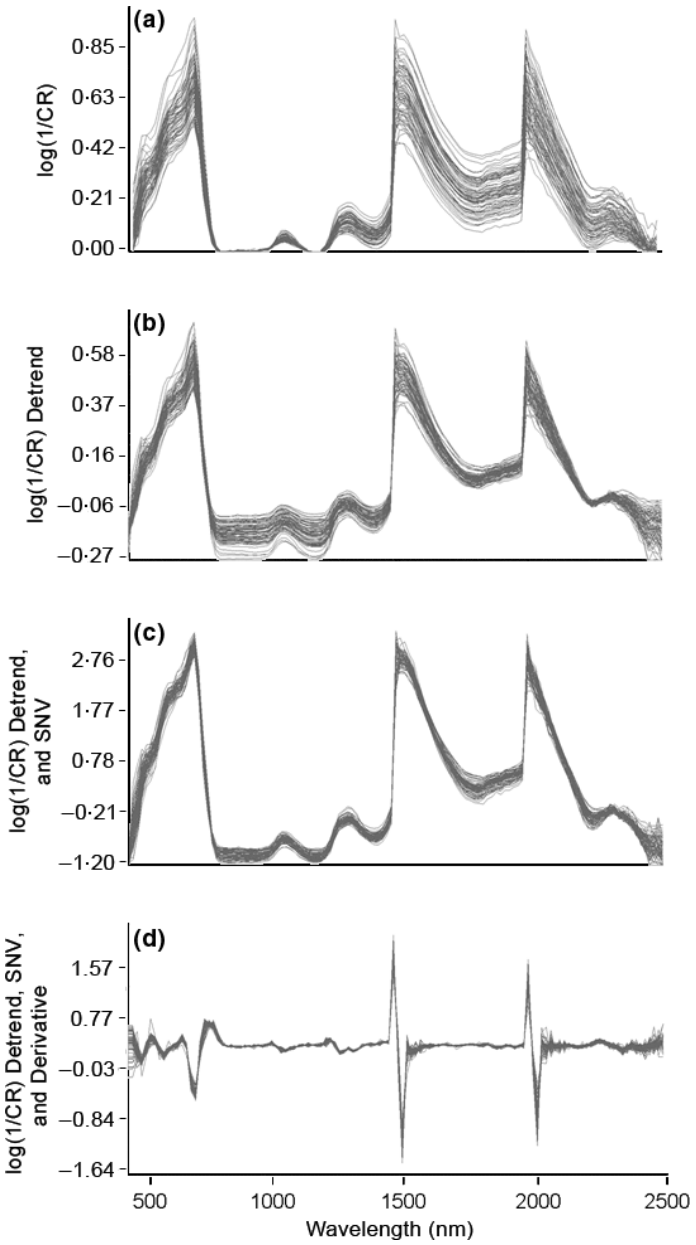

Figure 10.3 Spectral transformations applied to the maximum continuum-removed (CR) HyMap reflectance data from 77 eucalypt tree canopies:
(a) pseudo-absorption spectra from the log(1/CR) data;
(b) detrended log(1/CR) spectra;
(c) standard normal variate (SNV) scatter correction applied to the detrended, log(1/CR) spectra;
(d) a Savitzy-Golay derivative based spectral smoothing routine (e.g., 2221) applied to the SNV, detrended log(1/CR) spectra: 2221 = the second derivative (2) was calculated with a primary smoothing of 2 nm (2) across a gap size of 2nm (2) and no secondary smoothing (1).
Reprinted from "Using imaging spectroscopy to estimate integrated measures of foliage nutritional quality" by K. N. Youngentob et al., 2012, *Methods in Ecology and Evolution*, 3, p. 420.

Calibration equations from the transformed mean, median and max imagery spectra can then be developed using common regression methods. Three methods are recommended and explained here; partial least squares regression (PLSR) based on all wavebands (Wold 1975), step-up and step-wise regression (Weisberg 1980). PLSR is a multivariate extension of multiple linear regression that determines the independent linear

combinations of the predictor variables (i.e. wavebands) that explain the maximum covariation with the response variables (i.e. chemical concentrations). Thus, PLSR compresses the independent variables into factors, similar to a principal component regression. We recommend the modified PLSR described by Shenk and Westerhaus (MPLS, 1991a), which essentially normalises (i.e., zero mean, unit variance) the chemical concentrations and reflectance values at each wavelength. PLSR requires cross-validation to prevent over-fitting the model (described below). Step-up and stepwise regression can also be used to develop models based on a subset of wavebands. Step-up regression begins with a single waveband from the full spectrum and then adds subsequent wavebands to the regression model (Weisberg 1980). The waveband selected is the one that results in the largest increase in model-fit, which is assessed with the coefficient of determination, R^2. The model is run with the added variable and this process can be repeated to add additional terms. Stepwise regression is a variation of step-up regression that relies on an F test of significance to determine whether a previous term can be removed once a new term is added to the model.

Over-fitting is a common problem in linear regression models, resulting from a tendency of fitting procedures to want to exploit as large a number of predictor variables as possible to explain all the variation in a given training dataset. While the fit to training data is very good, it is likely to result in a regression model that is too complex to have any real predictive power for independent validation data (Weisberg 1980). The number of terms selected for a model requires consideration of the sample size, the closeness of fit and the contribution of each additional term. To avoid over-fitting a model, use a test-of-exact-fit to identify the maximum number of terms that could be expected to fit the population covariance matrix—based on the number of samples and wavebands (Bollen and Long 1993).

Model-fit can be further assessed using cross-validation (Elisseeff and Pontil 2002). Cross-validation provides an estimate of model error based on data resampling. For example, in 6-fold cross-validation, samples are split into 6 groups and trained six times on all but one group, which serves as validation data. A standard error of cross-validation (SECV) is obtained by pooling the residuals from each prediction and averaging the estimates of prediction error across the six repetitions. Obtaining an external estimate of prediction is not always feasible for small datasets. In these instances, cross-validation is appropriate because it enables a model to be trained and tested using all available data (Elisseeff and Pontil 2002). Two additional benefits of cross-validation are that it can be used to help identify the optimum number of terms for a model and outliers are easily identified from the prediction residuals (Shenk and Westerhaus 1991b, Baumann 2003). Although cross-validation is commonly used in spectrometry, some caution must be taken when interpreting model accuracy because the ability of the model to fit new data depends on how well the training-data represents the entire population. An additional indication of model stability can be obtained by comparing the training and testing standard errors from the cross-validation, which should be similar. Another caveat is that MPLS, step-up and stepwise regression assumes a linear relationship between leaf reflectance and concentrations of foliar biochemicals and ignores possible non-linear interactions that can result from multiple scattering effects (Borel and Gerstl 1994).

Select the best performing model for each foliar chemical constituent. If possible, test model accuracy using an independent testing dataset of trees in the imagery with known chemical values. If an independent dataset is not available due to sampling limitations, then use the cross-validation method described above to assess model performance. The best performing algorithms to predict each foliar chemical can then be applied to the entire image using the automated pixel selection method described by Huang *et al.* (2007) and crown delineation (Culvenor, 2003). Ensure that the same spectral transformations applied to the spectra used to develop the prediction algorithm are also applied to all modelled spectra in the imagery. It is also important to note that crown delineation can be highly challenging. The performance of various delineation algorithms are influenced by the spatial resolution of the remote sensing data and the architecture of the trees in the imagery. For high-spatial resolution data, the Tree Identification and Delineation Algorithm (TIDA) described by Culvenor (2002), can provide a reasonable estimation of tree crowns and canopy branch clusters.

References

Asner, G.P., Martin, R.E., Knapp, D.E., Tupayachi, R., Anderson, C., Carranza, L., Martinez, P., Houcheime, M., Sinca, F., Weiss, P. (2011). Spectroscopy of canopy chemicals in humid tropical forests. *Remote Sensing of Environment*, 115, 3587-3598.

Barnes, R.J., Dhanoa, M.S. & Lister, S.J. (1989). Standard normal variate transformation and de-trending of near-infrared diffuse reflectance spectra. *Applied Spectroscopy*, 43, 772-777.

Baumann, K. (2003). Cross-validation as the objective function for variable-selection techniques. *TrAC Trends in Analytical Chemistry*, 22, 395-406.

Bollen, K.A. & Long, J.S. (1993). *Testing Structural Equation Models*. Sage, London.

Borel, C.C. & Gerstl, S.A.W. (1994). Nonlinear spectral mixing models for vegetative and soil surfaces. *Remote Sensing of Environment*, 47, 403-416.

Clark, R.N. & Roush, T.L. (1984). Reflectance spectroscopy: Quantitative analysis techniques for remote sensing applications. *Journal of Geophysical Research*, 89, 6329-6340.

Culvenor, D. (2002). TIDA: an algorithm for the delineation of tree crowns in high spatial resolution remotely sensed imagery. *Computers and Geosciences*, 28, 33-44.

Culvenor, D. (2003). Extracting individual tree information: A survey of techniques for high spatial resolution imagery. In, M.A. Wulder & S.E. Franklin (Eds.), *Remote Sensing of Forest Environments: Concepts and Case Studies* (pp.255-277). Kluwer Academic Publishers, Dordrecht, The Netherlands.

Curran, P.J. (1989). Remote-sensing of foliar chemistry. *Remote Sensing of Environment*, 30, 271-278.

Dhanoa, M.S., Lister, S.J., Sanderson, R. & Barnes, R.J. (1994). The link between multiplicative scatter correction (MSC) and standard normal variate (SNV) transformations of NIR spectra. *Journal of Near Infrared Spectroscopy*, 2, 43-47.

Ebbers, M.J.H., Wallis, I.R., Dury, S., Floyd, R. & Foley, W.J. (2002). Spectrometric prediction of secondary metabolites and nitrogen in fresh Eucalyptus foliage: towards remote sensing of the nutritional quality of foliage for leaf-eating marsupials. *Australian Journal of Botany*, 50, 761-768.

Elisseeff, A. & Pontil, M. (2002). Leave-one-out error and stability of learning algorithms with applications. In, J.A.K. Suykens (Ed), *Advances in Learning Theory: Methods, Models, and Applications* (p. 415). IOS Press, Leuven, Belgium.

Huang, Z., Turner, B.J., Dury, S.J., Wallis, I.R. & Foley, W.J. (2004). Estimating foliage nitrogen concentration from HYMAP data using continuum removal analysis. *Remote Sensing of Environment*, 93, 18-29.

Huang, Z., Xiuping, J., Turner, B.J., Dury, S.J., Wallis, I.R. & Foley, W.J. (2007). Estimating nitrogen in eucalypt foliage by automatically extracting tree spectra from HyMap data. *Photogrammetric Engineering and Remote Sensing*, 73, 397-401.

Kavanagh, R.P. & Lambert, M.J. (1990). Food selection by the greater glider (Petauroides volans)--is foliar nitrogen a determinant of habitat quality. *Australian Wildlife Research*, 17, 285-299.

Kokaly, R.F., Asner, G.P., Ollinger, S.V., Martin, M.E. & Wessman, C.A. (2009). Characterizing canopy biochemistry from imaging spectroscopy and its application to ecosystem studies. *Remote Sensing and Environment*, 113, 578-591.

Kokaly, R.F. & Clark, R.N. (1999). Spectroscopic determination of leaf biochemistry using band-depth analysis of absorption features and stepwise multiple linear regression. *Remote Sensing of Environment*, 67, 267-287.

Majeke, B., van Aardt, J. & Cho, M.A. (2008). Imaging spectroscopy of foliar biochemicals in forestry environments. *Southern Forests*, 70, 275-285.

Richards, J.A. & Jia, X. (2006). *Remote Sensing Digital Image Analysis: An Introduction*. Birkhauser: Springer, Berlin.

Shenk, J.S. & Westerhaus, M.O. (1991a). Population structuring of near-infrared spectra and modified partial least-squares regression. *Crop Science*, 31, 1548-1555.

Shenk, J.S. & Westerhaus, M.O. (1991b). New standardisation and calibration procedures for near infrared reflectance spectroscopy. *Crop Science*, 31, 469-474.

Tsai, F. & Philpot, W. (1998). Derivative analysis of hyperspectral data. *Remote Sensing of Environment*, 66, 41-51.

Williams, J.E. & Woinarski, J. (1997). *Eucalypt Ecology*. Cambridge: Cambridge University Press.

Xiao, Q., Ustin, S.L. & MCPherson, E.G. (2004). Using AVIRIS data and multiple-masking techniques to map urban forest tree species. *International Journal of Remote Sensing*, 25, 5637-5654.

Weisberg, S. (1980). *Applied Linear Regression*. Wiley, New York.

Wold, H. (1975). Soft modeling by latent variables: The partial least squares approach. In, J. Gani (Ed.), *Perspectives in Probability and Statistics*. Academic Press, London.

Youngentob, K.N, Renzullo, L.J., Held, A.H., Jia, X., Lindenmayer, D.B., & Foley, W.J. (2012). Using imaging spectroscopy to estimate integrated measures of foliage nutritional quality. *Methods in Ecology and Evolution*, 3, 416-426.

Youngentob, K.N., Roberts, D.A., Held, A.A., Dennison, P.E., Jia, X., & Lindenmayer, D.B. (2011). Mapping two *Eucalyptus* subgenera using multiple endmember spectral mixture analysis and continuum-removed imaging spectrometry data. *Remote Sensing of Environment*, 115, 1115-1128.

Chapter 11. Tree crown delineation

A. Cabello-Leblic *[1]
[1] International Baccalaureate, Cordoba, SPAIN

*Corresponding author:
arantxacabello@gmail.com

Abstract

Forest inventories are essential if forest resources are to be effectively conserved and sustainably managed. The results of the forest inventory are used as a tool for decision-making in forest and environmental policy. Efficient forest management demands detailed, timely repeatable, and spatially explicit information. As high spatial resolution remotely sensed imagery and LiDAR data becomes more available, there is a great potential to allow the achievement of forest inventory at a single tree level. Numerous algorithms for automatic individual tree-crown detection and delineation have been developed to provide tree-based forest inventory measurements. Methods, however, need to be tested under a variety of forest conditions.

This chapter is a review of four of the most commonly used algorithms (local maxima detection, valley following, region growing and watershed segmentation) and gives a step by step case study methodology.

Key Points

- Tree Crown delineation is a desirable tool in forest management.
- The perfect algorithm to delineate individual trees does not exist. Instead, there are many that could and the suitability of each depends on the individual context.
- Most of the algorithms work well in open forests and coniferous forests but only few of them work well in deciduous and mixed forests.
- A simple methodology is shown to illustrate how to delineate tree crowns in a forest environment.

11.1 Introduction

Modern forest management objectives include timber production, maintaining biodiversity, meeting wildlife, environmental, and recreational needs, hence a better knowledge of forests structure is needed (Wang et al., 2004). The variables of interest in forest inventory usually determine the amount of trees by means of stem volume or biomass as well as stand structural information, health data or plant physiological data (Packalén et al., 2008). Under the forest conservation point of view, other variables are studied. These include: vegetation communities, invasive weeds, human induced changes, and disturbance impacts (e.g., fire and tropical cyclones).

With the increasing availability of high spatial resolution data and the computational power to process it more and more remote sensing research in forestry has focused on detecting and measuring the individual trees as opposed to obtaining stand level statistics. The individual tree crown delineation is a useful tool for mapping and analysing forest environments using high resolution remote sensing imagery. This technology is providing new opportunities for investigating and quantifying the structure and floristic of forests at both the stand and individual tree level (Bunting and Lucas, 2006). The use of very fine spatial resolution enables the representation of individual trees as a single polygon entity.

Over the last two decades a wide variety of tree crown detection and delineation algorithms have been developed. Although most of these methods have been successful in coniferous forests, often they do not work well in deciduous and mixed species forests (Jing *et al.*, 2012). However some good attempts (Bunting and Lucas, 2006; Held et al., 2001) to delineate crowns in tropical, deciduous or mixed species forest have also been carried out.

Light Detection And Ranging (LiDAR) data have emerged as sources for forest inventory analysis *(Fransson et al.*, 2000; Holmgren and Persson, 2004). Extracting individual tree information from LiDAR data can utilise some methods developed for high-resolution optical imagery (Chen *et a*l., 2006) and has also been the focus

of algorithm development. High sampling LiDAR point data provides detailed vertical structure of tree crowns, so researchers have utilised LiDAR measurements for extracting individual tree-based information such as crown diameter and tree height (e.g. Brandtberg, 2011; Chen *et al*., 2006; Holmgren and Persson, 2004). Research has also integrated LiDAR and high spatial resolution aerial imagery for individual tree analysis, since LiDAR provides accurate tree height information and optical images provide detailed spatial and spectral information (Ke and Quackenbush, 2011). In this chapter, a review of the most commonly used algorithms is presented as well as a case study where individual crown delineation has been carried out step by step.

11.2 Canopy reflectance considerations

The most important factor that acts on the optical properties of plant canopies is its geometrical structure (Guyot *et al*., 1989). The canopy reflectance derived from the remote sensing sensors is also influenced by shadowing within and between crowns (Asner and Heidebrecht 2002), which varies with their shape and structure, proximity to one another, and relative position within the vertical profile (Bunting and Lucas, 2006). Other influencing factors include reflectance contributions from non-photosynthetic material (e.g., primary branches) in the crown and the underlying soils and vegetation (Blackburn and Milton, 1997) and variations within and between species and growth stages as a function of foliar biochemistry, moisture content, internal structure and age of leaves (Lucas *et al*., 2004; Roberts et al., 1998)

Dense canopies of complex morphology create a challenge in crown delineation. Most of the algorithms already reviewed need a shadow falling between canopy crowns. However canopy crowns of different species may be too close to meet this requirement. Although multispectral sensors with high spatial resolution may have limited capacity to identify tropical tree species, due to a lack of fine spectral detail, some proportion of canopy and emergent trees can be located from these images.

11.3 Tree crown delineation methodologies

A variety of algorithms exists for the purpose of automated tree crown delineation and tree crown detection. These may be broadly categorised as local maxima/minima, template matching, region growing, and edge detection approaches. The effectiveness of each varies depending on the tree stand conditions and data source resolution.

Several studies combine tree detection and crown delineation in that detection is required prior to crown delineation (Culvenor, 2002; P Gong et al., 2002; Wang *et al*., 2004). Some even consider detection as equivalent to tree delineation, that is individual trees were detected once the crowns were delineated (Gougeon, 1995).

A pre-requirement for delineation of tree crowns is that the crowns should be at least visually recognisable as an object in the remote sensing images. In other words, the spatial resolution of the image should be much higher than the size of tree crowns. Remotely sensed images (aerial or satellite) with spatial resolution 10-100cm/pixel allow analysis of forested areas at the level of individual tree crown (Gougeon and Leckie, 2001). In the case of Aerial Laser Scanning data, if the number of laser pulses is increased to more than 5 measurements per square meter, individual trees can be recognised (Packalén *et al*., 2008).

11.3.1 Local maxima methods

These methods are based on the assumption of a mountainous spatial structure that is typical of forest images. They do not delineate the boundary of the crown, but rather provide a location of each crown. However, local maxima have been used as part of other methods that do define crown boundaries (Pinz, 1991). This algorithm identifies local maxima and examines brightness changes in concentric circles out from each maximum to determine if it is a tree crown and estimate the crown radius. Walsworth and King (1999) use local maxima and cost surfaces to identify crowns.

11.3.2 Valley-following algorithm

The valley-following algorithm was originally presented by Gougeon (1995) in a mature coniferous forest stand using 31cm imagery. The forest stand was characterised by moderate density and well-shaded gaps between neighboring trees due to intra and inter-specific competition. This method uses the fact that trees are often represented on high resolution imagery by bright areas surrounded by darker regions of shade, in a way forming a hill top and valley topography in the spectral image. The algorithm follows the valleys to separate trees and applies a rule-based approach to further refine and outline tree boundaries. The highest valued pixels generally correspond to a location on the crown where the sun orientation, viewing angle and tree geometry create a bright area on the crown. This is on the sunlit side of the tree usually near the crown apex. The algorithm has limitations where varying crown sizes can be problematic due to illumination variation within large crowns or self-shaded crowns (Gougeon, 1998).

11.3.3 Region growing algorithm

Region growing is an image segmentation approach used to separate regions and recognise objects within an image. This approach mainly depends on the assumption that the intensity of colour is high at the top of the tree but it is gradually decreased towards a tree's crown boundary. If different tree species are standing close to each other, the variation within a tree's crown is less than the variation among different trees. Starting at some seed pixel, neighboring pixels are examined one at a time and added to the growing region if they are sufficiently similar to the seed pixel. When a significant boundary is found, these pixels are labeled as belonging to the region specific to the seed pixel. For tree-crown delineation, treetops or tree location pixels can be used as seed points, and the differences between tree crowns and the background used to determine the criteria. Culvenor (2002) used local maxima to determine seed positions.

11.3.4 Watershed segmentation algorithm

The watershed transform can be classified as a region-based segmentation approach. The intuitive idea underlying this method comes from geography: the topographic relief of a landscape is flooded by water, and the dividing line of the domains of attraction of rain falling over the region are delineated by the watershed, Figure 11.1 (Serra, 1982).

Watershed segmentation is a way of automatically separating or cutting apart particles that touch. It first calculates the Euclidian distance map (EDM) and finds the ultimate eroded points (UEPs). It then dilates each of the UEPs (the peaks or local maxima of the EDM) as far as possible; either until the edge of the particle is reached, or the edge of the region of another (growing) UEP is reached. Watershed segmentation works best for smooth convex objects that do not overlap too much.

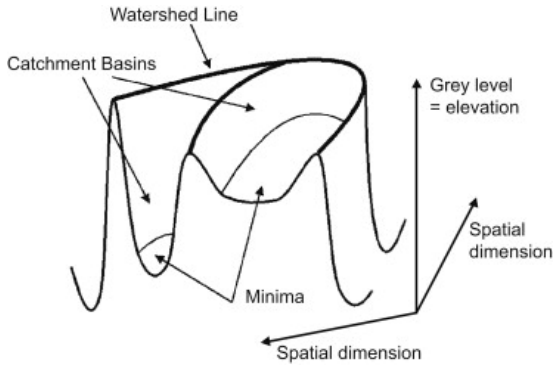

Figure 11.1
Topographic representation of a one-band image (Extracted from Tarabalka *et al.,* 2010).

A summary of the most popular algorithms applied to different conditions can be found in Table 11.1. When neighboring crowns are of different species their differences in spectral reflectance and absorption properties may be exploited in high resolution hyperspectral imagery (Ticehurst et al., 2001).

Table 11.1 Summay of tree-crown delineation algorithms and examples (Extracted from Yinghai and Quackenbush 2011).

	Applications		
Algorithms	Examples	Images	Forest conditions
Valley following	Gougeon (1995a)	MEIS-II image with 31 cm GSD	Mature coniferous plantation divided into compartments with uniform species such as red pine and red spruce
	Gougeon (1999)	CASI image with 60 cm GSD	49-year-old Douglas-fir plantations
	Leckie *et al.* (2003b)	CASI image with 60 cm GSD	Pure coniferous stands planted in 1979 and 1980
	Gougeon and Leckie (2006)	IKONOS image resampled to 50 cm pixels	Mature coniferous plantations with average tree age between 65 to 80 years, species included red pine, Scotch pine and white spruce
Region growing	Culvenor (2002)	Digital Multispectral Video image with 1 m GSD	60-year-old even-aged Mountain Ash forest
	Bunting and Lucas (2006)	CASI data with 1 m GSD	Mature forest stands with mixed species
	Pouliot *et al.* (2002)	Aerial image acquired by Kodak CIR 460 digital camera with 5 cm GSD	Black spruce and jack pine plantation established in 1994 with 1 m spacing
	Erikson (2003)	Digitized aerial photography with 10 cm pixel size	80-year-old coniferous stands, pure and mixed with Scotch pine, Norway spruce, birch and aspen
Watershed segmentation	Wang *et al.* (2004)	CASI image with 60 cm GSD	80-year-old white spruce plantation with small portions of Douglas fir
	Lamar *et al.* (2005)	Digitized aerial photography with 10 cm pixel size	Hemlock stands mixed with hardwood

11.4 Case study: Individual Crown delineation using ImageJ and ENVI

A simple step by step simple methodology to obtain individual tree crown delineation is presented in this section. Although this process is not as complex as many that can be found in the literature and may not yield the most accurate results, it is described here as it provides a simple and accessible workflow.

Two software are used in this case study: ImageJ and ENVI. ImageJ is an open-source Java based program so is freely available and in the public domain. No license is required. It can be downloaded from http://rsbweb.nih.gov/ij/download.html. ENVI (an acronym for "ENvironment for Visualising Images") is a software application used to process and analyse geospatial imagery. It is commonly used by remote sensing professionals and image analysts.

The crown delineation showed here is applied to a managed subalpine Eucalyptus forest located in Tumbarumba (New South Wales).

AISA Eagle (airborne imagine spectrometer for applications, SPECIM) was operated in a hyperspectral mode collecting 247 spectral channels in the visible and near infrared ranges of the solar spectrum from 400-970.

The steps followed in the image segmentation start with the calculation of the forest mask, followed by the application of a filter to smooth the mask. These two steps have been executed in ENVI while the next (thresholding and watershed segmentation) have been done with ImageJ.

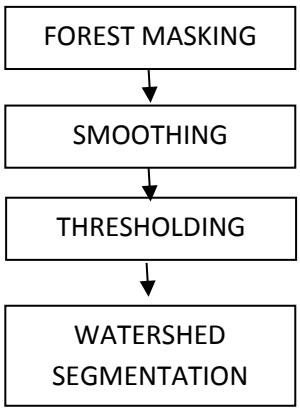

Figure 11.2 Crown delineation workflow.

2.3.1 Forest Masking

An important first step in any tree delineation and identification algorithm is the generation of a forest mask as this often defines the outer boundaries or crowns at the interface with non-forest areas.

Although generating the forest mask can be very easy, it is also a key step as it is possible to ignore some forested areas or include some non-forest areas.

When working with optical data the most common way of masking forests is through thresholding single band data or indices, including the green reflectance or near infrared channels and/or ratios that include the red edge (Bunting and Lucas, 2006). These approaches have a common problem associated and it is that most forested areas have photosynthetic active vegetation in the ground layer that, more than likely, is not going to be removed. However, when hyperspectral data are available other regions of the spectrum and hence other vegetation indices can be exploited depending on the type of forest that is found within the study area.

Eucalypts can be distinguished from the understorey vegetation because of their higher anthocyanin concentration. These pigments are responsible for the red to purple coloration of leaves (Stone *et al*., 2001). The Anthocyanin Reflectance Index 2 (ARI2)(Gitelson *et al*., 2001) was applied to the image allowing masking not only bare soil but also grass and shrubs.

$$ARI2 = \rho_{800}\left[\left(\frac{1}{\rho_{550}}\right) - \left(\frac{1}{\rho_{700}}\right)\right] \qquad \textbf{(equation 11.1)}$$

In this case there was a pine plantation that also needed to be masked.

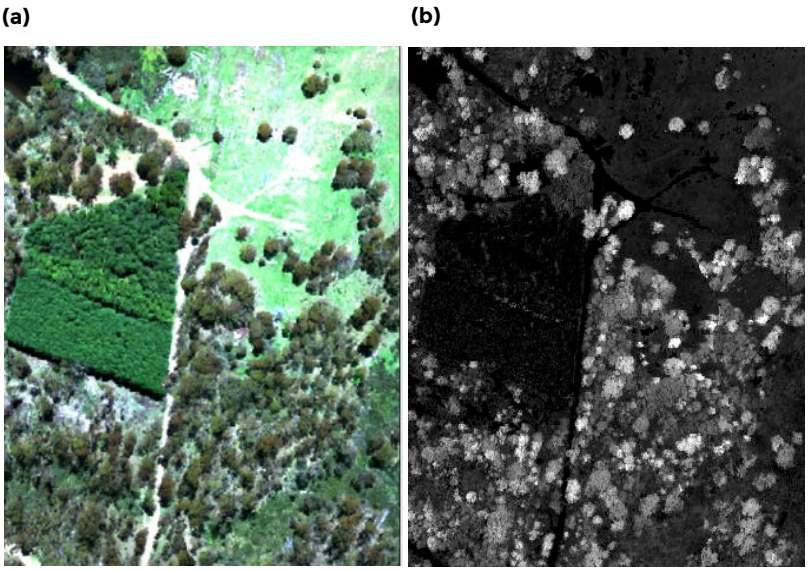

Figure 11.3 **(a)** True colour composition image
(b) Anthocyanin reflectance index 2

2.3.2 Smoothing

Image smoothing has been applied in several studies after geometric and radiometric correction in order to alleviate image noise caused by the sensor system Wang *et al*.(2004) applied a Gaussian smoothing filter, which preserves edge features better than a mean filter. For very high spatial resolution images, image smoothing can also reduce noise caused by small branches and their shadows within one crown (Ke and Quackenbush, 2011). Sometimes the smoothing makes the crown differentiation more difficult. Applying a filter or otherwise will depend of the type of canopy that is going to be segmented.

In this workflow a low pass Gaussian filter has been applied to the ARI2 image.

2.3.3 Thresholding

The objective of the segmentation is to distinguish the object from the background. To do that it is necessary to choose a threshold range identifying which pixels are set to the background colour and which to the foreground color.

The grayscale image is converted to binary by defining the grayscale cutoff point. Grayscale values below the cutoff become black and those above become white. The red areas will become the black portions in the binary image (Figure 11.4).

This point of the process is user dependent and the result of the segmentation will depend on it.

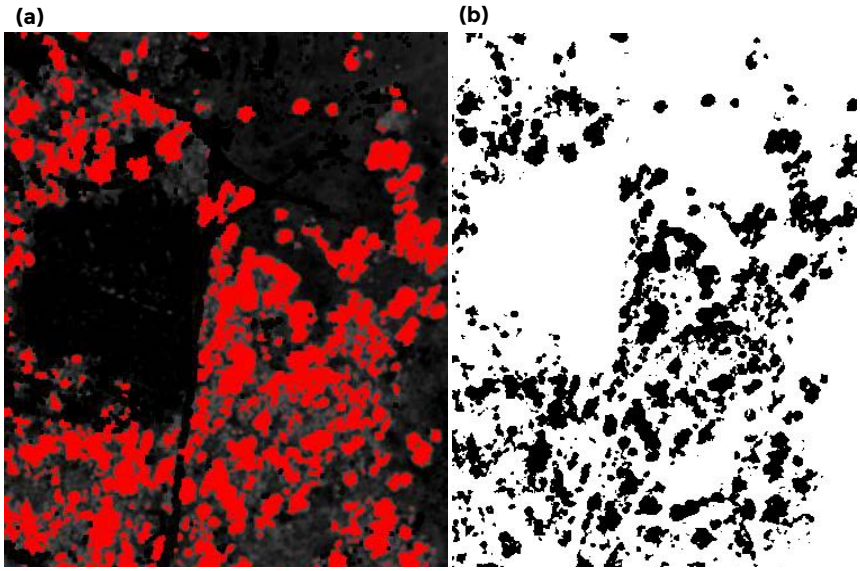

Figure 11.4 **(a)** Selected pixels as objects in red.
(b) Binary image resulted from thresholding.

2.3.4 Watershed algorithm

This algorithm is already implemented in ImageJ so the only step remaining is to apply it. The product of the watershed segmentation is a raster binary image. The raster can be used for further analysis as a mask or it can be vectorised.

There is an option also in ImageJ to count the particles obtained (crowns) and their size and position.

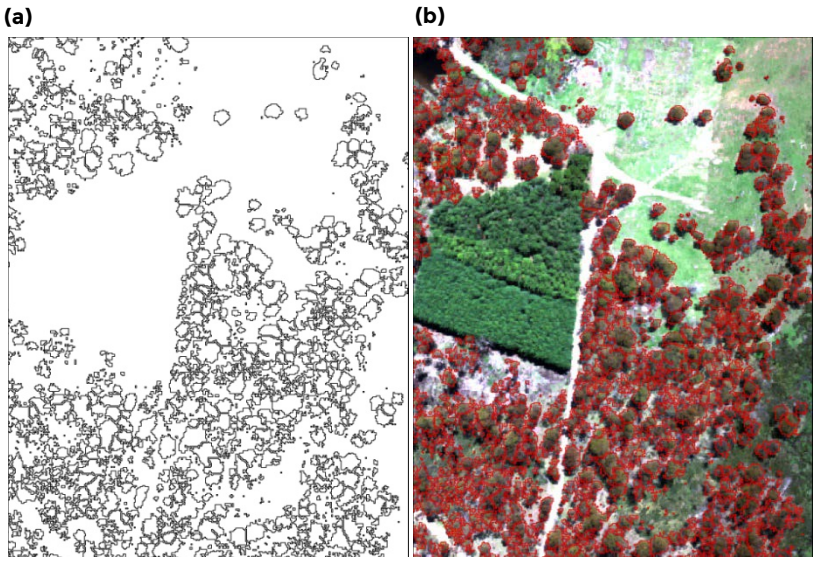

Figure 11.5 **(a)** Crown delineation vector layer
(b) Crown vectors overlaying the true colour composition image.

11.5 Conclusion

Individual tree delineation has great potential to derive meaningful forest characteristics such as stand density, species composition, health condition analysis or crown closure. Many tree crown delineation algorithms have been proposed during the last few years but their performance depends on the input imagery and the forest conditions under study. In this chapter, some of the most common tree crown delineation algorithms have been reviewed followed by a case study demonstration.

References

Asner, G., & Heidebrecht, K. (2002). Spectral unmixing of vegetation, soil and dry carbon cover in arid regions: comparing multispectral and hyperspectral observations. *International Journal of Remote Sensing* 23, 3939–3958.

Blackburn, G., & Milton, E. (1997). An ecological survey of deciduous woodlands using airborne remote sensing and geographical information systems (GIS). *International Journal of Remote Sensing.*18, 1919–1935.

Brandtberg, T. (2011). Automatic individual tree based analysis of high spatial resolution aerial images on naturally regenerated boreal forests. *Canadian Journal of Forest Research*. 29, 1464–1478.

Bunting, P., & Lucas, R. (2006). The delineation of tree crowns in Australian mixed species forests using hyperspectral Compact Airborne Spectrographic Imager (CASI) data. *Remote Sensing of Environment* 101, 230–248.

Chen, Q., Baldocchi, D., Gong, Peng, & Kelly, M. (2006). Isolating individual trees in a savanna woodland using small footprint lidar data. *Photogrammetric Engineering and Remote Sensing* 72, 923 – 932.

Culvenor, D.S. (2002). TIDA: an algorithm for the delineation of tree crowns in high spatial resolution remotely sensed imagery. *Computers & Geosciences* 28, 33–44.

Fransson, J.E.S., WaLter, F., & Ulander, L.M.H. (2000). Estimation of forest parameters using CARABAS-II VHF SAR data. *IEEE Transactions on Geoscience and Remote Sensing* 38, 720–727.

Gitelson, A.A., Merzlyak, M.N., & Chivkunova, O.B. (2001). Optical properties and nondestructive estimation of anthocyanin content in plant leaves. *Photochemistry and photobiology* 74, 38–45.

Gong, P., Sheng, Y., & Biging, G. S. (2002). 3d model-based tree measurement from high-resolution aerial imagery, *Photogrammetric Engineering & Remote Sensing* 68, 1203–1212.

Gougeon, F.A. (1995). A crown-following approach to the automatic delineation of individual tree crowns in high spatial resolution aerial images. *Canadian journal of remote sensing* 21, 274–284.

Gougeon, F.A. (1998). Automatic individual tree crown delineation using a valley-following algorithm and rule-based system. In Automated Interpretation of High Spatial Resolution Digital Imagery for Forestry (pp. 11–23) Natural Resources Canada, Canadian Forest Service, Victoria, B.C., Canada.

Gougeon, F.A., & Leckie, D.G. (2001). Individual tree crown image analysis—a step towards precision forestry. In proc. First Held International Precision Forestry Symposium.(pp 43–49). University of Washington, Seattle, Washington.

Guyot, G., Guyon, D., & Riom, J. (1989). Factors affecting the spectral response of forest canopies: a review. *Geocarto International* 3 3–18

Held, A., Ticehurst, C., & Lymburner, L. (2001). Hyperspectral mapping of rainforests and mangroves. In: IGARSS 2001. Scanning the Present and Resolving the Future. Proceedings. (pp. 2787–2789) International Geoscience and Remote Sensing Symposium (Cat. No.01CH37217). IEEE.

Holmgren, J., & Persson, Å. (2004). Identifying species of individual trees using airborne laser scanner. *Remote Sensing of Environment* 90, 415–423.

Jing, L., Hu, B., Noland, T., & Li, J. (2012). An individual tree crown delineation method based on multi-scale segmentation of imagery. *ISPRS Journal of Photogrammetry and Remote Sensing* 70, 88–98.

Ke, Y., & Quackenbush, L.J.L. (2011). A review of methods for automatic individual tree-crown detection and delineation from passive remote sensing. *International Journal of Remote Sensing* 32, 4725–4747.

Lucas, R.M., Rowlands, A.R., Niemann, O., & Merton, R. (2004). Hyperspectral sensors: Past, present and future, in Varshney, P.K., Arora, M.K. (Eds.), Advanced Image Processing Techniques for Remotely Sensed Hyperspectral Data (pp.11–49). Springer Berlin Heidelberg. Berlin, Heidelberg.

Packalén, P., Maltamo, M., & Tokola, T. (2008). Detailed Assessment Using Remote Sensing Techniques, in: Gadow, K. von. Pukkala, T. (Eds.), Designing Green Landscapes. (pp. 53–77). Netherlands. Springer Science+Business Media B.V.

Pinz, A. (1991). A computer vision system for the recognition of trees in aerial photographs. In James Tilton (Eds) Multisource Data Integration in Remote Sensing (pp 111-124) NASA Conference Publication. NASA

Roberts, D.A. DA, Nelson, B.W., Adams, J.B., & Palmer, F. (1998). Spectral changes with leaf aging in Amazon caatinga. *Trees* 12, 315–325.

Serra, J. (1982). Image analysis and mathematical morphology. New York: Academic Press,

Stone, C.A., Chisholm, L.B., & Coops, N.C. (2001). Spectral reflectance characteristics of eucalypt foliage damaged by insects. *Australian Journal of Botany.* 49, 687–698.

Ticehurst, C., Lymburner, L., & Held, A. (2001). Mapping tree crowns using hyperspectral and high spatial resolution imagery, in: *Third International Conference on Geospatial Information in Agriculture and Forestry. Denver, Colorado.*

Walsworth, N., & King, D. (1999). Image modelling of forest changes associated with acid mine drainage. *Computers & Geosciences.* 25, 567–580

Wang, L., Gong, Peng, & Biging, G.S.G. (2004). Individual tree-crown delineation and treetop detection in high-spatial-resolution aerial imagery. *Photogrammetric Engineering and Remote Sensing.* 70*,* 351–358.

Chapter 12. Measurement of above ground biomass

M.T. Schaefer[1]
[1]CSIRO Agriculture and Food

*Corresponding author:
Michael.Schaefer@csiro.au

Abstract

Biomass contained in vegetation is a crucial ecological variable for understanding the evolution and potential future changes of the climate system. This form of biomass is a larger global store of carbon than the atmosphere, and consequently, changes in the amount of vegetation biomass affect the global atmosphere by being a net source of carbon and having the potential to either sequester carbon in the future or to become an even larger source. The quantity of biomass contained in vegetation cover can also have a direct influence on local, regional and even global climate, particularly influencing the air temperature and humidity. Therefore assessment of biomass on a nation-wide and even global scale and the dynamics associated with it is an essential input to climate change forecasting models and mitigation and adaption strategies.

This section provides a basic definition of biomass and a brief review of biomass measurement in the field. After presenting a brief introduction to the concept of biomass, a discussion of the different validation methods and both remote sensing and *in situ* biomass measurement techniques is provided. These techniques are vegetation specific; it is proposed that remote or semi-remote sensing methods such as airborne laser scanning (ALS) and terrestrial laser scanning (TLS) are used in forests/woodlands, while more direct methods such as destructive sampling and *in situ* reflectance measurements are used in crops/pastures/grasslands.

Key points

- Vegetation biomass is a crucial ecological variable for monitoring and understanding the evolution and potential future changes of the climate system in a given ecosystem.
- Remote or semi-remote sensing methods such as TLS and ALS are proposed as rapid biomass assessment methods for forests and woodlands.
- Direct methods for biomass sampling such as destructive sampling are suggested for use in crops/pastures/grasslands.

12.1 Introduction

12.1.1 Biomass

Biomass is typically defined as the mass of live or dead organic matter in an ecosystem. Specifically vegetation biomass is a crucial ecological variable for understanding the evolution and potential future changes of the climate of a given area as the biomass per unit area (biomass density) is a direct measure of the sequestration or release of carbon between terrestrial ecosystems and the atmosphere.

Conceptually, biomass is usually divided into four subsections; above-ground biomass, below-ground biomass, dead mass and litter. Each of these sub-sections is defined as follows:

Above-ground biomass: consists of all living biomass above the soil, including stem, stump, branches, bark, seeds and foliage.

Below-ground biomass: consists of all living biomass of live roots. This includes fine roots (< 2 mm in diameter), small roots (2 – 10 mm in diameter) and large roots (> 10 mm in diameter). Fine roots are usually excluded from evaluation as these roots often are indistinguishable from soil organic matter or litter.

Dead mass: includes all non-living woody biomass that is not contained in litter, either standing, lying on the ground, or in the soil. Dead wood includes wood lying on the surface, dead roots, and stumps larger than or equal to 10 cm in diameter and greater than 1 m in length.

Litter: includes all non-living biomass with a diameter less than a minimum diameter chosen by a given country (for example 10 cm), lying dead, in various states of decomposition above the mineral or organic soil.

12.1.2 Biomass validation/estimation

Ecologists, research agriculturalists and foresters estimate biomass for a wide range of purposes, such as assessment of crop value, site productivity, grazing potential, regeneration, decomposition and fire effects, prediction of fire behaviour, to monitor carbon stocks, as well as to estimate potential future changes of the climate in the area (Catchpole and Wheeler, 1992).

There are a range of different methods that can be used to monitor vegetation biomass, however traditionally these methods are described as belonging to one of the following four classes;

(a) *In situ* destructive biomass measurements,
(b) *In situ* non-destructive biomass estimations (using equations, conversion factors or visual estimation),
(c) Inference from remote sensing (experimental stage), and
(d) Models describing biomass.

In the field, these techniques are often used on their own as well as in combination with one another, depending on the vegetation type that is being studied. There is a variety of techniques that fall under each of the above categories; hence it is worthwhile to consider the advantages and disadvantages of each of the different techniques in a range of situations and vegetation types (Catchpole and Wheeler, 1992).

From a TERN perspective, the vegetation types that will be focussed on include; forests (native and managed), woodlands, crops and grasslands (native and managed). Therefore, this document will outline traditional methods used to measure biomass and the techniques that TERN employs to measure the biomass in these vegetation types.

12.2 Review of techniques/methods of biomass estimation for different vegetation types

12.1.3 Woodlands and Forests (native and managed)

Above ground biomass for many natural and managed forests and woodlands has been monitored by forestry agencies through the collation of vegetation structural metric inventories. Traditionally, the total above ground biomass is typically estimated by applying allometric equations that relate field-based measurements (such as the diameter at breast height, DBH) of individual tree size to biomass (as determined through destructive sampling). A common limitation of this approach is that these equations are not available for many species and are not always applicable outside of the environmental envelope and size range for which they were originally developed. It is for this reason that errors in biomass estimation, particularly when the biomass

measurements are progressively scaled from individual trees to plot to region level, are introduced and propagated through measurements.

Major limitations also occur when using destructive sampling to determine the forest stand biomass as it is irreversible and cannot be used as a technique to monitor the biomass change over time. This form of sampling is commonly employed in managed forests and woodlands, however is not suitable for natural forests and woodlands due to the reasons stated above.

Remote sensing via satellite, airborne or terrestrial platforms often offer a faster, more cost effective alternative for collecting vegetation structural metrics than traditional field measurements such as recording the basal area or diameter at breast height etc.

Remote Sensing

Remote sensing satellites have considerable potential for monitoring forests on a regional or local scale. A number of studies have evaluated the utility of remote sensing data for mapping forest types and, to a lesser extent, for inferring forest stand parameters such as above ground biomass and vegetation density. For optical sensors, vertical observations of the forest canopy are based on spectral reflectance data collected in visible and infrared regions. It is understood that the reflectance data of a tree is governed by the properties of the tree foliage, including the chlorophyll pigments, which absorb a large part of the incoming red radiation, the leaf angle orientation and the leaf internal structure, which affect the infrared radiation (Le Toan *et al*., 1992).

The reflectance of the forest canopy will be influenced by the foliage type, the crown area, and the understory vegetation or soil, especially when the canopy is not fully closed. However, when the tree types or species are known, forest stand parameters can be inferred from the crown area, which is related to parameters such as density, height, and biomass (Le Toan *et al*., 1992). For example early reports by Franklin (1986) found that the visible reflectance of Landsat TM bands 1, 2, and 3 were strongly related to the amount of vegetation. While, Sader *et al*., (1989) found that the Normalised Difference Vegetation Index (NDVI), (which relates a ratio of the red and near infrared reflectance to the 'greenness' of the vegetation) calculated from Landsat TM data was sensitive to variations in the crown area and green biomass.

While optical and infrared techniques are effective in estimation of foliage biomass in forests, they arwell suited to direct estimation of the woody biomass. The use of synthetic aperture radar (SAR) data to estimate the woody biomass is based on the fact that scattering and attenuation of the radar by the foliage layer scales with frequency. Conversely, attenuation by 'woody' vegetation such as trunks, stems and branches, as well as the soil surface, is strong at all frequencies. In this way, radar backscatter at high frequencies (C- and X- bands) will be dominated by scattering processes in the crown layer of branches and foliage, while backscatter at lower frequencies *(P*- and L- bands) will be dominated by scattering processes involving the major woody biomass components i.e. trunks, stems and branches. (Ulaby *et al*., 1990; McDonald *et al*., 1991).

More recently airborne and terrestrial lidar (ALS and TLS) has been increasingly used to measure forest metrics from which biomass can be inferred such as vegetation density, basal area, tree height, leaf area index etc. These lidar instruments measure the three dimensional structure of a target (in this case a forest canopy) by interrogating it with laser radiation. In the simplest case, the time that is takes for the reflected radiation to return to the sensor is recorded and digitised into a three dimensional image. In this way, the forest structure can be accurately measured in high resolution from a leaf, to branch, to trunk level.

Airborne lidar has the capability to directly measure the structure of vegetation at a rapid rate as the aircraft flies over a forested area. This has brought a breakthrough in remotely collecting forest inventory data resources and therefore provides a superior choice for the remote sensing of above ground biomass compared with optical sensors that may suffer from saturation in the canopy spectral response when the canopy is dense and high in biomass (Lefsky *et al*., 2002).

Standard practice in establishing airborne lidar based models for estimating plot-level forest attributes involves the use of regression analysis for relating some carefully-selected lidar metrics to spatially coincident *in situ* measurements that are often temporally concomitant with the lidar data (Zhao *et al*., 2009). Upon

validation, these regressed models will be applied to the rest of the lidar data for prediction on a broader scale, from plot to regional level (Næsset and Bjerknes, 2001). The use of lidar for above ground biomass measurement generally follows this two stage procedure, where ground reference biomass is obtained by *in situ* destructive sampling or more often via comparisons with allometric equations. Past work by several different groups demonstrates promising results in estimating above ground biomass with lidar (Lefsky et al., 1999; Means et al., 1999; Nelson et al., 2004 and others).

The use of terrestrial laser scanning (TLS) as a forest inventory tool is becoming increasingly popular as it provides a relatively fast and labour inexpensive method of recoding three dimensional forest metrics. In terms of forest biomass estimation, TLS is commonly used in conjunction with allometric regression equations that are based on structural parameters such as tree height, stem count density, leaf area index, DBH and basal area. Combinations of such parameters are often used, however simple allometric equations relying on a single parameter, namely DBH, also exist (Seidel *et al*., 2012).

Another approach that has been used to extract biomass, in particular stem biomass, from TLS data is the use of stem reconstruction for individual trees from the TLS point cloud data (Yu *et al*., 2012). The method involves scanning the vegetated plot from multiple locations (one at the centre of the plot and six around the border of the plot), providing good data coverage of the plot and ensuring that each tree within the plot is covered by at least one scan. The tree stems are then automatically reconstructed using a modelling procedure. First the stem points were identified, a stem model was then reconstructed from the selected points and finally, the stem curve and diameters were estimated. The stem biomass can then be estimated based on measurements obtained from the reconstructed stem via linear regression using the TLS-derived DBH as a predictor (equation 1), or the volume of the reconstructed stem (equation 12.2) as a predictor (Yu *et al*., 2012).

$$\ln B = a + b\ln(DBH) \qquad \textbf{(equation 12.1)}$$

$$B = c + dV \qquad \textbf{(equation 12.2)}$$

Where *B* is the stem biomass in kg, *DBH* is derived from TLS in cm, *V* is the sum of the section volume calculated from the TLS stem reconstruction, and *a*, *b*, *c* and *d* are coefficient of the regression models (Yu *et al*., 2012).

12.2.1 Crops and Grasslands (native and managed)

The methods available for measuring biomass in a crop or pasture are often influenced by the morphology and phenology of crops and pastures, the climatic conditions and other logistical factors. The traditional methods used are primarily in situ in nature and include, physical destructive sampling, physical non-destructive sampling and electromagnetic pseudo-remote sensing techniques.

The *in situ* destructive method of direct biomass measurement involves harvesting the plants, drying the harvested portion of the plant and then weighing the green dry matter (GDM). These measurements can be undertaken on a single plant basis or on an area basis; for example in a square-metre quadrat. This is the most direct and accurate method for determining the biomass within a small unit area and is frequently extrapolated to estimate the total biomass over a larger area such as a paddock.

In the case of crops and pastures, the above ground biomass content of the crop or pasture is physically cut to a predetermined height of residue ('stubble') or harvested directly to bare soil (Figure 12.1). The resulting harvested vegetation is collected, sorted, dried in an oven and then weighed so that the projected GDM in kg/ha can be calculated.

Figure 12.1 Collecting crop biomass samples in the field by clipping the crop off using shears and leaving only short stubble or bare soil (extracted from Schaefer, 2012).

This method of biomass measurement provides an accurate measure of the plant material within the quadrats in question, generally a good estimate of the total green biomass per particular square metre, per row and possibly per that particular hectare in the crop or pasture. However, the accuracy of 'up-scaling' what is very localised measurement to an entire paddock, is prone to errors associated with the spatial variability of the crop and pasture at the paddock scale. If increasing the number of quadrats is necessary in order to account for the spatial variability at larger scale, then the technique has the major disadvantages of being labour intensive, time consuming, requires a significant amount of post processing and it becomes increasingly destructive to the crop or pasture due to the need for multiple samples across a field.

To address the limitations of destructive biomass measurement techniques described in the previous section (*viz*. time consuming, expensive to carry out and difficult to achieve on a large scale) a variety of other non-destructive physical biomass measurement techniques have been developed and reviewed throughout the literature, including visual assessment and objective height measuring devices. Specific examples include; visual assessment (Hutchinson *et al*., 1972; Campbell and Arnold, 1973), pasture height devices such as measuring sticks (Hutchings, 1991; Harmoney *et al*., 1997; Ganguli *et al*., 2000), weighted plate meters (Earle and Mcgowan, 1979; Scrivner *et al*., 1986; Laca *et al*., 1989; Gourley and McGowan, 1991), canopy intercept or point quadrat methods (Frank and McNaughton, 1990), electronic capacitance probes (Neal *et al*., 1976; Vickery *et al*., 1980; Sanderson *et al*., 2001; Serrano *et al*., 2011) and finally, pendulum sensors (Ehlert *et al*., 2003).

Each of the stated non-destructive techniques have their own advantages and disadvantages. However common disadvantages include limited and varying accuracies (generally producing errors from around ± 50 kg/ha to ± 500 kg/ha), lack of objectivity (for those using visual assessment techniques) and, in many cases, the requirement for trained or skill operators (Campbell and Arnold, 1973; Sanderson *et al*., 2001). The techniques described above are point sampling techniques, so large scale measurements across large areas is time consuming or can be unfeasible.

The use of electromagnetic sensing and spectral reflectance indices has been explored to estimate the biomass of crops, pastures and grasslands. These techniques use active and passive sensor technology to exploit the unique spectral features of green vegetation reflectance spectra (Figure 12.2).

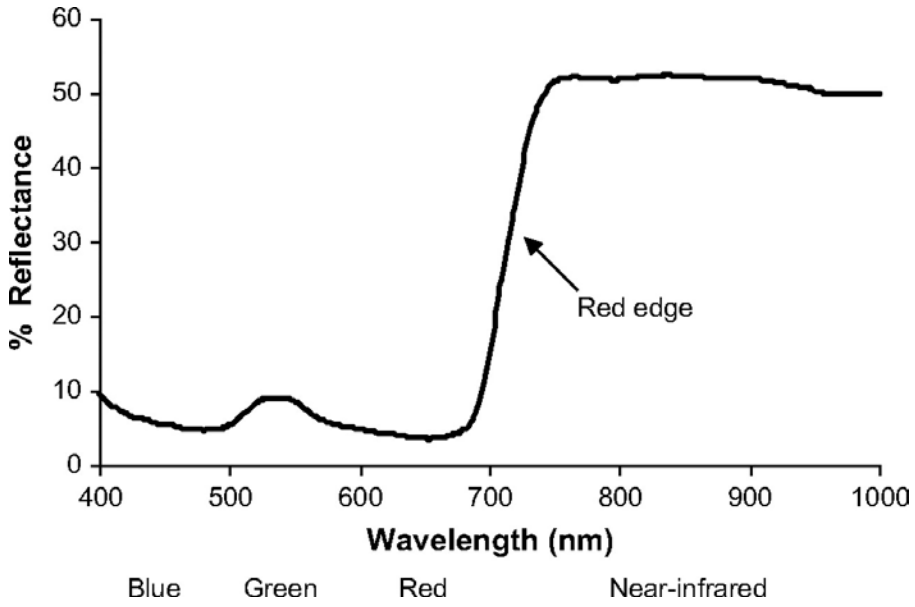

Figure 12.2 Typical green leaf reflectance spectrum for the range of 400-1000 nm, clearly displaying the 'red edge' in the range of approximately 680-750 nm. (Extracted from Blackburn, 2007).

A typical leaf reflects strongly in the green region of the spectrum (~550 nm) and due to chlorophyll, the dominant pigment within crop and pasture plant leaves, the spectrum exhibits a very low reflectance in the blue (~450 nm) and red (~650 nm) wavebands of the electromagnetic spectrum due to absorption by different leaf pigments. Blue and blue-green light are strongly absorbed by chlorophyll and xanthophylls, while carotenoids absorb light most strongly in the blue portion of the spectrum (Figure 12.2). It is for this reason that photosynthesising targets appear green when viewed in the visible wavelengths only. However, there is also a significantly higher region of reflected radiation in the near infrared (NIR) waveband (700-1200 nm) of the electromagnetic spectrum. The strong reflection of NIR radiation by plants is mainly due to multiple scatterings of the radiation at the air-cell interfaces within the leaf's internal tissue (Woolley, 1971). In the short-wave infrared wavebands (1200-2400 nm), reflectance decreases due to the absorption of light by water, protein and other carbon constituents (not shown in Figure 12.2, but refer to, for example Campbell, 1996; Lamb, 2000; Huang *et al*., 2007).

Of particular note in the reflectance spectrum of Figure 12.2, is the dramatic increase in reflectance that occurs in photosynthetically active leaves between the Red and the NIR portions of the electromagnetic spectrum. This sharp increase known as the 'red edge' occurs in the leaf reflectance between 680 nm and 750 nm which is the long wavelength limit of chlorophyll absorption (Horler *et al*., 1983). The red edge is a unique feature of the reflectance spectrum of green vegetation as it results from two optical properties of the plant tissue itself; high internal leaf scattering causing a large infrared reflectance, and chlorophyll absorption giving a low Red reflectance. These unique optical reflectance properties allow the direct estimation of biomass in pastures and grasses as well as the ability to distinguish live vegetation from other optical targets, such as dead vegetation, soil and water.

In contrast to living vegetation, bare soil and dead vegetation display a steady increase in reflectance with increasing wavelength between 400 and 900 nm (Figure 12.3), with no significantly higher reflectance in the green or NIR wavebands. The often high degree of contrast between photosynthetically active plant matter and soil or dead vegetation in the NIR wavelengths make the measurement of NIR reflectance an important means of delineating relative amounts of photosynthetically active biomass (PAB) against a soil or dead vegetation background in the field (Lamb, 2000; Serrano *et al*., 2000; Huang *et al*., 2007). It has also been demonstrated that the NIR reflectance is more sensitive to plant health than the visible wavelengths

(Campbell, 1996) and so via the spectral characteristics of the canopy, the influence of plant diseases, pests, nutrition and available water on plant biomass can also potentially be monitored.

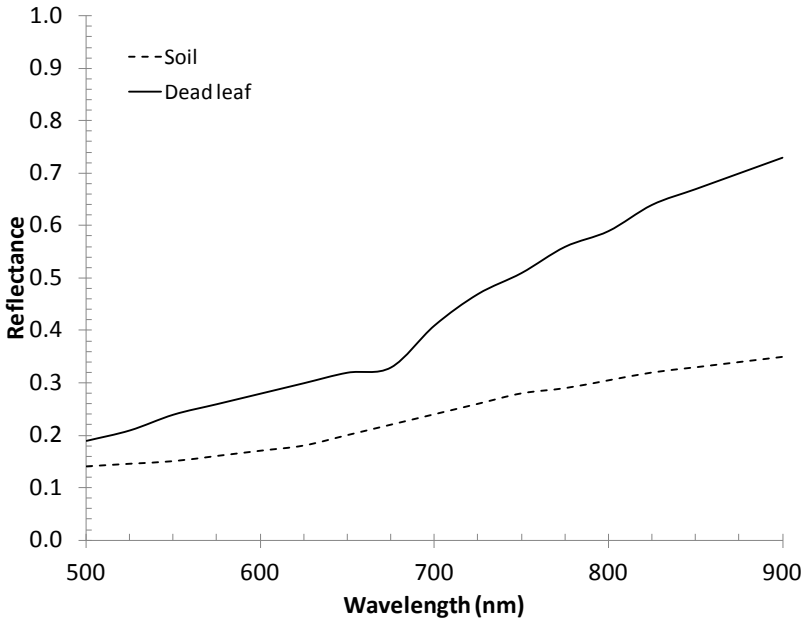

Figure 12.3 Measured reflectance spectra for a single senescent ryegrass leaf (*Lolium* spp.) and bare soil. (Adapted from Lamb *et al*., 2002).

The key spectral reflectance characteristics of photosynthetically active plant leaves and canopies described earlier have been used to develop one-dimensional spectral vegetation indices (VI) that highlight changes in the vegetation condition. These VI's generally exploit the significant difference in the reflectance of vegetation canopies in the green, red and NIR wavelengths (Lamb, 2000). One commonly used VI in remote sensing is the normalised difference vegetation index (NDVI), which is usually a number between +1 and -1 and it standardises the relative difference between the NIR reflectance 'peak' and the Red reflectance 'trough'. The NDVI was first described by Rouse *et al.* (1973), according to Equation 12.3;

$$NDVI = \frac{(Near\ Infrared) - (Red)}{(Near\ Infrared) + (Red)} \qquad \textbf{(equation 12.3)}$$

where 'Near Infrared' and 'Red' are the are the reflectances in each respective waveband. The NDVI is one of the most widely used and accepted indicators of plant vigour and relative biomass. It should also be noted here that the NDVI is technically valid for the NIR waveband ranging from 725-1020 nm and the red waveband spanning 570-680 nm. For this reason, when the NDVI has been determined by narrow wavelength-bandwidth systems, each waveband is usually denoted with a subscript denoting the particular wavelength of light used, e.g. NIR_{780} and Red_{658}.

Another commonly used vegetative index is the Simple Ratio (SR). Jordan (1969) states that the SR is given by Equation 12.4;

$$Simple\ Ratio = \frac{Near\ Infrared}{Red} \qquad \textbf{(equation 12.4)}$$

where 'Near Infrared' and 'Red' are, again, the reflectances in the NIR waveband and Red wavebands respectively. The NDVI and SR are one of the many VI's that researchers have used to estimate the LAI of a vegetative canopy (Serrano *et al.*, 2000; Aparicio *et al.*, 2002).

In the context of agricultural fields, there are a broad range of spectral indices based on the Red and NIR wavelengths which are potential candidates for estimating the quantity of green herbage mass in a pasture or crop. Indices such as NDVI and SR have well-known relationships to leaf pigment content, leaf water stress and green biomass (Jordan, 1969; Rouse *et al.*, 1973). Other Red and NIR-utilising indices such as the Soil Adjusted Vegetation Index (SAVI) designed to minimise soil induced variations (Huete, 1988) and the Non-Linear Vegetation Index (NLI), the Modified Non-Linear Vegetation Index (MNLI) and Modified Simple Ratio (MSR); are all designed to take into account non-linear relationships between surface factors that are encountered (Gong *et al.*, 2003; Haboudane *et al.*, 2004). Both the SAVI and MNLI include a 'transformation factor' L, designed to render them insensitive to soil or surface factors unrelated to the actual canopy. The value of L in both indices is selected to be 0.5 for intermediate vegetation densities (Huete, 1988; Gong *et al.*, 2003; Trotter *et al.*, 2010).

There are countless other indices that are all variations on the same theme of Red and NIR reflectance many of which are listed by Devadas *et al.* (2009) and Trotter *et al.* (2010). Several of these variations have been used to estimate biomass. Trotter *et al.* (2010) has provided an overview of the relative accuracies for several of the more common indices for use with an active optical sensor over a pasture paddock of Tall fescue (*Festuca arundinacea* var. Fletcher). From the indices that were examined it was found that the two that achieved the best correlation with GDM were the SAVI and the NLI, with a root mean square error (RMSE) of prediction of 288 kg/ha and 295 kg/ha respectively, midrange predictions included the NDVI with an error of 341 kg/ha while the MNLI performed the worst with a RMSE of prediction of 420 kg/ha. These values compare favourably with many of the 'traditional' non-destructive pasture measurement techniques discussed previously.

12.3 Specific steps for biomass measurement in different vegetation types

12.2.2 Crops, Pastures and Grasslands

To evaluate the amount of 'green' and 'dry' biomass of crops and pastures in the field, some factors such as the size of the study area, the vegetation type and the growing season need to be taken into account. If the study is to be a "once off" study, then measurements should be collected at the peak of the growing season, however if the study is to be on-going, then multiple measurements need to be taken at regular intervals throughout the growing season. The "gold standard" for biomass measurement in crops, pastures and grasslands is to use physically destructive techniques such as harvesting. However, due to the size of most study areas, a combination of destructive and non-destructive are used. The general steps are as follows.

Non-destructive sampling

1. Set out the field site to be sampled, with two 100 m transects orientated N, S, E, W.
2. Using an active Red/NIR reflectance sensor such as a CropCircle ACS-210 (Holland Scientific, Lincoln, NE USA) or a GreenSeeker (NTech Industries, Ukiah, CA USA), record the Red and NIR reflectance at a constant height of approximately 1 m above the canopy along each of the site transects (Figure 12.4).

Figure 12.4 Recording the Red and NIR reflectance using an "on-the-go" active reflectance sensor.

3. Record 'spot' reflectances at each of the sites marked for biomass harvesting using the destructive method (below).
4. Data is recorded onto an SD memory card for post processing to be carried out.
5. As the Red and NIR reflectance of the vegetation has been recorded, spectral vegetation indices (such as the NDVI and SR) can be calculated. These indices are then correlated with the above ground biomass of the site and cam be compared with other reflectance measurements obtained from remote sensing products such as MODIS etc.

Destructive sampling

1. Set out the field site to be studied with at least 10 random sites marked for harvesting of the vegetation (Figure 12.5).

Figure 12.5 Laying out a field site to begin taking biomass measurements.

2. Using grass clippers, the grass/crop is clipped to a short stubble length (around 1 cm) within a known size quadrat (Figure 12.6). Be sure to record a concurrent reflectance measurement before cuts are made for later calibration. Record the position using a GPS (optional).

Figure 12.6 Using grass clippers to cut the grass down to short length stubble within a steel quadrat laid on the ground.

3. The grass is collected in a paper sample bag for later analysis.

4. The bag containing the freshly clipped grass is weighed to determine the 'fresh' total biomass (Figure 12.7).

Figure 12.7 Weighing each of the biomass samples to determine the 'fresh' total biomass.

5. The grass/crop sample is sorted into green and dry/senesced vegetation so that each can be weighed separately.

6. The samples are dried in an oven at approximately 80^{o}C to remove any residual water that is present.

7. The samples are re-weighed to obtain the 'dry' biomass.

8. If several samples are collected in a given field site, the average of the measurements can be taken and up-scaled to determine the biomass in kg/ha.

9. The spatial distribution of above ground biomass can also be determined if the quadrat positions were recorded using a GPS.

12.2.3 Woodlands and Forests

The *in situ*, physical methods used to recording the above ground biomass of forest and woodlands are quite different to those stated for biomass measurements in crops and pastures. Condit (2008) provides a basic outline of the methods that a generally used. This outline states that;

1. Forest plots should in nearly all cases be 1 hectare in area, 100 m x 100 m in size.
2. Within each, all trees ≥ 100 mm in trunk diameter are measured, and a smaller sample of trees ≥ 10 mm but < 100 mm are also measured. In addition, a subsample of tree heights are measured and these trees are also cored for estimating wood density.
3. There are precise published formulae relating diameter, height, and density to tree biomass, so these data are converted into an estimate of the aboveground biomass in each hectare of forest.
4. In addition, fallen logs are counted and measured in order to estimate dead wood mass.
5. Tree height and wood density are also measured in a random subset of trees from each plot for use in the formulae estimating biomass.
6. In addition, surveys of dead trunks on the ground are necessary for measuring their carbon stocks.
7. Where it is possible, destructive harvesting of the trees/vegetation is undertaken. This process involves; cutting the tree down at ground level; measuring the trunk diameter D (cm) at 130 cm above ground level (DBH), as well as along the length of the tree to get trunk tapering information; total tree height H (m); wood specific gravity □(g cm^{-3}); leaf collection. Finally the total oven-dry AGB (kg) including that of the leaves is calculated.
8. This information is combined to evaluate existing allometric equations for the measurement of above ground biomass as well as the generation of new allometric equations.

Terrestrial Laser Scanning (TLS)

TERN Landscape Assessment is collecting terrestrial lidar data using two different scanners, a Riegl VZ400 and the dual wavelength echidna lidar (DWEL), for all of the calibration validation field sites around Australia. These scans when acquired correctly can quickly and easily provide and overall vegetation structural summary of the field site being examined. The method that is employed by TERN to collect TLS data at each site is as follows;

1. At each of the calibration/validation field sites, TLS measurements are also recorded (Figure 12.9). As each TLS produces a 360^{o} field of view point cloud of the immediate area of ground and canopy, a modified SLATS star transect is used.
2. 5 TLS scans are taken per site (Figure 12.8), 1 scan taken at the centre of the site, followed by 4 scans taken approximately 35 m from the centre along each of the NE, SE, SW and NW transect arms. By using this spatial configuration of scans, a complete site characterisation of the vegetation structural properties can be made.

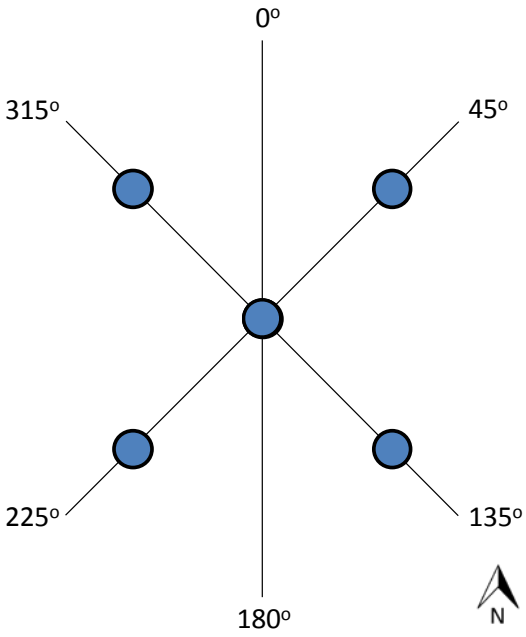

Figure 12.8 Modified SLATS Star Transect representing a single validation field site. Each of the blue dots indicates a TLS measurement position, allowing for a complete site structural characterisation to be made using this spatial configuration.

Figure 12.9 Recording TLS measurements and metadata in the field using a Riegl VZ400 Laser Scanner.

3. Once all the *in situ* vegetation measurements (DHP, TLS, DBH, basal area, vegetation species and plant canopy analyser) at each site have been recorded, post processing and collation of the data is carried out.
4. TLS point cloud data for each site is co-registered with each other. This includes the use of markers that have been manually placed within each TLS scan so that 'common' markers appearing in adjacent scans can be used to tie the two adjacent TLS scans together.
5. Once a complete site point cloud has been created by co-registering each of the point clouds. Vegetation metrics such as canopy height, tree height, tree density, basal area, LAI and DBH can be extracted from the TLS data to be used in biomass estimations.

Airborne Laser Scanning (ALS)

TERN's Landscape Assessment platform has collected airborne lidar data for all of the calibration/validation field sites around Australia. This involved using a commercial contractor to collect full waveform and discrete return laser data for each site. The data that are provided allow the retrieval of vegetation structural metrics such as tree height, canopy height, tree crown dimensions, fractional cover and others. The basic method/commercial setup for ALS acquisition was as follows;

1. The scanner was setup so that there was an outgoing pulse rate of 240 kHz, scanned at 135 lines per second.
2. Each scan line was an angular sweep through 45 degrees and contained 882 individual laser shots. The scan pattern was offset by 4 degrees from the vertical of the scanner coordinate system in order to compensate for wing dihedral and thus resulted in a symmetrical arrangement in aircraft coordinates.
3. The nominal flying height of 300 metres above ground over the planned area and a forward speed of 40 m/s is used which yields a homogeneous surface point distribution of 0.30 m in along-track as well as across-track directions. An example of an airborne lidar survey flight lines over a site is shown in Figure 12.10.
4. The scanner was mounted in the left-hand under-wing pod of one of the ARA research aircraft (VH-OBS).
5. Data from the lidar unit was logged on a Riegl DR560 data recorder containing two 500 GB hard disks, mounted in the luggage compartment of the aircraft.
6. The data was post-processed by the lidar provider to deliver industry standard LAS files (in .las format).
7. Each of the LAS files was then further processed to extract vegetation metrics to estimate biomass on a 'per plot' grid basis.

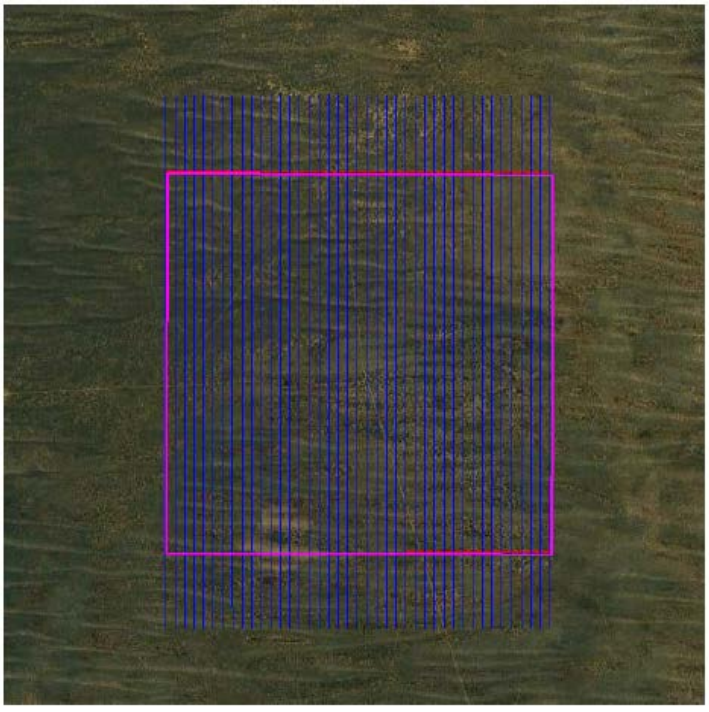

Figure 12.10 Lidar survey consisting of N-S oriented flight lines, spaced 125 m apart for a 5 km x 5 km study area.

12.4 Conclusion

The measurement of above ground biomass across a broad range of Australia's vegetated ecosystems will aid in the creation of a national coverage map of above ground biomass by TERN Landscape Assessment. The collation of data (both historical and current) to create a national map of above ground biomass will require the collaboration of several different agencies across the broader TERN network, commonwealth scientific organisations, as well as state and territory forestry agencies. These organisations contain a wealth of historical and up-to-date forestry data, and when used in conjunction with biomass data from targeted locations collected by TERN and its partners, the creation of a data rich national biomass map is entirely possible in the near future.

References

Blackburn, G. A. (2007). Hyperspectral remote sensing of plant pigments. *Journal of Experimental Botany*, *58*, 855-867.

Campbell, J. B. (1996) *Introduction to Remote Sensing* (New York (The Guliford Press)).

Campbell, N., & Arnold, G. (1973). The visual assessment of pasture yield. *Australian Journal of Experimental Agriculture and Animal Husbandry*, *13*, 263-267.

Catchpole, W. R., & Wheeler, C. J. (1992). Estimating plant biomass: A review of techniques, *Australian Journal of Ecology*, *17*, 121-131.

Condit, R. (2008). Methods for estimating aboveground biomass of forest and replacement vegetation in the tropics. *Center for Tropical Forest Science Research Manual*, 73 pages.

Devadas, R., Lamb, D., Simpfendorfer, S., & Backhouse, D. (2009). Evaluating ten spectral vegetation indices for identifying rust infection in individual wheat leaves. *Precision Agriculture*, *10*, 459-470.

Earle, D., & McGowan, A. (1979). Evaluation and calibration of an automated rising plate meter for estimating dry matter yield of pasture. *Australian Journal of Experimental Agriculture and Animal Husbandry*, *19*, 337-343.

Ehlert, D., Hammen, V., & Adamek, R. (2003). On-line sensor pendulum-meter for determination of plant mass. *Precision Agriculture*, *4* , 139-148.

Frank, D. A., & McNaughton, S. J. (1990). Aboveground biomass estimation with the canopy intercept method: a plant growth form caveat. *Nordic Society Oikos*, *57*, 57-60.

Franklin, J. (1986). Thematic Mapper analysis of coniferous structure and composition. *International Journal of Remote Sensing*, *7*, 1287-1301.

Ganguli, A. C., Vermeire, L. T., Mitchell, R. B., & Wallace, M. C. (2000). Comparison of Four Nondestructive Techniques for Estimatings Standing Crop in Shortgrass Plains. *Agronomy Journal*, *92*, 1211-1215.

Gong, P., Pu, R., Biging, G. S., & Larrieu, M. R. (2003). Estimation of forest leaf area index using vegetation indices derived from Hyperion hyperspectral data. *Geoscience and Remote Sensing, IEEE Transactions, 41*, 1355-1362.

Gourley, C., & McGowan, A. (1991). Assessing differences in pasture mass with an automated rising plate meter and a direct harvesting technique. *Australian Journal of Experimental Agriculture*, *31*, 337-339.

Haboudane, D., Miller, J. R., Pattey, E., Zarco-Tejada, P. J., & Strachan, I. B. (2004). Hyperspectral vegetation indices and novel algorithms for predicting green LAI of crop canopies: Modelling and validation in the context of precision agriculture. *Remote Sensing of Environment*, *90*, 337-352.

Harmoney, K. R., Moore, K. J., George, J. R., Brummer, E. C., & Russell, J. R. (1997). Determination of pasture biomass using four indirect methods. *Agronomy Journal*, *89*, 665-672.

Horler, D. N. H., Dockray, M., & Barber, J. (1983). The red edge of plant leaf reflectance. *International Journal of Remote Sensing*, *4*, 273-288.

Huang, W., Lamb, D. W., Niu, Z., Zhang, Y., Liu, L., & Wang, J. (2007). Identification of yellow rust in wheat using in-situ spectral reflectance measurements and airborne hyperspectral imaging. *Precision Agriculture*, *8*, 187-197.

Huete, A. (1988). A soil-adjusted vegetation index (SAVI). *Remote Sensing of Environment*, *25*, 295-309.

Hutchings, N. (1991). Spatial heterogeneity and other sources of variance in sward height as measured by the sonic and HFRO sward sticks. *Grass and Forage Science*, *46*, 277-282.

Hutchinson, K., McLean, R., & Hamilton, B. (1972). The visual estimation of pasture availability using standard pasture cores. *Grass and Forage Science*, *27*, 29-34.

Jordan, C. F. (1969). Derivation of Leaf-Area Index from Quality of Light on the Forest Floor. *Ecology*, *50*, 663-666.

Laca, E. A., Demment, M. W., Wincke, l. J., & Kie, J. G. (1989). Comparison of weight estimate and rising-plate meter methods to measure herbage mass of a mountain meadow. *Journal of range management*, *42*(1), 71-75.

Lamb, D. W. (2000). The use of qualitative airborne multispectral imaging for managing agricultural crops - a case study in south-eastern Australia. *Australian Journal of Experimental Agriculture*, *40*, 725-738.

Lamb, D. W., Steyn-Ross, M., Schaare, P., Hanna, M., Silvester, W., & Steyn-Ross, A. (2002). Estimating leaf nitrogen concentration in ryegrass (Lolium spp.) pasture using the chlorophyll red-edge: theoretical modelling and experimental observations. *International Journal of Remote Sensing*, *23*, 3619-3648.

Le Toan, T., Beaudoin, A., Riom, J., & Guyon, D. (1992). Relating forest biomass to SAR data. *IEEE Transactions on Geoscience and Remote Sensing*, *30*(2), 403-411.

Lefsky, M. A., Cohen, W. B., Acker, S. A., Parker, G. G., Spies, T. A., & Harding, D. (1999). Lidar remote sensing of the canopy structure and biophysical properties of Douglas Fir western hemlock forests. *Remote Sensing of Environment, 70*, 339–361.

Lefsky, M. A., Cohen, W. B., Parker, G. G., & Harding, D. J. (2002). Lidar remote sensing for ecosystem studies. *Bioscience*, *52*, 19–30.

McDonald, K., Dobson, M. C., & Ulaby, F. T. (1991). Modeling multifrequency diurnal backscatter from a walnut orchard. *IEEE Transactions on Geoscience and Remote Sensing*. *28*, 852-863.

Means, J. E., Acker, S. A., Harding, D. J., Blair, J. B., Lefsky, M. A., & Cohen, W. B. (1999). Use of large-footprint scanning airborne lidar to estimate forest stand characteristics in the western Cascades of Oregon. *Remote Sensing of Environment*. *67***,** 298–308.

Næsset, E., & Bjerknes, K. O. (2001). Estimating tree heights and number of stems in young forest stands using airborne laser scanner data. *Remote Sensing of Environment*. *78*, 328–340.

Neal, D. L., Currie, P. O., & Morris, M. J. (1976). Sampling herbaceous native vegetation with an electronic capacitance instrument. *Journal of Range Management*, *29*(1), 74-77.

Nelson, R., Short, A., & Valenti, M. (2004). Measuring biomass and carbon in Delaware using airborne profiling Lidar. *Scandinavian Journal of Forest Research*, *19***,** 500–511.

Rouse, J. W., Haas, R. H., Schell, J. A., & Deering, D. W. (1973). Monitoring vegetation systems in the great plains with ERTS. *Proceedings of the 3rd ERTS Symposium, NASA SP-351 I*, 309-317.

Sanderson, M. A., Rotz, C. A., Fultz, S. W., & Rayburn, E. B. (2001). Estimating forage mass with a commercial capacitance meter, rising plate meter, and pasture ruler. *Agronomy Journal*, *93*, 1281-1286.

Sader, S. A., Waide, R. B., Lawrence, W. T., & Joyce, A. T. (1989). Tropical forest biomass and successional age class relationships to a vegetation index derived from Landsat TM data. *Remote Sensing of the Environment*, *28*, 143-156.

Schaefer, M. T. (2012). Advanced optical sensing of biomass in plant canopies. In: School of Science and Technology, (Armidale NSW, Australia, University of New England).

Scrivner, J. H., Center, D. M., & Jones, M. B. (1986). A rising plate meter for estimating production and utilization. *Journal of Range Management*, *39*(5), 475-477.

Seidel, D., Albert, K., Fehrmann, L., & Ammer, C. (2012). The potential of terrestrial laser scanning for the estimation of understory biomass in coppice-with-standard systems. *Biomass and Bioenergy*, *47*, 20-25.

Serrano, J. M., Peca, J. O., Marques da Silva, J., & Shahidian, S. (2011). Calibration of a capacitance probe for measurement and mapping of dry matter yield in Mediterranean pastures. *Precision Agriculture*, 12(6), 860-875.

Serrano, L., Filella, I., & Peñuelas, J. (2000). Remote Sensing of Biomass and Yield of Winter Wheat under Different Nitrogen Supplies. *Crop Science*, *40*, 723-731.

Trotter, M., Lamb, D. W., Donald, G., & Schneider, D. (2010). Evaluating an active optical sensor for quantifying and mapping green herbage mass and growth in a perennial grass pasture. *Crop and Pasture Science*, *61*, 389-398.

Ulaby, F. T., Sarabandi, K., McDonald, K., Whitt, M., & Dobson, M. C. (1990). Michigan microwave scattering model. *International Journal of Remote Sensing*, *11*(7), 1223-1253.

Vickery, P., Bennett, I., & Nicol, G. (1980). An improved electronic capacitance meter for estimating herbage mass. *Grass and Forage Science*, *35*, 247-252.

Woolley, J. T. (1971). Reflectance and transmittance of light by leaves. *Plant Physiology*, *47*, 656-662.

Yu, X., Liang, X., Hyyppä, J., Kankare, V., Vastaranta, M., & Holopainen, M. (2012). Stem biomass estimation based on stem reconstruction from terrestrial laser scanning point clouds. *Remote Sensing Letters*, *4*(4), 344-353.

Zhao, K., Popescu, S., & Nelson, R. (2009). Lidar remote sensing of forest biomass: A scale-invariant estimation approach using airborne lasers. *Remote Sensing of Environment*, *113*, 182-196.

Chapter 13. Vegetation spectroscopy

L. Suarez*[1], N. Restrepo-Coupe[2], A. Hueni[3,4], L. A. Chisholm[4]

[1] Remote Sensing Centre, School of Mathematical and Geospatial Sciences, RMIT University

[2] Plant Functional Biology and Climate Change Cluster, University of Technology Sydney

[3] Remote Sensing Laboratories, Department of Geography, University of Zurich, Switzerland

[4] School of Earth and Environmental Sciences, Centre for Sustainable Ecosystem Solutions, University of Wollongong

*Corresponding author:
Lola.Suarezbarranco@rmit.edu.au

Abstract

Field spectroscopy involves the study of the interrelationships between the spectral characteristics of objects and their biophysical attributes in the field environment (Bauer *et al.*, 1986; Milton, 1987). When applied to vegetated surfaces, the spectral characteristics are function of the status, composition and structure of the elements measured. There are more elements that add undesired effects to the overall signal as the soil background or the viewing and illumination geometry. Like every other measurement in the field, it is very important to be familiar with the instrument used and conscious of good practices that ensure the acquisition of reliable measurements. Moreover, for the comprehensive use of the data in future studies, it is very important to document the measurement protocol and a proper collection of measurement auxiliary data. This chapter compiles some basic theory about photon-vegetation interaction and some guidelines for field spectroscopy measurement.

Key points

- Vegetation spectral response is function of leaf composition, age and phenology, plant architecture, illumination intensity and illumination/viewing angles.
- The key recommendations to follow when measuring in the field are: ensure constant illumination, avoid shadows or external elements within the instrument footprint and be sure the instrument and calibration panels are calibrated and in good state.
- There are different measurement set-ups and sampling designs (11.2.2 and 11.2.3), the operator must choose one and document it as part of the metadata of the measurement.
- It is very important to properly document the measurements with enough metadata allowing future users to understand how the data was taken (see 11.2.4 for metadata collection).

13.1 Vegetation spectral response

When an incident radiation ($W \cdot sr^{-1}$) reaches a surface, it is reflected, absorbed or transmitted. The sum of these three processes accounts then for the total of the incoming energy, being expressed most of the times in proportional units and their sum being equal to 1. Little of the incident visible (0.4–0.7 mm) or near-infrared (0.7–1.3 mm) energy is reflected directly from the outer surface of a leaf because the cuticular wax layer is nearly transparent to radiation at these wavelengths (Knipling, 1970). Hence, leaf reflectance is low in the visible, starting with very low values in the blue (0.4–0.5 mm), slightly higher in the green (0.5–0.6 mm), and again reaching a minimum in the red (0.6–0.7 mm) (Jackson, 1986) (Figure 13.1). The main responsible of the leaf low reflectance in the visible part of the electromagnetic spectrum is the leaf pigment pool (chlorophyll, carotens and xanthophylls). However, the influence of pigment composition does not affect the near-infrared region significantly (Gates and Tantraporn, 1952). Chlorophyll is mainly absorbing in the red visible portion of the spectrum and partially contributes to the absorption in the blue and the green together with other pigments as carotenes and xanthophylls (Jackson, 1986). In the near-infrared region, leaf absorption/reflection is mainly dependent on the leaf cell structural discontinuities; meanwhile, in the mid-infrared region (1.3–3 mm), water and other compound concentrations play a major role (Peñuelas and Filella, 1998).

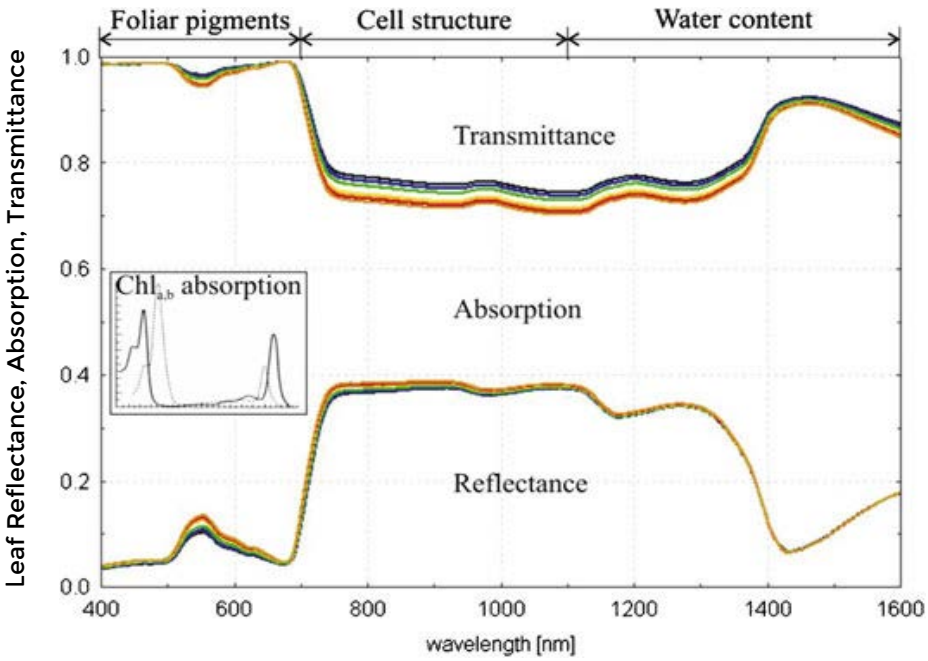

Figure 13.1 Reflectance, transmittance, and absorption of a leaf, the chlorophyll a and b absorption in the visible, and the regions affected by foliar pigments, cell structure, and water content.

Figure 13.1 Depicts the reflectance, transmittance, and absorption proportional values of a leaf specifying the spectral regions affected by pigment absorption, cell structure, and water content. The chlorophyll absorption spectrum is also presented with two characteristic peaks, in the blue and red regions.

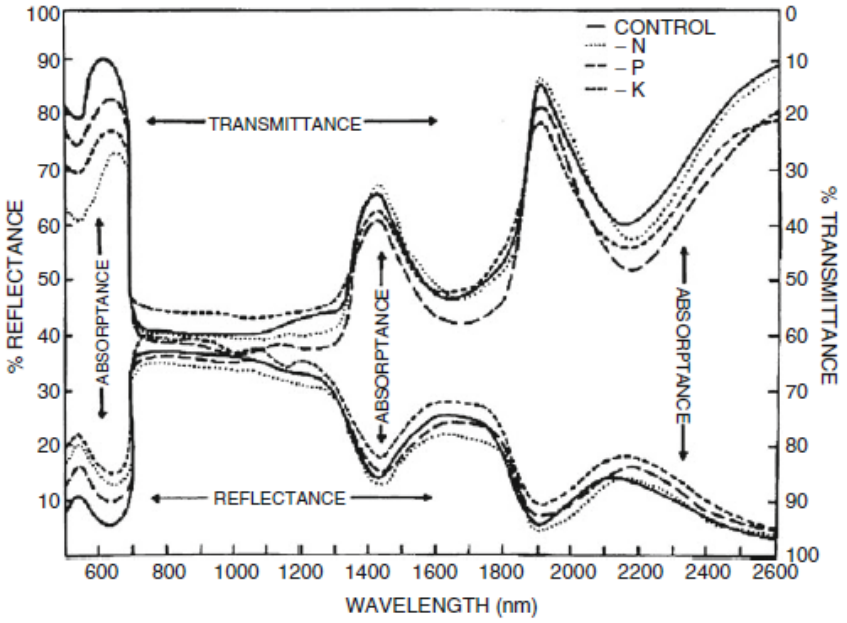

Figure 13.2 Reflectance and transmittance leaf spectra corresponding to healthy, nitrogen-, phosphorous-, and potassium-deficient leaves (Adapted from Al-Abbas et al., 1974).

The leaf spectrum is affected by several factors including leaf age, phenology, and a highly variable range of stressors, for example, nutrient and water deficiencies, and insects and other damaging agents. Figure 13.2 presents the differences in the reflectance and transmittance spectra of a healthy leaf and the spectra of leaves compared to those with nitrogen, phosphorous, and potassium deficiencies. As the impact of different nutrients in the electromagnetic spectrum generally overlaps, it is important to identify spectral regions where differences are driven by individual nutrients for a proper pathology assessment.

Periodic changes on meteorological drivers as precipitation, solar radiation and temperature, among others, influence different biological events (e.g. flowering, fruiting, etc.). These seasonal cycles and their relationship with biotic and physical drivers is known as phenology (see Phenology Validation section for definitions). At the leaf level, phenology is characterised by changes in photosynthetic capacity, spectral properties, and leaf chemistry. The phenology of temperate broadleaf and tropical deciduous species is generally straight forward with a clear and visible annual cycle that starts with springtime leaf-flux to autumn abscission at temperate areas and it is driven by the onset of the rainy and dry periods at tropical sites (e.g. leaf longevity of tropical deciduous is 6 to 9 months (Sobrado, 1994)). For eight savanna tree species, Eamus *et al*. (1999) showed a drop in assimilation rates (µmol m-2 s-1), foliar N content (mg g-1) and Specific Leaf Area (SLA, cm2 g-1) in June – Sep. If we assume that the phenology of the leaf spectral properties is a reflection of leaf chemistry (e.g. chlorophyll content and anthocyanin) and leaf traits (e.g. SLA), we should expect that reflectance, absorbance and the different vegetation indices (e.g. Enhanced Vegetation Index (EVI) and Photochemical Reflectance Index (PRI)) will also change. Patterns of shoot extension and refoliation of eucalypts differ from many of the commercially-important tree genera in the temperate Northern Hemisphere. Eucalypts have a very opportunistic leafing phenology, although rapid leaf expansion usually occurs in moderately synchronised seasonal flushes (Stone *et al* 2005). If we want to understand the phenology of leaf optical properties, it is required to follow a set sample of leaves through time. Figure 13.3 shows seasonal changes (occurred on a period of 3-months) in optical properties and the effect of leaf age on the spectra. Changes in reflectance and transmittance will be species specific, will have a different effect at the top-of-the-canopy and shaded leaves and in many cases they will be site specific, thus all this factors should be balanced when planning a field campaign and the design should be based on the objectives of the project (e.g. validation of satellite products, chemistry models, etc.). Optical measurements on a seasonal basis offer promise for future studies and are appropriate given sufficient resources.

Plant canopies are structurally diverse due to unique spatial patterns that different species adopt for intercepting light and even regulating the light (Atwell *et al* 1999). Thus, at canopy level, the interaction of radiation within the vegetation depends on the contribution of several components such as leaves, stems, soil background, illumination and view properties of each canopy element as well as on their number, area, orientation and location in space (Goel and Thompson, 2000; Koetz *et al.*, 2004).

In addition, the illumination and viewing geometry play a very important role in the resulting reflectance (Curtiss and Goetz, 1999; Perbandt *et al.*, 2010). The changes in the overall reflectance as function of the illumination geometry are defined in the Bidirectional Reflectance Distribution Function (BRDF) for each viewing angle. The BRDF of a particular canopy is dependent of the amount and disposition of the canopy elements, being highly affected by the total leaf area, foliage clumpiness and the leaf angle distribution.

As a consequence, indices or algorithms derived from leaf measurements are not applicable to canopy measurements. Some authors have overcome this problem by combining indices (Haboudane *et al.*, 2002) and some others have drawn upon model simulations of such effects (Cescatti, 1997; Combal *et al.*, 2002; Suarez *et al.*, 2009).

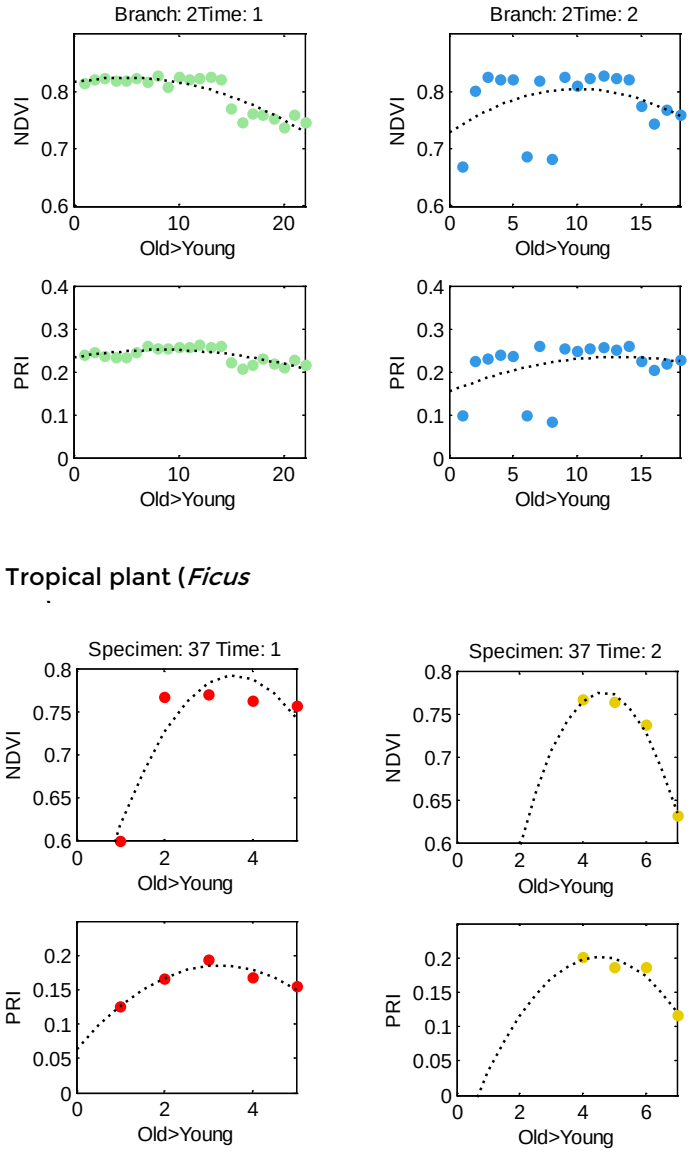

Figure 13.3 Relationships between relative leaf age (old to young along a branch), Normalized Vegetation Index NDVI (top panels) and the Photochemical Reflectance Index, PRI (lower panels). Leaf spectra obtained using an ASD portable spectroradiometer and a LI-1800 integrating sphere. Each point correspond to the mean of 6 measurements (each a 30 sample average) (a) initial (t1) NDVI (b) 3-months after (t2=t1+3months) NDVI Tropical plant, (c) initial (t1) PRI (d) 3-months after (t2=t1+3months) PRI Tropical plant. (e) initial (t1) NDVI (f) 3-months after (t2=t1+3months) NDVI agricultural plant, (g) initial (t1) PRI (h) 3-months after (t2=t1+3months) PRI agricultural plant.

13.2 Field spectroscopy measurement

There are a number of good practices or recommendations for the acquisition of spectral measurements in the field:

- Illumination conditions must be constant during the whole measurement (clear sky conditions, avoid cloud cover changes).
- The measured surface should not be shadowed by the operator or measuring structures. The operator should stand perpendicular to the solar plane, not shadowing the target and not being in the hotspot position to avoid possible backscattering on the target.
- The carrier (person or structure) cannot cover any area within the instrument footprint (see Figure 13.5 a). In the case of being in the proximity, the person should dress in low-reflective clothes; structures should not be of highly reflective materials (see http://discover.asdi.com/Portals/45853/docs/Measurements-paper-10-26-12.pdf for more information).
- Fibre optics must be handled with care. They are composed of a high number of individual fibres that are broken easily when folded. In case of rupture of part of the fibres, the instrument has to be recalibrated.
- Assure the instruments and reference panels have been calibrated.

13.2.1 Target selection

If the spectroscopy measurements are meant to be related to airborne/satellite imagery, targets should cover at least 3x3 pixels square to ensure a minimum of 1 pure image pixel. Spectrometer should capture only the target when performing the instrument calibration or data collection (see section 13.2.3.). In order to avoid unwanted BRDF effects on the measurements, targets should be as flat and levelled as possible. In the case of being selected for calibration purposes, the targets and the surrounding should be homogeneous in illumination and in the property needed to be validated. Areas that are half-shadowed or that have an adjacent element should be avoided because such elements can affect the measured spectra.

13.2.2 Spectral measurement set up

Leaf measurements

Leaf hemispherical reflectance and transmittance can be measured using an integrating sphere attached to a spectrometer. The resulting spectral characteristics will depend of the spectrometer used. The integrating sphere is used to create a perfectly diffuse illumination on the leaf and to record the hemispherical reflectance and transmittance (Figure 13.4. b).

For leaf directional reflectance measurements, a leaf clip can be used. Leaf clips can either have their own light source (e.g. ASD leaf clip; Figure 13.4 a) or use natural light, as for chlorophyll fluorescence measurements (Rascher *et al*., 2011). Leaf clips are including a reference material allowing the measurement of reflectance and radiance in case the attached spectrometer is calibrated for radiance measurements. For more information about illumination-viewing geometries in spectroscopy measurements, please refer to Schaepman-Strub *et al*. (2006).

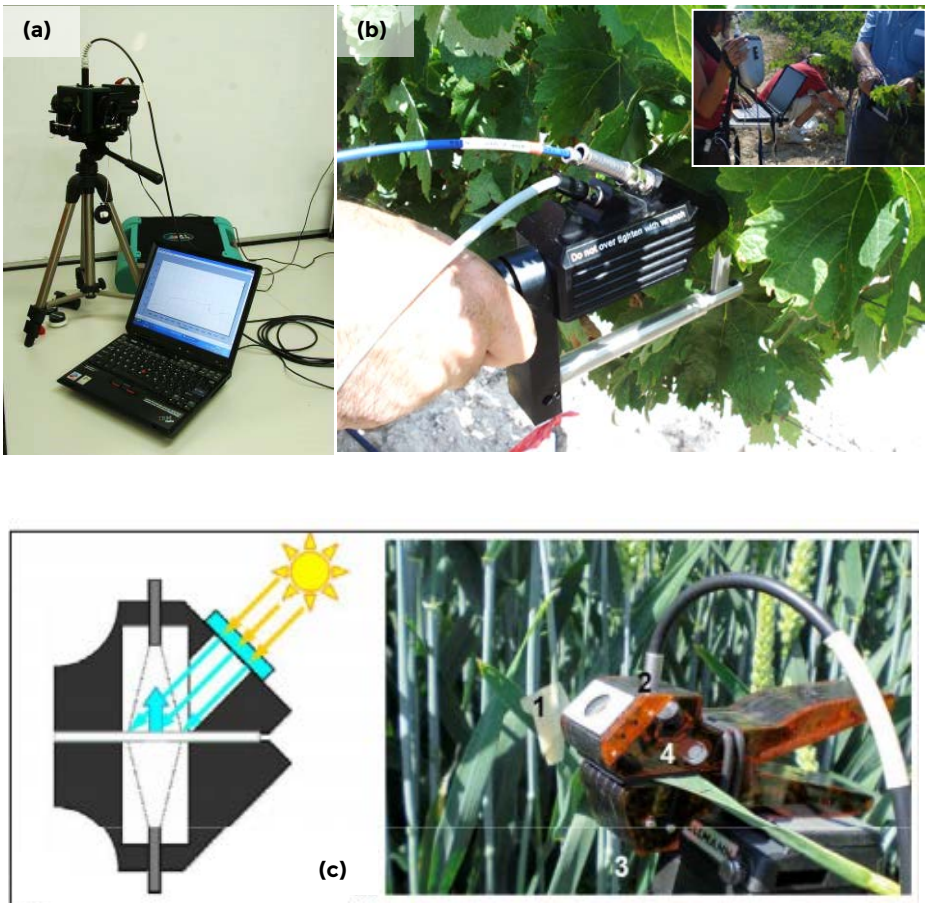

Figure 13.4 **(a)** Measurement set-up for leaf hemispherical reflectance and transmittance spectroscopy using an integrating sphere attached to a field spectrometer.
(b) Leaf biconical reflectance measured in the field with a leaf probe attached to a field spectrometer.
(c) Leaf probe to measure using natural illumination (from Rascher *et al.*, 2011).

Canopy measurements

Figure 13.5 **(a)** Direct walking transect measurements,
(b) use of field measuring structures on tree crowns where the bare fibre is attached to the structure pointing at nadir on the same point. For the measurement, the loose end of the fibre is attached to a field spectrometer. Portable measuring structures:
(c) and **(d)** using a cherry picker (Quantalab, Spain; Berni et al., 2009);
(e) telescopic pole attached to a motorbike (NASA JPL 'Reflectomobile', Thome et al., 1994); and
(f) a pole is used to reach to measure at a certain height without interfering the instrument footprint (RMIT University, Australia).

- **Direct measurements:** Direct measurements can be taken by pointing the fibre (using fore optics or not) on the canopy.

- **Fix measuring structures:** Bare fibres can be installed on fix measuring structures to get continuous measurements (installing the spectrometer in the field) or for punctual measurements by attaching a spectrometer to the fibre end. These structures could be used for individual crown monitoring or ecosystem biophysical parameters, now common in many eddy covariance sites (see Balzarolo et al. 2011)

- **Portable measuring structures:** Portable structures can be used for measurements at different heights. They include portable poles with a fibre attached to measure at a height up to 5-7 metres or portable platforms (up to 15 m, e.g. cherry picker). In both cases it is important to always be aware of the instrument footprint on the canopy and avoid the intrusion of the structure on such footprint.

13.2.3 Sampling designs

It is important to bear in mind the instrument footprint on the canopy. The theoretical footprint is function of the instrument field of view (FOV), orientation and the measuring height. The manufacturers provide a nominal solid included angular value per foreoptic but the methods used to determine this FOV parameter are not specified, and associated uncertainties are not made explicit (MacArthur *et al*., 2012). Figure 13.6 presents the equivalent footprint diameter corresponding to typical nominal field of view angles used in field spectroscopy measurements at nadir. When we are measuring a certain point on a surface we should be sure the footprint area belongs 100% to the target. Besides, it has been demonstrated that the real instrument FOV is irregular and most of the times exceeds the limits of the theoretical FOV (MacArthur *et al.*, 2012). This fact should be taken into account considering an instrument footprint larger than the nominal when taking spectral measurements. The nominal footprint diameter (*d*) can be calculated as [1] for nadir measurements with a α FOV and as [2] for measurements taken with a FOV α at a viewing angle β.

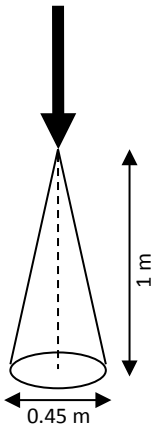

	Viewing angle (FOV)	Footprint diameter measuring at 1 m height
Bare fibre	25 deg	45 cm
Fore optics	10 deg	17.4 cm
	1 deg	1.74 cm

Figure 13.6 Left panel: Schema of the nominal footprint of an instrument measuring through a bare fibre at a 1 m distance. Right panel: Indicative nominal diameter of the footprint measuring at 1 m height with different viewing settings (bare fibre and 10 and 1 degrees foreoptics).

$$d = 2 * height * \tan(\alpha / 2) \quad \textbf{(equation 13.1)}$$

$$d = 2 * height * [\tan(\alpha / 2) - \tan(\beta)] \quad \textbf{(equation 13.2)}$$

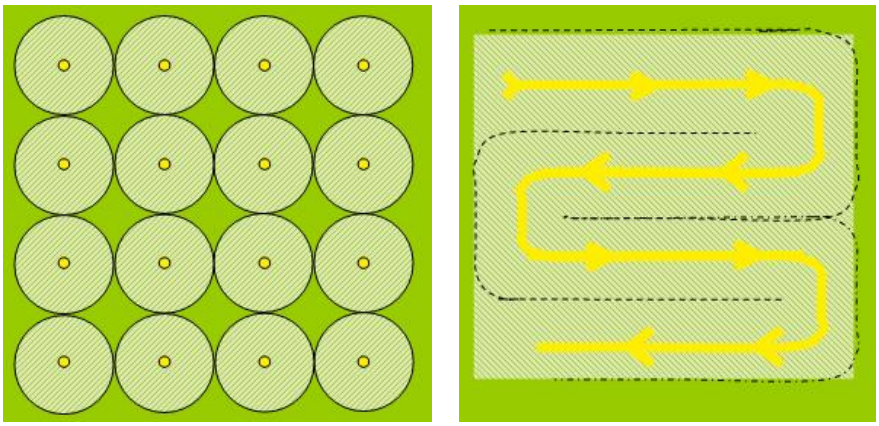

(a) (b)

Figure 1.7 Common sampling schemes used to get representative spectroscopy measurements of an area. **(a)** Based on individual points at an approximate distance of the theoretical footprint diameter. **(b)** Taking continuous measurements while walking over the sample surface.

In order to take a representative measurement of an object, several readings should be taken covering the whole object area. This can be done by taking punctual readings all over the target or by taking continuous measurements while walking pointing at the target (Figure 13.7). In both cases, it is important to maintain the right position with respect to the sun and if possible to walk on the surface area that has been already measured.

13.2.4 Metadata collection

In order to facilitate the long-term use of the spectral data, pertinent metadata has to be collected. There is a general set of metadata that should be collected for every spectral measurement.

General metadata includes:

- Date and location
- Sky conditions in case the sky is not completely clear
- Instrument and reference panel REF numbers (the one of the instrument is available in the header of the resulting file)
- Foreoptics used (This may be recorded by the instrument as well if set correctly)
- Additional comments

The measurements for specific experiments need additional metadata documenting relevant information of the target. In the case of measuring leaf or canopy spectra, the specific metadata includes:

- Scale (leaf or canopy)
- Species
- Other measurements taken (e.g. pigment content, specific leaf area, dry matter content, photosynthetic rate, conductance)
- Comments

In the case of measuring the canopy or leaves representing a tree, additional metadata includes:

- Height
- Diameter at breast height (DBH)
- Position of the crown relative to surrounding vegetation (emergent, isolated, part of the canopy)
- Approximate percentage cover
- Approximate crown diameter

- Extra comments (e.g. fork trees, specific existing damage, bended trunk, high decolouration etc.).

13.2.5 Data storage

Optimally, the spectral measurements and associated metadata should be stored within a spectral information system, such as SPECCHIO(V3). Essentially, at this stage the spectral data enters the lifecycle stages of data ingestion, metadata augmentation, information building and information retrieval. For details on the spectral information system based spectroscopy data lifecycle please refer to Chapter 14.

References

Al-Abbas, A. H., Barr, R., Hall, J. D., Crane, F. L., & Baumgardner, M. F. (1974). "Spectra of Normal and Nutrient Deficient Maize Leaves." *Agronomy Journal* 66 (1): 16–20.

Atwell, B.J., Kriedemann, P.E., & Turnbull, C.G.N. (eds) 1999 Plants in action: adaptation in nature, performance in cultivation, McMillan Education, 664 pp.

Balzarolo, M., Anderson, K., Nichol, C., Rossini, M., Vescovo, L., Arriga, N., Wohlfahrt, G., Calvet, J.-C., Carrara, A., Cerasoli, S., Cogliati, S., Daumard, F., Eklundh, L., Elbers, J.A., Evrendilek, F., Handcock, R.N., Kaduk, J., Klumpp, K., Longdoz, B., Matteucci, G., Meroni, M., Montagnani, L., Ourcival, J.-M., Sánchez-Cañete, E.P., Pontailler, J.-Y., Juszczak, R., Scholes, B., & Martín, M.P. (2011). Ground-Based Optical Measurements at European Flux Sites: A Review of Methods, Instruments and Current Controversies. *Sensors* 11, 7954–7981.

Bauer, M. E., Daughtry, C. S. T., Biehl, L. L., Kanemasu, E. T., & Hall, F. G. (1986). *IEEE Transactions on Geoscience and Remote Sensing*, GE-24, 65-75.

Berni, J.A.J., Zarco-Tejada, P.J., Suarez, L., & Fereres, E. (2009). Thermal and Narrow-band Multispectral Remote Sensing for Vegetation Monitoring from an Unmanned Aerial Vehicle. *IEEE Transactions on Geoscience and Remote Sensing*, 47, (3), 722-738.

Cescatti, A. (1997). Modeling the radiative transfer in discontinuous canopies of asymmetric crowns. II. Model testing and application in a Norway spruce stand. *Ecological modelling*, 101, 275-284.

Combal, B., Baret, F., Weiss, M., Trubuil, A., Macé, D., Pragnère, A., Myneni, R., Knyazikhin, Y., & Wang, L. (2002). Retrieval of canopy biophysical variables from bidirectional reflectance using prior information to solve the ill-posed inverse problem. *Remote Sensing of Environment*, 84, 1-15.

Curtiss, B., & Goetz, A.F.H. (1999) Field spectrometry: techniques and instrumentation, ASD Technical Guide. Boulder, CO.

Eamus, D., Myers, B., Duff, G., & Williams, D. (1999). Seasonal changes in photosynthesis of eight savanna tree species. Tree Physiol. 19, 665–671.

Gates D. M., & Tantraporn W. (1952). The reflectivity of deciduous trees and herbaceous plants in the infrared to 25 microns. *Science*, 115:613–616.

Goel N. S., & Thompson R. L. (2000). A snapshot of canopy reflectance models and a universal model for the radiation regime. *Remote Sensing Reviews*, 18(2), 197–225.

Haboudane, D., Miller, J. R., Tremblay, N, Zarco-Tejada, P. J., & Dextraze, L. (2002). Integration of Hyperspectral Vegetation Indices for Prediction of Crop Chlorophyll Content for Application to Precision Agriculture. *Remote Sensing of Environment*, 81(2-3), 416-426.

Jackson R. D. (1986). Remote sensing of biotic and abiotic stress. *Annu Rev Phytopathol*, 24:265–287.

Knipling E. B. (1970). Physical and physiological basis for the reflectance of visible and near-infrared radiation from vegetation. *Remote Sensing of Environment*, 1, 155–159.

Koetz B., Schaepman M., Morsdorf F., Bowyer, P., Itten, K., & Allgower B. (2004). Radiative transfer modeling within heterogeneous canopy for estimation of forest fire fuel properties. *Remote Sensing of Environment*, 92, 332–344.

MacArthur, A., MacLellan, C. J., & Malthus, T. J. (2012). The Fields of View and Directional Response Functions of Two Field Spectroradiometers. *IEEE Transactions Geoscience and Remote Sensing*, 50(10), 3892-3907.

Milton, E. J. (1987). Review Article Principles of field spectroscopy, *International Journal of Remote Sensing*, 8:12, 1807-1827.

Peñuelas J., & Filella I. (1998). Visible and near-infrared reflectance techniques for diagnosing plant physiological status. *Trends Plant Science*, 3(4):151–156.

Perbandt, D., Fricke, T., & Wachendorf, M. (2010) Effects of changing simulated sky cover on hyperspectral reflectance measurements for dry matter yield and forage quality prediction. *Computers and Electronics in Agriculture* 73, 230–239.

Rascher, U., Moreno, J., Damm, A., Schickling, A., Alonso, L., & Guanter, L. (2011). Current status on remote sensing of fluorescence from space. Proceedings of EARSeL, 31st EARSeL Symposium 2011, Prague, 30th May - 2nd June 2011 (Czech Republic).

Schaepman-Strub, G., Schaepman, M. E., Painter, T. H., Dangel, S., & Martonchik, J. V. (2006). Reflectance quantities in optical remote sensing- definitions and case studies. *Remote Sensing of Environment*, 103, 27-42.

Sobrado, M.A. (1994). Leaf age effects on photosynthetic rate, transpiration rate and nitrogen content in a tropical dry forest. *Physiologia Plantarum*, 90, 210–215.

Stone, C., Chisholm, L., & McDonald, S. (2005). Effects of leaf age and psyllid damage on the spectral reflectance properties of Eucalyptus saligna foliage, *Australian Journal of Botany*, 53(1), 45-54.

Suárez, L., Zarco-Tejada, P.J., Berni, J.A.J., González-Dugo, V., Fereres, E. (2009). Modelling PRI for Water Stress Detection using Radiative Transfer Models. *Remote Sensing of Environment*, 113, 730-744.

Thome, K. J., Biggar, S.F., Gellman, D.L., & Slater, P.N. (1994). Absolute-radiometric calibration of Landsat-5 Thematic Mapper and the proposed calibration of the Advanced Spaceborne Thermal Emission and Reflection Radiometer. Geoscience and Remote Sensing Symposium, IGARSS '94. Surface and Atmospheric Remote Sensing: Technologies, Data Analysis and Interpretation. Los Angeles, 8-12 August 1994.

Chapter 14. The Spectroscopy Dataset Lifecycle: Best Practice for Exchange and Dissemination

L.A. Chisholm[1], A. Hueni[2]

[1] School of Earth and Environmental Sciences, Centre for Sustainable Ecosystem Solutions, University of Wollongong
[2] Remote Sensing Laboratories, University of Zurich, Switzerland

*Corresponding author:
Laurie_Chisholm@uow.edu.au

Abstract

In today's information age, spectroscopy data management is a significant consideration for researchers and practitioners presenting challenges imposed by multi-disciplinary data producing activities. Such activities are a result of heterogeneous infrastructure and instrumentation, scientific experiments, high data rates and multi-user environments. When data is created, published, exported, imported, transformed and shared by different parties and used for different purposes, these actions form a data lifecycle. Creating a conceptualised model of this data lifecycle helps to better understand the nature of the data and the integration of previously disparate implementation efforts. The newly enhanced AUS-SPECCHIO spectral information system is presented within the context of a spectroscopy data lifecycle model for remote and proximal sensing activities, through a common set of lifecycle phases, features and roles established as best practice procedures.

Key points

- A spectroscopy database system that incorporates a metadata standard improves interoperability of processes related to, and data sharing of, spectral data.
- The spectroscopy data lifecycle is composed of six steps that, when implemented in series, results in the improvement of existing information on spectral data which facilitates data sharing and further analytical processes, thus assisting the researcher to more quickly achieve product development and/or publication of results.
- Several systems developed for the storage of spectroscopy data have arisen over the past decade, however, the newly enhanced AUS-SPECCHIO (SPECCHIO(V3)) has been established as the system of choice and best practice for the Australian proximal and remote sensing community.

14.1 Introduction

Field or laboratory spectroscopy are common techniques applied by different remote sensing user communities for various purposes, ranging from calibration/validation exercises to material identification (Milton *et al* 2009; Eisele *et al*. 2012; Haest, *et al* 2013). In all cases a large number of spectra tend to be collected, yet the value and sharing of such collections is often restricted because the data are stored in disparate silos with little, if any, metadata to aid their discovery. These datasets have significant potential to benefit the wider remote sensing community as well as to contribute to international spectral libraries to fill existing gaps in collections (Chisholm *et al* 2013). Spectral databases provide the means to store data in an organised manner, described by appropriate metadata documenting the sampling setup as well as the sampling conditions (Hueni *et a*l 2011). Spectral information systems take spectral databases a step further by making data held in the databases retrievable and usable by other users or systems and by adding processing functionalities that further transform the data or information held in the system, in turn generating more information. This could, for example, involve the generation of higher-level products or spectral data corrected for sampling equipment or sensor artefacts (Hueni *et al* 2012). Adopted by the Australian remote sensing community, and enhanced with funds provided by the Australian National Data Service Data Capture Program, (ANDS Project DC-10) AUS-SPECCHIO, is a system designed to support scientists in not only storing spectral data, but analysing the data using the full potential of combined metadata spaces (Wason and Wiley, 2000) and spectral spaces (Hueni et al 2012). The system incorporates a defacto metadata standard to improve interoperability and data sharing, has spatial search capabilities, and contains mechanisms to house validation data associated with spectra and several enhancements which facilitate ease-of-use for individuals

and research groups. As the basis of a Spectral Information System (SIS), it provides a model to assist a multi-disciplinary user base to conceptualise the spectroscopy data lifecycle. Through greatly improved management of existing and new data, increased data quality by applying algorithms to a centralised and well-defined data pool and quicker acquisition to product/publication cycles (Chisholm *et al* 2013), a guide of best practice in spectroscopy data management is presented.

14.1.1 Definitions

Table 14.1 provides definitions which attempt to remove ambiguity related to metadata standards, protocols, schemas and file formats apparent in the spectroscopy community.

Table 14.1 Metadata terms

Term	**Definition**
Metadata	Metadata are structured facts that describe information, or information services. Metadata facilitates information discovery and access, but also informs about the appropriate use of products and services. (ANZLIC 2011)
Metadata Standard	Defines what metadata should be reported/recorded and the grouping of the metadata attributes (elements) within this metadata set. It defines the semantics of each element. It is driven by science and the need to potentially allow a replication of the measurements. Metadata standards may differ between user communities, depending on their typical scientific questions. In its formalised version the metadata standard is equivalent to the metadata schema.
Protocol (Sampling Protocol, Field/Lab Protocol)	A protocol defines what data should be recorded in which way, i.e. it describes a procedure for the data collection in the field or laboratory. The protocol is based on a metadata standard, i.e. ensures that data are recorded adhering to the metadata standard.
Schema (Metadata Schema)	A schema is a formalised definition of a metadata standard, i.e. a particular structure that can hold the metadata elements of the standard. It defines the semantics of the elements. Schemas are defined using schema languages. A schema definition could e.g. be stored in the form of an XML Schema Definition (XSD).
File Format	A file format defines how metadata are written to a file and conforms to a schema, i.e. data are written to the file in a structure defined by the schema.
File	A file is written according to a file format and contains actual metadata.
Metadata Element (Metadata Attribute)	Definition of a component of a metadata schema by a name and a data type, e.g. Filename (String). It relates to one particular dimension of a metadata space.
Metaparameter	A value of a defined metadata element
Metadata Space	N dimensional space defined by metadata attributes. Each spectrum has a defined position with the metadata space, given by its metaparameters. Ideally, metadata spaces are orthogonal.

A practical example relating to some of these definitions is given in Figure 14.1. The plot reveals the positions of spectra in a two-dimensional metadata space. The space is defined by the metadata elements Latitude and Longitude. The actual metaparameters differ for each recorded spectrum.

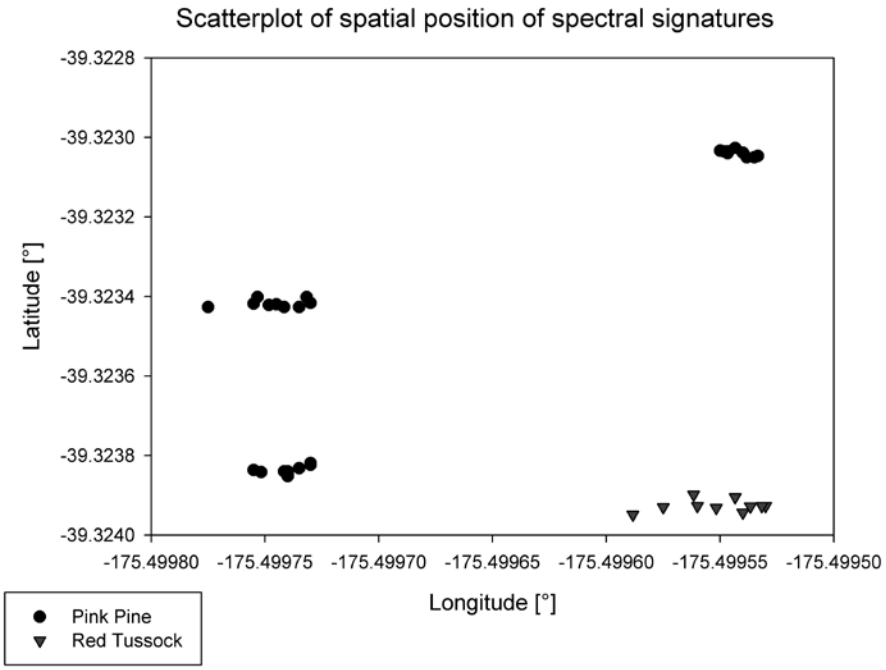

Figure 1.1 Example visualisation of a two-dimensional metadata space.

14.2 Spectroscopy Data Management Lifecycle

The generic lifecycle of spectroscopy data is comprised of six steps (Figure 14.2): (i) planning of sampling experiments, including the definition of sampling protocols adhering to a metadata standard; (ii) actual data acquisition, where data are acquired according to predefined sampling protocols; (iii) ingestion of the acquired spectral data into the SIS; (iv) augmentation of the automatically generated metadata by manually or semi-automatically adding further metadata parameters to the spectral data collection; (v) building further information by applying algorithms to spectral data and metadata; and (vi) retrieval of information for a particular purpose.

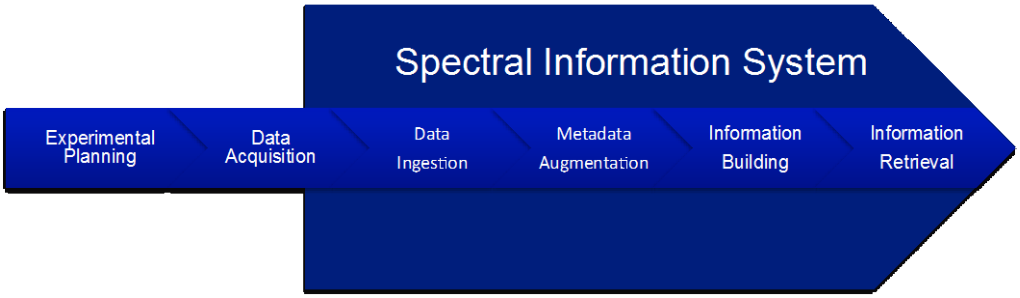

Figure 14.2 Generic spectroscopy data lifecycle.

The forte of a SIS is the building of information based on already existing information and the extraction of information by specification of metadata space restrictions (Figure 14.3). These processes are recurring throughout the lifecycle, in particular the extraction process. The generation of new information may either be the generation of higher-level spectral data, e.g. by calculating radiance from digital numbers, or the derivation of new metaparameters based on both spectral data and metadata, e.g. the estimation of biogeophysical parameters such as plant fluorescence.

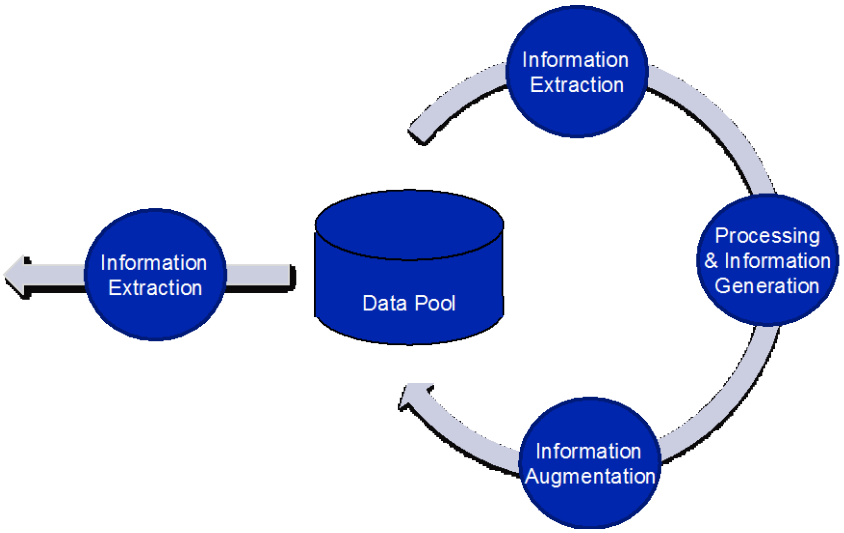

Figure 14.3 Recurring operations applied to spectral information held by a data pool.

14.2.1 Planning and Protocols

For any project, appropriate planning and application of relevant protocols for sampling and measurements is critical to success. The technical handbook within which this chapter lies, presents best practice guidelines for successful field validation and measurement in support of remote sensing campaigns, including logistical and overall design. For successful use of an SIS to support such research, consideration of the objectives of the field campaign is required to standardise the way in which spectra are collected and subsequently entered into the system. Once this foundation is established, it is appropriate to check available metadata standards regarding their applicability to the experiment at hand. The existing defacto metadata standard available in AUS-SPECCHIO may be enhanced by adding fields specifically related to the planned experiment.

Field protocols should make use of metaparameter names as defined by metadata standards. Ideally, the target SIS implements a metadata schema derived from a metadata standard, thus ensuring that a unique vocabulary is used. In the case of no existing metadata standard, metaparameter names to be used in the protocol may be adopted from the target SIS schema.

14.2.2 Spectroscopy Data Collection

In the broadest sense, spectroscopy is the use of light, sound or particle emission to study matter. More specifically, it refers to the measurement of radiation intensity as a function of wavelength and is often used to describe experimental spectroscopic methods (Crouch *et a*l 2007). A variety of spectral measurement sensors are available, such as spectrometers/spectroradiometers, spectrophotometers, spectrographs or spectral analysers, and thus, a range of methods are used to measure materials and acquire spectral data.

In optical systems, spectral reflectance measurements obtained on the ground *in situ* are collected by handheld spectroradiometers (Jensen 2007). There are numerous spectroradiometers on the market that may be used to collect spectral reflectance information, with many capable of obtaining data over the spectral region from 400 – 2500nm at approximately 10nm resolution (Jensen 2007). Specifically related to TERN Landscape Assessment objectives, there are well established procedures and protocols for the collection of spectroscopy data to investigate the spectral reflectance characteristics of a material (Chapters 6, 7, 8, 9, 10, 13), to calibrate optical sensors (Chapter 4), and assist with the acquisition of multispectral and hyperspectral remote sensor data (Chapters 15, 17).

Other bio-physical science disciplines which closely interlink with vegetation science and also rely upon spectroscopy as a basis for interpretation, analysis and modeling include the soil, mineralogical, and chemical sciences. For example, as outlined by Viscarra Rossel and McBratney 1998, proximal soil sensing refers to field-based techniques for collecting information on the soil from close by, or within, the soil, and often involves the combined use of optical, geophysical, electrochemical, mathematical and statistical methods. Similarly, Fourier Transform Infrared Spectroscopy (FTIR) is a form of spectroscopy which interprets the infrared absorption spectrum to quantitate components of materials, whether solid, liquid or gas. These proximal sensing disciplines produce spectroscopy data with a similar data lifecycle model, and with similar data management requirements. The development and use of a spectral library to identify materials relevant to such fields of study, with spectra often combined with additional data and/or techniques, e.g. x-ray diffraction, further exemplifies the need for a generic spectral information system which can support researchers across wide-ranging disciplines.

14.2.3 Data Ingestion

The process of data ingestion automatically extracts metadata and spectral data from files created by the spectroradiometers during data collection. Ideally, the SIS implements file readers capable of parsing the raw

files. By doing so, information may be based on the most basic data level, allowing a transparent generation of higher-level information within the SIS. Furthermore, the raw files usually include the highest number of metaparameters recorded by the instrument; any pre-processing applied before data ingestion is likely to reduce the metadata content, particularly if the pre-processing was developed with a focus on spectral data, thus often dismissing metadata.

14.2.4 Metadata Augmentation

Spectral data are by default described by metadata that are automatically generated during data ingestion process by the SIS. This basic metadata set needs augmenting with further data, not contained in the spectral input file. Typical data sources are the field protocols or laboratory reports, as in the case of, for example, chemical analysis carried out on collected samples. The task of the SIS is to simplify this augmentation process by: (a) allowing multiple updates, i.e. applying the same metaparameter value to a collection of spectra; and (b) enabling the semi-automated augmentation of metadata based on, for example, tabular data where a column is used to link the metaparameters to existing spectra.

The SIS supports not only the storage of metaparameters defined by a metadata standard, but facilitates the enhancement of the metadata space by adding new metadata attributes to the system.

14.2.5 Information Building

Editing or processing of data forms information. Information may be used to derive further information, hence adding to the pool of existing information; the notion of 'information continuum' refers to the fact that the value of information can be increased though the processing of existing information.

The information continuum of spectral data refers to either the processing level of the spectral data (Table 14.2) or metadata of the spectral data, which may be expanded by estimating or deriving new parameters from the existing information held by the SIS or by data assimilation processes utilising other sources as well, such as FLUX databases.

Table 14.2 Proposed processing levels for spectral databases

Level	Description
RAW	Raw, sensor generated files, stored as binary objects on a file system or in the database system. This forms the first tier of the DIKW hierarchy and allows regeneration of data/information at the following tiers.
Level 0	Spectral measurements as digital number (DN), described by auto-generated metadata augmented by user defined metadata parameters.
Level 1	Spectral measurements as radiances traceable to an international standard. Metadata as in level 0 but including information related to the data calibration process.
Level 2	Spectral measurements as factors (reflectance factors, transmittance, absorbance), corrected for reference panel deficiencies where needed (non-ideal reflective and Lambertian properties). Metadata as in level 1 but including information related to the data calibration process.
Higher level products	Products derived from the lower levels, similar to products generated in imaging spectrometer processing systems, such as estimated bio-geophysical properties.

The reasons for maintaining an information continuum within a SIS are to: (a) allow the tracing of effects via provenance down to the initially ingested data, (b) allow a selection of data at a specific processing level depending on the purpose, e.g. some analysis may require radiance while others may need reflectance factors, and (c) every additional metaparameter allows a refined selection of spectral data during information extraction, e.g. selection of spectra via their estimated fluorescence.

14.2.6 Information Extraction

Information extraction is a two stage operation: (i) selection of a subset of all spectral information held by the SIS, also referred to as information discovery; and (ii) provision of the selected subset via an electronic file adhering to standardised file formats or via an Application Program Interface (API) allowing direct data access of both spectral data and metadata in another processing/analysis environment.

The selection of spectral data is based on metadata space restrictions, i.e. constraints limiting the values of selected metadata space dimensions (Figure 14.4).

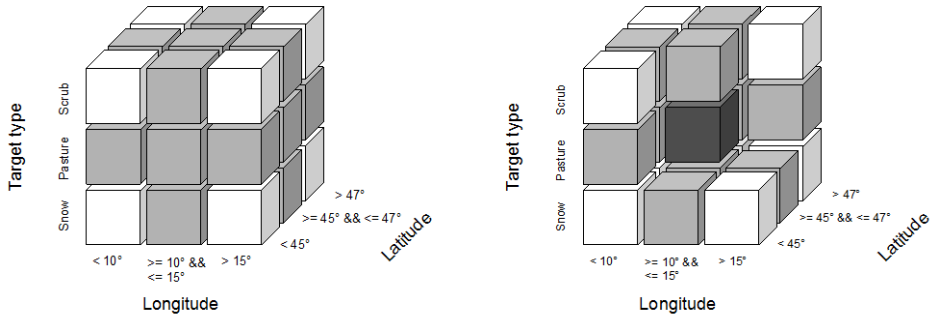

Figure 14.4 Visualisation of a subspace projection in a 3D metadata cube: constraints (light coloured) imposed on a cube (left) lead to a subspace (darkly coloured) (right).

14.3 Spectral Information Systems as a Tool to Assist Researchers

14.2.7 Existing Spectroscopy Data Storage Systems

A number of systems for the storage of spectroscopy data have been developed over the past decade. However, their use is not yet widespread due to a number of factors: (a) accessibility: some systems are proprietary solutions, accessible by a limited number of persons; (b) generic: some system focus only on one sensor type or one particular application; (c) long-term support: systems need maintaining and developing over time; (d) practicality: users do not want to be distracted from their primary objective by data management tasks and any convoluted and redundant interaction renders the system un-utilised.

Table 14.3 gives an overview of the current status and properties of selected spectral database systems, namely: SPECCHIO (Bojinski et al. 2003; Hueni et al. 2009), DLR Spectral Archive (Becvar 2008), SSI Hyperspectral.Info (Ferwerda et al. 2006), SSD's Spectral Library Database (Pfitzner et al. 2008) and SpectraProc (Hueni and Tuohy, 2006). Table 14.4 provides the versioning history of SPECCHIO.

Table 14.3 Attributes of selected spectral database systems as by September 2011, SPECCHIO(V2) updated to AUS-SPECCHIO in 2014.

System / Attributes	SPECCHIO V2	DLR Spectral Archive	SSI Hyperspectral Information	SSD's Spectral Library Database	SpectraProc
Institute	RSL, University of Zurich, Switzerland	DLR, Oberpfaffen-hofen, Germany	SSI, Australia	SSD, Darwin, Australia	Massey University, Palmerston North, New Zealand / A. Hueni
Website	www.specchio.ch	cocoon.caf.dlr.de	www.hyperspectral.info/	environment.gov.au/ssd/research/protect/rehabilitation.html	www.geo.uzh.ch/en/units/rsl/research/spectroscopy-spectrolab/research-fields/data-processing/spectroproc/
Main Data Source / Research Topic	Landcover/ Vegetation /Goniometry	?	Generic	Vegetation	Vegetation, Classification, Separability
Online accessible	✓	✓	✓	✗	✗
Publicly accessible	✓	~ ✓	✓	✗	✗
Multi-user capability	✓	✓	✓	-	✗

System / Attributes	SPECCHIO V2	DLR Spectral Archive	SSI Hyperspectral Information	SSD's Spectral Library Database	SpectraProc
Underactive development	✓	✗	✗	✓	✗
# of spectra available online	80'000	2008	A few dozen	NIL	NIL
# of install.	20	1	1	1	> 2
Database	MySQL	MySQL	MySQL	SQL Server	MySQL
Interface	Java and PHP	Web	PHP	-	Microsoft Windows C++/MFC and TCL/TK
Local installation possible	✓	✗	✗	✗	✓
Import formats	ASD binary, GER, Apogee, ENVI SLB, OO, ASCII, XML, FGI HDF5, SPECPR, UniSpec	ASD binary, ASCII	ASD binary ASD text GER, ASCII ENVI SLB	ASD binary	ASD binary
Export formats	CSV, ENVI SLB, XML, Direct access from Matlab and other scientific languages	Metadata zip file Zip file containing ASD binary files	ASCII, ENVI SLB, JCAMP	-	CSV, ENVI SLB, ARFF (University of Waikato, 2005)

Systems such as the USGS spectral library or the ASTER spectral library are not considered here, as they are not database systems per se, but rather static collections of reference spectra. They do have their benefits, but are not suited for the dynamic storage of field spectroscopy data, where many replicates per target are acquired and targets are observed over time and space.

14.2.8 AUS-SPECCHIO

SPECCHIO Version History

Table 14.4 Version history of SPECCHIO, updated to AUS-SPECCHIO in 2014.

Date	SPECCHIO Version	Comments
2002	0	• RSL internal only (one instance) • Redundant data storage • Cumbersome data entry • No granular data access rights • Single user system
2006	1.0	Complete redesign: • Enhanced metadata • Multiple OS: open source database, Java application • Greatly improved data input, storage and retrieval, group updates • Multi-user system • Easily installable • Online accessible • Multiple instances
2009	2.0	• Reference panel handling including uncertainties • Data Processing Extension (Space Concept) • Campaign import/export function
2010	2.1	• SVC HR-1024 support • Calibration metadata for instruments
2011	2.1.2	• Matlab integration
2012	2.2	• FGI HDF reader • Loading of FGI goniometer data -> 80'000 spectra online • New ASD binary file format reader • SPECPR reader • EAV: generic metadata upgrade • SPECNET upgrades and higher level processing
2013	3.0	• Major redesign and upgrade in the framework of ANDS DC-10 • Open source deployment • Web development in the framework of EuroSpec • Name alias to represent Australian version.

The new AUS-SPECCHIO version include an upgrade function that migrates existing data to new storage schemas and updates the system tables to support new functionality.

Installation options

Type	Details	Usage
Single User	Database and user application on same machine	Data ingestion and analysis during field trips. Personal data management and processing
Multi User Intranet	Database and application server on an intranet server	Data sharing with an organisation. Storage of confidential data.
Multi User Internet	Database and application server on a server connected to the Internet	Data sharing across organisations.

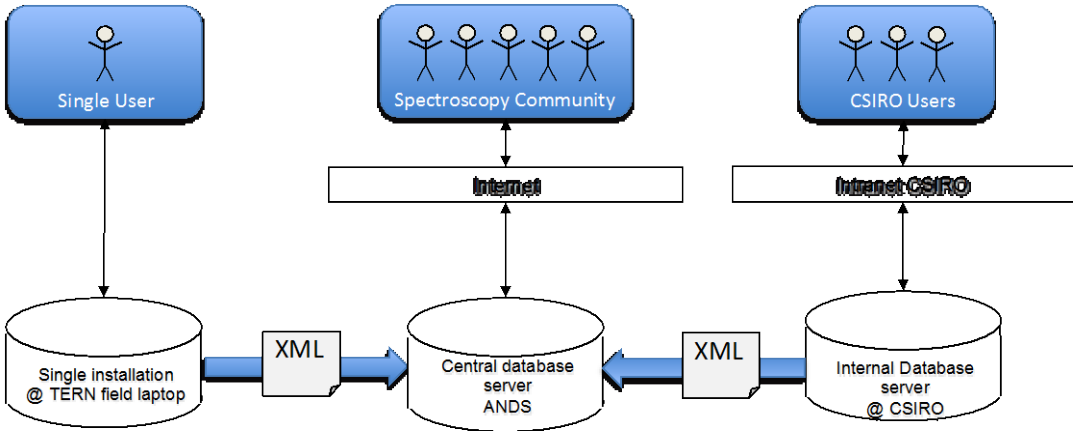

Figure 14.5 Possible system ontology

Exchange of Spectral Collections between Databases

AUS-SPECCHIO allows users to export spectral data collections as XML files and import collections into a different AUS-SPECCHIO database (Figure 14. 5). This function facilitates the preparation of a dataset on an in-house server and publishing an identical copy on an online accessible server.

Flexible Structuring of Data and Data Loading

Data are organised by campaigns, where a campaign is essentially a high-level container and could be anything from a few spectra captured in a single experiment to multi-temporal data, where new data are acquired on a regular basis. Data loading into AUS-SPECCHIO is based on parsing the file system under a specified campaign folder. The system supports delta loading, i.e. if new data are added to an existing campaign structure on the file system, a new load of a campaign will only ingest new files.

SPECCHIO replicates any hierarchical structure found under a campaign folder on the file system within the database, i.e. the hierarchy information that usually reflects the experimental setup and potential hypothesis is preserved. No hierarchy structure is enforced by the system; it is up to the users to structure their data. Examples of possible structures are show in Figure 14.6 and Figure 14.7.

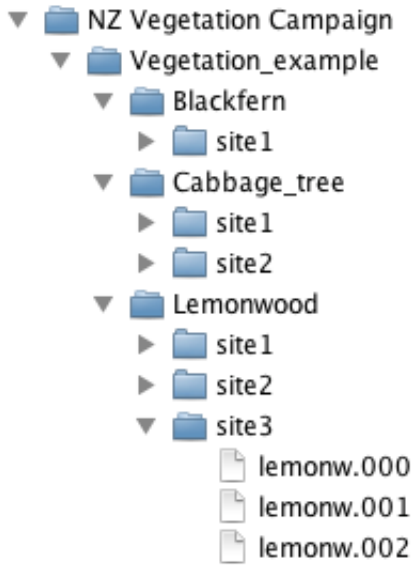

Figure 14.6 Example of a hierarchy, structured by species and sampling site.

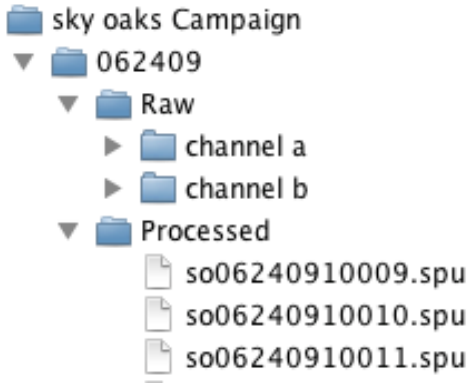

Figure 14.7 Example of a hierarchy, structured by processing levels and channels for the raw DN data.

Populating Metadata Using Adopted Metadata Standard to Facilitate Data Exchange

AUS-SPECCHIO uses a mixture of categorical system variables and EAV (entity-attribute-value) based metaparameters to store the metadata of a spectral data collection. The system is preconfigured with metadata elements grouped by categories, but may be easily extended to support further elements. Metadata

elements not included in the default installation can be easily added by a user with administrator rights, i.e. the vocabulary of element names is controlled by the administrators to avoid ambiguities.

At the time of publication, a generic metadata standard or schema defining metadata core elements, i.e. mandatory elements, is still elusive. Hence, the metadata schema defined within the current SPECCHIO version represents a de facto standard.

Within the ANDS DC-10 project, it is planned to implement checks for metadata compliance of spectral data collection metadata with a schema defined in a schema definition language. Such a function will facilitate a quality rating of the entered data based on their compliance level.

14.4 Links to Other Spectral Databases / Organisations

AUS-SPECCHIO provides cross-referencing to the TERN Landscape repository, which houses satellite/airborne image and lidar data and associated field validation data. In addition, the development provides a foundation which facilitates collaborative arrangements with US and European-based researchers with the aim to establish internationally-compatible databases, systems and tools related to spectroscopy data (SpecNet; EuroSpec). It is envisaged that these joint efforts will create a highly useful network of accessible systems which would foster the exchange of spectral data and thus, collaborative research amongst the international remote sensing community.

14.5 Conclusion / Summary

Within the complex environment of spectroscopy data acquisition and management, a common spectroscopy data lifecycle is presented. The spectral information system, AUS-SPECCHIO, is designed to facilitate best practice in spectroscopy data storage, exchange and dissemination in support of the Australian remote sensing community. Not only does the SIS provide a tool to share and discover existing spectral libraries, importantly it facilitates the capture of new datasets as they are formed, providing recorded, consistent metadata and a consistent method for publishing, discovering and assessing this information. AUS-SPECCHIO offers greatly improved management of existing and new spectroscopy data, increased data quality by applying algorithms to a centralised and well-defined data pool and quicker acquisition to product/publication cycles. The newly structured and enhanced version of SPECCHIO can serve as a potential model for international adoption.

References

ANZLIC, The Spatial Information Council of Australia and New Zealand. (2011). ANZLIC Metadata Profile Guidelines, Version 1.2. Online at: http://spatial.gov.au/system/files/public/resources/anzlic/ANZLICmetadataProfileGuidelines_v1-2.pdf.

Becvar, M., Hirner, A. (2008). DLR Spectral Archive. Online at: http://cocoon.caf.dlr.de/intro_en.html.

Bojinski, S., Schaepman, M., Schlaepfer, D. & Itten, K. (2003). SPECCHIO: a spectrum database for remote sensing applications. *Computers & Geosciences*, 29, 27-38.

Chisholm, L.A., Hueni, A., Ong, C., Wyatt, M., Malthus, T., Jones, S., & Lewis, M. (2013). SPECCHIO for Australia: taking spectroscopy data from the sensor to discovery for the Australian remote sensing

community, Proceedings of the International Geoscience and Remote Sensing Symposium (IGARSS 13), Melbourne, July 21-26, 2013.

Crouch, Stanley; Skoog, Douglas A. (2007). Principles of instrumental analysis. Australia: Thomson Brooks/Cole. ISBN 0-495-01201-7.

Eisele, A., Lau, I., Hewson, R., Carter, D., Wheaton, B., Ong, C., Cudahy, T.J., Chabriallat, S., & Kaufmann, H. (2012). Applicability of the thermal infrared spectral region for the prediction of soil properties across semi-arid agricultural landscapes, *Remote Sensing of Environment*, 4(11): 3265-3286.

Ferwerda, J. G., Jones, S.D., & Reston, M. (2006). A free online reference library for hyperspectral reflectance signatures. SPIE Newsroom, 1-2, http://spie.org/x8461.xml .

Haest, M., Cudahy, T., Rodger, A., Laukamp, C., Martens, V., & Caccetta, M. (2013). Unmixing the effects of vegetation in airborne hyperspectral mineral maps over the Rocklea Dome iron-rich palaeochannel system (Western Australia), *Remote Sensing of Environment*, 129, 17-31.

Hueni, A., Chisholm, L., Suarez, L., Ong, C., & Wyatt, M. (2012). Spectral information system development for Australia, in Proceedings of the Geospatial Science Research Symposium 2, RMIT, Melbourne, December 2012.

Hueni, A., Malthus, T., Kneubuehler, M., & Schaepman, M. (2011). Data exchange between distributed spectral databases, *Computers & Geosciences*, 37: 861-873.

Hueni, A., Nieke, J., Schopfer, J., Knewbuhler, M., & Itten, K. (2009). The spectral database SPECCHIO for improved long term usability and data sharing, *Computers and Geosciences*, 35(3): 557-565.

Hueni, A., & Tuohy, M. (2006). Spectroradiometer Data Structuring, Pre-Processing and Analysis - An IT Based Approach. *Journal of Spatial Science*, 51(2), 93-102.

Jensen, J.R. (2007) Remote sensing of the environment: an earth resource perspective, Prentice-Hall: NJ, 592pp.

Milton, E. J., Schaepman, M. E., Anderson, K., Kneubühler, M., & Fox, N. (2009). Progress in field spectroscopy. *Remote Sensing of Environment*, 113, S92-S109.

Pfitzner, K., Esparon, A., & Bollhöfer, A. (2008). SSD's spectral library database. In 14ARSPC: Proceedings of the 14th Australasian Remote Sensing and Photogrammetry Conference, Darwin NT, 30 September – 2 October 2008.

Viscarra Rossel, R.A., & McBratney A.B. (1998). Laboratory evaluation of a proximal sensing technique for simultaneous measurement of clay and water content. *Geoderma* 85, 19-39.

Wason, T. D. & Wiley, D. (2000). Structured Metadata Spaces. *Journal of Internet Cataloging*, 3(2/3), 263-277.

Chapter 15. Quality Assurance Steps for TERN Landscape Assessment Hyper-Spectral Data

M. Broomhall*[1], K. Johansen [2], D. Wu[2]

[1] Remote Sensing and Satellite Research Group, Department of Physics, Curtin University
[2] The Remote Sensing Research Centre / Joint Remote Sensing Research Program, School of Geography, Planning and Environmental Management, The University of Queensland

*Corresponding author:
Mark.Broomhall@curtin.edu.au

Abstract

Between January 2011 and June 2013, TERN's Landscape Assessment platform collected field, airborne hyper-spectral and airborne LiDAR data coincidently from nine locations across Australia. This chapter outlines a process to use for Quality Assurance (QA) of the airborne hyper-spectral data. All the data sets are available for the general public to download for use via the TERN Landscape Assessment Visualisation Portal (http://data.auscover.org.au/Portal2/) to support ecosystem science in Australia. This chapter explains how to geo-reference and atmospherically correct the hyper-spectral data and how to assess the quality of the geo-referencing, the spatial coverage of the data set and the spectral at-surface reflectance image pixel values when compared against in-situ spectrophotometer measurements of ground calibration targets. These QA methods may be used to any hyper-spectral image data set.

Key Points

- The hyper-spectral image data were delivered as a regridded nominal grid cell size (i.e. files where you select the pixel size yourself during processing in e.g. ENVI), as this allowed flexibility to select the most suitable pixel size for any application.
- It is important to check the absolute geometric accuracy and the relative geometric accuracy of flight lines to ensure the data deliverables meet the expectations outlined in the contract.
- On-ground spectral measurements collected coincidently with the airborne hyper-spectral image data can be used to quality assure the results of an image atmospheric correction.

15.1 Introduction

TERN Landscape Assessment have worked together with Airborne Research Australia (ARA) to deliver hyper-spectral data for a number of selected homogenous 5 km x 5 km field sites across Australia (Figure 15.1). This Quality Assurance (QA) procedure details the steps applied to the hyper-spectral image data, initially developed for the data captured for the Chowilla site in South Australia. It has been used as a guide to perform QA on the data for all other TERN Landscape Assessment sites. It is envisaged that the methods explained in this chapter can be used as a general guide for checking the quality of most types of high spatial resolution airborne hyper-spectral image data sets.

The nine TERN Landscape Assessment sites, which are all 5 km x 5 km include the following:

- Tumbarumba, NSW – 7 April 2011 (Hymap data)
- Chowilla, SA – 31 Jan & 1 Feb 2012 (Eagle/Hawk data)
- Watts Creek, VIC – 14 Apr 2012 (Eagle/Hawk data)
- Rushworth Forest, VIC – 15 Apr 2012 (Eagle/Hawk data)
- Zig Zag Creek, VIC – 17 Apr 2012 (Eagle/Hawk data)
- Credo, WA – 15 May 2012 (Eagle/Hawk data)
- Robson Creek, QLD – 13 & 14 Sep 2012 (Eagle/Hawk data)
- South East Queensland, QLD – 2 Feb 2013 (Eagle/Hawk data)
- Litchfield, NT – 27 May 2013 (Eagle/Hawk data)

The following additional surveys were also flown:

- A 14 km transect near Chowilla, SA – 31 Jan 2012
- A 1 km x 1 km at the Whroo flux site, VIC – 15 Apr 2012
- A 1 km x 4.7 km area near Robson Creek, QLD – 14 Sep 2012.

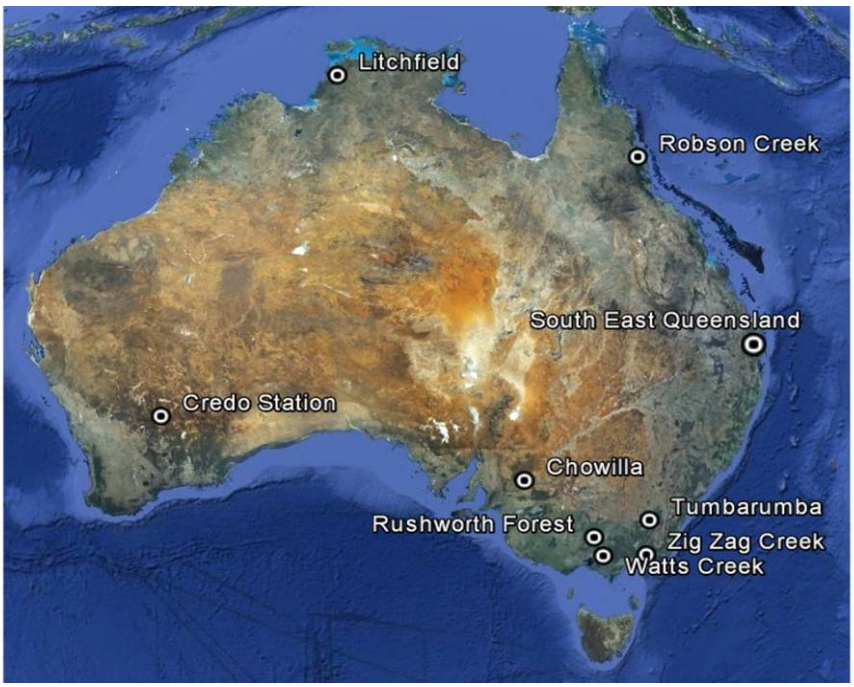

Figure 15.1 Map of Australia showing the location of TERN Landscapes campaign sites with hyper-spectral image data.

For eight of the nine surveys, the airborne hyper-spectral data covering the full spectral range from 400 nm to 2500 nm were collected using a research aircraft of Flinders University – ARA. A SPECIM AisaEAGLE II hyper-spectral scanner (VNIR) and a SPECIM AisaHAWK hyper-spectral scanner were mounted in underwing pods of ARA's ECO-Dimona research aircraft VH-EOS, each one together with its own OXTS RT4003 GPS/IMU navigation and attitude system (Figure 15.2). A NovAtel GPS Basestation was set up within or close to each of the survey sites to demonstrate that the required geometric accuracy was met (Hacker et al., 2013).

Figure 15.2 Specim Hawk hyper-spectral scanner mounted in the underwing pod of ARA's ECO-Dimona research aircraft.

The Eagle and Hawk instruments are manufactured by Specim (http://www.specim.fi/products/aisa-airborne-hyperspectral-systems/aisa-series.html). The Eagle instrument has 252 bands ranging from 400.7 nm – 999.2 nm with a silicon CCD detector giving 965 spatial pixels across the aircraft track. Swath width and pixel size depend on sampling duration and aircraft height at the time of sampling. The Hawk instrument has 241 bands

ranging from 993.1 nm – 2497.4 nm with a swath of 296 pixels with swath width and pixel size dependent on sampling duration and aircraft height at the time of sampling.

Based on the airborne data acquisition specifications (Table 15.1) and the inspection of the data, it is possible to produce Eagle and Hawk pixel sizes of around 30 cm and 1 m (nominal flight pattern altitude of 500 m above ground), respectively for most TERN Landscape Assessment sites. A las format and igm-file approach was used for the data delivery to avoid gridding the data onto fixed pixels, and hence leaving it up to the user to produce the required pixel size for their application. While it is not a common delivery mode, it was found scientifically more appropriate and provide more control to the data users to tailor the pixel size to any set application. The data format allows for selection of the pixel size when the data are geo-referenced. This will be covered below.

Table 15.1 Specifications for a hyper-spectral survey using the Chowilla site as an example.

Airborne Hyper-Spectral Data Acquisition Specifications	
Area	Chowilla, South Australia (shapefile provided)
Spatial Extent	• 5 km x 5 km • The 5 km x 5 km area will be centered on the flux tower located at E461899.4; N6237491 (34.0025°S; 140.5874°E) • UR: E464434.5; N6239956 • UL: E459423.8; N6239956 • LL: E459423.8; N6234973 • LR: E464434.5; N6234973 • UTM, Zone 54 • More than 99% of the area needs to be covered.
Date/Period of capture	• 31 Jan – 3 Feb 2012 • If rain or other unsuitable conditions persist within this period prohibiting data capture, two spare time windows have been identified as 12 – 25 Mar 2012 and 11-25 Apr 2012.
Acquisition parameters	• Pixel size ≤ 1 m x 1 m • 100+ spectral bands between 400 nm – 2500 nm; separate spectral data for the Eagle and Hawk, sampled simultaneously, but independently. • Flight strips should overlap at least 10% on each side • Flight strips should be collected along the principal plane of the sun ± 10º to reduce hotspots and cross-track illumination problems • Less than 5% cloud and cloud shadow within the 5 x 5 km study areas is highly desirable • Data to be only collected under dry canopy and ground conditions (i.e., not immediately after rainfall?).
Accuracy	• Demonstrated positional accuracy of +/- 1 m at 1σ in terms of absolute horizontal accuracy over flat terrain.
Field measurements	• The data provider will be responsible for setting up a ground station to acquire the appropriate calibration and validation data to assure and demonstrate that the specified absolute and relation geometric accuracies are achieved.
Deliverables	• Evidence/demonstration that the absolute horizontal accuracy specifications have been met as part of the delivery reporting specifications. The potential error budget within the IMU, GPS unit, IFOV, position of each flight line and any other factor should be included. • (1) EAGLE data delivered at the highest spatial resolution possible under the given illumination and other conditions. • (2) HAWK data delivered at highest spatial resolution possible under the given illumination and other conditions. • (3) Seamless hyper-spectral data set covering the spectral range from 400 nm to 2500 nm, i.e. a data set integrating both the EAGLE and HAWK data can be produced and delivered, but would require further funding.

Airborne Hyper-Spectral Data Acquisition Specifications	
	• For each of the three data sets above, the following product deliverables are required: o Hyper-spectral data delivered in ortho-rectified radiance units; o Hyper-spectral data can be delivered as ortho-rectified at-surface reflectance using the ATCOR4 processing tool for atmospheric correction (potential negative pixel values should be left instead of converting them to a value of 0), but would require some further funding • MGA, WGS84/GDA94, Eastings, Northings • IMG, TIFF or HDF format • A flight report including, but not limited to, the actual and planned acquisition parameters and information should be supplied: o Flight line ID and related information, including: o Flying starting time; o Altitude above AGL and MSL; o Heading; o Time of completing the flight line (duration); o Flying speed (ground speed); o Maximum off-nadir viewing angle along edge of strips; o Specify if IMU and GPS measurements relate to the exact sensor location; o Which DEM was used for the ortho-rectification; o Specification of all ancillary data and software used for processing. • All field survey control data used or derived from this contract must be supplied to ensure independent Quality Assurance (QA) of the survey operations. • The complete data set (raw and processed image and field data), metadata, and reporting should be supplied within 12 weeks of completed data capture (excluding time periods for capture of data in the context of other TERN Landscape surveys)

The following report will refer to steps taken using the ENVI software package and IDL programming language. It also refers to steps required to atmospherically correct the data to produce a surface reflectance product.

15.2 Geo-referencing

The radiometrically corrected radiance files for each flight line in band sequential (bsq) format with a header file for each radiance file were provided by the airborne data provider. The input geometry (igm) files store two bands for each flight line: one for the X coordinates (longitude or easting) and one for Y coordinate (latitude or northing). These igm files are used to geo-reference the hyper-spectral data as they contain the coordinate information for each original raw pixel.

15.2.1 Geo-referencing processing steps

1. It is recommended to create new sub-folders, for example GLT (Geographic Lookup Table), georef_rad_RGB and georef_rad_full_spectrum.
2. Start an ENVI session. The ENVI version used for this set of instructions was 4.7 but should be applicable to most versions.
3. From the file tab at the top of the ENVI bar select Open Image File and load the X and Y geometry coordinates bands for a single flight line from the igm sub-folder. All of the files in all of the sub-folders should have the same base filename for each flight line.
4. Select from the ENVI bar Map > Georeference from Input Geometry > Build GLT.

5. A popup window will ask for Input X geometry (select the X geometry coordinate band) and hit ok. It will then ask for Y Input geometry (select the Y geometry coordinate band).
6. Another window will pop up asking for Geometry Projection Information. For Input projection select UTM, the Datum is Geocentric Datum of Australia 1994. Leave the units as meters. The zone depends on where the flight lines are for. If you don't know click set zone and enter the lat/lon coordinates of the site and it will select the correct zone.
7. For the output information you can select what you would like but it is best to have the datum and projection the same. You can change units if you would like. It is suggested leaving this as meters as well.
8. A popup will announce that it is calculating parameters before another popup will arrive asking for Build Geometry Lookup File Parameters. This will have the maximum resolution Output pixel size and an Output rotation. Set the rotation to 0 and the pixel size is user selectable. Choose a GLT file name. This should be based on the flight line base file name and be saved in the GLT directory that was created earlier on. It is suggested putting _GLT at the end of the base name to denote the type of file.
9. Hit OK and it will build the GLT file. It is possible to create and save a number of these with different spatial resolutions. These will need to have unique file names however. They can be used later to create geo-referenced flight lines at the spatial resolution selected for the creation of the GLT file.
10. Go back to the ENVI bar and open the radiance .bsq file. If the GLT file is not loaded (will be if you have just created it), then load it. From Map on the ENVI bar select Georeference from Input Geometry > Georeference from GLT. Select the GLT file as the Geometry lookup file, select the radiance file as the Input data file. Hit OK and a popup window will appear. Choose a filename based on the base name of the flight line and save it to the folder previously created for the full spectrum images. Leave the background value as zero. It is suggested putting _GEO at the end of the base name. Click OK and the geo-referenced flight line will be produced.
11. Perform the same set of tasks as in step 10 but when you choose the radiance file there will be a button at the bottom left of the window allowing a subset to be chosen. Choose 3 bands that look like nice RGB images if possible as these will later be used to create a RGB representation. Choose bands that are not in an absorption feature. These files should be saved in the folders previously created for RGB images.
12. Repeat these steps for each flight line. If this is done manually then it will prove easier, probably, to create all GLT files first, then process all RGB files and finally process all full spectrum files. Processing scripts can be written in IDL that use the ENVI functions discussed above to batch process the files.

When all of these steps are run you will end up with a set of geo-referenced flight lines for the full spectrum and a set of geo-referenced flight lines with 3 bands for each flight line. The RGB versions can now be used to create mosaicked images, whereas the full spectrum will be used for further processing. It is important to note that the accepted geometric accuracy depends on the application. If the data are resampled to coarse resolution a larger RMS error in geometric accuracy is acceptable. For instance, when resampling to MODIS spatial resolution (250 m – 1 km), an absolute error of 10 - 20 m would likely be acceptable whereas for the same process at Landsat resolution (30 m), an absolute error of less than 5 m may be appropriate.

15.3 Verifying flight line alignment and spatial coverage by mosaicking the flight lines

As airborne instruments are at the mercy of wind and turbulence experienced by the aeroplane, it is possible that some of the survey area may have been missed as the plane pitches, rolls and yaws its way through the air. To check the coverage, ENVI can be used to mosaic the flight lines together now that they have all been geo-referenced. One of the reasons for creating the RGB files is that these are quicker to mosaic and the resultant files are far smaller. The steps to mosaic the RGB files together are as follows:

1. Go to the ENVI tab and click file > Open Image file. Open all the .bsq files from the RGB sub-folder that is for the survey flight lines. This section may contain .bsq files for cross lines or transect lines.
2. Go to the ENVI tab and select Map > Mosaicking > Georeferenced. A window will pop up.
3. In the window click Import > Import files and Edit properties. Select all files that appear in the list by clicking the first, scrolling to the last, holding shift and clicking the last.
4. Select 0 as the data value to ignore. Click OK. The same window will pop up for each selected file. Keep clicking OK until it goes away.
5. Once all the clicking has been done a thumbnail style image will appear in the original popup window. To avoid mosaicking cloud covered flight lines on top of cloud free flight lines, the 3-band flight lines can be either raised or lowered to different positions in ENVI to reduce the amount of cloud cover within the mosaicked images. From here go to the popup window tab and select File > Apply. Another window will pop up asking for Mosaic Parameters. Leave the output pixel sizes as it is, Resampling as Nearest Neighbour, background value as 0 and then chose a file name. Save it in the RGB sub-folder with any name you would like.
6. If there were a cross-sectional transects flown over the site, mosaic these separately using steps 1 to 5.

This will produce a mosaic of all of the flight lines. Load the mosaic into a RGB display. This will allow you to visually assess the alignment of flight lines. Identify features which can easily be assessed, e.g. artificial features such as roads, tracks, buildings, etc.

Maximise the scroll window. If you have a vector file such as a .shp file that has the boundaries of the site you can overlay this on the scroll window to make sure full coverage of the study area has been achieved. Make a note if it has not.

Next, check the image for holes. These might be on the edges of overlapping flight lines if the area has not been covered correctly, or may be inside the area if instrument perturbations during the flight have caused the flight lines to deviate too much. Using the Cursor Location / Value tool grab an approximate centre position of any holes you find. This is best done by examining the image window. If the data provider has provided a project report, compare the coverage percentage they have reported with you visual inspection to see if this is reasonable. You can also:

1. Overlay a shape or vector file of the survey area on the mosaicked image to see where the extents of the survey site are. The flight lines should extend well past the north and south edges.

2. In the image window go to Tools > Measurement tool. The Display measurement tool will pop up. In the window select Type > Polygon. Click the Zoom button.
3. In the scroll and image windows negotiate around searching for holes. Make sure the hole is fully displayed in the zoom window. Click the left mouse and draw around the edges of the hole. Right click the mouse to close the polygon. The pixel number inside the hole will be displayed as will the area of the hole in pixels squared. Write this down.
4. Find all the holes and record the areas of all the holes. Assuming the geo-referencing was done to 1 m, divide the resultant by the number of pixels within your study area, multiply by 100 and subtract the total from 100. This will give the percentage of coverage from the site.

It is expected that this will be close to 100% but there is generally a clause in the contract that stipulates leeway here, as it is not always possible to achieve complete coverage.

15.4 Spectral Analysis and Accuracy

Analysing the spectral response of the airborne hyper-spectral data requires data from a spectrophotometer (such as an ASD instrument) taken simultaneously with the overflights. TERN's Landscape Assessment platform had a set of three targets made of white, grey and black material, each with dimensions of 8 m x 8 m. These were sampled with ASD instruments during the overflights. If these types of targets are not available, then reasonably homogenous surfaces each with a range of brightness levels would suffice, e.g bare ground, road.

If possible collect atmospheric information while both airborne and surface sampling is occurring. The Lanndscape facility made use of Microtops Sunphotometers and Ozonometers (Figure 15.3) to collect, atmospheric pressure, aerosol optical depth, total column water vapour, temperature and total column ozone measurements. These measurements are used when performing atmospheric correction.

Figure 15.3 Microtops sunphotometer and ozonometer showing the instruments being geolocated and time synchronised using a GPS.

15.2.2 Atmospheric Correction

There are several methods available to atmospherically correct hyper-spectral data. Users of ENVI may have run FLAASH (Fast Line-of-site Atmospheric Analysis of Spectral Hypercubes) but other popular packages include ACORN (Amospheric CORrection Now) and ATREM (Atmospheric REMoval program). These packages are generally based on or created using a radiative transfer program such as MODTRAN or 6S.

Most atmospheric correction packages perform similarly with the same input conditions but the operator should be aware that there will be differences especially around parts of the spectra where there are strong atmospheric absorption features. If possible run more than one atmospheric correction program and compare.

15.2.3 Deriving in situ atmospheric measurements to use for atmospheric correction

Once you have decided which Atmospheric Correction (AC) package you are going to use, atmospherically correct any flight lines that have the surface targets in them. If the program requires atmospheric information such as Aerosol Optical Depth (AOD), Water Vapour (WV), ozone (O3), atmospheric pressure or temperature then this can be derived from the Microtops instruments.

The Microtops has an interface program, which will connect with the RS232 output from the instrument, through the supplied RS232 – USB convertor to the computer. When downloaded, the data will end up in a database that can be opened as a text file in e.g. Microsoft Excel. Each line in this file will give AOD, WV and O3 (assuming both instruments were used). These will be recorded with the time (generally UTC) so it should be possible to match up the atmospheric parameters when each flight line was captured. Care should be taken to ensure that cloud cover was not present when the Microtops data were retrieved. When readings are taken with the Microtops triplicate reading should be taken over about 30 seconds to a minute. If the results vary significantly over the triplicate samples there is a good chance that cloud has contaminated the readings and they should be discarded. If hemispherical photos were taken at the same time as the samples, check these to see if the sky is clear. When you are happy with the atmospheric data, you can move onto the atmospheric correction.

15.2.4 Using FLAASH for atmospheric correction

The following instructions relate to the FLAASH atmospheric correction module in ENVI. This assumes you have completed the geo-referencing steps above and have access to atmospheric data from the Microtops (or have guesstimates of these parameters) and have the metadata and .nav files from the airborne data provider.

1. The first step is to convert the geo-referenced full spectrum .bsq (band sequential) files to either .bil (band interleaved by line) or .bip (band interleaved by pixel). It is suggested using .bil format. Open the geo-referenced file prepared earlier, then select from the menu bar Basic Tool > Convert Data (BSQ, BIL, BIP). Enter a name and either hit OK or Queue. It is suggested that you queue this and repeat the process for all of the flight lines, as this conversion process will take a long time. When you have added all of the conversions to the queue, go to the menu bar and select File > ENVI Queue manager, select all of the queued jobs in the list in the popup window, then Execute Selected. Although of course it depends on the hardware being used to run ENVI, this conversion process can be lengthy. For instance, the

conversion from bsq to bil using the TERN Landscape Assessment hyper-spectral image data took between 20 to 30 minutes per flight line using a core i7laptop with 8GB of RAM that runs on Windows 7, resulting in between 13 to 20 hours to convert 40 flight lines. After the files have been converted to bil, the subsequent atmospheric correction step (described below) will take about the same time (when running FLAASH per flight line).

2. Once all of the files are converted, open one of the converted tiles, go to the menu bar and select Spectral > FLAASH. The FLAASH Atmospheric Correction Model Input Parameters window will pop up. Click Input Radiance Image and select the loaded file from the list. Another window will pop up (Radiance Scale factors). Select the Use single scale factor for all bands button and type in the scale factor. Now select an Output Reflectance File name and location, Output Directory for FLAASH Files and a Rootname for FLAASH files. Log, template, water vapour and cloud mask files will end up in the output directory. Template files can be re-used to quickly reload input parameters. This can be done by clicking the Restore button at the bottom right of the popup window and selecting a previous template file.

3. The next section of the FLAASH window requires specifics about the sensor. Most of the required information can be obtained from the .nav file for each flight line. These are text files that report sensor specific navigation information for each flight line. The columns in the file show scan line, time, latitude, longitude, altitude, heading, roll, pitch and speed. To get the scene centre location, scroll to the middle of the .nav file and select the values from the latitude and longitude columns. It is not essential that this is extremely precise; anywhere near the middle is fine. For the sensor type, click the button, then select Hyperspectral > AISA. The flight date can be derived from the flight line name. The first 4 digits represent MMDD. The sensor altitude can be derived from the .nav file. The 5th column shows sensor height in metres. Either extract these values and average them or guesstimate the approximate median or average value for the sensor height. Hopefully the range of sensor heights will be less than 100 m. If you have a site elevation estimate from GPS then use this. If in doubt, select a ground elevation of 0.3 to 0.4 km. The pixel size will be whatever was set when the data were geo-referenced. A kmz file with UTC flight time information of each flight line should be requested from the airborne data provider. An easy way to get the flight time is to use the flight line kmz file provided in the metadata. Open the .kmz file in Google Earth. In the Places menu under Temporary places you will see the flight line. Expand the entry for the flight line then check the box that says UTC. This will display the sensor position and time on the map. Select a time near the centre of the flight line as the flight time.

4. The third panel on the FLAASH window deals with selection of the atmospheric correction parameters. Select Tropical from the list of atmospheric models. This allows higher values of water vapour to be retrieved. Select Yes for Water Retrieval and select 1135 nm as the Water Absorption feature. Select the Rural Aerosol model and the 2-band (K-T) aerosol retrieval. The initial visibility can be set to 50 km for Australia as we generally have extremely clear skies. Select No for Spectral Polishing and No for Wavelength Recalibration.

5. Click Advanced settings at the bottom of the FLAASH window. Leave the Aerosol Scale Height as 1.5 km, the CO2 Mixing Ratio as 395.0, select No for Use Square Slit Function, Yes for Adjacency Correction, and No for Reuse MODTRAN Calculations. Select Modtran Resolution of 1 cm-1, Scaled DISORT for Modtran Multiscatter Model and 8 DISORT streams. Leave the Zentih Angle as 180 and the Azimuth angle as 0. The Azimuth angle will change if the flight line is not flown north or south. The sensor heading is measured in degrees east from north from 0 – 360. The FLAASH input is in degrees east from north but is 0 – 180 towards south and from -180 – 0 from south towards north. Select to use Tiled Processing and set the Output Reflectance Scale Factor to 10000 if not already set. This will output the reflectance product as an integer where the reflectance for any pixel value can be found by dividing by 10000. This reduces the size of the output file. Click ok on the advanced settings window then click Apply on the FLAASH window. FLAASH will now atmospherically correct your data and output it to the filename selected earlier.

6. Repeat this process for each flight line.

15.2.5 Comparing atmospherically corrected data to ASD spectral measurements

Easy method:

- Extract pixel values as text from the atmospherically corrected hyper-spectral data over the targets using the z profile tool.
- Output ASD as text using viewspec pro.
- Open both in Excel and plot one against the other

Harder method:

- The ASD files need to be resampled to the airborne hyper-spectral band responses using ENVI.
- Compare band by band the spectral target ASD values to the atmospherically corrected image target data.

15.5 Conclusions

This document provides instructions on how to open, geo-reference and atmospherically correct airborne hyper-spectral image data based on the experience of working on the TERN Landscape Assessment hyper-spectral data. This can be used to Quality Assure the data when delivered to assess the coverage, geometric accuracy and spectral integrity of the data.

References

Hacker, J., Lieff, W., & Mcgrath, A. (2013). Project Report. Report prepared by Airborne Research Australia, Flinders University for AusCover. Final version 25 March 2013.

Acknowledgements

Significant input to the hyper-spectral data acquisition and processing was provided by Jorg Hacker, Andrew McGrath and Wolfgang Lieff (ARA, Flinders University).

Chapter 16. Airborne LiDAR Acquisition and Validation

N. Quadros*[1], J. Keysers[1]
[1] Cooperative Research Centre for Spatial Information

*Corresponding author:
NQuadros@crcsi.com.au

Abstract

Background knowledge and experience on airborne LiDAR is required to optimise and exploit a LiDAR survey. A basic understanding of sensors, combined with knowledge of the various considerations which impact upon the quality of the products, is essential. The major considerations which impact upon a LiDAR survey are the extent, vertical accuracy, point spacing, ground cover types and temporal variations. Each of these factors needs to be considered when designing LiDAR survey specifications.

The LiDAR acquisition section of this chapter provides a brief outline of the most typical LiDAR sensors. Within the context of each sensor, the project and environmental considerations should be optimised to enhance the success of a LiDAR survey.

The technical specifications for designing a successful LiDAR survey can be complex and numerous. The Intergovernmental Committee for Surveying and Mapping (ICSM) Standard LiDAR Specifications provide a comprehensive template for commissioning an airborne LiDAR project.

To ensure that the LiDAR products meet the specifications and user requirements, the quality needs to be assured and the deliverables validated. The validation can either be against the required specifications, or against a set of requirements defined by the end use of the LiDAR data. The validation practices typically inspect the LAS and DEM data products, and any additional deliverables that are produced.

The LiDAR validation section of this chapter outlines the recommended steps which may be taken by a purchaser or end user to validate the project deliverables. The recommended validation checks include the delivery completeness, coordinate systems, vertical datums, extent, coverage, survey control, vertical accuracy, density, classification and reports. Additional checks may be performed for unique deliveries, or for specific applications requiring an analysis of particular components of the LiDAR products.

A standard airborne LiDAR Compliance and Quality Assurance Tool (QA^{4}LiDAR) has been developed by the Cooperative Research Centre for Spatial Information which was released to partners in early 2015. This tool implements the validation concepts presented in this chapter. The tool provides an easy to use, automated approach for several of the LiDAR checks described. The report produced by the software tool provides users with a simple guide to the quality of their LiDAR datasets.

Key Points

- The major considerations which impact upon a LiDAR survey are the extent, vertical accuracy, point spacing, ground cover types and temporal variations. Each of these factors needs to be considered when designing LiDAR survey specifications.
- Within the context of each sensor, the project and environmental considerations should be optimised to enhance the success of a LiDAR survey.
- The technical specifications for designing a successful LiDAR survey can be complex and numerous. The Intergovernmental Committee for Surveying and Mapping (ICSM) Standard LiDAR Specifications provide a comprehensive template for commissioning an airborne LiDAR project.
- The validation of LiDAR products can either be against the required specifications, or against a set of requirements defined by the end use of the LiDAR data. The validation practices typically inspect the LAS and DEM data products, and any additional deliverables that are produced.
- Recommended validation checks include delivery completeness, coordinate systems, vertical datums, extent, coverage, survey control, vertical accuracy, density, classification and reports. Additional checks may be performed for unique deliveries, or for specific applications requiring an analysis of particular components of the LiDAR products.

16.1 LiDAR Acquisition

Understanding the main LiDAR sensor characteristics and the impact of survey specifications on the LiDAR products is vital to selecting the optimal acquisition strategy. This section presents an overview of the main LiDAR sensor characteristics, followed by factors which should be considered before acquiring LiDAR data. These factors, or survey considerations, are divided into project considerations, which are independent of location, and environmental considerations, which vary depending upon the project area and location.

The considerations presented are aimed at creating an awareness of the factors involved in developing an effective LiDAR survey strategy. The overview does not provide enough detail to replace a knowledgeable and experienced LiDAR provider. The overview should enable users to understand competing factors in a LiDAR survey, some of which include:

- Spatial resolution vs. survey extent
- Acquisition flexibility vs. concurrent datasets
- Optimal conditions vs. stringent product delivery dates

Recognising the optimal balance between competing factors will make a critical difference to the success of a LiDAR survey.

16.1.1 LiDAR Sensors

There are a number of topographic LiDAR sensors on the market. Each has unique characteristics which can impact on the success and quality of a LiDAR survey. A few sensors are customised to survey particular environments or features. Most sensors can efficiently conduct a typical ground or feature survey.

The most commonly used LiDAR sensor uses discrete-return processing. A GPS/GNSS position, aircraft platform orientation, laser scan angle and range are used to accurately position each return. Figure 16-1 shows these features of an airborne LiDAR system. Most discrete-return sensors produce up to four points per laser pulse.

The alternative to discrete return sensors produce a full waveform product. The full waveform processing records the whole LiDAR signal as it passes through the atmosphere. This is especially useful for high-end vegetation applications, as the full waveform signal conveys more information about the structure of the vegetation canopy and understory. The downside of full waveform data is that it is significantly larger, requiring more storage space, and there are not as many tools for processing and analysing the data. For these reasons most projects use discrete-return for the capture of LiDAR data.

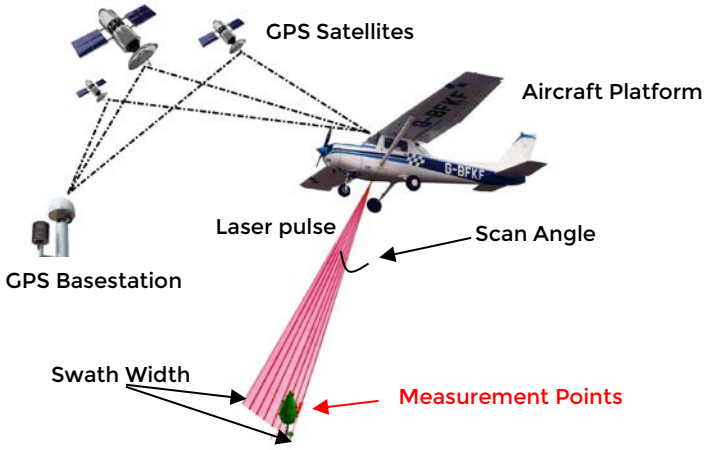

Figure 16-1 Airborne LiDAR Diagram

The main LiDAR sensor characteristics relevant to data capture can be divided into:

- Laser pulse
- Scanning method
- Data recording
- System precision and resolution
- Operational requirements

The major *laser pulse* characteristics are the wavelength, pulse length, beam divergence and eye-safe range. Most topographic LiDAR sensors use a wavelength of 1064nm, with varied pulse lengths and laser footprint sizes. Some LiDAR sensors are using the 1550nm wavelength for greater eye safety at higher power, and to further determine soil composition. The eye-safe distance dictates the minimum flying height of the laser platform. Most surveys can be adjusted so that they are flown to meet a particular footprint size, whilst maintaining an optimal flying height.

The *scanning method* is composed of the scanning pattern, mirror speed and scan angle. The main scanning patterns, some of which are shown in Figure 16-2, involve a rotating mirror, oscillating mirror, or rotating multi-facet mirror. The mirror speed and maximum scan angle are unique to each sensor. The scanning method will not significantly impact the vast majority of applications.

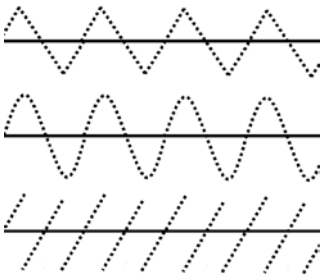

Figure 16-2 LiDAR scan patterns. Sawtooth oscillating mirror (top), sinusoidal oscillating mirror (middle) and rotating mirror (bottom).

The main *data recording* parameters consist of pulse frequency, maximum number of returns/pulse, minimum return separation distance and pulse detection method. The advent of multi-pulse LiDAR (shown in Figure 16-3) in systems in recent years has increased the pulse frequency due to the sensor emitting additional pulses before the previous pulse signal returns. The number of returns per pulse and their minimum separation will reflect the amount of detail returned from vegetation. The *system precision and resolution* is mainly concerned with the positioning accuracy, across-track and along-track point spacing and range precision. The *operational requirements* relate to the platforms, flying heights, acquisition duration and processing software.

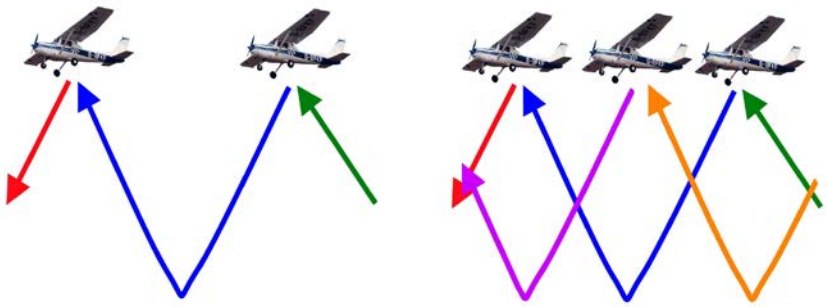

Figure 16-3 Single pulse (left) vs. Multi-pulse (right).

Bathymetric LiDAR sensors are used to measure the depths of the seafloor. These sensors have a number of different characteristics to topographic LiDAR sensors. The main differences are that they operate at a green wavelength of 532nm which is able to penetrate water (as shown in Figure 16-4), they have a more powerful laser which is not able to measure as frequently, and a larger laser footprint with great beam divergence in the water column. As this publication is focused on terrestrial ecosystems the discussion in this chapter is restricted to topographic LiDAR systems. For further information on Bathymetric LiDAR sensors refer to Quadros (2013).

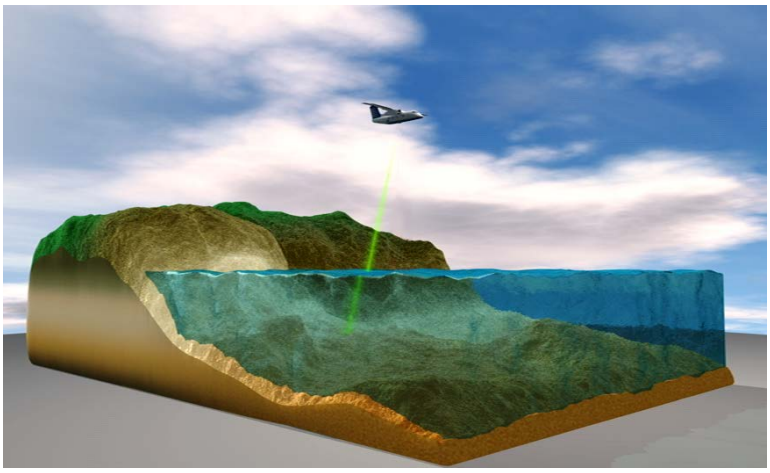

Figure 16-4 Bathymetric LiDAR sensor (Courtesy of Fugro LADS)

16.1.2 Project Considerations

The project considerations include the strategic survey decisions which are independent of location. Each consideration will have an impact on cost, quality and success of the survey. The main project considerations include:

- Survey extent and shape
- Accuracy, point spacing and object detection
- Vertical datums
- Budget and timelines
- Supplementary datasets

The *survey extent* has a major impact on the feasibility and efficiency of the LiDAR acquisition. Small survey areas may be more efficiently surveyed with alternative on-ground technologies. Likewise, large survey areas may be more efficiently surveyed with alternative technologies, such as satellite imagery or radar. The shape

of the survey area also impacts the survey efficiency. The longer the survey flight lines, the more efficient the survey operations. Longer flight lines are frequently attributed to regular shaped survey areas.

Accuracy generally refers to the absolute vertical accuracy of each point, which is how close the measured height values are to the true heights. A standard for most airborne LiDAR projects is to require an absolute vertical accuracy of ±30cm @ 95% confidence. The horizontal accuracy, although relevant, is less frequently discussed. The horizontal accuracy standard used within airborne LiDAR projects is ±80cm @ 95% confidence.

Depending upon the remoteness of a survey and the application, different absolute and relative vertical accuracy requirements can be considered. The remoteness of a survey can affect the accessibility and reliability of a dense survey control point network, which is required to generate a survey to a high absolute vertical accuracy. Lowering the absolute vertical accuracy requirement may be more practical in these areas.

Some applications rely on the measurement of features internal to the survey, and therefore should place more emphasis on the relative point accuracy, rather than the absolute accuracy. Applications which require the LiDAR heights to be integrated with other data, including other LiDAR surveys will require a more reliable absolute accuracy.

Point spacing refers to the horizontal distance between LiDAR measurements/footprints. Denser point spacing can substantially increase the cost and decrease the rate (flying speed) of a survey. Surveys which have an emphasis on only the ground definition generally require between 1.2-2 pulses/m^2 on the ground (e.g. Figure 16-5). Surveys which require definitions of non-ground features typically need more measurements at around 8-15 pulses/m^2, or even 30-35 pulses/m^2. The point spacing can be highly variable and specific depending upon the required application.

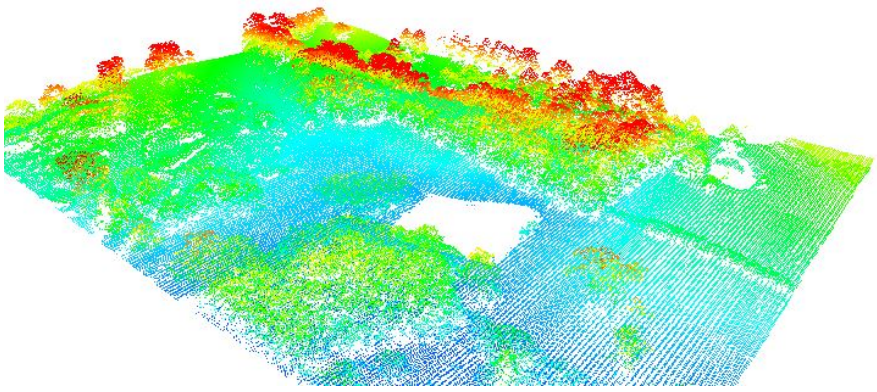

Figure 16-5 An example LiDAR project captured at 2 pulses/m^2

For particular applications, such as mapping power lines, the minimum *detectable object* size needs to be considered. The object detection is impacted by the flying height and target reflectivity. For instance, at lower flying altitudes thinner power lines can be detected. Figure 16-6 shows power line object detection in a LiDAR point cloud.

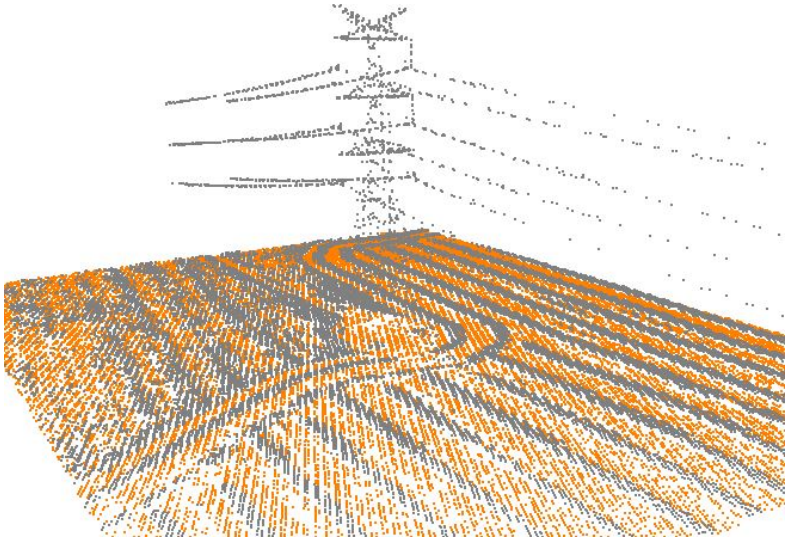

Figure 16-6 LiDAR surveyed power line corridor

The required *vertical datums* need to be considered when planning a LiDAR survey. The vertical datum is the reference surface to which all LiDAR heights are referred. In Australia heights are commonly referred to the Australian Height Datum (AHD). Alternative reference systems, such as the WGS84 or GRS80 ellipsoids, can also be used. Ellipsoid heights are provided via GPS/GNSS without the need for geoid corrections.

AHD heights are computed with the addition of a geoid model. AusGeoid09 is the currently accepted version. In areas where the geoid model accuracy does not meet the requirements, an additional correction to the data may be made. Storing LiDAR data referenced to the ellipsoid provides for easier updates, if changes are made to the geoid model or orthometric height datum.

The *budget and timeline* for the LiDAR survey will have very obvious implications on the chosen strategy and specifications. A higher budget will allow collection of more points, to greater accuracy and a larger extent for the survey. An increase in these factors will increase the timeline for acquisition and processing. An increase in the budget will frequently need a commensurate increase in the timeline for product delivery.

The cost of a survey is higher per area for inefficient surveys which require many aircraft turns. Surveys in remote areas are also likely to cost more, especially if aircraft transit is a high proportion of the flying time. Topographic LiDAR surveys have been quoted as low as AU$70 per km^2 for large regular areas. However, the typical survey cost for a discrete-echo airborne LiDAR survey is a round AU$150 per km^2 for a 300-1000km^2 survey.

Surveys typically require about one week of acquisition per 150km^2 of survey. The processing time for LiDAR data is at least six weeks after the completion of acquisition. Twelve weeks is generally used for a 300km^2 survey in ideal conditions with no new product development, and an average amount of point validation. As the classification quality and development of new products are increased, the processing time is also increased. The necessity of new products must be weighed against the survey schedule.

Supplementary datasets can be acquired concurrently with the LiDAR acquisition. These datasets can include video imagery, aerial imagery (Figure 16-7), and hyperspectral imagery. These datasets can be of varying resolution and quality.

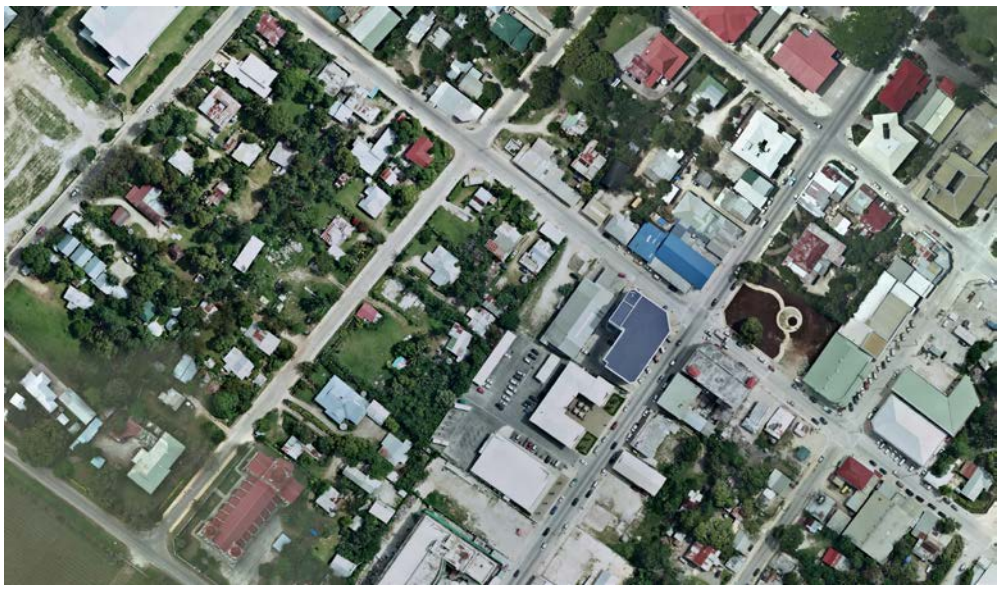

Figure 16-7 Concurrent aerial imagery captured during a LiDAR survey.

The downside of capturing concurrent imagery with LiDAR, is it limits acquisition to daytime operations. It is also important to note that image quality will not be the same as from a dedicated aerial imagery capture. If the same quality as a dedicated aerial imagery capture is required with the LiDAR, the acquisition times will be extremely limited given that high quality imagery requires no cloud, and limited sun glint and shadows. If the expectation of the imagery quality is lowered, concurrent imagery can be cost effective as part of the LiDAR capture.

LiDAR intensity is an important attribute to include within topographic LiDAR datasets. The intensity is a measure of the strength of the return signal. The addition of this information is inexpensive, as it is gathered whilst laser scanning however the information is invaluable for modelling ground types and habitats. Although, it is not a supplementary dataset in its own right, it is an important inclusion within any elevation deliverable. Figure 16-8 provides an example of LiDAR intensity imagery.

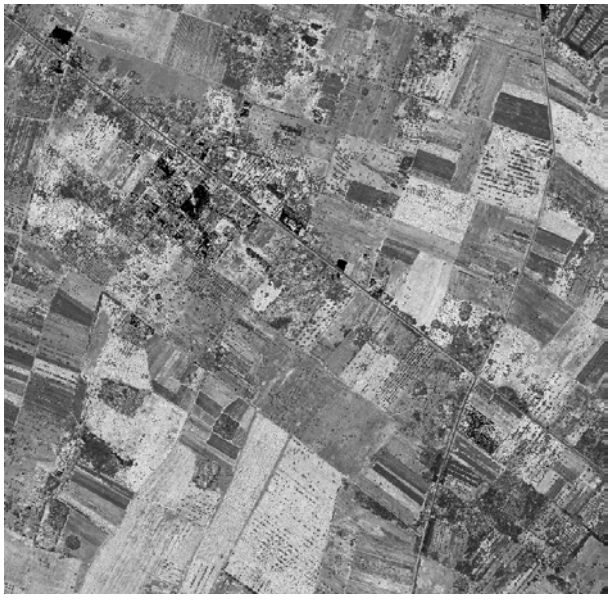

Figure 16-8 LiDAR intensity in an agricultural area

16.1.3 Environmental Considerations

The environmental considerations are dependent on location. These considerations require prior knowledge of the survey area, without which the success of the survey can be severely hampered. The main environmental considerations include:

- Terrain elevations - altitude and variability
- Ground cover types and ground penetration
- Temporal variations affecting acquisition - seasons, wind, smoke, cloud, fog, air traffic and daylight
- Environmental changes affecting ground measurement - foliage, tide, water flow and pooling

The *terrain elevations* directly impact the minimum flying height for the LiDAR acquisition. Acquisition generally plans the flying height around the highest elevation. Variable terrain heights will create variable swath widths as the distance between the ground and aircraft varies. To obtain complete coverage, the aircraft line spacing will provide for the minimum swath width. Flatter terrains are easier and more efficiently acquired.

Ground cover types affect many different aspects of the LiDAR acquisition depending upon whether the application involves ground points, non-ground points or both. The main ground cover types come under the broad categories of buildings/infrastructure, vegetation and water (Figure 16-9). The type of vegetation present will greatly affect ground penetration of the LiDAR pulse. Dense vegetation has the ability to completely block the LiDAR ground measurements. Dense low-lying vegetation can lower the reliability of the ground definition as these points may be mistaken for ground points. Some low-lying vegetation, such as reeds, can even mask the presence of water.

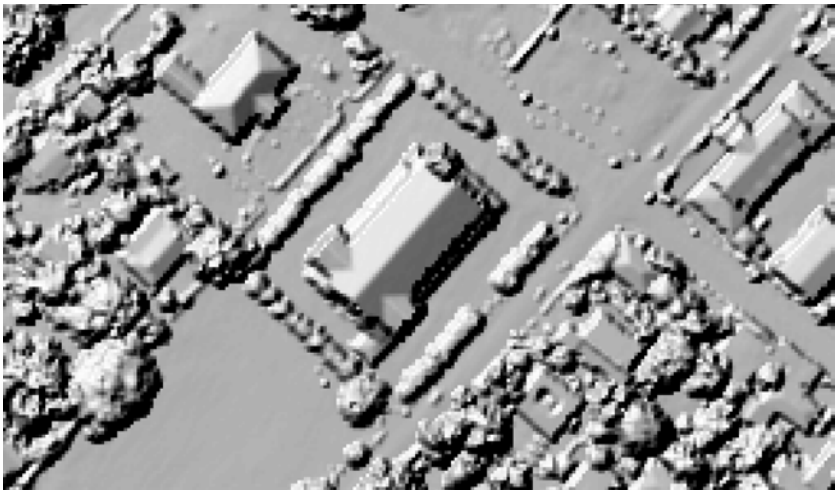

Figure 16-9 Features within a LiDAR survey

In moderately dense vegetation more pulses are required to obtain an adequate ground definition. Increasing the pulse density increases the likelihood of the ground being measured. The pulse density can be increased in a number of ways, such as lowering the acquisition speed, or providing multiple flights over the same area. If multiple flights are deemed appropriate, these can be confined to the areas requiring more ground points.

To increase the ground measurement probability the scan angle is reduced, so that measurements can obtain greater *ground penetration*. This is due to the increased vertical angle of the laser measurements. It is recommended that the maximum scan angle in vegetated areas is limited to between 30-40 degrees. It should be noted that the reduced scan angle will reduce the swath width, and therefore increase the amount of flying.

Temporal variations occur daily, monthly and seasonally. The seasons dictate the viability of a survey, particularly with regard to stand-by, or non-flying days. Whether the seasonal change is between summer and

winter, or wet and dry the impact can be significant. A survey performed in the optimal season can make significant savings on time and budget, as well as producing better quality products. The main seasonal factors which influence flying are winds, temperature, cloud-cover and rain-fall. The times when these factors have less influence on the survey are most optimal for acquisition.

The LiDAR sensor cannot penetrate clouds, rain, smoke, fog or dense haze. Therefore, surveys must be flown in clear atmospheric conditions. LiDAR is typically acquired at a flying height lower than the cloud cover.

LiDAR surveys can be flown during the day or night. Acquisition at night can help avoid on-ground features such as cars and human traffic that are more prevalent in the day. Around cities surveys are sometimes flown at night because it is easier to obtain flight clearances as there is reduced air traffic. Scheduling acquisition around busy airports can be difficult, and appropriate planning is required.

Environmental changes have a significant impact on the success of LiDAR surveys. In many environments, scheduling the survey around changes on the ground is pivotal to the ground data coverage.

In vegetated areas, reduced tree foliage and grass heights will enhance the ground penetration of the LiDAR pulse. The timing of the survey in these areas should coincide with leaf-off season if ground penetration is important (Figure 16-10).

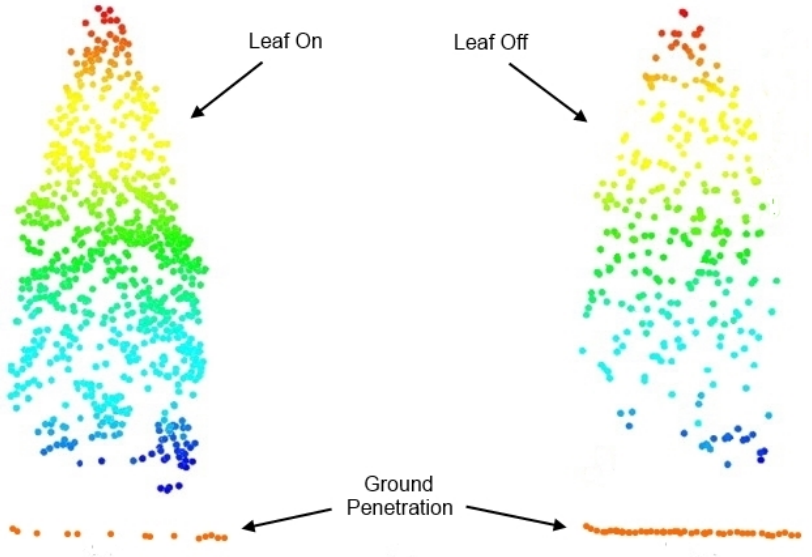

Figure 16-10 Ground penetration in leaf-off season compared to leaf-on

In areas of rivers and lakes, high water flows and low-lying water will reduce the effectiveness of the LiDAR. Greater coverage will be obtained when the volume of water is at a minimum.

In the coastal environment the tide will provide the seaward limit of the survey, given that topographic LiDAR does not penetrate water. To maximise the survey extent the survey can be conducted around low tide, however the cost and delays of restricting the survey to these times should be weighed against the benefit of the increased extent. It should be noted that the height of low tide varies between the spring and neap tide. To gain maximum coverage, data should be gathered during spring tides.

16.1.4 ICSM Specification Standard

It is not a simple process to create LiDAR specifications which comprehensively cover all aspects of a LiDAR acquisition project. To ease the process, the standard LiDAR acquisition specifications developed by the ICSM Elevation Working Group can be used. These specifications were developed to address traditionally inconsistent and diverse product specifications. The national base specifications define a consistent set of minimum products which ensure compatibility across projects and States.

There are a number of variables within the standard LiDAR specifications. Defining the variables, such as classification standards, requires knowledge of the LiDAR acquisition processes and outputs, within the context of the data application. It is recommended that LiDAR expertise be sought for defining these variables.

The LiDAR specifications are evolving and continue to be a working document. When using these specifications, an awareness of potential short comings experienced by other users, will reduce the likelihood of problems with delivered products.

It is recommended that the standard ICSM LiDAR specifications be used as a basis for commissioning airborne LiDAR projects. Prior knowledge of the project and environmental considerations should dictate the required edits and modifications to the document. To download the specifications go to:

http://www.icsm.gov.au/elevation/LiDAR_Specifications_and_Tender_Template.pdf

16.2 LiDAR Validation

LiDAR validation is vital in ensuring the LiDAR data meets the requirements of the intended application. It is especially important to perform the validation, or obtain a validation report, before using the data. Discovering short comings in the data during later analysis can cause significant setbacks for projects.

The most thorough checks to be performed are directly post-acquisition, or on receiving a dataset from the acquisition provider. If the user is the first person to analyse the LiDAR data there is a great risk of discovering an error. If obtaining data from a second party who has already performed some validation steps, the user should only perform additional checks within the context of the experience and thoroughness of the previous validation.

The LiDAR validation concepts and steps provided in this chapter cover the most important compliance and quality assurance (QA) checks. Validation is performed against an expected standard. The checks in this chapter are in response to the national ICSM standards. More application specific checks may be performed depending upon the data use.

Most LiDAR validation is concerned with the two core products shown in Figure 16-11; the LAS point cloud and DEM. These two products are the most commonly used, and provided by resellers. If additional products are to be used within an application, additional checks may be performed on these datasets.

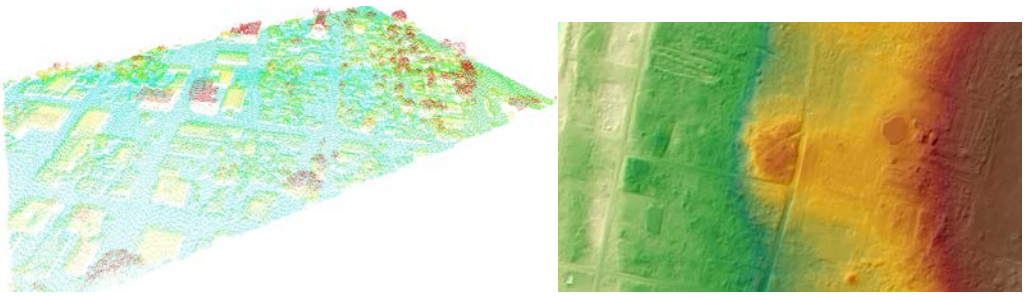

Figure 16-11 Example LAS point cloud (left) and LiDAR DEM (right)

Before beginning the validation of a LiDAR delivery, it is important to have a definitive list describing all the specifications and delivery requirements for each dataset. As each dataset passes or fails the validation for each requirement, it can then be ticked off against this list. For tiled datasets, a table listing every tile name with associated fields to tick off each requirement, such as whether it has been delivered, whether it is corrupt

and so on, is recommended. This table may be within the tile index polygon attributes, or you may wish to use a spreadsheet.

As the validation is performed and data are ticked off against the specification list and tile index table, it is useful to attribute elements with Pass, Fail, Conditional Pass, Pending, or N/A;

- PASS - Data is compliant and satisfies the QA measure, no further action is necessary.
- FAIL - Data is non-compliant and does NOT satisfy the QA measure. Resupply is required.
- CPASS - Conditional Pass means the data is not compliant and does NOT satisfy the QA measure, but is very close to satisfying the measure, and is acceptable.
- PENDING - The compliance and QA check has not been completed.
- N/A - The check is not applicable.

For some checks it is also appropriate to record values resulting from the QA, such as the absolute vertical accuracy or the point density measures. These values will support PASS, FAIL and CPASS results when reporting and requesting resupply.

16.1.5 Delivery Completeness

Delivery completeness is frequently overlooked as the first validation step, however is the most important for any dataset, including LiDAR. Identifying missing data during the later processing or analysis stages of the project can cause frustration and potentially significant setbacks.

The delivery completeness check looks for the presence of all expected products for a LiDAR project. This includes:

- All relevant tiles, swath files and mosaics for all datasets i.e. LAS, DEM, DSM etc.
- All the required ancillary information i.e. waveform data, GPS RINEX files, photographs etc.
- File naming and directory structure match the required conventions
- File formats are as specified
- Las headers and point source ID's (PSID) are valid
- Tile size is as specified, and the southwest corner of each tile is on a whole metre coordinate value
- Vector datasets contain the correct attributes
- All required metadata and reports
- Additional requirements are fulfilled i.e. statistics and pyramids

LiDAR datasets can contain a large number of files which can be corrupted during copying and data transfer. It is vital that all files are checked for readability, ensuring no files have been corrupted in the delivery.

Instructions:

This can be a time consuming process as ideally all data needs to be opened and viewed to ensure it is valid. It is not enough to simply check for the existence of files with a file manager application as this could overlook problems such as corrupt data or imagery tiles being delivered that don't contain actual data. As data are validated, tick items off against the specification list and tile index table.

1. Using a file manager application, ensure all ancillary information, metadata and reports have been delivered.
    a. Ensure files are of the required formats and use the required naming conventions.
    b. Open files to ensure they are not corrupt and contain the necessary information.
    c. If waveform data has been delivered, ensure there is a waveform data packet (WDP) file for each waveform LAS file.

2. View the tile index data and/or its properties in a GIS to ensure the tile size is as expected, that the tile origin and name is the south west corner of each tile and on a whole metre coordinate value, and the tile names are an attribute in the tile index.
3. For tiled datasets (i.e. LAS, DEM etc), check all tiles within each dataset have been delivered and tick off against the tile index table;
    a. Ensure the formats and naming conventions are correct. A quick check of a few tiles for each dataset will suffice, as consistency may be assumed.
    b. To check all tiles have been delivered, view the tiles and tile index in a GIS to ensure they are present, not corrupt and (at a coarse level) contain the necessary data.
        - *It is important to note that the number of tiles per dataset may not always match.* However, there should always be more LAS than DEM tiles. If discrepancies are found between the numbers of required and supplied tiles for any dataset, it is important to identify *why* the tile/s may be missing.
        - To check the reason for missing tile/s in a datasets, view in a GIS with contextual information such as imagery, coastline and/or water body data.
        - *There are a number of valid reasons why a tile may be missing, for example*; in inland areas LAS, contours and DEM usually have the same number of tiles unless there is a water body that causes a discrepancy. However, in coastal areas there can be more LAS tiles but less contour and DEM tiles e.g. the LAS can pick up a jetty extending into the sea whereas the ground points under the water are not captured so would not be in the contours or DEM.
    c. For LAS files it is worthwhile displaying the points by PSID to see if these values correctly represent the flight lines.
    d. As an additional validation step for LAS files, the open source LAStools lasvalidate can be run to check whether files conform to the LAS specification. This will also report whether the coordinate reference system is specified in the files which should be noted for the next section.
    e. Ensure you save or keep open the GIS projects with tiles loaded for following checks.
4. For swath datasets (i.e. unclassified LAS), check all swath files have been delivered and tick off against the lines in the trajectory shapefile;
    a. Ensure the formats and naming conventions are correct. A quick check of a few swaths files will suffice, as consistency may be assumed.
    b. To check all swaths have been delivered, view the swath files and trajectory shapefile in a GIS to ensure there is a swath file for each run line present in the trajectory shapefile and the IDs match. Ensure that files are not corrupt and (at a coarse level) contain the necessary data.
    c. Again, display LAS by PSID to ensure there is only one valid (non 0) PSID for all points in each swath.
5. Open and view all remaining spatial files i.e. non-tiled data such as mosaics, contours, control points etc. in a GIS. Save or keep open the data view for following checks.
    a. Ensure files are of the required formats and use the required naming conventions.
    b. Identify any data that is corrupt or doesn't contain the necessary information.
6. View the attribute tables of vector spatial files (i.e. flight trajectory, tile index, survey control, or contours) in a GIS to ensure the required attributes exist e.g. flight trajectories may require populated 'Date of Capture', 'Start Time' and 'End Time' attributes.
7. If there were any additional delivery requirements such as statistics and pyramids, ensure these exist for the relevant datasets.
8. Ensure all data and specifications checked have been ticked off against the specification list.

Checklist:

- ✓ Were all datasets delivered?
- ✓ Was all ancillary information delivered including waveform wdp files if relevant?
- ✓ Were all metadata and reports delivered?
- ✓ Were all tiles for all tiled datasets delivered?
- ✓ Were all swath files for swath datasets delivered?

- ✓ Was the tile index size and origin correct?
- ✓ Were all files of the specified formats?
- ✓ Were all files named correctly?
- ✓ Were vector spatial file attributes as specified?
- ✓ Did all spatial data open/read i.e. it was not corrupt and there were no glaring data omissions?
- ✓ Did PSIDs correctly represent flight lines in LAS files?
- ✓ Did LAS files conform to the LAS specification?
- ✓ Were any additional delivery requirements met?

Tools:

- File manager e.g. Windows Explorer
- GIS e.g. ArcGIS, Quantum GIS, GRASS GIS, SAGA GIS
- LAStools; lasvalidate

16.1.6 Coordinate System and Datum

The coordinates and height system of the LiDAR data need to support the data use. The horizontal coordinate system for all files should be checked for consistency and projection. LiDAR data in Australia is commonly projected to the Map Grid of Australia 1994 (MGA94).

The vertical datum is the surface to which all LiDAR heights are referenced. The Australian Height Datum (AHD) is used for most LiDAR surveys. AHD heights from LiDAR data are derived from ellipsoid referenced heights obtained from GPS/GNSS. Ellipsoid referenced LiDAR products can also be used for some applications. The typical ellipsoid product in Australia has LiDAR heights referenced to the GRS80 ellipsoid realised through GDA94.

AHD datasets typically use a geoid model to transform the ellipsoid heights to AHD. Currently, AusGeoid09 is the Australian standard. Where AusGeoid09 does not perform adequately, additional corrections may be applied to the heights of the LiDAR data so that they match the survey control.

The following aspects are checked as part of the coordinate system and datum check:

- The horizontal coordinate system of all spatial data
- The vertical reference system of all spatial data
- The geoid model applied to achieve AHD
- Whether any additional corrections were applied

Effective checking of the horizontal coordinate system requires spatial viewing of the data, as opposed to simply checking the data properties. It is possible that the horizontal coordinates may appear correct in the property definition however there may still be horizontal coordinate system problems if the data is located beyond the extent of the coordinate system. This would not become apparent until the data is viewed in a GIS. An example of a warning you may see when viewing such data in ArcMap is shown in Figure 16-12.

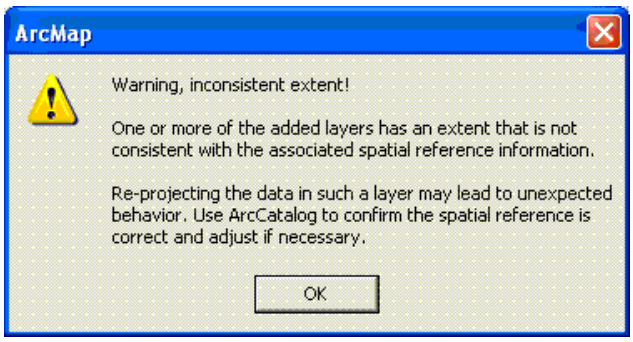

Figure 16-12 Coordinate system warning in ArcMap

Instructions:

1. Checking the horizontal coordinate system of spatial data should involve both investigating the coordinate system definition in the data properties, and viewing the data spatially to ensure it is located in the correct position compared to other data.
   a. If LAStools lasvalidate was run in the previous section on LAS files, you will already know whether the coordinate definition of the LAS files is correct. As an alternative to viewing LAS files, the open source LAStools lasinfo could be run which reports on points that fall outside of the bounding box, indicating a coordinate system problem.
   b. Use the GIS projects in which you have already loaded the data, to check it all appears in the correct location. If any data appears in the wrong location (see example in Figure 16-13), it most likely has a horizontal coordinate system issues.
   c. Investigate the spatial reference definition in the properties of any data in the wrong location to determine the problem and whether resupply or correction is required. For data that appears in the correct location, checking the spatial reference definition of a sample of each tiled dataset is sufficient.
2. The vertical reference of data is rarely specified within the properties of a dataset hence it is difficult to directly check. A basic check for the vertical reference is to compare the vertical datum/s required in the project specifications, to the information supplied in the project report regarding the vertical datums used. The absolute vertical accuracy check (section 16.2.5) may reveal problems with the reported vertical references.
3. Similarly, it is difficult to check the geoid model used directly from the data. Again, compare the specification with the project report information to ensure the geoid reported as used, was as specified.
   a. An additional option to check the geoid model used is to difference ellipsoid and AHD LAS and compare the difference to the specified geoid (i.e. AUSGeoid09), or difference the (AHD) DEM and specified geoid and compare the difference to the ellipsoid LAS. *Note that results are not expected to match exactly as you are comparing modeled and observed data. You should also be aware of any additional corrections applied.*
4. The project report should provide information on additional corrections that were applied to the data. Particularly, the magnitude of the shift, the computation for the shift and whether the shift was constant across the whole project, a tilted shift, or a modeled surface shift.
5. Ensure all data and specifications checked have been ticked off against the specification list.

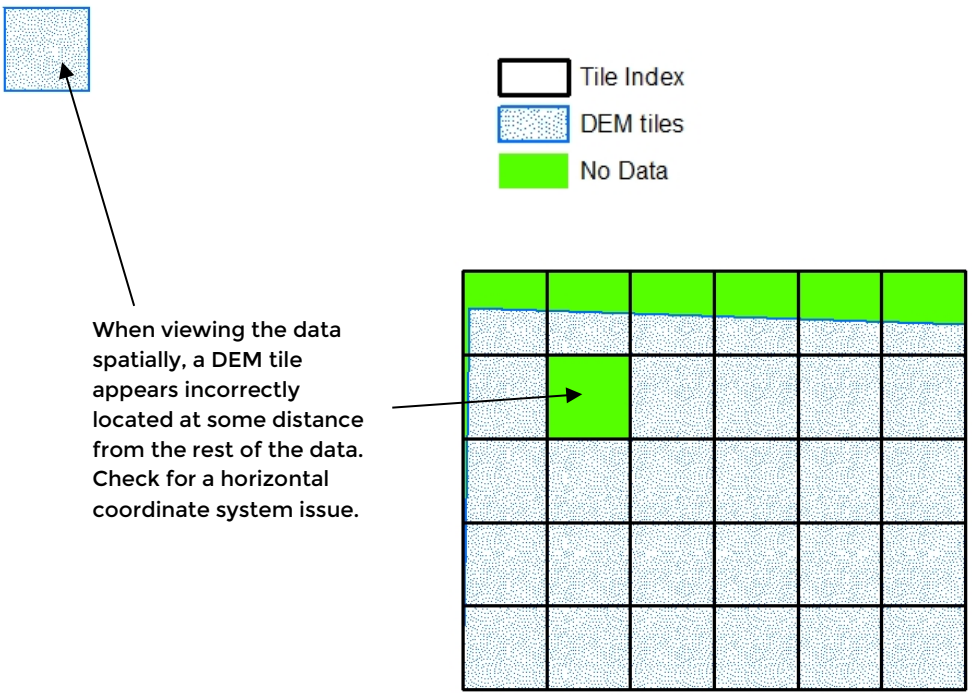

Figure 16-13 Example of a horizontal coordinate system error for one DEM tile.

Checklist:

- ✓ Were the horizontal coordinate systems of data correct?
- ✓ Were the vertical references of data correct?
- ✓ Was the specified geoid model applied?
- ✓ Were any additional corrections applied to achieve AHD?

Tools:

- GIS e.g. ArcGIS 10.1, Quantum GIS, GRASS GIS, SAGA GIS
- LAStools; lasinfo

16.1.7 Extent and Internal Coverage

The extent and internal coverage validation ensures that the LiDAR data covers the required area, and provides an assessment of the acceptability of any internal gaps. Figure 16-14 provides an example of the extent and internal coverage check.

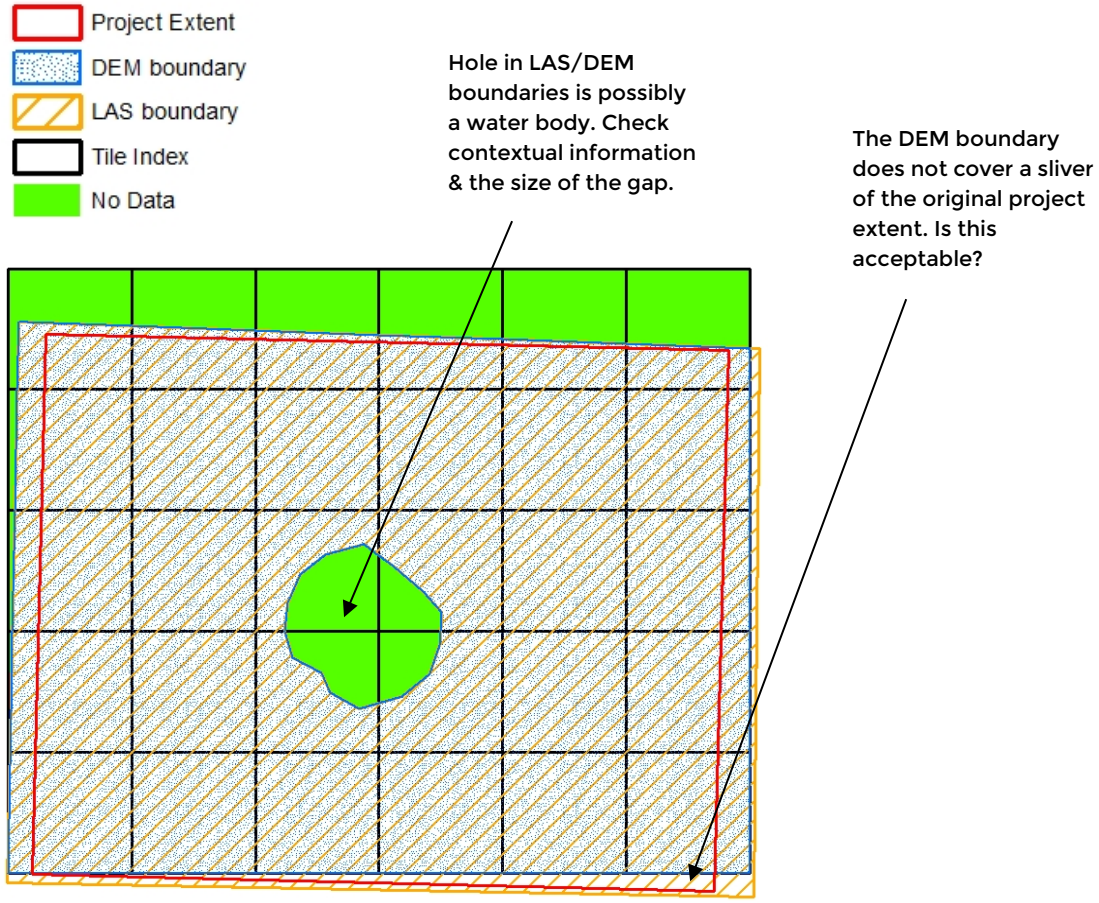

Figure 16-14 The extent and internal coverage check should display the required survey boundary, the tile index, and the boundary extents created for LAS and DEM.

The internal coverage provides an assessment of gaps within the LiDAR survey. Gaps can be caused inadvertently within the acquisition and processing, or can be a consequence of the on-ground features. Gaps between flight lines should not be present in the dataset. Gaps due to the presence of water are acceptable in the LiDAR point cloud. In the DEM the gap acceptability is determined by the interpolation rules defined in the specifications. Gaps between ground points can be assessed in the LAS point cloud to gauge the reliability of the DEM in areas under thick vegetation. In these areas the ground points are likely to be sparse.

Instructions:

This check is primarily for LAS and DEM tiled datasets.

1. Create an extent polygon for every LAS and DEM tile;
   a. For LAS files this could be achieved using a tool such as LAStools lasboundary (please check licensing requirements). *If using lasboundary apply internal holes and an appropriate concavity.*
   b. Alternatively, a raster surface could be created from the LAS with an appropriate cell size, and the raster converted to an extent polygon as in step c. However, this may not be worth doing if checking the DEM.
   c. For DEM files, a GIS could be used to create the extent polygons.

- *Do NOT simply convert the raster to polygon and dissolve the tiles into one extent as this can hide individual or small areas of pixels that are data voids.*
- One option is to create a DEM mosaic dataset and build footprints using the appropriate parameters for internal holes (ArcGIS).
- The alternative is to create binary DEM tile rasters representing areas of data versus data voids, and then mosaic (before conversion to polygon to avoid vertices at every pixel corner) and convert to polygon. Dissolve the polygon tiles but be careful of X and Y tolerances when dissolving as you need to maintain internal holes.

2. View the extent files created without fill (outlines only) in a GIS and ensure they cover the required extent of data capture.
   a. If the extent of the LAS and DEM data is correct, it can be assumed that the extent of other data will be correct. (Any gross extent errors for other datasets would have been noticed when viewing data for the *Delivery Completeness* check).
   b. If a whole dataset or any individual tiles do not overlap with the original extent polygon at all, it is most likely a horizontal coordinate system issue that would have been noticed in the *Coordinate System and Datum* check.
   c. If there appear to be missing tiles, ensure a valid reason was found for this in the *Delivery Completeness* check, otherwise data may require redelivery.
3. Ensure there are no internal gaps between parallel flight lines in the LAS data i.e. ensure there is complete coverage and flight line overlap. This can be done by viewing the LAS extents created overlayed with the flight line trajectories, or by using a tool such as LAStools lasoverlap (please check licensing requirements), which creates a raster showing how many flight lines cover each area of your extent (Figure 16-15).
4. Internal gaps due to the presence of water are acceptable in the LiDAR point cloud. Validate that any such gaps are legitimate water bodies by comparison to the intensity imagery, aerial imagery or any existing water body polygon data.
5. If there are internal gaps in the DEM data, be aware of the sizes of water bodies it is acceptable to triangulate across and when they should be voids e.g. the ICSM specifications state that acceptable sizes for non-tidal water bodies are of surface area greater than 625m^2, and non-tidal water courses greater than 30m nominal width.
6. Make note of any additional data supplied outside the original extent. All subsequent checks should only be conducted on data *within* the original specified extent as data outside the required extent is frequently not processed to the specified level.

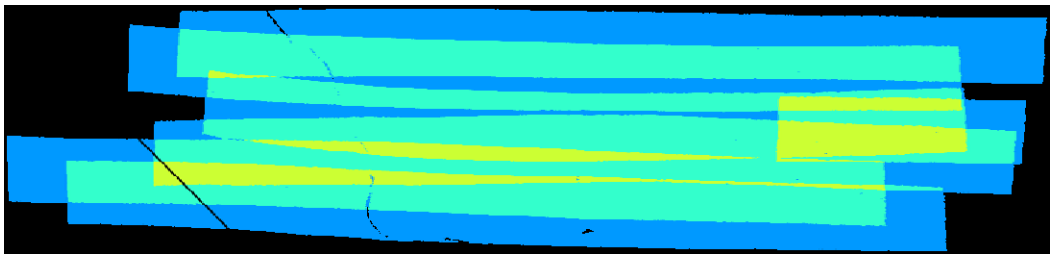

Figure 16-15 LAStools lasoverlap output example; blue represents coverage by one flight line, green by two and yellow by three (Isenburg, 2013)

Checklist:

- ✓ Was the specified capture extent met?
- ✓ Was there complete coverage i.e. no gaps between parallel flight lines?
- ✓ Were any internal holes found in the data legitimate?

Tools:

- GIS e.g. ArcGIS 10.1, Quantum GIS, GRASS GIS, SAGA GIS
- LAStools; lasboundary, lasoverlap

16.1.8 Survey Control

Survey ground control is used to check and/or correct the heights of the LiDAR data points. The survey control is generally gathered by the LiDAR acquisition company, however independently gathered survey control may be used to verify the heights of the LiDAR data.

There are two types of control points gathered during the ground control survey. High accuracy ground control points (GCPs) which are used to establish the datum in the survey area, and check points (CPs), which are subsequently gathered to assess the accuracy of the LiDAR data. Both sets of points should have their datum established independently of the LiDAR dataset.

Ground control points can be external to the survey area and should assess the geoid separation and variation of the reference surface and/or geoid model across the survey area. Check points need to be internal to the survey area. These should be gathered in open, flat areas to assess the fundamental absolute vertical accuracy of the LiDAR dataset.

The ground control points and check points need to be acquired to the same datum (reference surface) as the LiDAR data. Where applicable the points can be measured to both the ellipsoid and AHD surfaces, so that comparisons can be made to both sets of LiDAR products if acquired.

Ground control acquisition for a LiDAR survey is usually conducted with differential GPS. However, any existing ground points within a survey area may be used to assess the accuracy of the LiDAR data. The quality of the heights and their relationship to the ground surface need to be accounted for in any comparisons.

The ground control points and check points are gathered in open, flat ground so that the effects of slope and non-ground features are reduced. Check points should not be gathered too closely to non-ground features in the LiDAR survey. Sports ovals, car parks and roads generally make ideal check point sites.

Additionally, vertical reference points are often gathered in different cover and ground types to assess the supplemental LiDAR accuracy in areas of relevance to a project. The reference points may be gathered in different types of vegetation cover, or on different ground slopes such as around and along rivers. Supplemental accuracy checks are addressed in section 16.2.10.

Where possible photographs should be gathered and supplied with all points gathered as part of the project. Photographs can provide context for the points, especially if anomalies are found in comparisons with the LiDAR data.

Instructions:

There are *four* aspects to this check; openness/flatness rating, collection method, control point density, and control point distribution.

1. ***Openness/Flatness***
   a. Determine the suitability of the control points (CPs and GCPs) for use in vertical accuracy testing, by determining how open and flat the area surrounding each control point is. When analysing the suitability of points for the vertical accuracy assessment you will need to develop an acceptability system for openness and flatness. A suggested system is provided below.
   b. Rate the '<u>openness</u>' of the area around each control point;
      - Determine the percentage of non-ground classified (i.e. vegetation or building) LiDAR points out of all LiDAR points within a 10m radius of the control point.
      - Also check the classification of non-ground points and if there are any class 5 (high vegetation) or class 6 (buildings) within the 10m radius, that control point cannot be rated highly.
      - If your LiDAR data does not have the non-ground points classified, check the heights of unclassified points within the 10m radius and if there are any greater than 2m different to the control point, that control point cannot be rated highly.

- These steps may be done by adding the control points and LAS to a GIS, viewing the LAS by classification, buffering the control point and using identity, selection and measuring tools.

c. Rate the 'flatness' of the area around each control point;
   - Using only the LiDAR points classified as *ground* within a 2m radius of the control point, determine the height differences of these ground points to the control point and average these as absolute values. The American Society for Photogrammetry and Remote Sensing (ASPRS) suggest that slope should be less than 10% (ASPRS, 2014).
   - This may be done by adding the control points and LAS to a GIS, viewing the LAS by classification, buffering the control point, and using identify tools.

d. If the 'flatness' or 'openness' rating is unacceptable for a point, you may not want to use the control point in the following survey control checks or to test the absolute vertical accuracy of the data. Whether a control point is unacceptable is up to the user. You may decide to use all control points in the survey control and absolute accuracy check regardless.

2. Collection Method

a. Check the project report for the following information (you will require some knowledge of control surveys to determine whether the methods and explanations provided denote adequate survey technique);
   - Method used to collect GCPs
   - Explanation of GCP connection to AHD
   - Method used to collect CPs
   - Explanation of CP connection to AHD

3. Control Density

a. Check whether an adequate number of points were collected for the survey area i.e. the density of the control network. Determine the survey area from the original extent polygon or LAS extent created in the *Extent* check. The density of the control network is then rated in two modes as follows.

b. A Pass/Fail is given based on the following minimum points per square kilometer;
   - 0 - 100km^2: ≥5 CPs + minimum 3 GCPs
   - 100 – 400km^2: ≥20 CPs + minimum 5 GCPs
   - ≥400km^2: 20 CPs + 1 CP for every 50km^2 over 400km^2 + minimum 5 GCPs

c. In addition, a score can be given for the density of points per square kilometre (e) given by the following equation;

$$e = \frac{n}{a}$$ where a = project area (km^2)
n = number of CPs + internal GCPs

The score given will depend on the rating system you develop.

4. Control Distribution

a. Rate the distribution of CPs and internal GCPs across the survey area. The ICSM specification states that, the distribution 'must be established to adequately cover the full extent of the survey area, and be representative of the project area landscape'. This can be determined visually using the Figure 16-16 examples as a guide. A rating system will need to be developed.

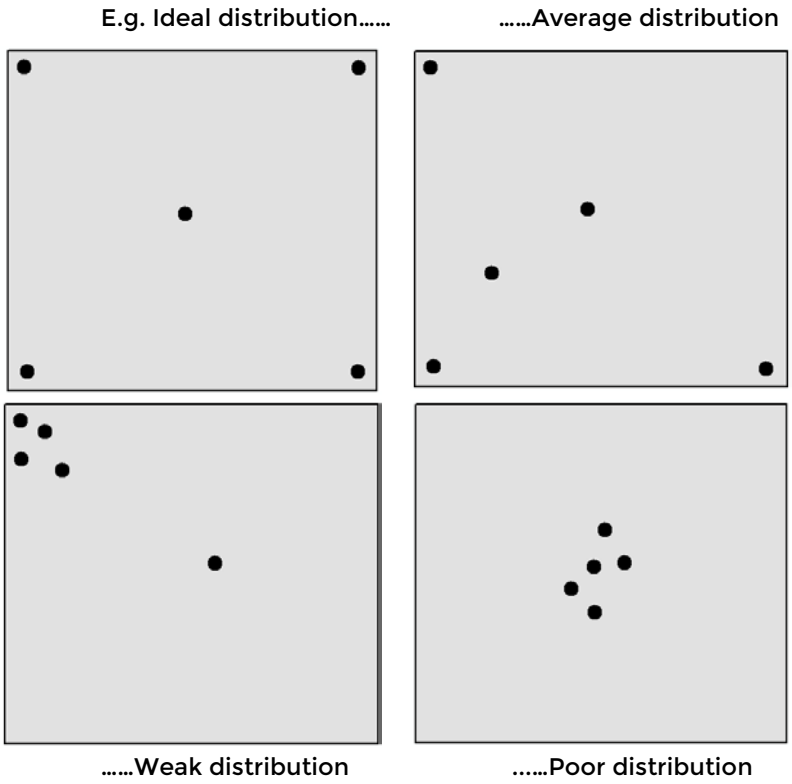

Figure 16-16 Example survey control distributions

5. The results of the control density and distribution checks can then be combined into an overall rating for the survey control and reported with the minimum number of points pass/fail results.

Checklist:

- ✓ Were all control points used in accuracy testing acceptable in terms of 'flatness' and 'openness'?
- ✓ Was the GCP report clearly written and presented?
- ✓ Was an appropriate method used to collect GCPs and connect them to AHD?
- ✓ Was an appropriate method used to collect CPs and connect them to AHD?
- ✓ Was the number of GCPs adequate for the survey area?
- ✓ Was the number of CPs adequate for the survey area?
- ✓ Was the density of CPs and internal GCPs acceptable?
- ✓ Was the distribution of CPs and internal GCPs acceptable?
- ✓ Was the overall survey control rating acceptable?

Tools:

- GIS e.g. ArcGIS 10.1, Quantum GIS, GRASS GIS, SAGA GIS

16.1.9 Vertical Accuracy

There are two types of vertical accuracy; absolute and relative. Absolute vertical accuracy refers to the alignment of the LiDAR data to the required vertical datum. The relative vertical accuracy refers to the internal alignment of the LiDAR data to neighbouring points within the dataset, particularly in regards to points gathered from adjacent flight lines.

Some applications rely on the accurate measurement of features within the survey, and therefore should place more emphasis on the relative accuracy. Depending on the application for which the validation is being performed a more detailed assessment can be performed on the absolute or relative vertical accuracy.

In Australia the absolute vertical accuracy is generally assessed for the orthometric products and/or the ellipsoid products. The orthometric products are usually referenced to the Australian Height Datum (AHD) – as determined by the published heights of local survey control marks within or adjacent to the project extent. The ellipsoid products are often referenced to the GRS80 ellipsoid realised through the GDA94 reference frame.

The fundamental absolute vertical accuracy standard used for most LiDAR surveys is ±30cm @ 95% confidence interval (1.96 x RMSE). Previous reporting of vertical accuracy has generally referred to ±15cm @ 68% confidence interval. The vertical accuracy of a LiDAR survey is assessed against ground points in open, flat areas.

The relative vertical accuracy is assessed by comparing the overlapping LiDAR points from adjacent flight lines.

Instructions:

Before using the control points (CPs and GCPs) internal to the survey area to test the absolute vertical accuracy of the LiDAR, determine how open and flat the area surrounding each control point is and hence its suitability for use in testing. You can use datasets with less reliable control points however this should be taken into account within the analysis. When analysing the suitability of points for the vertical accuracy assessment you will need to develop an acceptability system for openness and flatness. A suggested system was provided in section 16.2.4. Once you have decided which control points are acceptable to use in vertical accuracy testing, proceed with the below.

1. Compute the height differences between the LAS and acceptable LiDAR provider control points and hence the absolute vertical accuracy;

a. Interpolate the LAS data classified as ground in the vicinity of each control point (perhaps a 10m radius) into surfaces, using nearest neighbour or triangulation (TIN). Extract the LAS height ($Z_{data\ i}$) at each control point location from your interpolated surfaces and compute the differences between these and each associated control point height ($Z_{control\ i}$). This may need to be performed for both AHD and ellipsoid heights if applicable.

b. Use these height values to compute the RMSE and absolute vertical accuracy at 95% confidence interval for each type of control (ICSM, 2008).

$$RMSE = \sqrt{\frac{\sum(Z_{data\ i} - Z_{control\ i})^2}{n}}$$

$$Accuracy_Z = 1.96 \times RMSE_Z$$

c. Compare the computed accuracy values to the specified and reported accuracies (separately for AHD and ellipsoid values if applicable) to determine a pass or fail for each type of control.

d. Alternatively this can be done with LAStools lascontrol (please check licensing requirements).

2. Compute the height differences between the DEM and acceptable LiDAR provider control points and hence the absolute vertical accuracy;

a. This can either be done by directly extracting the DEM value at each control point (preferred method of ASPRS), or by interpolating the DEM height at each control point location using surrounding DEM cell values. This will only need to be performed for AHD as DEMs are always orthometric.

b. Use the DEM heights and associated control point heights to compute the RMSE and absolute vertical accuracy at 95% confidence interval for each type of control as per the equations for LAS in step 1.b.

c. Compare the computed accuracy values to the specified and reported accuracies to determine a pass or fail for each.

3. If any additional control (e.g. state benchmarks) or adjacent overlapping data with known accuracies exist, these can also be used to test the accuracy of the LAS and DEM in the same way.

To test the swath-to-swath relative vertical accuracy, the heights of the LAS ground point data must be compared across flight lines. This can be done via a profile sampling method or by creating difference rasters across the whole dataset. Within swath relative vertical accuracy can also be tested but is not addressed here.

1. Profiling;
   a. Load the LAS point data into a GIS and display the ground points only by elevation to visually check there is no flight line striping effect.
   b. Create a series of sample profiles perpendicular to the flight line direction, across each pair of adjoining flight lines to visually check the vertical alignment of ground points is acceptable.
   c. If a difference raster cannot be created, a sampling method could be used to estimate the relative vertical accuracy. Heights of neighbouring points classified as ground from pairs of adjoining flight lines could be differenced, averaged, and used as an estimate of the relative vertical accuracy.

2. Difference raster;
   a. Create a ground point elevation raster (DEM) per flight line (LAS files require that the flight line number is correctly attributed in the point source ID field of each point data record)
   b. Combine these rasters to produce a difference raster for the project showing the maximum difference between flight lines at every cell in the project area by following these steps;
      - Mosaic the flight line DEMs into one raster using a mean operator to get a surface of the average elevation
      - Subtract each flight line DEM individually from the average DEM and convert each difference flight line to absolute values
      - Mosaic the flight line difference rasters back into one raster using a maximum operator to get a surface of the maximum elevation difference
   c. Calculate the RMSE and relative vertical accuracy at 95% confidence interval using the formula in step 1.b. used for absolute vertical accuracy. The values in the relative vertical accuracy maximum difference mosaic are the result of '$Z_{data\ i} - Z_{control\ i}$'. Ignore no data values in the calculation i.e. only consider the areas of overlap.
   d. Alternatively, a tool such as *LAStools lasoverlap* could be used which produces a difference raster in a single step (Figure 16-17) but please check licensing requirements.

3. Compare the relative vertical accuracy results to the specified and reported accuracies.

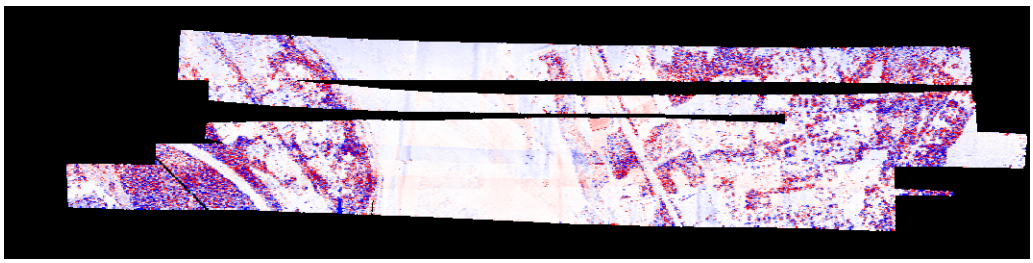

Figure 16-17 LAStools lasoverlap example output; colour ramp that maps blue to -2.5m, white to 0, and red to 2.5 (Isenburg, 2013).

Checklist:

- ✓ Were all control points used in accuracy testing acceptable in terms of 'flatness' and 'openness'?
- ✓ Was the absolute vertical accuracy of the data (LAS and DEM) relative to LiDAR provider control points within specification?
- ✓ Was the absolute vertical accuracy of the data (LAS and DEM) relative to any other control data within specification?
- ✓ Was the relative (or internal) vertical accuracy of the LAS data between flight lines acceptable?

Tools:

- GIS e.g. ArcGIS 10.1, Quantum GIS, GRASS GIS, SAGA GIS
- LAStools; lascontrol, lasoverlap

16.1.10 Density and Resolution

The density and resolution check assesses the point spacing (density) in the LiDAR point clouds, and the cell size (resolution) of the derived raster data products. These checks are performed to validate that the level of detail in the LiDAR data meets the user requirements.

The density validation can potentially evaluate five different point densities in the LiDAR point cloud. Each of which is listed in Table 16-1.

Table 16-1 Point Density Definitions

Point Density Type	Definition
All Point Density	The number of successful ground and non-ground point returns (1st, 2nd, 3rd AND last return) over a set area (e.g. more points are returned in vegetated areas due to the presence of 2nd & 3rd returns).
Ground Point Density	The number of successful ground point returns (1st, 2nd, 3rd OR last return) over a set area, which equates to removing all non-ground points from the point density (e.g. a typical ground point density required to generate a DEM is 2 points per square metre).
First return point density	The number of successful 1st (or last) returns over a set area which could be ground or non-ground (e.g. only by examining first return or pulse density will you find areas of greater density in a project).
Points at Nadir	The number of successful ground and non-ground point returns (1st, 2nd, 3rd AND last return) over a set area at nadir (e.g. 10% of swath width).
Pulse density	The number of outbound pulses (not necessarily successful returns) over a set area. This cannot be directly measured as non-successful returns are not recorded in LiDAR point clouds. However it can be simulated using 1st (or last) return and excluding data gaps to get a measure of 'pseudo-pulse density'.

The results of the point density check can vary within projects and between projects. The results will ideally yield densities per flight line, and can be plotted spatially to indicate areas of lower and higher densities, giving the user a sense of any areas of concern.

The all point density should show greater densities in vegetated areas as multiple returns will be recorded in a tree's canopy (Figure 16-18). The ground point density will potentially be lower in these areas as the ground can be obscured by the vegetation. The ground point density will also reveal areas of water. The first return point density should be relatively consistent across the project, with gaps only present between flight lines, if the coverage was inadequate, or in areas of water providing no returns. The points at nadir density, enables a density assessment for the whole project to be conducted without the influence of flight line overlap, or influences of a reduced point density at the outer swath.

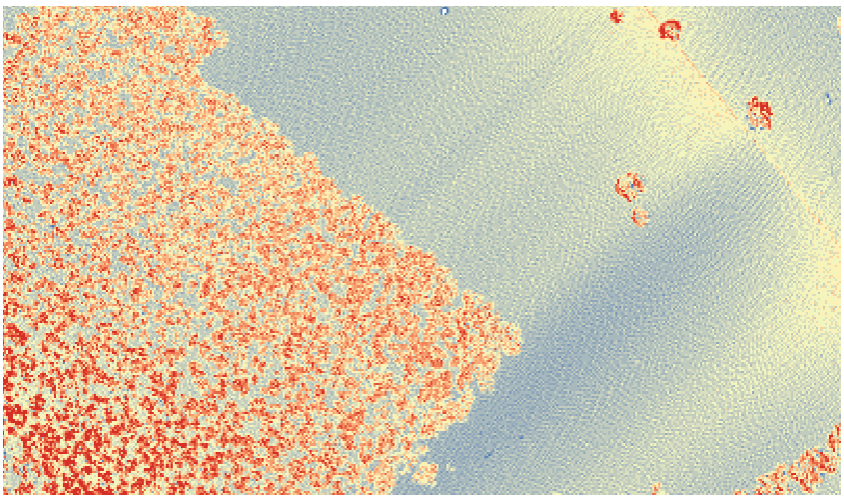

Figure 16-18 Example of an all point density raster, with high density areas in red (treed), and low density areas in blue (open ground).

The pulse density (Nominal Post Spacing - NPS) is used in the standard specifications as a requirement by the LiDAR provider however this cannot be directly measured as non-successful returns are not recorded in LiDAR point clouds. Therefore, the first (or last) return point density can be used to replicate the pulse density, creating a 'pseudo-pulse density'. In contrast to the other point densities, internal data gaps should be ignored in measuring the pseudo-pulse density as their inclusion will inadvertently lower the assessed pulse density.

Instructions:

This QA focuses on *All Point Density*, *Ground Point Density,* and *Pseudo-Pulse Density*, by producing density grids and/or statistics for each type of density. You may also wish to compute points at nadir.

1. Choose a cell size at which to produce the all and ground point density rasters. This should be between 2m and 10m. An appropriate value may be about 4 times the specified point spacing of the data to produce a good visual representation of density.

2. ***All Point Density;***
   a. Calculate the density using *all points* in every cell (of your chosen size) for every LAS tile. This may be best achieved by producing a density raster using your chosen cell size – this provides a visual representation of *All Point density*.
   b. To find the point density per metre squared, divide each cell density value by the cell size squared (or just use a 1m cell size to create the raster; however this will increase the storage size of your raster).
   c. Average the *All Point Density* cell values for each tile in the project and store this against your tile index for reporting. Include cell values with zero density so that gaps and water bodies are accurately represented.
   d. If you have the time to be meticulous, exclude cells on the boundaries of the project which may only be partially filled with data, to avoid incorrect low density values. However, depending upon the project, such boundary cells may not be statistically significant for project density results (although some tiles may fail), so this is optional.
   e. Average the *All Point Density* tile values for the project and include this on the final validation report.
   f. You may see higher density in overlap areas between flight lines depending on how your data were supplied (i.e. if overlap points were removed or retained – they should be retained).

3. ***Ground Point Density***
    a. Repeat steps 2.a – 2.e under *All Point Density* but this time for the density calculations only use *points classified as ground*.
4. ***Pseudo-Pulse Density***
    a. As the pulse density can vary for each flight line this density is reported per flight line not per tile, to avoid overlap points between flight lines skewing the results.
    b. Calculate the density using *first (or last) return points* in every cell, for every flight line in every LAS tile. Two filters will need to be applied for this density calculation; one to include only first (or last) return points and the other to include only points in the same flight line. The flight line of points can be identified by the points "Point Source ID" attribute in the LAS file.
    c. This may be best achieved by producing a density raster for every flight line in your project using a *1m cell size*.
    d. Average the pseudo-pulse density cell values for each flight line. For this density measure, exclude cell values with zero density from the averages as we are trying to simulate pulse density, and know non-successful returns are not recorded.
    e. Again, if you have the time to be meticulous, exclude cells on the boundaries of the project which may only be partially filled with data, to avoid incorrect low density values. However, depending upon the project such boundary cells may not be statistically significant for flight line density results, so this is optional.
    f. To determine if each flight line meets the point density specification, compare the averaged pseudo-pulse density value for each flight line to the specification and give each flight line a pass/fail.
5. To test the raster resolution, simply check the cell size property of the DEM and compare it to the specification.

Checklist:

- ✓ Did the pseudo-pulse density of the LAS data meet the NPS specification?
- ✓ Did the resolution of the raster data meet the specification?
- ✓ Were the ground point and all point density statistics acceptable?
- ✓ Did the ground point and all point density rasters appear free of density issues?
- ✓ Was the ground penetration (*Ground Point density*) in vegetated areas acceptable?

Tools:

- GIS e.g. ArcGIS 10.1, Quantum GIS, GRASS GIS, SAGA GIS
- LAStools; lasinfo, lasgrid (check licensing requirements)

16.1.11 Classification

Point classification is the process of categorising points to features. The classification validation may be skipped for projects which only require unclassified points. The typical point classifications are ground, low vegetation (0 – 0.3m), medium vegetation (0.3 – 2m), high vegetation (>2m), buildings and structures, spurious high/low point returns, model key points and water. Additional point classifications can be added for application specific features.

The typical classification process is both automated and manual. The level of manual inspection and editing will dictate the quality of the classification. Figure 16-19 shows a basic ground (orange points) and non-ground (grey points) classification product. The classification validation typically analyses the ground points via the DEM. Analysing the full point cloud classification can be a time consuming process and is typically performed by sampling areas of concern, or potential error. Such areas will have a variety of non-ground features, low-lying vegetation and water.

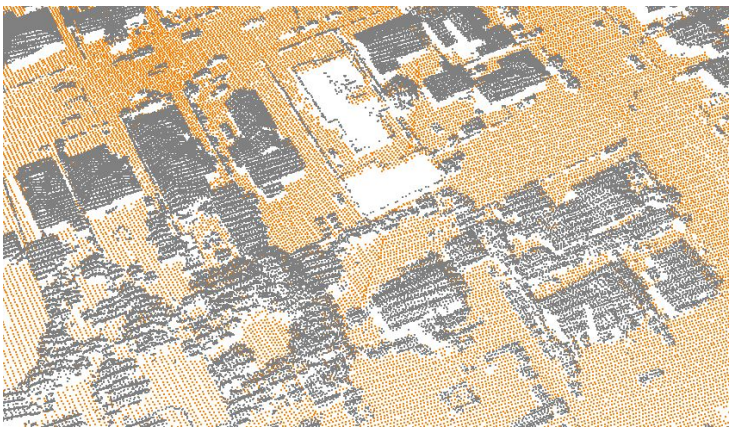

Figure 16-19 Ground and Non-Ground LiDAR Classification

The classification validation involves a visual inspection of the data, as well as a statistical analysis. The classification validation can be the most time consuming validation step as it is mostly a manual process. The statistical analysis needs to be interpreted by the user to identify any anomalies. For instance there should be buildings classified in urban areas, and there should not be vegetation with negative heights. If your survey required certain classes, the statistics will highlight whether these have been delivered.

Instructions:

1. ***Statistics***
   a. Produce the following classification statistics using a tool such as LAStools lasinfo or a GIS tool which extracts point file information and allows summary by classification;
      - Number of points in each class
      - Percentage of points in each class
      - Z minimum for each class
      - Z maximum for each class
   b. Statistics can be produced for the whole project, and/or on a tile or area (i.e. urban, rural) basis.
   c. If there are points in classes 0 or 1, make a note in the validation report that there remains unclassified point data.
   d. There should not be any class 12 'overlap' points, as points in flight line overlap areas are expected to be classified.
   e. Check that total point counts of each LAS dataset match i.e. AHD LAS, ellipsoid LAS and unclassified swath LAS (if applicable), should all have the same total number of points.
   f. Unclassified swath LAS should only contain point class 0.

2. ***Visual***
   a. First, decide whether to visually check every tile in the project, or whether to sample a reduced number of tiles.
   b. To check the ground classification, produce a mosaic of the DEM if one was not delivered and display it in a GIS along with the tile index. View the DEM mosaic using bilinear re-sampling and symbology from the current display extent (not the whole mosaic) to increase the colour variation when inspecting each tile area.
   c. If you wish to assess the classification of non-ground points, the LAS point data must be viewed which will be time consuming.
   d. When assessing the classification, display coincident aerial photography if available.
   e. Display *no data* values of the DEM in a contrasting colour to your DEM symbology so they can be easily differentiated.
   f. Display the edges (perhaps ~100m) of the surrounding tiles so edge issues can be detected.

g. Hill shades of the DEM tiles can also be created to assist visual assessment.
h. Display the DEM maximum and minimum values as part of the symbology and *note that if the DEM tile has a large elevation range it may be harder to spot errors.*
i. If checking all tiles, step through them one by one in a systematic manner (each tile may take from 5 seconds up to 15 minutes to check).
j. If sampling tiles, adopt an 'intelligent random sampling' approach i.e. target areas that are steep, urban, vegetated, coastal or near water bodies as these are more difficult to classify and hence prone to errors in classification.
k. If large error/s are found in a tile when sampling, it is advisable to check the eight surrounding tiles as well.
l. As each tile is checked, attribute the tile index to signify that the tile has been checked and identify if any errors were found.
m. If errors are found within a tile, create a polygon or point dataset to digitise the specific location of the problems and provide further explanation as part of the attributes. You may come across systematic errors as well as classification errors.
n. If deemed necessary, save screen grabs (i.e. jpegs) of any tiles with errors and hyper-link to these in the tile index.

Checklist:

- ✓ Were all required classes present?
- ✓ Was the data free of classes that the specification deemed must not be present?
- ✓ Were there any gross errors found i.e. trees with negative heights?
- ✓ Was there any unclassified data remaining?
- ✓ Were class 12 overlap points used?
- ✓ Did the total point counts of LAS datasets match?
- ✓ Was unclassified swath data all class 0?
- ✓ Did the visual check deem the classification acceptable?

Tools:

- GIS e.g. ArcGIS 10.1, Quantum GIS, GRASS GIS, SAGA GIS
- LAStools; lasinfo
- LAS viewer e.g. Mars, Fusion, Global Mapper, Fugro Viewer, FME, LiDAR Viewer

16.1.12 Reports

Identifying that all reports have been delivered with the appropriate content provides context to the survey outside of the datasets. The previous validation tests mainly relate to the LiDAR data and derived products. However, not all check elements can be identified easily within the data. The main details which influence the quality of the LiDAR should be reviewed in the survey report. Two important details to review are:

- The environmental conditions at the time of survey; and
- The scan angle of the LiDAR sensor.

Outside of these details, most other checks can be performed against the LiDAR data. If some of the previous validation steps are skipped, details of similar tests performed by the provider can frequently be found in the survey report. The validation results can also be compared to the provider's quality assurance testing results provided in the survey report.

Additional details, such as the flight equipment and parameters, can be found in the survey report. Although, the influence of these details on the LiDAR data are difficult to determine without prior knowledge of the sensor, platform and their parameters.

Instructions:

These things are difficult to detect from the data so the information on the project report can be used.

1. Compare the project report information with the original specification to ensure the following are as specified;
   a. Environmental conditions
   b. Scan angle

2. There are two additional options to check the scan angle.
   a. Check the LAS point information as the scan angle is an attribute in the LAS point data record "Scan Angle Rank (-90 to +90) – Left side" (however it is easy to manipulate).
   b. A more rigorous option would be to mathematically compare it to the flying height and swath width from the report information (see Figure 16-20). Beware that these parameters can vary over different types of terrain i.e. swath width will be smaller in higher terrain.

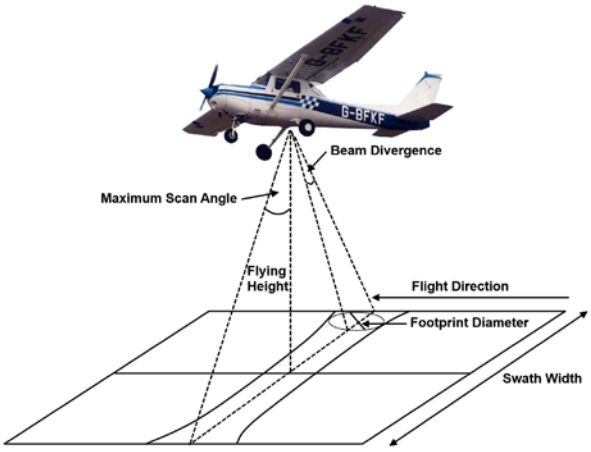

Figure 16-20 The scanning principle; the swath width and footprint diameter can be used to geometrically derive the scan angle.

Checklist:

- ✓ Were the environmental conditions as specified?
- ✓ Was the scan angle as specified?

16.1.13 Additional Products

The ICSM standard specifications contain three products in addition to the point and raster LiDAR data. These derived products are:

- Contours
- Fractional Cover Model (FCM)
- Canopy Height Model (CHM)

Each of these products can be validated. At the minimum their presence in the delivery should be checked if they are required. The fractional cover model and canopy height model (Figure 16-21) can have their values checked using the LiDAR points. For definitions of these layers check the standard LiDAR specifications. Checking a sample of points will enable the algorithm used to derive each model to be verified.

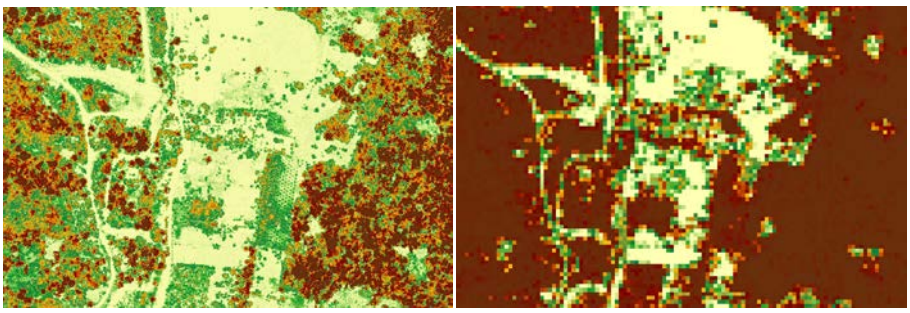

Figure 16-21 Example Canopy Height Model (left) and Fractional Cover Model (right).

The contours should be checked against the DEM for correct heights. They should also be checked for the number of vertices, line smoothness, topology and continuity.

Instructions:

1. Contours;
    a. Check the contour interval or height separation between successive contour lines via the attributes
    b. Check the topology of the contours or connections between contour lines have no intersections or dangles
    c. Check the continuity of the contours by checking lines of the same elevation are single continuous lines
    d. Check the number of vertices and smoothness of the contour lines by visualising the data at an appropriate scale
2. CHM check a sample of bins by subtracting the lowest points from the highest points in the LAS file and comparing to the equivalent location in the CHM. There should not be any negative values.
3. FCM check a sample of bins by using LAS file classifications to determine the percent of foliage in each bin, compare it to the equivalent location in the FCM. Values should range from 0-100.

Checklist:

- ✓ Were the contour vertices, smoothness, topology, and continuity acceptable?
- ✓ Was the CHM acceptable?
- ✓ Was the FCM acceptable?

Tools:

- GIS e.g. ArcGIS 10.1, Quantum GIS, GRASS GIS, SAGA GIS

16.1.14 Extra Validation

The LiDAR validation listed in this chapter covers the fundamental components of the LiDAR data. However, there are always additional and more rigorous checks which can be performed. The most obvious validation steps not outlined in the chapter are:

- Supplemental absolute vertical accuracy
- Horizontal Accuracy
- DEM and DSM Interpolation
- DEM Hydro Flattening

The four checks above are not typically performed on LiDAR data and their derived products. However, this does not mean that they cannot be performed should the need arise.

The supplemental absolute vertical accuracy can be checked if supplemental check points have been collected. These check points are gathered in different types of vegetation cover, or on different ground slopes such as around and along rivers. The absolute vertical accuracy check would be repeated using these points, omitting the flatness and openness check, and results summarised by land cover type.

The horizontal accuracy can be checked by comparing the intensity grid of the LiDAR data to independent aerial imagery and non-ground features. It can also be checked by collecting horizontal control points using non-ground features such as fence posts or building corners. These features can then have their position checked in the LiDAR data.

The DEM and DSM interpolation technique can be checked within the LiDAR data gaps. The interpolation algorithm and settings should match the user requirements. The interpolation rules can differ from project to project. It is now common that no interpolation is performed across large LiDAR point gaps on the raster data. Small gaps will have some interpolation performed to create the grid.

Hydro flattening is the process of leveling all DEM heights around a water body. The hydro flattening validation involves testing that the heights of all raster cell values around a lake or water body are equal. The DEM can also be checked for the amount of hydro flattening to see if it has been applied to all the expected locations.

16.1.15 Conclusion and Future Work

Numerous validation checks have been presented in this chapter. A selection of these checks may be performed depending upon relevance, and resources. A pass for all checks means the data is fit for use. Fails require either data redelivery or correction, if it is deemed the nature of the fail will impact upon the project analysis or outcomes.

Around mid 2015, some of the validation steps outlined in this chapter are to be included in an automated LiDAR compliance and quality assurance tool (QA^{4}LiDAR). This tool is currently being developed by the Cooperative Research Centre for Spatial Information (CRCSI), with the support of State and Commonwealth Governments. The software tool is aimed at providing an easy to use mechanism for contracting authorities, and data users to perform standard independent compliance testing on their LiDAR data. LiDAR providers can also use the tool and supply the output report to users.

QA^{4}LiDAR has been developed to complement the ICSM LiDAR Specification Template and ensure the validation is performed using a standard methodology. It has also been developed to ensure that LiDAR data is captured and delivered to Australian ICSM standards. QA^{4}LiDAR returns a standard compliance and QA report, as well as supporting information to the user. This report will provide transparency to the user on the quality of the LiDAR data.

References

American Society for Remote Sensing and Photogrammetry. (2014). ASPRS Positional Accuracy Standards for Digital Geospatial Data edition 1, version 1 <http://www.asprs.org/a/society/committees/standards/Positional_Accuracy_Standards.pdf>

Intergovernmental Committee on Surveying and Mapping. (2010). ICSM LiDAR Acquisition Specification and Tender Template version 1.0, <http://www.icsm.gov.au/elevation/LiDAR_Specifications_and_Tender_Template.pdf>.

Intergovernmental Committee on Surveying and Mapping. (2008). ICSM Guidelines for Digital Elevation data version 1.0, <http://www.icsm.gov.au/elevation/ICSM-GuidelinesDigitalElevationDataV1.pdf>.

Isenburg, M. (2013). lasoverlap raster, digital image, rapidlasso, <http://rapidlasso.com/category/quality-checking/>

Quadros, N. (2013). Unlocking the Characteristics of Bathymetric Sensors. LiDAR News Volume 3 Issue 6, p. 62-67.

Acronyms

AHD	Australian Height Datum
ASPRS	American Society for Photogrammetry and Remote Sensing
CHM	Canopy Height Model
QA4LiDAR	Compliance and Quality Assurance Tool for Airborne LiDAR
CP	Check Point
CRCSI	Cooperative Research Centre for Spatial Information
DEM	Digital Elevation Model
DSM	Digital Surface Model
FCM	Fractional Cover Model
GCP	Ground Control Point
GDA94	Geodetic Datum of Australia 1994
GIS	Geographic Information System
GPS/GNSS	Global Positioning System / Global Navigation Satellite System
GRS80	Geodetic Reference System 1980
ICSM	Intergovernmental Committee for Surveying and Mapping
LAS	LASer file format
LiDAR	Light Detection and Ranging
MGA94	Map Grid of Australia 1994
NPS	Nominal Post Spacing
QA	Quality Assurance
RINEX	Receiver Independent Exchange format
RMSE	Root Mean Square Error
TIN	Triangulated Irregular Network
WGS84	World Geodetic System 1984

Chapter 17. Australian examples of field and airborne TERN Landscape Assessment campaigns

K.Johansen[1]*, R. Trevithick[2], M. Bradford[3], J. Hacker[4], A. McGrath[4], W. Lieff[4]

[1] The Remote Sensing Research Centre / Joint Remote Sensing Research Program, School of Geography, Planning and Environmental Management, The University of Queensland

[2] Remote Sensing Centre / Joint Remote Sensing Research Program, Department of Science, Information Technology and Innovation

[3] CSIRO Land and Water

[4]Airborne Research Australia / Flinders University

*Corresponding author:
K.Johansen@uq.edu.au

Abstract

TERN's Landscape Assessment platform (also known as TERN Landscapes) has undertaken nine field and airborne campaigns within selected Australian biomes between January 2011 and June 2013 as part of the calibration and validation program to support the production of continental scale satellite based time-series of biophysical parameters. Many national and international approaches were reviewed during the development phase, and the field and airborne data collection approaches and protocols developed have been based on their suitability and adaptability to different Australian environments, while still upholding national and international standards. Another focus was also to ensure the data collected were suitable to multiple uses and purposes to support a wide range of ecosystem science, research and environmental management activities in Australia. This chapter will present an outline of the main activities involved in planning and executing the nine field and airborne campaigns and hence will provide a useful set of guidelines of things to consider when collecting field and airborne Light Detection and Ranging (LiDAR) and hyper-spectral data suitable for up-scaling to continental scale satellite based measurements.

Key points

- Ensure consistency and compatibility of field and airborne data;
- Select data collection approaches that reduce errors, allow daily backups and can be made readily available as soon as possible (e.g. Open Data Kit (ODK) forms);
- Always have contingency plans in case of weather, equipment breakdown or other unforeseen circumstances; and
- The type of environment being investigated will influence the way in which the most optical field and airborne data can be obtained.

17.1 Introduction

The TERN Landscape Assessment remote sensing data archive and access capability (www.auscover.org.au) was formally launched in the first half of 2010 and is one of several facilities of the National Collaborative Research Infrastructure Strategy (NCRIS) and Super-Science Education Investment Funded Terrestrial Ecosystem Research Network (TERN). The aim of TERN Landscape Assessment is to deliver consistent national time-series of remotely sensed biophysical parameters to support ecosystem research and natural resource management communities in Australia. These remote sensing products are based on past, current and future satellite image data sets with deliverables designed for Australian conditions. Biophysical remote sensing data products are developed based on satellite image data captured by the Landsat, Moderate Resolution Imaging Spectroradiometer (MODIS), Advanced Very High Resolution Radiometer (AVHRR) sensors among others. These products will enable assessment of how environmental variables change over time. National remote sensing time-series data sets are accompanied by consistently formatted metadata, which are considered to be equally important to the image data products. These data sets will be made publically accessible and retrievable through the online TERN Landscape Assessment portal. Another major focus area of TERN's Landscape Assessment platform is remotely sensed data calibration and validation of the continental scale time-series based on existing and new captures of high spatial resolution hyper-spectral and LiDAR airborne and field data.

TERN Landscape Assessment has carried out nine extensive airborne and field campaigns in Australia (Figure 17.1). Each site was selected to represent a dominant and/or conservation significant biome (Table 17.1) suitable for scaling up from field and airborne measurements to continental scale map products for calibration and validation purposes. Another focus by Lanndscapes has been to ensure that the collection of high quality and high spatial resolution field and airborne data of the selected biomes would encourage, foster and support ongoing and future research.

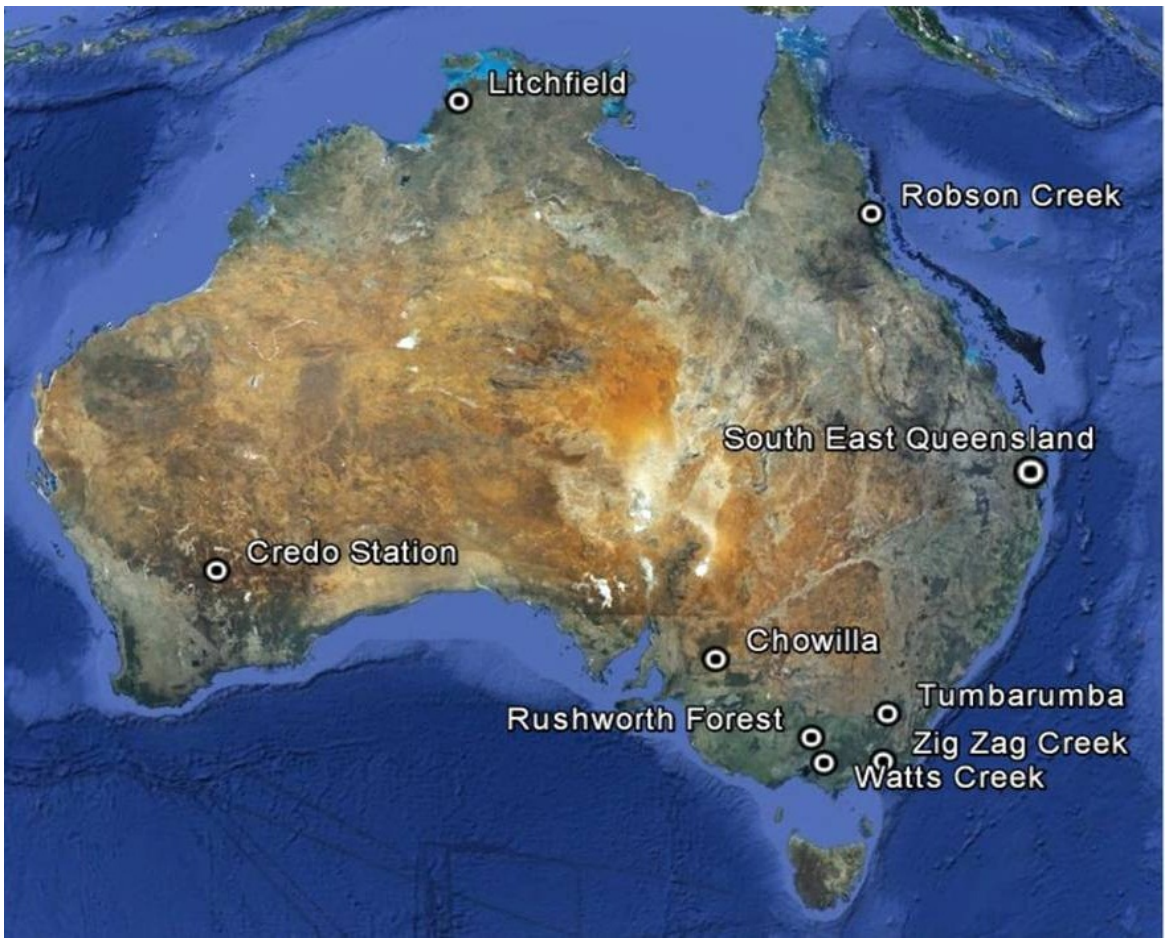

Figure 17.1 Map of Australia showing the location of field and airborne campaign sites carried out by TERN Landscapes between January 2011 and June 2013.

Table 17.1 Site name, location, data collection date, type of environment, and photos of each of the nine TERN Landscapes sites.

Site name	Site location	Date	Environment	Site Photo
Tumbarumba	South eastern New South Wales, 100 km south west of Canberra	8-14 Jan 2011	Temperature wet sclerophyll eucalypt forest with average tree height of 40 m. *Eucalyptus delegatensis* is the dominant species.	
Chowilla	North of the River Murray floodplains north of Renmark, South Australia	30 Jan - 3 Feb 2012	Semi-arid mallee ecosystem in dune and swale system covered with an open mallee woodland upper story with a chenopod and native grass understory.	
Watts Creek	70 km east of Melbourne, Victoria	5-9 Mar, 13-20 Apr, 1-3, 7 May, 9-16 Sep 2012	Open forest with a eucalypt overstorey greater than 40 m in height consisting mainly of mountain ash.	

Rushworth Forest	120 km north of Melbourne, Victoria	15 Apr, 3-6 May, 31 May and 6 Jun 2012	Open forest of red iron bark, red stringybark, red box, long leaf box and grey box.	
Zig Zag Creek	Eastern Victoria 300 km east of Melbourne, Victoria	16-20 Apr 2012	Dominated by shrubby dry forest and damp forest on the upland slopes, wet forest ecosystems which are restricted to the higher altitudes and grassy woodlands, grassy dry forest and valley grassy forest ecosystems are associated with major river valleys.	
Credo	Great Western Woodland 500 km north west of Perth, Western Australia	12-18 May 2012	Open woodland inter-dispersed with open, treeless areas. The main vegetation species are Salmon Gums reaching up to 20 m and Gimlet between 5-10 m, both with little understory. Salt bush and similar shrubs are also prevalent.	
Robson Creek	Lamb Range in the Wet Tropics World Heritage area 25 km south west of Cairns, Queensland	9-16 Sep 2012	Upland rainforest region at 700 m elevation. Notophyll vine forest with a tall canopy at around 40 m and high species diversity.	
South East Queensland	Multiple sites in South East Queensland, located in the Samford Valley, Karawatha Forest, and two mangrove sites near Brisbane Airport.	21 Jan 2013 - 6 Feb 2013	Samford site: on an improved (Paspalum dilatum) pasture with tall eucalypt species. Karawatha Forest: bushland with tall eucalypt species and patches of heatlands and Melaleuca swamps. Mangrove sites: Within Moreton Bay with *Avicennia marina* being the dominant mangrove.	 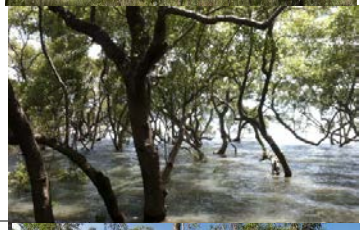
Litchfield	80 km south of Darwin, Northern Territory	27 May - 2 Jun 2013	Savanna, eucalypt open forests, dominated by *Eucalyptus miniata* and *Eucalyptus tetrodonta*.	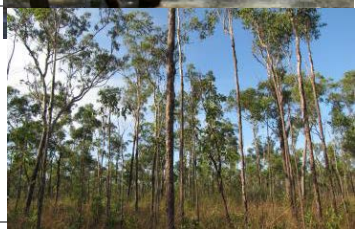

While the first field and airborne campaign in Tumbarumba, New South Wales was treated as a test site for development of field and airborne data collection approaches, field protocols, selection of suitable airborne data collection specifications, data post-processing procedures and data storage, the following eight campaigns have had a standard set of field and airborne data collected. While the field collection approaches and types of field data have been kept as consistent as possible, collection approaches have been refined and new types of field data added along the way (e.g. collection of Terrestrial Laser Scanning (TLS) data). The airborne data acquisition specifications and collection procedures have been kept consistent and carried out by Airborne Research Australia (ARA), Flinders University. The image processing approaches on the other hand have developed significantly to ensure the highest possible airborne data quality. Hence, a number of data versions have been supplied by ARA. As airborne data quality control and assurance are ongoing, new and refined airborne data post-processing approaches may be performed by ARA in the future to deliver new data versions consistently processed to the highest possible standard. These data sets will be made freely available via the online TERN Landscape Assessment Portal.

All the field and airborne image data provided by TERN Landscape Assessment are supplied with associated metadata. Well documented metadata for the airborne data have been developed and supplied by ARA. These metadata will also be freely accessible and retrievable via the online TERN Landscape Assessment Portal to support future ecosystem research in Australia. The data acquisition specifications were set to suit a large number of product and research purposes and ensure that the quality of the data meets short and medium term specification requirements for potential future research of Australian ecosystems.

One of the field and airborne campaigns, representing a mature stage of the data collection procedures and processing, is the Robson Creek campaign. Hence, the Robson Creek campaign is in many cases used in this book chapter as an example to illustrate and demonstrate the activities and outputs associated with the TERN Landscape Assessment field and airborne campaigns. TERN's Robson Creek Rainforest SuperSite is locally managed by CSIRO Tropical Forest Research and overseen by James Cook University. The site was chosen as a representative upland (400-1000 m) rainforest site with high plant and animal diversity, homogeneity of forest type and parent material, and all weather access. The Robson Creek site is critical to remote sensing of continental scale products, as it represents an area with the highest biomass in Australia and hence can be used to constrain and validate remotely sensed models.

The two main aims of each of the TERN Landscapes field and airborne data collection campaigns have been:

1. To demonstrate how hyper-spectral and LiDAR image data and field data can be collected in an accurate, timely and efficient manner to deliver products suited to TERN Landscapes calibration and validation activities as well as a range of TERN activities and international remote sensing calibration and validation work.
2. To collect field and airborne LiDAR and hyper-spectral image data over the selected sites to enable the production of maps of biophysical parameters, including (a) forest height, foliage projective cover, plant projective cover, vertical profiles, tree density, and leaf area index (LAI) from the LiDAR data and (b) reflectance, nitrogen, water content, canopy chlorophyll content, and photosynthetic and non-photosynthetic cover from the hyper-spectral data. Fusion of the LiDAR and hyper-spectral image data, as well as TERN Landscapes derived field and image data, may be used for deriving additional data sets including land cover maps and for developing scaling methods

17.2 Campaign Planning and Coordination

Each of the TERN Landscape Assessment field and airborne campaigns has required a substantial amount of planning and coordination to ensure optimal data were obtained and that airborne data and field measurements could be acquired simultaneously. The main activities required for planning and coordinating each of the field and airborne campaigned have included:

- Date selection of campaign (season, climate, people availability, availability of airborne facilities);
- People availability and ensuring the proper level of expertise was present for all field activities;
- Field equipment availability;
- Field data protocols and field sheets/Open Data Kit (ODK) forms;
- Allocation of field personnel for each of the field activities;
- Airborne data acquisition specifications;
- Flight planning and total station setup by ARA;
- Communication with ARA team before and during data collection;
- Logistics, including accommodation, transport, meals, site accessibility, communication, task distribution, training to build up expertise, and occupational health and safety requirements;
- Ensure backups of all data collected, proper data storage and data hand-over of all data to responsible person at the end of each campaign; and
- Backup plan if weather was unsuitable for airborne data collection, including identification of other suitable time windows and personnel available locally for collecting spectroradiometer measurements coincidently with airborne data campaign.

The timing of the field and airborne campaigns was for most of the campaigns dictated by the season to increase the likelihood of cloud free conditions to enable high quality airborne data to be collected. The collection of field data was not as dependent on the weather condition but for most activities, rain made data collection difficult and time-consuming. Once a suitable season for the TERN Landscape Assessment study sites had been identified, the selection of the dates of the field campaign were determined by the availability of the aircraft and ARA scientists operating them and suitable personnel within TERN Landscape Assessment. Most of the campaigns have relied on the availability of local personnel, but personnel from interstate has participated in all campaigns to ensure that the required level of expertise for equipment handling and field data collection was available to ensure data collection consistency and quality.

As much of the required field equipment as possible was obtained locally, i.e. from universities, government agencies and non-government organisations involved in the campaign, with additional instrumentation, such as spectroradiometers, ground calibration targets, terrestrial laser scanner, sunphotometer, etc. couriered to the site ahead of time. Prior to each campaign, it was ensured that at least one person with extensive experience in each of the field data collection activities were present to ensure the guidelines of the field data protocols were followed and all required data were correctly recorded on field sheets or on androids using ODK forms.

Airborne data acquisition specifications were developed to ensure the airborne LiDAR and hyper-spectral data collected were suitable for a large number of research and biophysical mapping applications. ARA has also provided a significant contribution towards the development of the data acquisition specifications to ensure the specifications were feasible and optimised where possible. Prior to each campaign, TERN Landscapes and ARA agreed on the most suitable airborne data collection procedure and ARA has provided flight planning information prior to each campaign to ensure all personnel in the field were informed. As some of the field sites did not have open areas suitable for deployment of ground calibration targets and spectroradiometer measurements to be carried out, airborne data for additional sites outside the target areas have in many cases been collected by ARA. ARA was also responsible for setting up a total station at each of the sites to demonstrate the geometric accuracy of the airborne data. Hence, regular and open communication between

TERN Landscapes personnel and ARA has been imperative to ensure the field and airborne data could be correctly integrated once collected.

A number of other logistics has been important for each of the TERN Landscape Assessment campaigns. As 10-20 people have been participating in each of the campaigns, booking of accommodation, transport and meals were required prior to the campaigns. Distribution of field tasks and responsibilities has also been done prior to each field trip to avoid miscommunication and ensure all required data were collected. Hence, communication prior and during the campaigns has been imperative, with regular phone meetings prior to the campaigns and briefings and de-briefings on a daily basis during the campaigns. One item specifically highlighted prior to each of the campaigns was the need for daily backups of all collected data, proper data storage and assigning a responsible person for collecting and storing all collected data throughout the entire campaign. Occupational health and safety (OHS) requirements have been very important to follow, as a large number of people participated in the campaigns in often very remote locations. The OHS requirements included but were not limited to risk assessments of all activities, assessment of the level of hazard, mitigation plans of all hazards, ensuring communication (satellite phones, walkie talkies), never working alone, always carrying first aid equipment and always having access to transport.

Finally, backup plans were put in place before each of the campaigns in case of poor weather conditions. The importance of this was highlighted during the first TERN Landscape Assessment campaign in Tumbarumba, New South Wales, where the weather prevented the acquisition of hyper-spectral data at the time of the field campaign. Hence, for all subsequent airborne campaigns, backup plans have been in place to ensure field measurements could be completed at a later stage if needed and that a team of people and equipment were available locally to collect spectroradiometer measurements of ground calibration targets at the time of a potentially delayed airborne hyper-spectral data collection.

17.3 Field Sampling Design

The general sampling design of TERN Landscape Assessment campaigns has depended on existing data sets and research being carried out within the focus sites. Generally, the size of the areas has been 5 km x 5 km. The 5 km x 5 km sites have been selected based on a number of criteria, mainly to ensure the following criteria were fulfilled:

- Homogenous sites to enable scaling-up approaches to MODIS type data;
- Representative biomes of Australia and/or biome with specific conservation value and/or of specific value for calibration and validation of continental scale data sets;
- Site with focus on research and long-term ecological monitoring;
- Data collection of use for multiple facilities within TERN; and
- Data collection to support ecosystem science in Australia.

As can be seen in Figure 17.2, the 5 km x 5 km sites have generally been very homogenous in terms of vegetation cover and structure or at least consistently mixed, and therefore suitable for scaling-up to MODIS type satellite image data. At many of the selected sites, a flux tower was installed or planned to be installed within the 5 km x 5 km area, which will allow measurements of energy, carbon and water exchange between the atmosphere and the ground and vegetation to be integrated with the field, airborne and satellite data collected by TERN Landscapes. Pheno-cams have been installed on some of the flux towers to allow photos to be taken every hour of the day throughout the year to study canopy and leaf phenology.

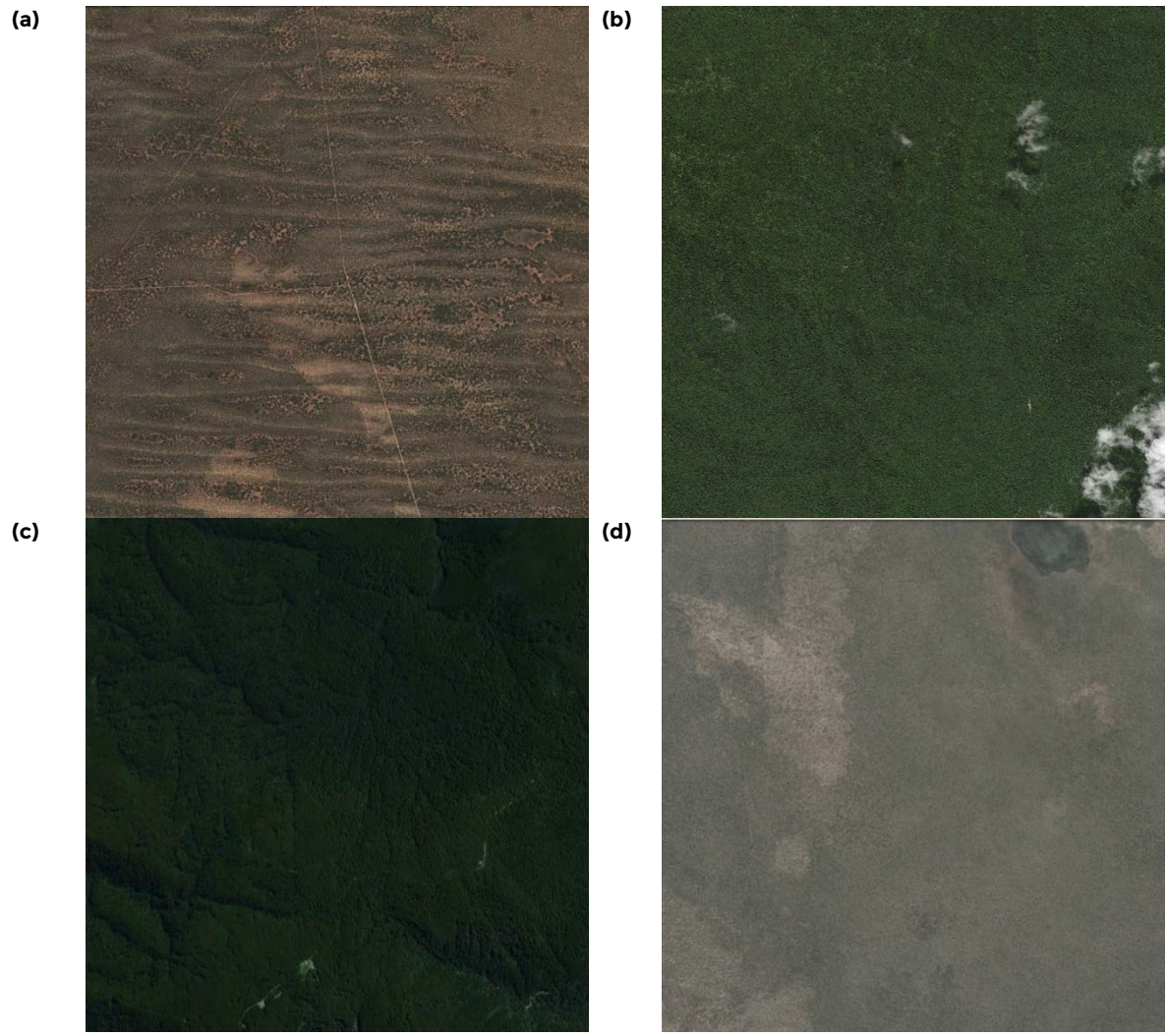

Figure 17.2 Examples of TERN Landscapes campaign sites of 5 km x 5 km, including the
(a) Chowilla site;
(b) Robson Creek site;
(c) Watts Creek site and
(d) the Litchfield site.

Within each 5 km x 5 km site, TERN's Landscape Assessment platform has collected a variety of vegetation structural measurements over 100 m x 100 m areas at different locations (Figure 17.3). The locations of these 100 m x 100 m areas were determined based on the following criteria:

- Ensure the field data collected were representative and captured the variability of the whole 5 km x 5 km site;
- Increase the sampling density (i.e. the number of 100 m x 100 m areas) around the location of the flux tower or other intensively sampled areas such as the 500 m x 500 m plot with all species identified within the Robson Creek site; and
- Ensure homogenous vegetation structure within the 100 m x 100 m area.

However, accessibility often restricted where sites could be located. For example, the Robson Creek site had significant elevation changes within the 5 km x 5 km area of around 700 m. As many areas were too steep to get to and to safely carry out the fieldwork, this limited the spread of sites to be within a few hundred metres of the two main dirt roads intersecting the study area.

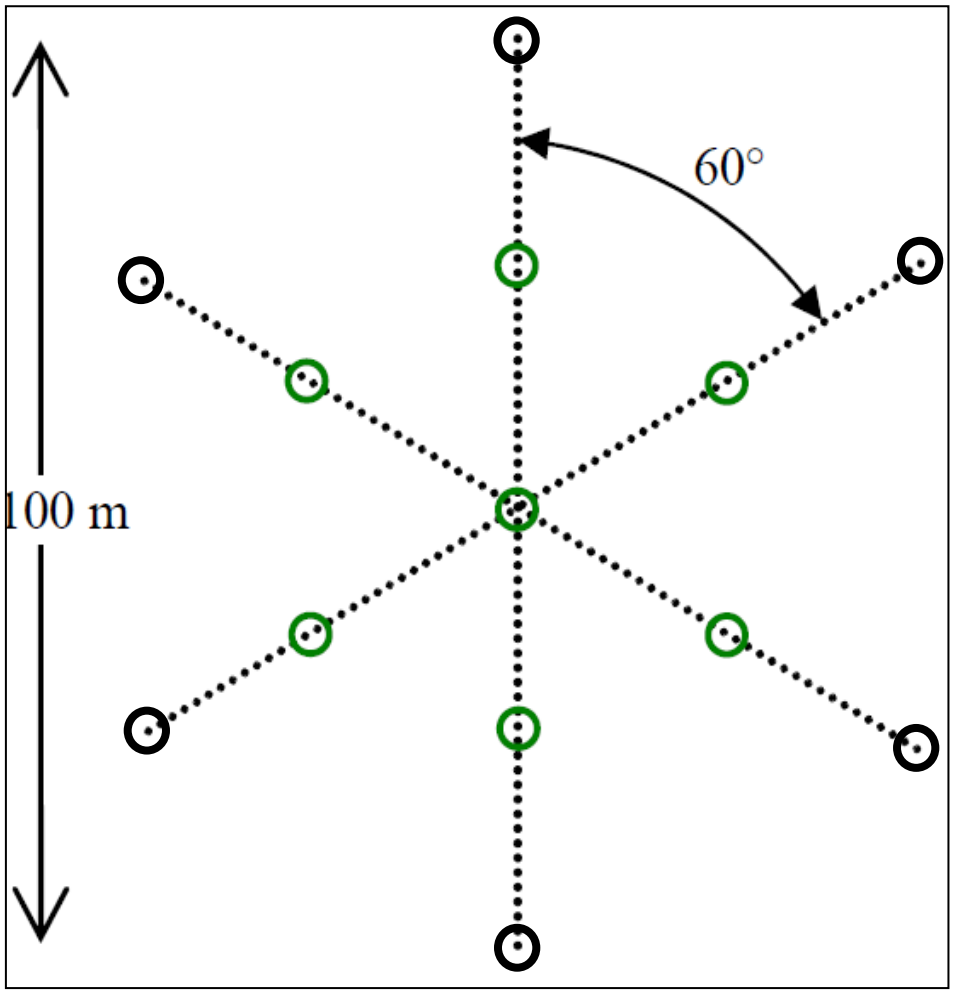

Figure 17.3 Layout of the 100 m x 100 m area within which vegetation structural measurements were obtained.

Within each 100 m x 100 m area, three 100 m tape measurements were lined up facing north (0°) – south (180°), 60° - 240° and 120° - 300° and intersecting at the centre, which created a star shape with each of the six arms being 50 m in length from the centre point (Figure 17.3). A Differential Global Positioning System (DGPS) was used to obtain the position of the centre point of each star transect. Point based observations were made for each 1 m of ground cover, mid-storey and over-storey, following the approach outlined in Muir et al. (2011). This produced a total of 300 point based observations, which can be converted into a measure of fractional ground cover and foliage projective cover. Basal area is estimated at the centre point, as well as the 25 m mark along each of the six arms of the star transect. Vegetation structure, i.e. Diameter at Breast Height (DBH) at 30 cm and 130 cm from the ground, tree height to first branch, total tree height, and length of the major and minor axes of the tree crown, was recorded for all trees included in the basal area count at the centre point of the star transect (typically 10-25 trees). LAI was measured using either the LAI-2200 or the CI-110 (depending on light conditions) at set intervals (typically every 1 m) along the three 100 m transect lines. Hemispherical photos, using a fisheye lens, were collected at three different exposure levels at the centre point, as well as the 25 m and 50 m marks along each of the six arms of the star transect (a total of 13 locations). At the centre point and at a distance of 10 m from the centre point in the north, east, south and west directions, terrestrial laser scans were collected. Reflectors were set up to allow the five different scans to be geo-referenced to each other.

In addition to the star transects covering a 100 m x 100 m area, additional sites were visited within the 5 km x 5 km sites to complete a rapid sample of structural measurements. These included DBH and hemispherical photos at some campaign sites and, at other more recent sites, one terrestrial laser scan and hemispherical

photos collected at the location of the TLS and at a distance of 10 m from the TLS in the north, east, south and west directions. A Global Positioning System (GPS) position was derived of the TLS location.

Additional field measurements, including the setup of pheno-cams, collection of spectroradiometer measurements of ground calibration targets, sunphotometer and ozonometer measurements and hemispherical sky photos at the time of the airborne data capture, were also collected. These measurements were not part of the star transect setup. During some of the TERN Landscapes campaigns (Tumbarumba, Robson Creek, South East Queensland, Litchfield) leaf sample collection, species identification and leaf chemistry assessment have also been undertaken.

17.4 Campaign Example: Robson Creek

TERN's Robson Creek Rainforest SuperSite is located in the Wet Tropics Bioregion with significant conservation value, representing the largest continuous stretch of rainforest in Australia. As part of the work conducted by TERN's Ecosystem Processes platform, site selection and surveying of a 500 m x 500 m focus plot commenced in August 2009 with the first trees measured and surveyed in October 2009. Approximately 25,000 tree species have been identified, and associated tree height, DBH and GPS position have been collected. Vertebrate and invertebrate biodiversity and seedling surveys started in November 2009. Construction of a flux tower and associated soil and water sampling infrastructure commenced in June 2010, and was completed in mid-2013. Because of the extensive field based work within the area, TERN's Landscape Assessment facility conducted an intensive field and airborne campaign between 9 and 16 September 2012 to collect further data in this area and complement existing research and data sets. A total of 18 people from the University of Queensland, James Cook University, Royal Melbourne Institute of Technology, CSIRO and the Department of Science, Information Technology, Innovation and the Arts participated in the field campaign. In addition, a team of four people from ARA/Flinders University worked closely together with the TERN Landscape Assessment team to ensure high quality airborne LiDAR and hyper-spectral data were collected coincidently with the field data.

17.6.1 Robson Creek Study Area

The TERN Robson Creek Rainforest SuperSite is located approximately 30 km northwest of Atherton, in Far North Queensland, Australia (17^0 01' 12"S 145^0 37' 56"E, 700 m elevation). It lies in Danbulla National Park within the Wet Tropics World Heritage Area. Access to the site is 13 km past Tinaroo Falls township along Danbulla Forest Drive and approximately 1 km along the Mount Edith Presentation Road (Figure 17.4). The Landscape focus areas are shown in Figures 17.5 and 17.6. The climate of the area is considered seasonal with 61% of the annual rainfall occurring in the months of January to March (Danbulla Forestry). Mean annual rainfall at Danbulla Forestry ($17^0$09'36"S, $145^0$37'35"E, 4.5 km south of the plot) is 1597 mm (1921 - 1991), at Tinaroo Dam township ($17^0$10'07"S, $145^0$32'54"E, 10 km southwest) is 1255 mm (1954 - 2006), and at Kairi Research Station (17013'03"S, 145034'33"E, 11 km south-southwest) is 1248 mm (1913 - 2006). Mean monthly rainfall for Danbulla Forestry and Tinaroo Dam Township is shown in Figure 17.7. Mean monthly minimum and maximum temperatures for Kairi Research Station are shown in Figure 17.8 (BOM, 2006).

Figure 17.4 Location of the TERN Robson Creek permanent plot on the Atherton Tablelands, Queensland, Australia. The red line indicates access route.

Figure 17.5 Aerial view of the Robson Creek focus areas. TERN Landscapes conducted fieldwork within the white 5 km x 5 km area. The large yellow rectangle shows the outline of a WorldView-2 image captured on 19 September 2012. The small yellow square outlines the 500 m x 500 m plot, where all tree species have been identified and mapped. The red rectangle represents an additional area of LiDAR and hyper-spectral image data within which leaf samples were collected and ground calibration targets were deployed.

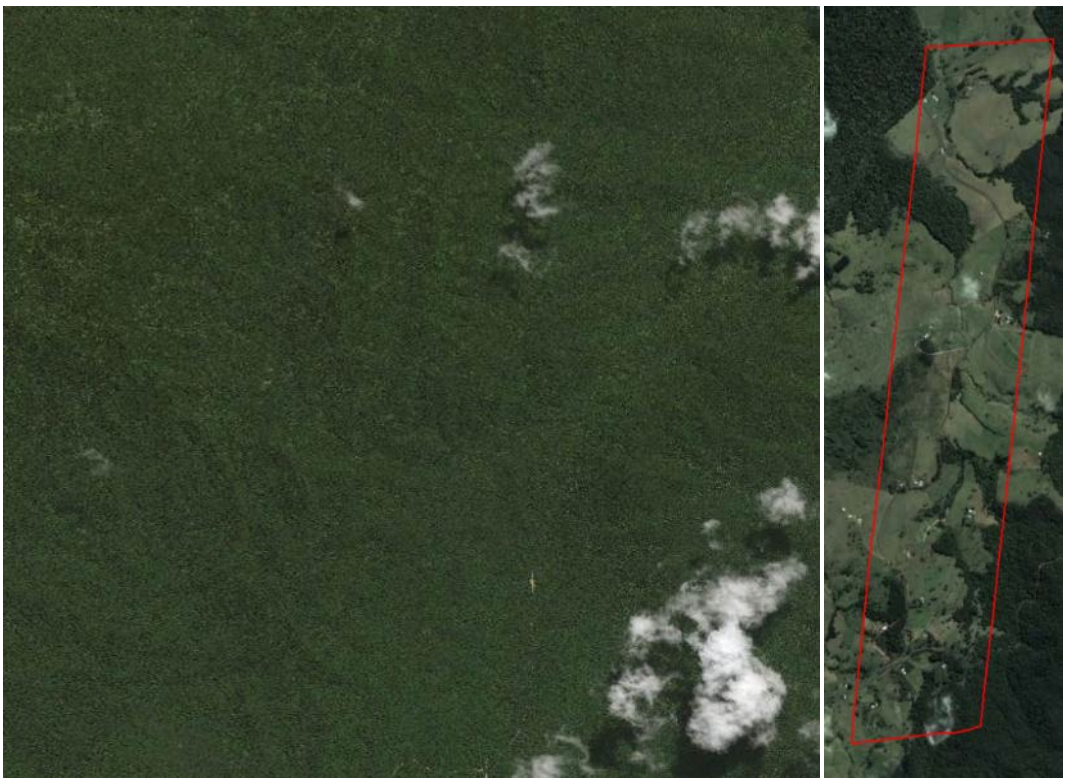

Figure 17.6 Aerial view of the TERN Robson Creek 5 km x 5 km site and the nearby site from where ground calibration targets were deployed and leaf samples were obtained.

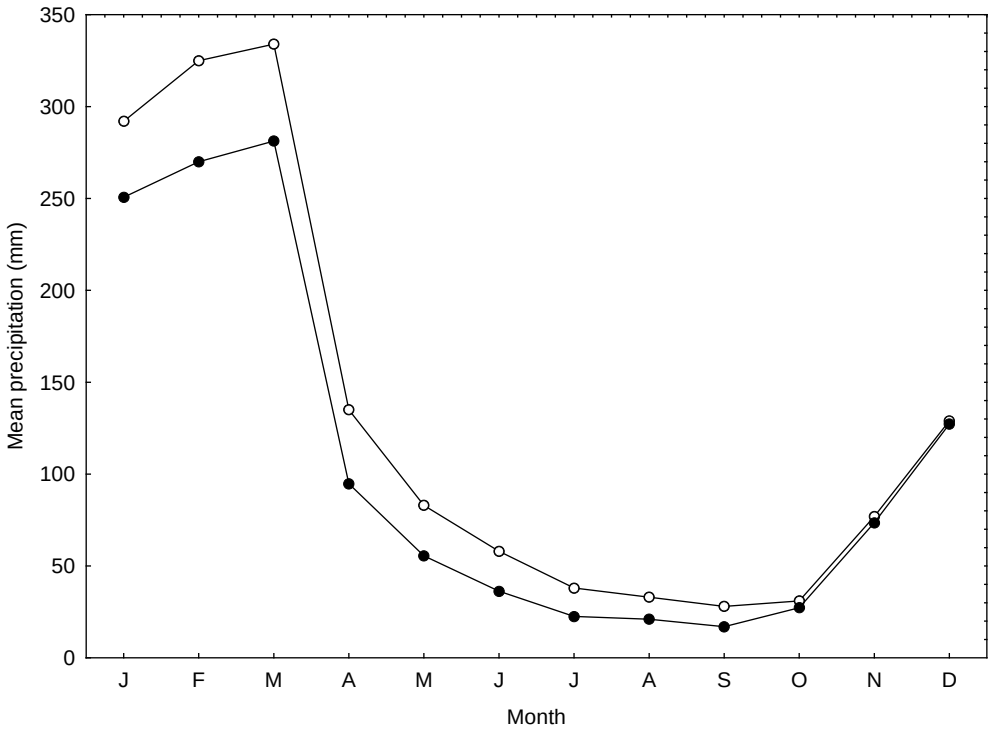

Figure 17.7 Mean monthly rainfall for Danbulla Forestry (○) and Tinaroo Dam Township (●).

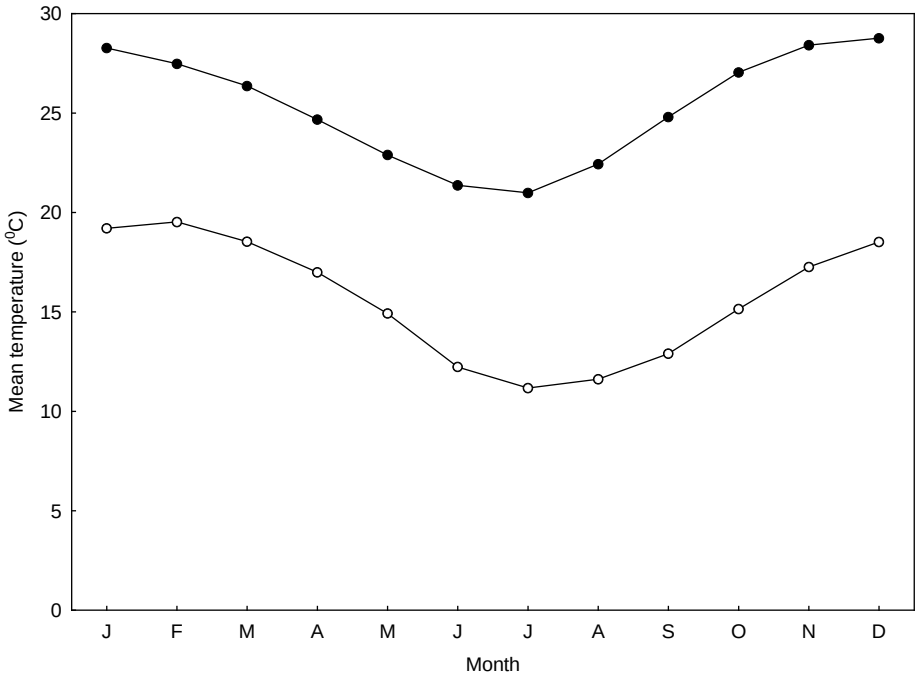

Figure 17.8 Mean monthly minimum and maximum temperatures for Kairi Research Station (11 km southwest of the plot).

The 500 m x 500 m plot is located at the southern base of the Lamb Range, which rises to 1276 m above sea level . The western edge of the plot runs parallel to, and 50 m east of the Mount Edith Presentation Road, which is on an alluvial flat adjacent to Robson Creek. The landform of the plot is moderately inclined with a low relief with a 30 m high ridge running north/south through the middle of the plot and a 40 m high ridge running north/south on the eastern edge of the plot. Three permanent creeks flow through the plot, joining with Robson Creek which in turn meets the Barron River approximately one kilometre south of the plot.

A detailed soil description of the CSIRO experimental plot 9, located 200 m to the north of the plot is given in Graham (2006). The parent material is a meta-sediment and soil fertility is considered low. The soil profile is described as having a Principal Profile Form Gn3.71 and affinities with the xanthozem Great Soil Group.

The plot is mapped as Regional Ecosystem (RE) 7.3.36a, complex mesophyll vine forest. The forest type changes to RE 7.12.16a, simple to complex notophyll vine forest, with increasing altitude to the north of the plot. Structurally the forest is very tall to extremely tall closed forest with canopy heights ranging from 23 to 44 m. Full floristic and structural details can be found in Bradford et al. (2014).

As is the case for all accessible areas of the Wet Tropics the plot has been selectively logged. The last logging in the Robson Creek area was undertaken between 1960 and 1969. The southern and central parts of the plot were logged in 1960-64, while the northeast and northwest corners were logged in 1964-1969. Silvercultural treatment of the surrounding Danbulla logging area was common place in the 1950's. Treatments included cutting and poisoning of unwanted species and promotion of valuable species and seed trees. Although no written evidence exists of such treatments on the plot, the presence of such activity cannot be dismissed.

Severe tropical cyclone Larry crossed the coast near Innisfail on the 20th March 2006. The northern edge of the eye passed just south of Atherton. However some areas removed from the eye received severe disturbance. The plot area received moderate to slight disturbance (Bradford/Unwin scale: Category 3, Metcalfe *et al.* 2008) with the winds coming from a north-westerly direction. Damage from severe tropical cyclone Yasi in February 2011 was minimal with moderate leaf and branch loss and only few stems > 10 cm DBH being uprooted.

17.5 Field Equipment

Field equipment was provided by a number of institutions for the Robson Creek campaign. For most TERN Landscape Assessment campaigns, the majority of the equipment used was obtained locally. However, for the Robson Creek campaign, Brisbane located Department of Science, Information Technology, Innovation and the Arts and the University of Queensland provided most of the equipment for the campaign. All field equipment used for the Robson Creek field campaign is presented in Table 17.2.

Table 17.2 List of field equipment used during the Robson Creek field campaign for each fieldwork activity.

Fieldwork Activities / Measurements	**Field Equipment**
Foliage projective cover and ground cover, including basal area and soil colour assessment (SLATS)	• DGPS omnistar • Field laptop point based observations • Backup sheets for FPC/ground cover point observations • 6 x 100 m tape measures • Densitometer and laser pointer • Basal area optical wedges • Munsell charts • Pegs • Marking tape • Digital camera
Vegetation structure (height, DBH, crown dimensions)	• Laser range finder • DBH tape measure • Tape measure
Leaf area index	• Licor LAI-2200 Plant Canopy Analyser • CI-110 Digital Plant Canopy Imager • 2 x SLR cameras • RGB fisheye lens • NIR fisheye lens • Tripod + monopod
Terrestrial laser scanning	• Riegl VZ400 terrestrial laser scanner and accessories
Leaf samples and leaf chemistry assessment	• 2 x Integrating sphere (for leaf optical measurements) • DGPS omnistar • Slingshot and attached rope • Leaf chemistry equipment (lab based)
Spectroradiometer measurements of ground calibration targets	• 2 x ASD Spectroradiometer (including panel and accessories) • Spectralon panel (for instrument inter-calibration) • White, grey and black ground calibration targets (8 m x 8 m) • DGPS omnistar
Atmospheric measurements	• Microtops Ozonemeter • Sunphotometer • Hemispherical photography (sky view)
Safety	• Walkie talkies • Maps • 12 x Compasses • Handheld GPSs (and AA Batteries)

17.6 Field Data Collection

For each of the TERN Landscape Assessment campaigns, a standard set of field based measurements has been collected. Because of equipment availability, field data collection protocol maturity and environmental variations between the times of data collection for the different TERN Landscape Assessment campaign sites, slight differences in field data type and collection methods have occurred. The aim of each of the TERN Landscapes campaigns was to collect as much field data as possible using as many of the following field data collection approaches:

- Statewide Landcover And Trees Study (SLATS) star transects for measuring ground and canopy cover, basal area and assessing soil colour;
- Vegetation structural measurements of trees included in the basal area count, including DBH at 30 cm and 130 cm, tree height, tree height to first branch, and major and minor axes of tree crowns;
- Hemispherical photography;
- Leaf Area Index measurements using the CI-110 and LAI-2200 instruments;
- Terrestrial Laser Scanning;
- Leaf samples and leaf chemistry assessment;
- Spectroradiometer measurements of ground calibration targets;
- Atmospheric measurements using a sunphotometer and ozonometer; and
- Installation of pheno-cams for ground and canopy cover phenology time-series observations.

An example of the types of data collected during the Robson Creek campaign can be seen in Table 17.3. It should be noticed that vegetation structural measurements collected by TERN for this campaign were limited because these were already available for many of the sites within the 5 km x 5 km area. Hence to save time and avoid duplication, tree height and DBH measurements were excluded, as the Australian Supersites Network had already collected these data. Using the Licor LAI-2200 Plant Canopy Analyser instrument for LAI measurements require a second sensor to be set up in an open area and the best results are obtained at dusk and dawn. Because of the canopy density within the Robson Creek site, no suitable open area was identified. Also, collecting the LAI-2200 measurements at dusk and dawn was deemed too dangerous because of the terrain and thorny plants. Hence, the CI-110 Digital Plant Canopy Imager instrument was used instead. At the time of the field campaign, the flux tower had not been installed. Therefore, no pheno-cams were installed at the time of the field campaign. Similar issues, affecting the type of field based measurements to be obtained, were encountered for the other TERN Landscape Assessment campaigns.

Table 17.3 Daily field measurements and associated weather condition for the Robson Creek campaign.

Date	Weather	Field Activities
8 Sep 2012	Cloudy	• Leaf species identification and tree tagging
9 Sep 2012	Cloudy	• Leaf species identification and tree tagging
10 Sep 2012	Cloudy	• Site and safety induction • Site location • Star transect 1 (including TLS scans, hemispherical photography and LAI using CI-110) • Leaf sampling • Spectral analysis of leaves using integrating sphere
11 Sep 2012	Rainy	• Star transect 2 (including TLS scans, hemispherical photography and LAI using CI-110) • Leaf sampling • Spectral analysis of leaves using integrating sphere

Date	Weather	Field Activities
12 Sep 2012	Cloudy	• Completed star transect 2 • Star transect 3 (including TLS scans, hemispherical photography and LAI using CI-110) • Leaf sampling • Spectral analysis of leaves using integrating sphere
13 Sep 2012	Mainly sunny, but some clouds	• Completed star transect 3 • Star transect 4 (including TLS scans, hemispherical photography and LAI using CI-110) • Leaf sampling • Spectral analysis of leaves using integrating sphere • LiDAR data collected for part of the site
14 Sep 2012	Sunny	• Spectrometer measurements of ground calibration targets • Irradiance measurements • Sunphotometer and Ozonometer measurements • Hemispherical sky photos • Leaf sampling • Spectral analysis of leaves using integrating sphere • LiDAR and hyper-spectral data collected for the whole site and the additional open area • Two rapid sites, including TLS and hemispherical photos
15 Sep 2012	Cloudy	• Leaf sampling • 10 rapid sites, including TLS and hemispherical photos

17.6.2 Measuring Ground and Canopy Cover, Basal Area and Assessing Soil Colour

The SLATS star transects are designed and used for collecting point based information on canopy cover, ground cover and basal area. The metric of overstorey vegetation cover adopted in many Australian vegetation classification frameworks is Foliage Projective Cover (FPC). Overstorey FPC is defined as the vertically projected percentage cover of photosynthetic foliage from tree and shrub life forms greater than 2 m height and was the definition of woody vegetation cover adopted by SLATS (Armston *et al*., 2009). Ground cover is the non-woody vegetation (forbs, grasses and herbs), litter, cryptogamic crusts and rock in contact with the soil surface.

Point based observations using a laser pointer (for ground cover) and a densitometer (for canopy cover) are obtained for each 1 m along the three 100 m long transects (Figures 17.3 and 17.9). The star transect is located within a vegetation structurally homogenous area to ensure that the 300 point based observations are representative for the selected area. The 300 observations are converted into a single value of fractional ground cover and a single value of FPC. The GPS position is recorded at the centre of the star transect (Muir *et al*., 2011). As part of the SLATS star transect, an optical wedge prism is used to estimate tree basal area. Basal area defines the area of a given section of land that is occupied by the cross-section of tree trunks and stems at their base. This is measured at a person's breast height (1.3 metres) and includes the entire diameter of every tree, including the bark. Basal area sweeps are recorded at the centre point as well as at a distance of 25 m from the centre point along each of the six transect arms (Figure 17.10). Soil characteristics and colour are also described as part of the star transect survey using Munsell Soil Color Charts.

(a)

(b)

Figure 17.9

(a) Pole with laser pointer and densitometer attached for point based observations of ground and canopy cover.

(b) The GPS position is recorded in the centre of the star transect.

(a)

(b)

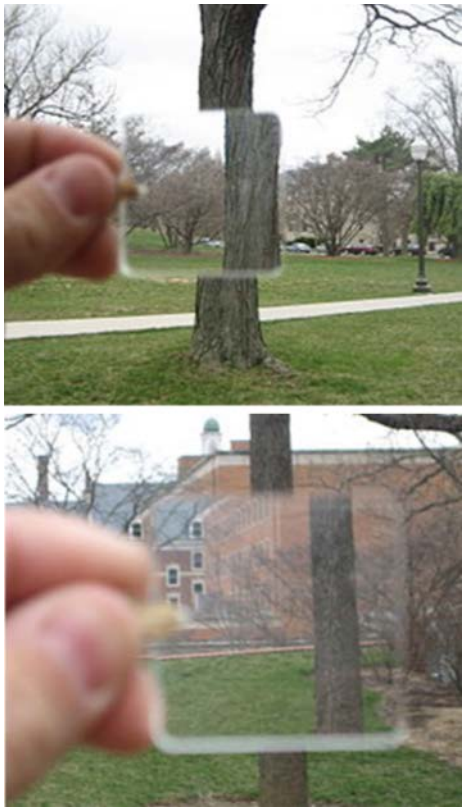

Figure 17.10

(a) Basal area sweep along transect line and

(b) Optical wedge inclusion and exclusion of trees. Source: http://en.wikipedia.org/wiki/Wedge_prism

17.6.3 Vegetation Structural Measurements

When the basal area sweep is performed in the centre of the star transect, trees which are counted as 'in' in the sweep have their structural characteristics measured and recorded. Diameter at Breast Height (DBH) is measured at 1.3 m and at 0.3 m using a DBH tape measure. The crown diameter major and minor axes are also measured by two people using a tape measure to determine the crown diameter, with one person standing under the canopy border on one side of the tree crown and the other person under the other side of the canopy border. Tree height, defined as the vertical distance from ground level to the uppermost point is measured. The height from ground level to the first branch is also recorded. A laser range finder, hypsometer or clinometers and tape measure are be used.

17.6.4 Hemispherical Photography

Hemispherical photography has been used in many studies of LAI (Chen et al., 1997; Robison & McCarthy, 1999). Hemispherical photos were collected from the centre point of the star transects, as well as at the 25 m and 50 m marks of each of the six transect arms. All photos are referenced to the central geographic location. A monopod may be used together with a level bubble to ensure the camera lens if facing vertically upwards (Figure 17.11). Three photos are collected at each sampling point, each with different exposures. Photos should be taken at dawn, dusk or during overcast conditions. During the time of the hyper-spectral data capture, hemispherical sky photos are taken every 10 minutes to record cloud cover during the airborne data capture (Figure 17.12).

(a)

(b)

Figure 17.11
(a) Collection of hemispherical photo
(b) Hemispherical photo example

(a)

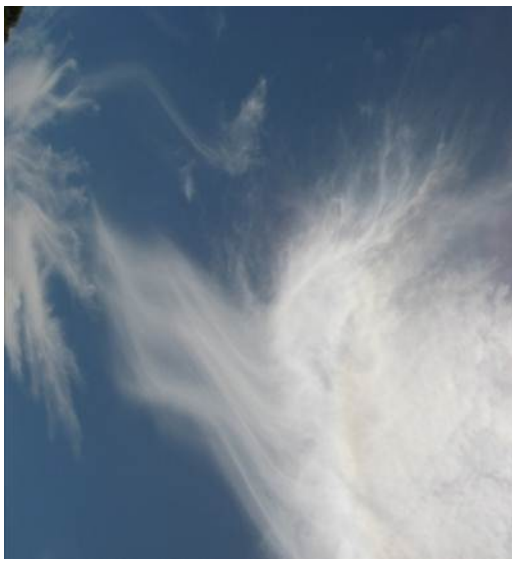

(b)

Figure 17.12
(a) Sky photos collected using (b)
(b) Hemispherical fisheye lens during the airborne hyper-spectral data capture.

17.6.5 Leaf Area Index Measurements Using the CI-110 and LAI-2200 Instruments

LAI data is collected at TERN Landscape Assessment sites using two separate instruments, the LAI2200 and the CI-110. The LAI-2200 Plant Canopy Analyser calculates LAI from radiation measurements collected both above and below the canopy with a fisheye optical sensor (148° field-of-view) (LI-COR, 2013). Hence, two sensors are needed, so one can be placed in an open area (above canopy measurements) (Figure 17.13) and the other one can be used for simultaneous below canopy measurements. The solar radiation is measured at five zenith angles. LAI estimates are based on four assumptions: (a) the foliage is black (no radiation is transmitted or reflected by the vegetation); (b) the foliage elements are small in comparison to the area of view of each sensor ring and the following guideline is applied: the distance between the sensor and the nearest leaf above it should be at least four times the width of the leaf; (c) the foliage is randomly distributed; and (d) the foliage is aziumuthally randomly orientated, in other words, leaves face all directions (LI-COR 2013). It is recommended that collection is carried out around dawn or dusk or during uniform overcast days. During TERN Landscape Assessment campaigns, LAI measurements have been collected with the LAI-2200 Plant Canopy Analyser along the three 100 m transects forming the star transects.

In situations where it has not been impossible to collect LAI-2200 measurements under the required conditions, the CI-110 Digital Plant Canopy Imager (Figure 17.14) has been used, as it allows a user-defined threshold to be set to discriminate between vegetation and sky, and hence can be used throughout the day, even in sunny conditions. A similar collection method, i.e. along the three 100 m transects forming the star transect, has been used.

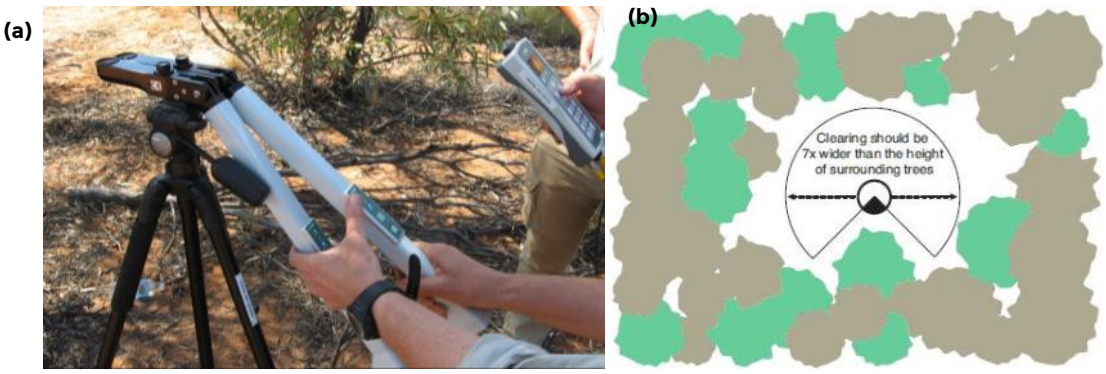

Figure 17.13
(a) Synchronising the clocks of both LAI-2200 sensors to ensure above and below
(b) Within clearing seven times wider than the height of surrounding trees canopy measurements can be related

Figure 17.14 CI-110 Digital Plant Canopy Imager used to derive LAI measurements.

17.6.6 Terrestrial Laser Scanning

Terrestrial Laser Scanning (TLS) data have been collected for most of the TERN Landscape Assessment sites. TLS data can be used to obtain more detailed structural characterisation of vegetation, including estimates of the number of trees per hectare, the distribution of stem diameters at breast height for assessing basal area, and estimates of tree height distributions, stem form, branching structure, the vertical distribution of foliage cover and plant area index (Figure 17.15). The sampling approach adopted by TERN Landscapes included five scan positions per site. One scan position was located in the centre of the star transect. The remaining four scans were obtained 10 m from the centre point in north, south, east and west directions. Reflectors visible in more than two scans were set up to ensure the scans could be geometrically related to each other (Figure 17.15).

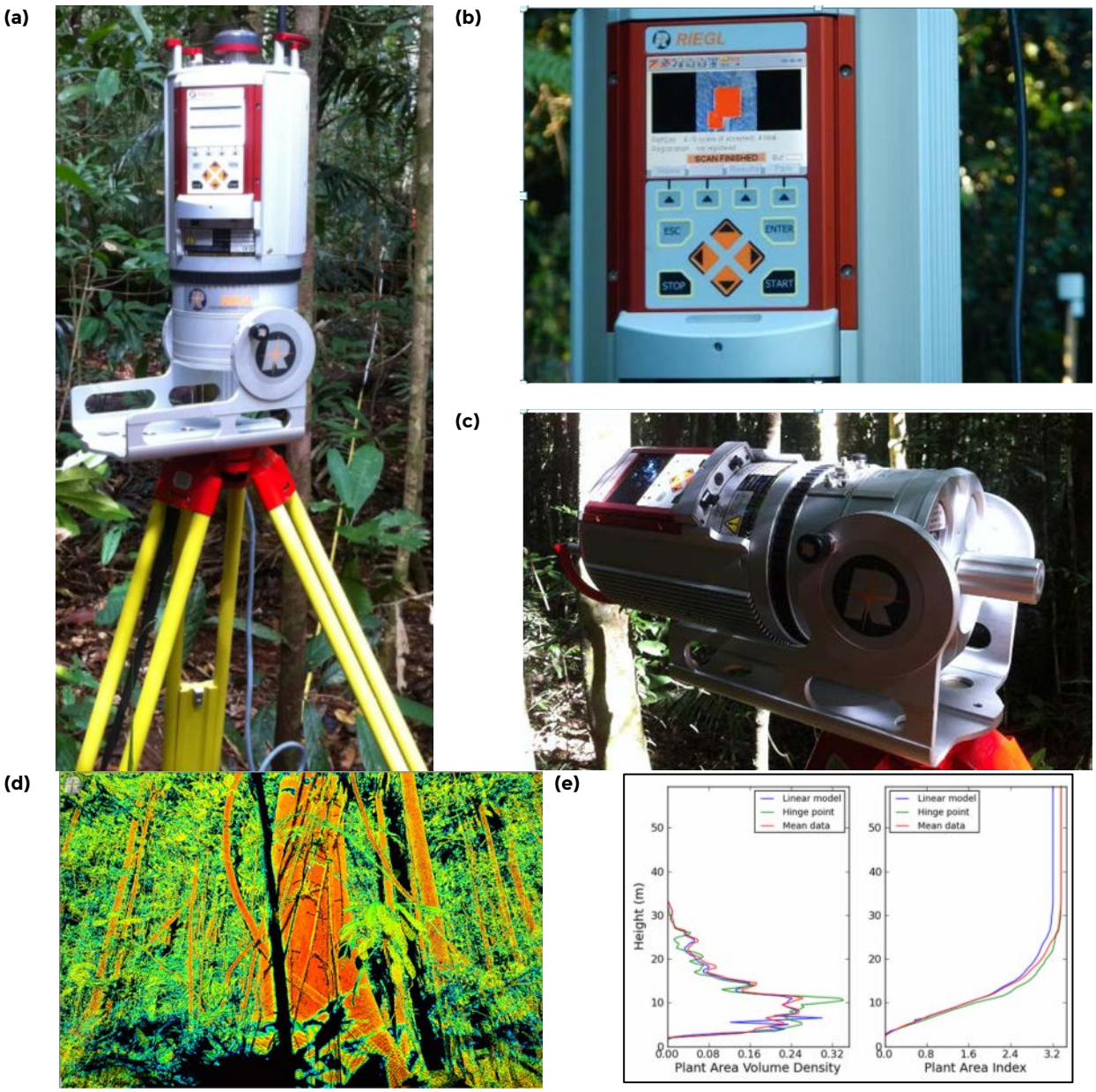

Figure 17.15
(a) Riegl VZ400 TLS,
(b) high resolution scan of reflectors,
(c) tilted TLS to obtain a full hemispherical scan,
(d) intensity output image from the Robson Creek campaign, and
(e) derived plant area volume density and plant area index from the Robson Creek campaign.

17.6.7 Leaf Samples and Leaf Chemistry Assessment

High temporal frequency satellite observations of landscapes are necessary to capture highly dynamic spatio-temporal patterns of vegetation growth and productivity and landscape processes of carbon and water fluxes. Satellite observations of landscape seasonality include co-varying phenological changes in vegetation foliage quantity, phenological variations in foliage quality (leaf age, pigment contents, nitrogen, leaf stress, etc.), and external variations in clouds, aerosols, and sun-view angle geometries. During some of the TERN

Landscape Assessment campaigns (Tumbarumba, Robson Creek, South East Queensland, Litchfield) leaf samples have been collected to support phenology studies and to map individual species and their leaf chemical properties from hyper-spectral data. These measurements help to: (1) document, understand, and validate seasonality profiles and patterns of landscape productivity; (2) verify satellite observations of dynamic seasonal responses of the landscape to climate drivers (rainfall, temperature, radiation, etc.), disturbance, and land use activities; (3) and provide the scientific basis for spectral reflectance characterisation of vegetation and help understand reflectance patterns at the micro-scale.

During the TERN Landscape Assessment campaigns, 3-5 samples of leaves per branch (youngest - middle and oldest leaf) and 3-4 branches (bottom to crown) were sampled from lower to upper branches to provide a proxy for age (Figure 17.16). The focus for these leaf samples was the dominant species within the TERN Landscape Assessment campaign site. To determine if whole tree/canopy leaves seasonally change their optical/biologic properties, a spectroradiometer and integrating sphere was used to assess leaf spectral reflectance and transmittance (Figure 17.16). All collected leaves were frozen for subsequent laboratory analysis of their chemical properties, e.g. chlorophyll, nitrogen, tannin, lignin and water.

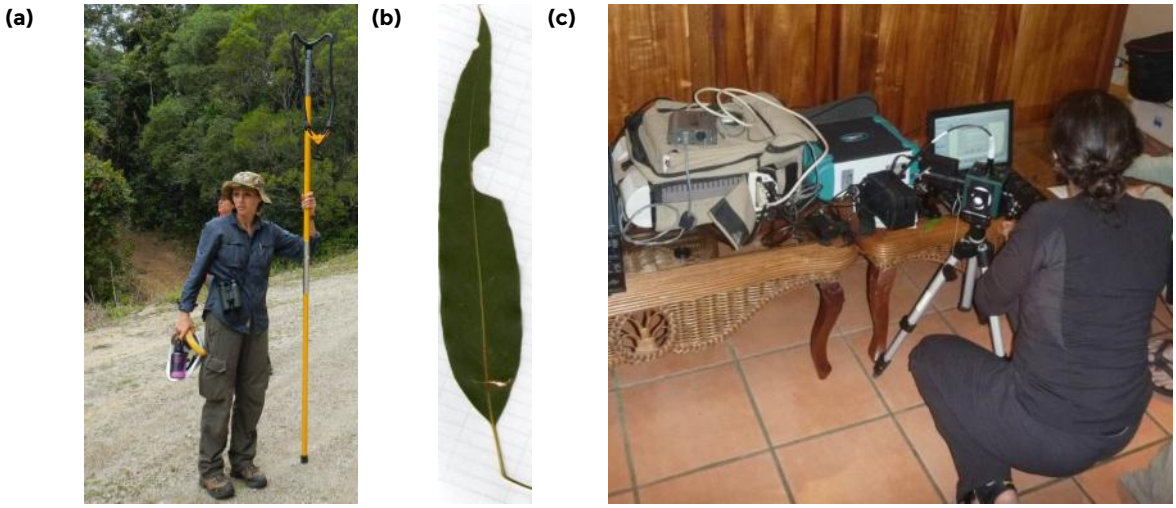

Figure 17.16
(a) Slingshot used to fire robe over branch to collect canopy leaves,
(b) leaf sample, and
(c) using a spectroradiometer and integrating sphere to assess leaf spectral properties.

17.6.8 Spectroradiometer Measurements of Ground Calibration Targets

Field spectroradiometer measurements have been collected for calibration and validation of at-surface reflectance of airborne hyper-spectral image data. Once the at-surface reflectance values of the hyper-spectral image data have been validated, the data can be used for scaling up to medium spatial resolution Landsat and MODIS data for calibration and validation of satellite based Nadir Bidirectional Reflectance Distribution Function (BRDF)-Adjusted Reflectance (NBAR) products. Calibration targets should be large (ideally, calibration targets should cover an area of at least 3 x 3 pixels of the airborne hyper-spectral data), homogeneous, spectrally featureless in the part of the spectrum to be investigated, Lambertian and encompass a range of albedo levels (bright to dark). Calibration targets can either be natural 'pseudo-invariant' features (asphalt, concrete, salt, sand, gravel, limed and painted surfaces) at the site or artificial targets specifically placed into the flight lines. TERN Landscapes have used three 8 m x 8 m standard canvas calibration targets in white, grey and black colours (Figure 17.17a-b). The site chosen to place these targets

should preferably in the centre of one of the flight lines (i.e. at the nadir view), flat and open. A spectralon reference panel was used every 5 minutes to optimise the spectrometer measurements to adjust the sensitivity of the detector according to the present illumination conditions (Figure 17.17c). In those cases where an additional spectroradiometer was available, irradiance was also measured (Figure 17.17d).

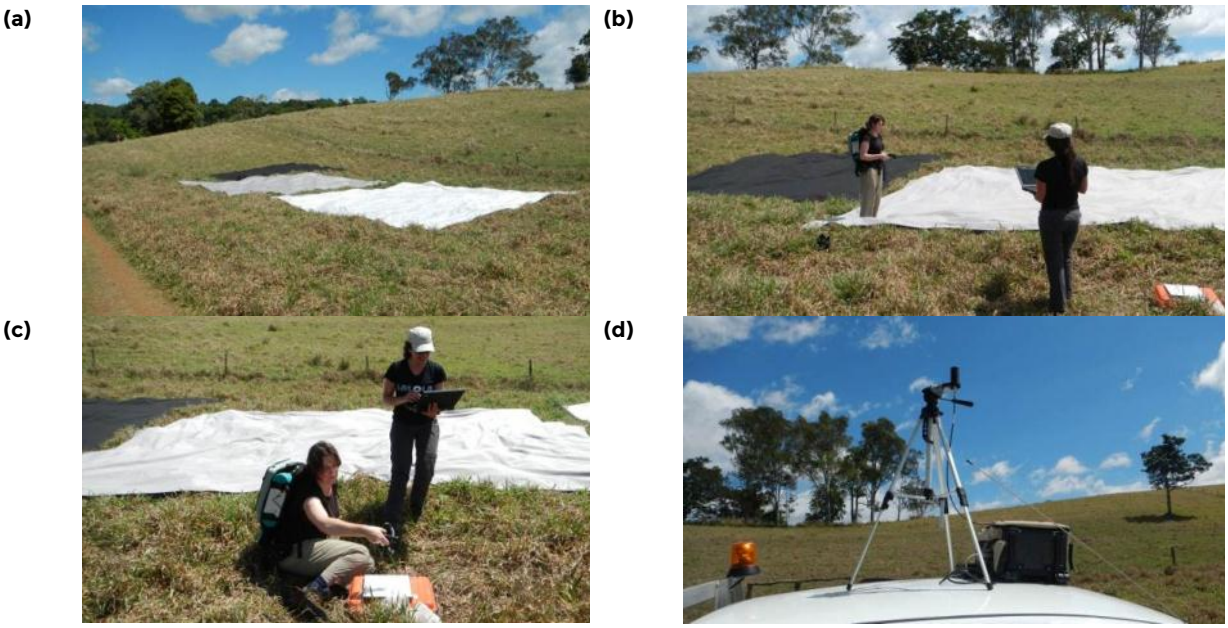

Figure 17.17
(a) White, grey and black 8 m x 8 m ground calibration targets,
(b) spectroradiometer measurements of ground calibration targets,
(c) using the spectralon panel to adjust the detector to the present illumination conditions, and **(d)** irradiance measurements.

17.6.9 Atmospheric measurements Using a Sunphotometer and Ozonometer

The acquisition of sunphotometer and ozonometer measurements is critical to capture data on atmospheric properties during airborne hyper-spectral imaging campaigns as well as for measurements coinciding with the overpass of satellite sensors. The atmospheric properties measured are used in the atmospheric correction of the remotely sensed image data. The Microtops instruments used by TERN's Landscape Assessment platform capture solar radiance data each in five wavelengths, which are used to extract information on aerosol optical depth, total column water vapour content, atmospheric pressure, temperature and total column ozone content (Figure 17.18). These observations are made regularly during the airborne hyper-spectral data capture at a set location within an open area.

Figure 17.18
Setup of Microtops sunphotometer and ozonometer on tripod with GPS receiver.

17.6.10 Pheno-Cams for Ground and Canopy Cover Phenology Time-Series Observations

For some of the TERN Landscape Assessment sites, pheno-cams, i.e. optical cameras, have been installed to automatically collect and store photos taken every hour throughout the year to study phenology of ground and canopy cover. Pheno-cams have been installed at about 3 m height on metal poles cemented into the ground for observation of ground cover, while pheno-cams for observation of canopy cover have been installed on flux towers present within the 5 km x 5 km TERN Landscapes sites.

(a)

(b)

Figure 17.19
(a) Pheno-cam installed on pole to assess ground cover phenology and **(b)** on flux tower to assess canopy cover phenology.

17.7 Field Data Storage

The field data processing and storage for all the TERN Landscape Assessment campaigns is managed within the TERN Landscape Assessment field data management system. The TERN Landscape Assessment field data management system consists of documentation, software/hardware and processes designed to facilitate the consistent collection, recording, storage and delivery of field data.

For the TERN Landscape Assessment campaigns, field data were collected following standardised protocols developed prior to field data collection. Supporting ancillary data were collected using standardised field data collection forms. All data collected in the field were downloaded and backed up after collection each day of the campaigns. Field forms were photographed and stored alongside instrument data in the backups.

On return from the field, data were collated and organised into a form enabling the data sets to be processed via Python scripts. These scripts are designed to upload ancillary data onto the TERN Landscape Assessment PostGIS spatial database, as well as rename instrument filenames to fit the Landscape file naming convention.

The TERN Landscape Assessment PostGIS database directly links to the Landscape GeoServer, which in turn links to the TERN Landscape Assessment Visualisation Portal. Delivery is therefore dynamic, with the information on the portal being the most up-to-date version of any given data set. Renamed instrument files are zipped and delivered by being placed within a directory linking to the Landscape Thematic Real-time Environmental Distributed Data Services (THREDDS) server. All data and relevant information are brought together both within the visualisation portal (through the use of popup windows specific to each data set) or within the data set metadata records. Both mechanisms contain links to all relevant data and metadata.

Futher information on the TERN Landscapes Assessment data management system, including access to system documentation (protocols, field forms etc), tools and processes, can be found on the TERN Landscape Assessment field data management home page on the TERN Landscapes Assessment xwiki (http://data.auscover.org.au/xwiki/bin/view/Field+Sites/WebHome). It should be noted, that the system is progressively evolving, so specific management steps may change over time.

17.8 Airborne Data Collection

The airborne data collection component of the first TERN Landscape Assessment campaign was undertaken by Hyvista, who used their Hymap sensor to collect hyper-spectral data and sub-contracted Vekta to collect discrete return LiDAR data. The subsequent eight airborne campaigns were all undertaken by ARA, Flinders University. Hence, only the ARA airborne data collection approaches are described in this section.

For the last eight TERN Landscape Assessment campaigns, airborne full waveform LiDAR and hyper-spectral data in the visible near infrared and shortwave infrared part of the spectrum were collected using the two research aircrafts of Flinders University – ARA (Figure 17.20). A Riegl Q560 LiDAR and two GPS/ Inertial Measurement Units (IMU) systems (OXTS RT4003 and NovAtel SPAN / LCI) were mounted in an underwing pod of one of ARA's ECO-Dimona research aircrafts. A SPECIM AisaEAGLE II hyper-spectral scanner (VNIR) and a SPECIM AisaHAWK hyper-spectral scanner (SWIR) were mounted in underwing pods of the second of ARA's ECO-Dimona research aircrafts. Each scanner had its own OXTS RT4003 GPS/IMU navigation and attitude system. A NovAtel GPS Base station was set up within or close to each of the TERN Landscape Assessment campaign sites to optimise the navigation data for the airborne data and to demonstrate the accuracy of the ensuing geo-referencing of all airborne data.

Figure 17.20 Diamond Aircraft HK36TTC ECO-Dimona over the Robson Creek site in September 2012.

This LiDAR scanner setup resulted in an outgoing pulse rate of 240 kHz, scanned at 135 lines per second. Each scan line is an angular sweep through 45 degrees and contains 882 individual laser shots. The scan pattern is offset by 4 degrees from the vertical of the scanner coordinate system in order to compensate for wing dihedral and thus result in a symmetrical arrangement in aircraft coordinates. For a nominal flying height of 300 m above ground and a forward speed of 40 m/s, this setup yields a homogeneous surface point distribution of 0.30 m in along-track as well as across-track directions. At a nominal flying height of 300 m above ground the specified footprint of the laser pulse on the ground has a diameter of < 0.15 m, resulting in an a priori average uncertainty of the horizontal position of any encountered target of 0.075 m. Due to the extreme terrain for some of the TERN Landscape Assessment campaign sites such as the TERN Robson Creek Rainforest SuperSite, a combination of north-south and east-west oriented flight lines were flown for the LiDAR data capture, in additional to a collection of terrain-following survey lines along the steepest slopes to ensure full coverage. For all other sites, either regular north-south or east-west patterns (with 125 m flight line spacing) were flown. The LiDAR surveys were usually flown in the early morning.

The SPECIM AisaEAGLE and AisaHAWK hyper-spectral scanners were mounted underneath each wing of one of the ARA research aircrafts. The AisaEAGLE has a silicon Charge Coupled Device (CCD) detector giving 965 spatial pixels across the aircraft track. The detector pixels are square, and from the nominal flight pattern altitude of 500 m above ground, these project to 0.33 m sampling. The AisaEAGLE was configured to return data in 252 spectral bands between 400 and 1000 nm, and exposure considerations led to a sampling rate of 30 - 45 lines per second for the TERN Landscape Assessment campaigns. The AisaHAWK hyper-spectral line scanner also has a detector array with square pixels. It images 296 spatial pixels across the flight track, and the nominal pattern altitude of 500 m was selected to give a projected sampling interval of 1 m on the ground. Since the AisaEAGLE pixels are smaller, the AisaHAWK resolution was the driver for the flight pattern. The instrument was configured to return data in 241 spectral bands between 990 and 2494 nm. The AisaHAWK was operated at 45 lines per second, for Signal-Noise-Ratio considerations.

With 1 m cross-track sampling, the AisaHAWK was the limiting instrument for line spacing, with a nominal swath of 296 m. This dictates a flight line spacing of less than 150 m to allow for disturbances of aircraft attitude and position, and for convenience of flight line management the same 125 m-spaced lines were specified as for the north-south LiDAR pattern. The flight pattern planned and flown for the hyper-spectral data collection was based on the imaging geometry of the instruments, along with the consideration of desiring imaging angles as close to orthogonal to the sun's incidence angle as possible, with the highest solar illumination angle. This resulted in a set of parallel, north-south runs, to be flown as close to solar noon as practicable (Figure 17.21).

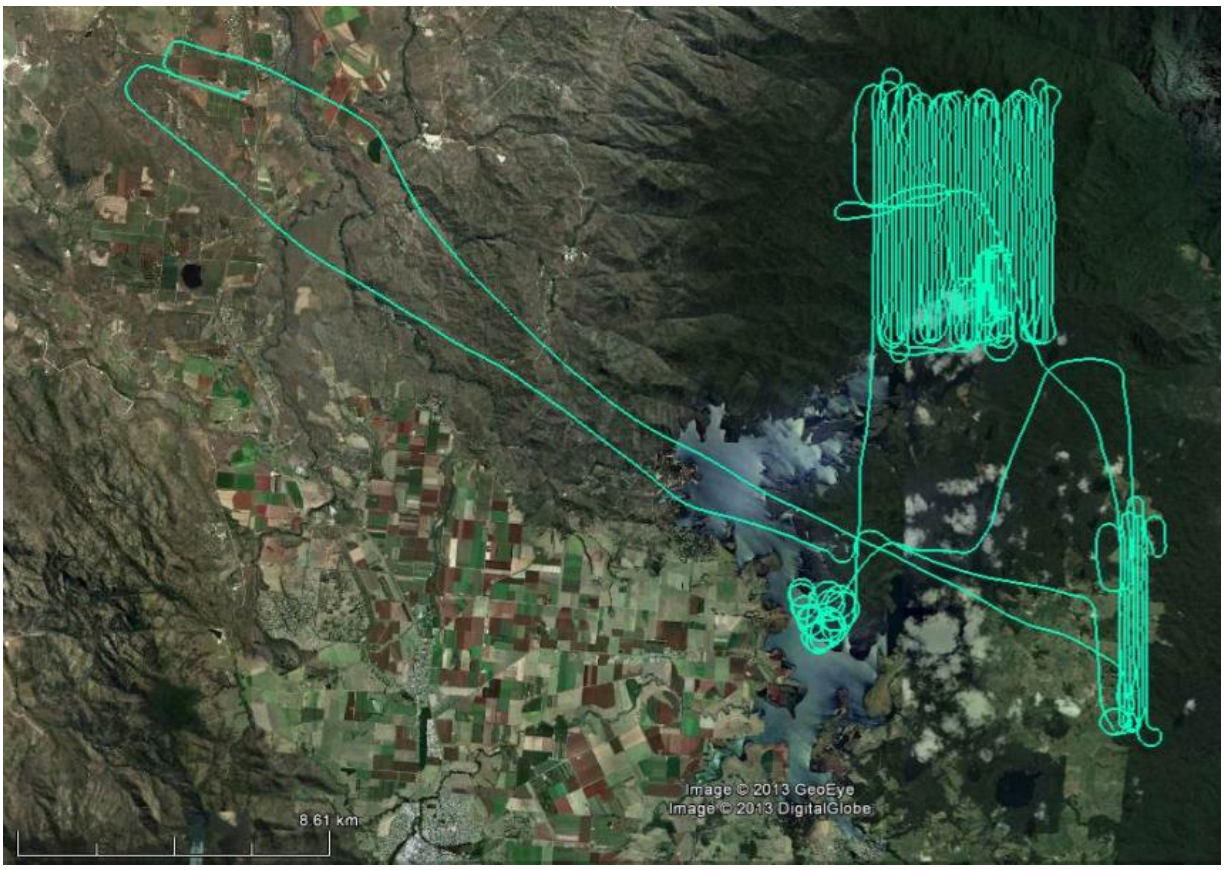

Figure 17.21 Flight pattern for the hyper-spectral data collection of the Robson Creek campaign, showing take-off and landing at Mareeba Airport, the 5 km x 5 km TERN Landscapes campaign site, and the additional site towards southeast where leaf samples were collected and the ground calibration targets were deployed.

17.9 Data Availability

The TERN Landscape Assessment field data sets typically consist of instrument files or measurements and a supporting shapefile of ancillary data (such as coordinates, date, and other observations). Associated metadata records for each data set contain details assisting users to determine the suitability of the data for their purposes, including abstract, licensing, contact details, spatial and temporal scales, etc. Additional information such as field collection protocols and associated reports are also publically available.

All field and airborne data collected, and associated metadata, can be freely downloaded from the TERN Landscape Assessment data servers. This occurs through either the TERN Landscape Assessment Visualisation Portal (http://data.auscover.org.au/Portal2/) or via the product's metadata records. Exploration of the data is most easily accomplished through the Visualisation Portal (Figure 17.22). A brief tutorial on how to use this portal can be found on the TERN Landscape Assessment xwiki: http://data.auscover.org.au/xwiki/bin/view/Field+Sites/Access+Field+Data).

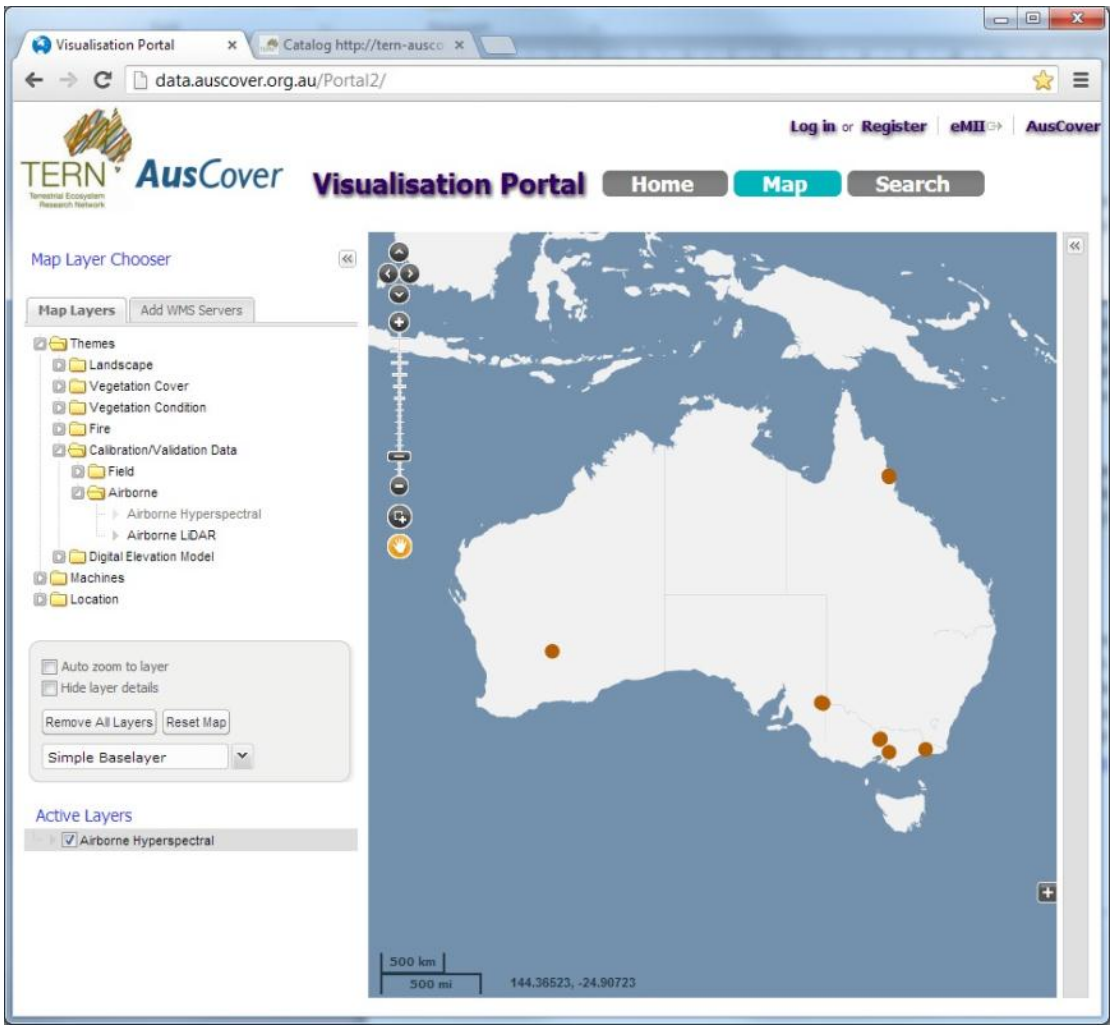

Figure 17.22 TERN's Visualisation Portal displaying the locations of the airborne hyper-spectral data.

Most of the information is available by direct download from the portal or via links to online sources. For instrument data sets (imagery, scans, data files, etc.), users are directed to the TERN Landscapes THREDDS server (Figure 17.23) for download via http. For most of these data sets, this is the most accessible way to download the data. However, for some of the larger and more complex data sets this is too time-consuming and cumbersome. For this reason an anonymous File Transfer Protocol (FTP) server has been setup to enable large scale transfer of the data sets (ftp://tern-auscover.science.uq.edu.au). Instructions on how to access the data sets via various FTP clients is provided on the TERN Landscape Assessment xwiki: (http://data.auscover.org.au/xwiki/bin/view/Field+Sites/FTP+Access).

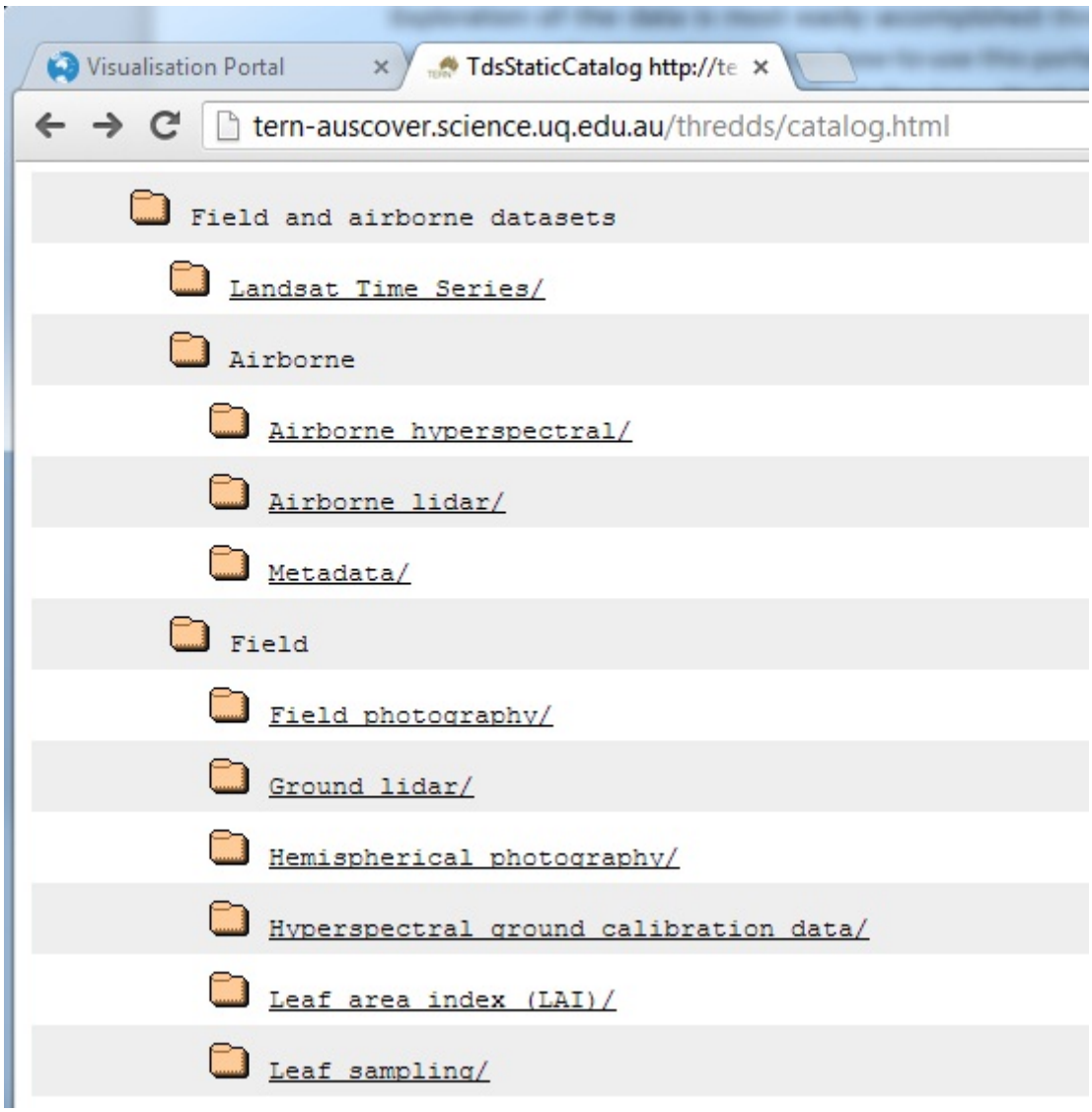

Figure 17.23 Field and airborne data sets present on the TERN Landscapes THREDDS server.

It should be noted that the field data sets are dynamic and updated as more data becomes available either through data becoming publically available or subsequent site visits. At no time can a field data set be considered 'complete' and data sets may be improved or added to at any time. As ARA is a university-based group and not a commercial data provider, and as such has its own research interests in the airborne and other data, on-going improvement of the processing algorithms will continue and amended data sets will become available. A typical example is ARA's current initiative to transfer the LiDAR full waveform data into the new open-source Pulsewave format. Some other sensors were flown simultaneously on the ARA research aircraft for some of the campaigns, including a 15 MPixel aerial camera, a 2048 pixel wide Tri-Spectral line scanner (red, green, near infrared) and an experimental single band linescanner. Data from these sensors will be available in the near future.

17.10 Summary

TERN's Landscape Assessment platform has undertaken nine field and airborne LiDAR and hyper-spectral campaigns between January 2011 and June 2013 as part of the calibration and validation program to support the production of Australian continental scale satellite based time-series of biophysical properties. This has resulted in the development of standardised field and airborne data collection approaches and protocols to ensure the consistency and quality of the data collected. While these approaches and protocols may be of use to others planning similar campaigns, it is worth highlighting that further improvements will still be made to existing approaches and protocols in the future. It should also be acknowledged that the type of environment being investigated will influence the way in which the most optical field and airborne data can be obtained. The field and airborne data collected by TERN are anticipated for multiple uses and are freely available via the online TERN Landscape Assessment Visualisation Portal to promote and support further ecosystem science and research in Australia in the future.

References

Armston , J.D., Denham, R.J., Danaher, T.J., Scarth, P.F. & Moffiet, T.N. (2009). Prediction and validation of foliage projective cover from Landsat-5 TM and Landsat-7 ETM+ imagery. *Journal of Applied Remote Sensing*, 3, 033540.

BOM (2006). Bureau of Meteorology. http://www.bom.gov.au/ [last accessed 16 April 2015].

Bradford, M.G., Metcalfe, D.J, Ford, A.J., Liddell, M.J., and McKeown, A.T. (2014) Floristics, stand structure and above ground biomass of a 25 ha rainforest plot in the Wet Tropics of Australia. *Journal of Tropical Forest Science*, 26, 543-553.

Chen, J.M., Rich, P.M., Gower, S.T., Norman, J.N. & Plummer, S. (1997). Leaf area index of boreal forest: Theory, techniques, and measurements. *Journal of Geophysical Research*, 102(D24), 29,429-29,443.

Graham, A.G. (ed.) (2006). *The CSIRO Rainforest Permanent plots of North Queensland. Site, Structural, Floristic and Edaphic Descriptions*. CSIRO and Cooperative Research Centre for Tropical Rainforest Ecology and management. Rainforest CRC, Cairns. 252pp.
http://www.jcu.edu.au/rainforest/publications/permanent_plots.htm [last accessed 16 April 2015]

LI-COR (2013). *LAI-2200 Plant Canopy Analyser Instruction Manual*. Publication Number: 984-14112. Lincoln, Nebraska, USA. http://envsupport.licor.com/docs/LAI-2200C_Instruction_Manual.pdf [last accessed 16 April 2015].

Metcalfe, D.J., Bradford, M.G. & Ford, A.J. (2008). Cyclone damage to tropical rainforests: species and community level impacts. *Austral Ecology*, 33, 432-441.

Muir, J., Schmidt, M., Tindall, D., Trevithick, R., Scarth, P. & Stewart, J.B. (2011). *Field measurements of fractional ground cover: a technical handbook supporting ground cover monitoring for Australia*. Prepared by the Queensland Department of Environment and Resource Management for the Australian Bureau of Agricultural and Resource Economics and Sciences, Canberra, November.

Robison, S.A. & McCarthy, B.C. (1999). Potential factors affecting the estimation of light availability using hemispherical photography in oak forest understories. *Journal of the Torrey Botanical Society*, 126(4), 344-349.

Acknowledgements

Many people and organisations have been involved in TERN Landscape Assessment field and airborne data collection campaigns. Every TERN Landscapes node and parties associated with the nodes are thanked for their input and participation in the field and airborne campaigns and for the post-processing and analysis of the obtained data. Also thank you to both Hyvista and Airborne Research Australia for the participation and involvement in the TERN Landscape Assessment campaigns.

Chapter 18. A calibration and validation framework to support ground cover monitoring for Australia

J.B. Stewart[1]*, J.E. Howorth[1]

[1] Australian Bureau of Agricultural and Resource Economics and Sciences

*Corresponding author:

Jane.Stewart@agriculture.gov.au

Abstract

To derive products from remote sensing requires reference sites to calibrate and validate the products. A national network of reference sites was established for this purpose to enable monitoring of ground cover using satellites. The location of field sites was guided by a national sampling strategy and associated sampling protocols. National standards were established for site descriptions and measurement of ground cover. Field teams were trained in these methods. More than 600 sites were measured over a 4 year field campaign and used to improve MODIS and Landsat-derived fractional cover products for Australia (both of which are described in Chapter 7). The data from the national network of sites are available via TERN.

Key Points

- A nationally agreed, reliable and cost-effective basis for measuring and mapping ground cover using satellite imagery has been implemented.
- An expanding, sensor-independent, national network of sites enables calibration, validation and improvement of remotely sensed fractional cover products.
- Future applications of the field data collected are possible with free data access under license.

18.1 Introduction

The amount of vegetation covering the soil—the ground cover— is a useful indicator of land condition. At the continental scale for Australia (>10^6 km^2) and within its states, ground cover monitoring supports assessment of environmental targets related to soil erosion and land management. Monitoring ground cover consistently over large spatial extents, at multiple spatial scales and through time is possible using remote sensing.

The 'Ground Cover Monitoring for Australia' project, funded by the Australian Government Department of Agriculture (DAFF, 2012), was established to develop and implement a nationally agreed, reliable and cost-effective basis for measuring and mapping ground cover using satellite imagery, and produce regular updates of ground cover conditions across Australia. Collaborating organisations were the Commonwealth Scientific and Industrial Research Organisation (CSIRO), New South Wales Office of Environment and Heritage, Northern Territory Department of Land Resource Management, Queensland Department of Science, Information Technology, Innovation and the Arts, South Australian Department of Environment and Natural Resources, Tasmanian Department of Primary Industries, Parks, Water and Environment, the Terrestrial Ecosystem Research Network (TERN) through their Landscape Assessment, Ecosystem Surveillance and Ecosystem Processes observatory platforms, Victorian Department of Economic Development, Jobs, Transport and Resources, and the Western Australian Department of Agriculture and Food. The project was managed by the Australian Bureau of Agricultural and Resource Economics and Sciences (ABARES), a research bureau within the Australian Government Department of Agriculture.

A national workshop in late 2009 scoped the tasks required to monitor ground cover across Australia using remote sensing (Stewart *et al.*, 2011). It was agreed that national, monthly monitoring of ground cover be completed using the MODIS-derived fractional vegetation product of Guerschman *et al*. (2009), also described in Chapter 7 of this handbook. This product estimates the percentage of the satellite pixel covered by green vegetation, non-green vegetation and bare soil. To use this product across Australia it was also agreed that extensive calibration and validation be supported by a national network of field sites.

A national sampling strategy (Malthus *et al.*, 2013) was developed to guide the location of sites. Standardised methods were also developed to measure ground cover in the field (Muir *et al.*, 2011). A national network of sites (NCI, 2015a) was established to calibrate, validate and improve remotely sensed fractional cover

products derived from both the MODIS and Landsat satellites (Chapter 7). Data from over 640 sites have now been collated under this project.

Figure 18.1 outlines the procedure adopted to improve the national remotely sensed ground cover maps outlined above using field site data. This chapter deals with the first three aspects—site selection, site characterisation and data collation—with some consideration of data analysis where it informed site selection. Bastin *et al*. (2012), DSITIA (2014) and Karfs *et al*. (2009) provide some examples of reporting ground cover levels and trends—this is an area of development.

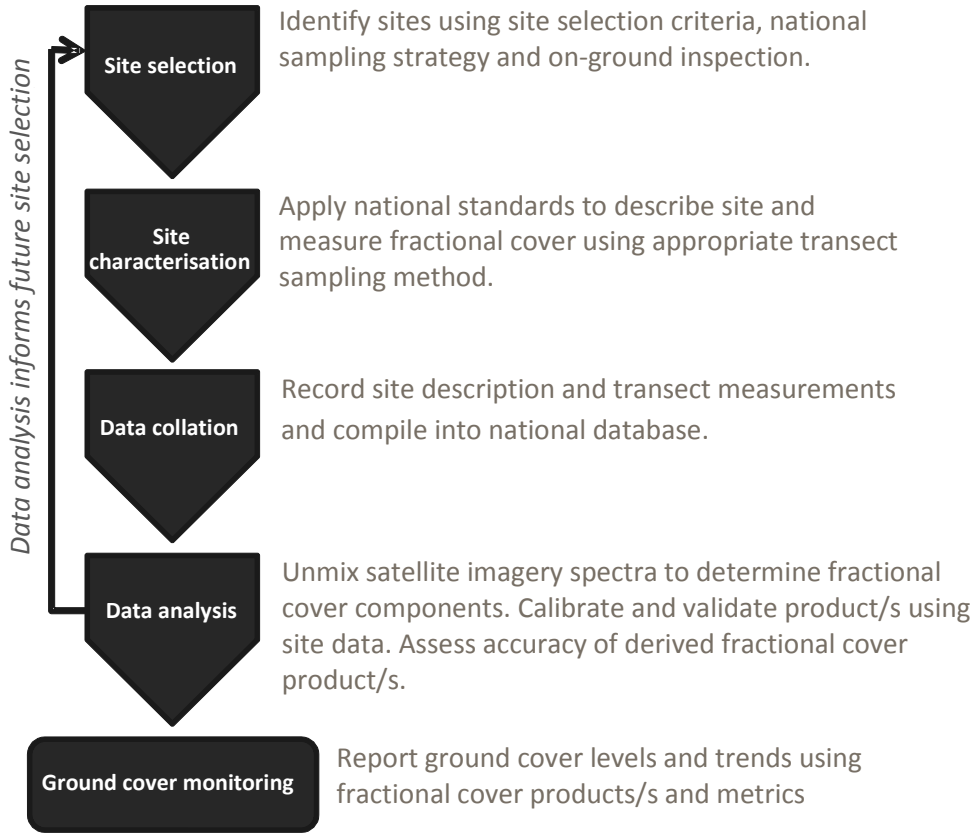

Figure 18.1 Procedure to create remotely sensed fractional cover products to monitor ground cover (modified from Muir *et al*. 2011).

18.2 Sampling strategy

With state agency partners, as listed earlier, a national network of ground cover reference sites was established. The location of these field sites was prioritised according to eight stratification principles that address variability and provide spatial representativeness across Australia. The stratification principles (Malthus *et al*., 2013), in order of priority, were:

1. Sample all non-woody vegetation types used for grazing and broadacre cropping—for assessment of ground cover under agricultural uses.

2. Target field validation effort at 90 per cent in rangeland areas and 10 per cent in broadacre cropping areas—the rangelands cover a large aerial extent of Australia's agriculture and its habitats are vulnerable to loss of ground cover and subsequent soil loss.
3. Select field sites with less than 12 per cent foliage projected cover or 20 per cent tree canopy cover—predominantly treed areas have a lower risk of soil erosion and it is also difficult to separate ground cover from tree cover.
4. Sample the full range of the ground cover components from 0 to 100 per cent.
5. Select field sites which are spatially homogeneous at the MODIS scale (500 metre pixel, 25 hectare in area)—to ensure a valid comparison between the field data and fractional cover estimates derived from the satellite data (at MODIS or finer scale).
6. Target key soil colours: gibber, red soils, black soils, bright soils, and others—to establish the influence of soil colour on the fractional cover product and highlight where useful improvements can be made.
7. Consider other issues such as soil moisture, timing of sampling and the need for repeat visits to sites—for their effect on algorithm unmixing and to establish the temporal reliability of the product.
8. Review to ensure an adequate number of sites in each priority environment.

The aim was to achieve an accuracy of at least +/- 15 per cent for all 3 components. The green vegetation component is estimated with the highest accuracy, followed by the bare soil component, with the non-green vegetation component the least accurate. To meet the needs of erosion modellers—identified as key users of the MODIS-derived fractional cover product—achieving an accuracy of +/- 15 per cent for the bare soil component was a priority.

The number of validation sites required to achieve this level of accuracy was difficult to estimate, but was notionally set at 1500. This sample size was based on the experience of the land cover product used in the National Carbon Accounting System (Furby, 2002) with 3000 validation sites, and the efficiencies gained using spectral unmixing in the fractional cover products. Sites were distributed systematically across the in-scope region—defined by the stratification principles above—to achieve maximum spatial representativeness. Malthus *et al*. (2013) recommended that the sampling effort be reviewed annually to assess the validity of the sample size estimate of 1500, the impact of ground cover sampling sites on reducing the uncertainty of the product, and where to focus future sampling sites.

18.3 Field handbook

To calibrate, validate, and improve remotely sensed fractional cover products, standard field data collection methods are required. A field handbook for measuring fractional cover (Muir *et al*. 2011) was trialled in all states and the Northern Territory by project partners. This handbook was then used to measure ground cover across the national network of ground cover reference sites. The handbook draws on ABARES (2011), Forward (2009), NCST (2009) and Tongway & Hindley (1995), for site description; and Brady *et al*. (1995), Scarth *et al*. (2006) and Schmidt *et al*. (2010) for the modified discrete point transect sampling methods. Further details are given under site characterisation.

18.4 Site selection

In addition to the stratification principles in the sampling strategy (Malthus *et al*., 2013), the following criteria from the field handbook were also used to locate sites (Muir *et al*., 2011):

- Acquire field data within one month of image acquisition.

- Locate a minimum of five sites per Landsat scene.
- Locate the edge of a site at least 100 metres from roads, powerlines or other features not characteristic of the vegetation being measured.
- Locate sites away from water run-on areas. Surface moisture can affect reflectance characteristics of the ground cover fractions.
- Locate sites on level or near-level ground. If selection of a sloped site is unavoidable, avoid western and southern slopes as these are affected by shadow due to winter and morning sun angles.

18.5 Site characterisation

18.5.1 Site description

Each site was described according to the categories in Muir *et al*. (2011) which consider:

- basic information on site visit—such as date, position, land use, plant growth stage, management phase, field observers
- vegetation attributes—such as structural formation, tree basal area, perennial vegetation percentage
- landform attributes—such as erosion, micro relief
- soil attributes—such as condition, strength, and colour.

A Global Positioning System (GPS), clinometer (to measure slope and tree height), optical wedge prisms or Haglöf Factor Gauge (for tree basal area), and Munsell Soil Color Charts were used to take these measurements.

18.5.2 Transect sampling methods

Fractional cover was measured at each site using a modified discrete point sampling method. This quantitative, time-efficient, and relatively objective method ensured repeatability between different operators (Booth *et a*l., 2006). Two different transect layouts for the discrete point sampling method were used.

For most vegetation communities, three 100 metre transects were laid in a star shape (Scarth *et al*., 2006). The transects were oriented at 0, 60 and 120 degrees from north. Measurements were made at each metre giving a total of 300 observations. This transect arrangement is shown in Figure 18.2a.

Where vegetation was in rows, as for cropping, two transects with 200 observations could be used (Schmidt *et al*., 2010). The lower complexity of cropping sites required fewer measurements to capture the variation. Transects were oriented at 45 degrees off-row to ensure adequate sampling both along and across rows. This transect arrangement is shown in Figure 18.2b.

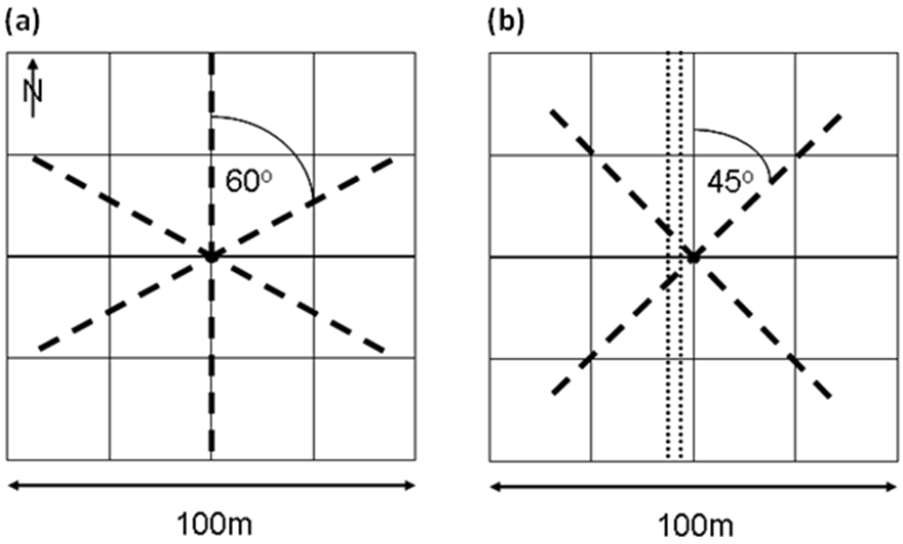

Figure 18.2 Transect layouts (a) in natural or pastoral environments; (b) in vegetation in rows, such as agricultural crops (adapted from Muir *et al*. 2011).

Equipment required for the transect measurements were tapes for the transects, a compass for tape placement, a telescopic pole attached with a laser pointer (for measuring the ground cover and low woody vegetation) and a densitometer (for measuring woody vegetation), and a digital camera for site photos.

18.6 Data collation

The data collected were entered into two electronic Microsoft Excel spreadsheets—the site description form and the transect form—and along with digital site photographs were provided to ABARES for inclusion in the ground cover reference sites database (Rickards *et al*., 2014).

The ground cover reference sites database used open source software—the object-relational database PostgreSQL with PostGIS to support geographic objects. The database can show the spatial locations of field sites in geographical information systems. The database consists of tables containing static data and views which calculate values from the tables. The data are available through the National Computer Infrastructure (NCI, 2015a), the TERN Australian Ecological Knowledge and Observation System (ÆKOS) Data Portal and Soils to Satellite website. Current data holdings (643 observations) are shown in Figure 18.3 for sites funded under the 'Ground cover monitoring for Australia' project.

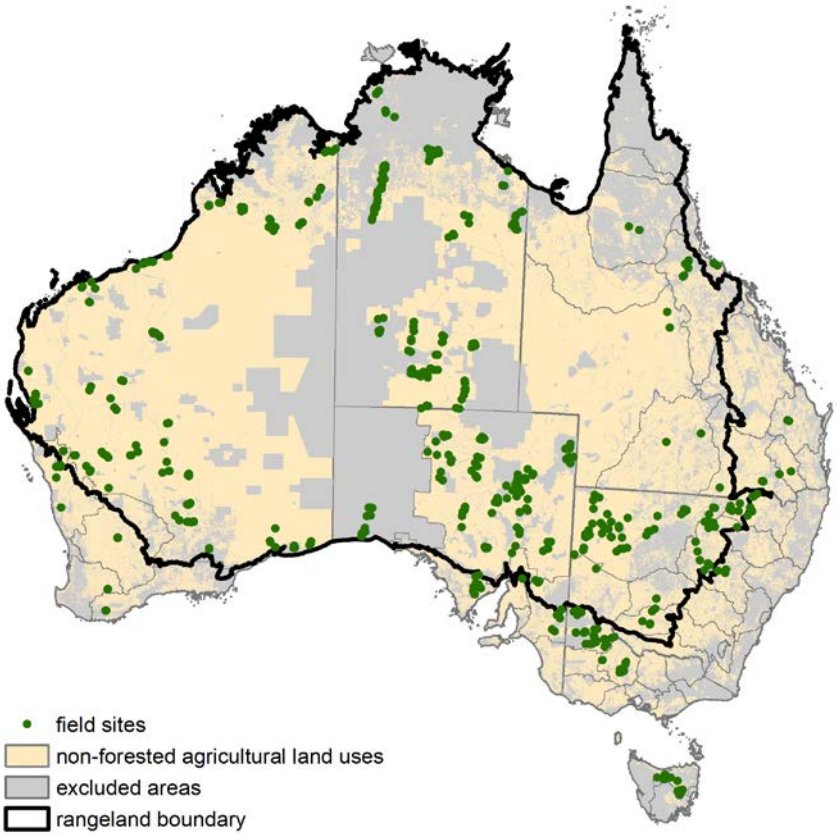

Figure 18.3 Location of the 643 ground cover observations (at 596 sites) measured under the project to August 2014 using the methods of Muir *et al*. (2011). 507 of these observations are available to download at the National Computational Infrastructure (NCI, 2015a).

18.7 Data analysis

Field site data were used to validate the MODIS-derived fractional cover product. Data analysis was completed according to Malthus *et a*l. (2013):

1. Assess site heterogeneity—rank sites on their heterogeneity to determine if heterogeneity affects product error.
2. Assess site validation data obtained—(i) identify cover fractions which are under-represented and (ii) determine that sites spatially represent the priority regions based on land use, vegetation type and soil colour, to inform priorities for future field campaigns.
3. Compare field data with MODIS-derived fractional cover—statistically assess the degree of agreement between site observations and the fractional cover predicted by the product to inform model accuracy.
4. Assess priorities for revisiting sites—for temporal accuracy to detect change at the same location.
5. Improve the product—as well as additional sites consider, for example, use of further spectral information and alternative satellite sensors to improve the estimates of fractional cover from the product.

Guerschman *et al*. (2012) recalibrated the MODIS-derived vegetation fractional cover product from 2009 using existing site data, predominantly from Queensland and its Statewide Landcover and Trees Study (SLATS) (359 sites, 567 observations). Bias in the estimates of non-green vegetation and bare soil was eliminated and the root mean square error (RMSE) in the estimates of the three cover fractions was also reduced. The aim is to reduce the RMSE to below 10-15 per cent by further improvement to the fractional cover product. The effect

of soil colour and soil moisture on product performance is also to be resolved. A new version of the product was released by CSIRO in 2014 (Guerschman *et al*., 2015). This version (3.0) utilises the sites funded under this project as well as other sites that have measured fractional cover according to, or compatible with, the national standards of Muir *et al*. (2011), such as under the SLATS operating in Queensland and New South Wales and TERN Landscape Assessment sites (913 sites, 1171 observations). Version 3.0 has a RMSE of 13, 18 and 17 per cent for the green vegetation, non-green vegetation and bare soil fractions respectively. It uses the approach of Scarth *et al*. (2010) which is used to produce Landsat-derived fractional cover estimates (see Chapter 7 for further information). Thus a combined Landsat/MODIS fractional cover product is now possible calibrated and validated with the same set of field observations.

Figure 18.4 shows the per cent green vegetation, non-green vegetation and bare soil for the sites funded under the 'Ground cover monitoring for Australia' project (643 observations). This is an example of how to identify data gaps in the cover fractions. Stewart et al. (2014) provide recommendations for future field campaigns based on an analysis of observations against the stratification principles of the sampling strategy (Malthus *et al*., 2013).

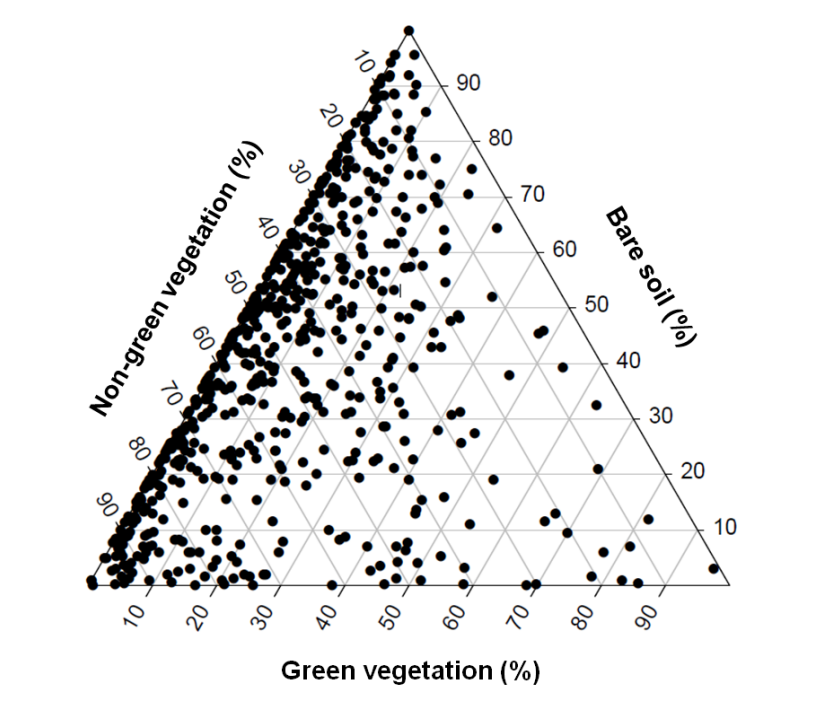

Figure 18.4 Tri-plot of the 643 ground cover observations measured under the project to August 2014 using the methods of Muir et al. (2011). The tri-plot shows the distribution of observations based on the per cent green vegetation, non-green vegetation and bare soil measured at a site.

18.8 Lessons learnt and future directions

This project established a national network of ground cover reference sites with data collected by a number of different field operators over a number of years. To ensure high quality data from such a collaborative project it is recommended to:

- use consistent field methods
- apply a sampling strategy and sampling protocols
- use data entry tools to minimise errors
- use an accessible database
- establish clear data licenses
- annually review data collected—to identify issues, prioritise future sites, and provide feedback on the completeness of the data received.

18.8.1 Consistent field methods

The field handbook of Muir *et al*. (2011) provides the national standards for collecting site data. Another important step to achieve data quality was for the different field teams in each state and the Northern Territory to be trained by experienced field operators from the Queensland Department of Science, Information Technology, Innovation and the Arts in these methods. These training exercises were also an opportunity for field teams to have input into the methods so they were indeed applicable nationally. Refresher training before each field campaign was also valuable for many field teams, especially where different operators joined the team or worked together. Feedback from each field campaign to the Australian Bureau of Agricultural and Resource Economics and Sciences (ABARES) was also crucial to make improvements to the data entry forms.

18.8.2 Applying the sampling strategy and sampling protocols

In addition to the sampling strategy stratification principles (Malthus *et al*., 2013), sampling protocols were provided to the field teams to assist with site selection. These sampling protocols (Stewart *et a*l., 2012; Stewart *et al*., 2013) provided the datasets, framework and rationale where a shift in focus was required for locating sites. Before each field campaign the states and Northern Territory submitted likely site locations for consideration by ABARES, the project coordinator. From November 2011, Landsat 5 imagery was not available to assist with site selection, and Landsat 7 imagery was used instead. Landsat 7 imagery severely restricted where sites could be located, as only the centre portion (30 km of 185 km) of the imagery is useable. Field campaigns now use the new Landsat 8 imagery (launched in February 2013), increasing the potential sample area for locating suitable sites to measure. After each field campaign a report was provided to ABARES with the data, listing the locations of the sites, the amounts of the cover components at each site and any issues faced in locating, describing and measuring sites.

18.8.3 Data entry tools

Data entry is a known source of error—transcribing from a paper form to an electronic form. Use of the electronic forms was encouraged as they contained built-in checking, but they were not always practical to use in the field. Recent developments in portable apps for tablets (White *at al*., 2012) and smart phones (R. Trevithick, pers. comm.) that conform to the field handbook of Muir *et al*. (2011) will make future data entry

easier. Attributes such as vegetation species and soil colour were commonly completed incorrectly requiring follow-up by ABARES.

18.8.4 Database interoperability

The individual site data were compiled into a PostGIS database (Rickards *et al.*, 2014) for analysis and spatial display. Fractional ground cover measurement collected by other programs are not accommodated within the database, as such published data can be extracted via the TERN ÆKOS Data Portal. This is the case with the TERN Ecosystem Surveillance observational data which uses a similar method to Muir *et al.* (2011) but requires many more (1010) transect measurements to be collected over the same area at a site (White *et al.*, 2012). Rickards *et a*l. (2014) provides a procedure to translate the TERN Ecosystem Surveillance rangelands point intercept observations into vegetation cover fractions to use in calibration or validation of remotely sensed fractional cover.

18.8.5 Data licensing

ABARES is the data custodian of the site data collected by the state agency partners under the 'Ground cover monitoring for Australia' project. All publishable data (507 observations) are provided to TERN with metadata under the conditions of the Creative Commons Attributions-ShareAlike 3.0 Licence. Unpublished data was withheld for privacy reasons—many (136) of the sites collected on private land. Provision of data aligns with the TERN Data Licencing Policy. All site data are available to select users under a more restrictive data licence. Future field campaigns would encourage landholder consent to publish data.

18.8.6 Data review

Having a national network of ground cover reference sites has already seen improvements in the MODIS-fractional cover product (Guerschman *et al.*, 2012; Guerschman *et al.*, 2015; NCI, 2015b) and the development of a national annual Landsat fractional cover product (JRSRP 2012a) and Landsat persistent green product (JRSRP, 2012b). The MODIS and Landsat fractional cover products are described in Chapter 7 whereas the persistent green product is described in Chapter 8. As the network of sites has expanded, these products can also further represent conditions across Australia. Together with other providers, the network (as at August 2014) totals 1259 sites (1714 observations) (Rickards *et a*l., 2014). Future field campaigns can be even more strategic in locating sites to fill identified data gaps. State-based efforts and TERN activities, such as the TERN Landscape Assessment sites and the TERN Ecosystem Surveillance plots, will provide additional data to the national network of sites—not just for monitoring ground cover but also total vegetation cover, and its components, including foliage projective cover.

References

ABARES (2011). *Guidelines for land use mapping in Australia: principles, procedures and definitions, a technical handbook supporting the Australian Collaborative Land Use and Management Program* (4th ed.). Canberra: Australian Bureau of Agricultural and Resource Economics and Sciences. Available at: http://data.daff.gov.au/brs/data/warehouse/pe_abares99001806/GuidelinesLandUseMappingLowRes2011.pdf (pdf, 3.81MB).

Bastin, G., Scarth, P., Chewings, V., Sparrow, A., Denham, R., Schmidt, M., O'Reagain, P., Shepherd, R. & Abbott, B. (2012). Separating grazing and rainfall effects at regional scale using remote sensing imagery: A dynamic reference-cover method. *Remote Sensing of Environment*, *121*, 443–57. http://dx.doi.org/10.1016/j.rse.2012.02.021.

Booth, D. T., Cox S. E., Meikle, T. W. & Fitzgerald, C. (2006). The accuracy of ground cover measurements. *Rangeland Ecology & Management*, *59*, 179–88.

Brady, W. W., Mitchel, J. E., Bonham, C. D. & Cook, J. W. (1995). Assessing the power of the point-line transect to monitor changes in plant basal cover. *Journal of Range Management*, *48*(2), 187–90. Available at: https://journals.uair.arizona.edu/index.php/jrm/article/view/9011/9623.

DAFF (2012). *Ground cover monitoring for Australia: Factsheet November 2012*. Canberra: Department of Agriculture, Fisheries and Forestry. Available at: http://www.agriculture.gov.au/natural-resources/soils/monitoring/ground-cover-monitoring-for-australia.

DSITIA (2014). *Guide to Using FORAGE Version 1.4*. State of Queensland (Department of Science, Information Technology, Innovation and the Arts). Available at: http://www.longpaddock.qld.gov.au/forage/forage_user_guide.pdf (2.60MB).

Guerschman, J. P., Hill, M. J., Renzullo, L. J., Barrett, D. J., Marks, A. S. & Botha, E. J. (2009). Estimating fractional cover of photosynthetic vegetation, non-photosynthetic vegetation and bare soil in the Australian tropical savanna region upscaling the EO-1 Hyperion and MODIS sensors. *Remote Sensing of Environment*, *113*(5), 928–45. http://dx.doi.org/10.1016/j.rse.2009.01.006.

Guerschman, J. P., Oyarzabal, M., Malthus, T. J., McVicar, T. M., Byrne, G., Randall, L. A. & Stewart, J. B. (2012). *Validation of the MODIS-based vegetation fractional cover product*. CSIRO Land and Water Science Report. Canberra: CSIRO Land and Water. Available at: http://www.clw.csiro.au/publications/science/2012/SAF-MODIS-fractional-cover.pdf (pdf, 6.3MB).

Guerschman, J. P., Scarth, P., McVicar, T. R., Malthus, T. J., Stewart, J. B., Rickards, J. E., Trevithick, R. & Renzullo, L. J. (2015). Assessing the effects of site heterogeneity and soil properties when unmixing photosynthetic vegetation, non-photosynthetic vegetation and bare soil fractions from Landsat and MODIS data. *Remote Sensing of Environment*, *161*, 12-26. http://dx.doi.org/10.1016/j.rse.2015.01.021.

Forward, G. (2009). *Manual of proposed national minimum standards for roadside erosion survey*. DWLBC Report 2009/24, Government of South Australia, through Department of Water, Land and Biodiversity Conservation, Adelaide. Available at: http://nrmonline.nrm.gov.au/catalog/mql:2245.

Furby, S. (2002). *Land cover change: specifications for remote sensing analysis*. National Carbon Accounting System technical report No. 9. Canberra: Australian Greenhouse Office. Available at: http://pandora.nla.gov.au/tep/23322.

JRSRP (2012a). *Fractional cover-Landsat, Joint Remote Sensing Research Program algorithm, Australia coverage*. Queensland: Joint Remote Sensing Research Program. Available at: http://data.auscover.org.au/xwiki/bin/view/Product+pages/Landsat+Fractional+Cover.

JRSRP (2012b). *Landsat persistent green vegetation mosaic of Australia 2000-2010*. Queensland: Joint Remote Sensing Research Program. Available at: http://data.auscover.org.au/xwiki/bin/view/Product+pages/Persistent+Green-Vegetation+Fraction.

Karfs, R. A., Abbott, B. N., Scarth, P. F. & Wallace, J. F. (2009). Land condition monitoring information for reef catchments: a new era. *The Rangeland Journal*, *31*, 69–86.

Malthus, T. J., Barry, S., Randall L. A., McVicar, T., Bordas, V. M., Stewart, J. B., Guerschman, J. P. & Penrose, L. (2013). *Ground cover monitoring for Australia: Sampling strategy and selection of ground cover control sites*. Canberra: CSIRO. Available at: http://data.daff.gov.au/brs/data/warehouse/9ic/9icl/2013/gcmssd9ica_00120130308/grndCovMonAustSampStratAndSelGrndCovCont_v1.0.0.pdf (pdf, 2.2MB).

Muir, J., Schmidt, M., Tindall, D., Trevithick, R., Scarth, P. & Stewart, J.B. (2011). *Field measurement of fractional ground cover: A technical handbook supporting ground cover monitoring in Australia*. Prepared by the Queensland Department of Environment and Resource Management for the Australian Bureau of Agricultural and Resource Economics and Sciences, Canberra. Available at: http://data.daff.gov.au/brs/data/warehouse/pe_hbgcm9abll07701/HndbkGrndCovMontring2011_1.0.0_HR.pdf (pdf, 81.20MB).

NCI (2015a). *Australian ground cover reference sites database - ABARES*. Canberra: National Computational Infrastructure. Available at: http://remote-sensing.nci.org.au/u39/public/html/modis/fractionalcover-sitedata-abares/.

NCI (2015b). *Fractional cover - MODIS, CSIRO Land and Water algorithm, Australia coverage*. Canberra: National Computational Infrastructure. Available at: http://remote-sensing.nci.org.au/u39/public/html/modis/fractionalcover-clw/.

NCST (2009). *Australian soil and land survey field handbook* (3rd ed.). National Committee on Soil and Terrain. Melbourne: CSIRO Publishing.

Rickards, J., Stewart, J., McPhee, R. & Randall, L. (2014). *Australian ground cover reference sites database 2014: User guide for PostGIS*. Canberra: Australian Bureau of Agricultural and Resource Economics and Sciences. Available at: http://remote-sensing.nci.org.au/u39/public/html/modis/fractionalcover-sitedata-abares/doc/Gcov_database_user_guide_2014_20140915.pdf (pdf, 1.10MB).

Scarth, P., Byrne, M., Danaher, T., Hasset, R., Carter, J. & Timmers, P. (2006). State of the paddock: monitoring condition and trend in groundcover across Queensland. *Proceedings of the 13th Australasian Remote Sensing and Photogrammetry Conference*, 20–24 November 2006, Canberra.

Scarth, P., Roder, A. & Schmidt, M. (2010). Tracking grazing pressure and climate interaction - the role of Landsat fractional cover in time series analysis. *Proceedings of the 15th Australasian Remote Sensing and Photogrammetry Conference*. http://dx.doi.org/10.6084/m9.figshare.94250.

Schmidt, M., Tindall, D., Speller, K., Scarth, P. & Dougall, C. (2010). *Ground cover monitoring with satellite imagery in agricultural areas and improved pastures*. Final report to the Bureau of Rural Sciences, State of Queensland (Department of Environment and Resource Management). Available at: http://www.agriculture.gov.au/abares/aclump/Documents/Ground_cover_monitoring_with_satellite_imagery.pdf (pdf, 3.23MB).

Stewart, J. B., Rickards, J. E., Bordas, V. M., Randall L. A. & Thackway, R. M. (2011). *Ground cover monitoring for Australia–Establishing a coordinated approach to ground cover mapping: Workshop proceedings Canberra 23–24 November 2009*. Canberra: Australian Bureau of Agricultural and Resource Economics and Sciences. Available at: http://data.daff.gov.au/brs/data/warehouse/pe_abares99001799/Groundcover_mapping-workshop_proc_11.pdf (pdf, 1.50MB).

Stewart, J. B., Randall, L. A., Rickards, J. E. & Bordas, V. M. (2012). *Ground cover monitoring for Australia: Progress report to June 2011*. ABARES Technical report 12.1. Canberra: Australian Bureau of Agricultural and Resource Economics and Sciences. Available at:

http://data.daff.gov.au/brs/data/warehouse/gcmfap9abll080/GroundCoverMonitoringAust_v.1.0.0.pdf (pdf, 2.13MB).

Stewart, J. B., Rickards, J. E. & Randall, L.A. (2013). *Ground cover monitoring for Australia: Progress report July 2011 to June 2012*. ABARES Technical Report 13.5. Canberra: Australian Bureau of Agricultural and Resource Economics and Sciences. Available at: http://data.daff.gov.au/data/warehouse/9aal/9aalc/GrndCovMon4Aust/PrgRptJun2012/GrndCov_PrgRpt_Jun2012V1.0.0.pdf (pdf, 4.67MB).

Stewart, J. B., Rickards, J. E., Randall, L. A., McPhee, R. K. & Paplinska, J. Z. (2014). *Ground cover monitoring for Australia: Final report July 2012 to June 2013*. ABARES Technical Report 14.1. Canberra: Australian Bureau of Agricultural and Resource Economics and Sciences. Available at: http://data.daff.gov.au/data/warehouse/9aal/9aalc/GrndCovMon4Aust/FinRptJun2013/GrndCov_FinRpt_Jun2013V1.0.0.pdf (pdf, 4.68MB).

Tongway, D. J. & Hindley, N. (1995). *Manual for soil condition assessment of tropical grassland*. Canberra: CSIRO Division of Wildlife and Ecology.

White, A., Sparrow, B., Leitch, E., Foulkes, J., Flitton, R., Lowe, A. J. & Caddy-Retalic, S. (2012). *AusPlots Rangelands Survey Protocols Manual, Version 1.2.9 2012*. South Australia: University of Adelaide Press. Available at: http://www.tern.org.au/rs/7/sites/998/user_uploads/File/AusPlots%20Rangelands%20manual%20versions/AusPlots%20Rangelands%20Survey%20Protocols%20Manual%20v1.2.9%20HiRes.pdf (pdf, 25.58MB).

Glossary

Bare soil	Fraction of bare soil, which includes soil crust, disturbed soil, rock and cryptogam, expressed as a percentage. This fraction has also been referred to as bare ground.
Green vegetation	Fraction of green vegetation covering the soil surface, expressed as a percentage. This fraction has also been referred to as photosynthetic vegetation.
Non-green vegetation	Fraction of non-green vegetation, which includes litter and dry attached vegetation, covering the soil surface expressed as a percentage. This fraction has also been referred to as non-photosynthetic vegetation.
Project	Ground cover monitoring for Australia project
Product	MODIS-derived fractional vegetation product of Guerschman et al. (2009). Most current version is Guerschman et al. (2015).

Chapter 19. Terrestrial LiDAR for measuring above-ground biomass and forest structure

K. Calders[1*], P. Wilkes[2,3], M. I. Disney[2,3], J. Armston[4,5], M. Schaefer[6], W. Woodgate[6]

[1] Ghent University, Belgium
[2] University College London, UK
[3] National Centre for Earth Observation, UK
[4] University of Maryland, USA
[5] Joint Remote Sensing Research Program, University of Queensland, AUS
[6] Commonwealth Scientific and Industrial Research Organisation, AUS

*Corresponding author:
kim.calders@ugent.be

Abstract

Uptake of terrestrial laser scanning (TLS, or terrestrial LiDAR) technology for monitoring ecosystems has significantly increased over the recent years. This chapter gives guidance on available instruments, fieldwork protocols and data analysis for estimating aboveground biomass (AGB) and 3D forest structure.

This chapter describes data acquisition and analysis tools for (i) geometric modelling and (ii) gap probability monitoring. These two approaches have potentially different data requirements, and hence different fieldwork planning. Guidance is given to determine the fit-for-purpose workflow for estimating AGB and forest structure using terrestrial LiDAR.

Key Points

- Geometric modelling of TLS data requires accurate (sub-cm) co-registration of multiple scan locations to minimise occlusion in the point cloud. Gap probability monitoring allows for fast analysis and only requires single scans for the plant area volume density (PAVD i.e. the volume of plant material per unit canopy volume) as a function of canopy height. Mutiple registered scans are required for 3D modelling of canopy gap probability (i.e. voxelization), wheras vertical PAVD profiles are not horizontally discrete and only require single scans.
- We currently recommend the use of retro-reflective targets to aid co-registration. Fully-automated reflector-less registration algorithms are available but are an active area of research and still need proper testing (i.e. quantifying the effect of ecosystems, instrument characteristics and sampling design on the resulting point clouds) before being deployed in an operational context.
- Sampling strategies for geometric modelling should aim for minimal occlusion and uniform point density in order to provide consistent point cloud quality throughout the plot. This may require sampling over a larger area than the plot size, particularly for smaller plots.
- Estimating AGB requires (i) segmentation of the full point cloud into single trees; (ii) geometric modelling to estimate volume; and (iii) conversion of volume to AGB using wood density.

1.1 Background

Large area mapping based on remote sensing (satellite) data rarely record the type of forest structural and dynamic information we require at plot-level (1 ha to sub-ha scales) directly. These broad-scale mapping approaches generally use models, ancillary data or various simplifying assumptions to extract structural information. However, these data offer a synoptic view over large or otherwise inaccessible areas. Terrestrial laser scanning (TLS), or terrestrial LiDAR, is a ground-based remote sensing approach that can measure 3D vegetation structure (i.e. the location and size of canopy constituents) to centimeter or even millimeter accuracy and precision. Figure 1.1 shows an example of a TLS point cloud captured with a RIEGL VZ-400 instrument (Calders et al., 2016).

Figure 1.1: Example of a segmented TLS point cloud from Wytham Woods, UK. Single trees extracted for a 20 x 100 m transect. Data captured with a RIEGL VZ-400 instrument. (a) Top view; (b) Side view [Image provided by K. Calders]

Recent advancements in TLS show great potential to provide calibration/validation data for passive and active air/spaceborne data. It also provides better quantified (and, generally, reduced) uncertainty and more traceability for traditional forest inventories (Newnham et al., 2015; Anderson et al., 2015). However, at the fine (sub-ha plot) scale, it has been difficult to incorporate rapid and robust assessment of accurate ground reference data of 3D forest structure into existing surveying and mapping strategies. This is in part due to the relatively recent development of such detailed structural data and the consequent lack of consistent methods and tools for processing and analysing these data in conjunction with more traditional survey and monitoring methods (Calders et al., 2015a). The potential of TLS for forest monitoring was first demonstrated more than a decade ago, but has not yet reached its full potential, for the reasons outlined above. A range of scientific and commercial scanners are currently available and the most common ones are listed in Table 1.1.

The focus of TLS in the past 15 years has been to present a more objective and robust tool to measure forest structural metrics that are historically accepted for inventories (e.g. tree height, diameter at breast height, crown dimensions). However, this does not fully exploit the detailed vegetation structural information contained in terrestrial LiDAR scans. Two general modeling approaches are used to derive forest metrics from the acquired 3D data: *gap probability* and *geometric modelling*. These two streams not only provide different products, they also require different fieldwork considerations. Gap probability measurements consider individual samples within a plot, whereas geometric modelling requires individual tree measurements to be derived from multiple scan locations co-registered to a common coordinate system. The latter can require deployment of highly-reflective targets in the field that act as tie-points between different scans; this increases the time required in the field. Recent work on reflector-less registration algorithms is promising (Kelbe et al., 2016), but more testing (i.e. quantifying the effect of ecosystems, instrument characteristics and sampling design on the performances of these algorithms) is required before we would recommend using this in an operational context. Examples of applications from gap probability measurements are the assessment of vertical plant profiles (i.e. the amount of plant material, the area (m^2) or volume (m^3) per m^3 of canopy volume, as a function of canopy height), monitoring phenological dynamics, quantifying within-canopy light environment properties or analysing animal habitats. Geometric modelling of the point cloud data provides explicit 3D quantitative structure models (QSMs) that can be used to calculate woody volume (and can

subsequently be converted to above-ground biomass using wood density) or study tree and stand architecture. QSMs (but also point cloud data) can be used to support and complement traditional forestry measurements such as diameter and tree height. 3D quantitative data can provide information beyond these inventory traditional measurements, such as branch size, crown size and shape.

Table 1.1: Overview of commonly used commercial and scientific TLS instruments

Instrument	**RIEGL VZ-400**	**Leica C10**	**Leica HDS7000**	**Optech ILRIS-HD**	**FARO Focus3D X 330**	**Trimble TX8**	**CBL**	**DWEL**
Commericial (C)/Scientific (S)	C	C	C	C	C	C	S	S
Ranging method	Time-of-flight	Time-of-flight	Phase-shift	Time-of-flight	Phase-shift	Time-of-flight	Time-of-flight	Time-of-flight
Maximum # returns	Multiple	Single	Single	Single	Single	Single	2	Multiple
Wavelength [nm]	1550	532	1500	1535	1550	1500	905	1064 & 1548
Range [m]	0.5 – 350 (high speed) 0.5 – 600 (long range)	0.1-300	0.3-187	3 – 1250	0.6 - 330	0.6 - 120	40 (max)	1 - 40
Samples/sec	42,000–122,000	50,000	101,6000	10,000	122,000-976,000	1,000,000	~ 23,500	2000
Beam Divergence [mrad]	0.3	0.1	< 0.3	0.150	0.19	0.177	15	2.5
Weight [kg]	9.6	13	10	14	5.2	11	3.4	22
Temperature range [deg C]	0 - 40	0-40	0-45	-20 – 40	5 – 40	0-40	NA	NA

19.1 Geometric modelling

19.1.1 Fieldwork considerations

When designing a sampling strategy for capturing data at plot level, it is important to consider that the resulting point cloud needs to:

1. Capture a large proportion of the target canopy to:
    a. be spatially representative and account for occlusion; and
    b. sample a wide range of view angles
2. Have a uniform point density across the scanning domain.
3. Be easily co-registered with the required degree of accuracy.

It is essential for the co-registration that the overall scan pattern forms a continuous "chain" where each scan location is linked to the next and previous locations (Figure 1.2A). A number of different configurations have been trialled dependent on stem and understory density. For example, when understory vegetation is dense a higher resolution sampling grid has been used e.g. 10 m x 10 m, to ensure adequate sampling of the canopy through the understory as well as occlusion of adjacent scan locations; whereas, if the understory is more open, a 20 m x 20 m sampling grid has been used (Wilkes et al., 2017). In very dense vegetation, a clear view of the tree upper canopy may not always be possible; however, it is important to continue a regular scanning "chain" to aid co-registration.

If the understorey is sufficiently open, a sampling configuration as presented in Figure 1.2B can be used. Targets are set out on a per row basis where once the end of a row is reached all targets are shifted on to the next row. For the first and last rows, targets are set out in a similar pattern outside of the grid. Targets are also located outside of the plot at the beginning and end of each row. For example, moving left to right in Figure 1.2B, targets outside Row 1 and between Row 1 and 2 are used when scanning Row 1. Once Row 1 is complete, the targets outside of Row 1 are moved to between Row 2 and 3 and Row 2 is scanned. In this example, four targets are used per quadrant, where a quadrant is bounded by a scan location at each corner.

An alternative sampling pattern applicable to more dense vegetation is presented in Figure 1.2C. From Scan Location 1 a set of 6 targets are located in view of the scan aperture between Scan Location 1 and Scan Location 2, once scanning is completed the scanner is moved to Scan Location 2. Before scanning at Scan Location 2, a second set of 6 targets is located between Scan Location 2 and 3. This can be a time-consuming process given that the placement of targets ideally requires consideration of target visibility from multiple, adjacent, scan locations. The more dense the vegetation, the more important and difficult this process becomes. After scanning is completed at Scan Location 2, the scanner is moved on to Scan Location 3 and the targets between Scan Location 1 and 2 are moved to between Scan Location 3 and 4. Once the end of a row is reached, scanning continues down the next row. The rows are linked by placing targets between the first and last scans positions of the adjacent rows as illustrated between Scan Locations 22 and 23 in Figure 1.2C.

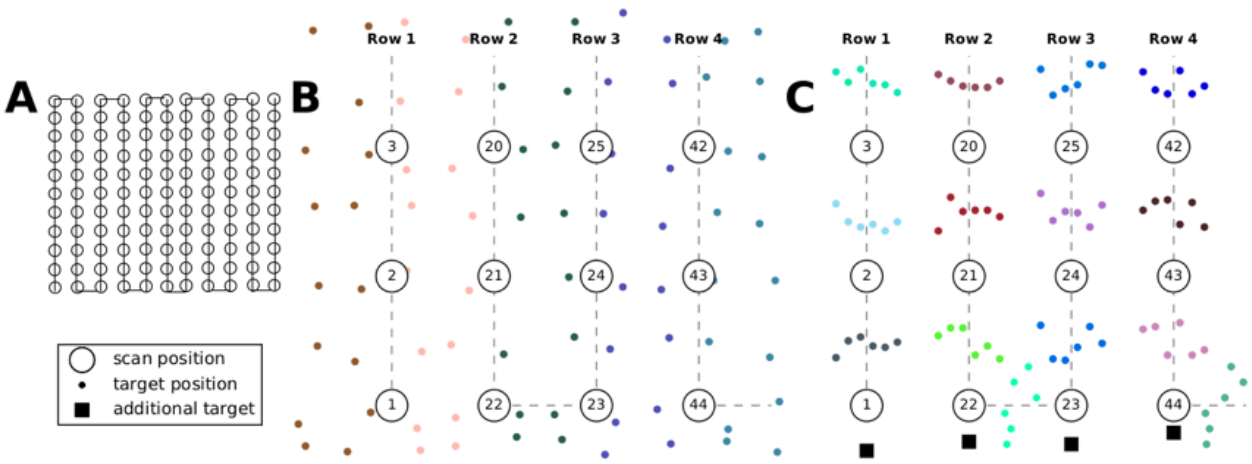

Figure 1.2: Sampling pattern configurations for capturing TLS data over large area, where scan locations are linked by a continuous ”chain” (A). Examples of sampling patterns where targets are common between rows (B) and between scan locations (C) [Figure from Wilkes et al., 2017].

Some TLS instruments, such as the RIEGL VZ-400, do not acquire a full hemispherical scan. In these situations, an additional scan is acquired from the same sampling location with the scanner tilted at 90° from the vertical to complete sampling of the full hemisphere. If tilted scans are required, to ensure targets are in the instrument's field of view, it is common practice to align the scanner at each location so that the tilt scan is perpendicular to the direction of the scanning transect i.e. the scanner's rotation axis is perpendicular to the sampling transect. If using the method described in Figure 1.2C it is important to include an extra target on the outside of the grid at the beginning and end of the scanning chain e.g. Scan Location 1, or at the end of a row Scan Location 22 and 23 in Figure 1.2C. This is to compensate for the lack of targets outside the grid, thereby, reducing roll and pitch errors when co-registering the tilt and upright scans.

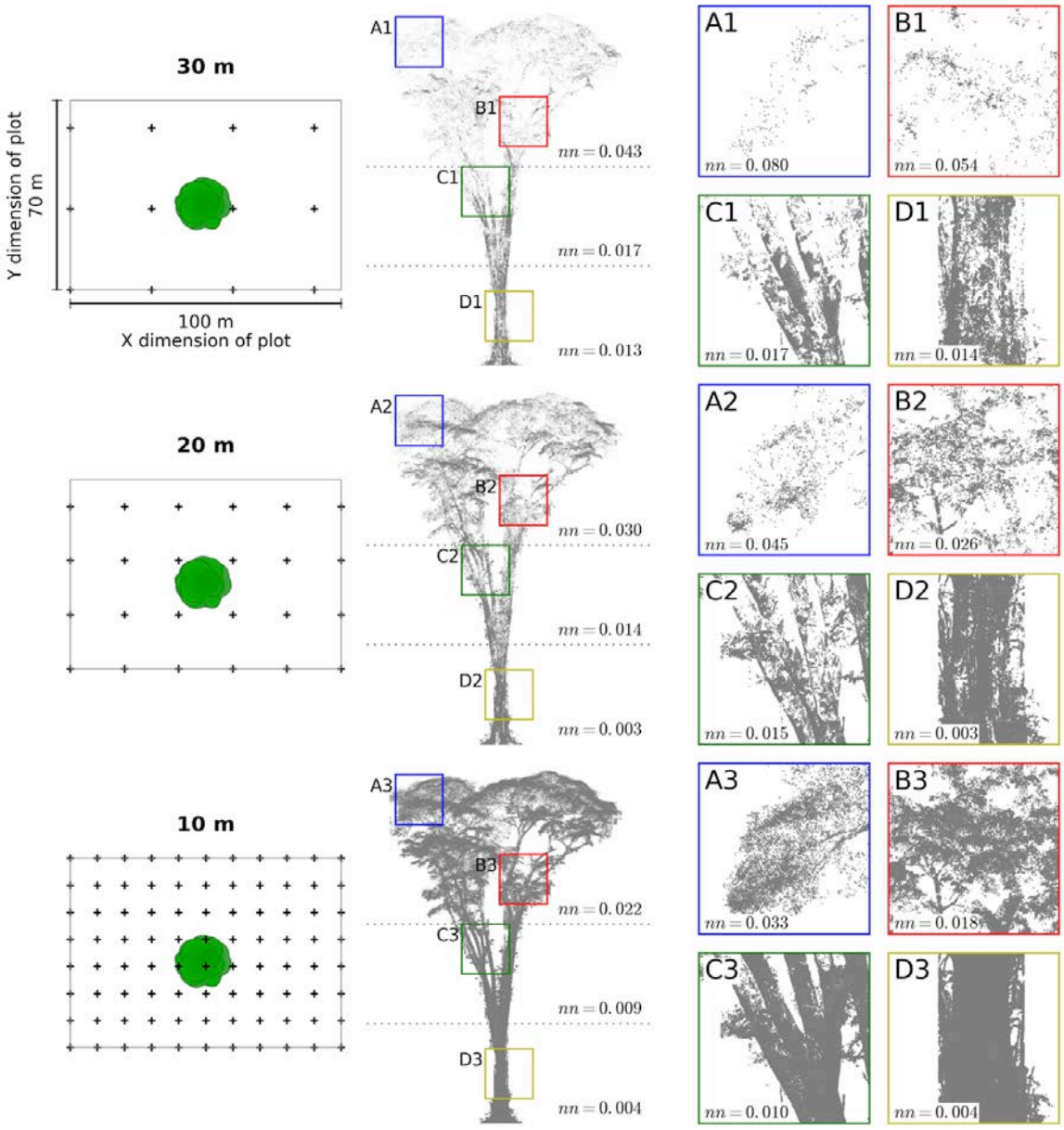

Figure 1.3: A comparison of mean nearest neighbour distance (nn) for points that comprise an individual tree derived using 10, 20 and 30 m grid sampling densities.
(Left column) The location of sample points (+) and location and extent of the target tree.
(Middle column) Point cloud representations of the sampled tree including mean nearest neighbour distance for different canopy heights.
(Right column) Subset 3 m x 3 m x 3 m voxels for different areas of the tree, locations are identified in the middle column. The tree has been extracted from the Ankasa AfriSCAT plot in Ghana [Figure from Wilkes et al., 2017].

The number of scan locations is also an important consideration, particularly in tall or dense forest canopies. A sparse sample grid can save time and resources, particularly for large area field campaigns and monitoring programs. However, this may cause issues with co-registration and result in heterogeneity in point density across the plot. When extracting a single tree (Figure 1.3), decreasing the sample density significantly decreases the fidelity of branching structure towards the top of the canopy and potentially leading to more uncertainty in derived outputs sensitive to these canopy components.

For accurate geometric modelling of forest plots, we recommend scanning over a one ha square plot, on a 10

m x 10 m grid, where reflective targets are set out in a 'rolling' format. This protocol has been adopted across a number of forest types, from dense tropical rainforest to commercial conifer plantations (Wilkes et al., 2017). It should be noted these recommendations are drawn from using a high specification time-of-flight RIEGL VZ-400 TLS instrument (RIEGL Laser Measurement Systems GmbH) and subsequent post-processing using RiScanPro. The conclusions drawn are intended most directly for users of this instrument in forested environments. However, the presented sampling framework and other recommendations could be modified to suit coarser resolution or lower powered instruments.

The methods currently employed by TERN to collect TLS data at each site are described below. To enable high fidelity reconstruction of the entire canopy at core one ha forest sites, we recommend taking into account the guidelines above to modify this design (adding more scan locations) when understory is dense and/or trees are tall, i.e. > 25 m.

1. At each of the TERN calibration/validation field sites, TLS measurements are recorded using a RIEGL VZ-400 (Figure 1.4). Metadata is collected on Android mobile devices using forms developed with the Open Data Kit (ODK) (http://opendatakit.org/).

Figure 1.4: Recording TLS measurements and metadata in the field using a RIEGL VZ-400 Laser Scanner (Credit: Remote Sensing Centre, Queensland Department of Science, Information Technology and Innovation).

2. Seven TLS scan locations are acquired per site in a radial configuration designed to be coincident with point intercept transects (Figure 1.5). One position is located at the centre of the site, followed by six scans taken approximately 33.3 m from the centre along each of the transect arms at 0, 60, 120, 180, 240 and 300 degrees from magnetic north. By using this radial configuration, scan locations have equal spacing and any location within 50 m radius of plot centre has a maximum horizontal distance of 16.6 m to any other scan location.
3. At each scan location an upright and tilted (90 degree from vertical) RIEGL VZ-400 scan is acquired to ensure uniform sampling for 0-360 degree azimuth and 0-130 deg zenith. An angular shot density of 0.04 degrees is currently used.
4. Depending on the tree density of a site, between 12 and 24 retro-reflective targets are typically deployed at each site to allow co-registration of scans. Between 2 and 4 targets are placed in each 60 degree segment between transects. To ensure retro-reflective targets are within the field of view of the upright and tilt scans, the tilt scans have the TLS aligned parallel with the transect.

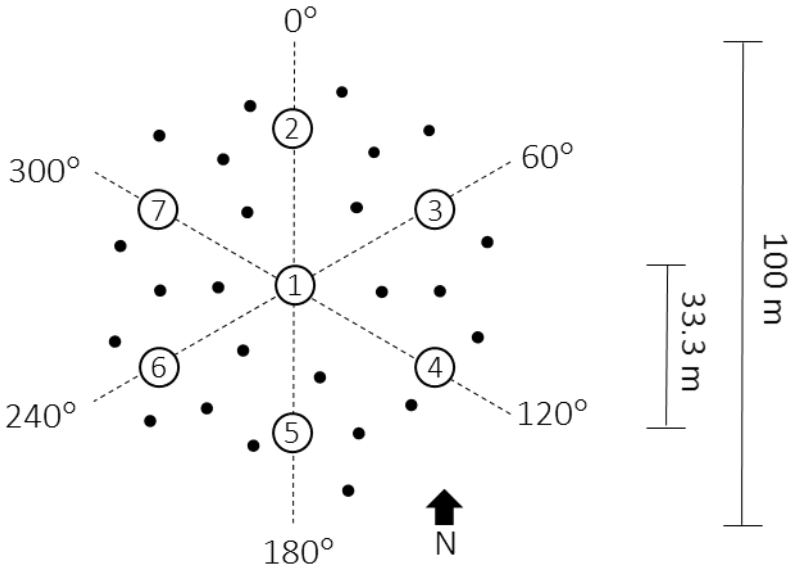

Figure 1.5: Radial sampling configuration for TERN Landscape Assessment sites, where scan locations are coincident with point intercept transects also acquired at each site. One scan is located at the plot centre, and the remaining six scans are located at 33.3 m from centre along each transect. This results in equal spacing between scan locations and a maximum horizontal distance of 16.6 m to any scan location within 50 m radius of plot centre. The location number indicates the order of acquisition. The black dots are example reto-reflective target placements; there should be an equal number of targets in each 60 deg slice, but they can be distributed randomly within the slice.

19.1.2 Estimating above-ground biomass

After data collection and data registration of individual scans to a common project coordinate system, three steps are required to estimate AGB:

1. Extract single trees from the full point cloud;
2. Derive volume estimates from the single tree point clouds;
3. Convert volume to AGB using estimates of wood density.

The extraction of single trees is time-consuming, and it is advised to use a semi-automated or automated workflow if many trees need to be extracted. Burt (2017) uses a C++ library based on the open-source Point Cloud Library (Rusu & Cousins 2011) for the extraction of single trees. This method was used in Calders et al. (2015b), and extracts single trees in four steps: (i) identification of individual stems through segmentation of the ground plane; (ii) RANSAC (Schnabel, et al., 2007) cylinder fitting to these stems and application of a series of pass-through filters with respect to the unfiltered point cloud to extract the individual trees; (iii) sequential identification of clusters defined by point density in height bins along the length of the tree to remove noise and unrelated vegetation; and (iv) visual inspection against the whole point cloud and, if needed, manual removal of unrelated vegetation from other trees. Figure 1.1 shows an example of a segemented leaf-off point cloud into single trees. Point clouds from leaf-on trees require leaf removal before geometric modelling. Burt (2017) and Disney et al. (2018) describe leaf separation methods that are based on geometrical descriptors in the point cloud.

Geometric modelling translates the 3D point cloud of a single tree into a quantitative structure model (QSM) that allows for the calculation of volume (Figure 1.6). These volume estimates can then be converted to AGB using wood density. Different geometric primitives (e.g. circular cylinder, elliptical cylinder, circular cone or

polygonal cylinder) can be used for the generation of QSMs. Åkerblom et al. (2015) found that the circular cylinder was most robust in the context of well-bounded volumetric errors and overcoming noise and gaps in the TLS data. Two commonly used QSM methods are those of Raumonen et al. (2013) and Hackenberg et al. (2015). Both methods use cylinder-fitting, and a comparison of both methods in Hackenberg et al. (2015) showed that volume estimates from both methods were broadly comparable in terms of accuracy and fidelity. Disney et al. (2018) discuss the issues of TLS acquisition for AGB, including sources of uncertainty. Uncertainty can be related to the TLS data (registration error, occlusion, wind and noise) or quantitative structure model (QSM) reconstruction (segmentation error and geometric structure error due to cylinder versus real shape).

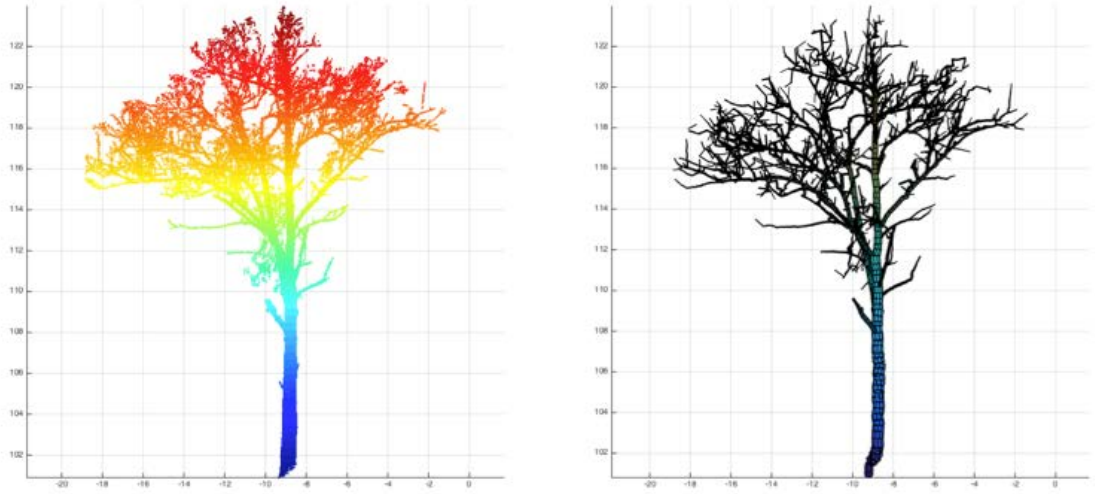

Figure 1.6: Point cloud (left) and corresponding QSM (right) using the method of Raumonen et al. (2013). [Image provided by K. Calders]

19.2 Gap probability modelling

19.2.1 Fieldwork considerations

Acquiring TLS data to estimate vertical gap probability profiles requires no co-registration of individual scans. This implies that data collected for geometric modelling can be used to estimate vertically resolved gap probability, but not the other way around. Data collection for PAVD profiles can be done at a relatively low point density. Calders et al. (2014) showed very little difference in the profiles generated from $0.04^\circ \times 0.04^\circ$ angular sampling and a subsampling with a factor of two. A resolution reduction of a factor 50 (i.e. keeping only 2% of the data) will still follow the general shape of the vertical plant profiles, but the PAVD profile will differ locally. Quantifying horizontial variation in directional canopy gap probability using voxelization methods does require co-registration of scans and higher point cloud densities (Hancock et al., 2017). The number of individual scans varies and depends on, e.g., available resources, structural heterogeneity within the plot or plot size. Examples of different sampling designs previously used in Australia are visualised in Figure 1.7 and Figure 1.5. These designs were selected based on the existing plot layout. As for any TLS data acquisition, scanning during rain should be avoided and low wind speeds are preferred.

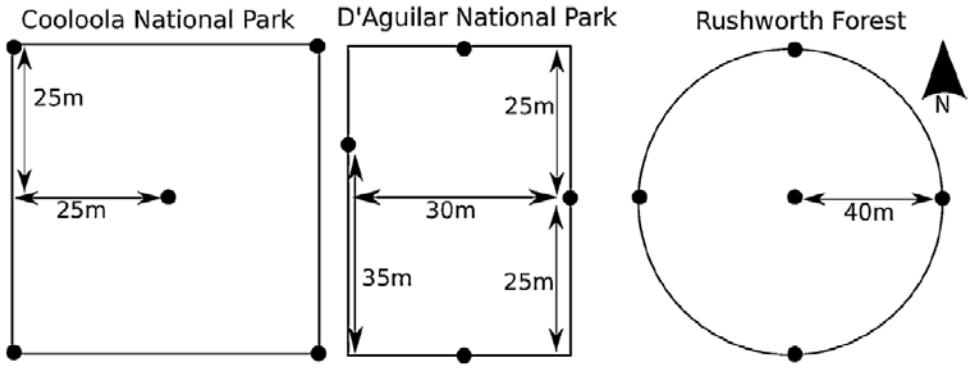

Figure 1.7: Different TLS sampling designs for Cooloola National Park (QLD), D'Aguilar National Park (QLD) and Rushworth Forest (VIC). Scan locations are indicated with a black dot. [Modified from Calders et al., 2014]

19.2.2 Estimating forest structure and AGB

Vertical plant profiles are calculated from estimates of the vertically resolved gap probability (*Pgap*(θ; *z*), derived from TLS data (Jupp et al., 2009). *Pgap*(θ;z) is calculated as 1−(∑wi(zi<z, θ))/N(θ),where w=1/ns with ns the number of returns for the outgoing pulse. An integrated *Pgap* over the upward hemisphere is equivalent to the canopy openness metric (Jennings et al., 1999).

The zenith angles (θ) are measured by the TLS instrument and *z* is the vegetation height above the reference height. Figure 1.8 shows the cross section of a zenith ring ranging from zenith angle θ_1 to θ_2. These zenith rings are typically five degrees. Figure 1.8 illustrates that not correcting for height will not influence the total gap fraction as a function of zenith angle (*Pgap* (θ)), but estimates of *Pgap*(θ; z) may be different to *Pgap*(θ; h). In other words, the total plant area index (PAI) would be the same for the corrected or uncorrected heights since it is the integral of the whole canopy, but vertical plant profiles would be different (Zhao et al., 2013).

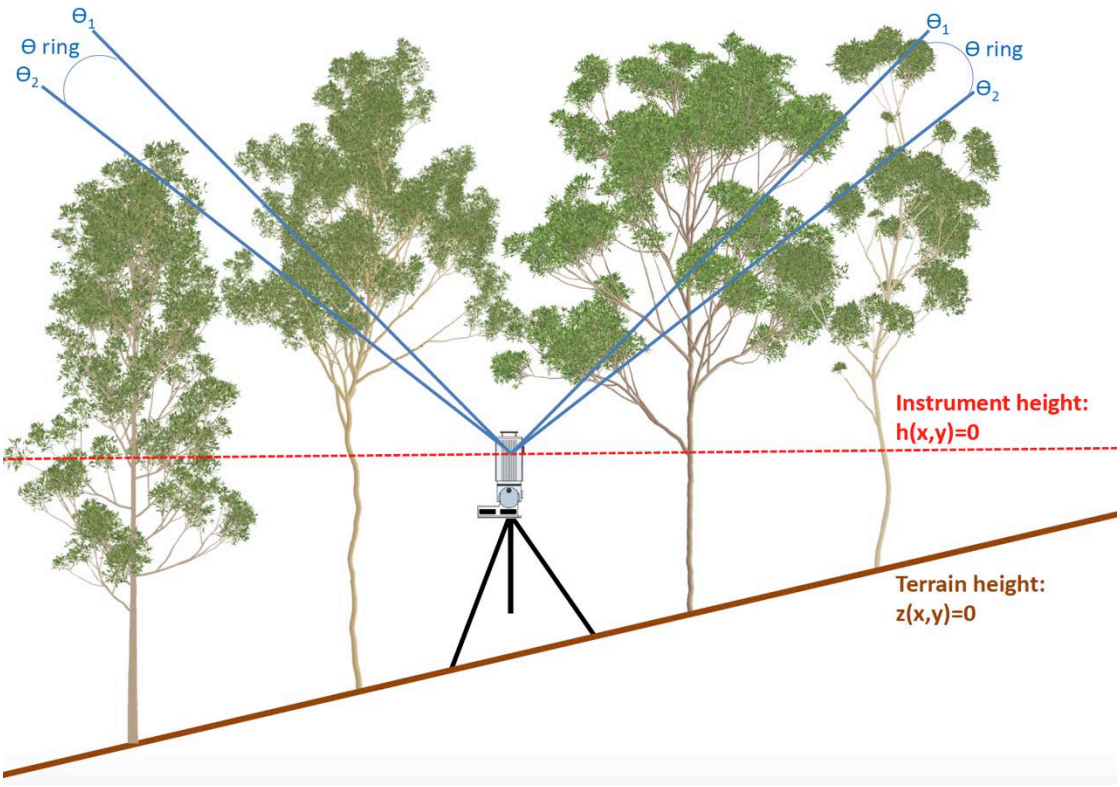

Figure 1.8: Illustration of TLS gap probability estimates. LiDAR heights are recorded with respect to the origin of the instrument (red line) and not to the true topography (brown line). The blue lines represents a cross section of a zenith ring. These zenith rings are used to calculate the vertically resolved gap fraction. [Image provided by K. Calders]

Terrain correction can be done by: (a) plane fitting through single scan data; (b) the use of a DTM from co-registered TLS data; or (c) the use of an independent DTM from e.g. airborne LiDAR. Separation of ground and near-ground plant material is unreliable when using plane-fitting, and DTM correction is preferred when extending the vertical profiles down to the ground.

The open source library Pylidar has implemented the calculation of vertical plant profiles and can be accessed at http://pylidar.org/. An example pylidar_canopy command-line for calculating a vertical plant profile from a RIEGL scan is demonstrated below:

$ *pylidar_canopy -i [in_rxp] -o [vpf] -w -p -r [plane_report] --minzenith 35 --maxzenith 70*

This will generate a vertical plant profile [vpf] from input scan [in_rxp], using weighted multiple returns and using the Jupp et al. (2009) method for the zenith interval 35 - 70 deg. A plane correction (Calders et al., 2014) has been applied in this example and the [plane_report] provides additional information such as slope and aspect of the study site. The resulting vertical profile and the effect of the topographic correction is visualised in Figure 1.9.

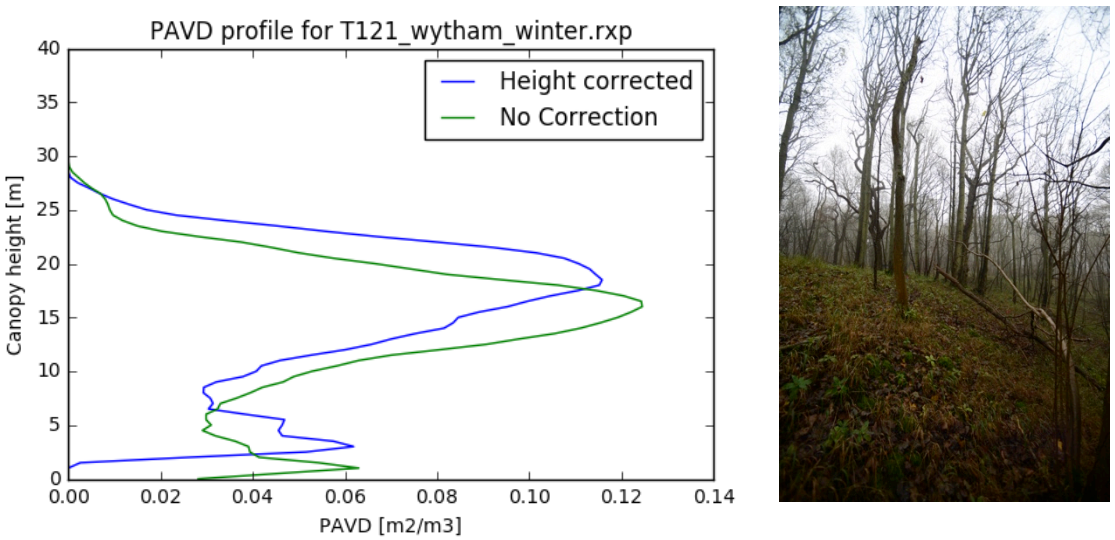

Figure 1.9: Comparison of vertical plant profile with and without height corrected through plane fitting for a leaf-off scan in Wytham Woods, UK. Total effective PAI is 1.54.

The use of vertical profiles for estimating AGB has not been published to date. Preliminary work on pre and post harvest profiles in Rushworth Forest demonstrates the potential for monitoring changes in AGB using gap probability analysis (Figure 1.10). More research is required to link these profiles to absolute quantities of AGB.

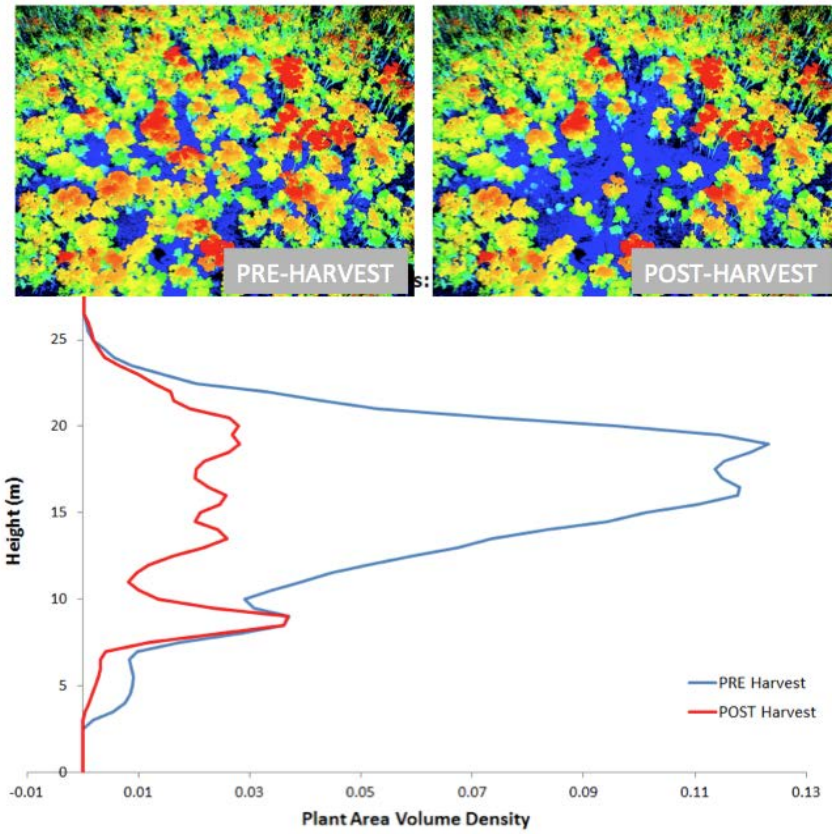

Figure 1.10: Rushworth Forest (RUSH07, VIC) pre- and post-harvest profiles in centre of plot (radius 40m). [Image provided by K. Calders]

19.2 Conclusions and Future Projections

TERN Landscape Assessment is currently collecting terrestrial LiDAR data using three different scanners, a RIEGL VZ-400, the dual wavelength echidna lidar (DWEL) and CBL, for all of the calibration validation field sites around Australia. These TLS scans, when acquired correctly, can quickly and easily provide an overall vegetation structural summary of the field site being examined. Table 1.1 lists the specification of the different instruments, and the appropriate scanner (e.g. maximum range, portability, resolution) should be selected depending on which tree and forest variables that want to be measured, as well as the ecosystem. Current technological developments of TLS instruments have produced more lightweight and compact scanners, such as the CBL and Leica BLK360. The new RIEGL VZi-series and Leica BLK-360 also support on-board automated registration, but this requires further testing in forest environments before being deployed in an operational context.

Mobile LiDAR sensors such as the ZEB-1 and ZEB-REVO are lightweight and do not require the use of reflectors and can potentially be used to quickly assess forest structure (Bauwens et al., 2015). However, the current resolution and maximum range of these instruments is limited (approx. 30 m), which might be problematic in more complex ecosystems and tall forests. Recent developments in autonomous ground-based LiDAR instruments will help us to increase the temporal resolution of 3D data. The VEGNET IML is designed to create daily vertical plant profiles and can, potentially, assist in monitoring changes in AGB and forest structure (Portillo-Quintero et al., 2014).

Acknowledgements

Wytham Woods TLS data has been collected within the Metrology for Earth Observation and Climate Project (MetEOC-2) within the European Metrology Research Programme (EMRP) funded by the EMRP participating countries within EURAMET and the European Union under Grant ENV55. M. Disney acknowledges the support of the UK's NERC Natural Environment Research Council (NERC) National Centre for Earth Observation (NCEO), and under grants NE/N00373X/1 and NE/P011780/1. K. Calders is funded by BELSPO (Belgian Science Policy Office) in the frame of the STEREO III programme – project 3D-FOREST (SR/02/355).

References

Åkerblom, M., Raumonen, P., Kaasalainen, M., and Casella, E. (2015). Analysis of geometric primitives in quantitative structure models of tree stems. *Remote Sensing*, 7(4), 4581-4603.

Anderson, K., Hancock, D., Disney, M. I. and Gaston, K. J. (2015) Is waveform worth it? A comparison of LiDAR approaches for vegetation characterisation. *Remote Sensing for Ecology and Conservation*, 2, 5-15.

Bauwens, S., Bartholomeus, H., Calders, K. and Lejeune, P. (2016) Forest inventory with terrestrial LiDAR: A comparison of static and hand-held mobile laser scanner. *Forests* 7(6), 127

Burt, A. (2017) New 3D Measurements of Forest Structure, PhD Thesis, University College London, unpublished.

Calders, K., Burt, A., Origo, N., Disney, D., Nightingale, J., Raumonen, P. and Lewis P. (2016). Large-area virtual forests from terrestrial laser scanning data. In IEEE International Geoscience and Remote Sensing Symposium (IGARSS 2016), 10-15 July 2016, Beijing, China. p. 1765-1767.

Calders, K., Newnham, G., Armston, J., Disney, M.I., Schaaf, C., and Paynter, I. (2015a) Terrestrial LIDAR for forest monitoring, Chapter 2.10. In book: A sourcebook of methods and procedures for monitoring and

reporting anthropogenic greenhouse gas emissions and removals associated with deforestation, gains and losses of carbon stocks in forests remaining forests, and forestation, Edition: GOFC-GOLD Report version COP21-1, Publisher: GOFC-GOLD Land Cover Project Office, Wageningen University, The Netherlands.

Calders, K., Newnham, G., Burt, A., Murphy, S., Raumonen, P., Herold, M., Culvenor, D., Avitabile, V., Disney, M., Armston, J. and Kaasalainen, M. (2015b) Nondestructive estimates of above-ground biomass using terrestrial laser scanning. *Methods in Ecology and Evolution*, 6, 198-208.

Calders, K., Armston, J., Newnham, G., Herold, M. and Goodwin, N. (2014) Implications of sensor configuration and topography on vertical plant profiles derived from terrestrial LiDAR. *Agricultural and Forest Meteorology*, 194, 104-117.

Disney, M. I., Boni Vicari, M., Calders, K., Burt, A., Lewis, S., Raumonen, P. and Wilkes, P. (2018) Weighing trees with lasers: advances, challenges and opportunities, Royal Society Interface Special Issue on Royal Society meeting '*The terrestrial laser scanning revolution in forest ecology'* 8: 20170048.

Kelbe, D., van Aardt, J., Romanczyk, P., van Leeuwen, M., and Cawse-Nicholson, K. (2016). Marker-free registration of forest terrestrial laser scanner data pairs with embedded confidence metrics. IEEE *Transactions on Geoscience and Remote Sensing*, 54(7), 4314-4330.

Hackenberg, J., Spiecker, H., Calders, K., Disney, M. and Raumonen, P. (2015) SimpleTree - An Efficient Open Source Tool to Build Tree Models from TLS Clouds. *Forests,* 6, 4245-4294.

Hancock, S., Anderson, K., Disney, M., & Gaston, K. J. (2017). Measurement of fine-spatial-resolution 3D vegetation structure with airborne waveform lidar: Calibration and validation with voxelised terrestrial lidar. *Remote Sensing of Environment*, 188, 37-50.

Jennings, S.B., Brown, N.D., & Sheil, D. (1999). Assessing forest canopies and understorey illumination: Canopy closure, canopy cover and other measures. *Forestry*, 72(1), 59-73.

Jupp, D. L. B., Culvenor, D. S., Lovell, J. L., Newnham, G. J., Strahler, A. H., and Woodcock, C. E. (2009). Estimating forest lai profiles and structural parameters using a ground-based laser called echidna. *Tree physiology*, 29, 171-181.

Newnham, G.J., Armston, J.D., Calders, K., Disney, M.I., Lovell, J.L., Schaaf, C.B., Strahler, A.H., and Danson, F.M. (2015) Terrestrial Laser Scanning For Plot Scale Forest Measurement. *Current Forestry Reports,* 1, 239-251.

Newnham, G., Armston, J., Muir, J., Goodwin, N., Tindall, D., Culvenor, D., Puschel, P., Nystrom, M., and Johansen, K. (2012). Evaluation of terrestrial laser scanners for measuring vegetation structure. CSIRO Sustainable Agriculture Flagship.

Portillo-Quintero, C., Sanchez-Azofeifa, A., Culvenor, D., 2014. Using VEGNET in-situ monitoring LiDAR (IML) to capture dynamics of plant area index, structure and phenology in Aspen Parkland Forests in Alberta, Canada. *Forests* 5, 1053–1068.

Raumonen, P., Kaasalainen, M., Markku, A., Kaasalainen, S., Kaartinen, H., Vastaranta, M. et al. (2013) Fast automatic precision tree models from terres-trial laser scanner data. *Remote Sensing*, 5, 491–520.

Rusu, R.B. & Cousins, S. (2011) 3D is here: point Cloud Library (PCL).In IEEE International Conference on Robotics and Automation 2011 (ICRA 201 1), 9–13May 2011, Shanghai, China.

Schnabel, R., Wahl, R., & Klein, R. (2007). Efficient RANSAC for point-cloud shape detection. Computer graphics forum, 26:2, 214-226.

Wilkes, P., Lau, A., Disney, M., Calders, K., Burt, A., Gonzalez de Tanago Menaca, J., Bartholomeus, H., Brede,

B. and Herold, H. (2017). Data Acquisition Considerations for Terrestrial Laser Scanning of Forest Plots. *Remote Sensing of Environment*, 196, 140-153.

Zhao, F., Yang, X., Strahler, A. H., Schaaf, C. L., Yao, T. et al. (2013). A comparison of foliage profiles in the Sierra National Forest obtained with a full-waveform under-canopy EVI lidar system with the foliage profiles obtained with an airborne full-waveform LVIS lidar system. *Remote Sensing of Environment*, 136, 330-341.

TERN

tern.org.au

Effective field calibration and validation practices

August 2018

TERN is supported by the Australian Government through the National Collaborative Research Infrastructure Strategy.